DOCTORAL THESIS

Efficient High-Speed Small Craft: Performance in Calm Water and Waves

Rasul Niazmand Bilandi

Efficient High-Speed Small Craft: Performance in Calm Water and Waves

RASUL NIAZMAND BILANDI

TALLINN UNIVERSITY OF TECHNOLOGY
School of Engineering
Estonian Maritime Academy
This dissertation was accepted for the defence of the degree of Doctor of Philosophy (Ph.D.)
on 19/11/2024

Supervisor: Ph.D., Assistant Professor Abbas Dashtimanesh
                          Tallinn University of Technology
                          Tallinn, Estonia
                          and
                          Department of Engineering Mechanics, SCI KTH Royal
                          Institute of Technology Stockholm, Sweden

Opponents: Ph.D., Alessandro Iafrati
                          Istituto di Ingegneria del Mare
                          Consiglio Nazionale delle Ricerche
                          Rome, Italy

                          Ph.D., Shan Wang
                          Assistant Professor at the Centre for Marine
                          Technology and Ocean Engineering
                          Instituto Superior Técnico
                          University of Lisbon
                          Lisbon, Portugal

Defence of the thesis: 20/12/2024, Tallinn

Declaration:
Hereby I declare that this doctoral thesis, my original investigation and achievement, submitted for the doctoral degree at Tallinn University of Technology has not been submitted for doctoral or equivalent academic degree.

Rasul Niazmand Bilandi

----
                                                              signature

European Union
European Regional
Development Fund

Investing
in your future

Tõhusad kiirekäigulised väikelaevad: jõudlus rahulikus vees ja lainetes

RASUL NIAZMAND BILANDI

Contents

Abstract

Efficient High-Speed Small Craft: Performance in Calm Water and Waves

Based on the recent International Maritime Organization (IMO) strategy to reduce greenhouse gas emissions, there is a growing demand for more efficient ships. To achieve reductions in emissions, it is essential to understand how various aspects of vessel design – such as hydrodynamics, propulsion systems, and automation – affect performance. However, IMO regulations primarily target large ships and largely neglect smaller vessels, such as high-speed craft, which are prevalent in certain areas. This regulatory gap highlights the need for more research and stricter controls on these smaller craft. The Baltic Sea, especially in Scandinavia, has a high per capita concentration of high-speed craft, with Finland, Sweden, and Norway among the leaders in boat ownership. With approximately 3.5 million leisure boats operating near coastlines in the Baltic, the rise in high-speed craft exacerbates pollution, disrupts shipping traffic, and poses safety risks to coastal residents. To address these issues, developing more efficient high-speed craft is crucial. Innovative hull designs, such as stepped hulls, can significantly mitigate their environmental impact and help safeguard the Baltic Sea's ecological and economic health.

Stepped hulls can significantly reduce frictional resistance by strategically placing steps in the hull bottom to ensure flow separation at the steps and adequate ventilation in the lee of the steps. However, the choice of longitudinal location and height of the steps is crucial. Inadequate choice of step location and step height can result in a step that does not function well, which can increase resistance, leading to higher fuel consumption, reduced dynamic performance, compromised seaworthiness, stability issues, decreased crew safety, and shortened structural fatigue life. Understanding the hydrodynamic principles of a planing hull is essential to grasp the rationale behind a stepped design. A step helps maintain trim at high speeds, avoiding increased drag resistance and improving fuel efficiency. Furthermore, in planing hulls with outboard engines, hull-propeller interaction is minimal, underscoring the importance of optimizing the hull design for maximum fuel efficiency.

Despite their potential, there are no specific guidelines for stepped hull design. Various step designs can be used to reduce resistance and improve fuel efficiency, but their optimized shape and arrangement, as well as their effects on seakeeping and manoeuvering motions, are still unknown to naval architecture community. To fill this gap, this thesis aims to investigate the hydrodynamics of different stepped hulls by developing new advanced computational and mathematical models along using experiment towing tests to identify which step solutions can lead to a efficient hull form, considering performance in calm water and waves.

The study involved three phases to optimize the dynamics of stepped planing hulls. Phase One focused on straight-stepped planing hulls, where a mathematical model using a 2D+t framework and a CFD setup using the finite volume method (FVM) were developed to simulate hull performance in calm water and dynamic motion in regular waves. The models were validated against experimental results for the performance of straight-stepped hulls in calm water. However, due to a lack of experimental data for stepped hulls in regular waves, non-stepped hull data were used to validate the nonlinear motion. A verification analysis between the two models in regular waves demonstrated

strong agreement, highlighting their suitability for early-stage design and parametric studies of straight-stepped planing hulls. Notably, this phase focused on straight steps, without considering swept steps.

Phase Two introduced swept steps to the bottom of a new series of stepped hulls, which were developed and tested at the towing tank of the Dipartimento di Ingegneria Industriale della Università degli Studi di Napoli "Federico II." Eight models with forward-swept steps of varying heights and positions were evaluated for resistance in calm water. These models featured transparent bottoms to allow for observation of wetted surfaces and vortical flow phenomena behind the steps. Performance varied significantly across different speed ranges, with the C04 hull (a single forward-swept step at 48.3% of the hull length and step height of 0.91% BTC) showing superior performance at very high speeds (Fr_B = 3.9–4.97). Among double-stepped hulls, the C08 hull, featuring an additional aft step at 31.6% of the hull length, also performed well. Due to the limitations of towing tank tests in accurately capturing pressure distribution and flow separation, detailed CFD investigations were conducted. The CFD analysis, which compared wetted surface shapes with experimental data, demonstrated that CFD could accurately predict wetted surface shapes. The analysis revealed that the overset mesh approach outperforms the morphing grid method in terms of numerical uncertainty and validation for complex planing hulls.

Phase Three extended the study to irregular wave conditions using CFD modelling to explore the dynamic responses of stepless, single-stepped, and double-stepped hulls with straight steps. Discrepancies between CFD and experimental results were analysed by focusing on time history data and identifying peak and trough values using a local Maxima/Minima approach. Statistical analyses revealed complex and nonlinear motion patterns, highlighting the challenges and insights into high-speed planing hull dynamics in irregular seas. The findings indicated that the most extreme vertical acceleration outliers for the double-stepped hull at the highest speeds were 31% lower than those of the non-stepped hull, while the single-stepped hull showed a 9% reduction compared to the non-stepped hull.

Overall, this comprehensive approach – integrating mathematical modelling, towing tank experiments, and CFD simulations – offers valuable insights into optimizing stepped hull designs for diverse operational conditions, advancing naval architecture practices, and enhancing vessel performance across various speed ranges. The findings from this study can be applied to the design and development of more efficient and environmentally friendly high-speed crafts. Future research could investigate the effects of swept steps with varying heights and positions in irregular waves, as well as the impact of different step configurations on dynamic stability and manoeuvering motions, such as circle turns and zig-zag manoeuvres.

Lühikokkuvõte

Tõhusad kiirekäigulised väikelaevad: jõudlus rahulikus vees ja lainetes

Tuginedes viimasele Rahvusvahelise Mereorganisatsiooni (IMO) strateegiale kasvuhoonegaaside vähendamiseks, on tekkinud kasvav nõudlus tõhusamate laevade järele. Heitkoguste vähendamiseks on oluline mõista, kuidas erinevad laevadisaini aspektid nagu hüdrodünaamika, jõuseadmed ja automatiseerimine mõjutavad laeva sooritusvõimet. Samas on IMO regulatsioonid suunatud peamiselt suurtele laevadele, jättes väiksemad alused, nagu osades piirkondades laialt levinud kiirkaatrid, suuresti tähelepanuta. See regulatiivne lünk toob seoses väiksemate alustega esile vajaduse täiendavate uuringute ja rangemate kontrollide järele. Läänemerel, eriti Skandinaavias, on kiirkaatrite arv elaniku kohta kõrge, kusjuures Soome, Rootsi ja Norra kuuluvad kõige arvukamate paadiomanike hulka. Ligikaudu 3,5 miljonit lõbusõidulaeva sõidavad Läänemerel rannikulähedases piirkonnas, kusjuures kiirkaatrite arvu suurenemine süvendab saastet, häirib laevaliiklust ja kujutab ohtu rannikupiirkondade elanike turvalisusele. Nende probleemide lahendamiseks on oluline arendada tõhusamaid kiirkaatreid. Innovatiivsed keredisainid, nagu astmelised kered, võivad oluliselt vähendada nende keskkonnamõju ja aidata kaasa Läänemere ökoloogilise ja majandusliku tervise säilitamisele.

Astmelised laevakered võivad märkimisväärselt vähendada hõõrdetakistust. Astmete pikisuunaline asukoht ja kõrgus on üliolulised – strateegiliselt kere põhjal paigutatud astmed tagavad voolu eraldumise astmetel ja piisava ventilatsioon/õhutus astmete vahel. Vale astmete asukoha ja kõrguse valik võib põhjustada astme ebaefektiivsust suurendades takistust ning läbi selle tõsta kütusekulu, vähendada dünaamilist sooritusvõimet, kahjustada meresõiduomadusi, viia stabiilsusprobleemide, meeskonna ohutuse vähenemise ja konstruktsiooni eluea lühenemiseni. Mõistmaks astmelise disaini kontseptsiooni, on hädavajalik mõista glisserite (veepinnal libisev lamedapõhjaline kiirmootorpaat) hüdrodünaamilisi põhimõtteid. Astmed aitavad säilitada aluse väiksemat trimmi kõrgetel kiirustel, vältides suurenenud takistusjõudu ja tõhustades kütusesäästlikkust. Lisaks on päramootoriga glisserite kere ja sõukruvi interaktsioon minimaalne, rõhutades kere disaini optimeerimise tähtsust maksimaalseks kütusetõhususeks.

Hoolimata nende potentsiaalist, puuduvad spetsiifilised juhised astmeliste keredе disainiks. Erinevaid astmete disaine saab kasutada takistuse vähendamiseks ja energiatõhususe parandamiseks, kuid nende optimeeritud kuju ja paigutus ning nende mõju meresõiduomadustele ja manööverdusvõimele on laevaehituse kogukonnas veel teadmata. Selle lünga täitmiseks on käesoleva doktoritöö eesmärk uurida erinevate astmeliste keredе hüdrodünaamikat, töötada välja uusi arvutuslikke- ja matemaatilisi mudeleid ning viia läbi eksperimentaalseid mudelkatseid, et tuvastada, millised lahendused võivad viia kütusesäästliku keredisainini, võttes arvesse sooritusvõimet rahulikes vetes ja lainetes.

Uuring astmeliste glisserite optimeerimiseks hõlmas kolme etappi. Esimene etapp keskendus sirgete astmetega glisseritele, kus töötati välja matemaatiline mudel, kasutades 2D+t raamistikku, ja arvutusliku vedelikudünaamika (CFD) seadet, mis põhineb piiratud mahtude meetodil (FVM), et simuleerida kere sooritusvõimet rahulikes vetes ja dünaamilist liikumist korrapärastes lainetes. Mudeleid valideeriti eksperimentaalsete

katsete tulemustega sirgete astmetega kerede sooritusvõime kohta rahulikes vetes. Kuna eksperimentaalsed andmed astmeliste kerede kohta regulaarsetes lainetes olid puudulikud, kasutati mitte-astmeliste kerede andmeid mittelineaarse liikumise valideerimiseks. Kontrollanalüüs kahe mudeli vahel regulaarsetes lainetes näitas tugevat vastavust, rõhutades nende sobivust varajases staadiumis disaini ja sirgete astmetega glisserite parameetrilisteks testideks. See etapp keskendus peamiselt sirgetele astmetele, jättes kõrvale astmed (swept step)

Teine etapp tutvustas uut astmeliste kerede seeriat, mida arendati ja katsetati Napoli Ülikooli "Federico II" tööstusinseneeria osakonna katsebasseinis. Kaheksat erineva kõrguse ja asendiga üheastmeliste vöörisuunalise kere (single forward-swept step) mudelit hinnati takistuse suhtes rahulikes vetes. Mudelitel oli läbipaistev põhi, mis võimaldas vaadelda märgunud pindu ja keerisvoolu nähtusi astmete taga. Sooritusvõime varieerus oluliselt erinevate kiirusvahemike puhul, kusjuures C04 kere (ühe vöörisuunalise astmega 48,3% kere pikkusest ja astme kõrgus 0,91% BTC) näitas väga suurte kiiruste (Fr_B = 3.9–4.97) puhul parimat sooritusvõimet. Kahe astmega kerede seas oli hea sooritusvõime ka C08 kerel, millel oli lisaks aste ahtris 31,6% kere pikkusest. Katsebasseini katsete piirangute tõttu, mis ei võimalda täpselt jäädvustada rõhujaotust ja voolu eraldumist, viidi läbi üksikasjalikud CFD uuringud. CFD analüüs, mis võrdles märgunud pindade kujusid eksperimentaalsete andmetega näitas, et CFD suudab täpselt ennustada märgunud pindade kujusid. Analüüs näitas, et ülekattuvate võrkude lähenemisviis ületab morfoloogilise võrgustiku meetodi keeruliste glisserkerede puhul nii numbrilise ebamäärasuse kui ka valideerimise osas.

Kolmas etapp laiendas uuringut ebakorrapäraste lainetingimuste jaoks, kasutades CFD modelleerimist, et uurida sirgete astmetega, ühe astmega ja kahe astmega kerede dünaamilisi reaktsioone. CFD ja eksperimentaalsete tulemuste vahelisi lahknevusi analüüsiti, keskendudes ajalooliste andmete ja tipp- ja miinimumväärtuste tuvastamisele, kasutades lokaalse Maxima/Minima lähenemisviisi. Statistilised analüüsid paljastasid keerulised ja mittelineaarsed liikumismustrid, tuues esile kõrgete kiirustega glisserkerede dünaamika ebakorrapärastes meretingimustes. Tulemused näitasid, et kõige äärmuslikumad vertikaalse kiirenduse kõrvalekalded kahe astmega kerel kõrgeimatel kiirustel olid 31% madalamad kui mitteastmelisel kerel, samas kui ühe astmega kere näitas võrreldes mitteastmelise kerega 9% vähenemist.

Kokkuvõttes pakub see terviklik lähenemine – matemaatilise modelleerimise, katsebasseini eksperimentide ja CFD simulatsioonide integreerimine – väärtuslikke teadmisi astmeliste kerede disaini optimeerimiseks erinevates töötingimustes, edendades laevaehituspraktikaid ja parandades laevade sooritusvõimet erinevates kiirusvahemikes. Selle uuringu tulemusi saab rakendada tõhusamate ja keskkonnasõbralikumate kiirkaatrite disainimisel ja arendamisel. Tulevased uuringud võiksid keskenduda erineva kõrguse ja asendiga astmete mõjule ebakorrapärastes lainetes, samuti erinevate astmekonfiguratsioonide mõju dünaamilisele stabiilsusele ja manööverdusvõimele, nagu pöörded ja siksakmanöövrid.

List of Publications

This thesis comprises publications from the following peer-reviewed journals:

I   Niazmand Bilandi, R., Tavakoli, S., Dashtimanesh, A. (2021). Seakeeping of double-stepped planing hulls. Ocean Engineering, 236, 109475. https://doi.org/10.1016/j.oceaneng.2021.109475.

II   Vitiello, L., Mancini, S., Niazmand Bilandi, R., Dashtimanesh, A., De Luca, F., & Nappo, V. (2022). A comprehensive stepped planing hull systematic series: Part 1 - Resistance test. Ocean Engineering, 266, 112242. https://doi.org/10.1016/j.oceaneng.2022.112242.

III Niazmand Bilandi, R., Dashtimanesh, A., Mancini, S., & Vitiello, L. (2023). Comparative study of experimental and CFD results for stepped planing hulls. Ocean Engineering, 280, 114887. https://doi.org/10.1016/j.oceaneng.2023.114887.

IV Niazmand Bilandi, R., Mancini, S., Dashtimanesh, A., Tavakoli, S. (2024). A revisited verification and validation analysis for URANS simulation of planing hulls in calm water. Ocean Engineering, 293, 116589. https://doi.org/10.1016/j.oceaneng.2023.116589.

V   Niazmand Bilandi, R., Tavakoli, S., Mancini, S., Dashtimanesh, A. (2024). Dynamic Motion Analysis of Stepless and Stepped Planing Hulls in Random Waves: A CFD Model Perspective. Applied Ocean Research 149:104046. doi: 10.1016/j.apor.2024.104046.

And the following relevant publications in peer-reviewed conference proceedings:

VI Dashtimanesh, A., Ghaemi, M. H., Wang, Y., Karczewski, A., Niazmand Bilandi, R., Hirdaris, S. (2022). Digitalization of High Speed Craft Design and Operation Challenges and Opportunities. Procedia Computer Science, 200, 566–576. https://doi.org/10.1016/j.procs.2022.01.254.

VII Niazmand Bilandi, R., Dashtimanesh, A., Tavakoli, S. (2023). Stepped Hulls Early Stage Design by Implementing 2D+t Method. In HSMV 2023 (pp. 23–32). IOS Press. https://doi.org/10.3233/PMST230005.

VIII Niazmand Bilandi, R., Mancini, S., Dashtimanesh, A., Lakatos, M. (2023). How to Improve Full-Scale Self-Propulsion Simulations? A Case Study on a Semi-Displacement Hull. In HSMV 2023 (pp. 265–274). IOS Press. https://doi.org/10.3233/PMST230034.

Author's Contribution to the Publications

Contribution to the papers in this thesis are:

I **Rasul Niazmand Bilandi:** Investigation, Software, Validation, Visualization, Writing – original draft. **Sasan Tavakoli:** Investigation, Software, Validation, Visualization, Writing – original draft. **Abbas Dashtimanesh:** Supervision, Conceptualization, Funding acquisition, Methodology, writing – review.

II **Luigi Vitiello:** Conceptualization, Methodology, Towing Tank Test, Visualization, Writing – original draft. **Simone Mancini:** Resources, Investigation, Data curation, Writing – review & editing. **Rasul Niazmand Bilandi:** Data curation, Formal analysis, Visualization, Writing – original draft. **Abbas Dashtimanesh:** Supervision, Writing – review & editing. **Fabio De Luca:** Data curation, Writing – review & editing. **Vincenzo Nappo:** Data curation, Formal analysis, model building & data analysis.

III **Rasul Niazmand Bilandi:** Software, Validation, Visualization, Formal analysis, Methodology, Writing – original draft. **Abbas Dashtimanesh:** Supervision, Conceptualization, Funding acquisition, Methodology, Formal analysis, Investigation, Project administration, Writing – review & editing. **Simone Mancini:** Software, Methodology, Writing – review & editing. **Luigi Vitiello:** Writing – review & editing.

IV **Rasul Niazmand Bilandi:** Conceptualization, Data curation, Formal analysis, Investigation, Methodology, Resources, Software, Validation, Visualization, Writing – original draft. **Simone Mancini:** Conceptualization, Data curation, Formal analysis, Investigation, Methodology, Software, Writing – review & editing. **Abbas Dashtimanesh:** Funding acquisition, Supervision, Writing – review & editing. **Sasan Tavakoli:** Formal analysis, Writing – review & editing.

V **Rasul Niazmand Bilandi:** Writing – original draft, Visualization, Validation, Software, Resources, Methodology, Investigation, Formal analysis, Data curation, Conceptualization. **Sasan Tavakoli:** Writing – review & editing, Investigation, Formal analysis, Resources. **Simone Mancini:** Writing – review & editing, Software, Resources, Formal analysis. **Abbas Dashtimanesh:** Writing – review & editing, Supervision.

1 Introduction

1.1 Background

In the present era, there is a concerted global need to achieve net-zero emissions across various sectors, including maritime transportation, which is responsible for around 80% of global transportation. This commitment is particularly noticeable in fields such as commercial shipping, military operations, and recreational activities, where significant technological and advancements scientific advancements are currently in progress. According to the International Maritime Organization (IMO) strategy, the global regulatory body for shipping, there is a target to reduce total GHG emissions by at least 50% by 2050 compared to 2008 levels. Additionally, indicative targets are set for 2030 (20% emissions reduction, striving for 30%) and 2040 (70% emissions reduction, striving for 80%).

Within the sea region, various types of ships and boats operate. Most of these small boats operate at high speeds. Presently, the estimated global count of recreational boats stands at 34 million, with leading countries in the Nordic and European regions being Finland (almost 1.2 million), Sweden (almost 1.0 million), Norway (almost 0.8 million), Italy (almost 0.6 million), and the Netherlands (almost 0.5 million) (ICOMIA, 2023). Approximately 3.5 million leisure boats actively navigate the Baltic Sea, primarily in coastal areas for recreational purposes (Moldanová et al., 2018). The growing number of high-speed craft in Nordic and European regions, particularly in the Baltic Sea, contributes to sea and air pollution, posing a threat to the ecosystem. Consequently, engineers must concentrate on crafting innovative hull designs or retrofitting solutions to alleviate these adverse effects, promoting the eco-friendliness of high-speed vessels – a necessity for realizing fuel consumption reduction goals outlined in the IMO strategy.

In past studies of high-speed craft, the focus has consistently been on two anti-synergetic needs: minimizing fuel consumption and hull resistance and improving comfort on board. Scholars have identified that by innovatively designing hulls, such as incorporating stepped and tunnelled forms, efficient use of energy and fuel and safer ride conditions may be achieved. Hence, achieving a harmonious balance between these requirements requires a thorough examination of how various basic design parameters can influence hull resistance, seakeeping behaviour, and manoeuvrability. This can be accomplished through methods like towing tank tests, Computational Fluid Dynamics (CFD) simulations, and mathematical modelling, and, most recently, Artificial Intelligence (AI) algorithms.

It's crucial to note that a step in hull design isn't primarily intended as a fuel-saving mechanism but rather as a solution to mitigate the significant increase in drag resistance experienced by standard planing hulls at very high speeds. At these velocities, standard planing hulls often suffer from decreased trim, leading to increased wetted surface area (friction resistance) and elevated pressure resistance when the bow enters the water. The step design helps maintain trim at high speeds, with ventilation being an incidental outcome.

Moreover, another critical aspect in optimizing planing hulls is the propulsive point, particularly the interaction between the hull and propeller. Typically, improving a vessel's fuel efficiency involves enhancing hull resistance, propeller efficiency, and the dynamic interplay between them. However, for planing hulls, especially those employing outboard engines, the impact of hull-propeller interaction is minimal. The flow dynamics

around planing hulls minimally disturb the water, resulting in hull-propeller interaction factors such as thrust deduction factor and wake fraction often approaching or exceeding 1. With outboard engines, the hull exerts negligible influence on the surrounding wave field, further diminishing the significance of hull-propeller interaction. Consequently, optimizing the hull design itself emerges as the primary avenue for achieving fuel efficiency gains in planing vessels, as potential savings from enhancing hull-propeller interaction remain limited.

Among different types of high-speed boats, stepped planing hulls have sparked tremendous interest in recent years, with researchers striving to understand their performance in both smooth and rough waters. These versatile vessels find application across various domains, including military operations, coast guarding, racing and leisure activities. Between 1950 and 2000, several scholars, including Rodstrom et al. (1953), Benen (1966, 1967), Clement (1967), Clement and Kobel (1991), Filling (1993), Gassman and Kartinen (1994) made notable contributions to understanding of stepped hull performance through conducting physical towing tank tests.

The early study dates back to 1950s, when Rodstrom et al. (1953) conducted systematic model experiments at the Swedish State Shipbuilding Experimental Tank, focusing on a single-step planing hull. They tested twenty-seven different single-step hull configurations, observing that seventeen of them exhibited porpoising behavior at maximum speed. The speed range for these tests was between $Fr_\nabla = 1$–5.4 (Fr_∇ greater than 3 is used to define planing operation). Their study covered various deadrise, while keeping the breadth, length of after-body, height of step, and bottom angle constant, demonstrated that the model with the least deadrise (Beta = 7.5 degrees) exhibited the lowest resistance, while not experiencing porpoising. Additionally, they investigated the effect of breadth variation at a constant length of after-body, height of step, and bottom angle, noting an 8% decrease in resistance with an increase in the breadth-displacement ratio from 1.28 to 1.60 at $Fr_\nabla = 4$. However, beyond this volumetric Froude number, porpoising was observed to occur. Further, they found that altering the angle between the keel lines of the fore and aft hulls could eliminate porpoising occurrence probability but at the expense of increased resistance. At $Fr_\nabla = 5$, they noted a 1.6% resistance decrease with a breadth-displacement ratio increase from 1.28 to 1.42 before porpoising onset. Their exploration of different step heights demonstrated that a step height of 10%B yielded the lowest resistance. Moreover, they studied the influence of the angle between the keel lines of the fore and aft hulls, determining that an angle of 0 appeared most satisfactory from a resistance perspective, up to speeds where porpoising occurred. In conclusion, based on their experiments, they suggested that a breadth-displacement ratio of 1.42, a length of after-body to breadth ratio of 2.46, a step height of 8.58% breadth, and a bottom angle of zero gives the optimal hydrodynamic performance.

In another set of experimental tests, Clement (1967) investigated the influence of the length-beam ratio (which refers to the overall length of the projected area to the maximum breadth over the chines) on two one-stepped planing hulls. Their investigation showed that the stepped hull with a lower length-beam ratio exhibited higher resistance compared to the other stepped model at volumetric Froude numbers below 2.6, albeit with slightly less resistance at volumetric Froude numbers above 2.6. Yet both stepped hulls demonstrated significantly lower resistance at high speeds than a representative stepless planing boat design. For instance, the resistance of the stepless hull was approximately 30 percents greater than that of the stepped hull. Consequently, an efficient configuration for one-stepped hulls was recommended based on those

experimental findings. Later, Clement and Kobel (1991) noted that a boat with a straight step (also called transverse step) has approximately 3% less drag compared to a boat with a step swept back at angle of 50 degrees, up to beam Froude number of 3.87 (Fr_B greater than 1.5 is used to define planing operation). Beyond this threshold, where the stagnation line intersects the straight step, the afterbody is partially washed by the main spray blister, resulting in increased drag. However, they observed that for all speeds above beam Froude number 3.87, a hull featuring a transverse step would experience larger resistance than a hull with a step swept back at angle of 40 degrees (for instance, 20% higher resistance at beam Froude number 4.63). They hypothesized that at this velocity, with the stagnation line positioned forward of the step, a very efficient balance between calm water performance and rough water performance can be achieved. They further observed that if a higher design speed is targeted, it can be accommodated by increasing the angle of sweepback. This implies that with the step parallel to the stagnation hull in the swept-back stepped hull, a very good level of efficiency in performance can be secured. They conducted that maintaining good planing efficiency up to high speeds can be achieved by providing the step with a sweepback angle ranging between 30 and 50 degrees.

Afterward, Filling (1993) conducted physical towing tank tests on stepped planing hulls at Webb Institute. In the initial phase of these tests, Filling (1993) evaluated a stepped planing hull configuration where the afterbody was set to be parallel to the forebody, allowing for freedom in trim and heave. Subsequently, in another test, Filling (1993) evaluated the forebody and afterbody separately to assess the lift and pitching moment generated by each planing surface. This analysis revealed that the presence of the front body led could potentially lead to an increase in lift force emerging in the rear body. Finally, in the last test, Filling (1993) investigated a stepped planing hull with the afterbody angled relative to the forebody, observing potential effects on dynamic trim. Filling (1993) found that stepped planing hulls are effective as load-carrying monohulls in service. Gassman and Kartinen (1994) expanded on Filling's work by examining the impact of adjustments to the Longitudinal Center of Gravity (LCG) and step position on stepped planing hulls. They utilized Filling's model hull for their experimentation, conducting tests within the speed range $Fr_{\overline{V}} = 1.07$–4.4. Three LCG positions were examined: 0%, 6%, and 9% of the hull length (1.2922 m), measured from the aft of the chine waterplane centroid (located 0.576 m forward of the transom). Each LCG position was assessed at step locations of 37.5%, 50%, and 62.5% of the hull length, measured from the forward of the transom, with the step height set at 10% of the beam. Their findings revealed that optimizing these variables can notably reduce resistance and wetted surface area, particularly at higher speeds. They concluded that positioning the LCG at 9% of the hull length measured from the aft of the chine waterplane centroid and placing the step at 50% of the hull length results in optimal performance in high-speed planing vessels.

In addition to the classical and modern studies conducted in between 1950 and 2000, other scholars have also made significant contributions to the understanding of hydrodynamic of stepped planing hulls. Notably, studies conducted at the U.S. Naval Academy (USNA) have provided further insights into the performance of stepped planing hull research through two sets of studies. Initially, Garland (2010) at USNA examined a single-stepped planing hull with varying step heights (2%, 4%, 6% of chine beam) across a speed range of $Fr_{\overline{V}} = 0.73$–4.54. Their findings demonstrated that the optimal resistance of a stepped planing hull would be acquired under a step design with height

of 0.04 % beam. They also noted minimal resistance changes with ventilation tubes behind the step compared to natural ventilation.

In the same year, Greg White (White & Beaver, 2010) at USNA explored the effects of steps and trim tabs on planing hulls' performance in calm waters and irregular waves. Testing four LCG positions (25.5%, 30.2%, 35.1%, and 40.09% of Length Between Perpendiculars (LBP) forward of the transom), they positioned steps at 33.64% LBP (forward step) and 18.89% LBP (rear step), with different heights: 0.87%B, 1.74%B, 3.47%B, 5.21%B, 6.94%B. Their study highlighted a double-stepped hull's superiority in achieving low trim and resistance, especially with a 6.94%B step height at Station 11 (assuming the hull is divided into 20 stations, and station 1 is transom). This configuration led to a notable 23% reduction in resistance at $Fr_{\overline{V}} = 4$, compared to a stepless planing hull with a trim tab. Additionally, they observed that a 0.87%B step height for the double-stepped hull with lift applied at Station 11 at $Fr_{\overline{V}} = 4$ experienced flow separation only from the rear step near the transom. However, flow separation was seen to emerge at both steps when the step height exceeded 0.87%B (White et al., 2012). More recently, Husser (2023) has examined the influence of forward and aft swept steps on planing hull performance in calm water and regular waves.

In addition to previous studies, researchers have explored stepped planing hull design complexities through systematic model-based experimentation. By changing hull forms systematically, question about hull form effect on the performance of a planing hull can be answered, which aids us in the optimization of design configurations. This approach also facilitates the development of regression formulas for building mathematical or AI models for performance prediction of the tested vessels (this can happen if the data is enough and reliable). Different research teams such as Taunton et al. (2010) and Lee et al. (2014) have followed this pathway and systematically tested model-scaled planing hull forms with a common aim to investigate the effects of different geometries, step positions, and heights on the hydrodynamic of the stepped planing hull (and compare their performance against those of stepless hulls with similar transverse sections and slenderness coefficients). Taunton et al. (2010) conducted towing tank tests on four deep-vee monohulls, installing one or two steps at various positions. Results showed significant resistance reduction when steps were added to a stepless hull, with decreases of 26.5% and 25.4% for single-stepped and double-stepped hulls, respectively, at maximum speed. In another set of experimental tests, Taunton et al. (2011) further explored vertical motions (i.e., wave-induced heave and pitch) of stepped and stepless planing hulls in irregular waves, observing differences in heave and pitch characteristics of these vessel. Notably, the research paper published by Taunton et al. (2011) was the last available documented research reporting and exploring motions of stepped planing hulls in either regular or irregular waves via systematic towing tank tests (please note that this statement is valid as of today).

In 2014, Lee et al. (2014) conducted physical tests on the Naval Surface Warfare Center 15 deadrise hull form (NSWC15E), studying calm-water performance two-stepped hulls by systematically changing step configuration and displacement. Their research aimed at assessing the impact of displacement on planning surface loading and its potential negative effects on calm-water performance of double-stepped hulls. Steps were positioned at 50% L (front step of the transom) and 25% L (rear step of the transom), with six different two-step body configurations investigated, featuring step heights of 0.7%, 1.4%, and 2.1%. All double-stepped hull configurations exhibited lower resistance values than the non-stepped configuration over planing regime, with the

lowest resistance observed when the front step height was 0.7%B, and the rear step height was 2.1%B. Furthermore, Lee et al. (2014) found that the effect of displacement did not significantly differ among the various step configurations. Despite being in the planing regime, all speeds tested resulted in ventilated steps, and increasing displacement did not sufficiently increase bottom loading to eliminate separated flow at the step. These studies offered valuable insights into stepped hull calm performance under effects of different step configuration and gravity loading. Apart from the fact that these experiments have helped us understand physics of stepped planing hulls, their data can be used for validating, calibrating and refining mathematical models and computational simulations used to analyze the performance of stepped hulls.

In parallel to conducting towing tank tests to evaluate the hydrodynamic characteristics of stepped planing hulls, researchers have increasingly turned to CFD simulations as a cost-effective alternative since late 2000s. Towing tank tests, while invaluable for validating design concepts, can be prohibitively expensive, particularly in the initial stages of design exploration. Consequently, CFD has emerged as a pivotal hydrodynamic tool in naval architecture, providing a virtual platform for conducting detailed hydrodynamic analyses. CFD benefits us in different ways. With CFD, researchers can sample hydrodynamic features such as pressure distribution and streamlines, enabling a deeper understanding of complex fluid dynamics around stepped planing hulls, including phenomena such as spray formation, water separation from the step, and water reattachment. These insights, often challenging to measure in towing tank tests, enhance comprehension of the hull's behaviour across various scenarios.

For further technical insights into the application of CFD simulations for stepped planing hulls in calm water conditions, researchers have referenced works by Brizzolara and Federici (2013), De Marco et al. (2017), Dashtimanesh et al. (2018), Di Caterino et al. (2018), Vitiello et al. (2020), Cucinotta et al. (2021), Park et al. (2022). These studies highlight how CFD simulations enable exploration of a broad spectrum of design parameters of stepless and stepped planing hulls and operating conditions, complementing and enhancing the understanding derived from physical experiments. In specific, this computational approach facilitates a deeper understanding of the complex air-water flow phenomena associated with stepped hulls, offering flexibility in rapidly exploring design variations.

However, to fully harness the potential of CFD simulations, it is essential to develop and refine the CFD setup. This entails investigating more detailed numerical aspects such as mesh refinement around the hull and steps, determining the optimal number of prism layers, and selecting appropriate turbulent models. Furthermore, while current applications primarily focus on steady-state situations, such as calm water conditions, there is a growing need to extend use of CFD modelling to reproduce motions of the vessel on other conditions, where absolute unsteady situations would emerge – examples are seakeeping and manoeuvering during which the vessel goes under transient movements. By addressing these challenges and refining CFD methodologies, researchers and naval architects can provide even greater insights into the hydrodynamic performance of stepped planing hulls, paving the way for more efficient and innovative design solutions (for example with a CFD modelling of seakeeping of planing hulls, holistic optimizations can be done).

Transitioning from CFD simulations to mathematical modelling represents a natural progression in the design process of stepped planing hulls. While CFD simulations offer detailed insights of the fluid flow around the vessel, they can be computationally

intensive, particularly in the early stages of design exploration. Thus, researchers have sought to develop simple, but reliable mathematical models that complement CFD analyses by providing efficient means of predicting hydrodynamic performance. These mathematical models are often built by combining physical laws (e.g. Newton Second Law), simple fluid dynamic theories (water entry of a wedge section), and empirical equations (plate frication coefficient), offering a streamlined approach to assessing design concepts and refining hull configurations.

The Savitsky method (1964) stands out as one of the most renowned mathematical approaches for the hydrodynamic design of planing hulls, relying on empirical equations. This method is based on a set of empirical equations most of which were formulated through systematic testing of planing surfaces in 1940s–1960s. There are some other mathematical models that were built in 1970s–2000s, most of which cover hydrodynamic of stepless planing hulls. But we limit our attention to a piece of research that was conducted in 2010, which started a new era in mathematical modelling of stepped planing hulls. This research was done by Savitsky and Morabito (2010). They conducted wave profile tests of planing hulls with a purpose to formulate the wake behind the transom. The motivation behind this research, was however, to build a new equation that gives the water surface profile behind steps incorporated on the bottom surface of planing hulls. The hypothesis behind their research was that the wake in the lee of step would be similar to the wake behind the transom (i.e., the surface behind the step does not affect the wake flow leaving a step). This hypothesis can be (no fully, but to an acceptable level) true as long as the wet length of body forward step is not relatively long. As such, they developed empirical formulas to calculate wake profiles leaving the transom. Building upon this work, Gray-Stephens (2020, 2021) conducted experimental and numerical measurements of nearfield longitudinal wake profiles, comparing their findings with the one formulate by Savitsky and Morabito (2010) and another one, which assumes wake behind the step can be formulated using a linear function. While Savitsky's Wake Equations demonstrated accuracy in predicting curves, the Linear Wake Assumption proved superior in estimating wake length in the x-direction, crucial for predicting flow separation from steps.

Despite its wide range of use and popularity, Savitsky's method has faced challenges in modelling the hydrodynamics of stepped planing hulls in calm water. The model should be modified to consider effects of ventilation on hydrodynamic forces acting on the vessel. This has been addressed just after the research conducted by Savitsky and Morabito (2010) by Svahn (2009) and Danielsson and Stromquist (2012). They attempted to extend Savitsky's method for one- and two-stepped hulls, respectively, with varying degrees of success. In the former, a single-stepped planing hull was modelled. The body was divided into two sub-bodies, and the wet surface of the former hull was found by estimating the ventilation length which was hypothesized to be the intersection of the keel and the wake leaving the step (wake was modelled using Savitsky and Morabito Equation). In the latter, hydrodynamic performance of a double-stepped planing hull was modelled and this time, the authors assumed that the wake behind the vessel has a linear ship. Dashtimanesh et al. (2017) used the similar approach and developed a simplified mathematical model for performance prediction of double-stepped planing hulls, based on Savitsky's formulas and linear assumption of the wake shape.

Another popular mathematical method used for hydrodynamic modelling of planing surfaces is, the 2D+t method, also termed the 2.5D method. It originates from a two-dimensional water entry scenario and evolves to encompass a three-dimensional

solution. The hypothesis behind this theory is that the three-dimensional planing problem can be either simplified to a water entry problem or modelled using a non-linear strip theory. It calculates the forces acting on the vessel using the sectional added masses or pressure acting on each 2D section of planing hulls, enabling the determination of forces on each section and subsequent calculation of 3D forces. Zarnick (1978, 1979), Martin (1978), and Payne (1994) pioneered its application, with Zarnick notably developing a nonlinear model for planing hull motion in waves. This method's foundation lies in Von Karman's added mass theory (1929), although concerns over its accuracy prompted researchers like Akers (1999), Troesch and Hicks (1994), and Garme (2005) to propose more precise solutions for sectional forces. Apart from the momentum theory, pressure-based simulations of water entry, such as those developed by Wagner (1932) and Algarin and Tascon (2014), are utilized to compute sectional hydrodynamic forces.

The 2D+t method shows potential in simulating various planing hull behaviours, including steady performances (Ghadimi et al., 2017), unsteady motion in waves (Tavakoli et al., 2020), and manoeuvering (Tavakoli & Dashtimanesh, 2017, 2019). Initially used for simpler planing hulls, it has evolved to model complex planing hulls, including stepped hulls, facilitating performance predictions in calm water with certain assumptions. The first mathematical model for stepped planing hulls was developed by Niazmand et al. (2019), predicting the hydrodynamic behaviour of two stepped hulls with straight steps. Subsequently, they expanded the model in 2020 to address asymmetric motion in doubled-stepped planing boats (Niazmand Bilandi et al., 2020). All these models were built through a linear wake assumption.

Stepped hulls have garnered attention for their fuel efficiency, leading researchers to develop various numerical and mathematical tools for performance prediction. However, reliable design tools for stepped hulls considering seakeeping and manoeuvering motion are lacking at the present time. Fluid dynamics around stepped planing hulls are complex, and predicting their behaviour in waves is very challenging. Developing mathematical models for early-stage design allows for parametric studies on effects of basic design aspects on a very complicate hydrodynamic problem (such as seakeeping of a stepped hull in waves), saving time and costs, although final designs should undergo CFD simulations, and get some approvals for the design, which would permit final towing tank model tests of a designed hull (or a designed planing hull series). Considering the value of every different method, this study focuses on experimental, numerical, and mathematical aspects of stepped planing hulls. It utilizes the 2D+t method to predict performances in calm water and dynamic motion in waves. Due to the complexity of fluid flow around stepped planing hulls, CFD simulations using StarCCM+ software is employed to demonstrate the numerical method's capabilities in calm water and waves. The experimental test is conducted with forward-swept stepped hulls in calm water, providing essential validation for the mathematical model and CFD simulations. Addressing the lack of research on performance prediction and seakeeping behaviour of stepped hulls is crucial for their potential as fuel-efficient solutions. Additionally, the study emphasizes the importance of manoeuvering characteristics, laying the groundwork for future in-depth investigations.

1.2 Problem Statement and Scope

In recent years, stepped hull designs have emerged as a forefront area of research within the maritime industry due to their potential for enhancing fuel efficiency and performance, as stated earlier. Stepped hulls feature a unique design characterized by transverse steps or discontinuities on the hull's bottom surface. At high speeds, water flowing along the hull bottom can separate from the forebody at a step introduced in the hull. This creates an unwetted area on the afterbody if adequately ventilated. The separated water may reattach to the afterbody, and the lift generated by both the forebody and the afterbody must support the vessel's displacement. These steps ventilation, reducing hydrodynamic drag, and increasing lift, thereby improving speed and fuel efficiency if the step is chosen properly.

When designing steps for hulls, it's crucial to carefully consider several basic design parameters, as selecting the right ones is essential. These include not only the shape and depth of the step but also its longitudinal position along the hull and the method used for ventilation. Figure 1 illustrates primary step shapes: three the forward swept step, the transverse step, and the backward swept step. Each shape has distinct characteristics that affects the hull's performance and behaviour in water. Figure 2 demonstrates how changing step height, longitudinal step location, can affect the wetted surface and consequently affect resistance and fuel efficiency. Hence, given the limitations on time and towing tank availability, researchers have been constrained to altering and testing one major variable dealing with stepped hull design. By developing accurate mathematical models and numerical setups, investigating these parameters for designing stepped planing hulls, which are one of the most famous efficient hull forms, becomes accessible.

However, despite the importance of these variables for stepped planing hulls, there is still a lack of comprehensive understanding of their influence on hull performance in calm water and their general hydrodynamic behaviour, particularly in non-steady conditions such those appearing under the effects of wind-generated waves and swells along these emerging during manoeuvering. Although some studies have focused on the calm water performance of stepped hulls, the effects of step height and position, the number of steps, step shape, and ventilation length profile remain unknown.

Therefore, to address these gaps, the primary scope of this research is to advance stepped hull technology through a multifaceted approach involving mathematical modelling, CFD simulation, and experimental testing, as stated before. The overarching scopes are as follows:

- Development of Models and Methods for Hydrodynamic Design: Formulate comprehensive design methods for stepped high-speed craft (HSC) hydrodynamics, encompassing both calm water conditions and wave environments, using simplified mathematical models. These Models and Methods will provide invaluable insights for early-stage hull design and optimization of stepped planing hulls.
- Analysis and Comparison of Stepped Hull Configurations: Utilize advanced CFD simulation techniques to analyse and compare various stepped hull configurations under different operating conditions, including calm water and waves. By comprehensively evaluating these configurations, we aim to identify the most efficient and effective design parameters.

- Experimental Validation and Optimization: Conduct experimental studies, including towing tank tests and model-scale experiments, to validate CFD simulations and mathematical models. These experiments will allow for the optimization of hull performance and provide crucial validation for the numerical and theoretical approaches used in the design process.

Aligned with the defined scopes, this study endeavours to offer a substantial contribution to hydrodynamic design of stepped planing hulls, renowned for their remarkable fuel efficiency. Through meticulous investigation and analysis, the research seeks to enhance our understanding of the intricate dynamics involved in the optimization of these hull forms, thereby paving the way for advancements in maritime technology and sustainability (since it can lead to less fuel consumptions).
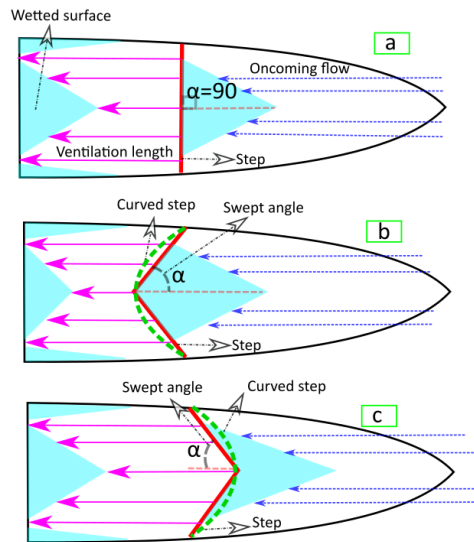

Figure 1. Various potential step concepts incorporated on the bottom surface of planing hulls that can be used as single-step, double-step, or triple-step designs (similar or a combination of all three): a) straight step, b) forward swept step, c) re-entrant vee-step.
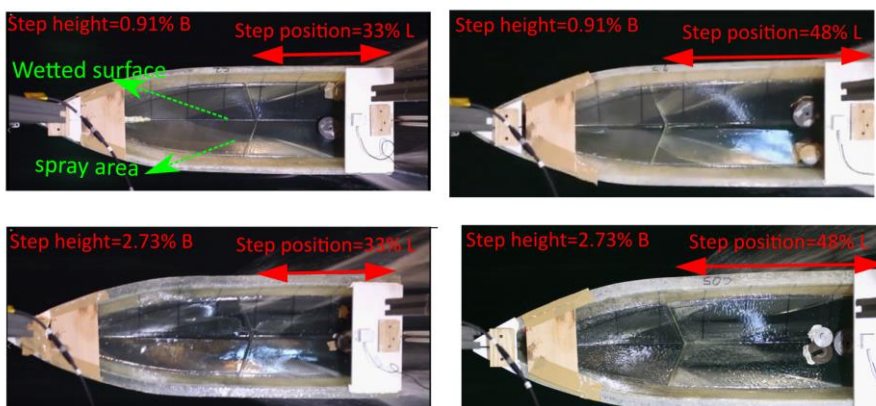

Figure 2. Effect of Changing Step Height and Longitudinal Position on Stepped Hull Performance at Fr_B=4.97 [P2].

1.3 Objectives

This study focuses on investigating the hydrodynamic performance and behaviour of stepped hull designs in both calm water and wave conditions. It encompasses the development of comprehensive design guidelines, analysis and comparison of various stepped hull configurations, and experimental validation and optimization of numerical and theoretical models. Specifically, the objectives include:

> **Objective 1:** Developing models to simulate the planing motion of stepped hulls in calm water and regular water waves, including a nonlinear mathematical model and a CFD model.
>
> **Objective 2**: Analysing an experimental campaign to systematically investigate a new series of stepped hulls by varying key design parameters such as step number, step height, and longitudinal step position.
>
> **Objective 3:** Modelling the flow behaviour around and beneath of stepped hulls in calm water using numerical methods, systematically varying design parameters like step numbers, step height, and longitudinal step position, while performing uncertainty and validation analyses.
>
> **Objective 4:** Creating a CFD setup to predict the dynamic responses of planing hulls in irregular waves, enhancing the accuracy of seakeeping performance assessments.

Through these objectives, we seek to address existing gaps in knowledge regarding stepped hull design and performance prediction. By combining theoretical, numerical, and experimental approaches, we aim to provide a holistic understanding of stepped hull behaviour and pave the way for the development of innovative solutions that maximize efficiency, and speed in stepped hull vessels.

Figure 3 illustrates the logical connections between the publications derived from the research conducted in this thesis and the overarching objectives. Each publication represents a significant milestone in the pursuit of understanding stepped hull behaviour and optimizing high-speed craft performance. The connections between the publications and objectives highlight the iterative nature of the research process, where findings from each publication inform subsequent investigations and contribute to the overall goal of maximizing efficiency, speed, and manoeuvrability in stepped planing hull.

The paper titled P1 investigates the development of mathematical models to simulate the planing motion of straight stepped surfaces in both calm water and regular waves. These models, based on the 2D+t theory method, lay the groundwork for understanding the fundamental principles governing stepped hull motion. Additionally, a CFD setup is designed to numerically replicate the motion of double-stepped planing hulls subjected to regular waves. This paper addresses the following research questions:

- Are the analytical equations and regression equations of non-stepped planing hulls valid for stepped planing hulls?
- Can 2D+t theory and linear wake assumption for the wake leaving be used to model dynamic motions of stepped planing hulls in water waves?
- Can CFD Simulation capture the motion of stepped planing hulls in regular waves?
- How does adding steps and changing step heights affect the dynamic response of the hull in regular waves?

In parallel, paper 2, named P2, conducts an extensive experimental campaign to systematically investigate a new series of forward swept stepped hull designs. By varying

key topological parameters such as step numbers, step height, and longitudinal step position, the aim is to gather empirical data to validate and refine the mathematical models and CFD simulations. This paper addresses the following research questions:

- How does the forward swept step shape affect the performance prediction of stepped planing hulls?
- How do changing step height, the position of the step, and adding a step on single forward swept stepped planing hulls affect performance prediction?

Furthermore, in Paper 3, named P3, CFD simulation setups are employed to model the flow behaviour around and beneath the new series of forward swept stepped hulls from P2 in calm water. Although towing tank tests are effective in predicting the hydrodynamic behaviour of stepped planing boats, there are limitations in studying some details. This study utilizes CFD to investigate the hydrodynamic behaviour of a stepped planing hull with eight different step configurations in detail. In parallel, Paper 4 investigates the Verification and Validation of CFD models in predicting the dynamic trim and hull resistance of complex high-speed planing hulls. This aims to provide a deeper understanding of V&V analysis in this specific field of application. The paper addresses the following research questions:

- How can Verification and Validation analysis in CFD simulations improve the prediction of dynamic trim and hull resistance in complex high-speed planing hulls?
- How accurately can CFD models predict fluid flow around and beneath forward swept stepped planing hulls?

Additionally, in Paper 5, named P5, the focus is on developing a CFD framework capable of predicting the dynamic responses of planing hulls in irregular waves. Through statistical analysis of the motions, the aim is to enhance the accuracy of seakeeping performance assessments for stepped hull vessels. This paper addresses the following research questions:

- Can a CFD setup predict the dynamic response of planing hulls in irregular waves?
- How does relying solely on spectra for generating irregular waves impact the dynamic response of planing hulls?
- How does adding a step on a planing hull affect dynamic response in irregular waves, as well as variations in PDF, Skewness and Kurtosis (indicators of statistical aspects of a time series), and Spectrum Analysis of Heave, Pitch, and Center of Gravity Acceleration?
- Which probability distribution functions follow heave, pitch, and CG vertical acceleration?

Overall, these efforts will provide a comprehensive understanding of stepped hull behaviour and contribute to the development of innovative solutions that maximize efficiency, and speed in high-speed craft, advancing environmentally friendly "Green Small Craft" technology.

Objective 1
P1
Predicting the motion of stepped planing hulls in both calm water and regular waves entails the development of mathematical models and Computational Fluid Dynamics (CFD) simulations

Motivates

Objective 2
P2
Conducting extensive experimental investigations into a new series of stepped hull designs

Motivates

Motivates

Objective 3
P3
Developing a comprehensive understanding of the hydrodynamics of stepped hull designs through CFD simulation setup

Guides

Objective 3
P4
Performing uncertainty and validation analyses of CFD setup for complex hulls, including stepped hulls

Constitutes

Objective 4
P5
Creating a CFD framework to predict dynamic responses of planing hulls in irregular waves and conducting statistical motion analysis.

Final

Advancing computational methods for eco-friendly "Green Small Craft" by optimizing hull performance in both calm water and waves.
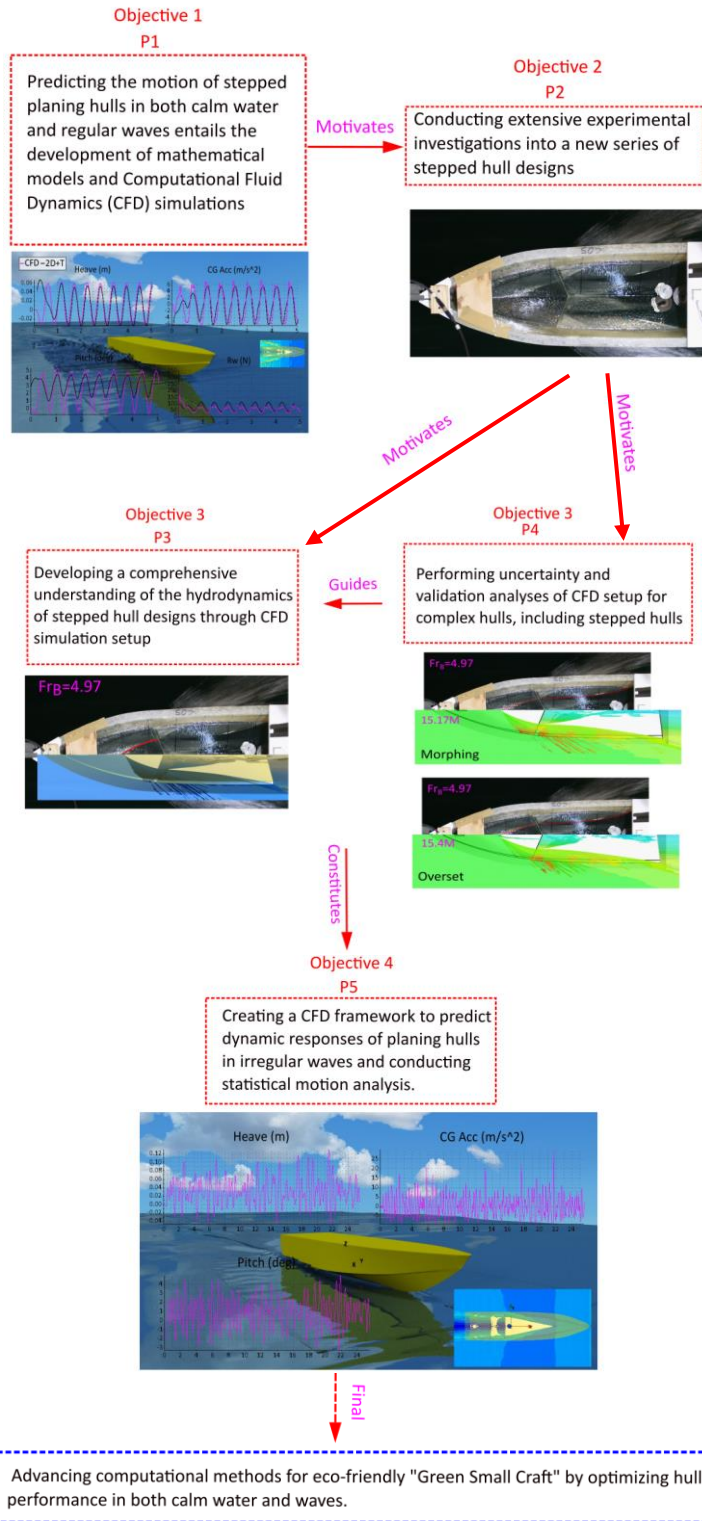
Figure 3. Logical relations between the publications and objective within the thesis.

1.4 Limitations

This thesis proposes calculations for the design of efficient high-speed craft, with stepped hulls being one of the renowned efficient hull forms. While the numerical, analytical, and experimental models presented in this study have provided valuable insights into the behaviour of steps on high-speed planing hulls, there are several limitations on the applicability of these models, which are as follows:

1.4.1 CFD Simulation Constraints

Despite its versatility, CFD simulation is subject to several limitations that may impact its accuracy and reliability. These include simplifying assumptions about fluid behaviour, uncertainties in turbulence modelling, boundary conditions, and numerical discretization methods, as well as issues with time-step size and grid resolution. Additionally, the nonlinear nature of planing hull motions poses challenges in accurately capturing their behaviour using any non-physical model. In the context of stepped hulls, accurately capturing the complex flow phenomena around and beneath the hulls may be challenging, particularly in regions of flow separation, reattachment, and ventilation. In calm water simulations, if the computed results exhibit oscillatory and non-monotonic behaviour, it provides further evidence that verification and validation analysis are crucial when using CFD models for design and industrial applications. Similarly, for simulations in regular waves, the limitations are similar to calm water simulation, but high-speed planing hulls exhibit oscillatory and nonlinear behaviour. Although there is no experimental data for stepped planing hulls in regular waves, data for planing hulls is available, and the validation of simulation setups can be done with this data.

Simulating irregular seas presents further difficulties due to the complex nature of wave groups. Moreover, the lack of comprehensive experimental and systematic data and verification studies on planing hulls in irregular seas compounds these challenges. Replicating irregular sea conditions in experimental tests is challenging, and conducting multiple runs for statistical analysis in towing tanks is resource-intensive. Additionally, the CFD model may still have some limitations in modelling the performance of the vessel for real-world scenarios. It only considered the single peak spectra, and no directional spreading was considered. This is just an idealisation of the sea, as in the real sea, different wave groups may emerge. This can be the topic of the next generation of CFD studies as the computational cost for such problems is very high, and there is a need to couple more complicated phase-resolving wave physics models (such as high-order spectral models, HOSM) and phase-average wave models (such as WaveWatchIII) with the CFD tanks.

Furthermore, the present model is not developed to consider fluid-solid interactions and related hydroelastic responses, which adds another layer of limitation to the current computational model. Additionally, our study is limited to head sea conditions, and the hull is restricted to heave and pitch free motion. Finally, the validity of our CFD model is still limited to wave-induced motions, and manoeuvering is not considered. The present results and CFD model do not consider bimodal seas and the interaction of different wave groups.

1.4.2 2D+t Method Limitations

While the 2D+t method provides valuable insights into the planing motion of stepped surfaces, it is based on simplifying assumptions and empirical relationships that may not fully capture the intricacies of stepped hull behaviour. Assumptions such as linear wake modelling and neglecting three-dimensional effects and the viscosity effect may limit the method's applicability to real-world scenarios, especially in conditions where nonlinear hydrodynamic phenomena dominate.

Additionally, the model is limited to deep water conditions and cannot consider shallow water effects. Planing hulls often operate in coastal seas, where performance may be affected by water depth. The current model is also developed for wedge water entry, assuming a flat wedge wall. However, planing hulls may have spray deflectors or double chines. Modelling such hulls with the 2D+t theory requires more advanced water entry models that can solve fluid flow around geometries other than a wedge.

The models are also limited to calm water and rough water conditions, without accounting for manoeuvring motions, which are crucial for real-world performance assessments. Incorporating manoeuvring motions would require advanced modelling techniques that capture the dynamic interactions between the hull and the fluid in more complex scenarios.

1.4.3 Towing Tank Test Constraints

While towing tank tests offer a controlled environment for studying hull behaviour, they are subject to certain limitations that may affect the accuracy and representativeness of results. These include scale effects, boundary condition uncertainties, and the inability to fully replicate real-world operating conditions such as wave-induced motions and dynamic effects. Additionally, towing tank tests may be resource-intensive and time-consuming, limiting the number of test configurations that can be explored within the scope of the research.

Acknowledging these limitations is crucial for interpreting the findings of this research accurately and understanding the constraints inherent in each methodology. Integrating multiple approaches and considering their respective strengths and weaknesses can contribute to a more comprehensive understanding of stepped hull behaviour and performance.

1.5 Thesis outline

This thesis is structured into four chapters, providing a comprehensive overview of the research, followed by five appended papers:

- **Chapter 1:** Introduces the thesis topic, outlining the objectives, scope, and limitations of the research. It also explains how the included papers contribute to a cohesive work and shows the logical relationships between the publications and the thesis objectives.
- **Chapter 2:** Details the methodologies used throughout the thesis, including the approaches and techniques employed in the research.
- **Chapter 3:** Presents the key findings and results of the research, emphasizing the most important outcomes.
- **Chapter 4:** Provides a discussion of the results and suggests potential directions for future research.
- **Appendix 1 [P1]**: Dynamic motion of stepped planing hulls in regular waves.

- **Appendix 2 [P2]**: Experimental study of a new systematic series of stepped planing hulls.
- **Appendix 3 [P3]**: Hydrodynamics of stepped planing hulls using the URANS solver.
- **Appendix 4 [P4]**: Verification and validation of complex planing hull hydrodynamics using the URANS solver.
- **Appendix 5 [P5]**: Dynamic motion of stepped planing hulls in irregular waves.

2 Methods for Efficient Planing Hulls Evaluation

This thesis explores into the evaluation of stepped planing hull performance, focusing on their hydrodynamic characteristics across various conditions such as calm water, regular waves, and irregular head waves. The methods employed for this evaluation are crucial in understanding the nuanced behaviour of stepped planing hulls. In the following, we provide an extended discussion of the methods utilized.

2.1 Experimental Method

The experimental approach involves conducting physical tests in controlled environments, such as model basins. These tests provide empirical data on hull behaviour, including resistance, motion response, and flow patterns around the hull. Through model-scale experiments and full-scale trials, valuable insights are gained into the performance of stepped planing hulls. Experimental methods also play a vital role in validating numerical simulations and theoretical models, ensuring their accuracy and reliability.

The calm water tests were conducted in the towing tank of the naval section of the Dipartimento di Ingegneria Industriale (DII) of the Università degli Studi di Napoli "Federico II". Dimensions of the basin are: length 137 m, width 9 m, deep 4,25 m, the tow carriage is able to develop a maximum speed of 10 m/s with a maximum acceleration of 1 m/s^2. The carriage system is equipped with advanced sensors and a data-acquisition device to measure key parameters during hydrodynamic testing. These include:

- Speed: Measured using a high-precision encoder with a resolution of 1.0 mm.
- Resistance: Assessed with a load cell of 0.003% accuracy and 0.005 N resolution.
- Trim: Evaluated by an accelerometer with an accuracy of ±0.1%.
- Sinkage: Determined using laser sensors with 0.5 mm accuracy.
- Weight and Ballast: Measured with a balance having an accuracy of ±0.1 N.

Additionally, a video camera mounted on the towing carriage captures the wetted surface, enabling detailed ventilation analysis near the step. For further information regarding the laboratory instrumentation used in the experimental tests and measurement techniques see P2.

Calm water tests followed ITTC procedures with a 10-minute interval between runs. The tests used a displacement of 30.705 N with trim conditions of +1°, -1°, and 0°, and speeds from 1.290 to 8.050 m/s. Data collected included speed, resistance, sinkage, trim angle, and recordings from three cameras.

A resistance dynamometer, connected via a Spectra™ rope, used the "Down-Thrust" method for high sensitivity to external forces. The model had 4 degrees of freedom, with restricted yaw and drift, stabilized by carbon fiber guide masts.

Sinkage was measured with lasers and processed using 3D CAD models. The dynamic wetted surface was estimated through video frame analysis of a transparent-bottom hull, accurately capturing water flow dynamics.
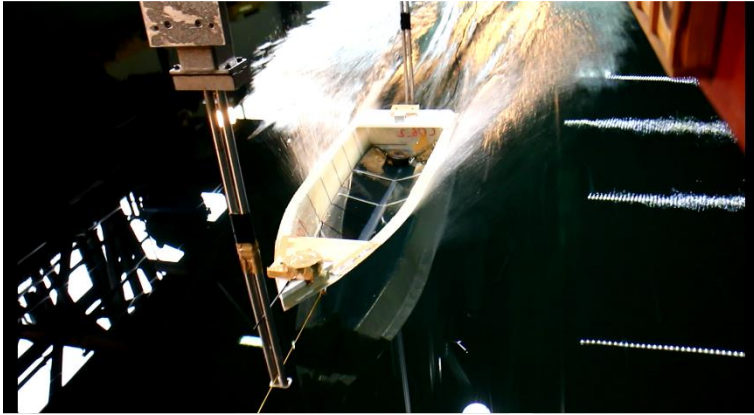
Fig. 4. Towing tank test with down-thrust methodology [P2].

2.2 Computational Fluid Dynamics (CFD) Simulation Setup

CFD simulation involves solving the governing equations of fluid flow numerically to predict hull performance. This approach allows for detailed analysis of flow behaviour around the hull, including turbulence effects, wave interactions, and pressure distributions. By discretizing the fluid domain into computational grids and employing appropriate turbulence models, CFD simulations can capture complex hydrodynamic phenomena. While CFD simulations offer flexibility and scalability, they are subject to various uncertainties, including turbulence modelling, boundary conditions, and grid resolution. Validation of CFD results against experimental data is essential to verify their accuracy and establish confidence in the simulation setup.

In this thesis, the dynamics of fluid motion are examined using the Reynolds-Averaged Navier-Stokes (RANS) equations. To accurately capture the deformation of the free surface, a volume fraction field is utilized. The detailed governing equations are omitted for brevity, but comprehensive discussions can be found in established CFD texts such as Ferziger et al. (2019) and Reynolds (1895). Additional references include P1, P3, and P5. Notably, P1 simulates stepped planing hulls in regular waves, P3 and P4 investigate these hulls in calm water, and P5 explores their behavior in irregular waves.

The motion of the vessel, treated as a rigid body, is governed by Newton's Second Law. The forces acting on the vessel are determined by integrating pressure and shear stresses over its surface. The specific governing equations for these calculations are not detailed here but are thoroughly covered in references like Su et al. (2012) and Tavakoli et al. (2020), as well as P1, P3, and P5.

For the CFD simulations, the Finite-Volume Method (FVM) is employed in conjunction with the Volume-Of-Fluid (VOF) model to manage two-phase flows. The interface between the air and water phases is accurately captured using a High-Resolution Interface Capturing (HRIC) scheme, which is based on the Compressive Interface Capturing Scheme for Arbitrary Mesh (CICSAM). Both fluids are modeled as incompressible Newtonian fluids, ensuring a realistic simulation of their behaviors.

To couple the pressure and velocity fields, the Semi-Implicit Method for Pressure-Linked Equations (SIMPLE) is used. This method is crucial for solving the discretized equations that govern fluid motion at each time step. A segregated flow

solver approach is applied for all simulations, streamlining the computational process by solving the momentum equations and the pressure correction equation separately.

For those seeking detailed information on the numerical methodologies and solver specifics, the Siemens PLM Star-CCM+ User's Guide, version 17.02.007 (SIEMENS PLM, 2022), provides extensive descriptions. Additional information regarding the numerical solver parameters used in this study is summarized in Table 1.

In Table 2, the boundary conditions utilized for all simulation setups are outlined. A no-slip boundary condition is applied to the body hull to accurately represent the interaction between the hull surface and the fluid. The velocity inlet boundary condition is used at the top, sides, and inlet of the simulation domain to define the flow characteristics entering the computational domain. Conversely, a pressure outlet boundary condition is employed at the outlet to manage the flow leaving the domain. Additionally, a symmetry boundary condition is considered for all setups to optimize computational efficiency and accurately reflect the physical symmetry of the problem. Figure 5 provides a comprehensive overview of the different boundaries employed in the irregular wave simulations and the mesh used for overset mesh motion, as published in paper P5. Moreover, in all simulations presented in this thesis, the initial location of the free surface is determined based on the draft obtained from the hydrostatic analysis to ensure accurate capture and simulation of the free surface in the numerical model.

These carefully chosen boundary conditions ensure that the simulations are both accurate and efficient, capturing the essential physics of fluid-structure interactions and providing reliable data for the analysis of planing hull performance.

This thesis aims to enhance the understanding of fluid dynamics in maritime applications, particularly in the performance analysis of planing hulls under various conditions. By employing advanced CFD techniques and robust numerical methods, the insights gained can significantly improve the design and optimization of marine vessels. These contributions are expected to advance the field of naval architecture, leading to more efficient and effective vessel designs.

Table 1. Solver settings for stepped hulls.

Item	P1	P3	P4	P5
Software version	STAR-CCM+, 2011, Version 13.04.	STAR-CCM+, 2022, Version 17.02.007.	STAR-CCM+, 2022, Version 17.02.007.	STAR-CCM+, 2022, Version 17.02.007.
solver	Implicit unsteady	Implicit unsteady	Implicit unsteady	Implicit unsteady
Implicit scheme	SIMPLE	SIMPLE	SIMPLE	SIMPLE
Convection term	2nd order	2nd order	2nd order	2nd order
VOF scheme	HRIC	HRIC	HRIC	HRIC
VOF Surface	Regular wave	Flat wave	Flat wave	Irregular waves
Turbulence model	Realizable $k - \varepsilon$	k-Omega SST	k-Omega SST/ Realizable $k - \varepsilon$	Realizable $k - \varepsilon$
Temporal Discretization	2nd order	1st order	1st order	2nd order

Iteration per time step	10	5	5	10
Mesh motion	Overset	Overset	Overset/ Morphing	Overset
Overset Interpolation scheme	Linear	Linear	Linear	Distance-weighted interpolation
Wall treatment	All y+ wall treat	All y+ wall treat	All y+ wall treat	All y+ wall treat

Table 2. The boundary conditions for all simulation setup of stepped hulls.

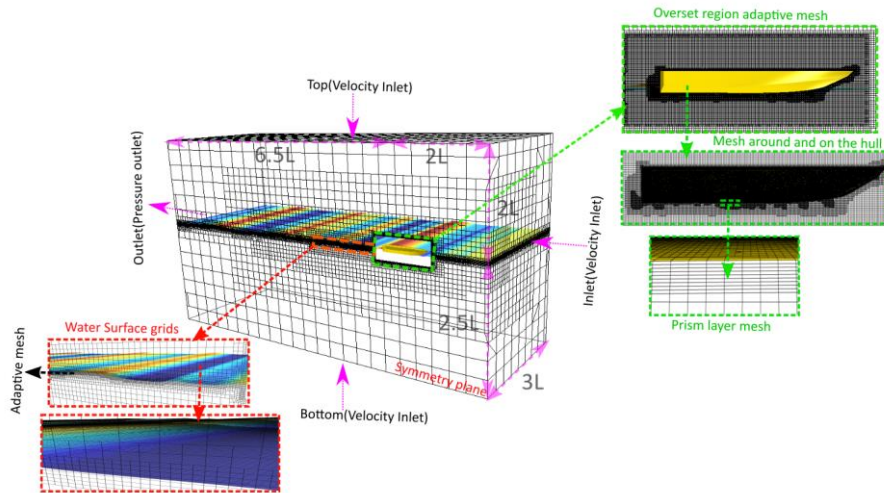|	No-slip (wall)	Symmetry	Velocity inlet	Pressure outlet
Velocity	$v_x = v_y = v_z = 0$	$\boldsymbol{U} = 0$	$\boldsymbol{U} = v_x$	$\dfrac{\partial \boldsymbol{U}}{\partial \boldsymbol{n}} = 0$
Pressure	$\dfrac{\partial p}{\partial \boldsymbol{n}} = 0$	$\dfrac{\partial p}{\partial \boldsymbol{n}} = 0$	$\dfrac{\partial p}{\partial n} = 0$	$p = 0$
Volume fraction	$\dfrac{\partial \Psi}{\partial \boldsymbol{n}} = 0$	$\dfrac{\partial \Psi}{\partial \boldsymbol{n}} = 0$	$\Psi = 1$, for water $\dfrac{\partial \Psi}{\partial \boldsymbol{n}} = 0$, for air	$\Psi = 1$, for water $\dfrac{\partial \Psi}{\partial \boldsymbol{n}} = 0$, for air
Turbulent kinetic energy (k)	$k = 0$	$k = 0$	$k =$ constant	$k =$ constant
dissipation rate (ε)	$\varepsilon = 0$	$\varepsilon = 0$	$\varepsilon =$ constant	$\varepsilon =$ constant
dissipation rate (Omega)	Omega $= 0$	Omega $= 0$	Omega $=$ constant	Omega $=$ constant

Fig. 5. The computational domain, showing the applied boundary conditions and grid configuration, used for simulating a planing hull in irregular waves with an overset grid [P5].

2.3 2D+t Method

The 2D+t method, or two-dimensional plus time method, is a computational technique used to predict the planing motion of hulls based on two-dimensional sections and their time evolution. This approach simplifies the hull geometry into two-dimensional profiles and accounts for the time-dependent behavior of the hull in response to hydrodynamic forces. The primary advantage of the 2D+t method is its ability to provide rapid insights into hull performance, making it useful for preliminary design assessments and sensitivity analyses. However, this method may overlook three-dimensional effects and nonlinearities inherent in real-world conditions, necessitating its integration with more comprehensive methods such as CFD simulations for a complete understanding of hull behavior.

2.3.1 Application and Benefits

The 2D+t method is particularly valuable during the concept and preliminary design phases of high-speed vessels, where rapid and reasonably accurate performance predictions are crucial. This method is especially effective in predicting the performance of hard-chine sections, which are commonly used in high-speed crafts. By analyzing pressure distributions or momentum variations of 2D sections along the hull length, the 2D+t method calculates forces in both calm water and dynamic wave conditions. This capability aids designers in optimizing hull shapes to achieve desired speeds and performance metrics. The 2D+t method offers several benefits:

- **Rapid Assessment:** It provides quick performance predictions, allowing for efficient iteration during the design process.
- **Versatility:** The method can be applied to various conditions, including calm water and wave environments.
- **Design Optimization:** It assists in optimizing hull shapes by providing insights into how different design parameters affect performance.

Studies have validated the efficacy of the 2D+t method in both calm water (Niazmand Bilandi et al., 2019, 2020) and wave conditions (Tavakoli et al., 2020), underscoring its utility across a range of scenarios. The method's ability to provide accurate performance predictions, resistance calculations, and dynamic motion simulations makes it an invaluable tool in the early stages of hull design.

In this thesis, the 2D+t method has been developed for performance prediction of stepped planing hulls in calm water and dynamic motions in waves. This is achieved by using analytical and regression formulas originally developed for non-stepped hulls. The current research assumes that a hard-chine prismatic planing hull is moving forward with a velocity u corresponding to $\text{Fr}_B = u/(gB)^{-1}$ in calm water or waves. Two coordinate systems are considered:

- **Body Frame (Gxyz):** This frame moves forward with the vessel's speed and is placed under or above the CG on the calm waterline. The x-axis is parallel to the calm water and positive forward, while the z-axis is normal to the calm water and positive downward. The governing equations of the vessel's motion are formulated in this frame.

- **Hydrodynamic Frame (Oξηζ):** This frame is attached to the CG of the vessel, with the middle panel showing a cross-section of the vessel. These frames are illustrated in Figure 6.
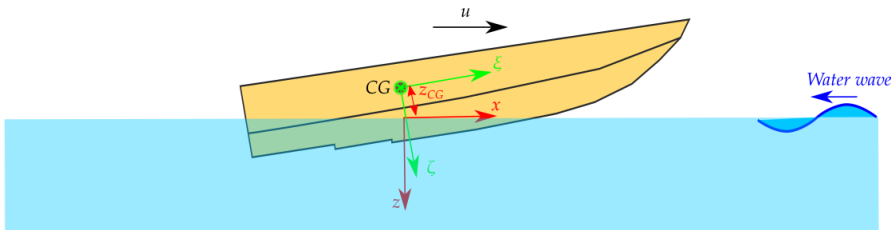
Figure 6. Illustration of frames for mathematical modeling of stepped planing hull in calm water and waves [P1].

2.3.2 Analysis of Sectional Forces

The 2D+t approach involves analysing the 2D sectional water entry problem at each time step to determine the sectional forces acting on the vessel, as shown in Figure 7. To evaluate these sectional forces, two methods are considered:

- **Pressure Method:** The pressure acting on the wall of the wedge is calculated using Wagner's water entry solution (Wagner, 1932). Based on the different phases displayed in Figure 7, the mean half-beam and its time derivative for the wedge section are determined. Integrating the 2D forces along the entire length of the boat provides the three-dimensional forces. Detailed procedures and mathematical formulations are available in Niazmand Bilandi et al. (2019, 2020) and updated comparisons with the CFD method in Niazmand Bilandi et al. (2023a).

- **Momentum Theory:** This method calculates hydrodynamic forces on the 2D wedge section using momentum variation and cross-drag flow (Payne, 1994). It depends on the instant added mass of the sections, with the formulation explained in [P1]. Sectional forces derived from this method are used to develop equations for heave force and pitch moment. To compute the hydrodynamic force acting on a single planing surface, forces from sections along the surface's length are integrated. The complete procedure and formulations are detailed in [P1].

For both methods, a transom correction function introduced by Garme (2005) is implemented to account for the effects of the transom/step. Additionally, the ventilation length from the steps is assumed to follow a linear pattern of separation from the step, known as the linear transom wave theory. Figure 8 illustrates how, by considering linear wake theory, the ventilation length behind the step is calculated. This comprehensive approach ensures a more accurate prediction of the forces acting on the hull, aiding in the optimization of hull design for improved performance.
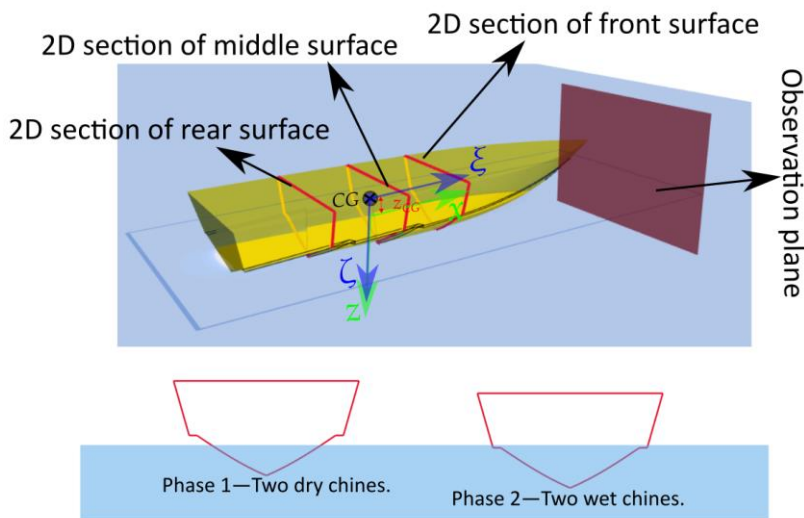
Figure 7: Schematic representation of the concept of the 2D+t theory for a double-stepped planing vessel navigating through calm waters.

Figure 8. The schematic of linear wake profile assumption.

2.3.3 Practical Applications

Both [P1] and Niazmand Bilandi et al. (2023a) demonstrate that the 2D+t theory can simulate the dynamic motion of stepped planing hull vessels in waves, allowing for the optimization of hull shapes for desired speeds in the early design stages. This method provides critical insights for the safe and efficient operation of high-speed crafts. However, due to the complex behaviour of stepped planing hulls in waves, it is recommended to use CFD simulations at the final design stage alongside the 2D+t method to ensure the reliability and accuracy of the results.

By combining the strengths of the 2D+t method and CFD simulations, designers can achieve a more comprehensive understanding of hull performance, leading to the development of high-speed vessels that are efficient, safe, and capable of superior performance in various conditions.

3 Results and Discussions

This section presents the key findings of the thesis, focusing on the extensive investigation of various parameters in the design of stepped planing hulls in calm water and waves, as published in journal and conference papers.

3.1 Progression Across Phases and Findings

Phase One involved developing a mathematical model and CFD setup to simulate the performance of straight-stepped planing hulls in calm water and regular waves. The models were validated with experimental data for calm water, but due to a lack of data on stepped hulls in wave conditions, data from non-stepped hulls were used (published in P1). The strong agreement between the models demonstrated their effectiveness for early-stage design and studies of straight-stepped hulls, as presented in a conference paper (Niazmand Bilandi et al., 2023a), which highlighted the need to explore swept steps in the next phase.

   Phase Two introduced swept steps to new hull models and evaluated their performance in calm water through experimental tests. The hulls were developed and tested at the towing tank of the Dipartimento di Ingegneria Industriale della Università degli Studi di Napoli "Federico II" (published in P2). To better understand pressure distribution and flow separation – critical factors in hull performance – detailed CFD investigations were conducted (published in P3). The experimental models featured transparent bottoms, allowing observation of wetted surfaces and vortical flow phenomena behind the steps, which enabled a verification and validation analysis for the numerical study of these complex hulls. The analysis revealed that the overset mesh approach was more accurate than the morphing grid method for complex hulls (published in P4). Insights gained from Phases One and Two underscored the importance of examining hull performance in irregular waves, leading to the initiation of Phase Three.

   Phase Three expanded the study to irregular wave conditions, using CFD modeling to analyze the dynamic responses of stepless, single-stepped, and double-stepped hulls with straight steps in random seas. Discrepancies between CFD and experimental results were analyzed by focusing on time history data and identifying peak and trough values using a local Maxima/Minima approach (published in P5). Understanding these analyses and the fluid flow of stepped planing hulls in random waves lays the groundwork for extending the mathematical model in the future for parametric studies of planing hulls in random wave conditions.

3.2 Straight-Step Performance: Model and CFD Development

In [P1], a mathematical model and CFD simulation setup for stepped planing hulls in calm water and regular waves were developed. The mathematical model is based on the 2D+t theory and linear wake theory from the steps. Figure 9 shows a sample of the calm water tests for the Taunton et al. (2010) model, named C2, at a Froude Number of 4.77. Initial values for heave and pitch were set, and simulations were run over time until convergence was achieved. Both CFD and 2D+t results closely matched the experimental data (dashed red line). Figure 9 compares results between the 2D+t method, CFD simulations, and experimental data, confirming the accuracy and reliability of the 2D+t method in predicting trim values and resistance within a reasonable range.
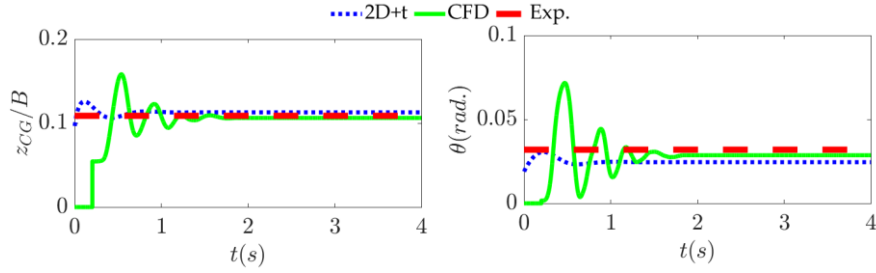
Figure. 9. Illustrated are the time histories of heave and pitch motions for a double-stepped planing hull in calm water at a Froude number of 4.77. The figure includes results from CFD simulations and the 2D+t method, alongside experimental measurements indicated by the red dashed line from Taunton et al.'s towing tank test (2010). This comparison demonstrates the precision of the simulation methods in capturing the hull's dynamic behaviour [P1].

Since there is no experimental data available to validate the mathematical model and CFD simulation setup for stepped planing hulls in regular waves, we relied on the non-stepped hull, known as the C2s model, for this purpose. The validation process utilized the 2D+t method and CFD simulations to predict heave, pitch motions, and the acceleration of the center of gravity in regular waves, using the C2s model depicted in Figure 10. Experimental data previously published by Tavakoli et al. (2020) were pivotal for this analysis. Table 2 illustrates the average error of the 2D+t and CFD methods in predicting the RAO for heave, pitch, CG acceleration, and resistance of the C2s model across various regular wave conditions, compared against towing tank test data. Figure 11 provides a snapshot of the time histories for heave, pitch, and vertical acceleration at the vessel's CG. These records indicate that both CFD and the 2D+t theory closely track the experimental data. While acknowledging the inherent limitations of the 2D+t theory compared to CFD, particularly in capturing the complexities of planing hulls in regular waves, it nonetheless demonstrates reasonable accuracy. Therefore, the 2D+t method proves valuable for conducting parametric studies on planing hulls. However, to ensure a robust final hull design, it is prudent to corroborate findings with comprehensive CFD simulations.
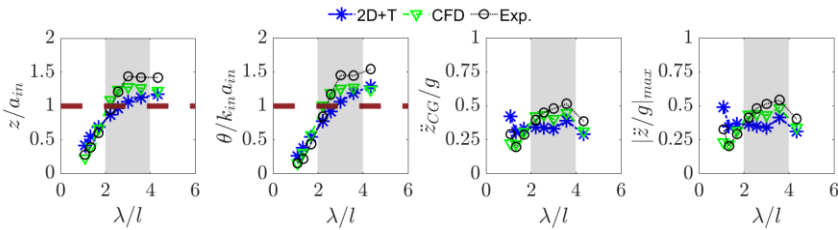
Figure 10. RAOs of heave, pitch, Vertical acceleration, and maximum value of the vertical acceleration C2s model at Fr_B = 2.28 (Tavakoli et al. (2020)).

Table 3. The average error of 2D+t method and CFD for prediction RAO heave, pitch, CG acceleration, and resistance in wave of C2s model of the Warped Hull Naples Systematic Series.

	z/a_{in}	$\theta/k_{in}a_{in}$	$\dfrac{\ddot{z_{CG}}}{g}$	$\dfrac{R_w}{\Delta}$
$Ave.E\%$ for CFD	10.53%	17.61%	12.42%	5.31%
$Ave.E\%$ for 2D+t	22.17%	20.52%	22.32%	9.6%
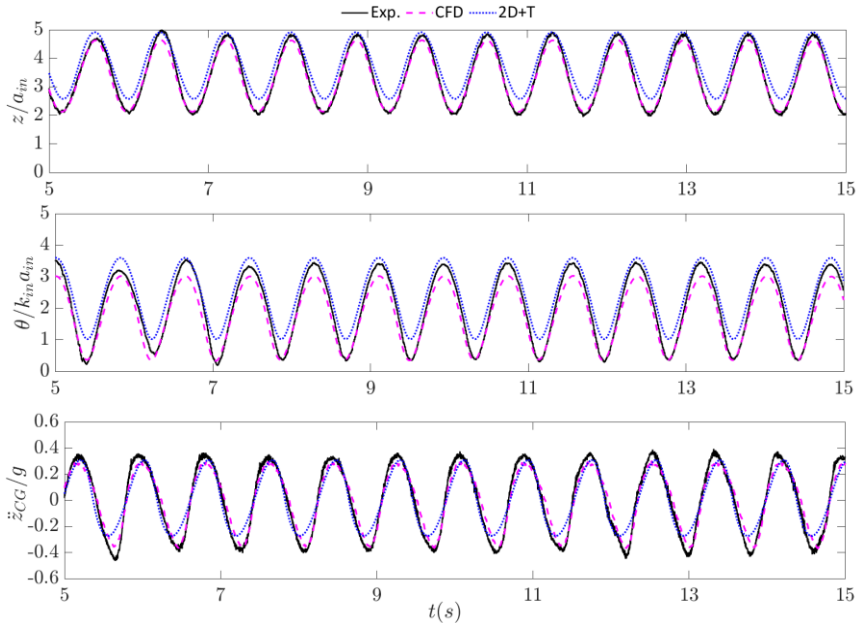
Figure 11. Time history samples of heave, pitch, and vertical acceleration at the center of gravity (CG) from experimental towing tank data, 2D+t data, and CFD simulations. These results are for a non-stepped planing hull, C2s, in regular waves with a wavelength of λ = 4.34L at Fr_B = 2.28. In the plots z/a_{in} denotes RAO of heave, $\theta/k_{in}a_{in}$ represent RAO of pitch and $\ddot{z}_{CG}/g$ reflects RAO of vertical acceleration at the CG.

Figure 12 provides a verification analysis between the 2D+t and CFD methods for a two-stepped planing hull, named C2. It displays three panels showing the RAO of heave, pitch, CG acceleration, and resistance at three beam Froude Numbers: 2.94, 3.83, and 4.77. The study covers a wide range of wavelengths, as presented in P1. Wavelengths ranging from 2L to 4L are marked in gray, indicating the range that can cause the highest response, which is of particular interest in this research. Both CFD and 2D+t models predict that heave resonance occurs in this marked area. At wavelengths greater than 2.0, the 2D+t model tends to compute weaker heave, pitch, and CG acceleration responses. This discrepancy between the two models is likely due to the CFD model's ability to account for fluid oscillations around the sections, whereas the 2D+t model assumes a high-frequency interaction between water and the solid body without considering fluid oscillation. This assumption can lead to smaller sectional forces as the waves become longer, making gravity effects more significant.

Despite the limitations of the 2D+t method, verification results show reasonable agreement between the 2D+t and CFD methods in predicting the RAO of double-stepped planing hulls. Additionally, the resistance of the vessel in waves is computed using both CFD and 2D+t models in Figure 12. Both methods exhibit similar behavior across a range of wavelengths and increasing speeds. The use of the 2D+t method represents a significant advancement in improving stepped planing hull design during the early stages for efficient and safe performance in various conditions. This method allows for a detailed parametric study on adding steps, changing step height, and adjusting the position of the step. Ultimately, integrating 2D+t with CFD simulations ensures more accurate and reliable results, enhancing the overall design and performance of high-speed vessels.
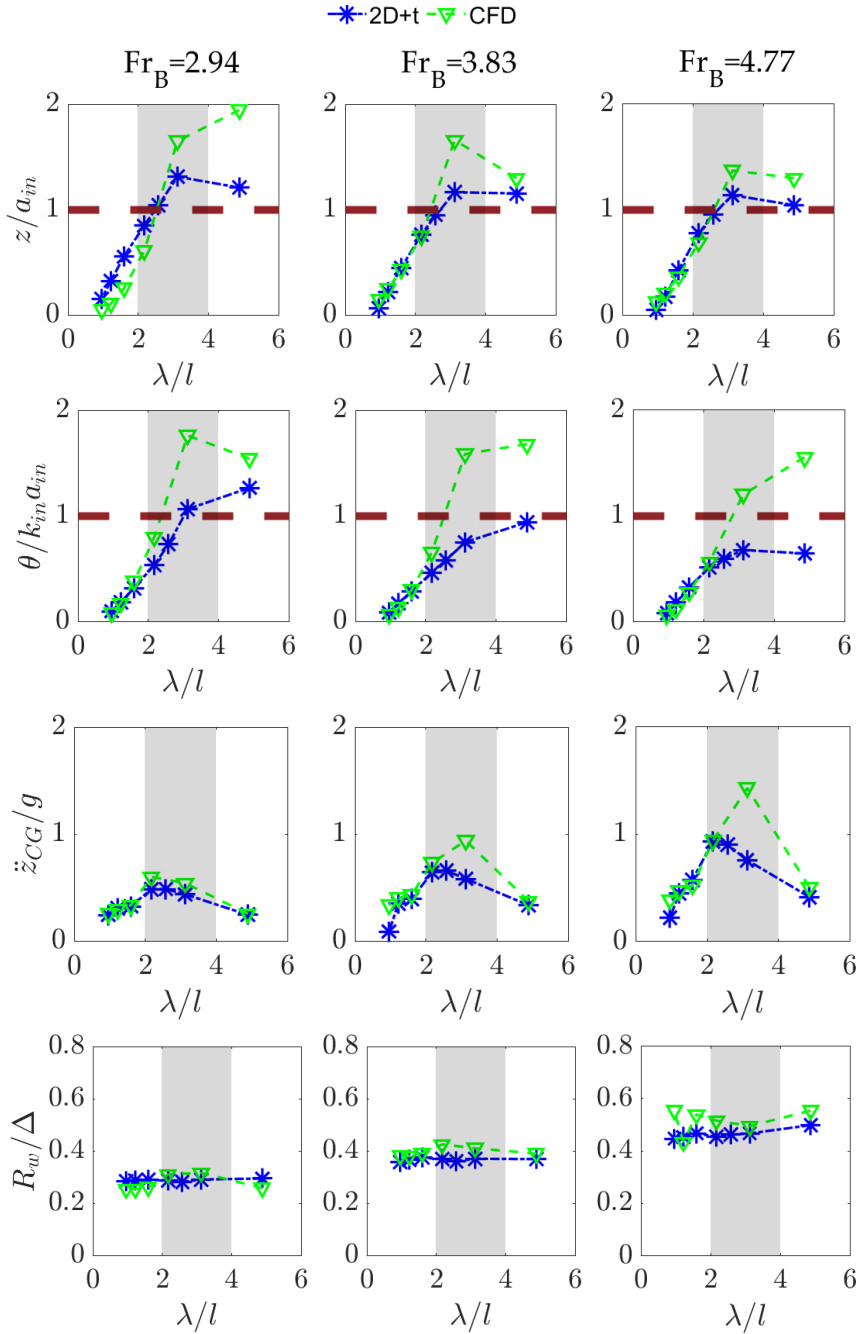
Figure 12. RAOs of heave, pitch, Vertical acceleration, and wave resistance of C2 hull at different operations speeds, Fr_B = 2.94, Fr_B = 3.83 and, Fr_B = 4.77. The dashed red line shows the wave amplitude, reference line. Wavelengths between 2L and 4L are shaded in gray, as they are of particular interest in this study for their potential to generate the highest response. In the plots, the RAO of heave represents z/a_{in}, the RAO of pitch is denoted as $\theta/k_{in}a_{in}$, the RAO of vertical acceleration at the center of gravity is shown as $\ddot{z}_{CG}/g$, and the RAO of wave resistance is expressed as R_w/Δ. Asterisk and triangle markers respectively show the 2D+t and CFD results ([P1], Niazmand Bilandi et al., 2023a).

In Niazmand Bilandi et al. (2023a), a parametric study was conducted on stepped planing hulls using the mathematical model (2D+t method) to explore the effects of altering step position and height in both calm water and waves. The objective was to identify the optimal step position and height by comparing these variations to a base hull, specifically the C2 hull. Eight different configurations with varying step heights and positions were examined. Detailed information about these cases is available in Niazmand Bilandi et al. (2023a).

In the base model, the forward step is positioned at 31% of the hull's length (L) with a height of 2.17% of the beam (B), while the aft step is located at 18.5% L with a height of 2.17% B. For Case 5, the forward step is positioned at 50% L with a height of 4.35% B, and the aft step is at 31% L with a height of 4.35% B. Performance predictions and dynamic motion analyses in regular waves using the mathematical model identified Case 5 as the most optimal design, exhibiting the lowest values of both wave resistance and added resistance compared to the base model. This indicates that the design parameters of Case 5 are well-suited to reducing wave resistance and enhancing vessel performance, making it a valuable reference for future vessel design optimization. In the final phase of the study, CFD simulations for Case 5 in calm water and regular waves were conducted to verify the accuracy of the mathematical model's results.

Figure 13 compares the wetted surfaces of the base hull and Case 5. Figure 14 presents the time histories of heave, pitch, vertical acceleration, and wave resistance for Case 5, as determined by both the 2D+t method and CFD simulations. While the results for heave, vertical acceleration, and wave resistance are consistent between the two methods, the pitch response shows some discrepancies. The 2D+t method tends to predict smaller pitch motions, likely due to an additional pitch damping moment, despite the similar heave response and vertical acceleration observed in both methods. These findings suggest that fine-tuning these parameters can lead to significant performance improvements, further validating the utility of the 2D+t method in the early stages of hull design. However, for a comprehensive understanding of the fluid dynamics around the hull, CFD simulations are essential in the final design stages. This research primarily focused on straight step shapes. The effects of different step shapes on performance prediction are discussed in [P2] and [P3].
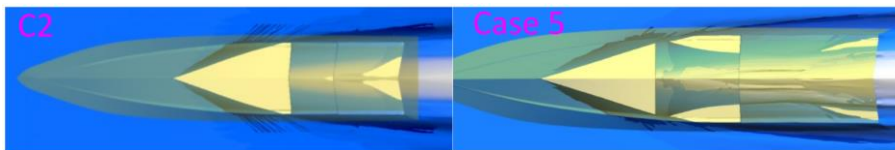
Figure 13. Comparison of the wetted surface areas for the base model (C2) and the optimal hull design (Case 5) at $Fr_B = 3.83$. The figure highlights the differences in wetted surface patterns, illustrating the hydrodynamic improvements achieved with the optimized step configuration in case 5 (Niazmand Bilandi et al., 2023a).
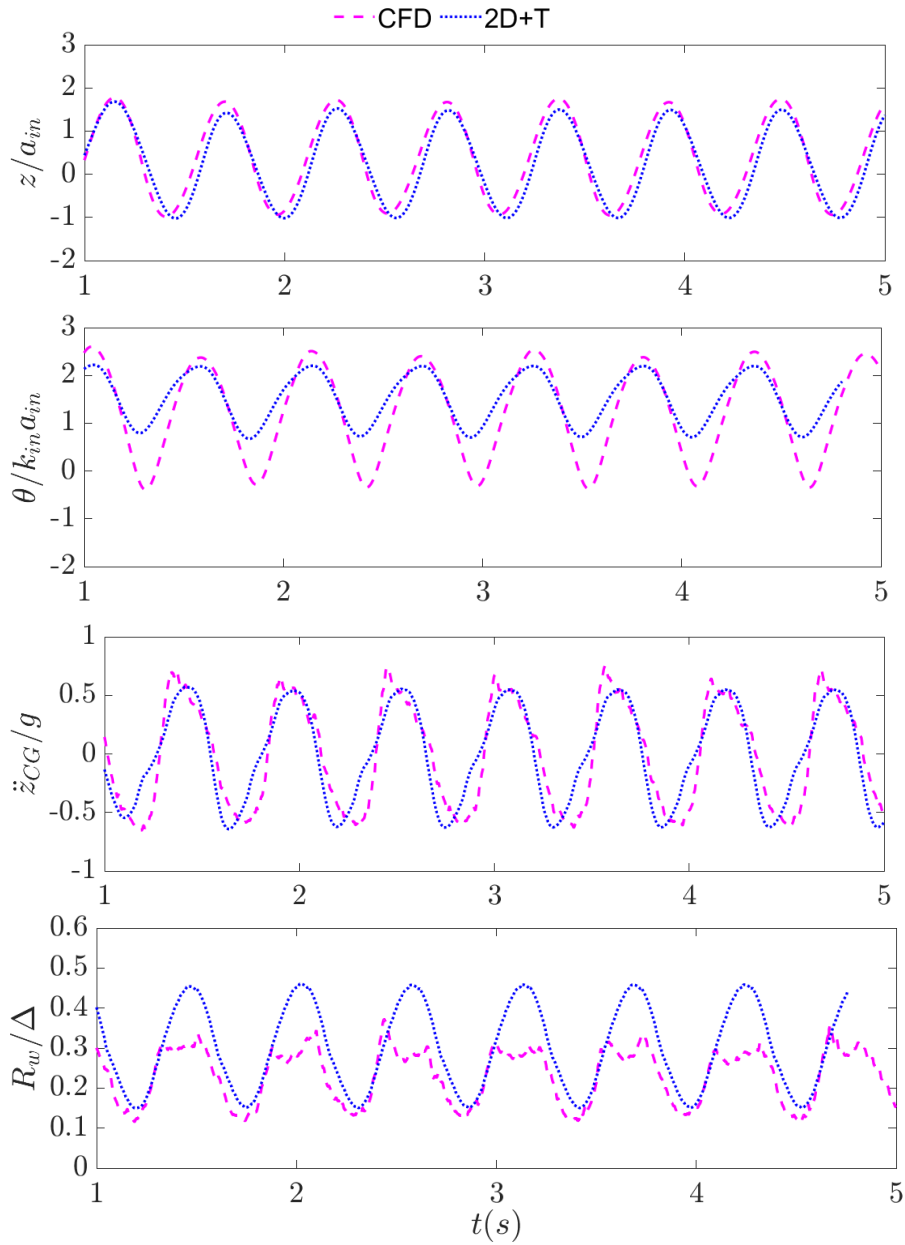
Figure 14. Comparison of CFD and 2D+t simulations for Case 5 in regular wave conditions with a wavelength of 3.12L at $Fr_B = 3.83$. This figure illustrates time history of the dynamic responses, including RAO of heave (z/a_{in}), RAO of pitch ($\theta/k_{in}a_{in}$), RAO of vertical acceleration at CG ($\ddot{z}_{CG}/g$), and RAO of wave resistance (R_w/Δ), as predicted by both methods. The results demonstrate the efficacy of the 2D+t method for preliminary design validation, with CFD simulations providing further accuracy and insight into complex fluid interactions (Niazmand Bilandi et al., 2023a).

3.3 Swept-Step Hulls: Experimental and CFD Analysis

In [P2], a systematic series of forward-swept stepped planing hulls, based on the systematic series of Taunton et al. (2011), has been developed. While Taunton et al. (2010) maintained a constant hull length and varied the L/B ratio, B, and step number (with identical step shapes), the present study (VMV Series) keeps the L/B ratio constant and focuses on the effects of various design parameters on hull performance, specifically resistance and running attitude. The design parameters considered include the number of steps, step height, and longitudinal step position. Eight hulls with different design parameters were developed, named C02, C03, C04, and C05 for single-stepped hulls, and C06, C07, C08, and C09 for double-stepped hulls.

Calm water tests for all eight hulls were conducted in the towing tank of the naval section of the Dipartimento di Ingegneria Industriale (DII) at the Università degli Studi di Napoli "Federico II," using three different static trim conditions (+1°, -1°, and 0° trim). The "Down-Thrust" methodology was implemented during towing tank tests to counteract the low weight and sensitivity to external forces of the hull models. This unique testing approach ensures the model remains free from equipment and instrumentation weights, replicating the real system of forces on the hull at full scale. More details about the procedure and results are provided in [P2].

A notable finding from the experimental campaign is the observation of the hulls' bottom due to the transparent bottom, which allows for visualizing the wetted surfaces and ventilation in various step heights and positions. This is also beneficial for validating CFD simulations. Figure 15 illustrates the wetted surfaces and flow separation phenomenon on the aft body behind the step of C07 hull at maximum speed for three different conditions: Trimmed Forward (-1°), Trimmed Aft (+1°), and Even Keel (0°). For details on other hulls and speeds, refer [P2]. Figure 16 compares resistance, wetted surface, and trim values for all stepped hulls at Fr_B ranging from 0.8 to 4.96, with an even keel (0°). Analyzing the resistance test results in the very-high-speed range of Fr_B between 3.9 and 4.97, hull C04, which has one step located at 48.3%L with a step height of 0.91BTC, performs the best. Among the double-stepped hulls in the same speed range, hull C08 shows the best performance in calm water. In the high-speed range of Fr_B between 2.8 and 3.9, hull C05, with one step at 48.4%L and a step height of 2.73BTC, performs best. Hull C07 is the best-performing double-stepped hull in this range. For the medium-speed range of Fr_B between 1.9 and 2.8, hull C05 performs best, and for the low-speed range of Fr_B between 0.8 and 1.9, hull C06 performs best.

For a final decision on which step configuration offers the best performance, seakeeping in regular and irregular waves and dynamic stability should be considered. Experimental work is time-consuming and expensive, often requiring model scaling and not fully capturing the fluid dynamics around the hull. Therefore, CFD simulations are necessary to gain deeper insights into the fluid flow around the stepped hulls. In [P3] and P4, CFD simulations are considered for these hulls, with experimental methods used for validation.

Trimmed Forward (-1°)
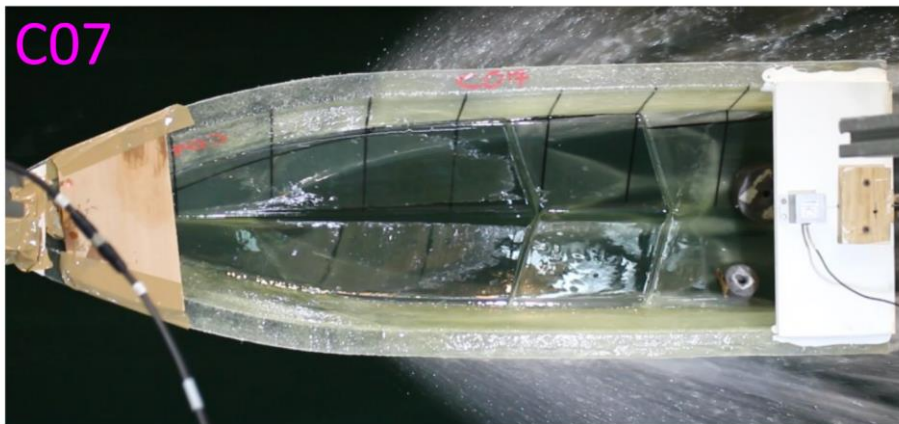
Even Keel (0°)

Trimmed Aft (+1°)

Figure 15. Wetted surfaces of C07 hull (double-stepped hull) at the maximum test speed condition ($Fr_B = 4.97$), shown at different static trim angles: Trimmed Forward (-1°), Trimmed Aft (+1°), and Even Keel (0°). For details on other hulls and speeds, refer [P2].
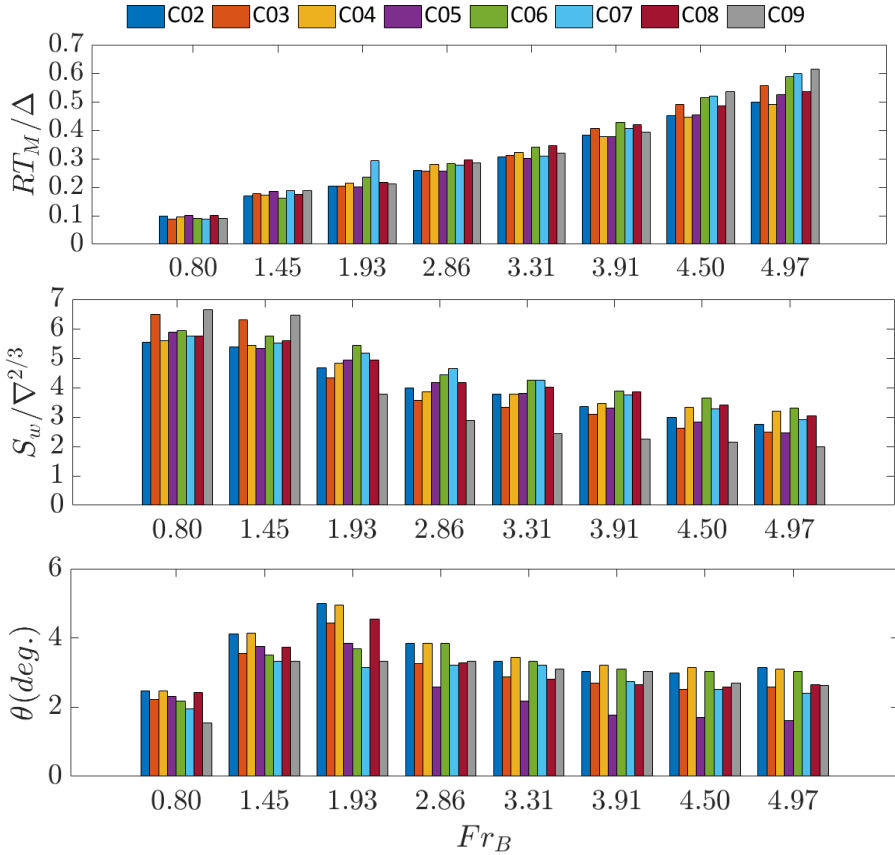
Figure 16. Comparison of resistance, wetted surface, and trim values for all stepped hulls at various operational speeds, with an even keel (0°). The data includes comprehensive measurements taken under different speed conditions. For further details and in-depth analysis of the data, refer to [P2].

In [P3], a CFD method is employed to investigate the hydrodynamic behavior of a new systematic series of forward swept-stepped hulls with eight different step configurations (known as the VMV systematic series). This study aims to provide a comprehensive analysis of how varying step configurations affect hull performance, including resistance and dynamic trim, under different operating conditions. Additionally, it seeks to understand the flow behavior around and beneath these hulls, and the pressure distribution on them using numerical methods, which are challenging to capture with experimental results.

Figure 17 shows a sample of validation results comparing CFD simulations with experimental data for C07 hull. The comparison illustrates the accuracy of CFD in predicting the dynamic wetted surface, resistance, trim angle, and sinkage of the hulls. For details on other hull configurations, refer [P3]. Table 4 presents the average error in predicting these parameters for all models, demonstrating that CFD can reasonably predict the performance of these types of stepped planing hulls. The low average errors indicate the robustness of the CFD approach in replicating the experimental results.

In Figure 18, the fluid flow around and beneath the C05 hull in the spray and ventilation areas is shown for both CFD and experimental results, indicating reasonable accuracy. The visualization of the spray area and ventilation zones using CFD aligns

closely with experimental observations, showcasing the method's capability to capture complex flow phenomena.

Furthermore, the study highlights the advantages of using CFD for design optimization. By simulating different step configurations, designers can evaluate the impact of each configuration on performance metrics such as resistance and trim without the need for extensive physical testing. This approach not only saves time and resources but also allows for rapid iteration and refinement of hull designs.
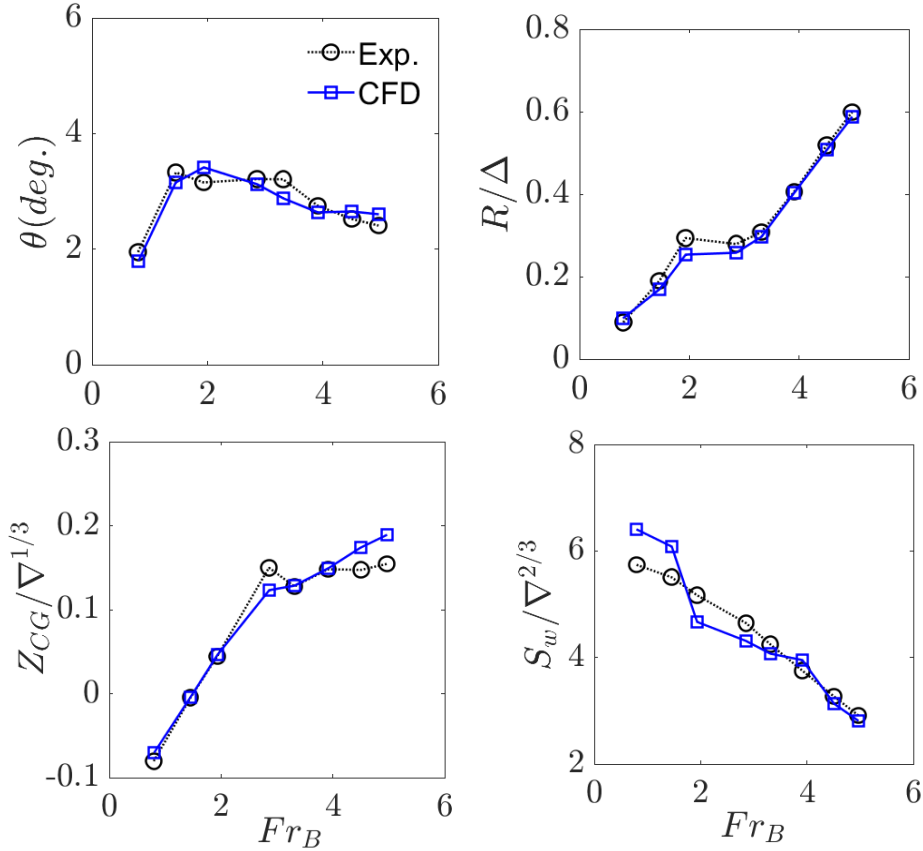
Figure 17. Comparison of the CFD results against the experimental results of Vitiello et al. (2022), from the left to the right, are: dynamic trim, resistance, sinkage, and wetted surface, for the C07 hull. For details on other hull configurations, refer [P3].

Table 4. The average error for prediction trim angle, sinkage, resistance, and wetted surface.

Models	C02	C03	C04	C05	C06	C07	C08	C09
$Ave. E_\tau \%$	7.98%	3.05%	6.06%	4.85%	2.14%	0.04%	5.39%	1.41%
$Ave. E_{Z_G} \%$	6.85%	1.52%	4.06%	3.91%	4.06%	0.03%	3.44%	0.8%
$Ave. E_R \%$	5.16%	0.04%	1.18%	5.48%	2.40%	3.81%	1.88%	1.39%
$Ave. E_w \%$	5.55%	6.72%	4.66%	2.29%	3.97%	0.22%	7.71%	9.11%
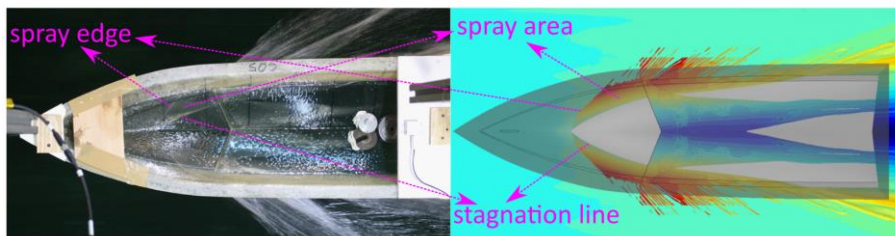
Figure 18. The spray area for the C05 hull at Fr_B = 3.31 [P3].

Estimating the wetted surface of a hull is typically complex and requires underwater cameras and CAD software. However, using transparent models can simplify the process. [P2] used transparent-bottom hulls in towing tank tests, capturing video frames with a mounted camera and analyzing them with 3D CAD software to estimate the wetted surface accurately.

In CFD simulations, a threshold value of 0.5 for the fluid volume fraction is used to determine the wetted surface. Figure 19 compares the wetted surfaces of C07 hull obtained through CFD and towing tank tests, showing that the results are generally similar at all speeds. For other hulls refer in [P3].
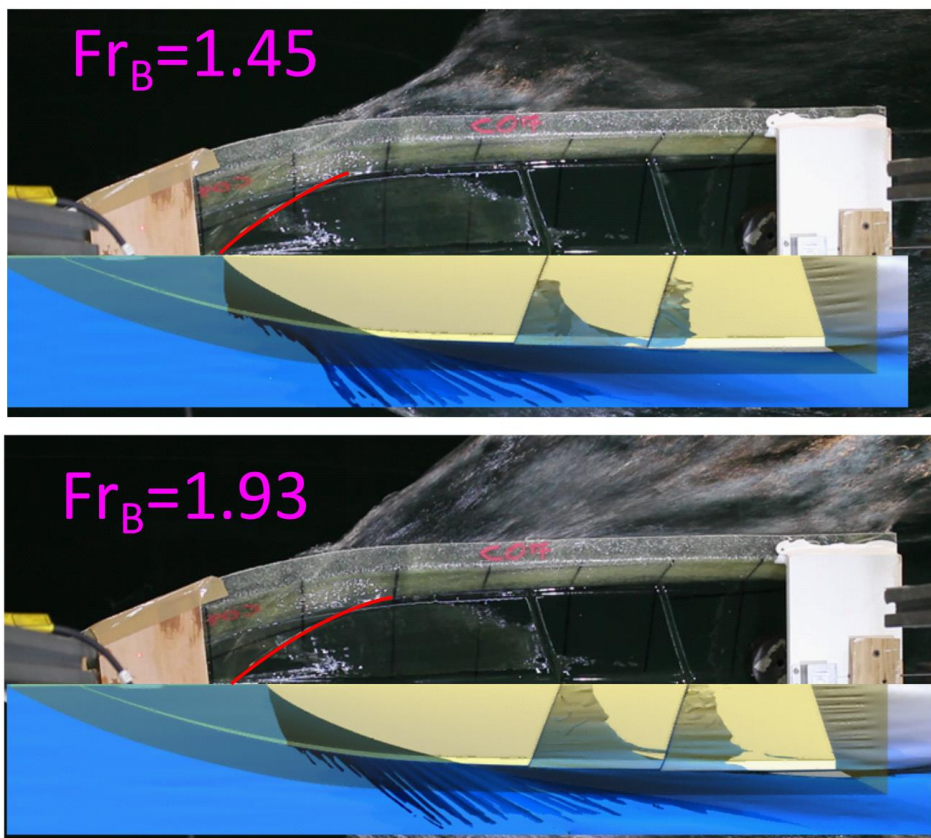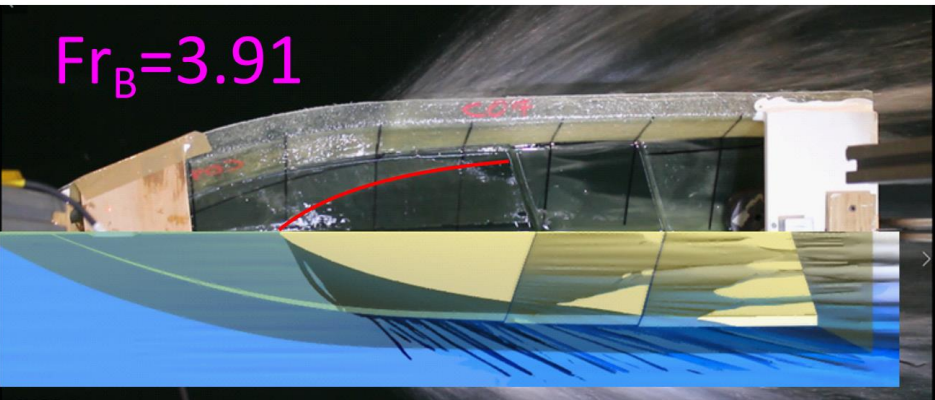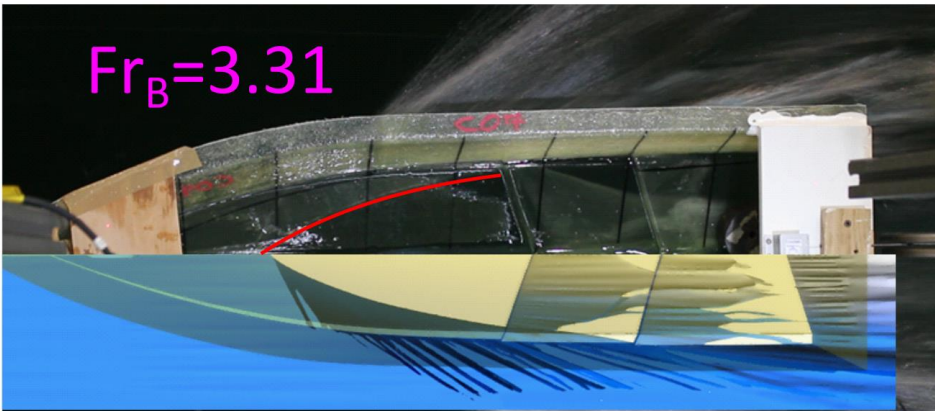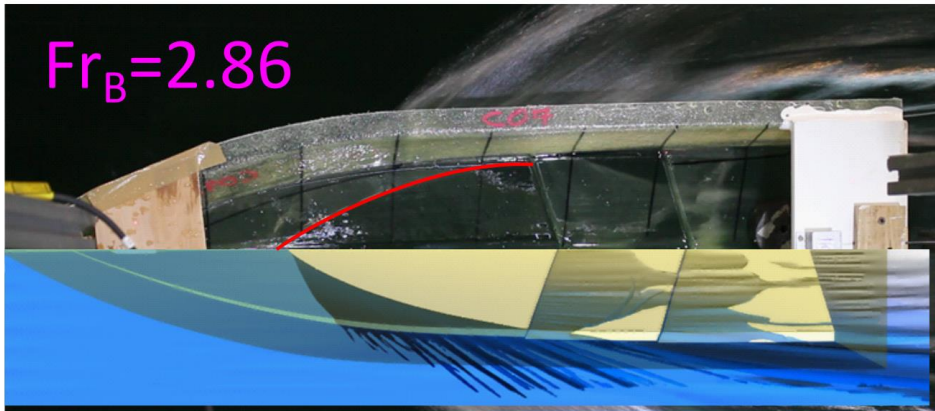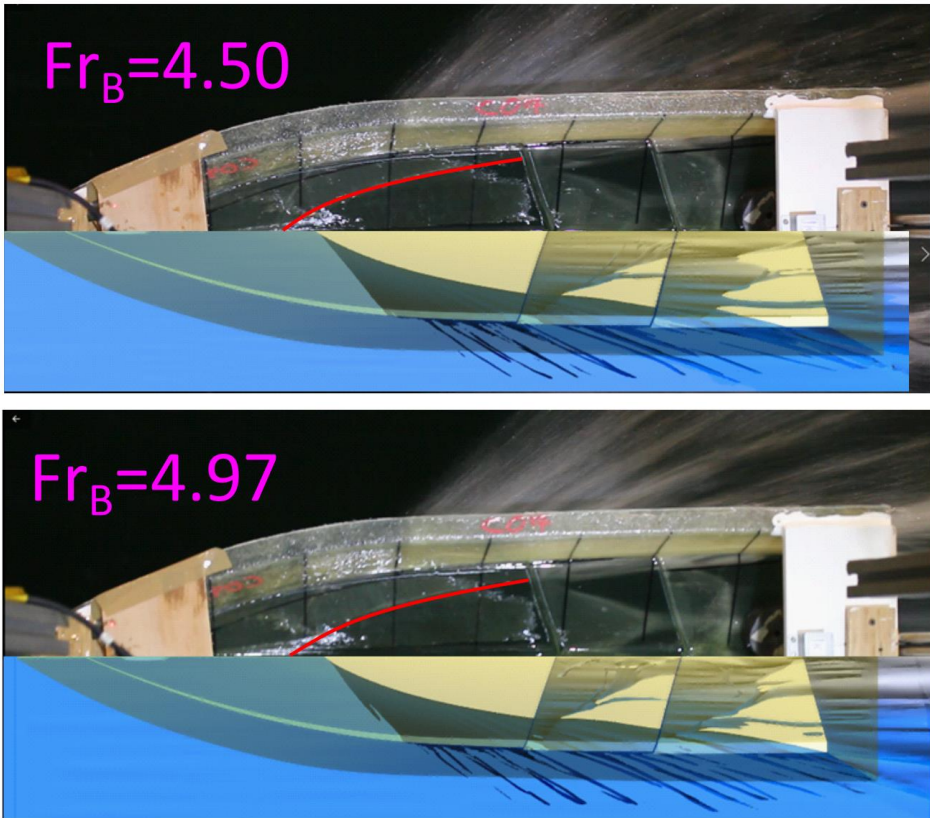
Figure 19. Comparison of numerically calculated wetted surfaces with the experimental results of Vitiello et al. (2022) for C07 hull (double-stepped hull). The CFD results are juxtaposed with towing tank test data, demonstrating a consistent agreement across various speeds. For details on other speeds and hull configurations, refer [P3].

CFD simulations offer detailed insights into pressure distribution and flow patterns that are difficult to observe experimentally, thereby providing a comprehensive understanding of hydrodynamic performance. Figure 20 illustrates water volume fractions at different velocities, demonstrating how step configurations influence flow patterns in C07 hull (double-stepped hull). As speed increases, airflow behind the step (indicated by green vectors) intensifies, potentially exiting through either the chine or the transom. Volume fractions range from 0 (indicating full air) to 1 (indicating full water), with intermediate values indicating mixed phases.

Higher step heights, whether in single-step or two-step hulls, create diverse flow patterns aft of the step, influenced by its positioning. This airflow-water mix often forms vortices directed towards subsequent steps or the transom. Straight steps typically produce small air-water bubbles without significant vortex formation, whereas forward-swept steps are more conducive to vortex generation. Flow beneath the hull can be directed to the transom via the spray rail, reducing spray resistance. These observations suggest potential avenues for optimizing stepped planing hull designs in future studies.

FrB=1.45

FrB=1.93

FrB=2.86

FrB=3.31

FrB=3.91

48
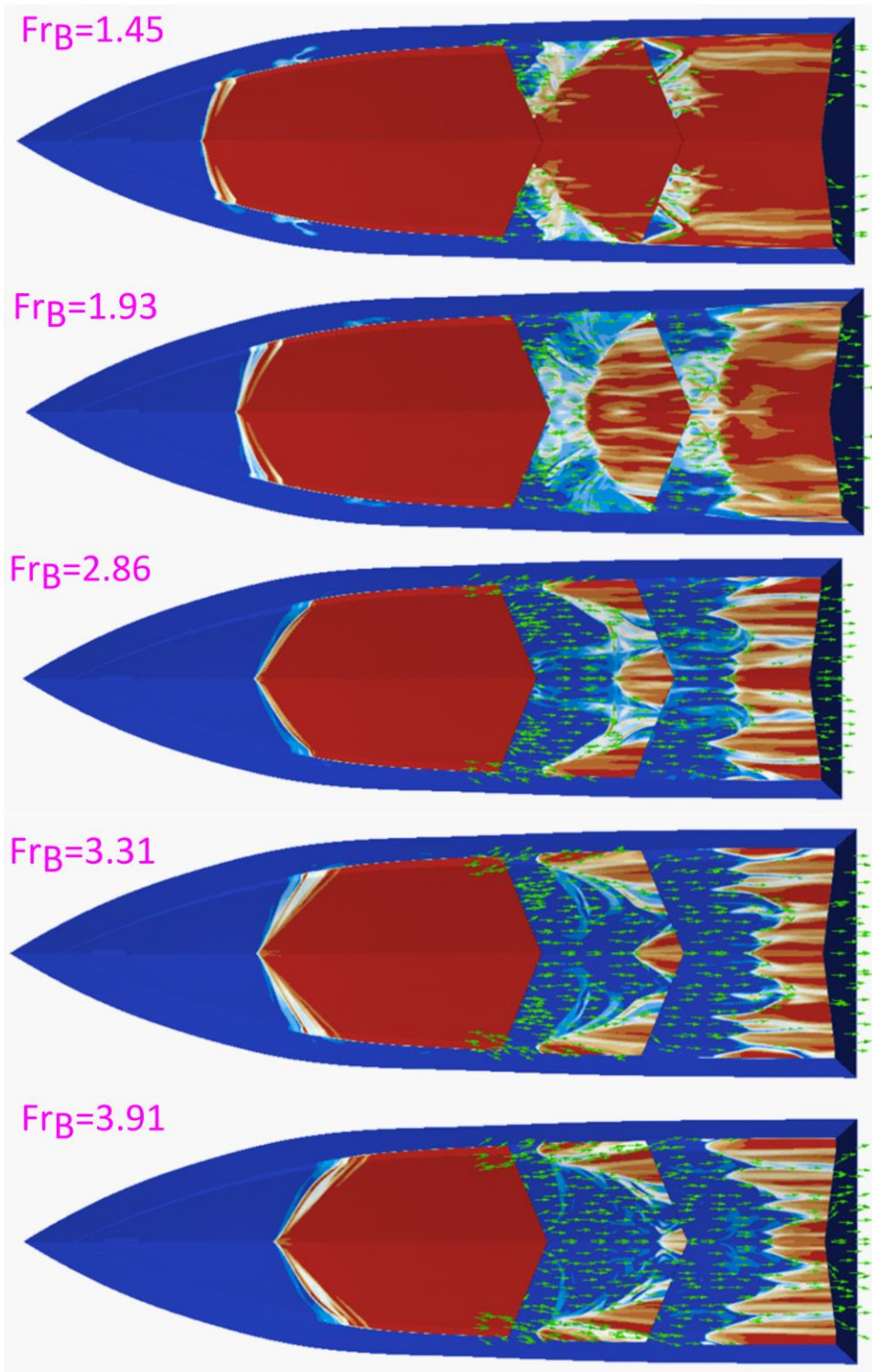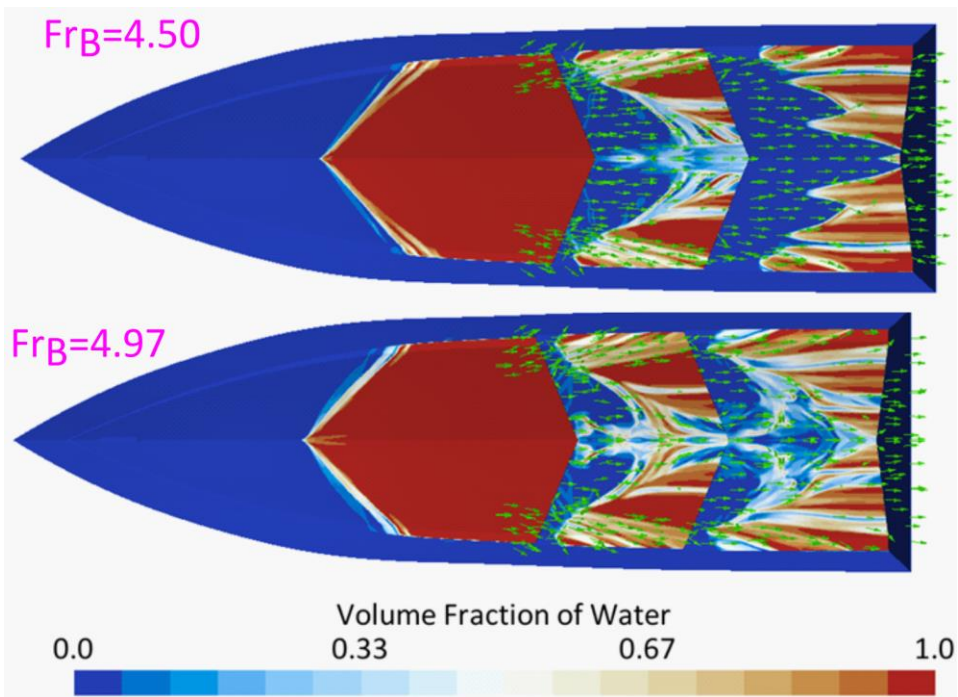
Figure 20. Calculation of the water volume fraction influenced by hydrodynamic forces, showing areas of water (red) and airflow (green vectors) resulting from the step configuration for C07 hull (double-stepped hull). This figure highlights the interaction between water and air at different velocities, illustrating the effects of step height and positioning on flow patterns and spray dynamics. For information on other hull configurations, refer to [P3].

Figure 21 illustrates the pressure distribution on the bottom of the C07 hull, showing two pressure zones for a single-step hull and potentially three for a two-step hull, depending on flow separation. Changes in hull geometry, step addition, height adjustments, or positioning affect pressure distribution and the center of lift force.

Fr$_B$=1.45

Fr$_B$=1.93

Fr$_B$=2.86

Fr$_B$=3.31

Fr$_B$=3.91
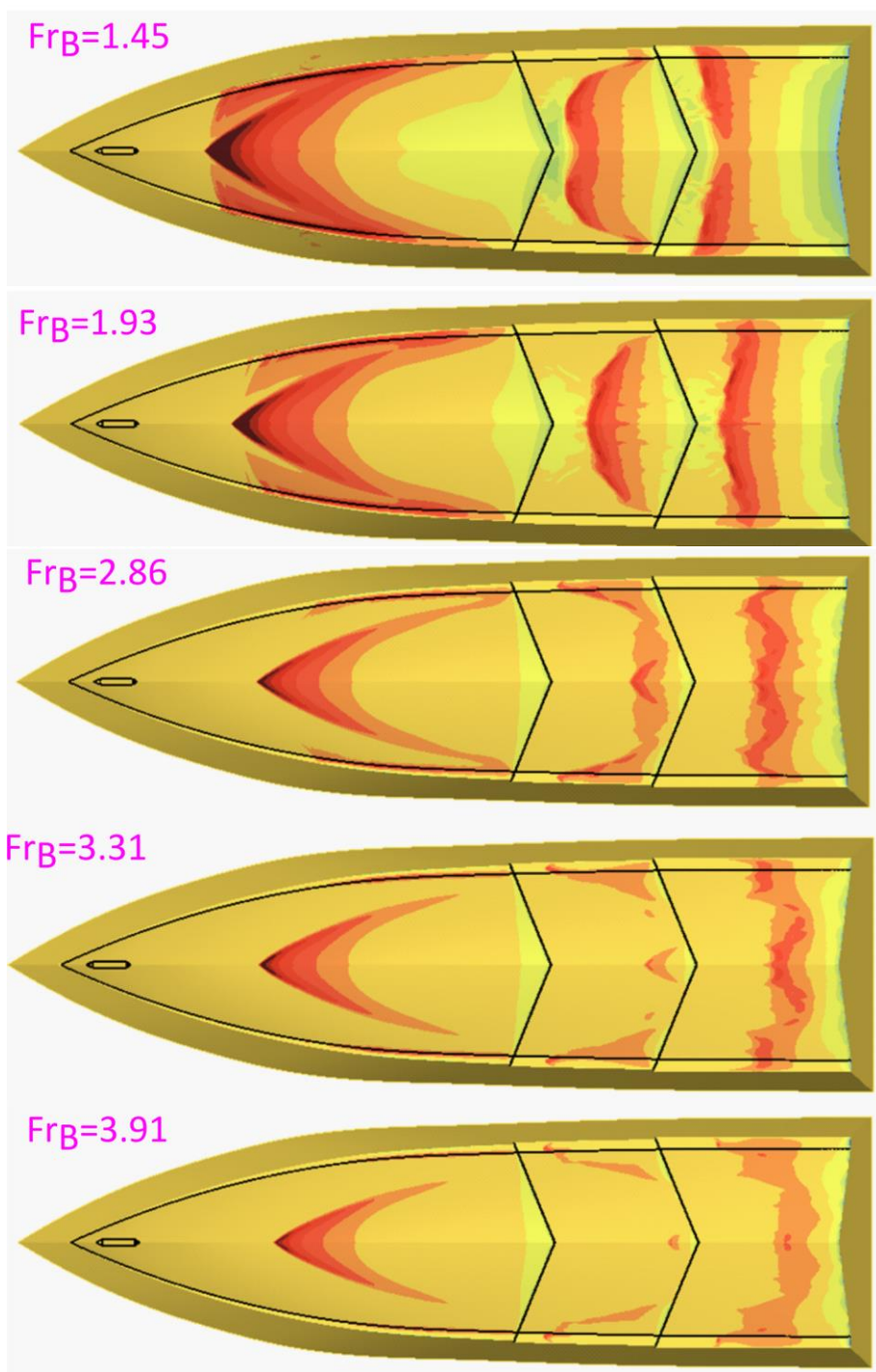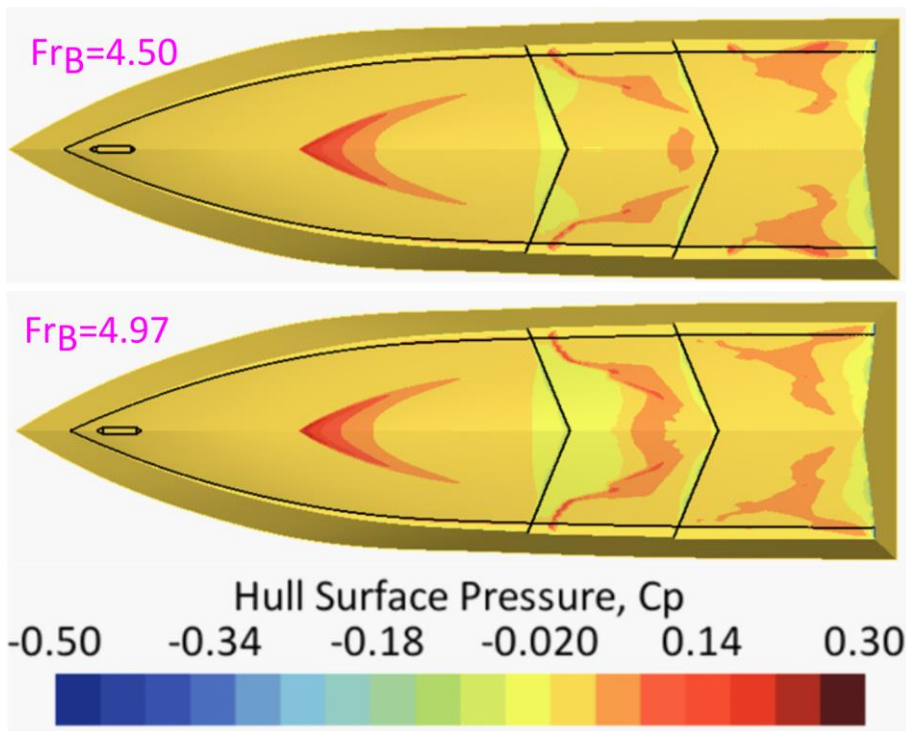
Figure 21. Pressure contours on the bottom of the C07 hull (double-stepped hull). This figure displays the distribution of pressure across the hull surfaces, demonstrating how changes in step height and position impact the pressure zones. For additional hull configurations, refer to [P3].

In Figure 22, the wake profile formation from the steps of the C07 hull at different Froude numbers is depicted along the 1/4 beam section and centerline. CFD predicts these profiles, which are challenging to replicate experimentally. The consistency with experimental data on wetted surfaces suggests similar wake profiles can be expected. Formulating predictions for wake profiles remains a potential focus for future research.

In conclusion, CFD proves effective in investigating the hydrodynamic behavior of forward swept-stepped hulls, offering accurate predictions and valuable insights into flow characteristics that complement experimental methods. However, rigorous Verification and Validation (V&V) of CFD models remains crucial to ensure reliability and applicability in practical design contexts.
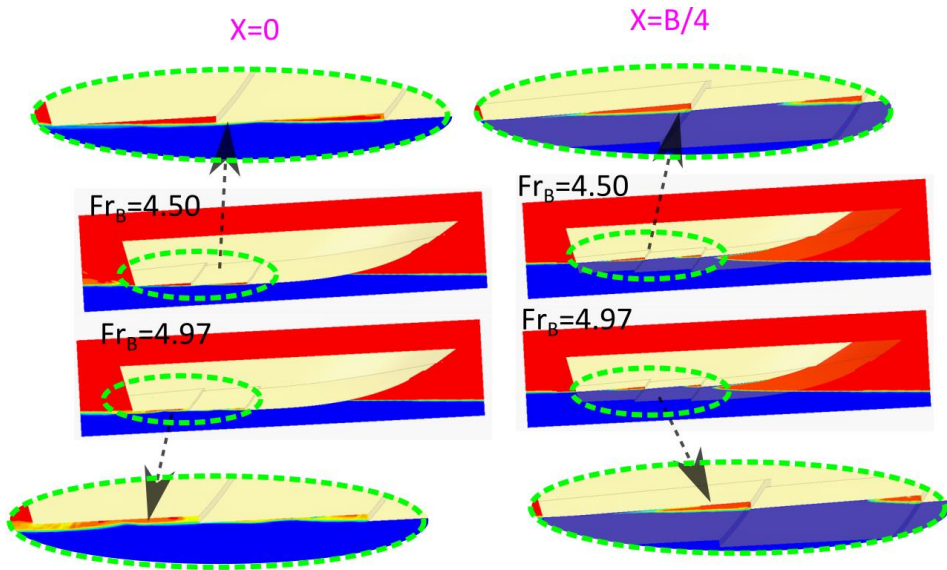
Figure 22. Wake profile formation resulting from the steps at two maximum Froude numbers, depicted along the 1/4 beam section (X=B/4) and centreline (X=0) for C07 hull (double-stepped hull). This figure illustrates the wake dynamics and flow separation patterns influenced by the step configurations, highlighting how the presence and positioning of steps affect the water flow and subsequent wake profiles.

In [P4], the study focuses on the V&V of CFD models in predicting the dynamic trim and hull resistance of high-speed planing hulls. The goal is to offer a deeper understanding of V&V analysis in this specific field, ensuring that CFD simulations are both accurate and reliable. This validation process is crucial for establishing the credibility of CFD models in naval architecture and for guiding future hull design optimizations based on CFD results.

Therefore, for this paper the V&V procedure is performed for complex planing hull, for the C05 stepped hull and C1 interceptor hull. These models have been previously designed and tested by De Luca and Pensa (2017) and [P2]. Both hull types being investigated have bottom 'discontinuities' causing flow separation. Analysing them together allows us to study the effects of these discontinuities on hydrodynamic behaviour, enhancing our understanding and contributing to a more comprehensive V&V analysis. The verification results for mesh and time step are obtained using SIEMENS PLM Star-CCM+ with two mesh motion techniques: overset/chimera and morphing mesh methods. Discretization uncertainties are estimated using a least squares method in a Matlab-based code. The results are validated by comparing them with towing tank tests from De Luca and Pensa (2017) and [P2]. Figure 23 presents a block diagram of the Least Squares method, detailing the systematic steps involved. This method is crucial in numerical simulations for accurately estimating grid and time step uncertainty, especially in complex flow phenomena, where accuracy and reliability are paramount.

calculating of $\mathcal{P}$ from minimum Eq. (3) and Eq. (4)

The $\mathcal{P}$ value that exhibits the lowest standard deviation is selected.

Yes ← $\mathcal{P} > 0$ → No

Anomalous data behavior

Data disregarding

$0.5 \leq \mathcal{P} \leq 2$ — No → $\mathcal{P} > 2$ — No → $\mathcal{P} < 0.5$

Yes

Yes

Yes

The discretization error is calculated using Eq. (2)

Discretization error can be computed using Eqs. (6) and (7) with the smallest standard deviation σ among the four possible fits (Eq. (8) to (11)).

Discretization error can be computed using Eqs. (6), (7), and (12) with the smallest standard deviation σ among the six possible fits (Eq. (8) to (11) and Eqs. (13), (14)).

No ← $\sigma < \Delta_f$ ← No — $\mathcal{P} \geq 2.1$ — Yes

$F_S = 3$

$F_S = 3$

Yes ↓ $F_S = 1.25$

$\sigma < \Delta_f$ — No

Yes

$F_S = 3$

uncertainty

$$U_f(f_i) = F_S \varepsilon(f_i) + \sigma + |f_i - (f_0 + \varepsilon(f_i))|$$

uncertainty

$$U_f(f_i) = 3\frac{\sigma}{\Delta_f}(\varepsilon(f_i) + \sigma + |f_i - (f_0 + \varepsilon(f_i))|)$$

Figure 23. Block diagram illustrating the implementation of the Least Squares method utilized in this study to assess mesh and time-step uncertainty for trim and resistance values of the C05 stepped hull. For detailed equations and further information, refer to [P4].

Figures 24 show the impact of time-step uncertainty on trim and resistance for the two hulls. For the C05 hull, using overset and morphing mesh techniques, the average time-step uncertainty errors are 0.93% for resistance and 2.29% for trim with overset, and 2.34% for resistance and 1.14% for trim with morphing mesh. This indicates limited impact of time-step changes on results. The resistance uncertainty is more critical than trim. Overset techniques have lower temporal uncertainty compared to morphing mesh, but accuracy also depends on grid and experimental uncertainties.
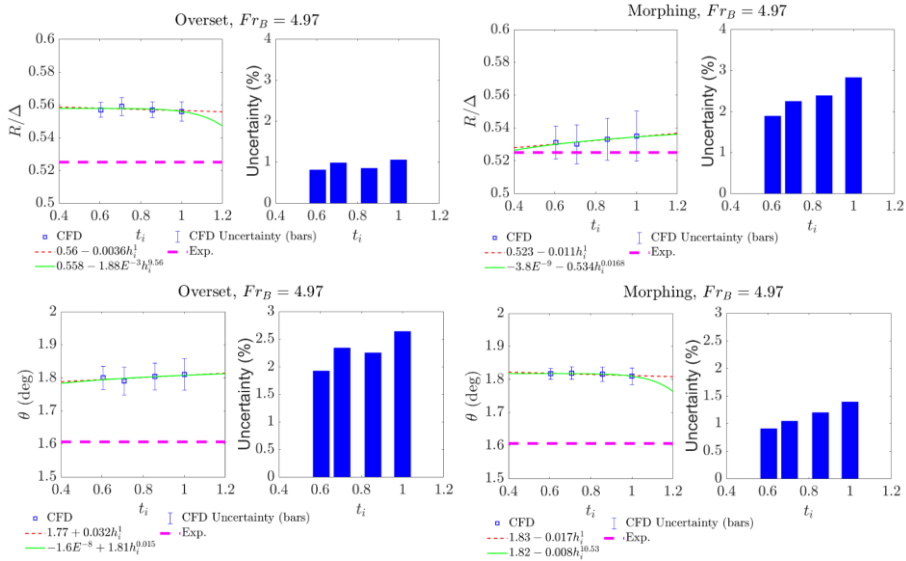
Figure 24. Time-step uncertainty error assessment for trim and resistance values of the C05 stepped hull, conducted using the least squares method. The evaluation uses overset and morphing mesh techniques at a Froude Number of 4.97, with mesh configurations of 15.4M for the overset technique and 15.17M for the morphing technique [P4].

Figure 25 depicts the grid uncertainty analysis of trim and resistance for the C05 stepped hull at a maximum beam Froude number of 4.97. Detailed grid uncertainty analyses for other Froude numbers can be found in [P4]. The symbol U_D in the figures denotes experimental or data uncertainty. For trim values, the apparent order of convergence $\mathcal{P}$ is less than 0.5 for the overset mesh technique, indicating first-order convergence. In contrast, the morphing mesh technique shows $\mathcal{P}$ greater than 2 for all Froude numbers except 1.93 and 3.91, suggesting higher-order convergence except for those specific cases, where it aligns with both first and second-order estimations.

Regarding resistance values, the overset mesh technique exhibits $\mathcal{P}$ less than 0.5, indicating first-order convergence. Conversely, the morphing mesh technique $\mathcal{P}$ greater than 2 for most Froude numbers except 3.31, 3.91, and 4.97, where $\mathcal{P}$ drops below 0.5. Therefore, a first-order error estimator is employed across all cases to quantify uncertainties. As speed increases (beam Froude Number), discrepancies between numerical and experimental results grow, particularly noticeable in the 8.9M and 11.2M mesh setups, predominantly in the overset mesh technique. This discrepancy is attributed to intensified turbulent flow, which introduces greater uncertainty in the simulations.
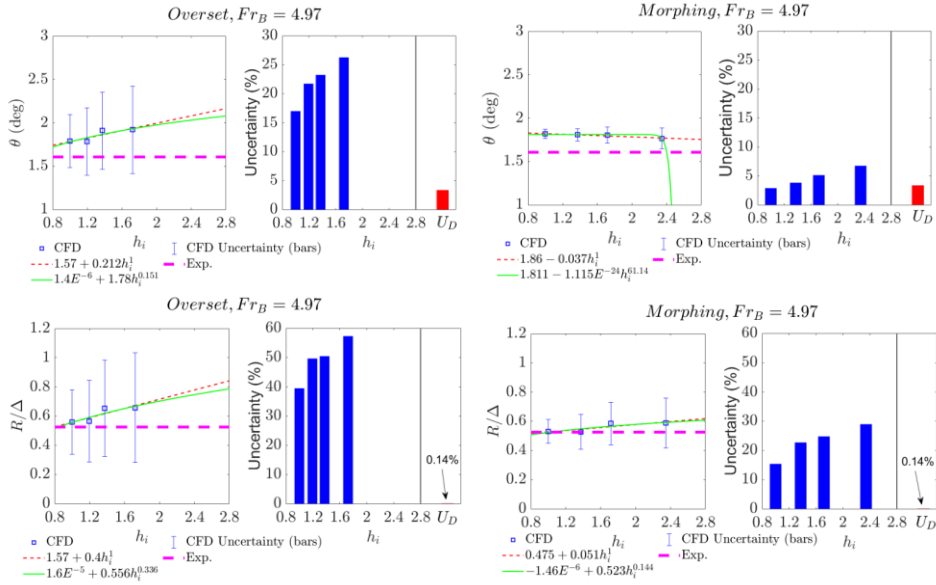
Figure 25. Mesh uncertainty error assessment for trim and resistance values of the C05 stepped hull, conducted using the least squares method. The evaluation uses overset and morphing mesh techniques at a Froude Number of 4.97. Results for other Froude numbers are detailed in [P4].

After calculating mesh uncertainty (U_G) and time step uncertainty (U_{TS}), the simulation uncertainty (U_{SN}) can be determined by taking the square root of the sum of their squares. These uncertainties for both CFD setups in predicting the trim angle and resistance force of the C05 hull are listed in Table 4.

Table 5. Simulation Uncertainty Error of C05 stepped hull for Mesh Configurations 15.4M (Overset) and 15.17M (Morphing) [P4].

Fr_B	Overset					
	$U_{G_R}\%$	$U_{TS_R}\%$	$U_{SN_R}\%$	$U_{G_\tau}\%$	$U_{TS_\tau}\%$	$U_{SN_\tau}\%$
1.93	3.70%	0.93%	3.82%	11.85%	2.29%	12.07%
2.86	12.19%	0.93%	12.23%	18.55%	2.29%	18.69%
3.31	16.23%	0.93%	16.26%	25.55%	2.29%	25.65%
3.91	23.45%	0.93%	23.47%	5.87%	2.29%	6.30%
4.50	28.18%	0.93%	28.20%	17.52%	2.29%	17.67%
4.97	39.51%	0.93%	39.52%	17.00%	2.29%	17.15%
	Morphing					
1.93	7.34%	2.34%	7.70%	3.29%	1.14%	3.48%
2.86	1.71%	2.34%	2.90%	2.12%	1.14%	2.41%
3.31	4.30%	2.34%	4.90%	4.60%	1.14%	4.74%
3.91	4.36%	2.34%	4.95%	3.49%	1.14%	3.67%
4.50	16.34%	2.34%	16.51%	1.96%	1.14%	2.27%
4.97	15.42%	2.34%	15.60%	2.91%	1.14%	3.13%

To validate the CFD setups used in this research, an essential indicator called the Uncertainty Value (U_V) is introduced. U_V is calculated as the square root of the sum of the squares of the experimental or data uncertainty (U_D) and the simulation uncertainty (U_{SN}). This value is crucial because stepped hulls present unique challenges in simulation due to their complexity, particularly in predicting resistance and wetted surfaces, which require exceptionally fine meshes near the step.

The validation process compares U_V with the percentage error |E|, calculated as (EXP-CFD)/EXP, where EXP is the experimental value and CFD is the CFD value. Validation is achieved when U_V is greater than or significantly greater than |E|. If U_V is less than |E|, it indicates modeling issues or inadequate mesh configurations. Tables 5 and 6 summarize the validation studies for the C05 stepped hull and C1 interceptor hull, categorizing validation outcomes as "yes," "yes, at U_V level of uncertainty" (where U_V is twice |E|, or "No." Tables 5 and 6 show that the CFD model using the overset technique successfully validated the resistance for all Froude numbers except 1.93, while the morphing mesh method only validated resistance for Froude numbers ≥ 3.91. The overset technique also validated the trim angle for all Froude numbers, whereas the morphing mesh technique only validated trim for Froude numbers 2.86 and 3.31. Figure 26 compares the wetted surface area observed in towing tank tests with that monitored in CFD simulations, focusing on a Froude Number of 4.94. It displays results from both mesh motion techniques and illustrates the impact of cell number on the ventilation area.

Table 6. The validation results for the resistance of the C05 stepped hull using two different mesh configurations (15.4M for Overset and 15.17M for Morphing) across various speeds [P4].

Fr_B	Overset				
	$E_R\%$	$U_{D_R}\%$	$U_{SN_R}\%$	$U_{V_R}\%$	validation achieved
1.93	7.10%	0.33%	3.82%	3.83%	No
2.86	3.84%	0.27%	12.23%	12.23%	Yes, at UV level of Uncertainty
3.31	2.09%	0.22%	16.26%	16.26%	Yes, at UV level of Uncertainty
3.91	-1.65%	0.18%	23.47%	23.47%	Yes, at UV level of Uncertainty
4.50	-5.97%	0.15%	28.20%	28.20%	Yes, at UV level of Uncertainty
4.97	-6.47%	0.14%	39.52%	39.52%	Yes, at UV level of Uncertainty
	Morphing				
1.93	10.55%	0.33%	7.70%	7.71%	No
2.86	6.37%	0.27%	2.90%	2.91%	No
3.31	5.23%	0.22%	4.90%	4.90%	No
3.91	3.23%	0.18%	4.95%	4.95%	Yes
4.50	0.28%	0.15%	16.51%	16.51%	Yes, at UV level of Uncertainty
4.97	-1.11%	0.14%	15.60%	15.60%	Yes, at UV level of Uncertainty

Table 7. The validation results for the trim values of the C05 stepped hull using two different mesh configurations (15.4M for Overset and 15.17M for Morphing) across various speeds [P4].

Fr_B	$E_R\%$	$U_{D_R}\%$	$U_{SN_R}\%$	$U_{V_R}\%$	validation achieved
			Overset		
1.93	4.06%	2.65%	12.07%	12.36%	Yes, at UV level of Uncertainty
2.86	1.48%	2.65%	18.69%	18.88%	Yes, at UV level of Uncertainty
3.31	0.67%	3.04%	25.65%	25.83%	Yes, at UV level of Uncertainty
3.91	-7.92%	3.26%	22.5%	22.73%	Yes, at UV level of Uncertainty
4.50	-5.24%	3.47%	17.67%	18.01%	Yes, at UV level of Uncertainty
4.97	-11.49%	3.39%	17.15%	17.49%	Yes
			Morphing		
1.93	5.36%	2.65%	3.48%	4.38%	No
2.86	3.19%	2.65%	2.41%	3.58%	Yes
3.31	0.76%	3.04%	4.74%	5.63%	Yes, at UV level of Uncertainty
3.91	-5.78%	3.26%	3.67%	4.91%	No
4.50	-4.59%	3.47%	2.27%	4.15%	No
4.97	-13.30%	3.39%	3.13%	4.61%	No
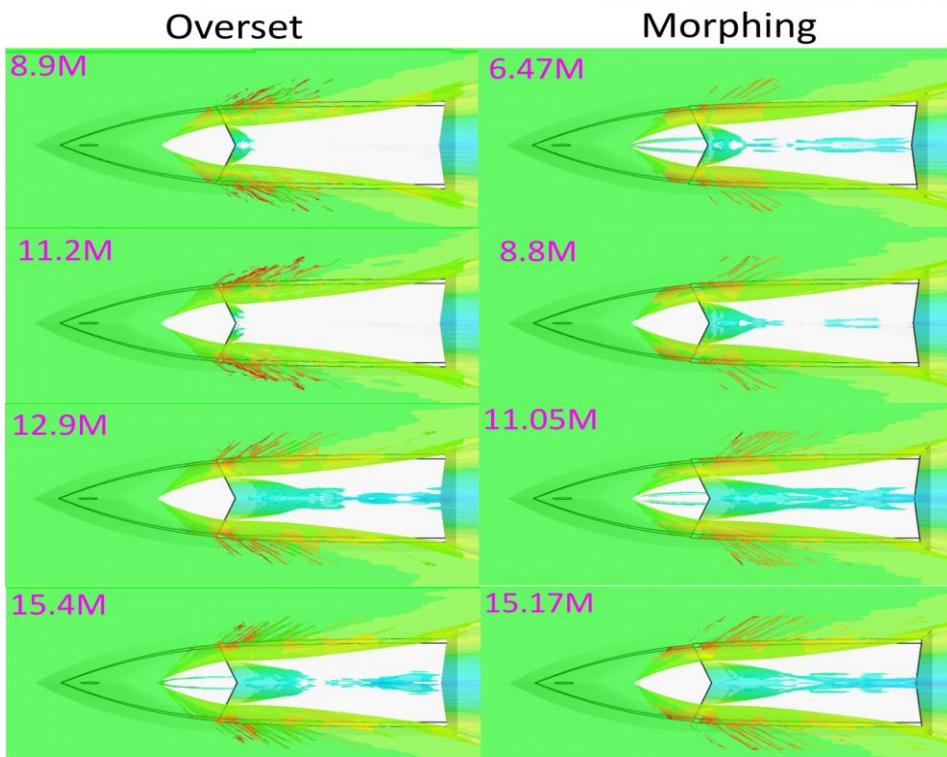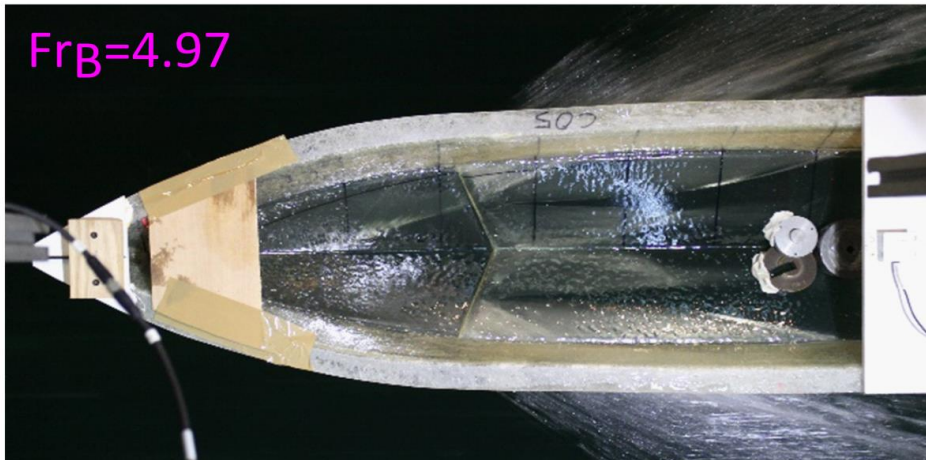
Figure 26. Comparison of wetted surface area and ventilation in CFD simulations of the stepped C05 hull using Overset mesh and Morphing mesh techniques, varying mesh densities, and towing tank test results at Froude number 4.94. Results for other Froude numbers are detailed in [P4].

These studies (P1, P2, P3, and P4) establish a comprehensive framework for optimizing the design of stepped planing hulls in calm water and regular waves by integrating experimental and computational methods to enhance performance and safety. However, the dynamic motion of planing hulls in irregular or random waves still requires investigation. Advances in CFD simulations now allow for highly accurate predictions in a

wider range of wave conditions, which are essential for understanding the nonlinear dynamics of these hulls. [P5] will focus on CFD simulations of stepless and stepped planing hulls in random waves.

3.4 Performance of Stepped Hulls in Random Seas: A CFD Perspective

In [P5], the commercial CFD software SIEMENS PLM STAR-CCM+ is used to model the dynamic behavior of stepless and stepped planing hulls in irregular waves. The aim is to create a CFD model for simulating these hulls in random waves, providing a thorough understanding of their statistical behavior, including the highest values and exceedance probabilities of motions, as well as the relationship between these probabilities and statistical indexes like skewness and kurtosis. Additionally, the study aims to understand the spectra of heave, pitch, and accelerations of stepless and stepped planing hulls. For this purpose, we have chosen the C hull, designed and tested by Taunton et al. (2011), because experimental results are available for one, two, and non-stepped hulls tested under different irregular conditions (shown in Table 7).

Table 8. Simulation particulars for seakeeping models in irregular waves (Taunton et al., 2011).

Configuration	Model	u (m/s)	Fr_B	Hs (m)	T_P (s)	k (m^{-1})	$\kappa = k\,{}^{Hs}\!/_2$
case 12	C	6.25	2.94	0.092	2.57	0.609	0.028
case 13	C	10.1	4.71	0.092	2.57	0.609	0.028
case 14	C	12.05	5.67	0.092	2.57	0.609	0.028
case 15	C	12.05	5.67	0.092	1.72	1.360	0.063
case 16	C	12.05	5.67	0.046	2.57	0.609	0.014
case 17	C	12.05	5.67	0.138	2.57	0.609	0.042
case 19	C	6.25	2.94	0.092	1.72	1.360	0.063
case 27	C1	6.25	2.94	0.092	2.57	0.609	0.028
case 28	C1	10.1	4.71	0.092	2.57	0.609	0.028
case 29	C1	12.05	5.67	0.092	2.57	0.609	0.028
case 30	C2	6.25	2.94	0.092	2.57	0.609	0.028
case 31	C2	10.1	4.71	0.092	2.57	0.609	0.028
case 32	C2	12.05	5.67	0.092	2.57	0.609	0.028
case 33	C2	12.05	5.67	0.092	1.72	1.360	0.063

Initially, it is crucial to Ensure that adequately many waves are encountered during simulations for accurate statistical calculations in irregular seas. The background domain is generated using the same grid configuration as in the seakeeping simulations. Table 8 compares wave characteristics between theoretical JONSWAP, experimental data, and current CFD results.

Table 9. Wave characteristic comparison: theoretical JONSWAP vs. experimental data vs. current CFD results [P5].

	Definition	Theoretical	CFD	Error CFD with theoretical	Exp.
H_S (m)	significant wave height	0.092	0.086	6.5%	0.109
$\bar{H}$ (m)	average wave height	0.0575	0.054	6%	0.0687
$\bar{T}$(s)	mean wave period	2.15	2.075	3.5%	2.21

The analysis of discrepancies between CFD simulations and experimental results focuses on time history data to identify peak and trough values. The amplitudes of pitch and heave motions, as well as CG acceleration relative to the mean, are extracted from these time histories. Mean, RMS, and ratio (r) values for crests and troughs are then compared to experimental data. The ratio (r) for maxima is the proportion of negative values among all maxima, while for minima, it is the proportion of positive values. The following factors contribute to discrepancies between CFD results and experimental data:

- High-speed planing hulls exhibit nonlinear behavior, which intensifies with speed.
- Nonlinearity affects the time histories of motions and accelerations.
- Time history data of mechanically generated waves from towing tank tests should be used to generate irregular waves in CFD simulations, not just spectra (Judge et al., 2020).
- Accurate comparisons require ensuring similar numbers of motions in CFD and experimental data.
- Differences in recorded motions can impact parameters like 1/3 and 1/10 values, especially with larger motions.
- A lack of comprehensive experimental data on wave time histories and recorded motions complicates analysis.
- Minor variations in wave elevation time histories can significantly affect response parameters such as heave, pitch, and CG acceleration, even if energy spectra and significant wave height match.
- Detailed attention to towing tank test response characteristics, including time history of waves, number of motions, probability distributions, individual maxima/minima, and statistical analysis values (1/3, 1/10, 1/100 peaks), is necessary.

Discrepancies in mean, RMS, and maxima/minima of heave and pitch between CFD and experimental data arise from these inherent variations. For an example comparison, Figure 27 shows the distribution parameters of heave, pitch motion extremes (maxima and minima), and gamma distribution parameters of minima CG acceleration for the C2 (double-stepped) hull under various operating conditions. Comparisons for other hulls are detailed in [P5]. These comparisons illustrate the favorable accuracy of the CFD model in capturing the statistical behavior of accelerations for both stepless and stepped hulls.
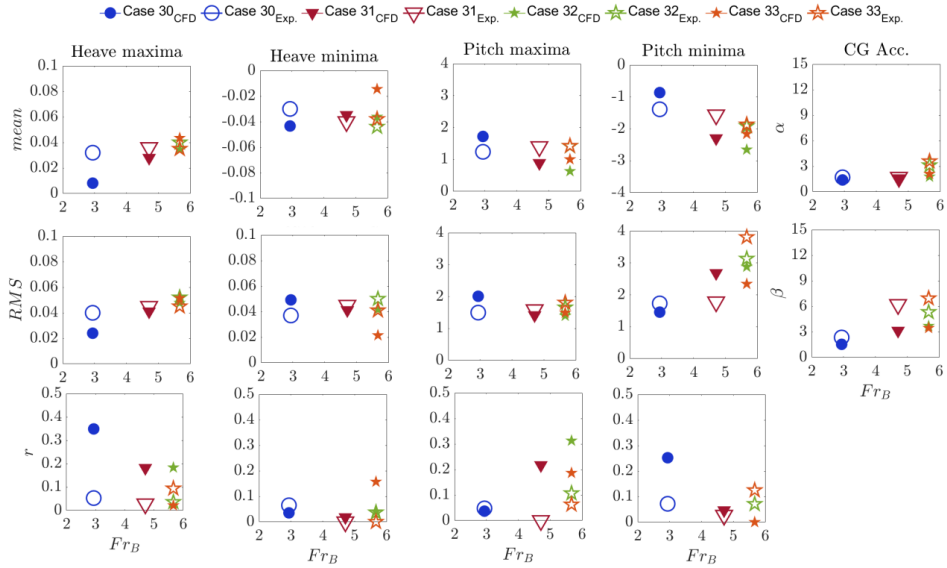
Figure 27. Comparison of distribution parameters for heave and pitch motion extremes (maxima and minima), as well as gamma distribution parameters of minima CG acceleration, between experimental (unfilled) and CFD (filled) data for the C2 (double-stepped) hull under various operating conditions. For other cases, refer to [P5].

The probability distributions of heave, pitch, and CG acceleration offer crucial insights into the dynamic behavior of planing hulls under various wave conditions. Unlike conventional ships, whose seakeeping behavior follows linear analysis methods due to the linear relationship between local wave elevation and vessel motions and accelerations, planing hulls exhibit a nonlinear relationship. This nonlinearity results in complex time histories of motions and accelerations, characterized by sharp peaks and flat troughs, making linear analysis methods unsuitable (ITTC, 7.5-02-04-05, 2014; ITTC, 7.5-02-07-02.1, 2014). The intensity of this nonlinearity increases with speed.

In this research, the probability distributions of heave and pitch motions, along with CG accelerations derived from CFD simulations, are analyzed to identify the appropriate probability distribution functions that match them. The heights, maxima, and minima of heave/pitch motions and vertical accelerations are normalized using the Root-Mean-Square (RMS) of the data. Figure 28 illustrates the probability distributions of heave, pitch, and CG acceleration for the C (case 14), C1 (case 29), and C2 (case 32) hulls under the same sea conditions and speed. Deviations from the expected distributions, as seen in Figure 28 for heave, pitch, and CG acceleration, are attributed to the presence of sharp peaks and flat troughs in the time histories, highlighting the nonlinear nature of high-speed vessel responses. For other cases, refer to [P5]. These findings are consistent with prior research by Fridsma (1971), Begovic et al. (2016), and De Luca and Pensa (2019).

These results underline the importance of considering nonlinear effects when analyzing the seakeeping performance of planing hulls. The accurate prediction of probability distributions enhances our understanding of vessel motions and accelerations, which is critical for designing safer and more efficient high-speed vessels.
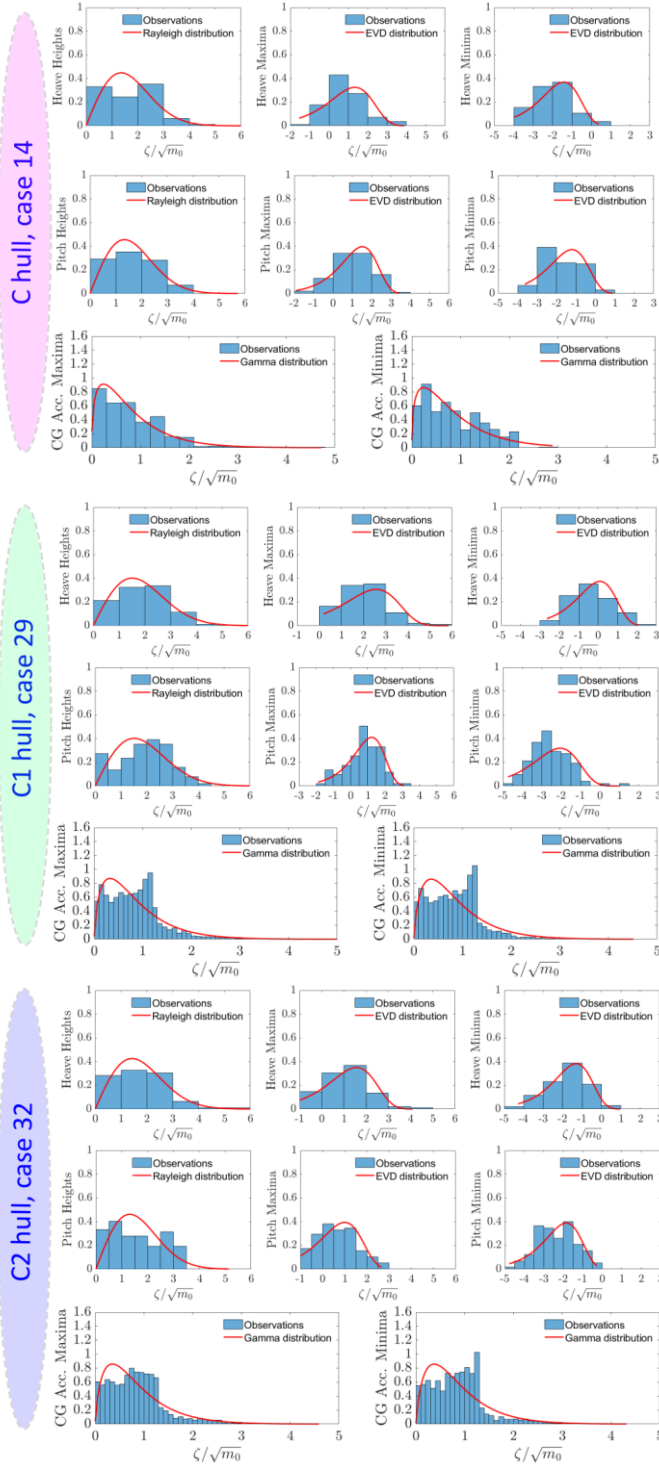
Figure 28. Statistics of normalized heights, maxima, and minima for heave, pitch motions and CG acceleration for the C (case 14), C1 (case 29), and C2 (case 32) hulls under the same sea conditions and speed. For other cases, refer to [P5].

To investigate the impact of speed and wave steepness on heave and pitch motion, as well as CG vertical acceleration, a statistical analysis of CFD measurements was conducted (refer to [P5]). The analysis considered a range of statistical indicators, including the mean, 1/3, 1/10, and 1/100 highest values, as defined in Table 9 for dynamic response analysis of hulls in random waves.

Table 10. Statistical indicators for dynamic response analysis of hulls in random waves.

Indicator	Description
Mean Value	Shows the central tendency of the data, indicating the typical dynamic response of each hull.
1/3 Highest	Provides insight into the extreme or upper-tail behaviour of the recorded motions.
1/10 Highest	Offers a better understanding of extreme events during the vessel's ride.
1/100 Highest	Identifies the most extreme outliers, informing us of the most extreme events.

Figures 29 depict the statistical analysis for heave and pitch motion, along with CG vertical acceleration for hulls C, C1, and C2, under identical sea conditions and operational speeds (e.g., cases 12, 27, 30; cases 13, 28, 31; and cases 14, 29, 32). The effects of adding steps to the hull on these statistical parameters are explored.

In the context of seakeeping, it is essential to monitor the heave and pitch range of motion when adding one or two steps to the hull, ensuring these parameters remain within acceptable limits established for non-stepped hulls. For range of heave motion statistical indicators of present hulls, consider the following points:

- The mean value, representing the central tendency, is overdamped across all hulls. However, the mean heave response for the hull with one step (case 29) is higher than the other two hulls at the highest speed, while the hull with two steps has the lowest mean value.
- The 1/3 highest values for the hull with one step are consistently higher than the other two hulls at all speeds, while the hull with two steps shows lower values.
- The 1/10 highest values are similar for all three hulls, with the hull with one step being higher at the highest speed.
- The 1/100 highest values for the hull with one step at lower speed (case 27) are lower than the non-stepped hull, but higher for other cases.

And for range of pitch motion statistical indicators of present hulls, consider the following points:

- The mean and 1/3, and 1/10 highest values for hulls with steps are higher than the non-stepped hull at higher speeds but lower at the smallest speeds.
- The 1/100 highest values vary, with the hull with one step being 7% higher at the smallest speed and 4% higher at the highest speed, while the hull with two steps is 20% higher at the smallest speed and 4% lower at the highest speed.

However, the most critical factor is the statistical indicator of vertical acceleration at the center of gravity (CG). High accelerations not only compromise the comfort of passengers and crew but also present significant operational challenges for cargo

handling. Additionally, phenomena such as slamming can generate substantial loads, thereby affecting the fatigue life of the vessel's structure. Ensuring that vertical accelerations are minimized is essential for maintaining both the structural integrity and operational efficiency of the vessel. Table 10 shows the percent changes in the statistical indicators of vertical acceleration at the CG when steps are added to the hull compared to non-stepped hulls. For range of vertical acceleration at the CG statistical indicators of present hulls, consider the following points:

- The mean value for hulls with steps is lower than the non-stepped hull at all speeds.
- The 1/3, 1/10, and 1/100 highest vertical acceleration values for stepped hulls are higher at the smallest speed but lower at mid and high speeds.
- The most extreme outliers of vertical acceleration for the hull with two steps at the highest speed are 31% lower than the non-stepped hull, and for the one-stepped hull, 9% lower.

Table 11. Percent change in statistical indicators of vertical acceleration at the center of gravity for stepped vs. non-stepped hulls.

	$\dfrac{CG_{H_{mean}}}{g}$	$\dfrac{CG_{H_{1/3}}}{g}$	$\dfrac{CG_{H_{1/10}}}{g}$	$\dfrac{CG_{H_{1/100}}}{g}$
	C1			
Case 27	-7%	93%	60%	33%
Case 28	-64%	-79%	-75%	-59%
Case 29	-65%	-66%	-48%	-9%
	C2			
Case 30	-15%	133%	69%	39%
Case 31	-64%	-78%	-69%	-32%
Case 32	-67%	-73%	-64%	-31%
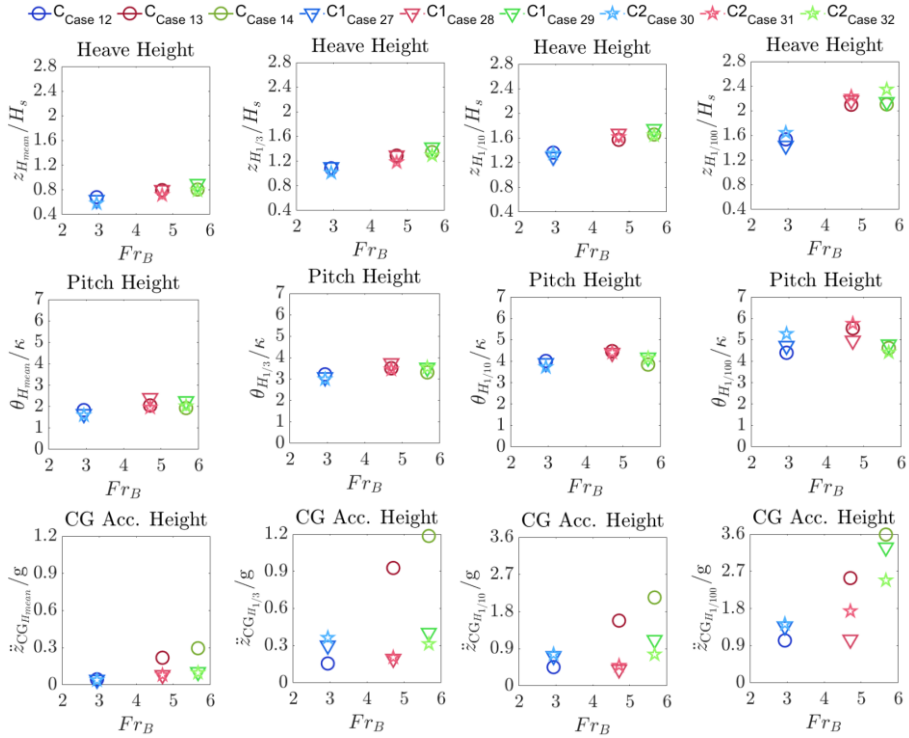
Figure 29. Effect of step configurations on heave, pitch, and CG acceleration statistics with increasing Froude numbers in identical irregular wave conditions [P5].

Figures 30 and 31 present the probability density functions (PDFs) and Exceedance Probability Functions (EPFs) for wave profiles, heave, pitch, and CG acceleration of non-stepped hull C (Case 14), one-stepped hull C1 (Case 29), and two-stepped hull C2 (Case 32) planing hulls under identical wave and operating conditions. In Figure 29, the solid red curve represents a Gaussian distribution, with its peak indicating the mean value. When a PDF follows this Gaussian curve, it implies that the recorded signal exhibits Gaussian behaviour. Figure 30 displays the EPFs for crest height in wave profiles, heave, pitch, and CG acceleration, with the solid red curve representing the Rayleigh distribution. Greater divergence from the Rayleigh curve indicates stronger nonlinearities and a higher likelihood of extreme events.

The skewness (S) and kurtosis (K) values shown in Figures 30 and 31 for heave, pitch motions, and CG acceleration provide insights into the vessel's behaviour in random waves. Skewness measures the asymmetry of each response cycle, while kurtosis assesses the peakedness. High kurtosis values suggest a greater likelihood of extreme events. Generally, CG acceleration is not expected to follow a normal distribution. High kurtosis in CG acceleration indicates a higher probability of extreme events, potentially causing discomfort, injury, or damage. A positive CG acceleration value signifies that large accelerations are mostly upward.

In Figure 30, the PDFs of recorded water waves generated in the numerical tank align with the Gaussian distribution, suggesting no nonlinearities in wave propagation. The PDFs of recorded heave motions and vertical acceleration are positively skewed for all cases, with the one-stepped hull (C1, Case 29) showing the highest skewness.

The pitch motion PDFs for all cases closely match the Gaussian distribution. Additional case PDFs can be found in [P5].

In Figure 31, deviations from the Rayleigh distribution in the EPF data indicate that the data is not well-represented by the Rayleigh distribution. A kurtosis value greater than 3.0 causes significant divergence from a normal EPF. The kurtosis values for heave and vertical acceleration are lower for the two-stepped hull than for the non-stepped and one-stepped hulls under the same sea conditions and speeds, indicating fewer extreme events for the two-stepped hull. The kurtosis values for pitch displacement are similar across all three hulls and remain below 3.0.
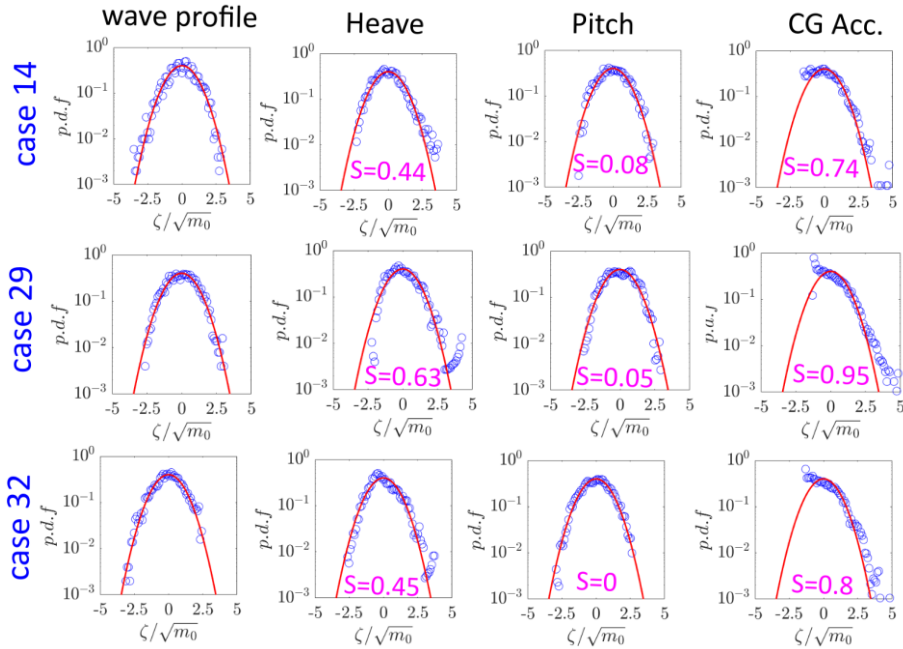
Figure 30. Probability Density Functions for wave profiles, heave, pitch, and CG acceleration of the non-stepped hull, C (case 14), one-stepped hull, C1 (Case 29), and two-stepped hull, C2 (Case 32) planing hull under same wave and operating conditions. The solid red curve represents a Gaussian distribution, and S represent the skewness value. For other cases, refer to [P5].
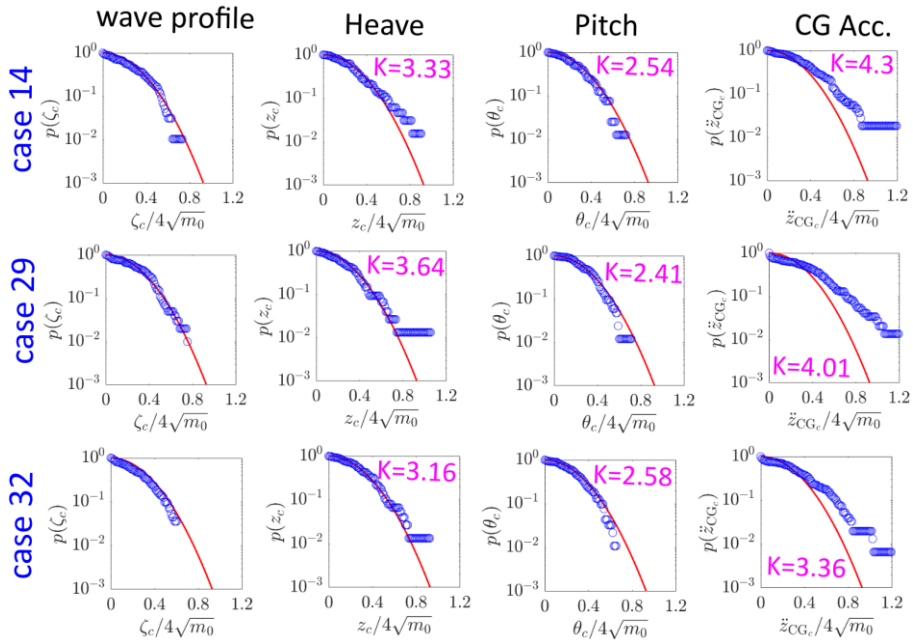
Figure 31. Exceedance Probability Functions for crest height in wave profiles, heave, pitch, and CG acceleration of the non-stepped hull, C (case 14), one-stepped hull, C1 (Case 29), and two-stepped hull, C2 (Case 32) planing hull under same wave and operating conditions. The solid red curve represents the Rayleigh distribution function, and K represent the kurtosis value. For other cases, refer to [P5].

4 Conclusions

Stepped planning hulls have become a noteworthy design for safe water operations. Properly designed stepped hulls can enhance fuel efficiency. Their motion follows nonlinear dynamics due to the varying wetted area of the vessel over time. This thesis investigates the hydrodynamic performance and dynamic behavior of stepped planing hulls under various operating conditions, aiming to optimize fuel efficiency at high speeds through strategic step placement and design.

In the initial phase of the thesis, a mathematical model based on the 2D+t approach was developed to replicate the hydrodynamic performance and unsteady motion of straight-stepped boats in calm water and head sea conditions. This model utilizes the solution of a high-frequency radiation problem, known as the Wagner problem, to calculate sectional forces by applying the momentum variation law or pressure distribution variation. Additionally, a simplified model was used to estimate the ventilation area behind each step. Concurrently, a CFD model was employed to simulate the hydrodynamic performance and unsteady motion of stepped boats in calm water and waves. Due to the lack of experimental seakeeping tests for stepped boats, the CFD model was crucial for verifying the mathematical model. The CFD model was also validated for non-stepped planing hulls in regular waves. Key findings from the analysis include:

- **Model Validation and Performance:** Both the 2D+t model and the CFD model effectively predict vessel performance in calm water conditions. However, the 2D+t model shows significant errors at low speeds due to unrealistic assumptions. In regular waves, both models produced similar results, validating the 2D+t model's reliability for simulating the unsteady motion of double-stepped hulls, despite some discrepancies in long waves.

- **Effects of Step Design on Vessel Performance:** The mathematical model provided valuable insights into how step design impacts unsteady planing motion in regular waves. Tests on stepless and double-stepped boats in head waves revealed that the double-stepped design enhances vessel performance by reducing heave and pitch responses and vertical acceleration. This improvement results from dividing the wetted area into three parts, which increases damping forces and decreases wave loads.

- **Influence of Step Heights:** mathematically modelled of two double-stepped boats with different step heights showed that a shorter front step reduces heave motion, particularly in the resonance zone, but increases vertical acceleration. This behaviour is due to the larger wetted area, which raises both total damping and exciting forces. It shows that the mathematical model can simulate different step height and also position of step.

- **Model Enhancements and Design Guidelines:** The mathematical model's accuracy for simulating the unsteady planing motion of double-stepped hulls can be improved by incorporating the oscillation motions of sections and providing a more precise prediction of the transom wave. For design guidelines, a designer can use a mathematical model, such as the 2D+t theory, to investigate the effects of different parameters on the hull through systematic

series analyses. This approach allows the designer to select the optimal range for their design. Following this initial analysis, CFD simulations can verify the results obtained from the mathematical model and ensure they fall within a reasonable range. CFD simulations also facilitate the evaluation of full-scale models. Finally, experimental tests can be conducted on the finalized hull design. This comprehensive procedure enhances accuracy and saves both time and money.

In the second phase, calm water resistance experiments were conducted at the towing tank of the naval section of the Dipartimento di Ingegneria Industriale (DII) at Università degli Studi di Napoli "Federico II." These experiments involved eight models of a new stepped hull series, each featuring a forward-swept step with varying heights and positions. All models were constructed with a transparent bottom to quantify the wetted surface and observe vortical flow phenomena behind the steps. Due to the low weight of the models, making them sensitive to externally applied forces, the towing tank tests implemented the "Down-Thrust" methodology.

Understanding pressure distribution under stepped planing hulls and streamlines during flow separation from steps and chines is challenging with towing tank tests alone. Therefore, a CFD method was employed to investigate the hydrodynamic behavior of the forward-swept stepped planing hulls in detail, with eight different step configurations. The uncertainty of CFD models in predicting the dynamic trim and hull resistance of one forward-swept stepped hull was also assessed using four different grids and two mesh motion approaches—overset and morphing mesh. Fitted convergence trends based on the least squares method were used to estimate the grid and time step uncertainties for each CFD simulation, proving to be the most robust method for obtaining these estimates. The comparative analysis showed that the choice of mesh technique and number of cells significantly affect the accuracy of CFD simulations. The overset mesh technique exhibited better performance across a wider range of Froude Numbers examined in the validation analysis, particularly for the forward-swept stepped hull validated at the UV level of uncertainty. Key findings from the analysis include:

- **Step Height and Flow Separation:** Increasing the step height of a stepped planing hull from 0.91% BTC to 2.73% BTC leads to flow separation behind the step and creates a high-pressure region at reattachment points. This high-pressure region generates additional lift, significantly affecting the trim angle. The lowest trim angles were observed in C05 for single-stepped hulls and in C07 for two-stepped hulls. Optimal step heights can significantly enhance performance.
- **Step Placement Effects:** The positioning of steps on single-stepped hulls significantly impacts their performance characteristics. Moving the step forward from a position slightly behind the centre of gravity reduces resistance at high speeds, despite increasing the wetted surface area. This forward placement acts akin to a reverse deflector, effectively minimizing spray drag and overall resistance. Conversely, adding a step near the transom (transformed from one step to two steps) decreases trim but increases both wetted surface area and resistance. Placing a step forward in the hull alters the dynamic trim angle, reducing it at lower step heights and increasing it at higher step heights during high-speed operations. The impact on wetted surface area varies with step

height, influencing overall resistance, particularly evident in configurations with higher step heights due to increased spray formation. These findings underscore the critical role of step placement in optimizing the hydrodynamic performance of single-stepped hull designs.

- **Two-Stepped Hull Optimization:** Rearranging the rear step towards the bow at lower step heights in two-stepped hull designs, exemplified by the C08 model, effectively reduces hull drag by mitigating or preventing spray formation. However, with higher step heights like those in the C09 model, where flow separation occurs, shifting the step forward increases hull resistance due to intensified spray formation. These insights underscore the importance of strategic step placement in enhancing performance and minimizing resistance in two-stepped hull configurations.

- **Optimal Performance Across Speed Ranges:** The performance of different hull configurations varies significantly across distinct speed ranges. In very-high-speed conditions ($Fr_B = 3.9$–4.97), hulls with specific characteristics, such as C04 (single step at 48.3%L, step height 0.91% BTC), demonstrate superior performance. Among double-stepped hulls, C08 stands out for its effectiveness in calm water at these speeds. Moving to the high-speed range ($Fr_B = 2.8$–3.9), hull C05 (single step at 48.4%L, step height 2.73% BTC) emerges as the top performer, with C07 leading among double-stepped designs. For medium-speed conditions ($Fr_B = 1.9$–2.8), hull C05 continues to exhibit optimal performance, while hull C06 excels in the low-speed range ($Fr_B = 0.8$–1.9). These findings emphasize the critical role of step position and height in optimizing hull performance across various speed regimes.

- **Impact of Step Height on Flow Patterns:** Increasing the step height in both single-step and two-step hulls creates a mixed flow pattern in the dry back part of the step, influenced by the step position. This pattern, consisting of a mixture of air and water that leads to vortex formation, is directed to the next step or the transom. For straight steps, these flow patterns typically consist of small bubbles made up of air and water, and vortex formation is generally not observed. However, vortex generation becomes more likely when the step is forward-swept.

- **CFD and Experimental Validation:** CFD models and experimental tests are essential for validating the hydrodynamic performance and dynamic behaviour of stepped hulls. CFD helps in understanding pressure distribution, streamlines, and flow behaviour, complementing physical experiments.

The third phase of this study utilized CFD modelling to investigate planing hull behaviour in irregular waves. It aimed to analyse the dynamic responses of stepless, single-stepped, and double-stepped hulls, providing insights into their performance under random wave conditions. This phase also sought to establish a robust CFD model capable of simulating real sea conditions, offering advantages over traditional experimental methods in towing tanks, which are costly and time-consuming.

The analysis encompassed a comprehensive statistical examination of CFD results, focusing on probability distributions, statistical metrics such as skewness and kurtosis, Exceedance Probability Functions (EPF), and spectral characteristics of heave, pitch, and vertical acceleration across different hull configurations. These insights significantly enhance the understanding of planing hull dynamics in irregular waves, benefiting naval architecture design and advocating for the adoption of CFD simulations. Key insights include:

- **Complex Motion Patterns:** High-speed planing hulls, whether stepped or non-stepped, exhibit intricate and non-linear motion and acceleration patterns in irregular waves. These patterns, characterized by sharp peaks and flat troughs, challenge traditional linear analysis methods used for slower vessels.
- **Extreme Event Probability:** High kurtosis values indicate a higher probability of extreme events, influencing hull design considerations for safety and performance. A kurtosis value greater than 3.0 indicates a significant departure from a normal EPF. For heave and vertical acceleration, the kurtosis values exceed 3 for all three hull types at maximum speed under the same wave conditions, indicating a higher probability of extreme events. Notably, the double-stepped hull exhibits lower kurtosis values compared to the non-stepped and single-stepped hulls, suggesting a reduction in extreme events. In contrast, the kurtosis values for pitch displacement remain below 3.0 for all three hulls, indicating a less significant departure from normality under the same conditions.
- **Extreme Value Analysis:** At both low and high speeds, the double-stepped hull generally shows better performance with lower extreme values, whereas the single-stepped hull exhibits mixed results with some higher extreme values, particularly in vertical acceleration at low speed.

Overall, double-stepped hulls tend to offer more consistent improvements in stability and performance, especially at high speeds, compared to single-stepped hulls and non-stepped hulls.

Future research on stepped planing hulls should focus on enhancing mathematical models to include additional degrees of freedom, such as roll motion, and developing models for irregular wave conditions, including head waves, following waves, beam waves, and oblique waves, as well as maneuvering motions like circle turns and zig-zag maneuvers. Advancements in the 2D+t model should account for yaw angles, compute maneuvering forces, and analyze heeled and yawed hulls. Investigating the effects of ice on stepped hull performance, despite its complexity, remains crucial. CFD models require further development to incorporate the effects of steps on the maneuvering motions of planing hulls in calm water and waves, using both free-sailing and captive approaches, and to address dynamic stability. Additionally, employing 6DOF simulations of unsteady planing in various sea conditions, including following waves, beam waves, and oblique waves, will provide deeper insights. These efforts will enhance the design, performance, and versatility of stepped planing hulls, leading to safer and more efficient marine vessels.

Abbreviations

CFD	Computation Fluid Dynamics
CICSAM	Compressive Interface Capturing Scheme for Arbitrary Mesh
CG	Centre of Gravity
EPF	Exceedance Probability Function
Exp	Experimental data
FFT	Fast Fourier Transform
FVM	Finite Volume Method
HRIC	High-Resolution Interface Capturing
HSC	High Speed Craft
IMO	International Maritime Organization
ITTC	International Towing Tank Conference
LBP	Length Between Perpendicular
PDF	Probability Density Functions
RANS	Reynolds Average Navier-Stokes
RAO	Response Amplitude Operator
RMS	Root-Mean-Square
SIMPLE	Semi-Implicit Method for Pressure-Linked Equations

Symbols

a_{in}	Amplitude of the incoming wave (m)
B	Maximum Beam of the boat (m).
B_{TC}	Chine breadth at transom (m).
$Fr_B = u/(gB)^{-1}$	Beam Froude Number (-).
$Fr_\nabla = u/(gB)^{-1}$	Beam Froude Number (-).
g	Gravity acceleration (m/s^2).
$Gxyz$	Body fixed frame (Coordinate system).
$\hbar_{s_\square}$	Step height (m).
H_s	Significant wave height (m).
$\overline{H}$	Average wave height.
k	Wave number (m^{-1}).
K	Kurtosis.
κ	Wave steepness.
L	Length over all (m).
L_{V_i}	The ventilation area for each planing surface (m)
L_{wl}	Length of waterline (m).
L_{CG}	Longitudinal position of centre of gravity (CG) with respect to transom (m).
Δ	Mass of the boat (Kg).
m_n	nth order spectral moment.
n	Normal unite vector.
$O\xi\eta\zeta$	Hydrodynamic frame (Coordinate system)
p	Fluid pressure (N/m^2).
r	Ratio of negative values among the maxima values divided by the total number of maxima values. Similarly, for the minima values, represents the ratio of positive values among the minima values divided by the total number of minima values.
R	Resistance (N).
S	Skewness.
S_w	Wetted surface (m^2).
t	Time (s).
T_{in}	Wave period (s).
T_p	Peak wave period (s).
$\overline{T}$	Mean wave height.
u	Boat speed (m/s).
$\boldsymbol{U} = [v_x, v_y, v_z]$	Velocity field in the fluid domain (m/s).
$Z, \dot{Z}, \ddot{Z}$	Heave displacement (m), speed (m/s), and acceleration (m/s^2).
Z_{Hmean}	Mean of highest height of heave (m).

$Z_{H1/n}$	Mean of 1/n highest height of heave (m).
$\ddot{Z}_{Hmean}$	Mean of highest height of CG acceleration (m/s^2).
$\ddot{Z}_{H1/n}$	Mean of 1/n highest height of CG acceleration (m/s^2).
$\theta, \dot{\theta}, \ddot{\theta}$	Pitch angle (rad), velocity (rad/s), and acceleration (rad/s^2).
θ_{Hmean}	Mean of highest height of pitch angle (rad).
$\theta_{H1/n}$	Mean of 1/n highest height of pitch angle (rad).
θ_j	Local Pitch angle (rad)
λ	wavelength (m)
∇	Displaced volume (m^3).
Ψ	Volume fraction of the water-air flow (-).
ω	Wave angular frequency (rad/s).
ω_p	Peak wave angular frequency (rad/s).

References

Akers, R. H. (1999). Dynamic Analysis of Planing Hulls in the Vertical Plane. Proceedings of the Society of Naval Architects and Marine Engineers, New England Section.

Algarín, R., & Tascón, O. (2014). Analysis of Dynamic Stability of Planing Craft on the Vertical Plane. Ship Science and Technology, 8(15), 35–43.

Begovic, E., Bertorello, C., Pennino, S., Piscopo, V., & Scamardella, A. (2016). Statistical analysis of planing hull motions and accelerations in irregular head sea. Ocean Engineering, 112, 253–264. https://doi.org/10.1016/j.oceaneng.2015.12.012

Benen, L. (1966). General resistance test of a shallow step planing hull with application to a hydrofoil configuration (DTMB Report 2169).

Benen, L. (1967). General resistance test of a stepped planing hull with application to a hydrofoil configuration (NSRDC Report 2320.).

Brizzolara, S., & Federici, A. (2013). Designing of planing hulls with longitudinal steps: CFD in support of traditional semi-empirical methods. Proceedings of Design and Construction of Super & Mega Yachts.

Clement, E. P. (1967). Effect of Length-Beam Ratio on the Performance of a Stepped Planing Boat with an Adjustable Stern Stabilizer (NSRDC Report 2552). https://apps.dtic.mil/sti/citations/AD0825515

Clement, E. P., & Koelbel, J. G. (1991). Effects of step design on the performance of planing motorboats. 4th Biennial Power Boat Symposium. The Society of Naval Architects and Marine Engineers. https://repository.tudelft.nl/islandora/object/uuid:d3ed95a2-d82b-45d8-a593-ad67ddb31f6b

Cucinotta, F., Mancini, D., Sfravara, F., & Tamburrino, F. (2021). The Effect of Longitudinal Rails on an Air Cavity Stepped Planing Hull. Journal of Marine Science and Engineering, 9(5), Article 5. https://doi.org/10.3390/jmse9050470

Danielsson, J., & Strømquist, J. (2012). Conceptual Design of a High Speed Superyacht Tender Hull Form Analysis and Structural Optimization. Independent Thesis Advance on Naval System.

Dashtimanesh, A., Esfandiari, A., & Mancini, S. (2018). Performance Prediction of Two-Stepped Planing Hulls Using Morphing Mesh Approach. Journal of Ship Production and Design, 34(03), 236–248. https://doi.org/10.5957/JSPD.160046

Dashtimanesh, A., Tavakoli, S., & Sahoo, P. (2017). A simplified method to calculate trim and resistance of a two-stepped planing hull. Ships and Offshore Structures, 12(sup1), S317–S329. https://doi.org/10.1080/17445302.2016.1262809

De Luca, F., & Pensa, C. (2017). The Naples warped hard chine hulls systematic series. Ocean Engineering, 139, 205–236. https://doi.org/10.1016/j.oceaneng.2017.04.038

De Luca, F., & Pensa, C. (2019). The Naples Systematic Series – Second part: Irregular waves, seakeeping in head sea. Ocean Engineering, 194, 106620. https://doi.org/10.1016/j.oceaneng.2019.106620

De Marco, A., Mancini, S., Miranda, S., Scognamiglio, R., & Vitiello, L. (2017). Experimental and numerical hydrodynamic analysis of a stepped planing hull. Applied Ocean Research, 64, 135–154. https://doi.org/10.1016/j.apor.2017.02.004

Di Caterino, F., Niazmand Bilandi, R., Mancini, S., Dashtimanesh, A., & Carlini, M. (2018, June 21). A Numerical Way for a Stepped Planing Hull Design and Optimization. https://doi.org/10.3233/978-1-61499-870-9-220

Ferziger, J. H., Perić, M., & Street, R. L. (2019). Computational Methods for Fluid Dynamics. Springer.

Filing, J. (1993). Experimental Procedure and Analysis of Stepped Planing Hulls with Applications to Motor Yachts. Patrol Vessels, and Fast Ferries, Webb Institute, Glen Cove, NY.

Fridsma, G. (1971). A Systematic Study of the Rough-Water Performance of Planing Boats. Irregular Waves—Part 2. https://apps.dtic.mil/sti/citations/AD0728788

Garland, W. R. (2010). Stepped planing hull investigation. United States Naval Academy.

Garme, K. (2005). Improved time domain simulation of planing hulls in waves by correction of the near-transom lift. International Shipbuilding Progress, 52(3), 201–230.

Gassman, W., & Kartinen, S. (1994). An investigation into the effects of the step location and the longitudinal center of gravity location on the performance of stepped planing hulls. Webb Institute, Glen Cove, NY.

Ghadimi, P., Tavakoli, S., Dashtimanesh, A., & Zamanian, R. (2017). Steady performance prediction of a heeled planing boat in calm water using asymmetric 2D+T model. Proceedings of the Institution of Mechanical Engineers, Part M: Journal of Engineering for the Maritime Environment, 231(1), 234–257. https://doi.org/10.1177/1475090216638680

Gray-Stephens, A., Tezdogan, T., & Day, S. (2020). Numerical Modelling of the Nearfield Longitudinal Wake Profiles of a High-Speed Prismatic Planing Hull. Journal of Marine Science and Engineering, 8(7), Article 7. https://doi.org/10.3390/jmse8070516

Gray-Stephens, A., Tezdogan, T., & Day, S. (2021). Experimental measurement of the nearfield longitudinal wake profiles of a high-speed prismatic planing hull. Ship Technology Research, 68(2), 102–128. https://doi.org/10.1080/09377255.2020.1836552

Husser, N. A. (2023). Experimental and Numerical Investigation of Forward and Aft Swept Stepped Planing Hulls in Calm Water and Regular Waves. https://vtechworks.lib.vt.edu/handle/10919/113915

ICOMIA. (2023). Recreational boating industry statistics 2022. Surrey: International Council of Marine Industry Associations (ICOMIA.org).

ITTC, 7.5-02-04-05. (2014). ITTC – Recommended Procedures and Guidelines, Seakeeping Tests.

ITTC, 7.5-02-07-02.1. (2014). ITTC – Recommended Procedures and Guidelines, Seakeeping Experiments.

Judge, C., Mousaviraad, M., Stern, F., Lee, E., Fullerton, A., Geiser, J., Schleicher, C., Merrill, C., Weil, C., & Morin, J. (2020). Experiments and CFD of a high-speed deep-V planing hull–part II: Slamming in waves. Applied Ocean Research, 97, 102059.

Lee, E., Pavkov, M., & McCue-Weil, L. (2014). The Systematic Variation of Step Configuration and Displacement for a Double-step Planing Craft. Journal of Ship Production and Design, 30(02), 89–97. https://doi.org/10.5957/jspd.2014.30.2.89

Martin, M. (1978). Theoretical Prediction of Motions of High-Speed Planing Boats in Waves. Journal of Ship Research, 22(03), 140–169. https://doi.org/10.5957/jsr.1978.22.3.140

Moldanová, J., Fridell, E., Matthias, V., Hassellöv, I.-M., Jalkanen, J.-P., Tröltzsch, J., Quante, M., Johansson, L., Karl, M., Malutenko, I., Ytreberg, E., Eriksson, M., Sigray, P., Karasalo, I., Peltonen, H., Hasenheit, M., Granhag, L., Mawdsley, I., Aulinger, A., … Piotrowicz, J. (2018). Sustainable Shipping and Environment of the Baltic Sea region: Final Report. In Sustainable Shipping and Environment of the Baltic Sea region [Report]. SHEBA.

Niazmand Bilandi, R., Dashtimanesh, A., & Tavakoli, S. (2019). Development of a 2D+T theory for performance prediction of double-stepped planing hulls in calm water. Proceedings of the Institution of Mechanical Engineers, Part M: Journal of Engineering for the Maritime Environment, 233(3), 886–904. https://doi.org/10.1177/1475090218797784

Niazmand Bilandi, R., Dashtimanesh, A., & Tavakoli, S. (2020). Hydrodynamic study of heeled double-stepped planing hulls using CFD and 2D+T method. Ocean Engineering, 196, 106813. https://doi.org/10.1016/j.oceaneng.2019.106813

Niazmand Bilandi, R., Dashtimanesh, A., & Tavakoli, S. (2023a). Stepped Hulls Early Stage Design by Implementing 2D+T Method. In HSMV 2023 (pp. 23–32). IOS Press. https://doi.org/10.3233/PMST230005

Park, S., Wang, Z., Stern, F., Husser, N., Brizzolara, S., Morabito, M., & Lee, E. (2022). Single- and two-phase CFD V&V for high-speed stepped planing hulls. Ocean Engineering, 261, 112047. https://doi.org/10.1016/j.oceaneng.2022.112047

Payne, P. R. (1994). Recent developments in "added-mass" planing theory. Ocean Engineering, 21(3), 257–309. https://doi.org/10.1016/0029-8018(94)90002-7

Reynolds, O. (1895). IV. On the dynamical theory of incompressible viscous fluids and the determination of the criterion. Philosophical Transactions of the Royal Society of London. (A.), 186, 123–164. https://doi.org/10.1098/rsta.1895.0004

Rodstrom, R., Edstrand, H., & Bratt, H. (1953). The transverse stability and resistance of single step boats when planing. Nr. 25, The Swedish State Shipbuilding Experimental Tank, Goteborg, Sweden

Savitsky, D. (1964). Hydrodynamic Design of Planing Hulls. Marine Technology and SNAME News, 1(04), 71–95. https://doi.org/10.5957/mt1.1964.1.4.71

Savitsky, D., & Morabito, M. (2010). Surface Wave Contours Associated with the Forebody Wake of Stepped Planing Hulls. Marine Technology and SNAME News, 47(01), 1–16. https://doi.org/10.5957/mtsn.2010.47.1.1

SIEMENS PLM. (2022). STAR CCM+ User's Guide Version 17.02.007.

Su, Y., Chen, Q., Shen, H., & Lu, W. (2012). Numerical simulation of a planing vessel at high speed. Journal of Marine Science and Application, 11(2), 178–183. https://doi.org/10.1007/s11804-012-1120-7

Svahn, D. (2009). Performance Prediction of Hulls with Transverse Steps [M.Sc.]. KTH Centre for Naval Architecture.

Taunton, D. J., Hudson, D. A., & Shenoi, R. A. (2010). Characteristics of a series of high speed hard chine planing hulls - part 1: Performance in calm water. International Journal of Small Craft Technology, 152, 55–75. https://doi.org/10.3940/rina.ijsct.2010.b2.96

Taunton, D. J., Hudson, D. A., & Shenoi, R. A. (2011). Characteristics of a series of high speed hard chine planing hulls - part II: Performance in waves. International Journal of Small Craft Technology, 153, B1–B22. https://doi.org/10.3940/rina.ijsct.2011.b1.97

Tavakoli, S., & Dashtimanesh, A. (2017). Running attitudes of yawed planing hulls in calm water: Development of an oblique 2D+T approach. Ships and Offshore Structures, 12(8), 1086–1099. https://doi.org/10.1080/17445302.2017.1316555

Tavakoli, S., & Dashtimanesh, A. (2019). A six-DOF theoretical model for steady turning maneuver of a planing hull. Ocean Engineering, 189, 106328. https://doi.org/10.1016/j.oceaneng.2019.106328

Tavakoli, S., Niazmand Bilandi, R., Mancini, S., De Luca, F., & Dashtimanesh, A. (2020). Dynamic of a planing hull in regular waves: Comparison of experimental, numerical and mathematical methods. Ocean Engineering, 217, 107959. https://doi.org/10.1016/j.oceaneng.2020.107959

Troesch, A. W., & Hicks, J. D. (1994). The Efficient Use of Simulation in Planing Hull Motion Analysis. Naval Engineers Journal, 106(1), 75–85. https://doi.org/10.1111/j.1559-3584.1994.tb02799.x

Vitiello, L., Mancini, S., Niazmand Bilandi, R., & Nappo, V. (2020). An Overview of Stepped Hull Performance Evaluation: Sea Trial Data vs Full-Scale CFD Simulation. https://doi.org/10.3233/PMST200026

Von Karman, T. H. (1929, October 1). The impact on seaplane floats during landing. https://ntrs.nasa.gov/citations/19930081174

Wagner, H. (with NASA). (1932). Phenomena Associated with Impacts and Sliding on Liquid Surfaces. http://archive.org/details/nasa_techdoc_20010003513

White, G., & Beaver, W. (2010). Stepped-hull High-speed Boat Model Test EW-07-10. U.S. Naval Academy, Annapolis, MD.

Zarnick, E. (1978). A Nonlinear Mathematical Model of Motions of a Planing Boat in Regular Waves (Technical Report DTNSRDC-78/032,). David Taylor Naval Ship

Research and Development Center. https://apps.dtic.mil/sti/citations/ADA052039

Zarnick, E. (1979). A Nonlinear Mathematical Model of Motions of a Planing Boat in Irregular Waves (Technical Report DTNSRDC/SPD-0867-01). David Taylor Naval Ship Research and Development Center. https://apps.dtic.mil/sti/citations/ADA078605

Acknowledgements

I wish to express my deepest gratitude to my supervisor, Prof. Abbas Dashtimanesh, for his guidance and unwavering support throughout the doctoral process. I also extend my sincere thanks to Prof. Simone Mancini and Dr. Sasan Tavakoli for their valuable insights and advice on this research. My heartfelt thanks go to Dr. Fabio De Luca and Dr. Luigi Vitiello for their essential support during the experimental study.

I would like to take this opportunity to thank the professors, colleagues, and staff members of the Estonian Maritime Academy for their continuous support and assistance during my doctoral program.

Lastly, I am profoundly grateful to my wife for her unwavering support and dedication throughout this journey. My heartfelt thanks also go to my parents and siblings for their constant encouragement and support. Their backing during challenging times has been invaluable, and without them, the completion of this thesis would not have been possible.

In closing, I would like to say, **"To be willing is to be able."**

Tallinn, 2024   Rasul Niazmand Bilandi

Appendix 1 (Publication I)

[P1] Niazmand Bilandi, R., Tavakoli, S., Dashtimanesh, A. (2021). Seakeeping of double-stepped planing hulls. Ocean Engineering, 236, 109475. https://doi.org/10.1016/j.oceaneng.2021.109475

Seakeeping of double-stepped planing hulls

Rasul Niazmand Bilandi [a], Sasan Tavakoli [b], Abbas Dashtimanesh [a],[*]

[a] *Estonian Maritime Academy, Tallinn University of Technology, Tallinn, Estonia*
[b] *Department of Infrastructure Engineering, The University of Melbourne, Parkville, 3052, VIC, Australia*

ARTICLE INFO

ABSTRACT

The double-stepped design of lifting surfaces, planing in water, has been seen to benefit the calm-water performance by distributing forces over the washed area. The unsteady motion of such surfaces in waves, however, is not well understood. It is not clear how steps can influence the response of a planing vessel operating in waves. In the presented research, this problem is analyzed by developing a model, which is established using a 2D + t framework. Meanwhile, a CFD set-up is also designed to numerically replicate the motion of double-stepped planing hulls subjected to gravity waves. It is demonstrated the results of both models agree. Performing mathematical simulations, it is demonstrated that a double stepped design can decrease the heave and pitch responses of the vessel in the resonance zone. More importantly, mathematical data confirms that wave-induced motions of a vessel are highly sensitive to the heights of steps. A vessel with a shorter front step has smaller vertical responses, especially over the resonance zone, while it may have larger vertical acceleration at high-speeds. This is caused by the larger washed area of the middle surface, which can increase damping forces, while it allows larger wave forces to impact the vessel.

1. Introduction

The need to design high-speed stable boats has derived naval architects to seek many different types of hullforms since early 1900s. Among different types of designs, planing hulls have always been considered as one of the popular hullforms, that can well operate at high-speeds. These vessels have been used for high-speed operations in the sea since the early 20 century. In the late 1950s and early 1960s, a new generation of planing hulls emerged (Savitsky, 1985). A step, which leads the water flow to be separated from it, was proposed to be added to their bottom (Fig. 1). At the first stage, such a design was found to be very interesting and attracted the attentions of different groups of boat designers. A set of papers and reports, including the calm water performance of these hulls, were published in 1960s–1980s (e.g. Clement and Pope, 1961; Clement and Desty, 1980). But it was eventually reported that, due to the unbalanced distribution of hydrodynamic pressure over the wetted surface of a single-stepped boat, the occurrence probability of instability may be intensified at high-speeds.

The problem with the instability of single-stepped boats slowed down their applications in coastal seas. In the early 2000s, a new design approach for stepped boats was suggested. Instead of one, two transverse steps were used on the bottom, which, on the whole, were seen to modify the pressure distribution over the entire length of boats. This type of design, which is known as double-stepped hullform, was seen to lead to smaller resistance force and trim angle, the angle between baseline and calm water line. The good performance of this type of vessel attracted renewed attention of boat designers. There is an accumulative series of research analyzing their performance in calm-water conditions, confirming their satisfactory performance in a smooth sea.

The steady planing problem of the double-stepped planing hulls has been well understood. Experimental studies have been performed (Taunton et al., 2010; Lee et al., 2014), Numerical and mathematical approaches have also been used to model their calm-water performance (Veysi and Ghassemi, 2016; De Marco et al., 2017; Dashtimanesh et al., 2018; Niazmand Bilandi et al., 2018; Niazmand Bilandi et al., 2019a, Esfandiari et al., 2019; Du et al., 2019). Hydrodynamic of double-stepped planing hulls in waves, however, is unclear. The steps lead to ventilation

---

* Corresponding author.
E-mail address: abbas.dashtimanesh@taltech.ee (A. Dashtimanesh).

Nomenclature

$\mathscr{A}_{zz}, \mathscr{A}_{z\theta}$	Linear added mass coefficients caused by vertical and angular accelerations
$\mathscr{A}_{\theta\theta}, \mathscr{A}_{\theta z}$	Angular added mass coefficients caused by vertical and angular accelerations
$a, \dot{a}$	2D added mass (Kg/m), and its time derivative (Kg/s)
a	Amplitude of the wave (m)
B, B_{WL}	Maximum Beam of the boat (m), and its beam at water line (m)
$c, \dot{c}$	Half beam of spray (m) and its time rate (m/s)
C_f	Frictional drag coefficient (-)
$d_\perp$	Normal distance from the wall of the vessel
D_t	Material derivative
$\mathscr{D}_f, \mathscr{D}_p, \mathscr{D}_s$	frictional drag, pressure frictional force and spray frictional force (N)
$\mathbf{F}$	force vector
$F = [F_x, F_y, F_z]$	Fluid force acting on the vessel (N). Different components refer to the surge, sway and heave forces
$f_{\mathscr{W}\mathscr{S}}^{2D}$	2D buoyant force (N/m)
$\mathrm{Fr_B} = u/(gB)^{-1}$	Beam Froude Number (-)
$\mathbf{f_b}$	Body force (N)
$\mathscr{F}$	Fluid force acting on the 2D section (N)
f_{z_i}, m_{θ_i}	Fluid force (N) in heave direction and moment (N-m) in the pitch direction on a single planing surface
$F_z^\star, M_\theta^\star$	Fluid force (N) in heave direction and moment (N-m) in pitch direction excluding the added mass contributions
g	Gravity acceleration (m/s^2)
$Gxyz$	Body fixed frame (Coordinate system)
h_s	Step height (m)
$h_{\mathscr{W}}(x)$	Water depth (m)
i	i-th planing surface
I	Mass moment of inertia (Kg-m^2)
κ	Wave number (m^{-1})
L_{CG}	The longitudinal position of the centre of gravity (CG) for transom (m)
L_{V_i}	The ventilation area for each planing surface (m)
$L_K^\oplus$	total keel length washed by water and the ventilation areas (m)
L_1, L_2, L_3	Length of each planing surface (m)
m	Mass of the boat (Kg)
$M = [M_\varphi, M_\theta, M_\psi]$	Moment vector (N-m). Different components refer to the heel, pitch and yaw moments
$\mathscr{M}$	Added mass forces (Kg/m)
$\mathscr{M}_i^\bullet, \mathscr{M}_i^{\bullet\bullet}$	Added mass moments (N-m)
$\mathbf{M}$	mass Matrix
$\mathbf{n}$	Normal unite vector
$OXYZ$	Earth frame (Coordinate system)
$O\xi\eta\zeta$	Hydrodynamic frame (Coordinate system)
p	Fluid pressure (N/m^2)
$\mathrm{R_E}$	Reyonlds number
$\mathscr{S}_i$	Wetted surface (m^2)
t	Time (s)

T	Wave period (s)
$\mathscr{T}_i$	Transom reduction function (-)
u	Boat speed (m/s)
u_τ	frictional velocity (m/s)
$\mathscr{U}$	Relative forward speed of 2D section (m/s)
V_{CG}	The Vertical position of the CG (m)
$\mathscr{V}, \dot{\mathscr{V}}$	Relative vertical speed (m/s) of a 2D section and its time rate (m/s^2)
$v = [v_x, v_y, v_z]$	Velocity field in the fluid domain (m/s)
W	Weight of the boat (N)
w_z	Vertical velocity of the wave
x_b	Bow position with respect to CG (m)
x_{s_1}	Step position with respect to CG (m)
x_{s_2}	step position with respect to CG (m)
x_T	Transom position with respect to CG (m)
$\mathcal{X}, \dot{\mathcal{X}}, \ddot{\mathcal{X}}$	displacement, velocity, acceleration vector
$\mathcal{Z}, \dot{\mathcal{Z}}, \ddot{\mathcal{Z}}$	Heave displacement (m), speed (m/s), and acceleration (m/s^2)
β	Deadrise angle of the vessel (deg)
β_j	Local deadrise angle of the vessel (deg)
Υ	The numerical domain
$\Upsilon_\mathbf{B}$	The part of the numerical domain occupied by the rigid body
Λ_B	Rigid body boundary
Λ_I	Inlet boundary
Λ_L	Left-patch boundary
Λ_O	Outlet boundary
Λ_S	Symmetry boundary
Λ_{SB}	Bottom boundary
Λ_U	Top boundary
γ_i	Spray angle
δC_f	Frictional drag coefficient due to hull roughness (-)
ε	Phase shift of the wave (-)
$\wp$	Wave steepness (-)
ζ	Water surface elevation (m)
$\theta, \dot{\theta}, \ddot{\theta}$	Pitch angle (rad), velocity (rad/s), and acceleration (rad/s^2)
θ_j	Local Pitch angle (rad)
λ	wavelength (m)
ν	Kinematic viscosity (m^2/s)
μ_a	Air viscosity (Kg/m-s)
μ_{eff}	Viscosity of the mixture of water (μ_t) and air (μ_a) at any point in the domain (Kg/m-s)
μ	Turbulent viscosity of the flow (Kg/m-s)
μ_w	Water viscosity (Kg/m-s)
ρ_{eff}	Density of the mixture of water (ρ_w) and air (ρ_a) at any point in the domain (Kg/m^3)
ρ_a	Density of the air (Kg/m^3)
ρ	Density of the water (Kg/m^3)
σ	Normal stress tensor
ω	wave angular frequency (rad/s)

areas and distribute forces over the bottom of the vessel (Garland and Maki, 2012). Added mass and damping forces/moments of the middle body are expected to be scant compared to the front and rear surfaces as the middle surface is nearly dry. Compared to a stepless design, the performance of a double-stepped body in waves can be different. To understand the effects of steps on the performance of planing hulls,
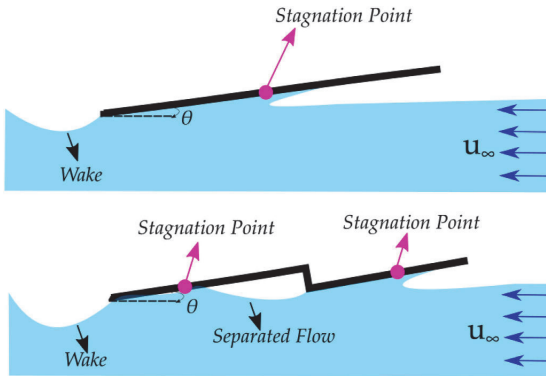
Fig. 1. A sketch showing the effects of step on the fluid motion around a planing surface with trim angle of θ. In the lee of a step, water flow is separated and re-attaches the rear lifting surface, causing a second lift force which is comparable to the one acting on the front surface.

exposed to water waves, their dynamic motion should be modeled.

The dynamic of ships in waves, also known as seakeeping, has been modeled by many researchers since the early 1950s. ideal flow assumption, zero-viscosity hypothesis, and the linear potential theory are used to model the problem. Using these assumptions, Radiation along with Diffraction problems emerge. Solutions to these problems give the added mass, damping force, and exciting force at different frequencies. The linear theory and these two problems are well explained in Newman (1977).

Radiation and Diffraction problems have been seen to be solved in the frequency domain by applying different analytical methods. Laplace Equation governs domain, which represents the continuity equations for an incompressible fluid flow with zero-viscosity. Depending on the physics of the problem, different methods including Eigenfunction matching, Multiploe methods, Green Integration among others can be used. A very deep overview of these methods is presented in Linton and McIver (2001).

For the case of ships, the strip theory can also be used (Salvesen et al., 1970; Ogilvie and Tuck, 1969), which utilizes the sectional damping and added mass coefficients of ship section, those which can be computed by using Lewis Section. The Radiation problem related to a two-dimensional cylinder is solved and then is mapped to the sections of the ship. This method has been seen to be valid for the case of displacement hulls.

For the case of a planing hull, advancing in water waves, some difficulties emerge. Since the vessel positions itself at a non-zero dynamic trim angle and the Centre of Gravity (CG) locates at a different level compared to zero-speed condition, hydrodynamic pressure turns into an important contributor to the generation of fluid forces. In this case, the linear potential assumption can lead to different physics which is far from what happens in reality, and classical frequency-dependent added mass and damping coefficients may not be consistent with real physics. Simply stated, the response of the vessel in the vertical direction is expected to be high and it starts to oscillate, leading to large variation in the wetted area of the vessel. In this situation, added mass and damping coefficients are likely to be response-dependent, which is different from the classical linear theory definition. Therefore, non-linear-based models can have been more accurate in this case.

Zarnick (1978) developed a nonlinear model for the mathematical replication of the motion of planing hulls in waves. The problem was solved in the time domain, while another time-scale was used to model the motion of the sections of the boat, i.e., the sectional motions of the boat were modeled through a qusie-steady approach. The sectional forces were found using added mass forces. The model gave

response-dependent added mass forces and exciting forces. It was seen that it can simulate the motion of vessels with a high level of accuracy. The model is also known as the 2D + t method.

The application of Zarnick's model was later extended to other planing motions, such as steady performance and asymmetric/drift motions, where the model was expected to be consistent with real physics to a higher level (Xu et al., 1999; Sebastiani et al., 2008; Ghadimi et al., 2016; Dashtimanesh et al., 2019). The reason was that Zarnick's model assumes that sectional forces emerge from the added mass forces, and the frequency of fluid motion around the section is infinite. The model has been seen to be used for modeling of the maneuvering motion of planing hulls, and acceptable performance of the model is reported, while its accuracy is still required to be modified (Tavakoli and Dashtimanesh, 2019).

In the recent year, the 2D + t method is used to simulate steady performance of the double stepped planing hulls (Niazmand Bilandi et al., 2020). This model is developed by assuming that the water separation from step follows the transom wave theories. The general idea comes from the work of Savitsky and Morabito (2010), who formulated the transom wave in the lee of the vessel, aiming to provide a non-sophisticated formulation for performance prediction of stepped planing hulls. Niazmand Bilandi et al. (2020) used this idea by simplifying it. They assumed that the transom wave has a linear shape as the water flowing toward the lifting surface behind the step travels a relatively small distance. In such a condition, the steep waves cannot be developed and a linear shape can be assumed for the water flow, separated from the step. It has been observed that it has a great level of accuracy. But, no mathematical model has been developed for the unsteady motion of double-stepped hulls, subjected to water waves, while there is a pressing need to simulate seakeeping of these hulls, as explained earlier.

Meanwhile, the Computational Fluid Dynamics, CFD, has been applied for simulation of seakeeping of ships and boats in the last two decades. It has been reported that CFD models can predict the response of the ships/boats exposed to water waves with reliable accuracy. CFD models solve turbulent viscous flow around ships/boats, allowing us to model high-order phenomena, such as turbulent dissipation, emerging during the mutual interaction between water waves and ships (e.g. in Huang et al., 2020). Of course, such a phenomenon cannot be easily modeled through mathematical modeling as many simplifications occur when these models are developed. While CFD models are very popular and accurate, they are time-consuming. They are not recommended to be used in the case a boat/ship has not been designed. They are better to be utilized in the last stages of the design of a ship. The comparison between mathematical and CFD models can let us know how their results can differ.

For the case of double-stepped planing hulls, experimental tests, highlighting their seakeeping in head sea condition, lacks at the current stage. Therefore, CFD models can be used to model their problem, and their results can be compared against those of 2D + t model. Of course, such a comparison cannot be considered as a validation study, but it can provide important messages regarding the performance of both models. Low differences between their results can show that they both are performing well enough to be used for improving our understanding of the problem.

The present paper aims to fill the gap in modeling of planing motion of stepped surfaces in water waves by offering two models, including a nonlinear mathematical model and a CFD one. The mathematical model is established by extending the Zarnick's method for double-stepped planing hulls. The CFD model is developed based on a Finite Volume Method, and an overset technique, which is applied to model the rigid body motion. The 2D + t model and an example of the CFD set-up, that can be used to simulate vertical motions of a double-stepped planing hull, were previously presented in a conference proceeding (Niazmand Bilandi et al., 2019). But, the details of the 2D + t model and the way that it is developed were not presented. In addition, the presented results

were restricted to one forcing condition, and one design. In the present research, the 2D + t model is explained in detail. Moreover, a wide range of results is presented, which provides us with an understanding regarding the effects of step on the vertical motion of double-stepped planing hulls, advancing in waves.

The present paper is outlined as follows: The mathematical model and CFD model are respectively presented in Sections 2 and 3. The validity of models in replication of the steady performance of the vessel in calm water is evaluated in Section 4. A comparison between the results of CFD and the mathematical model is presented in Section 5. Results of the paper are presented in Section 6, and it is shown how a double-stepped design can affect the dynamic response of a planing vessel in waves. Section 7 includes the concluding remarks.

2. The 2DOF mathematical model

2.1. Formulating the dynamic motion

Consider a hard-chine vessel with two bottom steps operates at planing regime, which is identified as $Fr_B > 2.0$. Here $Fr_B = u/(gB)^{-1}$, and represents beam Froude Number. u is the speed of the vessel, B is its beam, and g is the gravity acceleration. The water surface, the interface between water and air, may have elevation, i.e., water waves can exist.

Assume that water waves are monochromatic, unidirectional, and propagate toward the boat with an encounter angle of π. The angle between wave direction and boat speed is defined as the encounter angle. The boat is supposed to perform in an open sea condition, i.e., the spatial domain is not bounded at all. The water depth is assumed to be deep enough to satisfy a deep-water wave condition.

Surface waves are assumed to be linear and no wave breaking and modulation instability occur, i.e., linear wave theory, also known as Airy Theory, governs the surface waves. The water surface elevation, at any point, therefore, obeys

$$\zeta = a\cos(\kappa X - \omega t + \varepsilon). \tag{1}$$

In Eq. (1) a is the amplitude of wave, $\omega = 2\pi/T$ is the wave angular frequency, $\kappa = 2\pi/\lambda$ is the wave number, and ε is the phase shift of the wave. T is the wave period and λ is the wave number. κ is found using the deep-water dispersion equation, given by

$$\kappa = g^{-1}\omega^2. \tag{2}$$

Heave and pitch motions are assumed to be induced by water waves. Sway and yaw motions are assumed to be scant and are neglected. No roll motion is also allowed. Assuming that thrust force passes through the CG of the vessel, motion equations can be formulated as

$$m.\ddot{\mathcal{Z}} = F_z + W,$$
$$I\ddot{\theta} = M_\theta. \tag{3}$$

In Eq. (3) m and I are mass and pitch inertia of the vessel. F_z and M_θ respectively refer to vertical force and pitching moment generated by fluid flow. W is the weight force.

Eq. (3) shows the relative motion of a body frame attached to CG of the vessel, with respect to a hydrodynamic frame which advances with the vessel, and never has any oscillations. Both frames are right-handed and are positive downward. Both of these coordinate systems are shown in Fig. 2.

2.2. Model development

The body of a double-stepped planing hull consists of three lifting surface, including front, corresponding to $x \in [x_{s_1}, x_b]$, middle, $x \in [x_{s_2}, x_{s_1}]$, and rear, $x \in [x_T, x_{s_2}]$, surfaces. x_{s_1} and x_{s_2} respectively refer to the longitudinal positions of the front and rear steps in body frame. x_b and x_T refer to the longitudinal positions of the bow and transom in the aforementioned frame.

The length of each planing surfaces is found as

$$L_1 = x_b - x_{s_1}, \tag{4}$$

$$L_2 = x_{s_1} - x_{s_2}, \tag{5}$$

$$L_3 = x_{s_2} - x_T. \tag{6}$$

It is hypothesized that heave force and the pitching moment acting on the body of the double-stepped planing hull can be divided into three components, each of which separately acts on one of aforementioned lifting surfaces. Therefore the fluid vertical and angular forces are rewritten as

$$F_z = \sum_{i=1}^{3} f_{z_i},$$
$$M_\theta = \sum_{i=1}^{3} m_{\theta_i}. \tag{7}$$

In Eq. (7), f_{z_i} and m_{θ_i} respectively denote the heaving and pitching forces acting on a single planing surface.

It is hypothesized that water, flowing toward the surface behind each step, tends to travel linearly. The schematic of this assumption is drawn in Fig. 3. This assumption is known as the linear transom wave theory and has been observed to be relatively true for the case of double-stepped planing hulls when water partiality washes the planing surfaces (Dashtimanesh et al., 2018). Following this theory, the ventilation area corresponding to each planing surface, identified with i, may be written as

$$L_{V_i} = \frac{h_{s_{i-1}}}{\tan(\theta + \theta_i)} \qquad \forall i \in \{2, 3\} \tag{8}$$

Here, $h_{s_{i-1}}$ is the height of each step, θ is the pitch angle and θ_i is the local pitch angle.

Note that the basis of assumption made to compute the wetted area behind step can be found in the work of Savitsky and Morabito (2010). They hypothesized that the profile of the water surface behind a step is similar to that of a transom wave. They performed a series of experimental tests and reported non-sophisticated equations to compute the
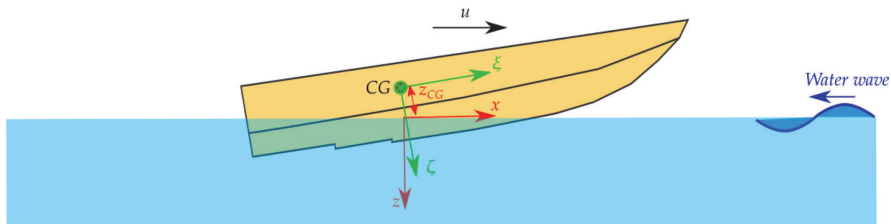
Fig. 2. Pictograph of a double stepped planing vessel exposed to monochromatic waves. The vessel advances with speed of u, corresponding to $Fr_B = u/(gB)^{-1}$. Water waves propagate toward the vessel, representing a head sea forcing condition. Hydrodynamic forces, generated by the fluid flow, are formulated in a hydrodynamic-frame, shown by $\xi\eta\zeta$. An earthly-framed coordinate system, shown by xyz, is used to derive the equations of the motion.
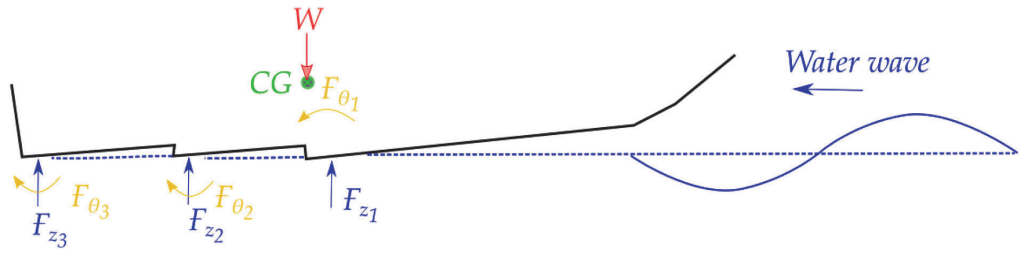
Fig. 3. The schematic of linear wake profile assumption used for establishment of the 2D + t model.
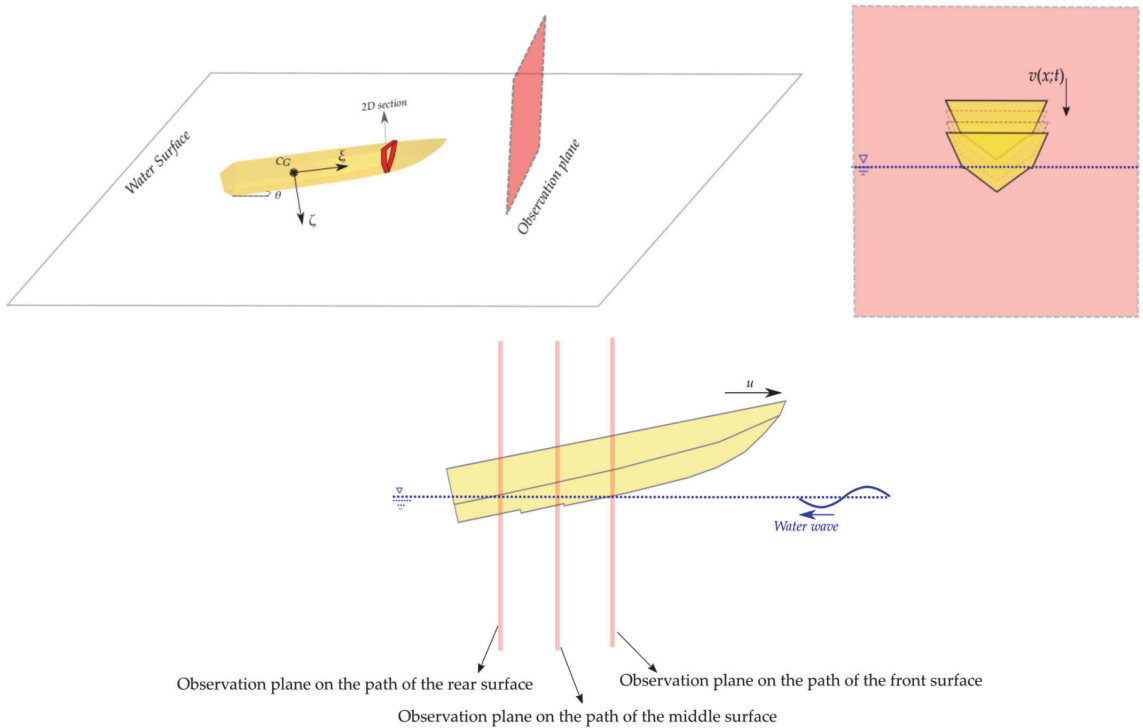
Fig. 4. The concept of 2D + t theory for a planing hull. The upper panel shows a planing hull passing through a fixed plane, marked with red color. As it can be seen from a front view (left), the three-dimensionless motion can be represented by a water entry problem. The lower panel shows how the method can also be used for a double-stepped planing hull. Three observation plans are used, and then three water entry problem emerge. (For interpretation of the references to color in this figure legend, the reader is referred to the Web version of this article.)

water surface profile. In the present research, their hypothesis is simplified, and the transom wave is assumed to have a linear shape. The reason for such a simplification is that the wetted surface of each planing surface is small, and thus the developed transom wave is not steep.

2.2.1. Sectional forces

The sectional forces of the vessel are found using the 2D + t model. A water entry problem is used to replicate the planing motion at any time-step. To understand this method, it is required to view the problem from an observation plane locating in the path of the vessel as shown in upper panel of Fig. 4. This theory can also be used for the double-stepped hulls by assuming that three water entry problems occur as displayed in lower panel of Fig. 4.

Consider that a wedge section enters water. Hydrodynamic force acting on a section is assumed to be generated by momentum variation

and cross drag flow (Payne, 1995), which is given by

$$\mathscr{F} = -D_t(a\,\mathscr{V}) + C_{CD}\left(\rho c\,\mathscr{V}^2\right). \tag{9}$$

Here, D_t is the material derivative, a is the added mass of the section, $\mathscr{V}$ is the relative vertical speed of the section, C_{CD} is the cross flow drag coefficient, c is half-wetted beam for of each section, and ρ is the fluid density. The first term of Eq. (9), found using a Lagrangian approach, can be expanded as

$$D_t(a\,\mathscr{V}) = a\,\dot{\mathscr{V}} + \mathscr{V}\,\dot{a} - \mathscr{U}\partial_x\,(a\,\mathscr{V}). \tag{10}$$

Here, $\mathscr{U}$ is the relative longitudinal speed of a section. The method for computation of added mass and watted length of section is explained in Appendix A.

Overall, the above equations show that sectional forces are found using momentum variation, which depends on the instant added mass of the section. The added mass of the section is computed by utilizing the solution of a water-entry problem. *i.e.*, a radiation problem with an infinite-frequency, known as Wagner Solution, is applied and then added mass of the section is formulated. Such a hypothesis might not fit with the real physics. When a vessel oscillates in any direction, fluid motion around any section of it is likely to oscillate with the same frequency. But such an inconsistency has been found not to be a big worry as the water entry problem has been reported to have proper accuracy in computation of the sectional forces of a boat advancing in waves.

The relative local speeds of any section of the vessel are computed by using the heave speed of the boat ($\dot{z}$), pitch rate ($\dot{\theta}$), vertical velocity of the free surface, and boat speed (u), as

$$\mathscr{V} = (\dot{z} - w_z)\cos(\theta + \theta_j) + u\sin(\theta + \theta_j) - \dot{\theta}\xi, \tag{11}$$

$$\mathscr{U} = u\cos(\theta + \theta_j) - (\dot{z} - w_z)\sin(\theta + \theta_j). \tag{12}$$

Here, w_z is the vertical speed of the fluid motion caused by the water waves. To find more accurate sectional force, it is also assumed that gravity can generate buoyant forces, which can be calculated by

$$f^{2D}_{\mathscr{H}\mathscr{S}} = 0.5(2\rho g c h_{\mathscr{W}}(x)). \tag{13}$$

Here the product of c and $h_{\mathscr{W}}(x)$ gives the sectional wetted area. Here, $h_{\mathscr{W}}(x)$ is the sectional water depth, that varies locally. *g* is the gravity acceleration constant. This wetted area includes the additional area caused by water-pile up, known as Wagner Condition. Sectional forces are used to derive equations for heave force and pitch moment later.

2.2.2. Hydrodynamic forces acting on the body

Hydrodynamic force acting on a single planing surface is computed separately. To do so, it is needed to integrate forces of sections over the length of the surface. Sectional force contains, momentum variation, cross drag and buoyant forces as shown earlier. Equations (14) gives the integration of sectional forces in heave direction as follows

$$f_{z_i} = \left(\int_{L_i} \mathscr{T}_i(x) \left(-D_t(a\mathscr{V}) + C_{CD}(\rho c\mathscr{V}^2) \right) dx \right) \cos(\theta + \theta_j)$$
$$+ \int_{L_i} \mathscr{T}_i(x) f^{2D}_{\mathscr{H}\mathscr{S}} dx \quad \forall i \in \{1,2,3\} \tag{14}$$

In this equation, $\mathscr{T}_i$ is the transom modification function. The upper and lower limits of integration have been presented in Eqs. (4) through (6). Note that the direction of buoyant force is different from that of the sectional forces computed by (13). The transom and steps, are all, hypothesized to modify the sectional forces, i.e., the Kutta condition governs at steps and transom, and thus forces should converge zero at related sections. A transom modification function can be implemented to serve this aim mathematically. This function will be presented later.

By computing the moment of sectional forces with respect to centre of gravity, the pitching moment of each single surface is formulated as

$$m_{\theta_i} = \int_{L_i} \left(\mathscr{T}_i(x) \left(-D_t(a\mathscr{V}) + C_{CD}(\rho c\mathscr{V}^2) \right) \right) x dx + \int_{L_i} \mathscr{T}_i(x) f^{2D}_{\mathscr{H}\mathscr{S}} x dx \quad \forall i$$
$$\in \{1,2,3\} \tag{15}$$

The effects of transom on sectional forces are activated by using a tangent hyperbolic function. This function gives a value of zero as $x \to x_{\mathscr{T}_i}$, and also converges 1.0 as $x \to \infty$. Such a behaviour agrees with the real physics. The aforementioned function was proposed by Garme (2005), and is given by

$$\mathscr{T}_i(x) = \tanh\left(\frac{2.5}{\mathscr{C}}(x - x_{\mathscr{T}_i}) \right) \quad \forall i \in \{1,2,3\} \tag{16}$$

Here $\mathscr{C}$ is a coefficient that determines the location at which transom effects emerge. This coefficient is a function of beam Froude Number and approaches ∞ as Fr$\to\infty$. $\mathscr{C}$ is recommended to be found by (Garme, 2005)

$$\mathscr{C} = 0.34 B \mathrm{Fr}_B \quad \forall i \in \{1,2,3\} \tag{17}$$

For more technical information regarding Eqs. (16) and (17) and the way they have been formulated, please refer to Garme (2005). The effects of transom function on sectional forces appear at different stations, that are given by

$$x_{\mathscr{T}_i} = x_{s_i} \quad \forall i \in \{1,2\} \tag{18}$$

$$x_{\mathscr{T}_i} = x_T \quad \forall i \in \{3\} \tag{19}$$

The equations for three-dimensional forces can be developed by summing the sectional forces. Integration of the 2D forces over the entire length of each planing surface gives the three-dimensional force. Thus, the three-dimensional heave force of each lifting surface is formulated as

$$f_{z_i} = \left(-\left(\mathscr{M}_i \cos(\theta + \theta_i) \right) \ddot{z} + \mathscr{M}_i^\bullet \ddot{\theta} + \mathscr{M}_i^{\bullet\bullet} \dot{\theta} \left(\dot{z}\cos(\theta + \theta_i) - u\cos(\theta + \theta_j) \right) \right.$$
$$+ f^{①}_{z_i} + f^{②}_{z_i} + f^{③}_{z_i} + f^{④}_{z_i} + f^{⑤}_{z_i} + f^{⑥}_{z_i} + f^{⑦}_{z_i} \right) \cos(\theta + \theta_i)$$
$$+ \left(\int_{L_i} \mathscr{T}_i(x) f_{\mathscr{H}\mathscr{S}} \right) dx \quad \forall i \in \{1,2,3\} \tag{20}$$

By using the same approach, the pitching moment, generated by the water flow, is formulated as

$$m_{\theta_i} = \left(\mathscr{M}_i^\bullet \cos(\theta + \theta_i) \right) \ddot{z} - \mathscr{M}_i^{\bullet\bullet} \ddot{\theta} + \mathscr{M}_i^{\bullet\bullet} \dot{\theta} \left(\dot{z}\sin(\theta + \theta_i) - u\cos(\theta + \theta_j) \right)$$
$$+ m^{①}_{\theta_i} + m^{②}_{\theta_i} + m^{③}_{\theta_i} + m^{④}_{\theta_i} + m^{⑤}_{\theta_i} + m^{⑥}_{\theta_i} + m^{⑦}_{\theta_i}$$
$$+ \left(\int_{L_i} \mathscr{T}_i(x) f^{2D}_{\mathscr{H}\mathscr{S}} \right) x dx \quad \forall i \in \{1,2,3\} \tag{21}$$

Note that the force and moment, presented in equations (20) and (21), are three-dimensional and formulated by the expansion of the two-dimensional forces. Each of the above equations contains several terms. The first three terms indicate the added mass contribution in the body frame. These terms are a result of integration of sectional added mass terms are shown with $\mathscr{M}_i$.

The fourth terms in Equations (20) and (21), are products of added mass force and velocities, which is an absolute nonlinear term. Some terms are shown by superscripts bounded in a circle. These terms refer to the forces/moments generated by integration of the added mass rate along with cross drag force.

Formulations for these terms are all presented in Appendix B. Note that, terms that are indicated with ①-④ are wave forces, and others refer to response-dependent damping forces/moments. Last terms in both equations are the buoyant forces/moments. These terms represent the stiffness mechanism contribution to total forces/moments acting on the vessel advancing in waves. Note that it was previously described that forces are in vertical direction.

Added mass forces/moments, that are shown with $\mathscr{M}$ are given by

$$\mathscr{M}_i = \int_{L_i} \mathscr{T}_i(x) a \, dx \quad \forall i \in \{1,2,3\} \tag{22}$$

$$\mathscr{M}_i^\bullet = \int_{L_i} \mathscr{T}_i(x) a \, x dx \quad \forall i \in \{1,2,3\} \tag{23}$$

$$\mathscr{M}_i^{\bullet\bullet} = \int\limits_{L_i} \mathscr{T}_i(x)a\,x^2 dx \qquad \forall i \in \{1,2,3\} \tag{24}$$

2.2.3. Motion equations

The movement of the boat is formulated using the rigid-body law as explained earlier. Forces are substituted in the motion equation, and give a set of differential equations as

$$(\mathrm{m}+\mathscr{A}_{zz})\ddot{z}+\mathscr{A}_{z\theta}\ddot{\theta}=F_z^{\star}+W \tag{25}$$

$$\mathscr{A}_{\theta z}\ddot{z}+(I+\mathscr{A}_{\theta\theta})\ddot{\theta}=M_\theta^{\star}$$

Here, the summation of $\mathscr{M}$ terms are defined as the added mass coefficients, and are extracted from the fluid forces, and transferred to the left hand side of both equations, which helps us to simulate the problem over the time domain. Added mass terms are shown with $\mathscr{A}_{zz}$, $\mathscr{A}_{z\theta}$, $\mathscr{A}_{\theta z}$ and $\mathscr{A}_{\theta\theta}$. Equation (25) governs the motion of the vessel advancing in waves and is needed to be solved over the time.

The rest of the forces are kept in the right hand side of the equations and are formulated as

$$F_z^{\star} = \sum_{i=1}^3 f_{z_i} - \mathscr{A}_{zz}\ddot{z} - \mathscr{A}_{z\theta}\ddot{\theta}, \tag{26}$$

$$M_\theta^{\star} = \sum_{i=1}^3 m_{\theta_i} - \mathscr{A}_{\theta z}\ddot{z} - \mathscr{A}_{\theta\theta}\ddot{\theta}.$$

Added mass coefficients are given by

$$\mathscr{A}_{zz} = \sum_{i=1}^3 \mathscr{M}_i \cos^2(\theta+\theta_i) \tag{27}$$

$$\mathscr{A}_{z\theta} = -\sum_{i=1}^3 \mathscr{M}_i^{\bullet} \cos\ (\theta+\theta_i), \tag{28}$$

$$\mathscr{A}_{\theta z} = -\sum_{i=1}^3 \mathscr{M}_i^{\bullet} \cos\ (\theta+\theta_i) \tag{29}$$

$$\mathscr{A}_{\theta\theta} = \sum_{i=1}^3 \mathscr{M}_i^{\bullet\bullet} \tag{30}$$

Equations (28 and 29) present $\mathscr{A}_{z\theta}$ and $\mathscr{A}_{\theta z}$. The instant values of these two added mass terms are equal. It important to note that the added mass terms are influenced by the response of the vessel. Simply stated, they are time-dependent and are different from the classical added mass coefficients formulated in linear theory. Moreover, it should be noted that the force and moment, identified with a * superscript contain damping, restoring and non-linear mechanisms. The formulation developed for added mass coefficients, and forces, show that the developed model treats the problem by considering non-linearities of the fluid motion. Under such an assumption, the problem is not solved in the frequency domain. Instead, it is solved over the time, which will be explained.

The motion equation of double-stepped planing hull can be is re-written in a vector form as

$$\mathbf{M}\ddot{\mathscr{X}} = \mathbf{F}^{\star}, \tag{31}$$

where, $\mathbf{M}$ is the mass Matrix, and $\mathscr{X} = [z(\mathrm{t})\ \theta(\mathrm{t})]$ is the displacement vector. $\mathbf{F}^*$ is the force vector. The mass matrix and force vector are defined as

$$\mathbf{M} = \begin{bmatrix} \mathrm{m}+\mathscr{A}_{zz} & \mathscr{A}_{z\theta} \\ \mathscr{A}_{\theta z} & \mathrm{I}+\mathscr{A}_{\theta\theta} \end{bmatrix}, \tag{32}$$

At any time interval, the acceleration vector is found as

$$\ddot{\mathscr{X}} = \mathbf{M}^{-1}\mathbf{F}^{\star}, \tag{33}$$

Using acceleration vector, velocity vector, $\dot{\mathscr{X}}$, and displacement vector, $\mathscr{X}$ are computed as

$$\dot{\mathscr{X}} = \int \ddot{\mathscr{X}}\mathrm{dt}, \tag{34}$$

$$\mathscr{X} = \int \dot{\mathscr{X}}\mathrm{dt}. \tag{35}$$

in each time step. There will be a phase lag between waves and the motion of the vessel. But, the phase lag of the vessel is not of interest in the present research, and we will not present the related data.

In the case that the wave height is set to be zero, the steady motion of the vessel is replicated. The vessel reaches the dynamic equilibrium. In this condition, the vertical force, generated by fluid, equals the weight force. In addition, the pitching moment is zero as the center of pressure settles at CG.

2.2.4. Drag forces

The drag force is assumed not to have any contribution in vertical motions of the vessel. It is hypothesized that this force is only generated by water flow and air drag is assumed to be nil. Three different components are assumed to cause the drag acting on the bottom of the vessel, as

$$\mathscr{D} = \mathscr{D}_f + \mathscr{D}_p + \mathscr{D}_s, \tag{36}$$

Here $\mathscr{D}_f$, is the frictional drag that is generated by the shear stresses near the wall of the vessel. $\mathscr{D}_p$ is the drag force that is induced by the hydrodynamic pressure. Note that for the case of a planing surface, pressure distribution in longitudinal direction is not symmetric at all, and it is expected that pressure generates a large amount of force. $\mathscr{D}_s$ is the spray drag, that is common to occur in the bow of planing surfaces, as an amount of water jet flows toward the bow of the vessel, leading to generation of spray.

The idea used for computation of hydrodynamic forces, is also used to compute the drag forces, i.e, drag force acting on each planing surface is computed separately and then the total drag forces are computed. Drag forces are found by

$$\mathscr{D}_f = \sum_{i=1}^3 d_{f_i}, \tag{37}$$

$$\mathscr{D}_p = \sum_{i=1}^3 d_{p_i} \tag{38}$$

$$\mathscr{D}_s = \sum_{i=1}^3 d_{s_i}. \tag{39}$$

The frictions drag force of each planing surface, denoted with d, is computed by using the ITTC recommendation (ITTC, 1978) as

$$d_{f_i} = 0.5\left(C_f + \delta C_f\right)\rho u^2 \mathscr{S}_i, \tag{40}$$

where C_f is the frictional drag coefficients and δC_f is the additional friction coefficient due to roughness of the surface. $\mathscr{S}_i$ is the area washed by water. Wetted area of each planing surface is computed by

$$\mathscr{S}_i = \frac{2b}{\cos(\beta+\beta_j)}\ . \tag{41}$$

The frictional drag coefficient is found by

$$C_f = 0.075(\log\mathrm{R}_\mathrm{E}-2)^{-2} \tag{42}$$

where R_E is the Reynolds number. Reynolds number of the whole planing vessel is used for each planing surface as

$$R_E = \nu^{-1} u L_K^\oplus \tag{43}$$

Here, ν is the kinematic viscosity of water. $L_K^\oplus$ is the total summation of the keel length washed by water and the ventilation areas, given by

$$L_K^\oplus = \sum_{i=1}^{3} L_{K_i} + \sum_{i=2}^{3} L_{V_i}, \tag{44}$$

Keel wetted length of each surface can be computed by

$$L_{K_i} = \int_{\bar{x}_{k_i}}^{x_{\mathcal{T}_i}} dx. \tag{45}$$

The drag force generated by pressure is found as

$$d_{p_i} = \left(\int_{L_i} \mathcal{T}_i(x) \left(-D_i(a \mathcal{V}) + C_{CD}(0.5\rho c \mathcal{V}^2) \right) dx \right) \sin(\theta + \theta_i) \quad \forall i$$
$$\in \{1, 2, 3\} \tag{46}$$

The spray drag acting on each planing surface is computed by

$$d_{s_i} = f_i^\oplus \cos(\gamma_i) \qquad \forall i \in \{1, 2, 3\} \tag{47}$$

where $f_i^\oplus$ is given by

$$f_i^\oplus = \frac{C_f (0.5\rho \mathcal{V}^2) B^2}{4 \sin(\gamma_i) \cos(\beta + \beta_i)} \qquad \forall i \in \{1, 2, 3\}, \tag{48}$$

γ_i is the angle between the whisker spray edge and the keel line in waterplane area, given by

$$\gamma_i = \tan^{-1} \left(\frac{\pi \tan(\theta + \theta_i)}{2 \tan(\beta + \beta_i)} \right) \qquad \forall i \in \{1, 2, 3\} \tag{49}$$

Here, β_i is the local effective deadrise angle. The formulations presented for computation of the spray drag are all taken from Savitsky et al. (2007).

3. The numerical model

Consider a three-dimensional spatial domain with a Cartesian right-handed coordinate system of $OXYZ$. The vessel is assumed to be exposed to waves in this domain, which is spanned within $X_O < X < X_I$, $Y_L < Y < Y_R$ and $-H < Z < H_a$. A schematic showing this domain and the vessel is presented in Fig. 5. The velocity field in the whole domain is presented by $\mathbf{v}(\mathbf{x}; t) = [v_x(\mathbf{x}; t) \; v_y(\mathbf{x}; t) \; v_z(\mathbf{x}; t)]^T$ which may vary over the time.

Consider that fluid around the vessel, which can contain the mixture

of water and air, is viscous, and also incompressible. Continuity of the mass flow and momentum conservation hold the domain in this condition. Hence, Reynolds Averaged Navier-Stokes equations, RANS, govern the motion of fluid at any point in the fluid domain, as

$$\nabla \cdot \mathbf{v} = 0, \tag{50}$$

$$\partial_t(\rho \mathbf{v}) + \nabla \cdot (\rho \mathbf{v} \mathbf{v}) - \nabla \cdot (\mu \nabla \mathbf{v}) = \nabla p - \mathbf{f_b} + \nabla \mathbf{v} \cdot \nabla \mu \qquad \text{in } Y/Y_B \tag{51}$$

Here, ρ is the density of the mixture of the air and water. p in the above equations refer to the pressure. Also, μ is the dynamic viscosity of the air-water mixture. The fluid flow is assumed to be turbulent, and turbulent viscosity is expected to affect the shear stresses, and thus the velocity field. A k-ε model is used for this aim. Details of the turbulent model are explained in Appendix C.

The two-phase flow is modeled using a volume fraction method. A fraction, shown by γ, is defined, which represents the fraction of water over air at any point. A conservation equation governs on this fraction in the whole domain as

$$\partial_t(\gamma) + \nabla \cdot (\rho \mathbf{v} \gamma) = 0 \qquad \text{in } Y/Y_B \tag{52}$$

Viscosity and density of the fluid in every point of the domain are found locally as

$$\mu = (1 - \gamma)\mu_{\text{air}} + \mu_{\text{water}} \tag{53}$$

$$\rho = (1 - \gamma)\rho_{\text{air}} + \rho_{\text{water}} \tag{54}$$

A numerical wave maker is prescribed at $X = X_F$, that generates surface waves as

$$\zeta(X_F, t) = a \exp(-i\omega t), \tag{55}$$

which propagate toward the vessel, where $i = \sqrt{-1}$. Water waves are expected to follow the linear water wave theory as they are set to have gentle steepness. Waves propagate toward the left end of domain and are damped at Λ_O and Λ_L in Λ_L order to stop any reflection of wave energy from boundaries of the domain. This forcing conditions replicates a head sea wave condition, which is modeled in the present research.

Water and air are prescribed to flow toward the boat from Λ_I with a velocity of $-u$. Also, flow with velocity of $-u$ is also set on Λ_L, which provides and open water condition around the vessel. The zero-gradient pressure and zero-gradient velocity govern on every point of Λ_O, which matches with an outlet boundary condition. On the walls of the boat a no-slip condition is satisfied, i.e., $u|_{\mathbf{x} \in \Lambda_B} = d_t \Lambda_B$. As the vessel has no yaw and sway motion, and also is not heeled, the fluid motion is expected to be symmetry with respect to the XZ plane. Therefore, a symmetry
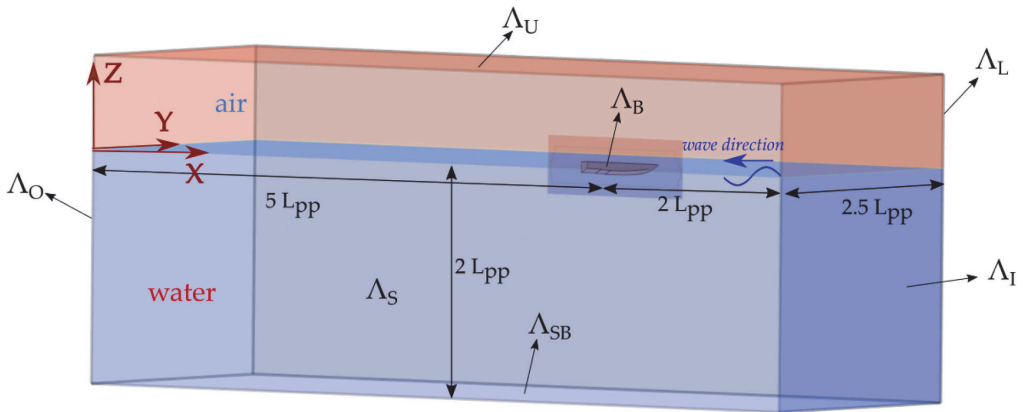
Fig. 5. Numerical domain used for replication of the dynamic response of a double-stepped planing surface in water waves.

Table 1
Summary of the boundary conditions applied to the numerical domain.

Boundary	Symbol	Type	Wave damping
Hull surface	Λ_B	No-slip wall	-
Inlet	Λ_I	Velocity inlet	-
Outlet	Λ_O	Pressure outlet	✓
Top	Λ_U	Velocity inlet	-
Bottom	Λ_{SB}	Velocity inlet	-
Left-patch	Λ_L	Velocity inlet	✓
Symmetry	Λ_S	Symmetry plane	-

boundary, shown by Λ_S, is defined, which accelerates the simulations and reduces the storage of data as well.

The upper patch of the domain, Λ_U, is set to act as an inlet with a constant velocity, being equal to that of the vessel. This provides a perfect open-sea condition. All the aforementioned boundaries conditions are summarized in Table 1.

Motion equations can be solved using rigid body equations over the time. The force, F, and moment, M, vectors acting on the planing body are computed as

$$F = \iint\limits_{\Lambda_B} (p + \sigma).n d\Lambda_B \tag{56}$$

$$M = \iint\limits_{\Lambda_B} (p + \sigma).n \times r \, d\Lambda_B \tag{57}$$

Here, σ is the normal stress tensor, n is the normal vector and r is the distance vector. The solution of a rigid body dynamic equations, provides the values of instant heave and pitch of the solid body over the time. All the presented equations, including the fluid and rigid body motions, are solved by using a CFD code, StarCCM+ (STAR-CCM+, 2011). An implicit approach is used for decomposing the unsteady terms. The temporal terms are discretized by applying a 2nd order method. The convection terms are decomposed by embarking a 2nd order method. The gradient discretization is performed through Hybrid Least Squares (LSQ) approach. The fluid equations are numerically solved by using a SIMPLE, (Semi-Implicit Method for Pressure Linked Equations) algorithm. The Algebraic System of equations is numerically solved by applying an AGM (Algebraic Multi-Grid) method. The two-phase flow is solved by using the VOF method as explained earlier. The convection of the VOF is modeled by using an HRIC (High-Resolution Interface Capturing) method. The dynamic response of the rigid body is solved by employing a DFBI (Dynamic Fluid Body Interaction) planar motion carriage framework. The mesh motion is treated with an overset technique. The rigid body is placed in a region which moves with the planing vessel. Therefore, no re-meshing or deformation of the cells occurs over time. An interpolation between the background region and the overset region is performed by utilizing a linear method.

The computation grid is generated by using the toolbox of the CFD code, StarCCM+ (STAR-CCM+, 2011), as well. The strategy for grid design is based on the previous numerical researches highlighting the wave-ship/wave-structure interaction. Examples can be found in Tezdogan et al. (2015), Mousaviraad et al. (2015) and Huang et al. (2019). Cells are set to be fine near the free surface and the hull surface, where
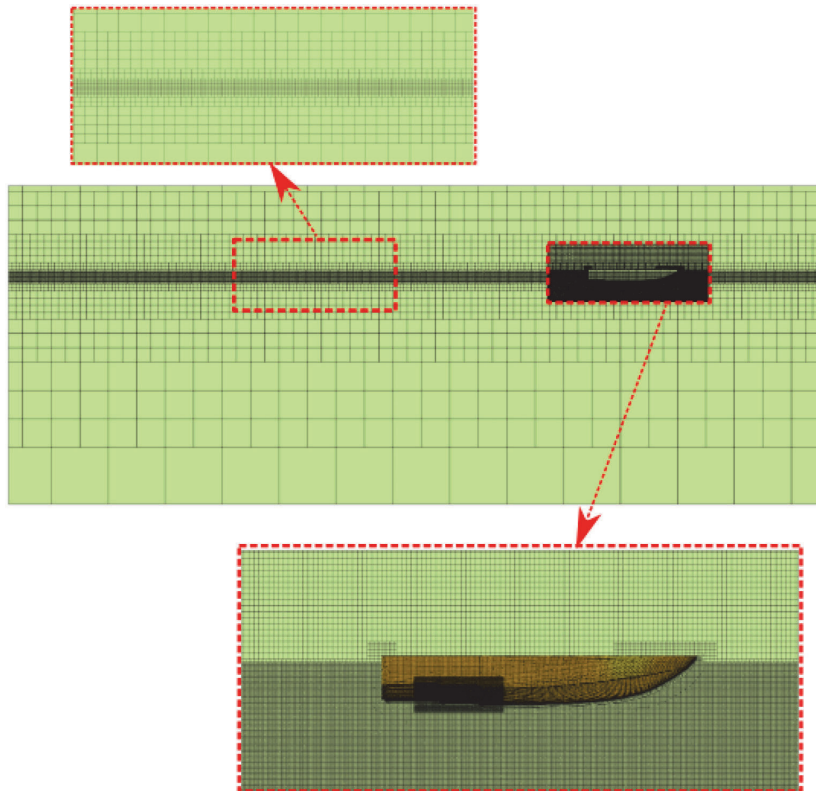
Fig. 6. Designed mesh for discretization of the spatial domain. The middle panel shows the entire domain. The upper and lower panels respectively show close-up views of the cells around the free surface and the vessel.

fluid is expected to be strongly turbulent and shear stresses should be computed with a high level of accuracy. Higher resolution is applied for the cells covering the wake of the vessel to ensure that the wake effects are captured and modeled properly. Since an overset method is used for dynamic simulations, cells are not deformable at all. A layout of the mesh used for the simulation of the problem is shown in Fig. 6. Please note that it is ensured that the wave height locates in about 20 cells. Different grids are generated using a mesh refinement ratio of $\sqrt{2}$. The summary of these grids is shown in Table 2. A mesh sensitive study is performed and it is found that G_3 can be used for numerical replication of the problem. The summary of the mesh sensitive study is presented in Appendix D. Also, the accuracy of the model in the generation of gravity waves is evaluated in Appendix E.

A personal computer, PC, equipped with a 3.1 GHz Intel 12-processors and 36 GB memory, is used to run simulations. Each simulation is run over 60,000-time steps. Every single simulation required nearly ~100 h on the machine.

4. Case conditions

Mathematical and numerical simulations are performed for two sets of planing models. These models are designed and presented in two of the previous research (Taunton et al., 2010; Lee et al., 2014) highlighting performance of stepped planing hulls. Effects of step and their location on the resistance and running attitude of planing hulls are evaluated and discussed in the related papers.

The first planing model set is designed at the University of Southampton by Taunton et al. (2010). Effects of two steps on the performance of a planing model were studied, and it was observed that two steps can highly decrease the resistance of the vessel. The stepless and double-stepped boats are named as models C and C2, respectively. Both vessels have similar body plans and are 2 m long, but one has two transverse steps, located at 0.158L and 0.31L. The mean deadrise angle of these vessels is 22.5°, which is the most common deadrise angle used for planing hulls performing in the real sea. Body plans of the models are shown in Fig. 7, and their dimensions, as well as other principal characteristics, are listed in Table 3.

Dynamic motions of models C and C2 are simulated in the head sea condition in the present research by applying both CFD and 2D + t models. A comparison between the obtained results can be very helpful in verifying the accuracy level of the 2D + t model. In addition, dynamic responses of model C and C2 are compared against each other. This can improve our understanding of the effects of steps on the movement of a planing craft in waves.

The second planing model set is designed in Virginia Tech in the early 2010s. The related hulls are developed to study the effects of step height on the performance of a double-stepped planing surface. Two models, including Case 4 and Case 6 are selected to be studied in the present research. The first mode, Case 4, has two steps with different heights of 0.007B and 0.021B. The second one, named Case 6, has two steps with similar heights of 0.014B.

A comparison between dynamic responses of cases 4 and 6 can increase our understanding of the influence of the step height on the dynamic response of a double-stepped planing craft in waves. Details of these two models are also presented in Table 3. The body lines corresponding to these models are shown in Fig. 7.

Table 2
Different grids used for modeling the problem.

Grid Name	Grid Number (Million)
G_1	2.010235
G_2	2.452366
G_3	2.778091
G_4	3.025686

The wave forcing condition used in the current research is also presented in Table 4. Waves cover a wide range of wavelengths, that can provide us with RAO plots. All waves are set to have gentle steepness. These forcing conditions are selected from the research of Begovic et al. (2014), who studied the unsteady motion of warped planing hulls.

5. Calm water performance tests: A validation study

Before performing a study on dynamic responses, calm water performance of the different hulls are computed using CFD and 2D + t methods, aiming to check their validity in computing hydrodynamic forces, and the equilibrium condition of the double-stepped vessels in calm water condition.

It is very important to note that there is no experimental work highlighting the dynamic of double-stepped craft advancing in planing regime. Therefore, we have first validated both CFD and 2D + t methods in modeling the calm water performance. Then, we have compared dynamic motion results computed by these two models against each other in the next Section.

The calm water experiments are performed by setting waves to have a steepness of zero in both models. Thus, the water surface will be in equilibrium condition. The boat has heave and pitch motions, both of which converge to steady values. Steady heave and pitch give dynamic trim angle and CG rise-up of the vessel.

5.1. Calm water tests for models C and C2

A sample of the calm water tests of model C and C2 at Froude Number of 4.77 is shown in Fig. 8. As seen initial values are set for heave and pitch, and then simulations are run over time up to the time they converge. Both CFD and 2D + t results are observed to provide results close to experimental data, dashed red line.

As mentioned earlier, steady planing simulations are run for every single Froude Numbers to model the calm-water operation of model C2, i.e, similar to what is presented in Fig. 8, the motion of the model C2 in a calm-water condition is run for all speeds and the data is found. The summary of simulations is presented in Fig. 9. Trim angle and resistance of the vessel are both presented. Trim angle of the vessel is expected to reach small values at high beam Froude Numbers, i.e, Fr > 4. Both CFD and 2D + t models are seen to follow this behavior. At small Froude Numbers, a peak in trim angle vs. Fr plot can be seen. CFD model can well capture this peak. But 2D + t method is not able to do so. There might be some reasons for this fact. The most probable one is the low speed of the vessel, which can affect the validity of the 2D + t model. At such a speed, for instance, the transom might not get fully dried, and the ventilation may not follow the linear wake theory. Also, the 2D + t theory is expected to have better accuracy at higher speed, where the solution of the infinity-frequency water penetration assumption used for commutation of sectional forces is likely to be consistent with the physics of the motion.

Computed values for the drag are also presented in Figure. The drag force becomes larger by the increase in Froude Number as it should. CFD and 2D + t model are seen to provide data with good accuracy. Both of these methods, however, can slightly over-predict the drag force at very high-speed. Note that, the CFD results have been previously presented in Niazmand Bilandi et al. (2020) as the same set-up was used. Here it should be clarified that the CFD setup, used in the present research is an extension of what was performed in Niazmand Bilandi et al. (2020). The key difference between the CFD set-up used here, and the one used in the previous research is the ability of the present set-up in modeling of the wave-induced simulations. The data presented in this sub-section is related to the calm-water performance operation, and thus the extended set-up, which is able to model the wave-induced motion of the vessel, is not run for this case. Therefore, the data of the previous research is plotted in Fig. 9. Please note that the CFD results that are presented in Section 6, and also Appendix F, are run with the CFD set-up designed in
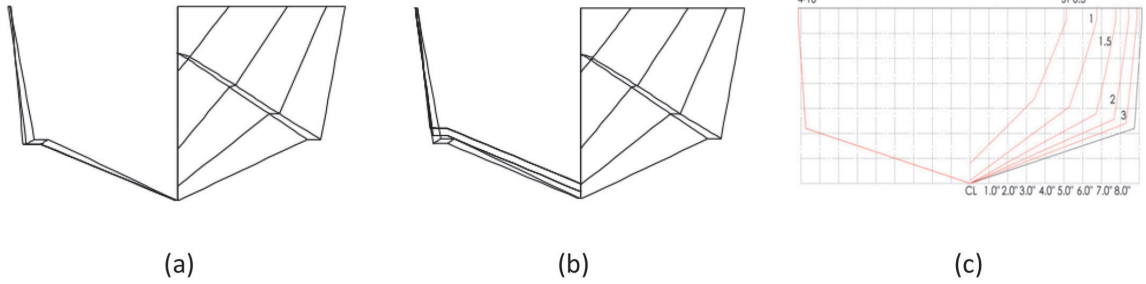
Fig. 7. Body plans of the cases studied in the present study. Model C (a) and model C2 (b), which are studied by Taunton et al. (2010). Model Lee et al. (2014) (c): Case 4 and Case 6.

Table 3
Main particulars of the studied planing models.

Parameter	Model C	Model C2	Case 4	Case 6
L/B	4.348	4.378	4.44	4.44
$\Delta/\rho g B^3$	0.255	0.255	0.451	0.451
β (°)	22.5	22.5	15	15
LCG (%L from transom)	33	33	40	40
L_{s_1}/L	NA	0.31	0.5	0.5
L_{s_2}/L	NA	0.158	0.25	0.25
Height of the front step/B	NA	0.0174	0.007	0.014
Height of the rear step/B	NA	0.0326	0.021	0.014

Table 4
Generated waves.

Wave Condition	ω (rad/s)	a(m)	κ (1/m)	$\epsilon = \kappa \times a$	λ/L
1	2.513	0.045	0.644	0.029	4.88
2	3.142	0.035	1.006	0.035	3.12
3	3.770	0.032	1.449	0.046	2.17
4	4.398	0.02	1.972	0.039	1.59
5	5.026	0.02	2.575	0.051	1.22
6	5.655	0.02	3.260	0.065	0.96

the present research. All of the results in Section 6 are related to wave-induced motions of a double-stepped planing hull.

5.2. Calm water tests for cases 4 and 6

Trim angle and drag force of cases 4 and 6 are also simulated by using the steady simulations of the 2D + t model. The CFD simulations of the wave-induced motions are only performed for model C2, the results of which are presented in Section 6. The reason is that CFD simulations

need a long time to be performed, which is nearly ~100 h. This time is much longer compared to the time the mathematical model is run. In addition, the set-up for the CFD model is designed to provide some additional data, which can be used for evaluating the behavior of the developed mathematical model. As it was mentioned earlier, there is no experimental data highlighting seakeeping of stepped planing hulls. Hence, CFD runs are performed to evaluate the differences between the results of CFD and 2D + t model in the computation of wave-induced motions of the vessel, which are present in Section 6. To sum, CFD simulations are not run for cases 4 and 6.

The computed values are compared against experimentally measured data. The computed trim angle is seen to be close to the experimental data, but it diverges from experiments at the highest speed. For the Case 6, this divergence is not significant. Overall, 2D + t method has seen to have reasonable accuracy level in modeling of the
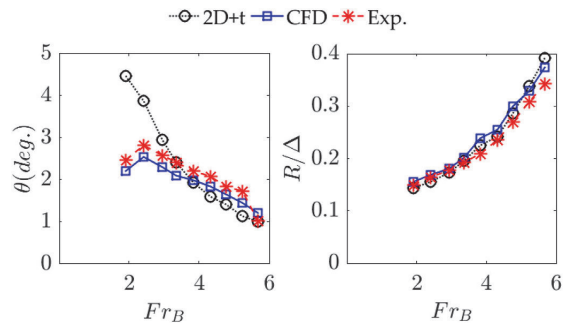
Fig. 9. Dynamic trim angle and resistance of model C2 at various Froude Numbers. CFD results are also presented in Niazmand Bilandi et al. (2020).
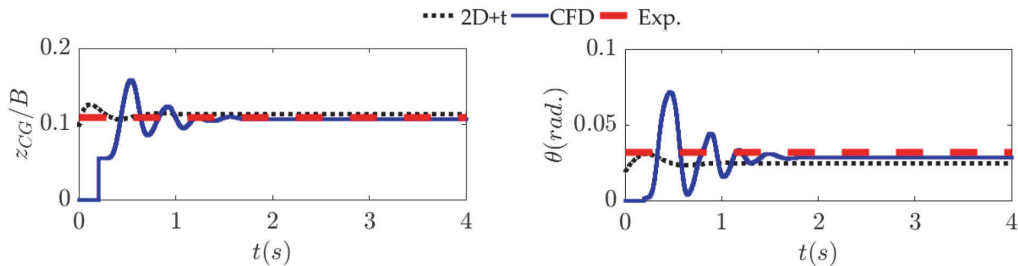
Fig. 8. Sample of the time history of heave and pitch motion of a double stepped planing hull advancing in still water at Froude Number of 4.77: Simulations performed by CFD and 2D + t method are plotted. The red dash line shows the value measured in towing tank test by Taunton et al. (2010). (For interpretation of the references to color in this figure legend, the reader is referred to the Web version of this article.)

steady performance of the Case 4 and Case 6.

The steady heave values, computed by both CFD and 2D + t models, are seen to follow each other. Some differences might be caused by the errors in the prediction of the trim angle. As it was seen, the trim angle was under-predicted. So, the vessel settles down at a lower height to establish the balance between the weight and fluid vertical force.

The related data is shown in Fig. 10. 2D + t model is again seen to follow the experimentally measured drag forces. There are still some over-predictions, which are seen to be greater for Case 6. To summarize, the 2D + t model is seen to provide a reasonable level of accuracy in computation of the performance of the cases 4 and 6. There are some errors, the source of which can be studied in future.

6. CFD vs. mathematical model

In the previous section, both models were used to reproduce the steady performance of double-stepped planing hulls advancing in still water. Runs were performed over the time to evaluate their accuracy level in prediction of the steady performance. The accuracy level of both methods were observed to be promising.

In this section, the results of CFD and 2D + t models in replication of unsteady planing motion are compared against each other. As mentioned earlier, no experimental based published paper/report highlighting regular wave effects on stepped planing surfaces is available. Therefore, it is attempted to compare the results obtained by CFD and 2D + t against each other to verify that both methods can work relatively accurate. But one point should be mentioned here. The present simulations are performed for the case of double-stepped planing hulls. The accuracy of the 2D + t model in simulation of wave-induced motions of stepless boats has been previously observed in a wide range of studies. In addition, another version of the present CFD model, which was designed to model wave-induced motions of a stepless boat, was previously tested by the authors. Motions of a hard-chine vessel, operating in regular waves, was modeled by CFD and 2D + t model. The results were presented in Tavakoli et al. (2020). Note that, the CFD set-up used in the related paper was different from the one used here. The difference was the mesh structure around the vessel, which was particular to a stepless boat. So, it can be concluded that an early version
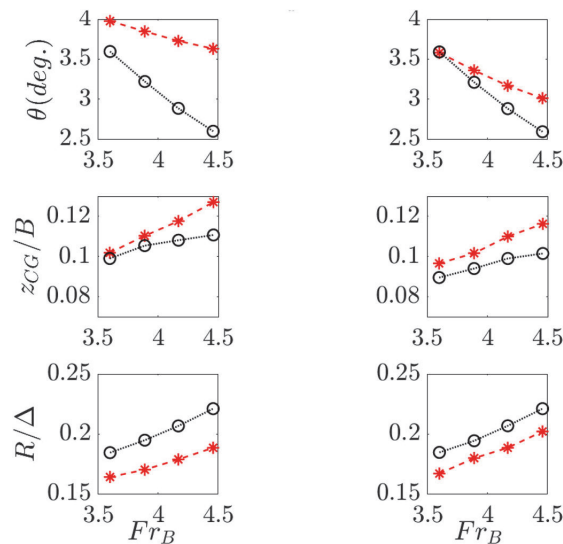
of the present CFD set-up, has been previously seen to compute the vertical motions of stepless boat, advancing in waves, with a fair level of accuracy.

Model C2 is tested in all forcing conditions at two beam Froude Numbers of 2.94 and 3.83. Heave and pitch response along vertical acceleration at CG are sampled at each time step. The data are presented in this section.

Fig. 11 shows the heave response of the model C2. Two panels are displayed, showing the heave RAO at two beam Froude Numbers of 2.94 and 3.83. The wavelengths ranging from 2L to 4L are marked with gray color as they can cause the highest response, and are of interest in the present research. The reference line, referring to wave amplitude, is also plotted (the dashed red line). If the plotted data is below the line, it imposes that rigid body motions are smaller than that of the waves. Otherwise, it signifies that the rigid body motion is greater compared to wave motion.

As observed, both CFD and 2D + t model predict that heave resonance occurs at the marked area. At wavelengths larger than 2.0, 2D + t model has seen to compute weaker heave response. The inconsistency between two models can cause such a difference. The CFD model can compute water fluid oscillation around the sections, but 2D + t model do not consider oscillation for fluid flow, instead it assumes that water and solid body mutually interact with a very high frequency. It can lead to smaller sectional forces as the waves become longer inasmuch as gravity effects becomes more significant. It is interesting to note that authors have seen such a difference between CFD and 2D + t results in stimulation of heave response of a stepless boat. Readers who are interested are invited to find related technical discussions in Tavakoli et al. (2020).

Pitch response of model C2 is presented in Fig. 12. The dashed red line shows the reference line, referring to the wave steepness. It can be seen that both CFD and 2D + t models capture a reassurance at a wavelength being between 2L and 4L at speed of 6.25 m/s. At the higher speed, it can be seen that both models predict that the pitch response converges a constant value as wavelengths becomes longer than 2L. Again, the CFD model predicts higher values. The possible reason for the differences between the results of the two models is assumptions made for each of them. The 2D + t model neglects the gravity and computes sectional forces for an infinite frequency. This might lead to larger damping forces, and smaller exciting forces, especially over the resonance zone, where motions are significant.

Vertical acceleration of model C2 at its CG is computed by both methods. The related data is shown in Fig. 13. Both models have predicted that vertical acceleration can reach higher values at resonance zone. But 2D + t model gives large values for vertical accelerations induced by short waves, e.g., 1L. Such a difference can be attributed to the method by which forces are computed. It has been previously

Fig. 10. Dynamic trim angle, vertical position of CG, and resistance of Case 4 (Left) and Case 6 (right) at various beam Froude Numbers. Circle and asterisk symbols respectively show the CFD and experimental data.

Fig. 11. Heave response of model C2 in waves. The dashed red line shows the wave amplitude, reference line. Circle and square markers respectively show the 2D + t and CFD results. (For interpretation of the references to color in this figure legend, the reader is referred to the Web version of this article.)
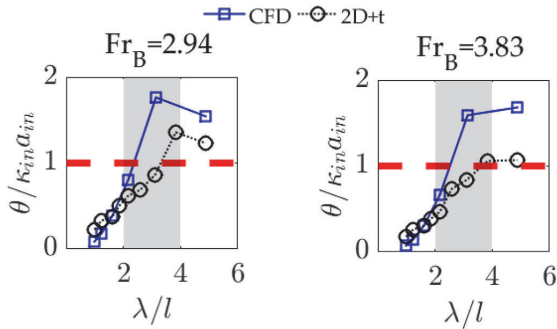
Fig. 12. As of Fig. 11, but for pitch response. The dashed red line shows the wave steepness, reference line. (For interpretation of the references to color in this figure legend, the reader is referred to the Web version of this article.)

Fig. 13. As of Fig. 12, but for vertical acceleration at CG.

observed that when waves are short, 2D + t model might compute negative sectional forces that can lead to large variation of vertical force in a single cycle, which consequences in larger vertical accelerations compared with what is computed by CFD. Technical information can be found in Tavakoli et al. (2020). Moreover, note that the mathematical model neglects the contribution of viscous forces as well. When the bow of the vessel re-enters water, viscous pressure can also contribute (Huang et al., 2021). This can also be another reason for larger vertical acceleration that the 2D + t model computes at small frequencies.

Examples of the time histories of heave, pitch and vertical acceleration, computed by both CFD and 2D + t models, are also presented in Appendix F. These results are not presented in this Section as they might make the paper hard to follow.

As it was explained earlier, it is impossible to evaluate the accuracy of 2D + t model in reproducing the unsteady motions of a double-stepped boat subjected to waves as no experimental data is available. Instead its results were compared against a CFD model in this section. It was seen that their data follow each other at most of forcing conditions. There are some differences between the computed data, especially at long waves. The inconsistency between the models, which is related to the way sectional forces are computed, is likely to be the main reason. Also, the turbulent nature of the flow, especially the water jet flowing toward the middle and rear surfaces can also cause extra shear stresses that are excluded from the 2D + t model. But it is important to note that turbulence is expected to be stronger for the case of shorter waves as their orbital velocity is higher.

7. Effects of step on dynamic responses of a double-stepped boat

In the previous sections, the performance of 2D + t model in computing the dynamic response of a double-stepped vessel operating in planing mode was evaluated. It was observed that it can compute the running attitudes and resistance of a hard-chine stepped planing boat advancing in smooth water with a good level o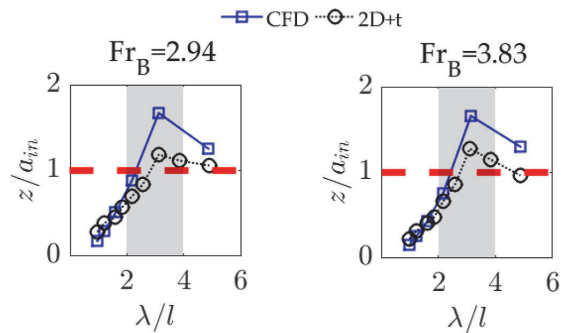f accuracy, especially at higher speeds. Then it was shown how it computes the dynamic response of a double-stepped boat under the forces of head sea waves.

The comparison between the results of CFD and 2D + t models show that the 2D + t model can provide reliable data and can be applied for improving our understanding of the unsteady planing motion of double-stepped boats. In this section, this model is used for this aim.

7.1. Adding two steps to the bottom

Heave and pitch responses of model C and C2 are found by using the developed mathematical model. Motions of these two vessels were mathematically replicated at four different beam Froude Numbers, ranging from 1.9 to 4.77. Waves with different frequencies were generated to have RAO plots with enough wavelengths.

Heave response of both models are shown in Fig. 14. At the two lower speeds, heave responses of both models seem to be over-damped, and do not reach a significant peak value in the resonance zone. At very long waves, such as $\lambda = 3L$, heave responses of both models converge to 1.0. Model C2 is observed to have smaller response at most of the forcing conditions. At the longest wave, heave response of this model is slightly larger compared to that of model C.

At the $Fr_B = 3.83$, heave response of model C reaches its maximum value at a wavelength ranging between $2L$ to $4L$. Waves can also resonate heave response of model C2. But, heave response corresponding to resonance of model C2 is much smaller compared to that of model C at this speed.

Finally, at the highest beam Froude Number, no resonance emerges in heave response of model C2, while a resonance is seen to emerge in the heave response of model C. At the all forcing conditions, model C is found to have greater heave response.

Pitch responses of both model C and C2 are presented in Fig. 15. It can be seen that, at the lowest speed pitch response of both models is over-damped, i.e, pitch amplitude is not highly intensified at frequencies near the natural frequency of both vessels. Model C2 is seen to have smaller response at most of the forcing conditions at this speed.

At the higher speeds, the pitch response of model C becomes larger, and resonance occurs. But model C2 is not affected in that way. Resonance only occurs when model C2 advances at Froude Number of 4.77. At larger Froude Number, response is seen to be over-damped and pitch response is observed to be below, or nearly equal the steepness of the incoming wave. In addition, it is obvious that model C2 has smaller pitch response at all speeds.

Vertical acceleration of both models are shown in Fig. 16. As seen, vertical acceleration of both models increases by the increase in speed which agrees with the previous observations. Model C has been found to have larger vertical acceleration at its CG. At the highest speed, vertical acceleration of model C reaches up to 1.7g, which is quite large and can be very harmful for the crew of the vessel.

Overall, it is observed that model C2, which has two transverse steps, has a better performance in head sea condition. i.e, its heave and pitch responses as well as vertical acceleration at CG are smaller compared to those of model C. This provides us with an important message that a double-stepped design can affect the hydrodynamic behavior of a vessel advancing at planing regime. One of the main reasons that leads to such a better performance is likely to be the changes in the wetted surface pattern of the vessel. Three different surfaces which are partially washed by waves can increase the damping forces and moments, which reduce the heave and pitch response of the vessel in resonance zone. Note that, the effects double-stepped design on heave and pitch responses was seen
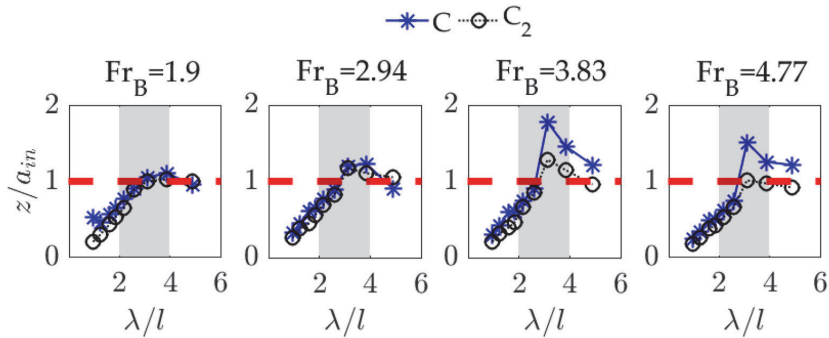
Fig. 14. Heave response of models C and C2.
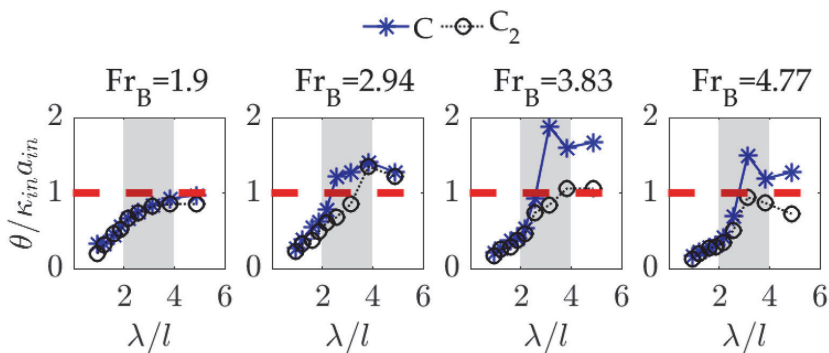
Fig. 15. As of Fig. 14, but for pitch response. The dashed red line shows the steepness of the incoming wave. (For interpretation of the references to color in this figure legend, the reader is referred to the Web version of this article.)
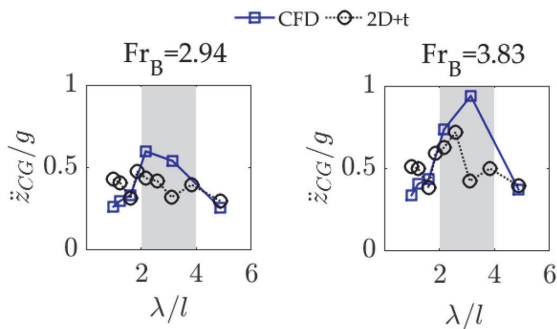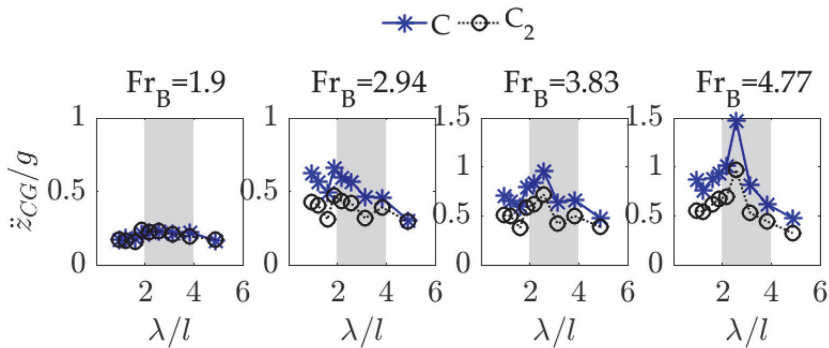

Fig. 16. As of Fig. 15, but for vertical acceleration.

to be more significant at the two higher speeds. This matches with the physics of problem. As the speed of a double stepped hull increases, effects of step on flow pattern becomes greater and leads to larger ventilation area, and also it reduces the dynamic trim angle.

7.2. Step height

In this sub-section, vertical motions of two different double-stepped hulls are mathematically simulated in head sea condition. One of the hulls, Case 4, has a shorter front step, and the other, Case 6, has two steps with similar heights. Sectional half-beam and deadrise angle of these two hulls are the same.

Heave responses of Case 4, triangle markers, and Case 6, cross markers, are displayed in Fig. 17. Pitch response of Case 4 is seen to be smaller compared to that of case 5 at higher speed. In addition, vertical motion of this vessel, Case 4, is not resonated by waves at the marked area, and the heave response plot is showing an over-damped behavior. Note that, at smaller Froude Number, $Fr_B = 3.89$, heave response of Case 4 is seen to be larger, compared to Case 6, at short waves.

Pitch response of cases 4 and 6 are plotted in Fig. 18. Both models
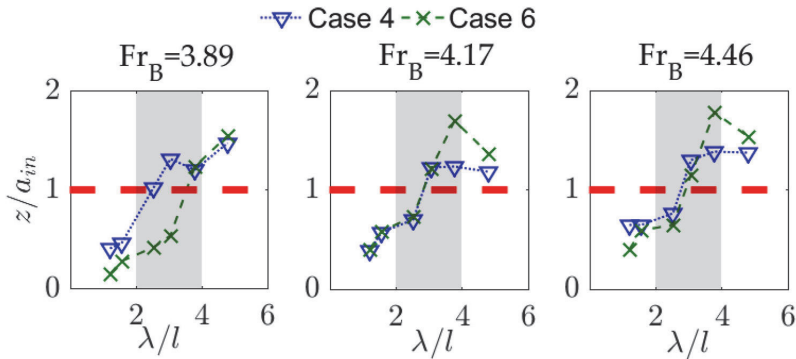
Fig. 17. Heave response of cases 4 and 6.
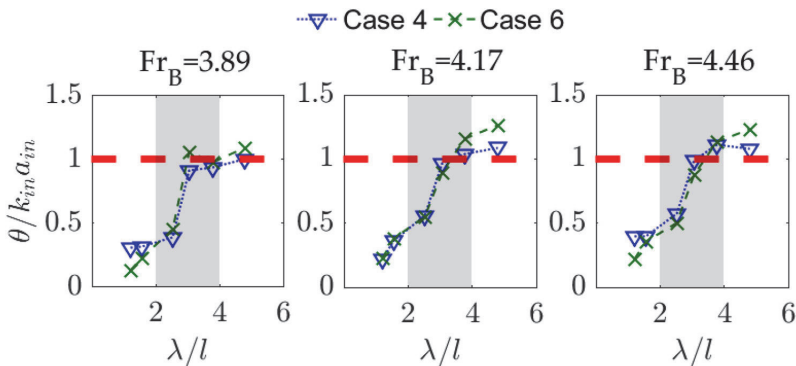
Fig. 18. As of Fig. 17 but for pitch response.
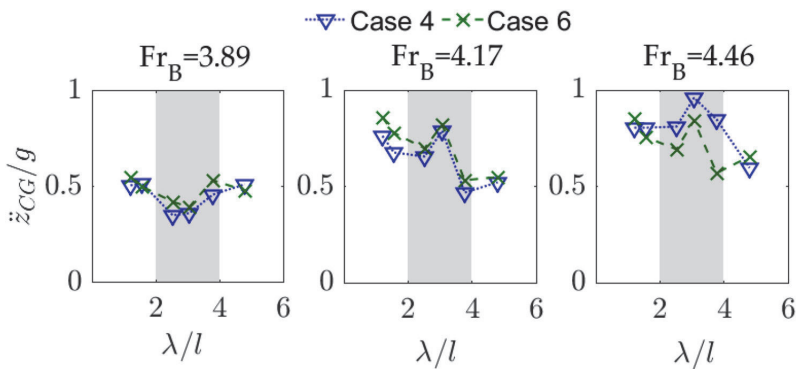
Fig. 19. As of Fig. 18 but for vertical acceleration at CG.

show an over-damped behavior in pitch direction. Their responses are seen to be very close to each other. At longer waves, Case 4 is seen to have smaller response. But at very short waves, it can have larger response.

Vertical acceleration of cases 4 and 6 are displayed in Fig. 19. It can be seen that vertical acceleration of both models follow each other at the lower Froude Numbers. At the higher-speed, however, vertical acceleration of Case 4 is seen to be relatively larger compared to that of Case 6.

The differences at the highest speed are not significant, but it can reach up to 1.3g at some forcing conditions.

On the whole, the results presented in this subsection confirmed that the response of the dynamic of a double-stepped boat is sensitive to proportion of step heights. Heave response of the vessel is highly influenced by the step height. When the front step is set to be shorter, heave motion is highly decreased and a very weak resonance might occur. But, it can lead to larger vertical acceleration at CG of the vessel

when speed is increased. Such a phenomenon is expected to be affected by distribution of the wetted area of the vessel. Compared to a case for which both steps have similar heights, larger area of the middle body, and less area of the rear body, are washed the water flow. Such a wet area pattern is expected to influence the damping forces/moments of the vessel by increasing them, i.e, when front step is shorter, damping force increases. Therefore, heave response is reduced and a very weak resonance might occur. But, the larger wet area can allow a larger volume of water to periodically impact the vessel, causing a larger vertical force. In this condition, the vertical acceleration is expected to be larger.

8. Concluding remarks

Double-stepped planing hulls have been turned into one of the interesting designs that can be used for a safe operation in water. Their motion obeys nonlinear theories and is far from being linear, as the wet area of the vessel varies over time.

In the current research, a mathematical model, based on the 2D + t, was developed to replicate the unsteady motion of double-stepped boats in head sea condition. The model uses the solution of a high-frequency Radiation problem, known as Wagner, to compute sectional forces by applying momentum variation law. A simplified model was also applied to compute the ventilation area behind each step.

In parallel, a CFD model was used to simulate the unsteady motion of the double-stepped boats in waves. This model was applied due to the lack of available experimental seakeeping tests of double-stepped boats.

Both models were found to be valid enough to be used for performance prediction of the vessel in calm water conditions. The related simulations were performed by setting the water waves to be zero, which resembles a smooth water test. The 2D + t model was seen to have large errors at low speeds, where the assumptions of the 2D + t model are expected to be inconsistent with reality.

Rough water tests then were carried out. Results of both models were compared against each other, showing their results follow each other. There were some differences in long waves. Heave and pitch responses computed by 2D + t model were seen to be smaller, which is expected to be linked to the assumptions of the 2D + t model. This model is based on the infinite-frequency Radiation problem, which simplifies fluid motion around the section when unsteady motions occur. When waves become longer, such an assumption can lead to inconsistency with the physic of the problem. But, the relative agreement between CFD and 2D + t results confirmed that the 2D + t model is reliable enough to be used for simulation of the unsteady motion of double-stepped hulls.

The mathematical model was used to improve the understanding of the effects of steps on the unsteady planing motion in waves. Vertical motions of a stepless boat and a double-stepped hull were both mathematically replicated in head sea by using the 2D + t method. It was seen that the stepped design can positively affect the performance of the vessel. Heave and pitch responses were both seen to be reduced when two steps were added to the bottom of the vessel. Vertical acceleration was also seen to be reduced when two steps were added to the bottom of the vessel. For the case of a double-stepped boat, the wetted area pattern

is divided into three sub-areas, on which the hydrodynamic pressure is distributed. Such a change in the wetted area pattern of the vessel is likely to be the main reason that reduces vertical motions of double-stepped boats.

Two double-stepped boats with similar sectional deadrise angles and beams were also mathematically modeled in the head sea condition. The main difference between these two designs was the step heights. In one case, both steps have the same heights. But the other vessel had a shorter front step. Quantitative comparison between the results demonstrated that in the case the front step is shorter, heave motion, especially in the resonance zone, is reduced, while vertical acceleration may be increased. A shorter front step may increase the washed area of the middle surface. A larger washed area can increase the total damping force, and also can increase the exciting force. Therefore, such behavior was observed for the vessel with a shorter front step.

The model developed in the present research provided an understanding of the unsteady planing motion of double-stepped hulls. The performance of the model can be modified by consideration of oscillation motions of the sections and also by assuming a more accurate prediction for the transom wave. In addition, the model can be further developed to consider more degrees of freedom. Specifically, the roll motion can be considered in the model, which is likely to be very important for the case of high-speed vessels as they might show unstable behavior in the transverse direction. More importantly, as was mentioned before, experimental studies, highlighting wave-induced motions of double-stepped planing hulls are lacking at the present stage. It is very vital to perform systematic experimental studies on the motions of double-stepped planing hulls exposed to water waves. This can provide us with an understanding of the unsteady motion of double-stepped planing through experimental observations. In addition, the data provides us with a benchmark that can be used for the validation of mathematical or numerical simulations.

CRediT authorship contribution statement

Rasul Niazmand Bilandi: Investigation, Software, Validation, Visualization, Writing – original draft. **Sasan Tavakoli:** Investigation, Software, Validation, Visualization, Writing – original draft. **Abbas Dashtimanesh:** Supervision, Conceptualization, Funding acquisition, Methodology, writing – review.

Declaration of competing interest

The authors declare that they have no known competing financial interests or personal relationships that could have appeared to influence the work reported in this paper.

Acknowledgments

Appendix A Sectional added mass of a wedge entering water

The sectional added mass of a solid wedge shape body entering water is found using the Wagner Solution as

$$a = \frac{\pi}{2} \rho c^2 \tag{A.1}$$

Here c is the half wetted beam of the solid body and vary over time. Time rate of added mass is found by computing derivative of Equation (A.1) with respect to time as

$$\dot{a} = \pi \rho c \dot{c} \tag{A.2}$$

As explained earlier. c is a function of time. Therefore, its time rate emerged as we compute the differential of the right side of equation A.2. Half-wetted bam of the section and its time rate are calculated through

$$c = (1 + \psi)c_0 \tag{A.3}$$

$$\dot{c} = (1 + \psi)\dot{c}_0 \tag{A.4}$$

where $1 + \psi$ is the water-pile up that is found by applying Wagner condition. For the case of a Wedge shape body entering water with constant speed, $1 + \psi$ is found to be $\pi/2$. c_0 refers to the transverse location of intersection between calm water line water, and is computed using the shape function of the section. When water reaches the chine, it values converges to a constant number, being equal to the half-beam of the vessel. It is, therefore, computed by

$$c_0 = \begin{cases} h_{\mathscr{W}}(x)/\tan(\beta) & h_{\mathscr{W}}(x) < z_c \\ 0.5B & h_{\mathscr{W}}(x) \geq z_c \end{cases} \tag{A.5}$$

Time rate of c_0 is also computed by

$$\dot{c}_0 = \begin{cases} \dot{h}_{\mathscr{W}}(x) \Big/ tan(\beta) & h_{\mathscr{W}}(x) < z_c \\ 0 & h_{\mathscr{W}}(x) \geq z_c \end{cases} \tag{A.6}$$

Note that, $\dot{c}_0$ is set to be zero after chine wetting. It is important to mention that we have simplified the water entry simulation after chine wetting. In a real water entry problem, as the water reaches the chine, its is separated and can affect the fluid the motion around the solid body. But we have simplified the problem by neglecting such a phenomenon.

Appendix BIntegral terms emerged in three-dimensional forces

The integration emerged in the final three-dimensional forces acting on each planing surfaces are presented in this Appendix. Integration emerged in force are found by:

$$f_{z_i}^{\text{①}} = \left(\int_{L_i} \mathscr{T}_i(x) a d_t(w_z) dx \right) \cos(\theta + \theta_j) \quad \forall i \in \{1, 2, 3\} \tag{B.1}$$

$$f_{z_i}^{\text{②}} = -\left(\int_{L_i} \mathscr{T}_i(x) a w_z \dot{\theta} dx \right) \sin(\theta + \theta_i) \quad \forall i \in \{1, 2, 3\} \tag{B.2}$$

$$f_{z_i}^{\text{③}} = -\left(\int_{L_i} \mathscr{T}_i(x) a v d_x(w_z) dx \right) \sin(\theta + \theta_j) \quad \forall i \in \{1, 2, 3\} \tag{B.3}$$

$$f_{z_i}^{\text{④}} = \left(\int_{L_i} \mathscr{T}_i(x) a u d_x(w_z) dx \right) \cos(\theta + \theta_i) \quad \forall i \in \{1, 2, 3\} \tag{B.4}$$

$$f_{z_i}^{\text{⑤}} = \mathscr{V} \mathscr{U} \rho a \big|_{x_{\mathscr{T}_i}} \quad \forall i \in \{1, 2, 3\} \tag{B.5}$$

$$f_{z_i}^{\text{⑥}} = -\left(\int_{L_i} \mathscr{T}_i(x) \dot{a} \mathscr{V} dx \right) \quad \forall i \in \{1, 2, 3\} \tag{B.6}$$

$$f_{z_i}^{\text{⑦}} = -\left(\int_{L_i} \mathscr{T}_i(x) C_{CD} (\rho \mathscr{V}^2) b \, dx \right) \quad \forall i \in \{1, 2, 3\} \tag{B.7}$$

Integration that are emerged in the three dimensional moment are given by:

$$m_{\theta_i}^{\text{①}} = \left(\int_{L_i} \mathscr{T}_i(x) a d_t(w_z) x dx \right) \cos(\theta + \theta_j) \quad \forall i \in \{1, 2, 3\} \tag{B.8}$$

$$m_{\theta_i}^{\text{②}} = -\left(\int_{L_i} \mathscr{T}_i(x) a w_z \dot{\theta} x dx \right) \sin(\theta + \theta_j) \quad \forall i \in \{1, 2, 3\} \tag{B.9}$$

$$m_{\theta_i}^{\text{③}} = -\left(\int_{L_i} \mathscr{T}_i(x) a \mathscr{V} d_x(w_z) dx \right) \sin(\theta + \theta_j) \quad \forall i \in \{1, 2, 3\} \tag{B.10}$$

$$m_{\theta_i}^{\text{④}} = \left(\int_{L_i} \mathscr{T}_i(x) a \mathscr{U} d_x(w_z) x dx \right) \cos(\theta + \theta_j) \quad \forall i \in \{1, 2, 3\} \tag{B.11}$$

$$m_{\theta_i}^{\circledcirc} = \mathcal{V} \mathcal{U} x_{\mathcal{T}_i} \rho a|_{x_{\mathcal{T}_i}} \qquad \forall i \in \{1,2,3\} \tag{B.12}$$

$$m_{\theta_i}^{\circledcirc} = -\left(\int_{L_i} \mathcal{T}_i(x) \dot{a} \, \mathcal{V} x dx \right) \qquad \forall i \in \{1,2,3\} \tag{B.13}$$

$$m_{\theta_i}^{\circledcirc} = -\left(\int_{L_i} \mathcal{T}_i(x) C_{CD} \left(\rho \, \mathcal{V}^{-2} \right) b \right) x dx \right) \quad \forall i \in \{1,2,3\} \tag{B.14}$$

Appendix C. Turbulence model and $y+$ values

The k-ϵ model is used to simulate turbulence flow around the domain. The turbulent viscosity is hypothesized to be a function of kinetic energy, k, and its time rate dissipation, ϵ:

$$\mu_t = \rho C_\mu \frac{k^2}{\epsilon} \tag{c.1}$$

Turbulent kinetic energy and its dissipation are linked through two conservatives based equations as

$$\frac{\partial}{\partial t}(\rho k) + \nabla.(\rho v k) + \nabla.\left(\mu_{eff,k} \nabla k\right) = \nabla.\left(\mu_{eff,k} \nabla k\right) + \underbrace{P_k - \rho \varepsilon}_{S^k} \tag{c.2}$$

$$\frac{\partial}{\partial t}(\rho \varepsilon) + \nabla.(\rho v \varepsilon) = \nabla.\left(\mu_{eff,\varepsilon} \nabla \varepsilon\right) + \underbrace{C_{\varepsilon 1} \frac{\varepsilon}{k} P_k - C_{\varepsilon 2} \rho \frac{\varepsilon^2}{k}}_{S^\varepsilon} \tag{c.3}$$

where C_μ, $C_{\varepsilon 1}$, and $C_{\varepsilon 2}$ are constants that are equal to 0.09, 1.44, and 1.92 respectively.

To treat flow behaviour near walls of the vessel, a standard $y+$ model is used. $y+$ is defined to be calculated as

$$\frac{d_\perp u_\tau}{v} = y^+ \tag{c.4}$$

where $d_\perp$ is the normal distance from the wall of the vessel, u_τ is the frictional velocity, and v is the kinematic viscosity of water. The frictional velocity is related to the shear stress acting on the wall of the vessel as

$$u_\tau = \sqrt{\frac{|\tau_w|}{\rho}} \tag{c.5}$$

The $y+$ value is set to vary between 30 and 300 on the wall of model C2 when it advances in waves. Its distribution on the wall of the model C2 is shown in Fig. 20. Readers who are interested in reconstruction of the turbulent fluid motion around a planing vessel are referred to Hosseini et al. (2021).

Wall Y+

| 30 | 97.5 | 165 | 232.5 | 300 |
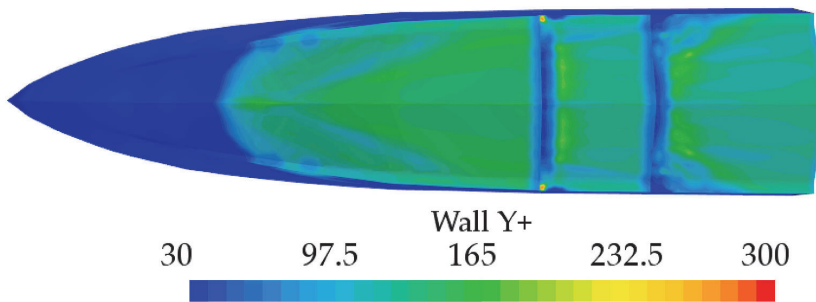
Fig. 20. Distribution of $y+$ on the bottom wall of model C2 for $Fn_B = 2.94$.

Appendix D. Mesh sensitivity study for CFD model

A sample of the mesh study is shown in this Appendix. Vertical motions of model C2 are numerically replicated in the fluid domain. Simulations are performed to replicate the motion of vessel at beam Froude Number of 3.83, and wavelength of 3.12L. Simulations are performed using all four generated grids. Heave and pitch responses are computed. The summary of data is shown in Fig. 21. It is observed that heave and pitch responses of the vessel converge by the increase of the cells.

The data presented in Fig. 21 ensures the fine gird, G_3, can provide reliable data, and grids with greater numbers of cell do not affect the simulations. Therefore, the fine grid is opted to use for modeling the unsteady planing motion of model C2 in different forcing conditions.
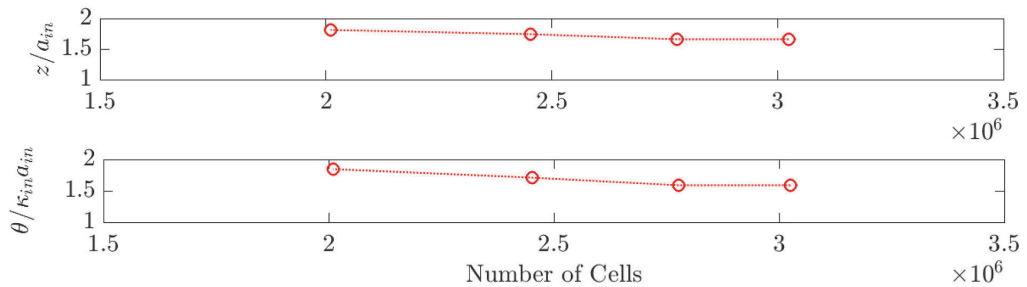
Fig. 21. Results of the performed mesh study. These results correspond to the heave and pitch motions of model C2. Froude Number is 3.83, and wavelength is 3.12L.

Appendix E. Wave generation by CFD model

Samples of generated waves by the numerical model are presented in this Appendix to evaluate the performance of CFD model in generation of water waves. Tests are performed in an open-water condition, and the numerical domain is vessel-free.

Water waves with a length of 1.6L, corresponding to the frequency of 0.7 rad/s are generated in the right end of the domain. Wave steepness is set to be 0.039. This condition matches with one of the forcing conditions used in the present research, 4th row of Table 4.

Time history of generated waves at a point, with a longitudinal position of 0.5L from the inlet, is shown in Fig. 22. Also, water surface elevation corresponding to linear wave, given by theory, is plotted in this Figure. It can be seen that the numerical data matches with the theory, showing that the CFD model is working well.
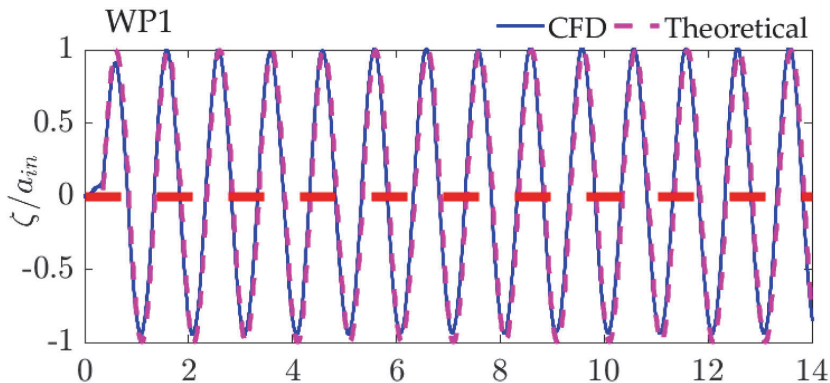
Fig. 22. Free surface elevation generated by CFD model in an open-water condition at a point with a distance of 0.5L from the wave maker. The results are also compared against Airy Theory to check the validity of the numerical technique.

A sample of water surface is shown in Fig. 23. The water surface elevation in the whole domain is shown. An uni-directional pattern for the waves is observed which ensures that the CFD model do not lead to any multi-directional waves. Therefore, it is guarantees that the generated wave model provides a clean fully head sea condition.
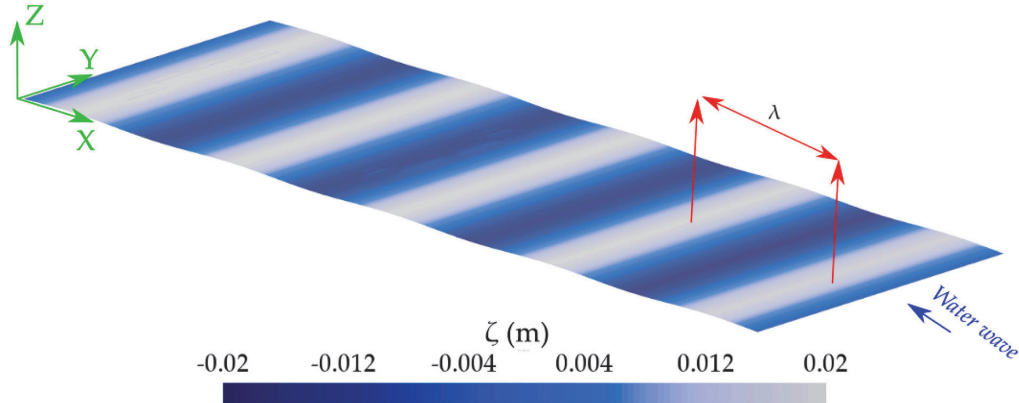
Fig. 23. Three-dimensional view of the uni-directional waves generated by the numerical model. The snapshot presented here corresponds to the wavelength of 1.6*L* and steepness value of 0.039.

Also, the time history of the wave waves at three different virtual wave probes are plotted. These probes, shown by WP1, WP2, and WP3, are located at longitudinal positions of 0.5*L*, 2.5*L*, 4.5*L* from the wave maker. Note that WP1 gives the water surface elevation presented in Fig. 23. Also WP2 locates where the CG of the vessel is located in the wave-body testes.

Time histories are plotted in lower panel of Fig. 24. Each time history is bounded with two different dotted lines, referring to a_{in} and $-a_{in}$. It can be seen that, the water is initially at rest, but as the wave energy reaches to the point, it starts to oscillate around its initial value, equilibrium condition. Water surface elevation at none of the probes is seen to go beyond the dashed lines. This means that the energy of waves is well damped at all boundaries, and therefore, no reflection effects emerges in simulation.
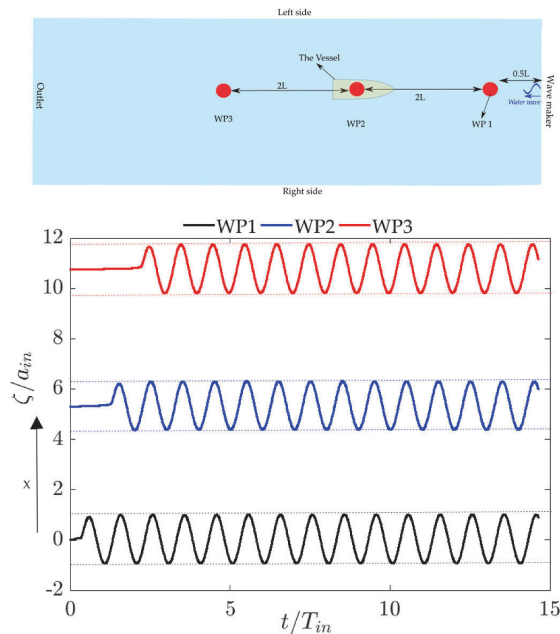
Fig. 24. Upper row shows the location of three different virtual wave probes. Note that the tests are vessel-free and the vessel with a low transparency is drawn to show the location of the vessel in the tank when its mutual interaction with waves is numerically modeled. Lower panels show the time histories of the mono-chromatic wave propagating in the numerical tank. Time history of water surface elevation is shown since the initial time to show how the generated gravity wave is developed. The second probe is placed at the CG of the vessel is located. Note that all results correspond to an open-water condition and the vessel is not placed in the domain.

Appendix F. Sample of time histories of the response of model C2

Samples of time histories of heave, pitch and vertical acceleration of model C2 are presented in this Appendix. Samples are extracted from both CFD and mathematical models, which are respectively shown by solid blue and dashed black plots in all Figures and panels.

The presented data cover two different beam Froude Numbers of 2.94 and 3.83, which correspond to speeds of 6.25 and 8.13 m/s, respectively. Two different forcing conditions with wavelengths of 1.59L and 3.12L are considered. The smaller wavelength represents a situation with small heave and pitch responses, but can have large vertical acceleration. The other wavelengths, however, can causes larger heave and pitch responses, but can induce smaller vertical acceleration.

Fig. 25 displays examples of the heave response of the model C2 over the time. As seen, heave response, computed by both models, show harmonic behaviour, and seems to follow a linear response. At the shorter wavelengths, CFD and 2D + t method are seen to fit very well. At the longer wavelength, there are some differences, and 2D + t method computes smaller response.
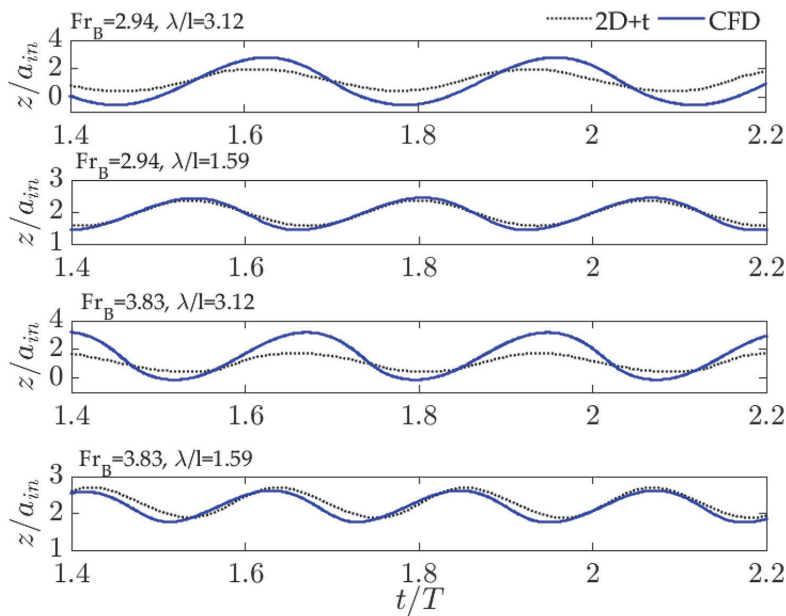
Fig. 25. Time histories of heave response of model C2. Results correspond to two different beam Froude Numbers of 2.94 and 3.83. Two different wavelengths of 1.59L and 3.12L are considered. Solid blue and dashed black plots respectively refer to CFD and 2D + t models.

Samples of pitch response of model C2 are shown in Fig. 26. As seen, like what was observed for heave response, time-dependent pitch of the vessel is harmonic. Both CFD and 2D + t model provides very similar results at shorter wavelength. At the longer wavelength, larger pitch response is computed by CFD model.
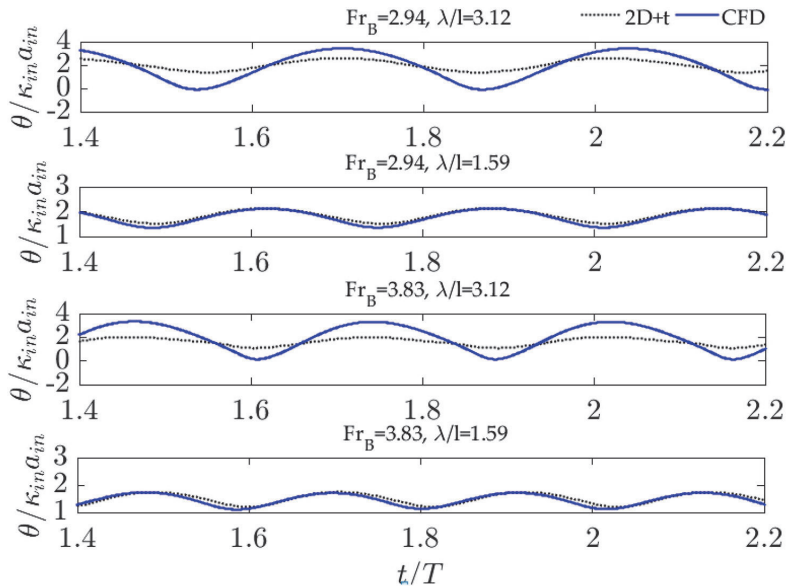
Fig. 26. Time histories of pitch response of model C2. Results correspond to two different beam Froude Numbers of 2.94 and 3.83. Two different wavelengths of 1.59L and 3.12L are considered. Solid blue and dashed black plots respectively refer to CFD and 2D + t models.

Time history of vertical acceleration at CG, computed by CFD and 2D + t models, are plotted in Fig. 27. This parameter is seen to show nonlinear behaviour. As apparent, crest of vertical acceleration is sharp. Crest is seen to be sharper at higher speed and shorter wave. The crest, corresponding to 2D + t model, is also seen to be skewed toward left. Physically, 2D + t model is more likely to compute larger spectral values for second and third harmonics.
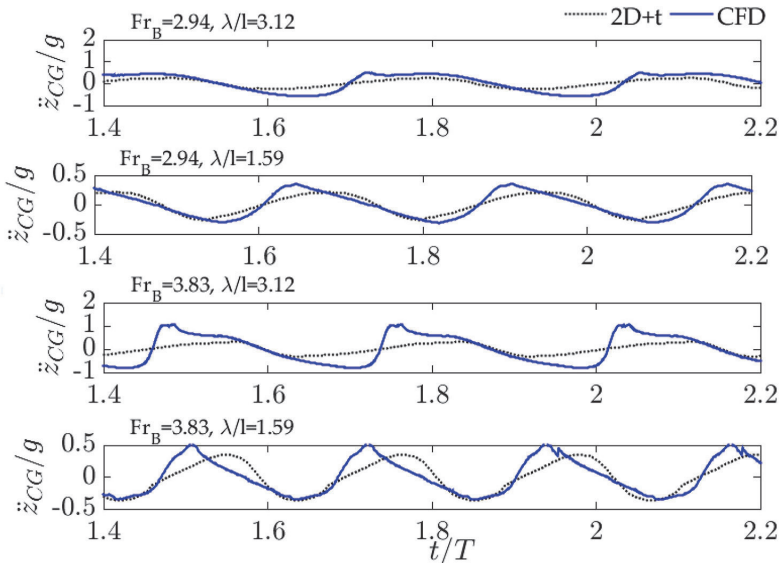
Fig. 27. Time histories of vertical acceleration of model C2 at CG. Results correspond to two different beam Froude Numbers of 2.94 and 3.83. Two different wavelengths of 1.59L and 3.12L are considered. Solid blue and dashed black plots respectively refer to CFD and 2D + t models.

References

Begovic, E., Bertorello, C., Pennino, S., 2014. Experimental seakeeping assessment of a warped planing hull model series. Ocean. Eng. 83, 1–15.

Clement, E.P., Desty, D.H., 1980. The BP Dynaplane High-Speed Research Boat. High-Speed Surface Craft. 3rd International Hovering Craft and Hydrofoil Exhibition.

Clement, E.P., Pope, J.D., 1961. Stepless and stepped planing hulls-graphs for performance prediction and design. Int. Shipbuild. Prog. 8 (84), 344–360.

Dashtimanesh, A., Esfandiari, A., Mancini, S., 2018. Performance prediction of two-stepped planing hulls using morphing mesh approach. Journal of Ship Production and Design 10, 5957. JSPD.160046.

Dashtimanesh, A., Enshaei, H., Tavakoli, S., 2019. Oblique-asymmetric 2D+ T model to compute hydrodynamic forces and moments in coupled sway, roll, and yaw motions of planing hulls. J. Ship Res. 63 (1), 1–15.

De Marco, A., Mancini, S., Miranda, S., et al., 2017. Experimental and numerical hydrodynamic analysis of a stepped planing hull. Appl. Ocean Res. 64, 135–154.

Du, L., Lin, Z., Jiang, Y., Li, P., Dong, Y., 2019. Numerical investigation on the scale effect of a stepped planing hull. J. Mar. Sci. Eng. 7 (11), 392.

Esfandiari, A., Tavakoli, S., Dashtimanesh, A., 2019. Comparison between the dynamic behaviour of the non-stepped and double-stepped planing hulls in rough water: a numerical study. Proc. IME M J. Eng. Marit. Environ. https://doi.org/10.1177/1475090219851917 (in press).

Garme, K., 2005. Improved time-domain simulation of planing hulls in waves by correction of the near-transom lift. Int. Shipbuild. Prog. 52 (3), 201–230.

Garland, W.R., Maki, K.J.A., 2012. Numerical study of a two-dimensional stepped planing surface. Journal of Ship Production and Design 28 (2), 60–72.

Ghadimi, P., Tavakoli, S., Dashtimanesh, A., 2016. Coupled heave and pitch motions of planing hulls at non-zero heel angles. Appl. Ocean Res. 59, 286–303.

Hosseini, A., Tavakoli, S., Dashtimanesh, A., Sahoo, P., Kõrgesaar, M., 2021. Performance prediction of a hard-chine planing hull by employing different CFD models. J. Mar. Sci. Eng. 9 (5), 481.

Huang, L., Ren, K., Li, M., Tuković, Ž., Cardiff, P., Thomas, G., 2019. Fluid-structure interaction of a large ice sheet in waves. Ocean. Eng. 182, 102–111.

Huang, L., Tuhkuri, J., Igrec, B., Li, M., Stagonas, D., Toffoli, A., Cardiff, P., Thomas, G., 2020. Ship resistance when operating in floating ice floes: a combined CFD&DEM approach. Mar. Struct. 74, 102817.

Huang, L., Tavakoli, S., Li, M., Dolatshah, A., Pena, B., Ding, B., Dashtimanesh, A., 2021. CFD analyses on the water entry process of a freefall lifeboat. Ocean. Eng. https://doi.org/10.1016/j.oceaneng.2021.109115.

Ittc, 1978. Performance Prediction. Method, pp. 1–9, 7.5 – 02. 03 – 01.4.

Lee, E., Pavkov, M., Mccue-Weil, W., 2014. The systematic variation of step configuration and displacement for a double-step planing craft. Journal of Ship Production and Design 30 (2), 89–97.

Linton, C.M., McIver, P., 2001. Handbook of Mathematical Techniques for Wave/structure Interactions. CRC Press.

Mousaviraad, S.M., Zhang, W., Stern, F., 2015. URANS studies of hydrodynamic performance and slamming loads on high-speed planing hulls in calm water and waves for deep and shallow conditions. Appl. Ocean Res. 51, 222–240.

Newman, N., 1977. Marine Hydrodynamics. MIT Press.

Niazmand Bilandi, R., Mancini, S., Vitiello, L., Miranda, S., De Carlini, M., 2018. A validation of symmetric 2D + T model based on single-stepped planing hull towing tank tests. J. Mar. Sci. Eng. 6, 136.

Niazmand Bilandi, R., Mancini, S., Dashtimanesh, A., Tavakoli, S., De Carlini, M., 2019. A Numerical and Analytical Way for Double-Stepped Planing Hull in Regular Wave, Viii International Conference on Computational Methods in Marine Engineering Marine 2019. Goteborg, Sweden.

Niazmand Bilandi, R., Dashtimanesh, A., Tavakoli, S., 2020. Hydrodynamic study of heeled double-stepped planing hulls using CFD and 2D+ T method. Ocean. Eng. 196, 106813.

Ogilvie, T.E., Tuck, E.O., 1969. A Rational Strip Theory for Ship motions(Report). University of Michigan, USA.

Payne, P.R., 1995. Contribution to Planing Theory 22 (7), 699–729.

Sebastiani, L., Bruzzone, D., Gualeni, P., et al., 2008. A practical method for the prediction of planing craft motions in regular and irregular waves. In: Paper Presented at: Proceedings for the 27th International Conference on Offshore, Mechanics and Arctic Engineering (OMAE 2008). Estoril, Portugal.

Salvesen, N., Tuck, E.O., Faltinsen, O., 1970. Ship motions and sea loads. Trans. - Soc. Nav. Archit. Mar. Eng. 78, 250–287.

Savitsky, D., 1985. Planing craft. Nav. Eng. J. 97 (2), 113–141.

Savitsky, D., DeLorme, M.F., Datla, R., 2007. Inclusion of whisker spray drag in performance prediction method for high-speed planing hulls. Mar. Technol. 44 (1), 35–56.

Savitsky, D., Morabito, M., 2010. Surface wave contours associated with the fore body wake of stepped planing hulls. Mar. Technol. 47 (1), 1–16.

STAR-CCM+, 2011. Version 13.04; CD-Adapco, Computational Dynamics-Analysis & Design. Application Company Ltd., Melville, NY, USA.

Tavakoli, S., Dashtimanesh, A., 2019. A six-DOF theoretical model for steady turning maneuver of a planing hull. Ocean. Eng. 189, 106328.

Tavakoli, S., Niazmand Bilandi, R., Mancini, S., De Luca, F., Dashtimanesh, A., 2020. Dynamic of a planing hull in regular waves: comparison of experimental, numerical and mathematical methods. Ocean. Eng. 217, 107959.

Tezdogan, T., Demirel, Y.K., Kellett, P., Khorasanchi, M., Incecik, A., Turan, O., 2015. Full-scale unsteady RANS CFD simulations of ship behaviour and performance in head seas due to slow steaming. Ocean. Eng. 97, 186–206.

Taunton, D.J., Hudson, D.A., Shenoi, R.A., 2010. Characteristics of a series of high speed hard chine planing hulls—Part I: performance in Calm Water. Int. J. Small Craft Technol. 152, B55–B77.

Veysi, S., Ghassemi, H., 2016. Numerical modeling of the stepped planing hull in calm water. Int. J. Eng. 29 (2), 236–245.

Xu, L., Troesch, A.W., Peterson, R., 1999. Asymmetric hydrodynamic impact and dynamic response of vessels. J. Offshore Mech. Arctic Eng. 121, 83–89.

Zarnick, E.E., 1978. A Nonlinear Mathematical Model of Motions of a Planing Boat in Regular Waves. David Taylor Naval Ship Research and Development Center, Bethesda Maryland.

Appendix 2 (Publication II)

[P2] Vitiello, L., Mancini, S., Niazmand Bilandi, R., Dashtimanesh, A., De Luca, F., & Nappo, V. (2022). A comprehensive stepped planing hull systematic series: Part 1 - Resistance test. Ocean Engineering, 266, 112242.
https://doi.org/10.1016/j.oceaneng.2022.112242
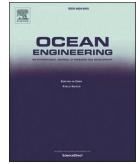
A comprehensive stepped planing hull systematic series: Part 1 - Resistance test

Luigi Vitiello [a,*], Simone Mancini [b], Rasul Niazmand Bilandi [c], Abbas Dashtimanesh [d], Fabio De Luca [a], Vincenzo Nappo [e]

[a] *Department of Industrial Engineering, University of Napoli" Federico II", 80125, Napoli, Italy*
[b] *Department of Hydro and Aerodynamics, FORCE Technology, 2800, Kgs. Lyngby, Denmark*
[c] *Estonian Maritime Academy, Tallinn University of Technology, 11712, Tallinn, Estonia*
[d] *Department of Engineering Mechanics, School of Engineering Science, KTH Royal Institute of Technology, 114 28, Stockholm, Sweden*
[e] *MV Marine S.r.l, Italy*

ARTICLE INFO

ABSTRACT

This work addresses the experimental study of a new systematic series of stepped planing hulls. Indeed, the interest in the stepped planing hulls is constantly growing, both in the industrial/commercial and academic fields. Designers and boat builders have been orienting toward the multi-stepped hulls solution to ensure good dynamic stability, reliable seakeeping and operability at high speeds. However, there is a lack of a comprehensive stepped hull systematic series with various step configurations including a forward V-shaped step, as typically used on modern boats. For the abovementioned reasons, a systematic series of eight different models of stepped hulls have been developed and tested. The towing tank tests have been carried out at the naval basin of the *Università degli Studi di Napoli "Federico II" Dipartimento di Ingegneria Industriale (DII)* in calm water at different speeds (Fr$_\nabla$ = 1.077–6.774) and for three different static trim conditions. All models are built with a transparent bottom to visualize the wetted surface and the eventual development of vortices generated behind the step. The eight models are defined by modifying three significant design parameters for stepped hulls (i.e. the number of steps, longitudinal step position, and step height).

1. Introduction

Nowadays, the design of high-speed craft is strongly conditioned by two anti-synergetic needs: the first is the reduction of fuel consumption and improvement of the speed, and the second is the improvement of comfort on-board (De Luca and Pensa, 2017). To reach a balance between these needs, it is necessary to study the effects of various parameters on hull resistance as well as seakeeping and manoeuvring motions. Several researchers have tried to develop a systematic series of planing hulls (Clement and Blount, 1963; Keuning and Gerritsma, 1982; Keuning et al., 1993; Kowalyshyn and Metcalf, 2006). However, these systematic series not only have not been developed for energy efficiency purposes but also their seakeeping and maneuvering behaviour have not been analysed in most of the cases. Just two systematic series report some considerations related to energy efficiency, specifically the Naples systematic series (De Luca and Pensa, 2017) and Southampton systematic series (Taunton et al., 2010). However, Naples systematic series is

mainly suitable for the low range of speeds in the planing regime. The Southampton systematic series, instead, based on the stepped hull form, was tested at a wide range of speeds.

Stepped planing hulls have sparked up a tremendous interest in recent years, and few researchers have tried to provide an understanding of their performance in smooth/rough water (Niazmand Bilandi et al., 2020a&2021). These vessels are used for a wide range of purposes (e.g. military & patrol, fishing, and leisure). However, due to the lack of available data about systematic studies of the stepped hulls, there still is a non-trivial question for the designers to define the height, the position, and the shape of the step(s). Indeed, there are only a few studies that have tried to measure the performance of stepped planing hulls in calm water and in waves.

From 1960 to 1990, a few authors (Clement and Pope, 1961; Moore, 1967; Clement and Desty, 1980) had some contributions in the performance prediction of stepped hulls. Clement and Koelbel (1991) studied the effects of the step design on the performance of planing boats. Clement and Koelbel (1992) and Clement (2003) published two reports

---

* Corresponding author.
E-mail address: luigi.vitiello@unina.it (L. Vitiello).

Nomenclature

A_T	Area of transom (m^2)
A_X	Area of maximum transvers section (m^2)
B	Breadth (m)
B_C	Maximum chine breadth (m)
B_r	Bias systematic uncertainty
B_{TC}	Chine breadth at transom (m)
c_j	Basis constant
Fr_∇	Volumetric Froude number
Fr_L	Froude number based on L_{WL}
Hs	Height of the step (mm)
K	Constant value
LSP	Longitudinal Step Position (mm)
L_{WL}	Waterline Length (m)
L_{OA}	Length overall (m)
Ns	Number of steps
P_r	Precision uncertainty
RT_M	Total model resistance (N)
S	Wetted surface (m^2)
$SDev_j$	Standard deviation of jth run
U	Uncertainty
U_r	Total uncertainty
U_k	k-input parameter uncertainty
V	Hull speed (m/s)
Z_G	Sinkage (m)

Z_O	Sinkage referred to the O of the coordinate system (m)
∇	Displacement volume (m^3)

Greek symbols

A	Constant value
Δ	Displacement weight (N)
ρ	Density (kg/m^3)
Λ	Expansion coefficient
$\Delta\tau$	Time step (s)
τ	Dynamic trim angle (deg)

Acronyms

CFD	Computational Fluid Dynamics
CNC	Computer Numerical Control
DAQ	Data acquisition device
DT	Down Thrust
EFD	Experimental Fluid Dynamics
FRP	Fibre Reinforced Plastic
ITTC	International Towing Tank Conference
LCB	Longitudinal Centre of Buoyancy
LCG	Longitudinal Centre of Gravity
PVC	Polyvinyl Chloride
RIB	Rigid Inflatable Boat
RSS	Root Sum Square
UA	Uncertainty Analysis

---

in which an efficient configuration of one-stepped hulls has been suggested.

In addition to those initial studies, Taunton et al. (2010, 2011) were one of the pioneers who carried out experimental work on two-stepped hulls. They provided a set of towing tank data that were suitable for the validation of numerical and mathematical models. Vitiello et al. (2012) also performed model experiments and sea trial tests on a two-stepped hull in the towing tank of the *Università degli Studi di Napoli "Federico II"*. White et al. (2012) have performed some experiments on two-stepped hulls and concluded that stepped hulls may improve the powering performance of planing boats only under certain conditions. Lee et al. (2014) have studied two-stepped hulls by various transverse step configurations and displacements. They observed that in all cases, two-stepped hulls led to a resistance reduction. Some researchers have also tried to develop numerical methods for calm water performance prediction of stepped hulls. Brizzolara and Federici (2013) used Computational Fluid Dynamics (CFD) to investigate the resistance reduction in stepped planing hulls. Sheingart (2014) investigated the influence of a cambered-shaped step on the performance of V-stepped planing hulls using a numerical method. Dashtimanesh et al. (2018) tried to develop a numerical setup based on the morphing mesh approach in CD-Adapco StarCCM+ in which the two-stepped planing hull was free to heave and pitch.

Moreover, some researchers have developed mathematical models to evaluate the stepped hulls performance. Svahn (2009) used the existing wake formulas (Savitsky and Morabito, 2010) and extended Savitsky's (1964) method for performance prediction of one-stepped hulls. Danielsson and Strumquist (2012) tried to develop Svahn's model for two-stepped hulls. However, they failed in the implementation of the wake formula for the two-stepped hull because of its range of applicability and other issues. Accordingly, Dashtimanesh et al. (2017) assumed a Linear Wake Pattern and presented a simplified mathematical model for performance prediction of double-stepped planing hulls based on Savitsky's formulas. Then, Niazmand et al. (2019 and 2020b) developed a mathematical model based on the 2D + T method for the performance prediction of two-stepped hulls.

It is worth mentioning although there are many studies about calm water performance of stepped hulls, the effects of step height and position, the number of steps and step shape are still unknown. The focus of most of the previous studies has been on transverse steps while transverse steps are not the case suitable for industrial/commercial applications where forward or backward V-shaped steps, instead, are largely implemented. To tackle this challenge, towing tank measurements can be used to provide an early understanding of the performance of boats with various step shapes, numbers, heights and positions.

Therefore, in the current work, an experimental campaign, conducted on a new systematic series of stepped hulls with various step configurations, has been designed at the naval section of *Dipartimento di Ingegneria Industriale (DII)* of the *Università degli Studi di Napoli "Federico II*. This study aims to measure resistance, trim, sinkage and wetted surface for eight stepped hull models with a systematic variation of relevant design parameters, i.e. step numbers, step height, and longitudinal step position in three different starting trim conditions. All models are built with a transparent bottom hull to visualize the complicated fluid flows underneath the stepped hulls. All experimental tests have been performed in calm water and it has been tried to capture the wetted surface during the towing tank tests. All the 3D CAD models are available on Github (Vitiello, 2022).

The remaining part of this work has been organized as follows: the Rigid Inflatable Boats (RIB) state of the art has been reported in section 2 where there is a market analysis of the boats similar to the parent's hull. A comparison based on the Gabrielli-von Karman efficiency transport diagram has been provided in addition to a review of available systematic series with and without steps. The description of the models' characteristics, as well as their building details, have been presented in Section 3. In section 4, the facilities with laboratory instrumentation and measurements devices have been described. Moreover, the test procedure has been discussed in Section 5. Results and Discussions along with uncertainty analysis have been reported in Section 6 and the paper has been finalized by a conclusion in Section 7. The towing tank test results are presented in Appendix A, the experimental uncertainty analysis is shown in Appendix B, and the wetted surface photos at all

speeds for all the models are available in Appendix C.

2. State-of-the-art

In this section, a market analysis of boats similar to parent's hull has been reported to have a better understanding of stepped hulls background. It is a comparison based on Gabrielli-Von Karman efficiency transport diagram by considering all available planing hulls systematic series (with and without steps). At the end of this section, a comparison between Taunton's Systematic Series (Taunton et al., 2010) and the present series has been shown.

2.1. Stepped hulls RIB

Table 1 has collected the state of the art of RIB available on the market. In this table have been listed the main boat data, in specific: length overall (L_{OA}), beam max (B), L/B ratio, sea trial power installed, weight/Sea trial power ratio, maximum speed during the sea trial test, $Ⓦ$, S/L, K-value, volumetric Froude number, and Transport efficiency (E_T), that according to Gabrielli and von Kàrmàn (1950), is defined as:

$$E_T = \frac{W \cdot V}{0.102 P_d} \qquad (1)$$

where V is the speed in m/s, W is the displacement in metric tonnes and the P_d is the propeller delivered power in kW. E_T is the weight/power ratio and represents the quality of the whole means of transport. The Gabrielli-von Karman transport efficiency index can be assumed as a sort of "efficiency" ranking based on the maximum speeds of the type of the hull available.

As reported on Gabrielli-von Karman graph in Fig. 1, on abscissa axis there is the volumetric Froude number and on the ordinate axis there is the Transport Efficiency. The hard chine hulls show the best efficiency index at very low Fr_{∇} numbers up to 0.8. At Fr_{∇} between 0.8 and 1.5, the round bilge hulls are the most efficient hulls, and at Fr_{∇} number between 1.5 and 6.0, the Surface Effect Ship (SES) shows the best efficiency index. Finally, for speeds growing up to Fr_{∇} 6.0, the stepped hulls have undisputed supremacy. Specifically, for volumetric Fr higher than 6, there are several stepped planing hulls above the threshold trend line of the hard chine hull, showing the best efficiency of the stepped hull at these extremely high speeds. The following stepped RIBs, in ascending order of Fr_{∇}, have a better Gabrielli-von Karman efficiency index comparing with hard chine hulls: Anvera 48, Technohull Omega 45, Magazzu MX 12 and MX 11, Buzzi 42, MV Marine Mito 31 (Fig. 2), Technohull 38 Grand Sport.

Fig. 1. Gabrielli-von Karman – transport efficiency index.

2.2. Systematic series overview

The state-of-the-art planing hull systematic series has been shown in Table 2 where there are 7 hard chine hull series and 2 stepped hull series.

Warped hard chine hulls (Naples Systematic Series - *NSS*) reported in De Luca and Pensa (2017) were designed at the naval section of the *Dipartimento di Ingegneria Industriale* (*DII*) of the *Università degli Studi di Napoli "Federico II"* as the VMV Stepped Hull series shown in this paper. The NSS series was designed with a deadrise angle constantly growing from astern to forward and by an A_T/A_X close to 1.0.

The other systematic series with a single chine (Hubble, 1974; Keuning and Gerritsma, 1982; Keuning et al., 1993; Taunton et al., 2010) have a constant deadrise angle along one-third of the hull.

Taunton's systematic series (Taunton et al., 2010) and the present VMV Series have the same B_{TC}/B_C ratio but with a different section geometry. In Taunton et al. (2010) a monohedric hull bottom with a constant deadrise angle of 22.5° is considered, on the contrary, in VMV Series there is warped bottom with a transom deadrise angle of 23.0° and an angle of 31.0° at the midship section. The following Table 2 summarizes the main hull data of the referenced series.

A detailed comparison between the Taunton's systematic series (Taunton et al., 2010) and VMV Series has been presented in Table 3. The main differences are related to, the hulls' dimensions, the

Table 1
The state of the art of RIBs.

Shipyard	Model (Commercial name)	L_{OA}	B	L/B	Δ	P	Δ/P	V_{max}	Ⓦ	S/L	Fr_{∇}	E_T
		[m]	[m]		[t]	[HP]		[Kn]				
Anvera	48	14.50	4.91	2.95	10.00	740	13.51	44	6.79	6.38	4.94	4.01
BSK Marine Skipper	NC 100C	9.85	2.90	3.40	2.68	800	3.35	70	7.15	12.31	9.80	1.58
BSK Marine Skipper	Desire 120S	12.40	3.50	3.54	6.50	1880	3.46	70	6.70	10.97	8.45	1.63
Buzzi	42 RIB sport	13.20	3.60	3.67	9.02	1730	5.21	70	6.39	10.64	8.00	2.46
Joker Boat	Clubman 30	9.50	3.28	2.90	4.00	600	6.67	48	6.03	8.60	6.28	2.16
Magazzù	MX-11 coupè	11.00	3.80	2.89	5.50	900	6.11	60	6.28	9.99	7.45	2.47
Magazzù	MX-12 gransport	12.00	4.80	2.50	6.00	900	6.67	60	6.66	9.56	7.34	2.70
MV Marine	Mito 29	8.65	3.30	2.62	2.87	600	4.78	58	6.14	10.89	8.02	1.87
MV Marine	Mito 31	9.35	3.30	2.83	3.20	600	5.33	60	6.40	10.83	8.15	2.16
MV Marine	Mito 40	12.14	3.86	3.15	5.98	900	6.64	53	6.74	8.40	6.49	2.38
MV Marine	Mito 45	13.50	4.18	3.23	5.65	740	7.64	44	7.64	6.61	5.44	2.27
Pirelli	1400	13.70	3.64	3.76	7.95	900	8.83	51	6.92	7.61	5.95	3.04
Pirelli	42	13.10	4.10	3.20	8.50	800	10.63	46	6.47	7.02	5.31	3.30
Tecnohull	seaDNA999	10.30	2.80	3.68	2.70	300	9.00	40	7.46	6.88	5.59	2.43
Tecnohull	38 Grand Sport	11.10	3.20	3.47	4.20	1350	3.11	103	6.94	17.07	13.37	2.16
Tecnohull	Explorer 40	12.10	3.50	3.46	4.50	900	5.00	60	7.39	9.52	7.70	2.02
Tecnohull	Omega 45	13.80	3.50	3.94	5.93	900	6.59	58	7.69	8.62	7.11	2.58

Fig. 2. Mito 31 body plan and profile.

Table 2
Planing hull systematic series – state-of-the-art.

Series	L/B range	⊗ range	B_{TC}/B_C
Clement and Blount (1963)	2.00	2.97	0.66
	7.00	8.46	
Keuning and Gerritsma (1982)	1.95	2.99	0.66
	6.82	8.36	
Keuning et al. (1993)	3.41	3.29	0.66
	7.00	8.25	
Hubble – A (1974)	3.20	4.0	0.35
	9.26	10.0	
Hubble – B (1974)	2.32	4.0	1.00
	9.28	10.0	
Kowalyshyn and Metcalf (2006)	3.24	4.98	0.96
	4.50	0.87	
Taunton et al. (2010)	3.77	6.25	1.00
	6.25	8.70	
Grigoropoulos and Loukakis (2002)	4.00	6.18	–
	7.00	10.00	
NSS De Luca and Pensa (2017)	3.24	4.83	0.95
	5.86	7.49	
VMV Stepped Series (present study)	3.41	6.24	1.00

Table 3
Comparison of main characteristics of two stepped hull series, Taunton et al. (2010) and VMV stepped Series (present study).

Model	Unit	Taunton model A	Taunton Model B	Taunton model C	Taunton model D	VMV Stepped Series (present study)
L	[m]	2.00	2.00	2.00	2.00	0.91
B	[m]	0.32	0.39	0.46	0.53	0.268
Δ	[N]	119.25	175.83	243.4	321.95	30.71
$L/\nabla^{1/3}$	[-]	8.7	7.64	6.86	6.25	6.24
L/B	[-]	6.25	5.13	4.35	3.77	3.41
β	[deg]	22.5	22.5	22.5	22.5	23
LCG	[%L]	0.33	0.33	0.33	0.33	from 0.30 to 0.34

displacements, and the design criteria of the hulls.

In Taunton et al. (2010), the length of the hulls has been kept constant and the L/B ratio, B, and step number (with the same step shape) have been varied. Instead, in the present study (VMV Series), L/B ratio has been kept constant and the main focus has been on the effects of

various design parameters on the hull performance (resistance and running attitude). The considered design parameters are including the Number of steps (Ns), Height of steps (Hs) and Longitudinal Step Position (LSP) explained in detail in the next sections.

3. Description of the hull models

3.1. Parent hull

The parent hull used in this study represents an example of a modern high-speed hull for Rigid Inflatable Boats (RIB). This hull can be a representative hull for typical pleasure or military high-speed craft. The parent hull comes from a RIB built by MV-Marine S.r.l., type Mito 31 (Fig. 2) powered with two outboard engines.

The assumed parent hull is a traditional stepped hull with longitudinal spray rails and without an artificial bottom cavity or artificially inflated air in the cavity and without the bracket for engines. The parent hull is a hard chine hull with two transverse steps with a forward V shape, with the Center of Gravity (CG) located in the center of the surface between the first and second steps. This step shape is different from the arrow-like and transverse bottom step is as reported in Sverchkov (2010). The parent hull performance data are available in Miranda and Vitiello (2014).

All models have the same main geometric dimensions (keel line, chine line, deadrise angle, displacement, LCG, step shape, step angle) of RIB Mito 31, with a 1:10 scale ratio.

Starting from the parent hull, the design parameters have been defined based on a critical review of the literature related to the stepped hull design. The specific design parameters, which have been selected to cover a wide domain of investigation, have been described as follows:

- Step Number (Ns): Following Peters (2010) and Akers (2003), the single or double-step choice depends on the length-to-beam ratio and speed. For instance, a low aspect-ratio lifting surface of a boat with a narrow beam requires two steps for lift.
- Step Height (Hs): Peters (2010) defines a minimum and maximum value for step height (31.8 mm–65.5 mm in full scale). Akers (2003) in accordance with Norman Skene (1938), specifies that high steps are not necessary and that experience shows steps as lower as 16 mm could be effective. Sailing at high speed, a high height of steps could affect the angle of attack of the flow on the eventual successive steps conditioning the buttock lines behind the first step.
- About Longitudinal Step Position (LSP), there are different approaches in the literature. The first one, in accordance with

Acampora and Racer (1995), Akers (2003) and Peters (2010), is based on the idea that it is necessary to have the LCG close to the forebody stagnation line to have a correct distribution of the vertical forces between forebody and after body (Savitsky and Morabito, 2010). The second one, according to Clement and Pope (1961), derives the LSP as a function of the main hull geometric parameters. However, the step is always further forward than the LCG. The third one, based on Clement (1964), defines a design approach for a stepped hull similar to hydrofoil boats or aeroplanes. This approach tries to find the optimum configuration of a lifting surface to obtain a maximum lift-drag ratio. The CG position, as well as the centre of pressure, are not negligible points since they could trigger dynamic instabilities phenomena.

Based on the abovementioned design parameters, the hull models of the present series have been generated by varying the number of steps (1 or 2), the Hs (20 mm and 60 mm, full scale), and the LSP, as summarized in Table 4.

3.2. Models identifications

All the models in the present study are identified with an Identification Number (ID). This ID is composed of six alphanumeric characters (i.e. C02_1_20_0), in particular:

- C02 – indicated the hull progressive number, from 2 to 9.
- 1 – Indicate the step number (1 or 2).
- 20 – Indicate the step height in mm (20 or 60 mm in full scale, the scale factor is 10).
- 0 – Indicate the Longitudinal Step Position: 0 for LSP = LCG; 1 for LSP 140 mm forward of LCG.

In Table 4, all models are reported with their geometric characteristics. O-XYZ is located at the intersection between keel line and transom with X-axis positive forward, Y-axis positive right hand, and Z-axis positive up.

3.3. Models building

The hull models for towing tank tests were designed with commercially available 3D CAD software. The 3D CAD files are available on the Github platform (Vitiello, 2022). To provide a full view of the water flow under the hull, the models have a full transparent bottom built only with high-gloss neopentylic gelcoat transparent surface and isophthalic transparent resin. The side of the model was built in Fibre Reinforced Plastic (FRP) with a surface of high-gloss neopentylic gelcoat transparent, isophthalic transparent resin and two layers of glass fibre Chopped Strand Mat (CSM) of 450 gr/m^2, to ensure the necessary structural strength.

The hull models are built with female moulds realized with a hand-made layup with composite materials. In order to build the female mould, in a hand-made layup, was manufactured a model for the mould. The model for the mould was designed in 3D CAD/CAM and the female mould was built in FRP, the two parts are built through the following step:

- milling of high-density PVC foam with CNC five-axis machine with a rough finish to build a *model for mould*;
- covered with a spray polyester paste;
- milling the foam covered with the polyester pastes with CNC machine five-axis with a good finish;
- spraying the polyester gelcoat;
- tooling in hand-made and after applying the polish and wax;
- spraying the polyester gelcoat for mould;
- laminating the FRP with glass CSM and isophthalic resin in hand-made layup;

CAD/CAM building process ensures that the model hull tolerances (for breadth, draught, and length) are in the range of ±0.5 mm, as requested by the ITTC procedures (7.5-01-01-01, 2002). In particular, the length manufacturing tolerance is less than 0.05%, and very special attention was paid to the shaping of chines and steps to ensure very hard edges.

4. Facility and equipment

The calm water tests were conducted in the towing tank of the naval section of the *Dipartimento di Ingegneria Industriale (DII)* of the *Università degli Studi di Napoli "Federico II"*. Details of the towing tank are outlined in Table 5. The front view of the tank carriage is shown in Fig. 3.

The details of the laboratory instrumentation implemented in the experimental tests and the measurement techniques are reported in Appendix A and also available in De Marco et al. (2017).

The dynamometer carriage is equipped with a Programmable Logic Controller, a sensor network and a Data-AcQuisition (DAQ) device. The sensors necessary for these tests are an encoder for measuring the speed carriage, the load cell for resistance measurement, the balance for models and ballast weights, a digital thermometer for acquiring the water temperature, an accelerometer for trim measurement, two lasers (one located at the stern and another located at the bow of the model) for sinkage measurement, two photo cameras and one video camera for sinkage measurement, wetted surface and the vortex phenomena recording.

The digital thermometer used during the tests allows a range from −5 °C to 40 °C, with an accuracy of 0.1 °C and a resolution of 0.1 °C as reported on the datasheet.

The dynamometer carriage speed was measured by a high-quality

Table 4
Geometric characteristics of the hull models.

ID number	Steps Number; (N_S)	Step Height (H_S)	Longitudinal Step Position (LSP)	Longitudinal Center of Buoyancy (LCB)
		[mm]	[mm]	[mm]
C02_1_20_0	1	2	0: step 1 = 300 mm	277
C03_1_60_0	1	6	0: step 1 = 301 mm	291
C04_1_20_1	1	2	+1.4: step 1 = 440 mm	276
C05_1_60_1	1	6	+1.4: step 1 = 441 mm	286
C06_2_20_0	2	2	0: step 1 = 147 mm step 2 = 300 mm	283
C07_2_60_0	2	6	0: step 1 = 149 mm step 2 = 302 mm	307
C08_2_20_1	2	2	+1.4: step 1 = 288 mm step 2 = 441 mm	282
C09_2_60_1	2	6	+1.4: step 1 = 290 mm step 2 = 443 mm	310

Table 5
Main particulars of the towing tank of *Università di Napoli "Federico II"*.

Parameter	Value	Unit
Length of the tank	137.0	m
Width of the tank	9.0	m
Depth of the tank	4.25	m
Maximum carriage speed	10.0	m/s
Max acceleration/deceleration	±1.0	m/s^2

Fig. 3. A front view of the carriage of the *Università di Napoli "Federico II"* towing tank.

encoder and a counter/timing card. The high-quality encoder was not fixed to any wheel drive of carriage and rolls without rolling resistance driven by the carriage (it gives 1000 pulses per one round, 1 pulse for each mm). The encoder sensor has an accuracy of 1 mm/m and a resolution of 1 mm. The period between two pulses was measured by a counter/timing card at 32 bits with a clock of 80 MHz. The card has a range from 1.25×10^{-8} s to 53.69 s; the clock at 80 MHz has an accuracy of $\pm 4 \times 10^{-3}$ MHz and a resolution of 1.25×10^{-8} s.

The resistance measurements were acquired by a high-quality load cell (precision class 0.003) with a conditioning-acquisition card. The specific load cell used in this test has a range up to 50 N, an accuracy of 0.003%, and a resolution of 0.005 N. The conditioning-acquisition card has a software programmed range of 50 N, an accuracy of 0.08%, 16-bit resolution, and a sampling rate up to 200 kSamples/s. For these measurements, the row data were oversampled at a rate of 10 kSamples/s and compressed at a rate of 500 Samples/s for ulterior reduction of the noise.

Running trim measurements were performed by an accelerometer and a conditioning-acquisition card. The accelerometer sensor has a range of 40 m/s^2, accuracy of $\pm 0.1\%$, and resolution virtually infinite. The conditioning-acquisition card has a software programmed range of 40 m/s^2, an accuracy of 0.1%, and a 16-bit resolution.

Sinkage was measured by two high-quality laser sensors and a conditioning-acquisition card. The two lasers have a range from 0.2 to 1 m, an accuracy of 0.5 mm, and a resolution of 0.05 mm. These laser devices were placed perpendicularly on the water surface, at two different positions (at the fore section and the aft section of the models). The conditioning-acquisition card has a software programmed range of up to 1 m, an accuracy of 0.1%, and a 16-bit resolution.

The weight of the model and ballast were measured with a scale with a range of 600 N, accuracy of ± 0.1 N, and resolution of 0.1 N.

5. Test procedure

Calm water measurements are performed following the ITTC procedures (7.5-02-02-01, 2011) with a stop (over 10 min) between two consecutive runs to ensure calm water condition. The displacement condition for resistance tests is 30.705 N with three different trim conditions ($+1°$, $-1°$, and $0°$ trim) and eight speeds: 1.290, 2.357, 3.131, 4.631, 5.368, 6.340, 7.301, and 8.050 m/s (Appendix A).

Speed, resistance, sinkage, trim angle and photo/video recording are the data acquired. Digital photos and videos for each run were acquired by three cameras, one in the right-fore hand, the second in the right-aft hand and the third camera with a 50 mm lens placed on the towing

carriage, in a perpendicular position to the model's centre of gravity. This third camera was set for the measurement of dynamic wetted surface and capturing the vortical flow under the hull.

The resistance dynamometer has been placed on the towing carriage and connected to the model through a quasi-inextensible rope Spectra™, which is a super fibre made by Honeywell©. The calm water resistance experiments are conducted with a "Down-Thrust" (DT) methodology according to Miranda and Vitiello (2014). The towed point is located in the intersection between the direction of thrust of engines and the keel line at the bow. In this way, the model tested has 4 degrees of freedom with only the yaw and drift motions restricted. To avoid any instability phenomena, the models have been built with two guide masts, realized in carbon fibre, located at the bow and at the stern, which engage two forks in stainless steel (Fig. 4). DT measurement solution ensures the high sensitivity of the hull model to the externally applied forces (*i.e.* the instrumentation weight). The DT procedures can be considered as a free running-like resistance test and this solution ensures reproducing the real system of forces exerted by the outboard engines and the same dynamics of the real boat.

The sinkage is calculated through the measurements of two lasers located in the fore and aft section of the model, acquired by a digital photo made with a 50 mm camera placed perpendicularly to the model's centre of gravity (CG) and elaborated with a 3D CAD model.

To estimate the dynamic wetted surface, as mentioned above, a hull with transparent bottom was built to ensure a full view of the water flow under the hull. The experimental wetted surface values are estimated through digital analysis of video frames acquired by a 50 mm camera put on CG. For each speed, the top view pictures (see Appendix C) acquired from the camera are post-processed with the 3D CAD software to measure the dynamic wetted surface.

6. Results and Discussions

The results of calm water resistance tests are presented in Appendix A. The experimental results are exposed in terms of non-dimensional total resistance (RT_M/Δ), dynamic trim angle (τ), non-dimensional dynamic sinkage ($Z_G/\nabla^{1/3}$), and non-dimensional dynamic wetted surface ($S/\nabla^{2/3}$). The results are raw data without a fairing post-process.

The uncertainty Analysis (UA) of the towing tank test results, reported in Appendix B, has been carried out following the ITTC procedures for uncertainty analysis in resistance towing tank tests (7.5-02-02-02, 2002). The UA shows a total uncertainty in an acceptable range for planing hull towing tank tests. The measures with the highest uncertainty are the sinkage and wetted surface. The wetted surface uncertainty is mainly related to the spray areas which are difficult to be estimated based on the recorded photos and videos.

An interesting finding of the present experimental campaign is the observation, thanks to the hulls' transparent bottom, of some vortices developing into the aft body region behind the step and partially continuing downstream in the wake. This vortex phenomenon has been detected only for hull models with a step height of 6 mm and appears at speeds greater than 2.36 m/s (Fr$_\nabla$ >1.97). This vortex phenomenon was already described in De Marco et al. (2017) and the towing tank video recording of the C03 hull was openly released on 2016 (Vitiello and Miranda, 2016). For more details, fluid flow and wetted surface pictures of present stepped hulls in trimmed forward condition at all speeds are reported in Appendix C.

Analyzing and comparing the resistance test results in the range of Fr$_\nabla$ between 5 and 6.7 (very-high-speed), the hull C04 trimmed aft has the best performance. In the range of Fr$_\nabla$ between 3.4 and 5 (high-speed), the best results are for the hull C05 trimmed aft. For the range of Fr$_\nabla$ between 2.6 and 3.4 (medium-speed range), the best hull is the C05 even keel, and in the range of Fr$_\nabla$ between 1.1 and 2.6 (low-speed range), the best results are for the hull C06 trimmed fore.

Regarding the effect of static trim angle on the hull performance, the experimental results are according to the general principles that for low
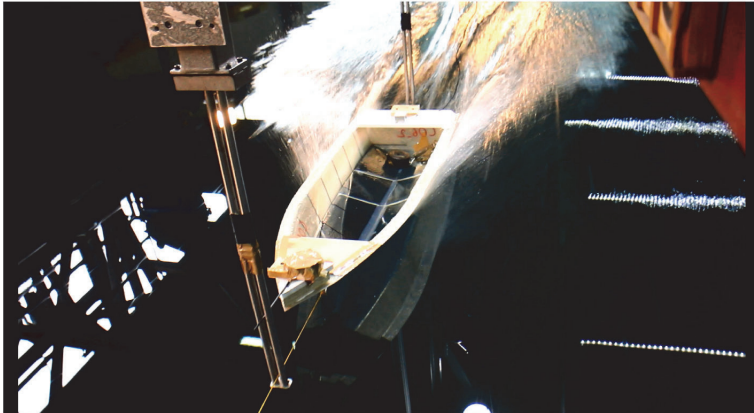
Fig. 4. Towing tank test with down-thrust methodology.

speeds a low resistance (compared with the even keel condition) is detected on the hull trimmed fore cases. On the contrary, at high speeds, low resistance (compared with the even keel condition) is detected on the hull trimmed aft cases.

Regarding the step geometric parameters, the results show that the single-step configuration is effective at almost all speed ranges (except at low speeds). Increasing the hull speeds, a decrement of step height allows a resistance reduction. Furthermore, moving forward the step (increasing LSP) at low speeds decrease the resistance.

7. Conclusions

Calm water resistance experiments have been conducted at towing tank of the naval section of the *Dipartimento di Ingegneria Industriale (DII) della Università degli Studi di Napoli "Federico II"*, on 8 models of a new stepped hull model series.

Towing tank tests are performed by implementing the "Down-Thrust" methodology since all the hull models are low-weighs and are sensitive to the externally applied forces, indeed the "Down-Thrust" methodology is able to keep free the model from the equipment and instrumentation weights. Furthermore, this testing methodology, developed exclusively for these towing tank tests, allows reproducing the real system of forces on the hull at full scale.

All models were built with a transparent bottom with the aim to quantify the wetted surface and observe the vortical flow phenomena on the area(s) behind the step(s). These vortex structures have been detected only in the hulls with a height step of 6 mm (model scale) and confirmed via CFD simulations, as reported in De Marco et al. (2017).

The results of calm water resistance tests are presented in Appendix A, where all values acquired are plotted against the volumetric Froude number (Fr$_\nabla$). In particular, the non-dimensional total resistance (RT$_M$/Δ), the dynamic trim angle (τ); the non-dimensional dynamic sinkage (Z$_G$/$\nabla^{1/3}$), and the non-dimensional dynamic wetted surface (S/$\nabla^{2/3}$) are shown for each hull in three different static equilibrium conditions: even keel, trimmed aft, and trimmed fore. The results for each model are shown in graphical and tabular ways. All the models' hull lines and the 3D CAD surface are openly available for research and investigation in the academic, technical, and practitioner communities.

The uncertainty analysis of the experimental results is performed in compliance with the ITTC guidelines and shows an acceptable level of accuracy.

The proposed VMV stepped hull planing series is intended to be a support to designers and boat builders that intend to design a stepped hull. In future works, the authors want to extensively apply the CFD tool on these hulls for both calm water and seakeeping tests with the idea to extend the present results for speed over Fr$_\nabla$ = 6.724 (over 50 knots in boat speed).

CRediT authorship contribution statement

Luigi Vitiello: Conceptualization, Methodology, Towing Tank Test, Visualization, Writing – original draft. **Simone Mancini:** Resources, Investigation, Data curation, Writing – review & editing. **Rasul Niazmand Bilandi:** Data curation, Formal analysis, Visualization, Writing – original draft. **Abbas Dashtimanesh:** Supervision, Writing – review & editing. **Fabio De Luca:** Data curation, Writing – review & editing. **Vincenzo Nappo:** Data curation, Formal analysis, model building & data analysis.

Declaration of competing interest

The authors declare that they have no known competing financial interests or personal relationships that could have appeared to influence the work reported in this paper.

Data availability

No data was used for the research described in the article.

Acknowledgements

Appendix A. Towing tank test results

Hull model C02_1_20_0

ID number	Steps Number; N_S	Step Height; H_S [mm]	Longitudinal Step Position; LSP [mm]	Longitudinal Center of Buoyancy; LCB [mm]
C02_1_20_0	1	2	0: step 1 = 300 mm	277
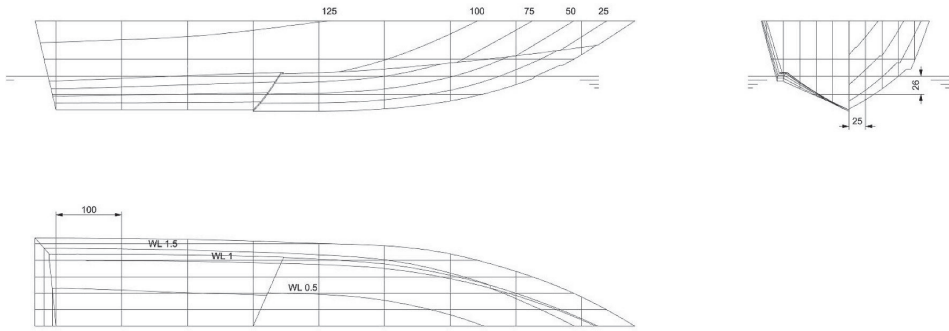
Fig. 5. C02 model lines plan: Sheer Plan, body plan, half breadth plan. Transversal section every 0.100 m, buttock line every 0.025 m, water lines every 0.026 m.

Hull model C02_1_20_0 - calm water towing tank test data

C2 evenkeel	V_M [m/s]	V_S [Knots]	Fr_L	Fr_∇	τ [deg]	Z_G [mm] + up	Z_O [mm] + up	$\dfrac{RT_M}{\Delta}$	$\dfrac{Z_G}{\nabla^{1/3}}$	$\dfrac{S_W}{\nabla^{2/3}}$
	1.29	7.93	0.47	1.077	2.46	−7.39	−19.99	0.100	−0.051	5.55
	2.36	14.49	0.87	1.968	4.13	5.31	−16.29	0.169	0.036	5.39
	3.13	19.25	1.15	2.614	4.99	14.46	−10.44	0.203	0.099	4.68
	4.63	28.47	1.70	3.865	3.84	19.46	1.26	0.259	0.133	3.99
	5.37	33.00	1.97	4.482	3.32	36.69	11.12	0.306	0.251	3.77
	6.34	38.98	2.33	5.290	3.04	23.77	7.87	0.382	0.162	3.36
	7.30	44.88	2.68	6.095	2.99	28.20	13.30	0.452	0.193	3.00
	8.05	49.49	2.96	6.724	3.16	30.56	14.36	0.498	0.209	2.75
C2 trimmed aft	V_M [m/s]	V_S [Knots]	Fr_L	Fr_∇	τ [deg]	Z_G [mm] + up	Z_O [mm] + up	$\dfrac{RT_M}{\Delta}$	$\dfrac{Z_G}{\nabla^{1/3}}$	$\dfrac{S_W}{\nabla^{2/3}}$
	1.29	7.93	0.47	1.077	2.64	−2.55	−16.95	0.104	−0.017	5.10
	2.36	14.49	0.87	1.968	4.53	7.68	−15.72	0.176	0.053	4.95
	3.13	19.25	1.15	2.614	2.46	5.06	−6.64	0.223	0.035	4.84
	4.63	28.47	1.70	3.865	2.41	18.33	6.63	0.296	0.125	4.71
	5.37	33.00	1.97	4.482	2.41	19.24	7.24	0.317	0.132	4.11
	6.34	38.98	2.33	5.290	2.46	28.85	16.85	0.365	0.197	3.20
	7.30	44.88	2.68	6.095	2.29	32.19	20.49	0.429	0.220	2.79
	8.05	49.49	2.96	6.724	2.46	31.25	19.25	0.472	0.214	2.55
C2 trimmed fore	V_M [m/s]	V_S [Knots]	Fr_L	Fr_∇	τ [deg]	Z_G [mm] + up	Z_O [mm] + up	$\dfrac{RT_M}{\Delta}$	$\dfrac{Z_G}{\nabla^{1/3}}$	$\dfrac{S_W}{\nabla^{2/3}}$
	1.29	7.93	0.47	1.077	2.24	−8.18	−18.68	0.088	−0.056	6.04
	2.36	14.49	0.87	1.968	4.08	−0.93	−20.73	0.169	−0.006	5.87
	3.13	19.25	1.15	2.614	5.29	24.28	−1.82	0.206	0.166	5.09
	4.63	28.47	1.70	3.865	4.77	38.09	14.99	0.264	0.260	4.27
	5.37	33.00	1.97	4.482	4.36	39.93	15.33	0.313	0.273	4.09
	6.34	38.98	2.33	5.290	4.13	22.22	−0.88	0.400	0.152	3.66
	7.30	44.88	2.68	6.095	4.02	41.41	21.88	0.483	0.283	3.23
	8.05	49.49	2.96	6.724	4.07	48.15	25.35	0.524	0.329	2.91
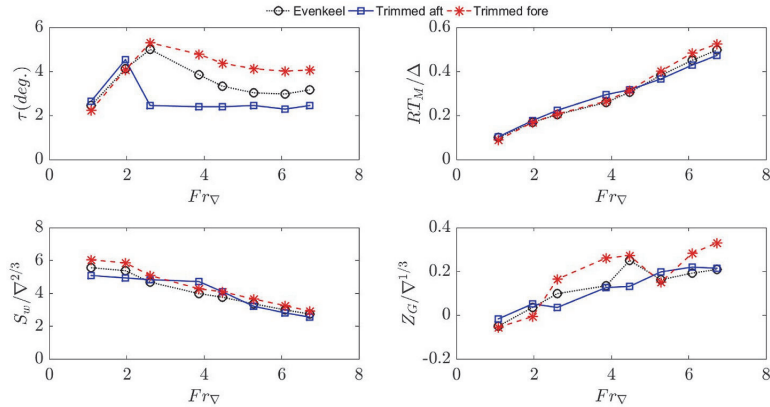
Fig. 6. Results of C02 hull for dynamic trim, resistance, wetted surface, and dynamic sinkage at states of even keel, trimmed aft, and trimmed fore.

Hull model C03_1_60_0

ID number	Steps Number; N_S	Step Height; H_S [mm]	Longitudinal Step Position; LSP [mm]	Longitudinal Center of Buoyancy; LCB [mm]
C03_1_60_0	1	6	0: step 1 = 301 mm	291

Fig. 7. C03 model lines plan: Sheer Plan, body plan, half breadth plan. Transversal section every 0.100 m, buttock line every 0.025 m, water lines every 0.025 m.

Hull model C03_1_60_0 - calm water towing tank test data.

C3 evenkeel	V_M [m/s]	V_S [Knots]	Fr_L	Fr_∇	τ [deg]	Z_G [mm] + up	Z_O [mm] + up	$\dfrac{RT_M}{\Delta}$	$\dfrac{Z_G}{\nabla^{1/3}}$	$\dfrac{S_W}{\nabla^{2/3}}$
	1.290	7.93	0.474	1.077	2.23	−11.68	−22.26	0.088	−0.080	6.48
	2.357	14.49	0.866	1.968	3.55	1.52	−17.99	0.178	0.010	6.29
	3.131	19.25	1.151	2.614	4.42	6.95	−15.30	0.204	0.048	4.32
	4.629	28.47	1.702	3.865	3.27	12.37	6.16	0.256	0.085	3.57
	5.368	33.00	1.973	4.482	2.87	20.39	7.20	0.312	0.139	3.33
	6.336	38.98	2.330	5.290	2.69	21.50	8.14	0.407	0.147	3.09
	7.301	44.88	2.683	6.095	2.52	22.15	9.07	0.491	0.151	2.62
	8.054	49.49	2.958	6.724	2.58	26.44	13.41	0.556	0.181	2.48
C3 trimmed aft	V_M [m/s]	V_S [Knots]	Fr_L	Fr_∇	τ [deg]	Z_G [mm] + up	Z_O [mm] + up	$\dfrac{RT_M}{\Delta}$	$\dfrac{Z_G}{\nabla^{1/3}}$	$\dfrac{S_W}{\nabla^{2/3}}$
	1.29	7.93	0.47	1.077	2.47	−5.26	−18.26	0.116	−0.036	6.07
	2.36	14.49	0.87	1.968	4.21	7.12	−14.78	0.189	0.049	5.89
	3.13	19.25	1.15	2.614	4.26	9.67	−3.23	0.209	0.066	4.59
	4.63	28.47	1.70	3.865	2.64	26.47	13.57	0.265	0.181	3.76
	5.37	33.00	1.97	4.482	2.18	23.39	13.49	0.305	0.160	3.00

(continued on next page)

(*continued*)

	V_M [m/s]	V_S [Knots]	Fr_L	Fr_∇	τ [deg]	Z_G [mm] + up	Z_O [mm] + up	$\dfrac{RT_M}{\Delta}$	$\dfrac{Z_G}{\nabla^{1/3}}$	$\dfrac{S_W}{\nabla^{2/3}}$
	6.34	38.98	2.33	5.290	1.89	25.51	15.61	0.369	0.174	2.32
	7.30	44.88	2.68	6.095	2.12	32.80	21.40	0.443	0.224	2.24
C3 trimmed fore	8.05	49.49	2.96	6.724	2.18	29.83	18.13	0.486	0.204	2.16
	1.29	7.93	0.47	1.077	1.89	−9.83	−16.73	0.090	−0.067	6.01
	2.36	14.49	0.87	1.968	3.67	2.11	−18.59	0.189	0.014	5.84
	3.13	19.25	1.15	2.614	3.95	0.41	−20.59	0.270	0.003	4.83
	4.63	28.47	1.70	3.865	4.24	19.23	−3.87	0.269	0.131	3.81
	5.37	33.00	1.97	4.482	3.95	4.77	5.97	0.332	0.033	3.62
	6.34	38.98	2.33	5.290	3.72	20.35	−0.35	0.413	0.139	3.04
	7.30	44.88	2.68	6.095	3.66	20.59	−0.11	0.500	0.141	3.02
	8.05	49.49	2.96	6.724	3.66	25.68	5.28	0.558	0.176	2.99
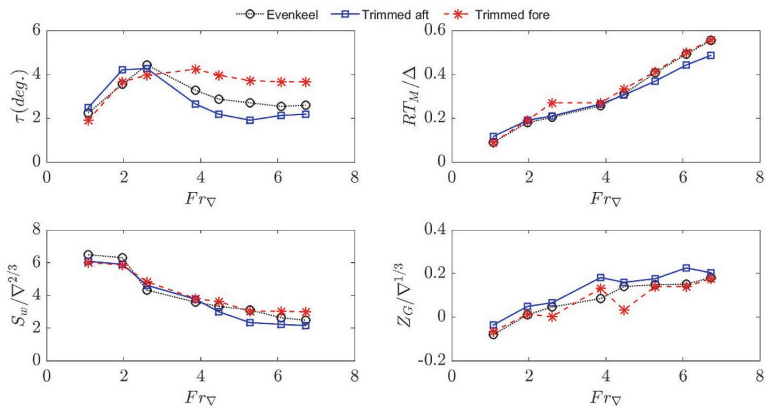
Fig. 8. Results of C03 hull for dynamic trim, resistance, wetted surface, and dynamic sinkage at states of even keel, trimmed aft, and trimmed fore.

Hull model C04_1_20_1

ID number	Steps Number; N_S	Step Height; H_S [mm]	Longitudinal Step Position; LSP [mm]	Longitudinal Center of Buoyancy; LCB [mm]
C04_1_20_1	1	2	+1.4: step 1 = 440 mm	276
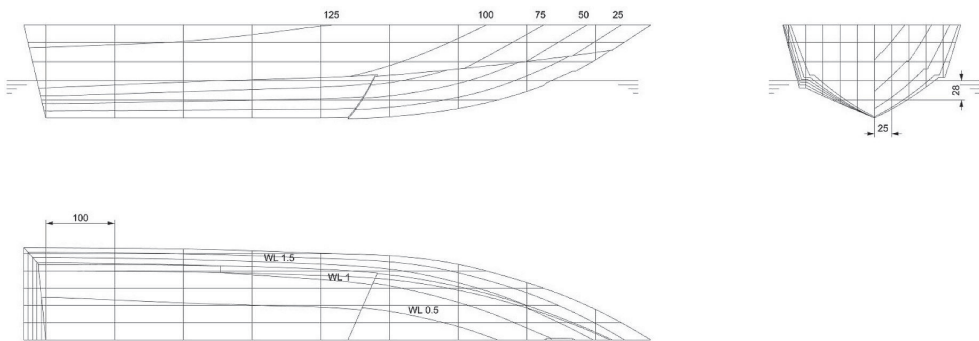
Fig. 9. C04 model lines plan: Sheer Plan, body plan, half breadth plan. Transversal section every 0.100 m, buttock line every 0.025 m, water lines every 0.028 m.

Hull model C04_1_20_1 - calm water towing tank test data.

	V_M [m/s]	V_S [Knots]	Fr_L	Fr_∇	τ [deg]	Z_G [mm] + up	Z_O [mm] + up	$\dfrac{RT_M}{\Delta}$	$\dfrac{Z_G}{\nabla^{1/3}}$	$\dfrac{S_W}{\nabla^{2/3}}$
C4 evenkeel										
	1.29	7.93	0.47	1.077	2.47	−6.84	−18.54	0.097	−0.047	5.59
	2.36	14.49	0.87	1.968	4.14	2.97	−17.73	0.172	0.020	5.42
	3.13	19.25	1.15	2.614	4.94	20.54	−6.16	0.213	0.140	4.82
	4.63	28.47	1.70	3.865	3.84	24.36	3.36	0.280	0.167	3.86
	5.37	33.00	1.97	4.482	3.44	28.43	10.43	0.322	0.194	3.78
	6.34	38.98	2.33	5.290	3.21	26.71	9.01	0.378	0.183	3.46
	7.30	44.88	2.68	6.095	3.15	27.12	12.12	0.447	0.185	3.34
	8.05	49.49	2.96	6.724	3.09	31.58	16.61	0.491	0.216	3.20
C4 trimmed aft										
	1.29	7.93	0.47	1.077	2.58	−5.19	−17.79	0.107	−0.035	5.69
	2.36	14.49	0.87	1.968	4.59	6.79	−17.81	0.187	0.046	4.49
	3.13	19.25	1.15	2.614	4.71	21.18	−3.42	0.215	0.145	3.96
	4.63	28.47	1.70	3.865	3.21	28.73	14.43	0.266	0.196	3.72
	5.37	33.00	1.97	4.482	2.74	26.78	11.48	0.304	0.183	3.25
	6.34	38.98	2.33	5.290	2.52	28.79	16.69	0.359	0.197	3.22
	7.30	44.88	2.68	6.095	2.35	27.32	15.32	0.418	0.187	2.95
	8.05	49.49	2.96	6.724	2.29	35.35	23.44	0.451	0.242	2.71
C4 trimmed fore										
	1.29	7.93	0.47	1.077	1.15	−7.43	−19.43	0.081	−0.051	6.20
	2.36	14.49	0.87	1.968	4.01	−1.04	−22.04	0.167	−0.007	6.02
	3.13	19.25	1.15	2.614	5.17	10.28	−16.72	0.212	0.070	5.73
	4.63	28.47	1.70	3.865	4.65	22.85	−1.15	0.288	0.156	4.48
	5.37	33.00	1.97	4.482	4.24	24.92	0.92	0.319	0.170	4.26
	6.34	38.98	2.33	5.290	4.07	22.42	1.42	0.400	0.153	3.99
	7.30	44.88	2.68	6.095	4.01	27.78	6.78	0.463	0.190	3.41
	8.05	49.49	2.96	6.724	3.96	27.84	6.84	0.513	0.190	3.27
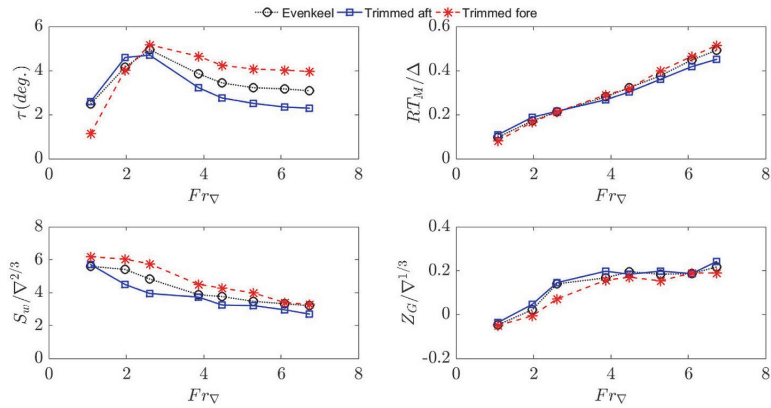
Fig. 10. Results of C04 hull for dynamic trim, resistance, wetted surface, and dynamic sinkage at states of even keel, trimmed aft, and trimmed fore.

Hull model C05_1_60_1

| ID number	Steps Number; N_S	Step Height; H_S [mm]	Longitudinal Step Position; LSP [mm]	Longitudinal Center of Buoyancy; LCB [mm]
C05_1_60_1	**1**	**6**	**+1.4: step 1 = 441 mm**	**286**
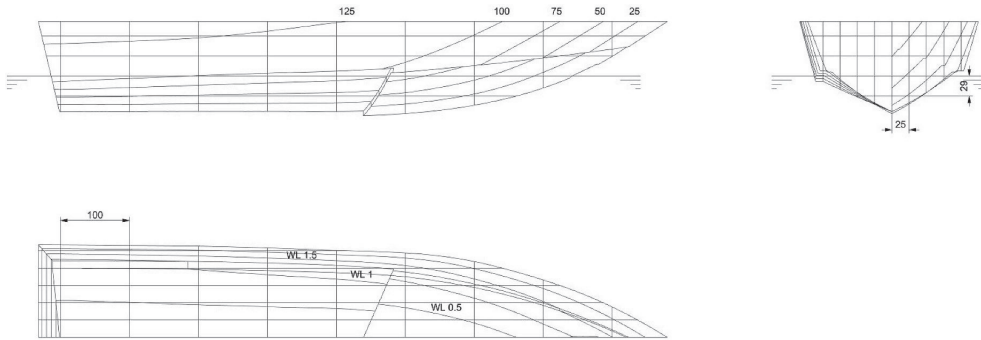
Fig. 11. C05 model lines plan: Sheer Plan, body plan, half breadth plan. Transversal section every 0.100 m, buttock line every 0.025 m, water lines every 0.029 m

Hull model C05_1_60_1 - calm water towing tank test data.

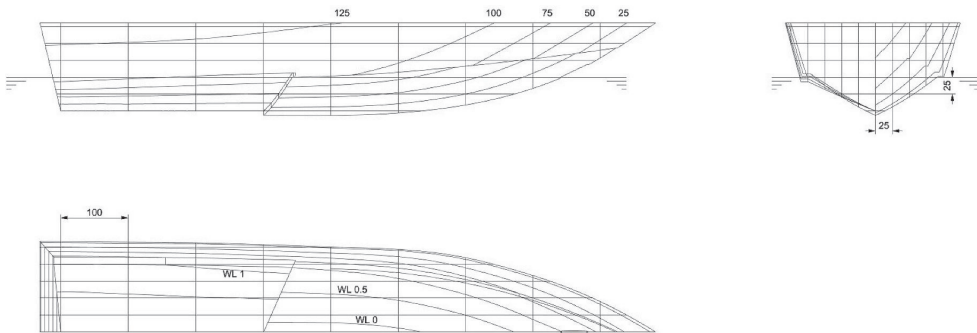| C5 evenkeel	V_M [m/s]	V_S [Knots]	Fr_L	Fr_∇	τ [deg]	Z_G [mm] + up	Z_O [mm] + up	$\dfrac{RT_M}{\Delta}$	$\dfrac{Z_G}{\overline{\nabla}^{1/3}}$	$\dfrac{S_W}{\overline{\nabla}^{2/3}}$
	1.29	7.93	0.47	1.077	2.30	−4.07	−17.02	0.103	−0.028	5.87
	2.36	14.49	0.87	1.968	3.75	7.10	−13.21	0.186	0.049	5.33
	3.13	19.25	1.15	2.614	3.85	13.30	−4.51	0.200	0.091	4.94
	4.63	28.47	1.70	3.865	2.58	19.17	12.15	0.258	0.131	4.18
	5.37	33.00	1.97	4.482	2.18	19.43	10.91	0.301	0.133	3.81
	6.34	38.98	2.33	5.290	1.78	21.72	11.39	0.378	0.148	3.31
	7.30	44.88	2.68	6.095	1.70	31.58	14.96	0.453	0.216	2.83
	8.05	49.49	2.96	6.724	1.61	27.58	14.83	0.525	0.189	2.45
C5 trimmed aft	V_M [m/s]	V_S [Knots]	Fr_L	Fr_∇	τ [deg]	Z_G [mm] + up	Z_O [mm] + up	$\dfrac{RT_M}{\Delta}$	$\dfrac{Z_G}{\overline{\nabla}^{1/3}}$	$\dfrac{S_W}{\overline{\nabla}^{2/3}}$
	1.29	7.93	0.47	1.077	2.52	−2.51	−14.91	0.112	−0.017	5.84
	2.36	14.49	0.87	1.968	4.08	9.04	−11.86	0.191	0.062	5.67
	3.13	19.25	1.15	2.614	3.78	4.99	−4.52	0.204	−0.034	4.42
	4.63	28.47	1.70	3.865	2.58	42.25	−2.17	0.256	0.289	3.88
	5.37	33.00	1.97	4.482	1.32	18.62	19.10	0.293	0.127	3.57
	6.34	38.98	2.33	5.290	0.92	21.32	21.84	0.365	0.146	2.93
	7.30	44.88	2.68	6.095	0.75	23.11	22.99	0.449	0.158	2.70
	8.05	49.49	2.96	6.724	0.69	24.19	24.53	0.511	0.165	2.21
C5 trimmed fore	V_M [m/s]	V_S [Knots]	Fr_L	Fr_∇	τ [deg]	Z_G [mm] + up	Z_O [mm] + up	$\dfrac{RT_M}{\Delta}$	$\dfrac{Z_G}{\overline{\nabla}^{1/3}}$	$\dfrac{S_W}{\overline{\nabla}^{2/3}}$
	1.29	7.93	0.47	1.077	2.00	−5.65	−17.85	0.093	−0.039	5.78
	2.36	14.49	0.87	1.968	3.61	4.93	−18.43	0.192	0.034	5.56
	3.13	19.25	1.15	2.614	3.36	8.42	−13.09	0.220	0.058	5.19
	4.63	28.47	1.70	3.865	3.43	18.98	0.69	0.265	0.130	4.62
	5.37	33.00	1.97	4.482	3.09	19.18	0.64	0.308	0.131	3.90
	6.34	38.98	2.33	5.290	2.92	22.73	4.18	0.382	0.155	3.44
	7.30	44.88	2.68	6.095	2.69	26.24	8.38	0.495	0.179	2.97
	8.05	49.49	2.96	6.724	2.52	28.97	9.68	0.569	0.198	2.61

Fig. 12. Results of C05 hull for dynamic trim, resistance, wetted surface, and dynamic sinkage at states of even keel, trimmed aft, and trimmed fore.

Hull model C06_2_20_0

ID number	Steps Number; N_S	Step Height; H_S [mm]	Longitudinal Step Position; LSP [mm]	Longitudinal Center of Buoyancy; LCB [mm]
C06_2_20_0	2	2	0: step 1 = 147 mm step 2 = 300 mm	283
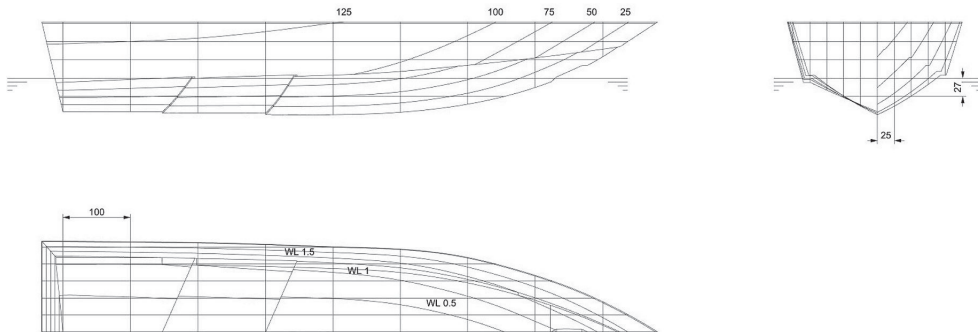
Fig. 13. C06 model lines plan: Sheer Plan, body plan, half breadth plan. Transversal section every 0.100 m, buttock line every 0.025 m, water lines every 0.027 m

Hull model C06_2_20_0 - calm water towing tank test data.

C6 evenkeel	V_M [m/s]	V_S [Knots]	Fr_L	Fr_∇	τ [deg]	Z_G [mm] + up	Z_O [mm] + up	$\dfrac{RT_M}{\Delta}$	$\dfrac{Z_G}{\nabla^{1/3}}$	$\dfrac{S_W}{\nabla^{2/3}}$
	1.29	7.93	0.47	1.077	2.18	−16.00	−17.00	0.090	−0.109	5.93
	2.36	14.49	0.87	1.968	3.50	−9.71	−16.71	0.163	−0.066	5.76
	3.13	19.25	1.15	2.614	3.68	−8.54	−14.54	0.236	−0.058	5.42
	4.63	28.47	1.70	3.865	3.85	10.17	1.12	0.284	0.070	4.45
	5.37	33.00	1.97	4.482	3.33	6.78	0.78	0.341	0.046	4.24
	6.34	38.98	2.33	5.290	3.10	15.00	3.00	0.427	0.103	3.89
	7.30	44.88	2.68	6.095	3.04	7.18	4.18	0.514	0.049	3.64
	8.05	49.49	2.96	6.724	3.04	24.75	8.39	0.589	0.169	3.30
C6 trimmed aft	V_M [m/s]	V_S [Knots]	Fr_L	Fr_∇	τ [deg]	Z_G [mm] + up	Z_O [mm] + up	$\dfrac{RT_M}{\Delta}$	$\dfrac{Z_G}{\nabla^{1/3}}$	$\dfrac{S_W}{\nabla^{2/3}}$
	1.29	7.93	0.47	1.077	2.60	−10.37	−19.62	0.101	−0.071	5.26
	2.36	14.49	0.87	1.968	3.75	−0.18	−14.52	0.168	−0.001	5.10
	3.13	19.25	1.15	2.614	4.73	9.36	−6.39	0.204	0.064	4.68
	4.63	28.47	1.70	3.865	3.05	13.54	10.43	0.273	0.093	3.75
	5.37	33.00	1.97	4.482	2.59	14.06	11.38	0.323	0.096	3.68

(*continued*)

	V_M [m/s]	V_S [Knots]	Fr_L	Fr_∇	τ [deg]	Z_G [mm] + up	Z_O [mm] + up	$\dfrac{RT_M}{\Delta}$	$\dfrac{Z_G}{\nabla^{1/3}}$	$\dfrac{S_W}{\nabla^{2/3}}$
	6.34	38.98	2.33	5.290	2.07	16.70	13.75	0.399	0.114	3.32
	7.30	44.88	2.68	6.095	2.01	21.27	19.17	0.473	0.145	3.12
C6 trimmed fore	8.05	49.49	2.96	6.724	2.01	24.99	21.42	0.527	0.171	2.90
	1.29	7.93	0.47	1.077	1.90	−12.79	−17.83	0.073	−0.087	5.69
	2.36	14.49	0.87	1.968	3.62	−2.27	−19.66	0.153	−0.016	5.53
	3.13	19.25	1.15	2.614	3.68	1.26	−18.27	0.234	0.009	5.48
	4.63	28.47	1.70	3.865	4.88	15.43	−7.78	0.279	0.105	4.71
	5.37	33.00	1.97	4.482	4.54	16.64	−5.46	0.338	0.114	4.19
	6.34	38.98	2.33	5.290	4.02	19.51	−1.32	0.424	0.133	3.99
	7.30	44.88	2.68	6.095	3.96	23.21	−1.46	0.511	0.159	3.78
	8.05	49.49	2.96	6.724	3.73	28.23	9.16	0.582	0.193	2.75
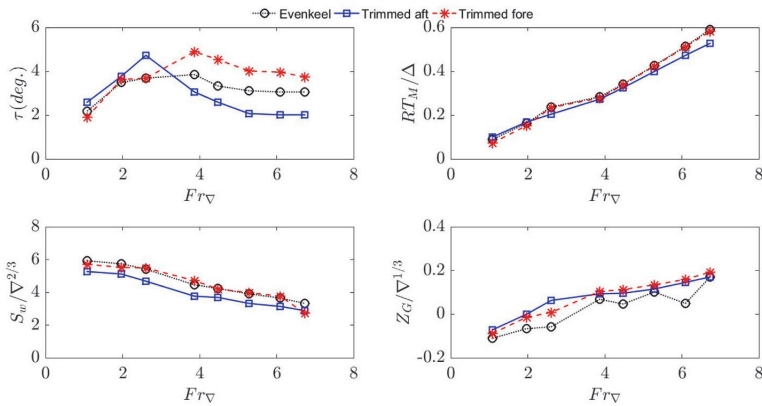
Fig. 14. Results of C06 hull for dynamic trim, resistance, wetted surface, and dynamic sinkage at states of even keel, trimmed aft, and trimmed fore.

Hull model C07_2_60_0

| ID number	Steps Number; N_S	Step Height; H_S [mm]	Longitudinal Step Position; LSP [mm]	Longitudinal Center of Buoyancy; LCB [mm]
C07_2_60_0	2	6	0: step 1 = 149 mm step 2 = 302 mm	307
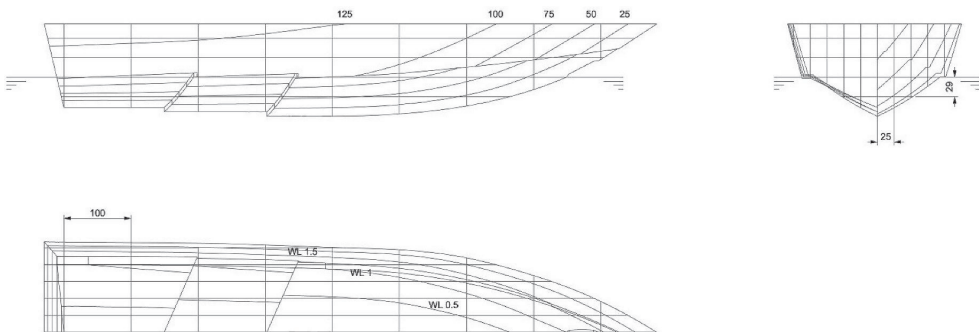
Fig. 15. C07 model lines plan: Sheer Plan, body plan, half breadth plan. Transversal section every 0.100 m, buttock line every 0.025 m, water lines every 0.029 m.

Hull model C07_2_60_0 - calm water towing tank test data.

| C7 evenkeel	V_M [m/s]	V_S [Knots]	Fr_L	Fr_∇	τ [deg]	Z_G [mm] + up	Z_O [mm] + up	$\dfrac{RT_M}{\Delta}$	$\dfrac{Z_G}{\nabla^{1/3}}$	$\dfrac{S_W}{\nabla^{2/3}}$
	1.29	7.93	0.47	1.077	1.95	−11.75	−21.73	0.089	−0.080	5.74
	2.36	14.49	0.87	1.968	3.33	−0.68	−18.05	0.189	−0.005	5.51
	3.13	19.25	1.15	2.614	3.15	6.51	−7.47	0.294	0.045	5.17
	4.63	28.47	1.70	3.865	3.21	21.94	5.68	0.279	0.150	4.64
	5.37	33.00	1.97	4.482	3.21	18.68	1.83	0.308	0.128	4.25
	6.34	38.98	2.33	5.290	2.75	21.67	7.31	0.406	0.148	3.75
	7.30	44.88	2.68	6.095	2.52	21.56	8.23	0.519	0.147	3.27
	8.05	49.49	2.96	6.724	2.41	22.60	10.27	0.599	0.154	2.91
C7 trimmed aft	V_M [m/s]	V_S [Knots]	Fr_L	Fr_∇	τ [deg]	Z_G [mm] + up	Z_O [mm] + up	$\dfrac{RT_M}{\Delta}$	$\dfrac{Z_G}{\nabla^{1/3}}$	$\dfrac{S_W}{\nabla^{2/3}}$
	1.29	7.93	0.47	1.077	2.30	−4.72	−14.30	0.104	−0.032	5.85
	2.36	14.49	0.87	1.968	3.29	4.55	−9.50	0.196	0.031	5.57
	3.13	19.25	1.15	2.614	3.80	12.33	−1.43	0.222	0.084	5.34
	4.63	28.47	1.70	3.865	2.88	22.28	11.33	0.261	0.152	4.60
	5.37	33.00	1.97	4.482	2.41	21.60	11.67	0.302	0.148	4.19
	6.34	38.98	2.33	5.290	1.95	28.38	11.76	0.401	0.194	3.64
	7.30	44.88	2.68	6.095	1.67	24.13	19.79	0.514	0.165	3.21
	8.05	49.49	2.96	6.724	1.72	24.64	19.95	0.605	0.168	2.86
C7 trimmed fore	V_M [m/s]	V_S [Knots]	Fr_L	Fr_∇	τ [deg]	Z_G [mm] + up	Z_O [mm] + up	$\dfrac{RT_M}{\Delta}$	$\dfrac{Z_G}{\nabla^{1/3}}$	$\dfrac{S_W}{\nabla^{2/3}}$
	1.29	7.93	0.47	1.077	1.72	−9.87	−18.38	0.084	−0.067	5.73
	2.36	14.49	0.87	1.968	3.50	−4.43	−22.74	0.189	−0.030	5.50
	3.13	19.25	1.15	2.614	3.82	0.23	−14.83	0.296	0.002	5.17
	4.63	28.47	1.70	3.865	4.24	12.39	−12.12	0.292	0.085	4.67
	5.37	33.00	1.97	4.482	4.19	14.08	−7.88	0.336	0.096	4.34
	6.34	38.98	2.33	5.290	3.90	18.48	−1.88	0.429	0.126	3.88
	7.30	44.88	2.68	6.095	3.56	17.94	−1.18	0.548	0.123	3.38
	8.05	49.49	2.96	6.724	3.33	22.17	4.69	0.646	0.152	3.03
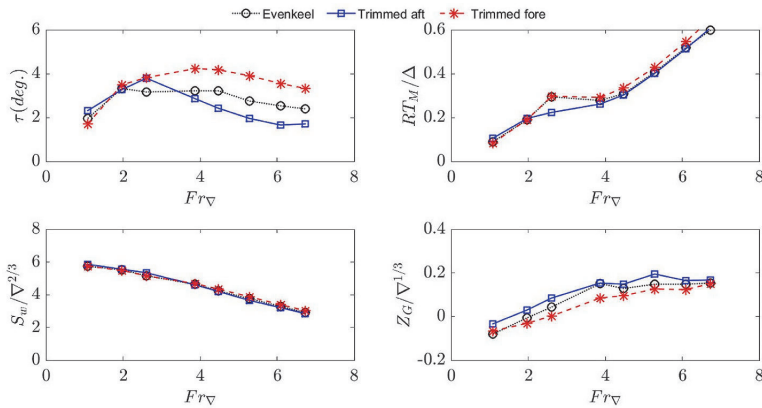
Fig. 16. Results of C07 hull for dynamic trim, resistance, wetted surface, and dynamic sinkage at states of even keel, trimmed aft, and trimmed fore.

Hull model C08_2_20_1

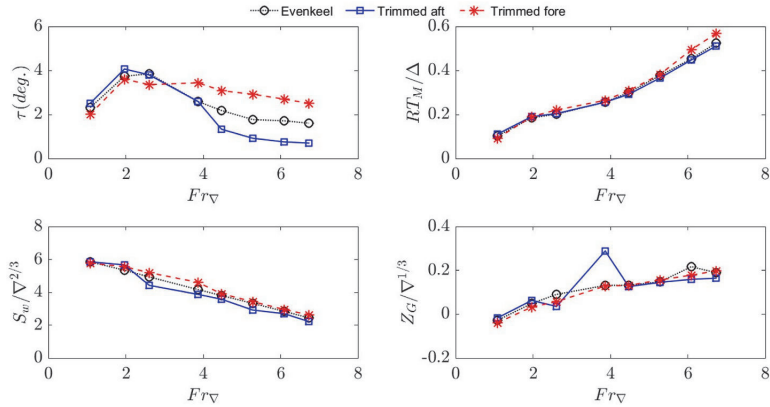| ID number	Steps Number; N_S	Step Height; H_S [mm]	Longitudinal Step Position; LSP [mm]	Longitudinal Center of Buoyancy; LCB [mm]
C08_2_20_1	2	2	+1.4: step 1 = 288 mm step 2 = 441 mm	282
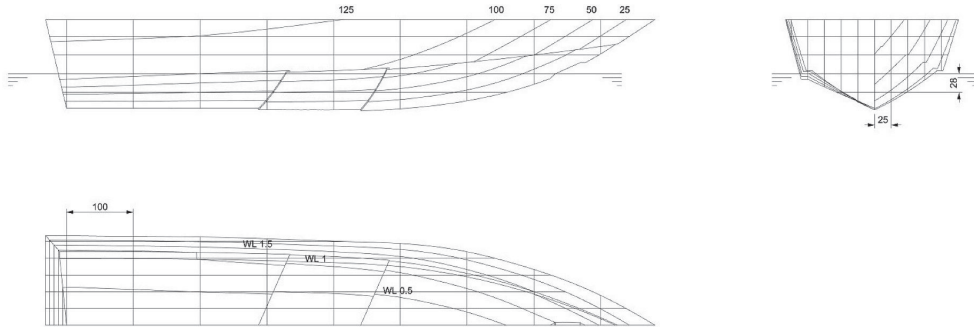
Fig. 17. C08 model lines plan: Sheer Plan, body plan, half breadth plan. Transversal section every 0.100 m, buttock line every 0.025 m, water lines every 0.028 m.

Hull model C08_2_20_1 - calm water towing tank test data.

| C8 evenkeel	V_M [m/s]	V_S [Knots]	Fr_L	Fr_∇	τ [deg]	Z_G [mm] + up	Z_O [mm] + up	$\frac{RT_M}{\Delta}$	$\frac{Z_G}{\nabla^{1/3}}$	$\frac{S_W}{\nabla^{2/3}}$
	1.29	7.93	0.47	1.077	2.42	−8.48	−20.11	0.101	−0.058	5.76
	2.36	14.49	0.87	1.968	3.74	−0.24	−17.82	0.175	−0.002	5.59
	3.13	19.25	1.15	2.614	4.54	9.54	−8.92	0.216	0.065	4.92
	4.63	28.47	1.70	3.865	3.28	20.99	6.03	0.296	0.143	4.18
	5.37	33.00	1.97	4.482	2.82	19.35	8.16	0.347	0.132	4.01
	6.34	38.98	2.33	5.290	2.64	19.97	8.57	0.419	0.137	3.85
	7.30	44.88	2.68	6.095	2.58	21.45	10.63	0.485	0.147	3.42
	8.05	49.49	2.96	6.724	2.64	28.20	18.06	0.536	0.193	3.04
C8 trimmed aft	V_M [m/s]	V_S [Knots]	Fr_L	Fr_∇	τ [deg]	Z_G [mm] + up	Z_O [mm] + up	$\frac{RT_M}{\Delta}$	$\frac{Z_G}{\nabla^{1/3}}$	$\frac{S_W}{\nabla^{2/3}}$
	1.29	7.93	0.47	1.077	2.59	−10.00	−17.69	0.111	−0.068	5.15
	2.36	14.49	0.87	1.968	4.37	3.11	−13.23	0.189	0.021	5.00
	3.13	19.25	1.15	2.614	4.20	9.32	−2.08	0.218	0.064	4.28
	4.63	28.47	1.70	3.865	2.64	12.34	11.70	0.279	0.084	3.66
	5.37	33.00	1.97	4.482	2.12	13.12	12.26	0.324	0.090	3.39
	6.34	38.98	2.33	5.290	1.84	16.40	15.50	0.390	0.112	3.14
	7.30	44.88	2.68	6.095	1.72	20.97	19.61	0.459	0.143	3.03
	8.05	49.49	2.96	6.724	1.84	24.67	21.50	0.491	0.169	2.62
C8 trimmed fore	V_M [m/s]	V_S [Knots]	Fr_L	Fr_∇	τ [deg]	Z_G [mm] + up	Z_O [mm] + up	$\frac{RT_M}{\Delta}$	$\frac{Z_G}{\nabla^{1/3}}$	$\frac{S_W}{\nabla^{2/3}}$
	1.290	7.93	0.47	1.077	2.25	−7.58	−18.84	0.091	−0.052	5.87
	2.357	14.49	0.87	1.968	3.80	−0.74	−19.03	0.173	−0.005	5.70
	3.131	19.25	1.15	2.614	4.55	5.61	−15.70	0.222	0.038	5.20
	4.629	28.47	1.70	3.865	3.85	18.46	−1.49	0.306	0.126	4.53
	5.368	33.00	1.97	4.482	3.57	19.00	2.99	0.359	0.130	4.06
	6.336	38.98	2.33	5.290	3.28	19.82	4.98	0.437	0.135	3.73
	7.301	44.88	2.68	6.095	3.22	24.17	10.17	0.508	0.165	3.37
	8.054	49.49	2.96	6.724	3.27	24.08	10.14	0.556	0.165	3.18
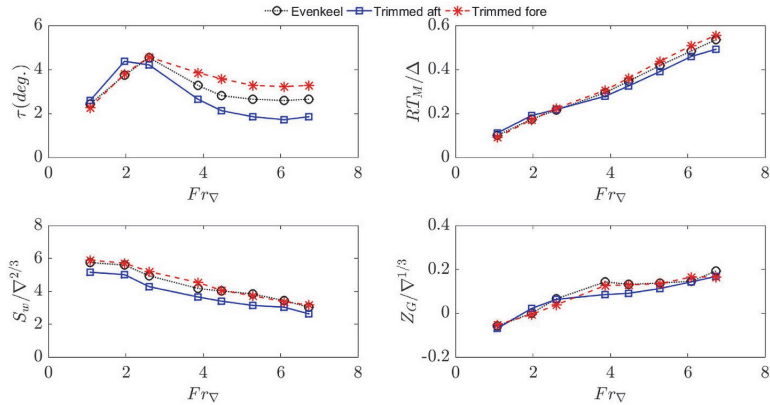
Fig. 18. Results of C08 hull for dynamic trim, resistance, wetted surface, and dynamic sinkage at states of even keel, trimmed aft, and trimmed fore.

Hull model C09_2_60_1

| ID number	Steps Number; N_S	Step Height; H_S [mm]	Longitudinal Step Position; LSP [mm]	Longitudinal Center of Buoyancy; LCB [mm]
C09_2_60_1	2	6	+1.4: step 1 = 290 mm step 2 = 443 mm	310
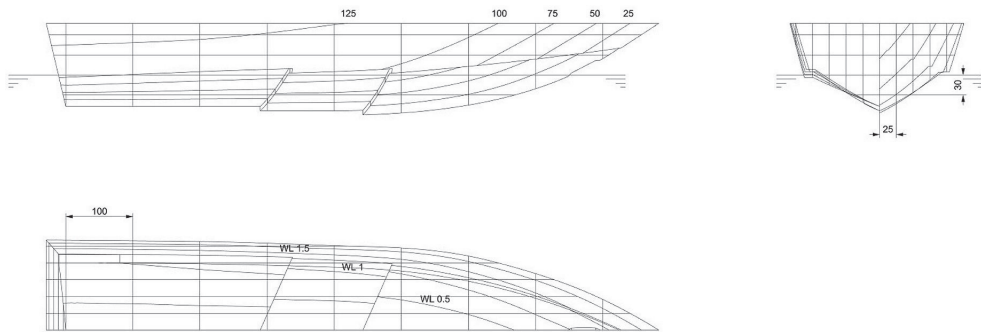
Fig. 19. C09 model lines plan: Sheer Plan, body plan, half breadth plan. Transversal section every 0.100 m, buttock line every 0.025 m, water lines every 0.030 m.

Hull model C09_2_60_1 - calm water towing tank test data.

C9 evenkeel	V_M [m/s]	V_S [Knots]	Fr_L	Fr_∇	τ [deg]	Z_G [mm] + up	Z_O [mm] + up	$\frac{RT_M}{\Delta}$	$\frac{Z_G}{\nabla^{1/3}}$	$\frac{S_W}{\nabla^{2/3}}$
	1.29	7.93	0.47	1.077	1.55	−10.35	−12.01	0.090	−0.071	6.64
	2.36	14.49	0.87	1.968	3.33	0.23	−15.04	0.188	0.002	6.45
	3.13	19.25	1.15	2.614	3.33	4.67	−11.16	0.213	0.032	3.78
	4.63	28.47	1.70	3.865	3.33	14.59	1.18	0.285	0.100	2.88
	5.37	33.00	1.97	4.482	3.10	17.15	2.57	0.319	0.117	2.44
	6.34	38.98	2.33	5.290	3.04	21.21	5.43	0.393	0.145	2.24
	7.30	44.88	2.68	6.095	2.70	24.47	6.24	0.535	0.167	2.14
	8.05	49.49	2.96	6.724	2.64	27.38	9.47	0.614	0.187	1.99
C9 trimmed aft	V_M [m/s]	V_S [Knots]	Fr_L	Fr_∇	τ [deg]	Z_G [mm] + up	Z_O [mm] + up	$\frac{RT_M}{\Delta}$	$\frac{Z_G}{\nabla^{1/3}}$	$\frac{S_W}{\nabla^{2/3}}$
	1.29	7.93	0.47	1.077	2.01	−10.01	−16.98	0.096	−0.068	6.68
	2.36	14.49	0.87	1.968	3.50	1.00	−14.58	0.209	0.007	6.49
	3.13	19.25	1.15	2.614	3.38	7.05	−4.60	0.216	0.048	4.08
	4.63	28.47	1.70	3.865	2.52	13.14	8.93	0.276	0.090	2.80

(continued on next page)

(*continued*)

|										
	5.37	33.00	1.97	4.482	2.18	15.19	11.50	0.321	0.104	2.54
	6.34	38.98	2.33	5.290	2.01	18.07	11.45	0.409	0.124	2.20
	7.30	44.88	2.68	6.095	1.84	23.54	18.57	0.535	0.161	2.10
	8.05	49.49	2.96	6.724	1.84	26.11	18.68	0.625	0.178	1.86
C9 trimmed fore	V_M [m/s]	V_S [Knots]	Fr_L	Fr_∇	τ [deg]	Z_G [mm] + up	Z_O [mm] + up	$\dfrac{RT_M}{\Delta}$	$\dfrac{Z_G}{\nabla^{1/3}}$	$\dfrac{S_W}{\nabla^{2/3}}$
	1.29	7.93	0.47	1.077	1.49	−10.69	−12.20	0.061	−0.073	6.64
	2.36	14.49	0.87	1.968	3.51	0.00	−18.16	0.188	−0.000	6.44
	3.13	19.25	1.15	2.614	2.76	1.86	−11.87	0.298	0.013	5.80
	4.63	28.47	1.70	3.865	4.03	15.16	−6.13	0.318	0.104	2.93
	5.37	33.00	1.97	4.482	4.03	17.30	−6.46	0.323	0.118	2.72
	6.34	38.98	2.33	5.290	3.85	21.64	−3.05	0.391	0.148	2.28
	7.30	44.88	2.68	6.095	3.97	26.35	−0.28	0.520	0.180	1.98
	8.05	49.49	2.96	6.724	3.22	28.35	8.25	0.648	0.194	1.68
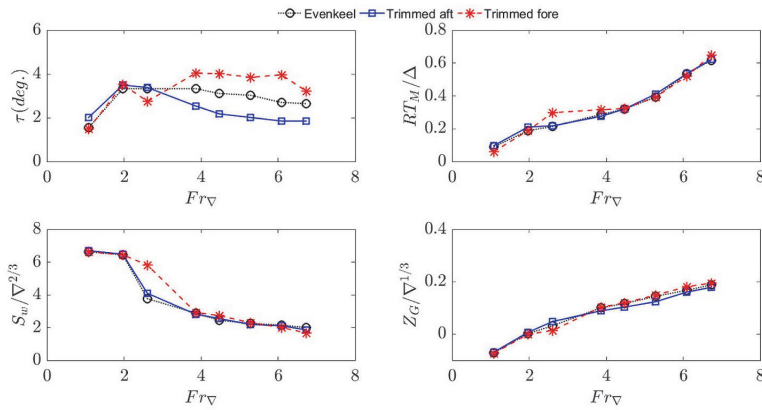
Fig. 20. Results of C09 hull for dynamic trim, resistance, wetted surface, and dynamic sinkage at states of even keel, trimmed aft, and trimmed fore.

Appendix B. Experimental uncertainty analysis

Uncertainty Analysis (UA) in Experimental Fluid Dynamics (EFD) has been also performed according to ITTC (7.5-02-02-02, 2002) only for C03 as reported in De Marco et al. (2017).

The UA was performed in two-phase: in the first phase for each variable *r* (model geometry, displacement, speed, resistance, density, running trim, and sinkage). In a second phase for non-dimensional coefficients (RT_M/Δ, τ, $Z_G/\nabla^{1/3}$, and $S/\nabla^{2/3}$). The methodology proposed for UA is in accordance with Coleman and Steele (1999), considering a confidence interval of 95% and a normal distribution with a large sample size with estimates of:

- bias (B_r), also called systematic uncertainty, is evaluated as the Root Sum of Square (RSS) of each elementary error source (i.e., calibration, data acquisition, data reduction, and conceptual bias) group of bias errors. Before every evaluation the elementary error sources have been divided and separately estimated;
- precision uncertainty, (P_r), also called random uncertainty, is calculated for each run, on the basis of $P_j(S) = K\,SDev_j$ where $K = 2$ is assumed according to the above-mentioned methodology and $SDev_j$ represents the standard deviation of *j*th run;
- total uncertainty U_r is an RSS of bias B_r and precision P_r.

All evaluation of bias, precision, and the uncertainties for non-dimensional coefficients (RT_M/Δ, τ, $Z_G/\nabla^{1/3}$, $S/\nabla^{2/3}$ and Fr_∇) are summarized in Table 6.

The uncertainty is assumed equal for all the other hulls of the VMV systematic series.

Table 6
Experimental uncertainty analysis

Description	Term	Speed								Units
		1.290	2.357	3.131	4.629	5.368	6.336	7.300	8.054	[m/s]
Model Speed										
	Fr_∇	1.077	1.968	2.614	3.864	4.481	5.289	6.094	6.723	[adim]
	B_V	6.97E-04	6.97E-04	3.13E-03	4.62E-03	5.36E-03	6.33E-03	7.29E-03	8.05E-03	[adim]
		22.62%	8.05%	4.73%	2.22%	1.66%	1.20%	0.90%	0.74%	% of B_{Fr_∇}
	B_∇	1.29E-03	2.35E-03	3.13E-03	4.62E-03	5.36E-03	6.33E-03	7.29E-03	8.05E-03	[adim]

(*continued on next page*)

Table 6 (*continued*)

Description	Term	Speed								Units
		1.290	2.357	3.131	4.629	5.368	6.336	7.300	8.054	[m/s]
		77.38%	91.95%	95.27%	97.78%	98.34%	98.80%	99.10%	99.26%	% of $B_{Fr\nabla}$
	$B_{Fr\nabla}$	1.47E-03	2.46E-03	3.20E-03	4.68E-03	5.41E-03	6.37E-03	7.33E-03	8.08E-03	[adim]
		0.14%	0.12%	0.12%	0.12%	0.12%	0.12%	0.12%	0.12%	% of Fr_∇
	$P_{Fr\nabla}$	4.38E-03	4.80E-03	5.22E-03	1.08E-02	1.36E-02	1.41E-02	2.08E-02	2.50E-02	[adim]
	$U_{Fr\nabla}$	4.61E-03	5.39E-03	6.13E-03	1.18E-02	1.47E-02	1.54E-02	2.21E-02	2.63E-02	[adim]
		0.43%	0.27%	0.23%	0.30%	0.33%	0.29%	0.36%	0.39%	% of Fr_∇
Model Resistance Ratio										
	R_{TM}/Δ	0.100	0.178	0.204	0.256	0.312	0.407	0.491	0.555	[N/N]
	B_R	6.62E-04	6.68E-04	6.71E-04	6.78E-04	6.86E-04	7.05E-04	7.25E-04	7.42E-04	[N/N]
		97.49%	97.54%	97.56%	97.61%	97.67%	97.78%	97.90%	98.00%	% of $B^2_{RT/\Delta}$
	B_Δ	1.06E-04	1.06E-04	1.06E-04	1.06E-04	1.06E-04	1.06E-04	1.06E-04	1.06E-04	[N/N]
		2.51%	2.46%	2.44%	2.39%	2.33%	2.22%	2.10%	2.00%	% of $B^2_{RT/\Delta}$
	P_R	4.08E-05	1.54E-07	1.54E-07	3.45E-07	2.25E-06	2.25E-06	2.25E-06	1.53E-06	[N/N]
	$U_{RTM/\Delta}$	6.72E-04	6.76E-04	6.79E-04	6.86E-04	6.95E-04	7.13E-04	7.33E-04	7.50E-04	[N/N]
		0.67%	0.38%	0.33%	0.27%	0.22%	0.18%	0.15%	0.14%	% of R_T/Δ
Trim Angle										
	τ	2.23	3.55	3.27	3.27	2.87	2.69	2.52	2.58	[deg]
	$B_{\tau\text{-cw}}$	0.001	0.001	0.001	0.001	0.001	0.001	0.001	0.001	[deg]
		0.01%	0.01%	0.01%	0.01%	0.01%	0.01%	0.01%	0.01%	% of B^2_τ
	$B_{\tau\text{-ix}}$	0.050	0.050	0.050	0.050	0.050	0.050	0.050	0.050	[deg]
		33.33%	33.33%	33.33%	33.33%	33.33%	33.33%	33.33%	33.33%	% of B^2_τ
	$B_{\tau\text{-iy}}$	0.050	0.050	0.050	0.050	0.050	0.050	0.050	0.050	[deg]
		33.33%	33.33%	33.33%	33.33%	33.33%	33.33%	33.33%	33.33%	% of B^2_τ
	$B_{\tau\text{-iz}}$	0.050	0.050	0.050	0.050	0.050	0.050	0.050	0.050	[deg]
		33.33%	33.33%	33.33%	33.33%	33.33%	33.33%	33.33%	33.33%	% of B^2_τ
	B_τ	0.087	0.087	0.087	0.087	0.087	0.087	0.087	0.087	[deg]
		3.88%	2.44%	2.65%	2.65%	3.02%	3.22%	3.44%	3.36%	% of B^2_τ
	P_τ	0.004	0.003	0.003	0.004	0.012	0.014	0.012	0.012	[deg]
	U_τ	0.087	0.087	0.087	0.087	0.087	0.088	0.087	0.087	[deg]
		3.89%	2.44%	2.65%	2.65%	3.04%	3.26%	3.47%	3.39%	% of τ
Sinkage										
	$Z/\nabla^{1/3}$	−0.080	0.010	0.048	0.085	0.139	0.147	0.151	0.181	[mm/mm]
	$B_{ZCG\text{-cw}}$	0.1	0.1	0.1	0.1	0.1	0.1	0.1	0.1	[mm]
		3.3E-03	3.3E-03	3.3E-03	3.3E-03	3.3E-03	3.3E-03	3.3E-03	3.3E-03	% of B^2_{ZCG}
	$B_{ZCG\text{-lf}}$	1.00	1.00	1.00	1.00	1.00	1.00	1.00	1.00	[mm]
		0.33	0.33	0.33	0.33	0.33	0.33	0.33	0.33	% of B^2_{ZCG}
	$B_{ZCG\text{-la}}$	1.00	1.00	1.00	1.00	1.00	1.00	1.00	1.00	[mm]
		0.33	0.33	0.33	0.33	0.33	0.33	0.33	0.33	% of B^2_{ZCG}
	$B_{ZCG\text{-lb}}$	1.00	1.00	1.00	1.00	1.00	1.00	1.00	1.00	[mm]
		0.332	0.332	0.332	0.332	0.332	0.332	0.332	0.332	% of B^2_{ZCG}
	B_{ZCG}	1.735	1.735	1.735	1.735	1.735	1.735	1.735	1.735	[mm]
		14.85%	114.14%	24.96%	14.03%	8.51%	8.07%	7.83%	6.56%	% of B^2_{ZCG}
	P_{ZCG}	6.365	7.120	6.846	4.046	8.755	5.870	6.556	4.864	[mm]
	$B^{1/3}_{Z/\nabla}$	0.016	0.012	0.014	0.017	0.023	0.024	0.025	0.028	[mm/mm]
		20.64%	115.04%	28.79%	20.06%	16.67%	16.45%	16.34%	15.77%	% of $Z/\nabla^{1/3}$
	$P^{1/3}_{Z/\nabla}$	0.025	0.024	0.024	0.019	0.036	0.030	0.032	0.032	[mm/mm]
	$U^{1/3}_{Z/\nabla}$	0.030	0.027	0.028	0.025	0.043	0.038	0.040	0.043	[mm/mm]
		−37.26%	261.37%	58.95%	29.82%	30.96%	26.01%	26.56%	23.52%	% of $Z/\nabla^{1/3}$
Model geometry										
	$S/\nabla^{2/3}$	6.730								[m²/m²]
	B_S	0.284								[m²/m²]
		80.81%								% of $B^2_{S/\nabla2/3}$
	$B^{2/3}_\nabla$	0.138								[m²/m²]
		19.19%								% of $B^2_{S/\nabla2/3}$
	$P^{2/3}_{S/\nabla}$	0.032								[m/m]
	$U^{2/3}_{S/\nabla}$	0.317								[m²/m²]
		4.72%								%of $S/\nabla^{2/3}$
Density										
	ρ	1000								[kg/m³]
	B_{r1}	0.071								[kg/m³]
		1.15%								% of B^2_ρ
	B_{r2}	0.07								[kg/m³]
		1.12%								% of B^2_ρ
	B_{r3}	0.655								[kg/m³]
		97.74%								% of B^2_ρ
	B_r	0.663								[kg/m³]
		0.066%								% of B_r
	P_r	1.00								[kg/m³]
	U_ρ	1.20								[kg/m³]
		0.12%								% of r

Appendix C. Visualization of the fluid flow on the bottom of stepped hulls

For a better understanding of wetted surfaces and flow separation phenomenon on the aft body behind the step of stepped hulls under analysis, the top-view snapshot in trimmed forward condition at all speed are shown.

Fig. 21. Wetted surfaces of C02 stepped hull at the different tested speeds - trimmed forward condition.

Fig. 22. Wetted surfaces of C03 stepped hull at the different tested speeds - trimmed forward condition.
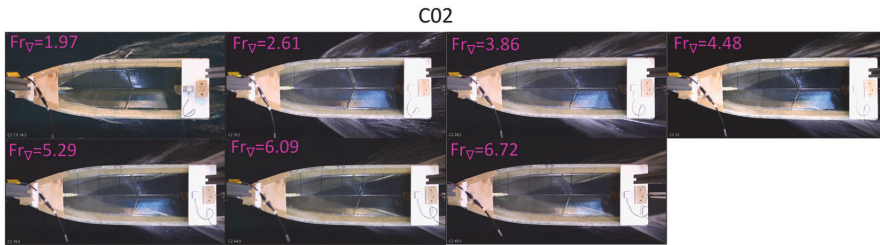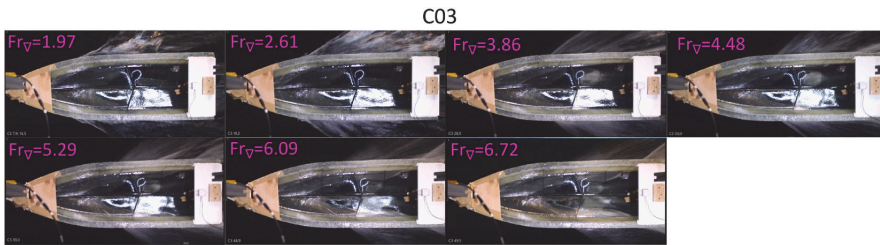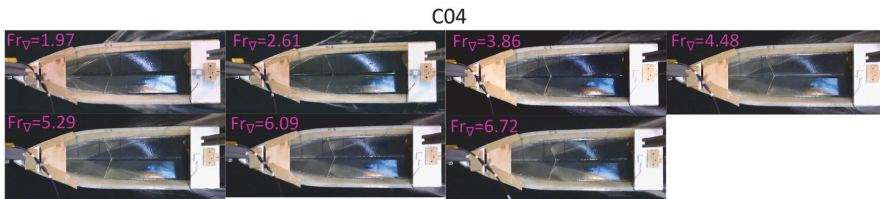

Fig. 23. Wetted surfaces of C04 stepped hull at the different tested speeds - trimmed forward condition.
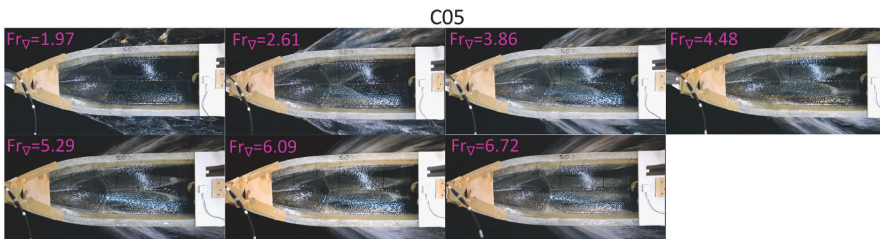

Fig. 24. Wetted surfaces of C05 stepped hull at the different tested speeds - trimmed forward condition.
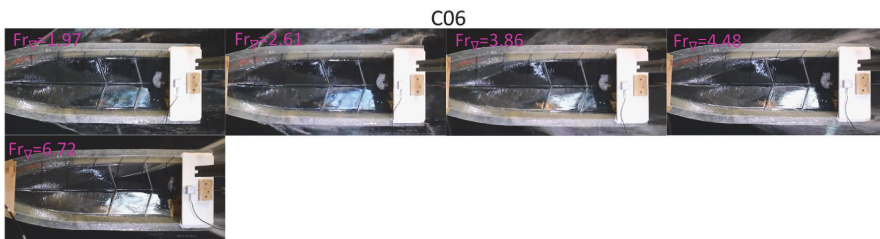
Fig. 25. Wetted surface of C06 stepped hull at the different tested speeds - trimmed forward condition.

C07
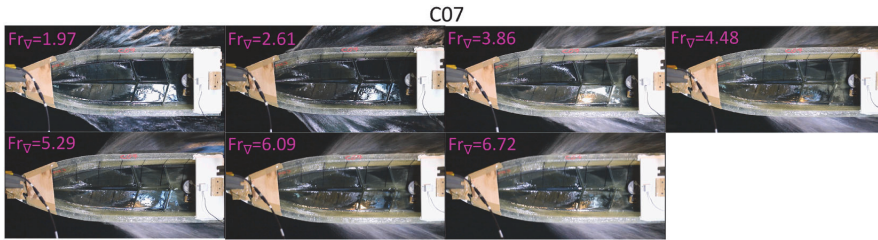
Fig. 26. Wetted surfaces of C07 stepped hull at the different tested speeds - trimmed forward condition.

C08
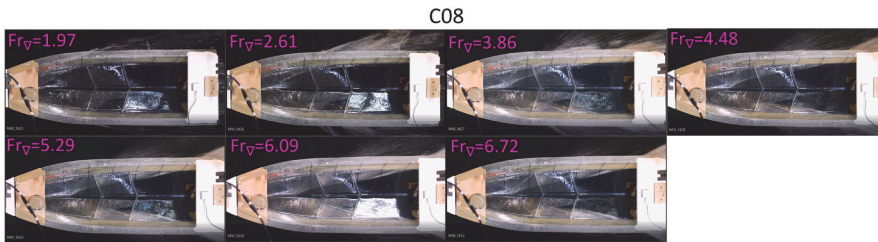
Fig. 27. Wetted surfaces of C08 stepped hull at the different tested speeds - trimmed forward condition.

C09
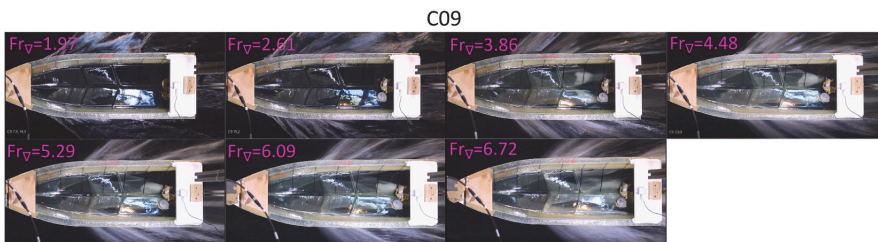
Fig. 28. Wetted surfaces of C09 stepped hull at the different tested speeds - trimmed forward condition.

References

Acampora, B., Racer, S.M., 1995. Design and operation of one of the World's Fastest Monohulls. Mar. Technol. 32.

Akers, 2003. Dancing a Fine Line. Professional BoatBuilder.

Brizzolara, S., Federici, A., 2013. Designing of planing hulls with longitudinal steps: CFD in support of traditional semi-empirical methods. In: Proceedings, Design, Construction & Operation of Super and Mega Yachts Conference, May 8–9, Genoa, Italy.

Clement, E.P., Pope, J.D., 1961. Stepless and Stepped Planing Hulls Graphs for Performance Prediction and Design. David Taylor Model Basin, US Naval Surface Warfare Center, Bethesda (MD).

Clement, E.P., 1964. A Lifting Approach to Planing Boat Design, DTMB Rep 1902.

Clement, E.P., Blount, D.L., 1963. Resistance tests of a systematic series of planing hull forms. Trans SNAME 71, 491–579.

Clement, E.P., Desty, D.H., 1980. The BP Dynaplane high-speed research boat. In: Paper Presented at High-Speed Surface Craft. Third International Hovering Craft and Hydrofoil Exhibition, Brighton, UK.

Clement, E.P., Koelbel, J.O., 1991. Effects of step design on the performance of planing motorboats. In: Paper Presented at Fourth Biennial Power Boat Symposium. The Society of Naval Architects and Marine Engineers, Miami, (FL), USA.

Clement, E.P., Koelbel, J.O., 1992. Optimized designs for stepped planing monohulls and catamarans. In: Paper Presented at HPMV-92, Intersociety High-Performance Marine Vehicles Conference and Exhibit; Washington (DC), USA.

Clement, E.P., 2003. A Configuration for a Stepped Planing Boat Having Minimum Drag. David Taylor Model Basin, US Naval Surface Warfare Center, Bethesda (MD).

Coleman, H.W., Steele, W.G., 1999. Experimentation and Uncertainty Analysis for Engineers. A Wiley Interscience Publication.

Danielsson, J., Strąmquist, J., 2012. Conceptual Design of a High-Speed Superyacht Tender Hull Form Analysis and Structural Optimization [thesis]. Marina System Centre for Naval Architecture, KTH University, Stockholm.

Dashtimanesh, A., Tavakoli, S., Sahoo, P., 2017. A simplified method to calculate resistance and trim of a two stepped planing hull. J Ship Offshore Struct 12 (Suppl. 1), 317–329.

Dashtimanesh, A., Esfandiari, A., Mancini, S., 2018. Performance prediction of two-stepped planing hulls using morphing mesh approach. J Ship Prod Des 34 (3), 236–248.

De Luca, F., Pensa, C., 2017. The Naples warped hard chine hulls systematic series. Ocean Eng 139, 205–236.

De Marco, A., Mancini, S., Miranda, S., Scognamiglio, R., Vitiello, L., 2017. Experimental and numerical hydrodynamic analysis of a stepped planing hull. Appl. Ocean Res. 64, 135–154. https://doi.org/10.1016/j.apor.2017.02.004.

Gabrielli, G., von Kàrmàn, T., 1950. What price speed? Specific power required for propulsion of vehicles. Mech. Eng. ASME 72 (10).

Grigoropoulos, G.J., Loukakis, T.A., 2002. Resistance and seakeeping characteristics of a systematic series in the pre-planing condition (Part I). Trans. SNAME 110, 77–113.

Hubble, E.N., 1974. Resistance of Hard-Chine, Stepless Planing Craft with Systematic Variation of Hull Form, Longitudinal Center of Gravity, and Loading, NSRDC Report 4307.

ITTC, 2002a. Recommended Procedures and Guidelines, 7.5-01-01-01.

ITTC, 2002b. Recommended Procedures and Guidelines, 7.5-02-02-02.

ITTC, 2011. Recommended Procedures and Guidelines, 7.5-02-02-01.

Keuning, J.A., Gerritsma, J., 1982. Resistance tests of a series of planing hull forms with 25 degrees deadrise angle. Int. Shipbuild. Prog. 29 (337).

Keuning, J.A., Gerritsma, J., van Tervisga, P.F., 1993. Resistance Tests of a Series Planing Hull Forms with 30 Degrees Deadrise Angle, and a Calculation Model Based on This and Similar Systematic Series, vol. 25. MEMT, Delft, The Netherlands.

Kowalyshyn, D.H., Metcalf, A., 2006. USCG Systematic Series of High-Speed Planing Hulls, vol. 114. Transactions of the Society of Naval Architects and Marine Engineers, Jersey City, USA.

Lee, E., Pavkov, M., Mccue-Weil, W., 2014. The systematic variation of step configuration and displacement for a double-step planing craft. J Ship Prod Des 30, 89–97.

Miranda, S., Vitiello, L., 2014. Propulsive performance analysis of a stepped hull by model test results and sea trial data. In: High-Speed Marine Vehicles Symposium. Naples.

Moore, W.L., 1967. Cambered Planing Surfaces for Stepped Hulls – Some Theoretical and Experimental Results. David Taylor Model Basin, US Naval Surface Warfare Center, Bethesda (MD).

Niazmand Bilandi, R., Dashtimanesh, A., Tavakoli, S., 2019. Development of a 2D+T theory for performance prediction of double-stepped planing hulls in calm water, Proceedings of the Institution of Mechanical Engineers, Part M. J. Eng. Marit Environ. 233 (3), 886–904.

Niazmand Bilandi, R., Vitiello, L., Mancini, S., Nappo, V., Roshan, F., Tavakoli, S., Dashtimanesh, A., 2020a. Calm-water performance of a boat with two swept steps at high-speeds: laboratory measurements and mathematical modeling. Procedia Manuf. 42, 467–474.

Niazmand Bilandi, R., Dashtimanesh, A., Tavakoli, S., 2020b. Hydrodynamic study of heeled double-stepped planing hulls using CFD and 2D+ T method. Ocean Eng 196, 106813.

Niazmand Bilandi, R., Tavakoli, S., Dashtimanesh, A., 2021. Seakeeping of double-stepped planing hulls. Ocean Engineering 236, 109475. https://doi.org/10.1016/j.oceaneng.2021.109475.

Norman, Skene, 1938. Elements of Yacht Design, sixth ed. Kennedy Bros., New York.

Peters, M., 2010. Peter on (Fast) Powerboats Part 2. Professional BoatBuilder, p. 127.

Savitsky, D., 1964. Hydrodynamic design of planing hull. Mar. Technol. 1, 71–95.

Savitsky, D., Morabito, M., 2010. Surface wave contours associated with the forebody wake of stepped planing hulls. Mar. Technol. 47, 1–16.

Sheingart, Z., 2014. Hydrodynamics of High-Speed Planing Hulls with Partially Ventilated Bottom and Hydrofoils. Master of Science thesis. Department of Mechanical Engineering, Massachusetts Institute of Technology, Cambridge.

Svahn, D., 2009. Performance Prediction of Hulls with Transverse Steps [thesis]. Marina System Centre for Naval Architecture, KTH University, Stockholm.

Sverchkov, A., 2010. Application of air cavities on high-speed ships in Russia. In: International Conference on Ship Drag Reduction (SMOOTH-Ships), Istanbul.

Taunton, D.J., Hudson, D.A., Shenoi, R.A., 2010. Characteristics of a series of high-speed hard chine planing hulls – part 1: performance in calm water. Trans. R. Inst. Nav. Archit. Part B Int. J. Small Craft Technol. 152 (2), B55–B74. https://doi.org/10.3940/rina.ijsct.2010.b2.96.

Taunton, D.J., Hudson, D.A., Shenoi, R.A., 2011. Characteristics of a series of high-speed hard chine planing hulls part 2: performance in waves. Trans. R. Inst. Nav. Archit. Part B Int. J. Small Craft Technol. 153 (1), B1–B22. https://doi.org/10.3940/rina.ijsct.2011.b1.97.

Vitiello, L., 2022. Github stepped hulls towing tank test [Online]. Available: https://github.com/LuigiVitielloDII/Stepped-Hulls-Towing-Tank-Test.git.

Vitiello, L., Miranda, S., 2016. Towing tank test of stepped hull C03 - university of Naples Federico II, Italy [Online]. Available: https://dx.doi.org/10.6084/m9.figshare.3466010.v1 [Accessed 2016].

Vitiello, L., Miranda, S., Balsamo, F., Bove, A., Caldarella, S., 2012. Stepped hulls: model experimental tests and sea trial data. In: 17th International Conference on Ships and Shipping Research – NAV2012; Naples, Italy.

White, G., Beaver, W., Vann, D., 2012. An experimental analysis of the effects of steps on high-speed planing boats. In: Paper Presented at the Third Chesapeake Power Boat Symposium; Annapolis (MD), USA.

Appendix 3 (Publication III)

[P3] Niazmand Bilandi, R., Dashtimanesh, A., Mancini, S., & Vitiello, L. (2023). Comparative study of experimental and CFD results for stepped planing hulls. Ocean Engineering, 280, 114887. https://doi.org/10.1016/j.oceaneng.2023.114887

Comparative study of experimental and CFD results for stepped planing hulls

Rasul Niazmand Bilandi [a], Abbas Dashtimanesh [b,*], Simone Mancini [c,d], Luigi Vitiello [c]

[a] *Estonian Maritime Academy, Tallinn University of Technology, 11712, Tallinn, Estonia*
[b] *Engineering Mechanics Department, School of Engineering Science, KTH Royal Institute of Technology, 114 28, Stockholm, Sweden*
[c] *Department of Industrial Engineering, University of Napoli" Federico II", 80125, Napoli, Italy*
[d] *Department of Hydro and Aerodynamics, FORCE Technology, 2800, Kgs. Lyngby, Denmark*

ARTICLE INFO

ABSTRACT

In recent years, research has been conducted on reducing resistance by adding steps on the bottom of high-speed craft. The most significant issue in the design of multi-stepped planing craft is the selection of an appropriate step configuration, i.e., step geometry, location, and height. This requires a general knowledge of the hydrodynamic behavior of each step configuration. Although the towing tank test is an effective method to predict accurately the hydrodynamic behavior of stepped planing boats, there are restrictions in studying some details. In this study, a Computational Fluid Dynamic (CFD) method is used to investigate the hydrodynamic behavior of a stepped planing hull with eight different step configurations in detail. Comparison of the results of trim angle, resistance, sinkage, wetted surface, and ventilation length of swept-stepped planing hulls for different step configurations at various Froude numbers shows that a maximum average resistance reduction occurs at $1.9 < \mathrm{Fr_B} < 4.0$ with the step height of 2.73% $\mathrm{B_{TC}}$ located at 48.46% L from the transom. There is also a lower resistance associated with a step height of 0.91% $\mathrm{B_{TC}}$ at 48.35% L distance from the transom at $\mathrm{Fr_B} > 4$. These results can be used to improve high-speed planing hull performances by utilizing an appropriate step configuration.

1. Introduction

Achieving optimal speed-power performance and reducing fuel consumption are paramount for planing hulls, as pointed out by Savitsky (1964). Compared to displacement hulls, planing hulls move faster and consume less fuel as they skim on the water surface instead of plowing through it (Doctors, 1985). To enhance these benefits, designers have incorporated transverse discontinuities known as steps on the bottom of planing hulls to reduce resistance and fuel consumption (Morabito and Pavkov, 2014). The steps divide the bottom of a planing hull into multiple planing surfaces, with a single-stepped hull having two planing surfaces and a double-stepped hull having three (Dashtimanesh et al., 2017; Niazmand Bilandi et al., 2019). Each planing surface generates a lift force and supports a portion of the boat's displacement (Savitsky and Morabito, 2010; Danielsson and Strumquist, 2012). Flow separation occurs when the flow passes from the step, reducing wetted surfaces, dynamic trim angle, and lowering the resistance, depending on the ventilation method (i.e., natural or boosted ventilation through a vent pipe) (Ricks et al., 2022). Lower resistance leads to reduced fuel

consumption for the same amount of horsepower. Thus, researchers have examined the effect of steps on the performance prediction of planing hulls using towing tank tests, numerical methods, and mathematical models. However, further research is required to explore the impact of various design parameters on the performance of stepped hulls.

Various towing tank test studies such as Rodstrom et al. (1953), Benen (1966, 1967), Clement (1967), and Filling (1993) have been performed to assess the effect of steps on performance prediction and fuel efficiency of stepped planing crafts. Rodstrom et al. (1953) examined the effect of deadrise angle, the height of the step, the angle between the fore and after body keel lines, and step position on a single-stepped planing hull with a test campaign conducted in the Swedish towing tank. Twenty-seven different single-step hull configurations were tested, and seventeen of them produced porpoises when they were run at maximum speed. The speed range for this test was between $\mathrm{Fr_\nabla} = 3.39–4.87$. In 1994, Gassman and Kartinen (1994) tested the effect of changing the Longitudinal Center of Gravity (LCG) and step position on a stepped planing hull in the speed range $\mathrm{Fr_\nabla} = 1.07–4.4$. Garland (2010) at the United States Naval Academy (USNA) worked on

Nomenclature

B	Breadth (m)	α	Volume fraction of the water-air flow ($-$)
B_C	Maximum chine breadth (m)	Δ	Displacement (buoyant) force (Kg)
B_{TC}	Chine breadth at transom (m)	θ	Dynamic trim angle (deg)
E	Comparison error	∇	Displaced volume (m^3)
$Fr_B = v/(gB)^{-1}$	Beam Froude Number	μ_a	Air viscosity (Kg/m-s)
g	Gravity acceleration (m/s^2)	μ_{eff}, ρ_{eff}	Viscosity and density of the mixture of water and air at any point in the domain (Kg/m-s), (Kg/m^3)
L	Length over all (m)	μ_t	Turbulent viscosity of the flow (Kg/m-s)
L_{wl}	Length of waterline (m)	ρ_w	Density of the water (Kg/m^3)
L_{CG}	Longitudinal position of center of gravity (CG) with respect to transom (m)	ρ_a	Density of the air (Kg/m^3)
		τ_{ij}	turbulent stress tensorAbbreviation
p	fluid pressure (N/m^2)	AMR	Adaptive Mesh Refinement
R	Resistance (N)	CFD	Computation Fluid Dynamics
S_w	Wetted surface (m^2)	CG	Center of Gravity
t	Time (s)	Exp	Experimental data
u	Fluid velocity (m/s)	HRIC	High-Resolution Interface Capturing
v	Boat speed (m/s)	ITTC	International Towing Tank Conference
Z_{CG}	Sinkage (m)	SIMPLE	Semi-Implicit Method For Pressure-Linked Equations
β	Deadrise angle of the vessel (deg.)	VOF	Volume of Fluid

a single-stepped planing hull with different step heights (2%, 4%, 6% of chine beam). Their test speed range was $Fr_\nabla = 0.73$–4.54 and they reported the lowest resistance value for step height of 4% of the chine beam. They also declared that by adding ventilation through tubes behind the step, the resistance changes were very small compared to the natural ventilation mode. Additionally, in the same year at USNA, Greg White (White and Beaver, 2010) conducted experiments on the effects of adding steps and trim tabs to the planing hull to improve power in calm water and reduce motion in irregular waves. Four different LCGs were tested (25.5%, 30.2%, 35.1%, and 40.09% of the L_{BP} forward of the transom). In this test, the steps were located at 33.64% L_{BP} (forward step of the transom) and 18.89% L_{BP} (rear step of the transom), and their heights were 0.87%B, 1.74%B, 3.47%B, 5.21%B, and 6.94%B. They found that the best combination of low trim and low drag could be achieved with a double-stepped hull, whose step height was 6.94%B with lift applied at Station 11 (Station 11 is the position along the hull and behind the transom, where the surface-piercing propeller is located). Accordingly, for the double-stepped planing hull with surface drives, the resistance value was reduced by 23% at $Fr_\nabla = 4$, compared to the stepless planing hull with trim tab. They also found that at the step height of 0.87%B for the double-stepped hull with lift applied at Station 11 at $Fr_\nabla = 4$, flow separation had only occurred from the rear step (close to the transom). Flow separation was observed for both steps when the step height exceeded this value (White et al., 2012). Furthermore, Husser (2023) recently conducted experimental and numerical investigations to analyze the impact of forward and aft swept steps on the performance of planing hulls in calm water and regular waves.

Systematic model-based experimental assessments of stepped planing hulls, such as Becker et al. (2008), Taunton et al. (2010), Lee et al. (2014), and Vitiello et al. (2022), can be employed to investigate the effects of different geometries, different step positions, and heights. Taunton et al. (2010) conducted towing tank tests on four deep-vee mono-hulls. One and two steps were installed at 31%L (forward step of the transom) and 19%L (rear step of the transom) on one of the hulls, named C. For the single-stepped hull, the steps height were 4%B and for the double-stepped hull, they were 2%B. According to their results, adding steps to a stepless hull (C) decreased its resistance by 26.5% for a single-stepped hull and 25.4% for a double-stepped hull at $Fr_\nabla = 7.12$ (maximum speed). Furthermore, Taunton et al. (2011) observed that in irregular waves, the acceleration motion of the center of gravity of

single-stepped and double-stepped hulls was reduced by 7% and 14%, respectively, compared to the stepless hull (C). In 2014, Lee et al. (2014) conducted tests on the Naval Surface Warfare Center 15 deadrise hull form (NSWC15E). The steps were placed at 50% L (front step of the transom) and 25% L (rear step of the transom). A total of six different two-step body configurations were investigated with step heights of 0.7%, 1.4%, and 2.1%. All of the double-stepped hull configurations showed a lower resistance value than the non-stepped configuration. Additionally, the lowest value of resistance was calculated for the configuration in which the front step height was 0.7%B (the lowest value of the step height) and the rear step height was 2.1%B (the highest value of the step height). In a recent study, Vitiello et al. (2022) tested a systematic series of eight planing hulls (called the VMV systematic series) with one and two swept steps under three static equilibrium conditions: even keel, trimmed aft, and trimmed fore. The present study uses a numerical approach to analyze the results of the VMV stepped hull systematic series (Vitiello et al., 2022).

Understanding pressure distribution under stepped planing hulls and streamlines and flow behavior during flow separation from steps and chines is difficult to achieve with towing tank tests. Thus, numerical methods have been incorporated into the analysis of stepped planing hulls. Although numerical methods require a great deal of time, they are cost-effective and have a reasonable level of accuracy when compared to towing tank tests.

Meanwhile, Computational Fluid Dynamics (CFD) has become an increasingly popular method for studying the hydrodynamic behavior of stepped hulls in calm water, with several researchers utilizing this technique, including Brizzolara and Federici (2013), Sheingart (2014), De Marco et al. (2017), Dashtimanesh et al., 2018Dashtimanesh et al., (2018), Dashtimanesh et al., (2019), Niazmand Bilandi et al. (2020 and 2021), and Park et al. (2022). In addition, Nourghasemi et al. (2017) and Husser and Brizzolara, (2021) have developed numerical setups to investigate the impact of swept angle on the performance of stepped planing hulls. Additionally, researchers have explored methods to improve the resistance of these hulls through the use of artificial air cavities, both experimentally and numerically, such as in the studies conducted by Cucinotta et al. (2018, 2019). In all of these studies, CFD was shown to be able to simulate stepped planing hull behavior with acceptable accuracy in calm water, but the use of techniques, such as morphing meshes or overset meshes, can be effective in improving the accuracy of the results (De Marco et al., 2017).

The purpose of the current study is to understand the flow behaviour around and below swept-stepped hulls using a numerical method and experimental results obtained by Vitiello et al. (2022). Therefore, this work focuses on simulating the performance prediction of new systematic series of swept-stepped hulls with different step configurations. To simulate the viscous fluid flow around the swept-stepped hulls, the commercially available CFD software Siemens PLM Star-CCM + has been used. The Unsteady Reynolds Averaged Navier-Stokes (URANS) equations with Overset and Adaptive Mesh Refinement (AMR) techniques have been implemented.

This paper is structured as follows. The problem is defined in Section 2 as well as the details of the hulls. In Section 3, the CFD governing equations on the problem and set-up details (numerical domain, boundary conditions, and computational grid) for the numerical method are defined. In Section 4, the main results of the paper are discussed. Section 5 concludes with concluding remarks. Errors of CFD results compared to towing tank test results are presented in Appendix A.

2. Problem definition

2.1. Forward-swept steps on planing hull performance

Stepped hulls are a common design feature in boats that can reduce resistance and wetted surfaces by inducing flow separation at the bottom of the vessel. However, the performance of a stepped hull depends on factors such as step type, height, and location. There are three main types of steps: straight, forward-swept, and backward-swept. This study investigates the impact of forward-swept steps on the performance of one- and two-stepped planing hulls in calm water using numerical simulations, building upon prior research in this field. By specifically examining the effects of this step type, our study provides valuable insights into the design and optimization of stepped hulls for improved performance and efficiency.

2.2. Studied models

This study investigates a numerical analysis of eight stepped planing hulls that were tested by Vitiello et al. (2022) at the *Università degli Studi di Napoli "Federico II" Dipartimento di Ingegneria Industriale (DII)*. The towing tank at the University Federico II of Naples has a maximum speed of 10 m/s and a maximum acceleration and deceleration of 1 m/s2. The carriage has been equipped with a sensor network and a Data Acquisition (DAQ) device, including an encoder, load cell, balance, thermometer, accelerometer, and laser. The thermometer has an accuracy of 0.1 °C and a resolution of 0.1 °C, with a range of −5 °C to 40 °C. The encoder has an accuracy of 1 mm/m and a resolution of 1 mm, with a period between two pulses measured at 32 bits with a clock of 80 MHz. The load cell has a range of up to 50 N, an accuracy of 0.003%, and a resolution of 0.005 N. The accelerometer has a range of 40 m/s2, an accuracy of ±0.1%, and virtually infinite resolution. The two laser sensors have a range of 0.2–1 m, an accuracy of 0.5 mm, and a resolution of 0.05 mm. The balance has a range of 600 N, accuracy of ±0.1 N, and resolution of 0.1 N. For further information regarding the laboratory instrumentation used in the experimental tests and measurement techniques see De Marco et al. (2017) and Vitiello et al. (2022).

C02 to C05 hulls are single-step, while C06 to C09 hulls are double-step. The principal characteristics and step details for each hull are shown in Tables 1 and 2, respectively. The models were all tested in calm water at different speeds (Fr$_B$ = 0.80–4.97) and in even keel conditions. Fig. 1 shows the body plans of all eight models. The commercial CFD code, Siemens PLM Star-CCM+, was used to calculate the performance of all eight models (Section 4).

Table 1
Principal characteristics of Vitiello et al. (2022) models (VMV Systematic Series).

Model Characteristics	Value
L (m)	0.91
B (m)	0.268
B_{TC} (m)	0.220
B_{TC}/B_C	1
β (°)	23
Δ (N)	30.71
$L/V^{1/3}$	6.24
L_{CG} (from transom) (%L)	From 30 to 34

Table 2
Step configuration details for the VMV Systematic Series hulls, Vitiello et al. (2022).

Cases	Position of forward step (%L)	Height of forward step (%B$_{TC}$)	Position of aft step (%L)	Height of aft step from forward step (%B$_{TC}$)
C02	32.967	0.91	NA	NA
C03	33.077	2.73	NA	NA
C04	48.352	0.91	NA	NA
C05	48.461	2.73	NA	NA
C06	32.967	0.91	16.154	0.91
C07	33.187	2.73	16.374	2.73
C08	48.461	0.91	31.648	0.91
C09	48.681	2.73	31.868	2.73

3. CFD model

3.1. Computational approach

The Reynolds Averaged Navier Stokes (RANS) equations are employed to study fluid flow around stepped hulls. It is assumed that the flow around the hull is incompressible and at a constant temperature to solve the equations. Therefore, the physical problem surrounding the stepped planing hull can be summarized in terms of continuity and momentum equations in a Cartesian framework as follows:

$$\frac{\partial u_i}{\partial x_i} = 0 \tag{1}$$

$$\frac{\partial(\rho u_i)}{\partial t} + \frac{\partial(\rho u_i u_j)}{\partial x_j} = -\frac{\partial p}{\partial x_i} - \frac{\partial \tau_{ij}}{\partial x_j} + g_i \tag{2}$$

where u is the fluid velocity, t is time, p is the pressure, τ_{ij} is the turbulent stress tensor, g_i is the force due to gravity. The stress tensor is given by

$$\tau_{ij} = \left(\mu_{eff} + \mu_t\right)\left[\frac{\partial u_i}{\partial x_j} + \frac{\partial u_j}{\partial x_i}\right] \tag{3}$$

where, μ_{eff} and μ_t are the effective dynamic viscosity and turbulence viscosity which is calculated with the k-omega SST model.

The Volume of Fluid (VOF) technique is used to model the free surface fluid interface by considering the High-Resolution Interface Capturing (HRIC) approach. The fluid phases (water/air) in each cell of the mesh are specified by phase volume fraction (α). α is a number between zero and one and is calculated by

$$\frac{\partial \alpha}{\partial t} + \nabla \cdot (\alpha u) = 0 \tag{4}$$

After that density and viscosity of the fluid are calculated as

$$\rho_{eff}(x_{cell}, t) = \alpha(x_{cell}, t).\rho_w + (1 - \alpha(x_{cell}, t)).\rho_a \tag{5}$$

$$\mu_{eff}(x_{cell}, t) = \alpha(x_{cell}, t).\mu_w + (1 - \alpha(x_{cell}, t)).\mu_a \tag{6}$$

The time step has been defined as the following equation suggested
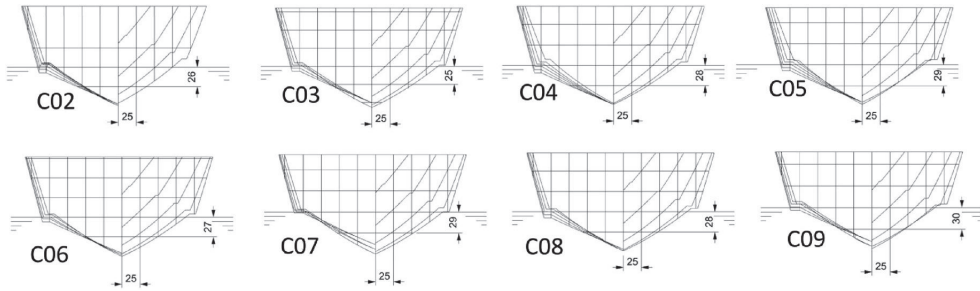
Fig. 1. Transversal body planes of the VMV hull models, Vitiello et al. (2022).

by the ITTC (ITTC 7.5-03-02-03):

$$\Delta_t = 0.005 \sim 0.01 \, \frac{L_{wl}}{v} \qquad (7)$$

where, L_{wl} is the length of the waterline (m), and v is the hull velocity.

Forces and moments acting on the stepped planing hull are solved in two degrees of freedom (pitch and heave) by the DFBI (Dynamic Fluid Body Interaction) approach implemented in the solver of the code Siemens PLM Star-CCM+. All details of the numerical solver are reported in Table 3. More details of the numerical method can be found in Siemens PLM Star-CCM + User's Guide, version 17.02.007 (Siemens, 2022).

3.2. Domain and boundary conditions

Fig. 2 shows a detailed description of the computational domain and boundary conditions of the numerical tank (L is the length of the hull). It is retained for all stepped hull geometries. Since the hull is in a zero-heel state and is completely symmetric, the numerical domain is considered to be axially symmetric for the hull. All dimensions of the numerical domain and the position of the boat are determined based on the CFD ITTC guidelines (ITTC 7.5-03-02-03).

For the inlet, up, side, and bottom boundary conditions, the velocity inlet boundary condition is used. It is specified that the outlet boundary condition is hydrostatic pressure. Symmetric boundary conditions are applied in the center plane. The surfaces of the hull are treated with a non-slip boundary condition. An overset region around the hull is used to calculate boat motions and fluid interactions. Overset boundaries are dynamic and move with the hull, while other boundaries are static. Fig. 2 shows a summary of boundaries. Additionally, the initial location of the free surface is determined based on the draft obtained from the hydrostatic analysis. Fig. 3 shows the free surface created in the numerical tank.

3.3. Mesh scheme

To solve the equations using the finite volume method, meshing is required and this is accomplished by using the CFD software Simens PLM Star-CCM+. It is important to note that mesh sizes and types vary according to the computational domain and the physics of the problem (calm water, waves, etc.). A trimmer mesh is applied to the free surface and a finer mesh is used around the hull and step position. The All-wall y + treatment applies a hybrid approach in the viscous sublayer region that emulates the low-y + wall treatment for fine meshes and the high-y + wall treatment for coarse meshes. As a result, y+ is limited to y+ < 130. Overset meshes are used to account for the motions of the hull in the computational domain. The Overset region is subjected to AMR in order to reduce the solution time and obtain more accurate results. AMR is an automated process that adjusts the mesh's fineness or coarseness based on the settings made during the solution. An overview of the mesh and the wall y + values of the walls is shown in Fig. 4.

A mesh convergence study was conducted to determine the number of meshes required for accurate results and to assess the convergence at four different mesh values, namely coarse (with a cell count of 6153456), medium (with a cell count of 7023456), fine (with a cell count of 8869701), and finest (with a cell count of 10153783). All four grid schemes had the same setting and only differed in the base size of the mesh. The results of the study are presented in Table 4 and Fig. 5a, which show the changes in trim and resistance with respect to different mesh sizes.

As can be seen from the results, convergence is reached at a mesh value of 8869701 cells. Fig. 5b displays samples of the time histories of trim and resistance calculated with Grid C using a mesh size of 8869701 cells.

4. Comparison analysis

4.1. Predicting the running attitudes and resistance of the models

The CFD tool is used to calculate the running attitudes and resistance of a systematic series of stepped planing hulls (Vitiello et al., 2022). Results, including the dynamic trim angle, resistance, sinkage, and wetted surface, are compared against experimental data in Fig. 6. For all models, CFD errors for the prediction of trim, resistance, sinkage, and wetted surface against experimental data are shown in Appendix A. For all cases, the CFD results are in line with experimental data, and for the regime in which the planing hulls operate, all data is nearly accurate. As the speed increases, the dynamic trim of the craft increases relative to displacement and the semi-planing regime (for $Fr_B < 1.5$). Once the semi-planing regime is completed, the trim reaches its maximum value. The trim value reaches its maximum for all hulls between beam Froude numbers 1.45 and 1.93, except for the C06 hull, which is at beam Froude number 2.86 in the experimental data. As the Froude number increases, the trim value in the planing regime decreases. In this case, the hull is

Table 3
Solver settings.

Item	Description
solver	Implicit unsteady
Convection term	2nd order
Turbulence model	k-Omega SST
Time step (s)	Equation (7)
Temporal Discretization	1st order
Iteration per time step	5
Mesh motion	Overset with Adaptive Mesh Refinement (AMR)
Overset Interpolation scheme	Linear
Wall treatment	Two-layer All y+
Water density	1000 kg/m³
Water viscosity	0.000934 Pa·s

Fig. 2. Computational domain and boundary conditions applied.
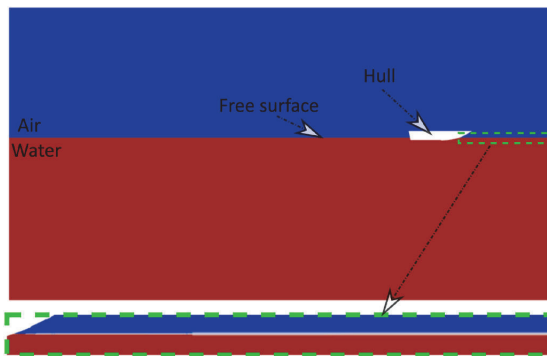
Fig. 3. Free surface in the numerical domain.

said to be in a planing regime when the sinkage value moves from negative to positive, as described in Garland (2010). According to the sinkage diagrams for these cases, the planing regime began when the sinkage value became positive (between beam Froude numbers 1.45 and 1.93), except for the C06 hull, where this occurred after a delay (at Fr_B = 2.86).

Table 5 shows the average error in predicting trim angle and sinkage by numerical models as compared to experimental data for all hulls.

The resistance value of stepped planing hulls is extremely important in the planing regime ($Fr_B > 1.5$), especially at high speeds. A comparison of the resistance of stepped hulls is presented in Fig. 6. The resistance of stepped hulls is directly related to the shape and value of the wetted surface as well as the water spray of the hull. Fig. 7 illustrates the wetted surface caused by water spray, determined numerically and experimentally.

It should be noted that wetted surfaces caused by the water spray area (mainly whisker spray area, Savitsky and Morabito, 2011) are not included in the experimental wetted surface values (due to the difficulties in precisely estimating them in towing tank tests) although the water spray resistance is accounted for in the experimental total resistance.

In Table 6, the average error in predicting the resistance value of all models is presented. The lowest and highest resistance values for $1.9 < Fr_B < 4.0$ are measured for C05 and C07 hulls, respectively. Additionally, for $Fr_B > 4.0$, the lowest and highest average resistance values are calculated for C04 and C09 hulls, respectively.

The C02 hull is a single-stepped hull with the lowest step height, and its step is almost at LCB (33% L). If the step height of C02 is multiplied by three and the longitudinal position of the step is kept constant (this is the specification for C03), the resistance value increases at all speeds. The new geometry increases the average resistance value for $1.9 < Fr_B < 4.0$ and $Fr_B > 4.0$ by 2% and 10%, respectively. In addition, the percentage of the wetted surface area of C03 is less than that of C02. Thus, step ventilation by increasing the step height in C03 has been done correctly, but the whisker spray resistance of the C03 hull is greater than that of the C02 hull, which increases the overall resistance of the C03 hull.

Increasing the longitudinal position of the step in the C02 hull by 48% L (in the forward direction) while keeping the step height (this is the specification for the C04 hull) increases the average resistance value by 4% for $1.9 < Fr_B < 4.0$ and decreases it by 1% for $Fr_B > 4.0$. In comparison to C02, C04 has a 0.7% increase in wetted surface area for $1.9 < Fr_B < 4.0$ and 14% for $Fr_B > 4.0$. It can be concluded that the resistance caused by the whisker spray is lower for C04 than for C02. This means that the reduction in whisker spray is caused by the forward movement of the step at a constant height.

In the final stage of single-step hulls, the longitudinal position of the C02 hull is increased by 48% L (in the forward direction) and the step height is tripled (this is called the C05 hull). These changes in hull geometry decreased the average resistance value by 1% for $1.9 < Fr_B < 4.0$ and increased it by 3% for $Fr_B > 4.0$ compared to the C02 hull. However, the average wetted surface of the C05 hull increased by 2% for $1.9 < Fr_B < 4.0$, while it decreased by 8% for $Fr_B > 4.0$ compared to the C02 hull. A comparison of the data indicates that the drag caused by whisker spray on the C05 hull is higher than that on the C02 hull at high speeds, which can be attributed to the higher step height on the C05 hull. According to CFD and towing tank testing at Fr_B = 3.31, Fig. 7 shows the whisker spray area.

Adding a step on the single-step C02 hull at 16% L (near the transom) and the same step height (C06 hull specifications) increases the hull's average resistance by 12% for $1.9 < Fr_B < 4.0$ and by 16% for $Fr_B > 4.0$. In addition, the average wetted surface increases by 16% for $1.9 < Fr_B < 4.0$ and by 21% for $Fr_B > 4.0$. Tripling the step height of C06 (specifications of C07 hull) increases the average resistance value by 2% for $1.9 < Fr_B < 4.0$ and by 1% for $Fr_B > 4.0$. Increasing the step height decreases the average wetted surface by 1% for $1.9 < Fr_B < 4.0$ and by 11% for $Fr_B > 4.0$. Increasing the step height decreases the wetted surface of the C07 hull but increases the spray resistance.

By adding a step at 16% L (near the transom) and keeping the same step height (C06 hull specifications), the hull average resistance is increased by 12% for $1.9 < Fr_B < 4.0$ and by 16% for $Fr_B > 4.0$. Additionally, the average wetted surface increases by 16% for $1.9 < Fr_B < 4.0$
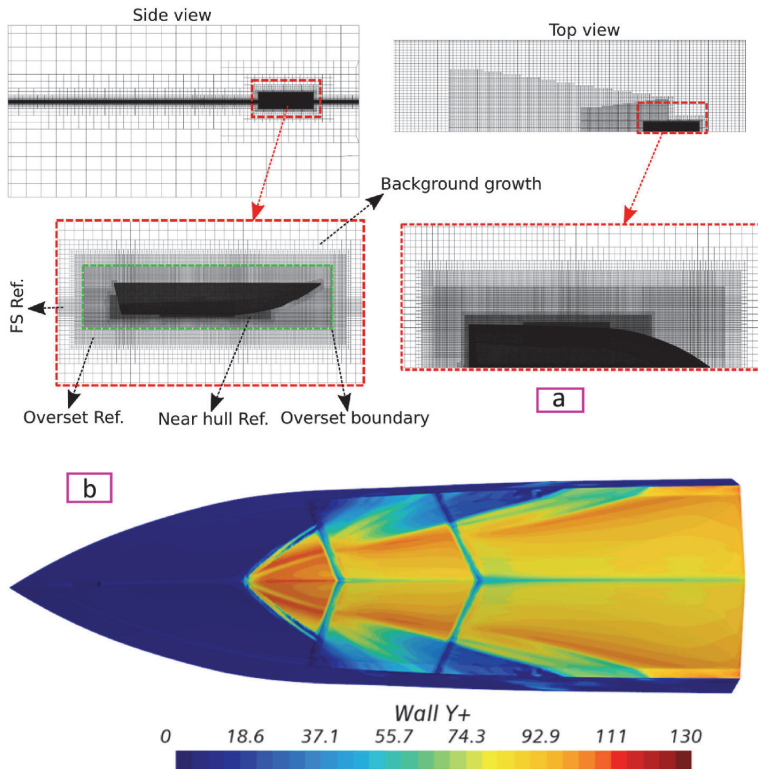
Fig. 4. (a) Computational grid views. (b) Wall y + on the C08 hull at $Fr_B = 4.97$.

Table 4
Mesh convergence study for C08 hull at $Fr_B = 4.97$.

Grid no.	Cell count	$\dfrac{R}{\Delta}$	E_R%	τ [deg]	E_τ%
A	6153456	0.692	29.10%	3.423	29.56%
B	7023456	0.638	19.03%	3.123	18.21%
C	8869701	0.553	3.17%	2.764	4.62%
D	10153783	0.550	2.61%	2.812	6.43%
Exp.	–	0.536	–	2.642	–

and by 21% for $Fr_B > 4$. A tripling of the step height C06 (specified for the C07 hull) increases the average resistance value by 2% for $1.9 < Fr_B < 4.0$ and by 1% for $Fr_B > 4.0$. As the step height is increased, the average wetted surface decreases by 1% for $1.9 < Fr_B < 4.0$ and by 11% for $Fr_B > 4.0$. As the step height increases, the wetted surface of the C07 hull decreases while the spray resistance increases.

In the C06 hull, the step (which is located at 16% L) can be moved forward (48% L) while keeping the step height the same (consistent with the C08 hull specifications), thereby reducing the average resistance value by 1% and 7% for $1.9 < Fr_B < 4.0$ and $Fr_B > 4.0$, respectively. As a result, the average wetted surface of the hull is reduced by 5% for $1.9 < Fr_B < 4.0$ and 7% for $Fr_B > 4.0$. Increasing the step height of the C08 hull to three times its original value (specifications of the C09 hull) decreases the average resistance value by 5% for $1.9 < Fr_B < 4.0$ but increases it by 12% for $Fr_B > 4.0$. As for the average wetted surface for both Froude number ranges ($1.9 < Fr_B < 4.0$ and $Fr_B > 4.0$), it decreased by 34% and 36%, respectively, compared to C08.

Among the two-stepped hulls, the C08 hull has the lowest average resistance value at the highest speed ($Fr_B > 4.0$), which increased by 9% compared to the single-stage C04 hull (which had the lowest measured resistance value among the single-stepped hulls). In addition, the average wetted surface of the C08 hull decreased by 1% compared to the C04 hull.

The C09 hull showed the greatest resistance at maximum speed among all hulls, and the lowest wetted surface value was measured for this hull at maximum speed. As a result of these results, it can be concluded that the C09 hull has a higher spray resistance at maximum speed.

Finally, it is important to note that adding a step can improve the longitudinal dynamic stability of the boat (e.g. by decreasing the dynamic trim angle, Blount and Codega, 1992); however if it is placed in the wrong position, it will increase the hull resistance, which is primarily related to the resistance to spray and the wrong reattachment point of the flow.

4.2. CFD-based wetted shape calculation vs towing tank measurements

Estimating the wetted surface of a hull through experimentation is a challenging task that typically requires the use of underwater cameras and post-processing with CAD software (e.g. Begovic and Bertorello, 2012). However, the use of transparent models can simplify the process. In towing tank tests, Vitiello et al. (2022) have used hulls with transparent bottoms to visualize the water flow beneath them. A 50 mm camera was mounted on the CG to capture video frames, which were then analyzed digitally to estimate the wetted surface values. They measured the dynamic wetted surface by post-processing the top-view images using 3D CAD software for each speed. This experimental approach provided an accurate and reliable method for estimating the dynamic wetted surface of the hulls.

(a)

(b)
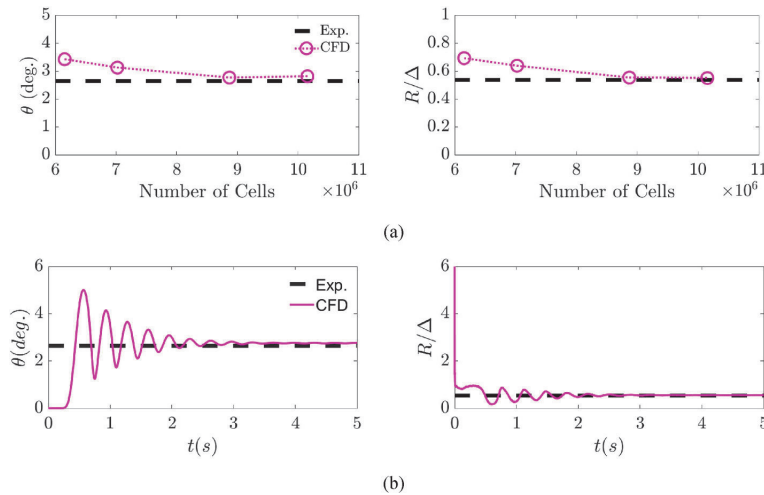
Fig. 5. a) Mesh convergence trends for C08 hull at $Fr_B = 4.97$, b) Time history of trim angle and resistance for C08 hull at beam Froude number 4.97 for grid number C.

To estimate the wetted surface in CFD simulations, a threshold value is defined for the fluid volume fraction in the post-process. This value represents the minimum fraction of the control volume that must be filled with fluid for the surface to be considered wetted. A common value for this threshold is 0.5, which means that if at least half of the control volume is filled with fluid, the surface is considered wetted.

The top views of the wetted surfaces of the single-stepped and double-stepped planing hulls, obtained by the CFD method (lower half of the figure) and towing tank test (upper half of the figure), are shown in Fig. 8. A comparison of the CFD and towing tank results shows that the wetted surface of the hulls is generally similar at all speeds. The average error in predicting the wetted surface value of all models using the numerical method is presented in Table 7.

For the C02 hull, where the step height is 0.91% B_{TC}, flow separation from the step did not occur at any speed (Fig. 8-a). The purpose of placing a step on the bottom of the planing hull is to separate the fluid flow and consequently reduce the dynamic trim angle and the resistance of the hull, otherwise, the performance of the step would be different, e. g., acting as a spray deflector (Molchanov et al., 2019). Therefore, for stepped planing hulls, it is essential to determine the height and position of the steps and the speed at which the flow separation begins. Another critical aspect of the stepped planing hull is that the stagnation line should not cross the step as this leads to heavy water sprays and significantly increases spray resistance (Fig. 8; Savitsky and Morabito, 2010). By increasing the step height of the C02 hull to 2.73% B_{TC} (C03 hull, Fig. 8-b), the flow has been separated from the step, and from the beam Froude number of 1.93, the average value of the wetted surface has decreased by 10%. As long as the stagnation line has not crossed the step (beam Froude number of 2.86), the total resistance in the planing regime is 1% lower than that of the C02 hull. The total resistance increases as soon as the stagnation line crossed the step.

Moving the longitudinal position of the step on the bottom of the C02 hull (C04 hull, Fig. 8-c) increased the wetted surface at all other speeds except Froude number 2.86, where the wetted surface decreased by 3% compared to C02. In the C04 hull, as in the C02 hull, the flow is not detached from the step. It can be concluded that the movement of the step has no effect on the onset of flow separation from the step, but its movement toward the front of the boat has a direct effect on resistance reduction, as it acts as a reverse spray deflector (Wielgosz et al., 2020).

As the step height of the C04 hull increased (C05 hull, Fig. 8-d), the wetted surface area increased except for the beam Froude number of

1.45 until the beam Froude number of 3.31. After beam Froude number 3.91, the wetted surface decreased significantly. As shown in Fig. 8-d, both the numerical and experimental methods performed step ventilation correctly. The increase in step height, which resulted in step ventilation decreased the resistance of the hull up to the beam Froude number of 3.91, but from the beam Froude number of 4.5, the resistance increased. It can be seen from the shape of the wetted surface that the resistance increased at high speeds due to the decreasing angle between the stagnation line and the keel and the stagnation line passing through the steps resulting in more spray resistance.

The C06 hull is a two-stepped planing hull created by adding a step to the bottom of the C02 hull. The shape of the wetted surface and the flow in the bottom of the hull are shown in Fig. 8-e. As seen from the figure, the additional step did not affect the flow separation at the step height of 0.91% B_{TC} and only increased the wetted surface and resistance for all speeds. It was found that the flow from both steps of the C06 hull was separated by increasing the step height to 2.73% B_{TC} (Fig. 8-f). Flow separation decreased the wetted surface for all speeds except for the two beams Froude numbers of 2.86 and 3.31, where the wetted surface increased by 5% and 0.03%, respectively. At the two beam Froude numbers of 4.5 and 4.97, the average wetted surface decreased by about 11%, while the average resistance increased by 1.22% due to the large spray caused by the passage of the stagnation line from the steps.

The C08 hull, whose wetted surface is shown in Fig. 8-g, was created by shifting the rear step of the C06 hull to the front. According to the experimental and numerical calculations, no flow separation was observed when the step was moved on the hull, and the step height was less than 1% B_{TC}. Compared to the C06 hull, the wetted surface has decreased at all speeds, and the average wetted surface reduction for the last two beam Froude numbers was about 7%. The resistance reduction was measured at the last three beam Froude numbers, which, considering that the height of the step was less than 1% B_{TC}, resulted in the step acting like a reverse spray deflector. A wetted surface of the C09 hull is shown in Fig. 8-h (the step height of the C08 hull has been increased to 2.73% B_{TC}). The average reduction in the wetted surface in planing mode (from $Fr_B = 1.93$ up to $Fr_B = 4.97$) was about 34.5% compared to the C08 hull. Additionally, the average resistance value in the planing regime up to beam Froude number 3.91 was reduced by 5% compared to C08. However, since beam Froude number 4.5, the average resistance value has been increased by 12%. As can be seen from the shape of the wetted surface, starting from Froude number 4.5, the angle between the
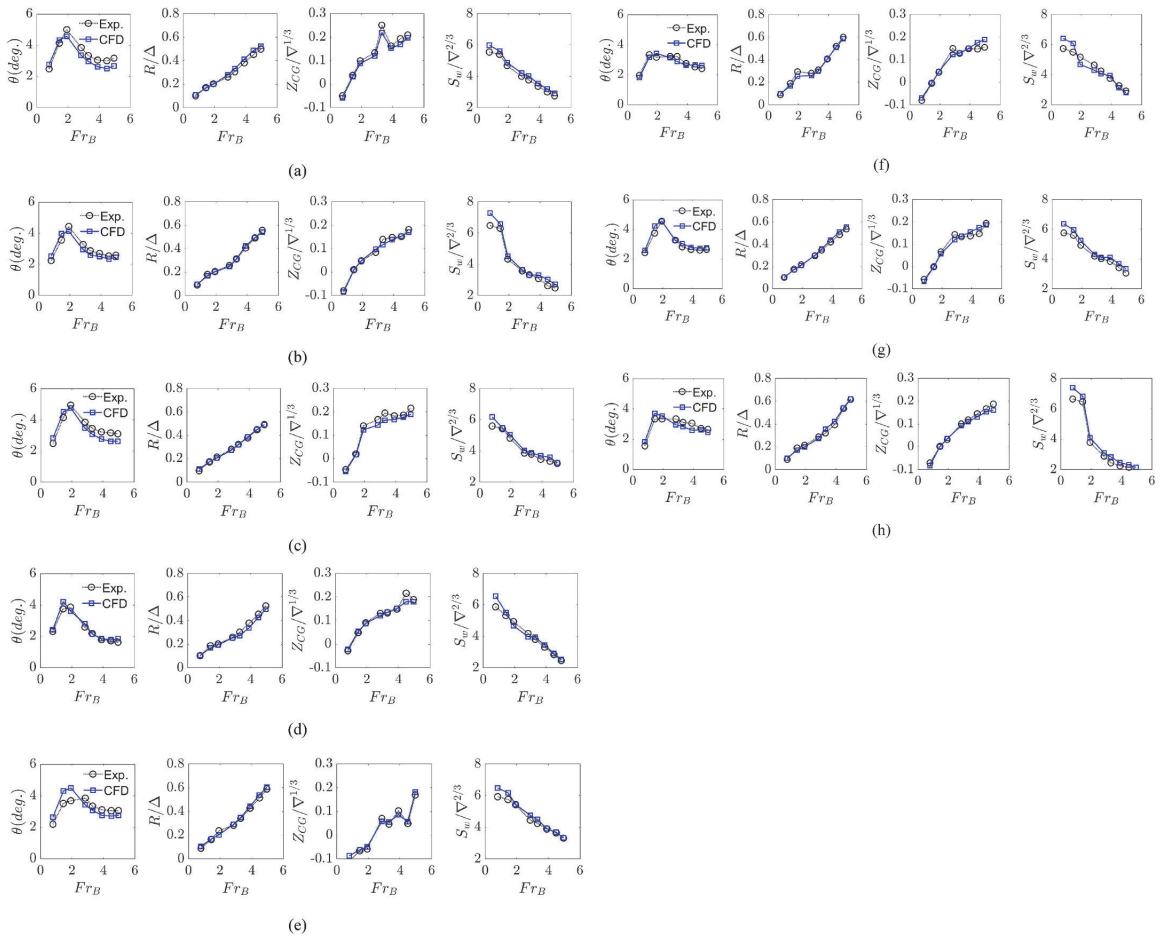
Fig. 6. Comparison of the CFD results against the experimental results of Vitiello et al. (2022), from the left to the right, are: dynamic trim, resistance, sinkage, and wetted surface, for the hull a) C02, b) C03, c) C04, d) C05, e) C06, f) C07, g) C08, and h) C09.

Table 5
The average error for prediction trim angle and sinkage.

Models	C02	C03	C04	C05	C06	C07	C08	C09
$Ave.\,E_\tau\%$	7.98%	3.05%	6.06%	4.85%	2.14%	0.04%	5.39%	1.41%
$Ave.\,E_{Z_G}\%$	6.85%	1.52%	4.06%	3.91%	4.06%	0.03%	3.44%	0.8%
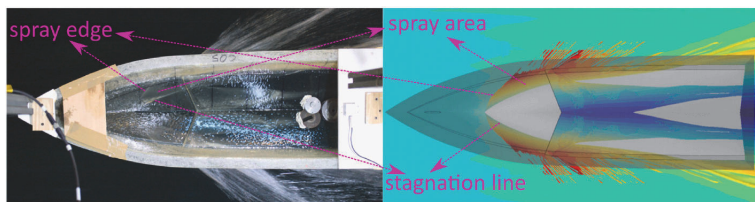
Fig. 7. The spray area for the C05 hull at $Fr_B = 3.31$.

Table 6

The average error for calculation resistance calculation.

Models	C02	C03	C04	C05	C06	C07	C08	C09
$Ave.\, E_R\%$	5.16%	0.04%	1.18%	5.48%	2.40%	3.81%	1.88%	1.39%

Fig. 8. Comparison of the numerically calculated wetted surfaces against the experimental results of Vitiello et al. (2022): a) C02, b) C03, c) C04, d) C05, e) C06, f) C07, g) C08, and h) C09.

keel and the stagnation line decreases, and the stagnation line intersects the step at a lower angle than the keel, thus increasing spray resistance.

4.3. Visualization of air and water flow on the bottom of stepped hull models by CFD

The volume fraction of water at various velocities is shown in Fig. 9

Table 7

The average error for calculation wetted surface.

Models	C02	C03	C04	C05	C06	C07	C08	C09
$Ave.\,E_R\%$	5.55%	6.72%	4.66%	2.29%	3.97%	0.22%	7.71%	9.11%
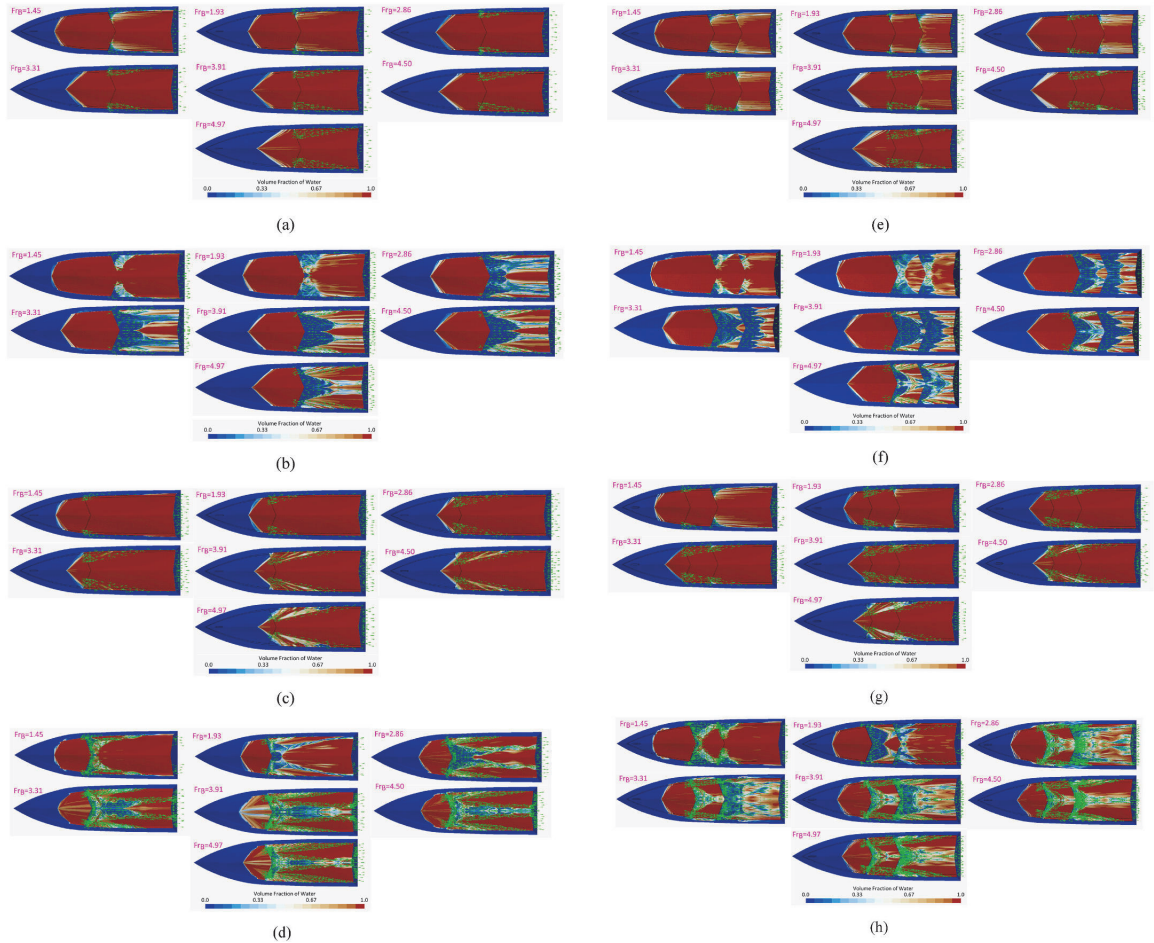
Fig. 9. Calculating the volume fraction of water due to hydrodynamic forces and the spray of water (red area) and also air flow (green vectors) due to the step for a) C02, b) C03, c) C04, d) C05, e) C06, f) C07, g) C08, and h) C09.

to determine the effects of the step on the wetted surface, ventilation, and spray flow. The airflow (green vector) becomes more apparent behind the step as the speed increases. This air stream (green vector) may exit the chine with the spray stream, or it may be directed to the transom and exit there. A volume fraction value of 0 (blue) indicates a full air phase, while a value of 1 (red) indicates a full water phase. A value between 0 and 1 represents the weight of the air-water mixture.

As the step height increases (whether for a single-step or a two-step hull), a mixed flow pattern is created in the dry back part of the step, which varies depending on the step position. The mixture of air and water, ending up in a vortex formation, is directed to the next step or transom (De Marco et al., 2017). Fig. 9 shows that this airflow enters the dry area of the steps via the chine or the main flow. In the case of straight steps, these flow patterns are formed by small bubbles, which are composed of a combination of air and water (see Lee et al., 2014). A

vortex usually is not detected in such cases but, on the other hand, this vortex generation becomes more likely when the step is forward-swept. It should be noted that the flow under the stepped hull can be directed to the transom through the spray rail, which reduces the spray resistance (Molchanov et al., 2019). This may be investigated for stepped planing hulls in future studies.

4.4. Calculating pressure on the bottom of stepped models by CFD

As the lift force supports the weight of the boat in a planing hull, a change in the boat's wetted surface will result in a change in the pressure distribution and, therefore, in the lift force distribution. Fig. 10 shows the pressure distribution on the bottom of stepped hulls C02 to C09. This figure illustrates the effect on the pressure distribution of adding the step, increasing the step height, and changing the step position. When
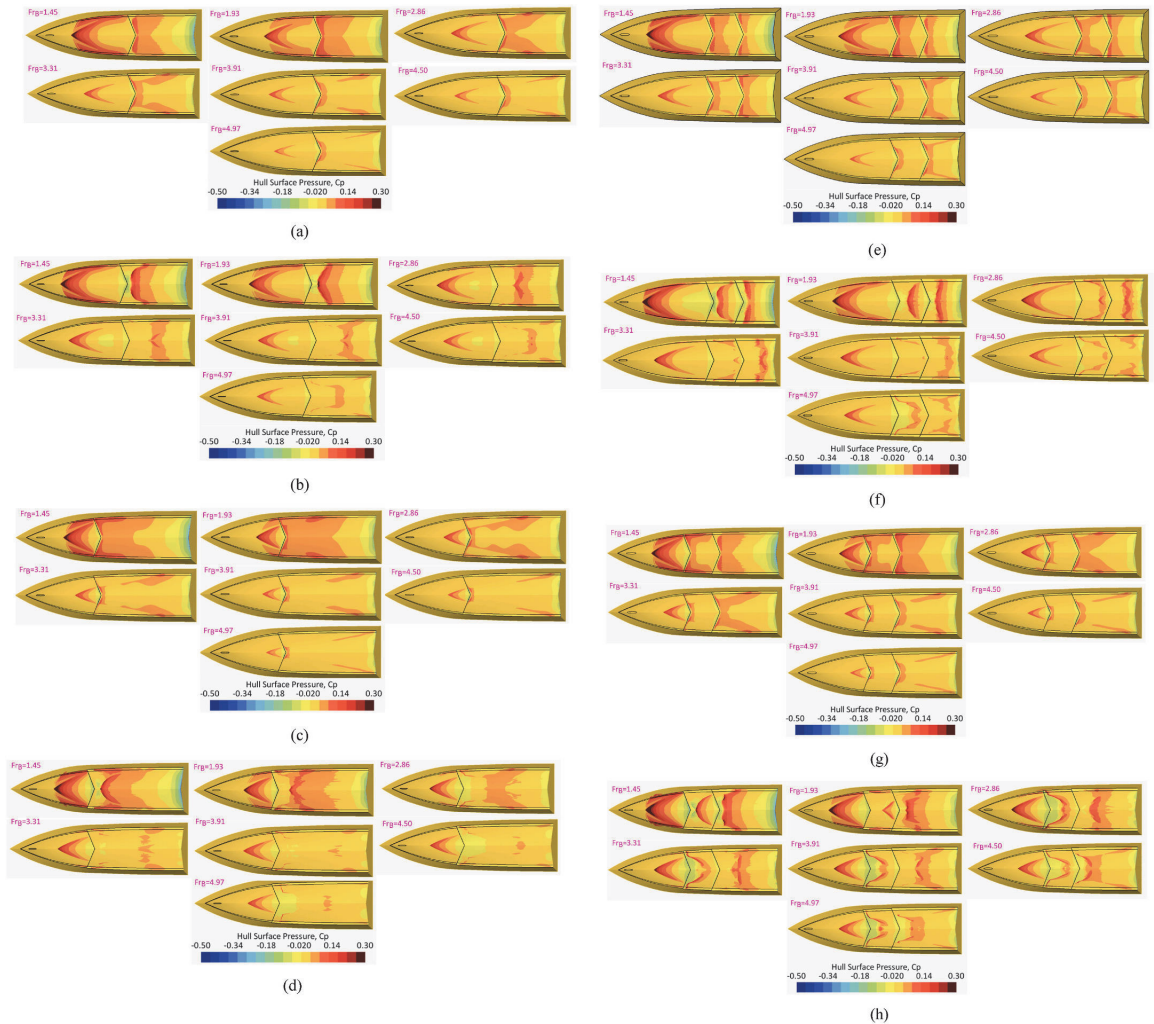
Fig. 10. Pressure contours on the bottom of the hulls: a) C02, b) C03, c) C04, d) C05, e) C06, f) C07, g) C08, and h) C09.

the flow in the step separates, the pressure distribution at the step location is interrupted, and a low-pressure region is created between the step and the back of the step. The pressure inside the cavity is almost equal to the atmospheric pressure. The pressure coefficient in Fig. 10 is defined as follows:

$$C_p = \frac{p}{0.5\rho_w v^2} \qquad (8)$$

The pressure distribution on the C02 hull is shown in Fig. 10-a. In this hull, the pressure distribution is greatest at the step and behind it, as the flow has not yet been separated from the step. When the step height is increased (C03 hull - Fig. 10-b) and the flow separation occurs, this high-pressure region is created after the ventilation region at the reattachment point. As a result of this high-pressure region, an additional lift force is generated, reducing trim angle and sinkage and improving the performance of the hull. Similar high-pressure regions can be seen in Fig. 8-c and 8-d following an increase in step height and flow separation. Additionally, as the flow is separated from the step, the pressure distribution near the chine is concentrated towards the keel (centerline).

The pressure distribution over a stepped hull bottom is also affected by the position of the steps. According to Fig. 10-a and 10-c, the pressure value at the stagnation line and at the step decreases with increasing distance from the transom.

By adding a step to the C02 hull (C06 hull - Fig. 10-e), three separate pressure zones are created at the bottom of the boat. The pressure distribution is highest at the location of the two steps and at the stagnation line of the forward planing region. When the step height of the C06 hull (C07 hull - Fig. 10-f) is increased for each step, the high-pressure region is transferred to the area after the step ventilation. For this hull, the pressure increases at the stagnation line of the forward planing region. When the position of the rear step in the C06 hull is moved forward (C08 hull - Fig. 10-j), the high-pressure region in the transom region becomes more sweeping and shifts towards the chine. Increasing the step height of the C08 hull (C09 hull - Fig. 10-h) results in a larger high-pressure region in the stagnation line of the forward planing region. The pressure distribution is also concentrated in the middle planing region and the stern zone after the step ventilation zone.

Fig. 10 shows that for all step configurations, the pressure

distribution concentrates on the centerline in the forward planing region as the speed increases. Additionaly, in the rear regions, it is mainly found in the chines.

To summarize, as seen in Fig. 10, changes in hull geometry alter the pressure distribution on the bottom of the hull and shift the center of lift force. For a one-step hull, two pressure zones are created, and for a two-step hull, three pressure zones are created, though this may depend on whether flow separation occurs. These changes in pressure distribution and lift force result from changes in the flow around and on the bottom of the hull.

5. Conclusion

In this paper, a comparative analysis has been conducted between towing tank test results and CFD simulations for swept-stepped planing hulls. Additionally, a numerical setup has been developed using CFD to better understand the hydrodynamic behavior and physical flow on these hulls. A systematic series of eight models of swept-stepped planing hulls have been selected to investigate the effects of adding a step, changing the step height, and changing the step position on performance prediction, resistance, wetted surface shape, and ventilation length. The results have been compared to experimental towing tests. The present numerical method predicts experimental trends with acceptable errors, with mean errors of 0.76% for trim, 0.34% for resistance, 2.76% for sinkage, and 4.85% for the wetted surface for all hulls. Based on the results of both the experimental towing tests and the numerical method, the following conclusions can be drawn:

- increasing the step height of a stepped planing hull from 0.91% B_{TC} to 2.73% B_{TC} leads to the flow separation behind the step and the formation of a high-pressure region at reattachment points. This high-pressure region generates additional lift, which significantly affects the trim angle. The lowest trim angle for single-stepped hulls was observed in C05 (step height = 2.73% B_{TC}, position = 48.46% L), and for two-stepped hulls, it was observed in C07 (step height = 2.73% B_{TC}, forward step position = 22.19% L, aft step position = 16.38% L). Additionally, at a Froude number of 4.97 (maximum speed), the trim angle of C02 was found to be higher than that of C03, C04, C05, C06, C07, C08, and C09 by 18%, 2%, 49%, 3.5%, 24%, 16%, and 16%, respectively. The absence of flow separation for a 0.91% B_{TC} step height in one- and two-step planing hulls was also noted.
- When the step of single-step hulls is located slightly behind the center of gravity (C02 and C03), moving the step towards the front of the hull at a constant step height (as in C04 and C05) leads to a decrease in resistance value at high speeds, despite an increase in the wetted surface area. This suggests that the forward swept step in the front part of the stepless hull acts as a reverse deflector, which reduces the spray drag and overall resistance.
- Adding a step to the near transom of a single-stepped hull (C02 or C03) causes a decrease in trim at high speeds but increases the wetted surface area and resistance (C06 or C07).
- Adding a step in the forward part of a single-stepped hull (C02 or C03) has been found to decrease the dynamic trim angle at the lowest

step height (C06 hull) and increase it at the highest step height (C07 hull) at high speeds. Additionally, the wetted surface area increases at a step height of 0.91% B_{TC} (C06 hull) and decreases at a step height of 2.73% B_{TC} (C07 hull). Consequently, resistance increases for both hulls, although this increase is greater for the C07 hull than the C06 hull due to the formation of sprays.

- For two-stepped hulls, when the rear step is moved towards the bow at lower step heights (without flow separation), as in the C08 hull, it is an effective way to reduce hull drag by avoiding or reducing sprays. However, at higher step heights, such as the C09 model where flow separation occurs behind the step, moving the step forward leads to an increase in hull resistance due to the formation of sprays.
- The C05 hull showed the lowest resistance value at Fr_B ranging from 1.9 to 4.0, while the C04 hull recorded the lowest resistance at Fr_B values higher than 4.0.
- The appearance of vortices behind the steps happens mainly for swept forward steps that can capture more air and consequently reduce the wetted surface area. However, the vortex generation may be accentuated by the model scale size, is the case for all flow detachment/separation phenomena in model scale.

Overall, this study provides valuable insights into the hydrodynamic performance of swept stepped planing hulls, but it is important to recognize its limitations. The investigation was limited to a systematic series of stepped hulls with specific design parameters, and the use of the RANS equations has limitations in predicting unsteady flow phenomena. Nonetheless, the study provides useful information about the performance of stepped hulls within the confines of the current simulation. Additionally, accurate modeling of the wetted surface and ventilation length of stepped planing hulls is complex and requires careful consideration of the threshold value used for the fluid volume fraction and the isosurface value used for free surface modeling, which can influence the accuracy of the results.

CRediT authorship contribution statement

Rasul Niazmand Bilandi: Software, Validation, Visualization, Formal analysis, Methodology, Writing – original draft. **Abbas Dashtimanesh:** Supervision, Conceptualization, Funding acquisition, Methodology, Formal analysis, Investigation, Project administration, Writing – review & editing. **Simone Mancini:** Software, Methodology, Writing – review & editing.

Declaration of competing interest

The authors declare that they have no known competing financial interests or personal relationships that could have appeared to influence the work reported in this paper.

Data availability

No data was used for the research described in the article.

APPENDIX A. Comparison error between CFD vs. towing tank test results in predicting the running attitudes and resistance of the models

C02														
v [m/s]	Fr_B	Fr_∇	τ_{Exp} [deg]	τ_{CFD} [deg]	$E_\tau\%$	$\dfrac{R_{Exp}}{\Delta}$	$\dfrac{R_{CFD}}{\Delta}$	$E_R\%$	$\dfrac{(Z_G)_{Exp}}{\nabla^{1/3}}$	$\dfrac{(Z_G)_{CFD}}{\nabla^{1/3}}$	$E_{Z_G}\%$	$\dfrac{(S_W)_{Exp}}{\nabla^{2/3}}$	$\dfrac{(S_W)_{CFD}}{\nabla^{2/3}}$	$E_{S_W}\%$
1.29	0.796	1.081	2.462	2.360	−4.14%	0.108	0.100	8.04%	−0.051	−0.059	16.37%	5.551	5.982	7.76%

(continued on next page)

R. Niazmand Bilandi et al.

Ocean Engineering 280 (2023) 114887

(*continued*)

C02														
v [m/s]	Fr_B	Fr_∇	τ_{Exp} [deg]	τ_{CFD} [deg]	$E_\tau\%$	$\dfrac{R_{Exp}}{\Delta}$	$\dfrac{R_{CFD}}{\Delta}$	$E_R\%$	$\dfrac{(Z_G)_{Exp}}{\nabla^{1/3}}$	$\dfrac{(Z_G)_{CFD}}{\nabla^{1/3}}$	$E_{Z_G}\%$	$\dfrac{(S_W)_{Exp}}{\nabla^{2/3}}$	$\dfrac{(S_W)_{CFD}}{\nabla^{2/3}}$	$E_{S_W}\%$
2.357	1.454	1.976	4.126	3.910	−5.23%	0.167	0.169	−1.25%	0.036	0.031	−15.25%	5.390	5.608	4.05%
3.131	1.931	2.625	4.987	4.950	−0.73%	0.199	0.203	−2.13%	0.099	0.089	−10.10%	4.678	4.860	3.90%
4.631	2.857	3.882	3.837	3.752	−2.21%	0.279	0.259	7.90%	0.133	0.120	−9.63%	3.991	4.206	5.39%
5.368	3.311	4.500	3.323	3.330	0.22%	0.332	0.306	8.37%	0.251	0.219	−12.78%	3.768	4.019	6.66%
6.34	3.911	5.314	3.037	3.000	−1.21%	0.411	0.382	7.53%	0.162	0.153	−5.62%	3.364	3.540	5.21%
7.301	4.504	6.120	2.986	2.879	−3.58%	0.487	0.452	7.79%	0.193	0.170	−12.06%	2.995	3.178	6.10%
8.05	4.966	6.748	3.155	3.055	−3.17%	0.523	0.498	5.05%	0.209	0.197	−5.76%	2.750	2.898	5.35%

C03														
v [m/s]	Fr_B	Fr_∇	τ_{Exp} [deg]	τ_{CFD} [deg]	$E_\tau\%$	$\dfrac{R_{Exp}}{\Delta}$	$\dfrac{R_{CFD}}{\Delta}$	$E_R\%$	$\dfrac{(Z_G)_{Exp}}{\nabla^{1/3}}$	$\dfrac{(Z_G)_{CFD}}{\nabla^{1/3}}$	$E_{Z_G}\%$	$\dfrac{(S_W)_{Exp}}{\nabla^{2/3}}$	$\dfrac{(S_W)_{CFD}}{\nabla^{2/3}}$	$E_{S_W}\%$
1.29	0.796	1.081	2.230	2.520	13.01%	0.096	0.088	8.24%	−0.080	−0.086	7.36%	6.480	7.291	12.51%
2.357	1.454	1.976	3.549	3.957	11.49%	0.169	0.178	−5.48%	0.010	0.010	−7.89%	6.291	6.571	4.44%
3.131	1.931	2.625	4.422	4.110	−7.06%	0.202	0.204	−0.90%	0.048	0.048	0.72%	4.321	4.519	4.58%
4.631	2.857	3.882	3.269	2.940	−10.06%	0.248	0.256	−3.24%	0.085	0.097	15.10%	3.573	3.627	1.49%
5.368	3.311	4.500	2.865	2.581	−9.92%	0.309	0.312	−0.82%	0.139	0.117	−16.33%	3.331	3.299	−0.94%
6.34	3.911	5.314	2.688	2.477	−7.85%	0.424	0.407	3.98%	0.147	0.138	−5.89%	3.086	3.309	7.21%
7.301	4.504	6.120	2.522	2.312	−8.32%	0.494	0.491	0.61%	0.151	0.153	0.81%	2.615	3.010	15.08%
8.05	4.966	6.748	2.579	2.433	−5.67%	0.540	0.556	−2.74%	0.181	0.170	−6.01%	2.479	2.711	9.35%

C04														
v [m/s]	Fr_B	Fr_∇	τ_{Exp} [deg]	τ_{CFD} [deg]	$E_\tau\%$	$\dfrac{R_{Exp}}{\Delta}$	$\dfrac{R_{CFD}}{\Delta}$	$E_R\%$	$\dfrac{(Z_G)_{Exp}}{\nabla^{1/3}}$	$\dfrac{(Z_G)_{CFD}}{\nabla^{1/3}}$	$E_{Z_G}\%$	$\dfrac{(S_W)_{Exp}}{\nabla^{2/3}}$	$\dfrac{(S_W)_{CFD}}{\nabla^{2/3}}$	$E_{S_W}\%$
1.29	0.796	1.081	2.470	2.827	14.47%	0.097	0.110	12.85%	−0.047	−0.055	16.96%	5.587	6.169	10.41%
2.357	1.454	1.976	4.139	4.519	9.17%	0.172	0.174	1.37%	0.020	0.017	−15.82%	5.425	5.451	0.49%
3.131	1.931	2.625	4.940	4.742	−4.01%	0.213	0.205	−4.13%	0.140	0.123	−12.37%	4.816	5.047	4.80%
4.631	2.857	3.882	3.845	3.470	−9.75%	0.280	0.273	−2.19%	0.167	0.144	−13.79%	3.858	4.019	4.17%
5.368	3.311	4.500	3.444	3.057	−11.24%	0.322	0.320	−0.63%	0.194	0.164	−15.58%	3.779	3.866	2.30%
6.34	3.911	5.314	3.209	2.746	−14.42%	0.378	0.386	2.06%	0.183	0.167	−8.50%	3.461	3.692	6.67%
7.301	4.504	6.120	3.152	2.610	−17.18%	0.447	0.450	0.59%	0.185	0.176	−5.13%	3.335	3.589	7.61%
8.05	4.966	6.748	3.094	2.614	−15.52%	0.491	0.489	−0.47%	0.216	0.189	−12.57%	3.197	3.225	0.86%

C05														
v [m/s]	Fr_B	Fr_∇	τ_{Exp} [deg]	τ_{CFD} [deg]	$E_\tau\%$	$\dfrac{R_{Exp}}{\Delta}$	$\dfrac{R_{CFD}}{\Delta}$	$E_R\%$	$\dfrac{(Z_G)_{Exp}}{\nabla^{1/3}}$	$\dfrac{(Z_G)_{CFD}}{\nabla^{1/3}}$	$E_{Z_G}\%$	$\dfrac{(S_W)_{Exp}}{\nabla^{2/3}}$	$\dfrac{(S_W)_{CFD}}{\nabla^{2/3}}$	$E_{S_W}\%$
1.29	0.796	1.081	2.304	2.407	4.45%	0.103	0.105	2.42%	−0.028	−0.023	−16.50%	5.870	6.543	11.45%
2.357	1.454	1.976	3.749	4.210	12.30%	0.186	0.168	−9.36%	0.049	0.055	12.62%	5.330	5.505	3.28%
3.131	1.931	2.625	3.853	3.610	−6.30%	0.200	0.191	−4.46%	0.091	0.089	−2.27%	4.939	4.683	−5.18%
4.631	2.857	3.882	2.584	3.650	8.35%	0.258	0.253	−1.72%	0.131	0.121	−7.30%	4.180	3.972	−4.96%
5.368	3.311	4.500	2.181	3.300	−2.55%	0.301	0.272	−9.78%	0.133	0.135	1.66%	3.807	3.944	3.62%
6.34	3.911	5.314	1.777	3.100	4.09%	0.378	0.340	−10.09%	0.148	0.152	2.09%	3.315	3.458	4.33%
7.301	4.504	6.120	1.700	2.940	3.89%	0.453	0.427	−5.68%	0.216	0.179	−17.02%	2.829	2.907	2.77%
8.05	4.966	6.748	1.606	3.000	14.60%	0.525	0.498	−5.16%	0.189	0.180	−4.57%	2.450	2.524	3.02%

C06														
v [m/s]	Fr_B	Fr_∇	τ_{Exp} [deg]	τ_{CFD} [deg]	$E_\tau\%$	$\dfrac{R_{Exp}}{\Delta}$	$\dfrac{R_{CFD}}{\Delta}$	$E_R\%$	$\dfrac{(Z_G)_{Exp}}{\nabla^{1/3}}$	$\dfrac{(Z_G)_{CFD}}{\nabla^{1/3}}$	$E_{Z_G}\%$	$\dfrac{(S_W)_{Exp}}{\nabla^{2/3}}$	$\dfrac{(S_W)_{CFD}}{\nabla^{2/3}}$	$E_{S_W}\%$
1.29	0.796	1.081	2.183	2.320	6.29%	0.090	0.103	14.78%	−0.109	−0.087	−20.19%	5.929	6.487	9.40%
2.357	1.454	1.976	3.505	3.990	13.84%	0.163	0.169	3.50%	−0.066	−0.062	−7.31%	5.757	6.178	7.33%
3.131	1.931	2.625	3.677	4.200	14.23%	0.236	0.202	−14.56%	−0.058	−0.049	−15.69%	5.423	5.431	0.14%
4.631	2.857	3.882	3.848	3.427	−10.95%	0.284	0.291	2.46%	0.070	0.059	−15.44%	4.447	4.753	6.88%
5.368	3.311	4.500	3.329	3.056	−8.21%	0.341	0.349	2.36%	0.046	0.055	18.75%	4.244	4.487	5.72%
6.34	3.911	5.314	3.100	2.754	−11.17%	0.427	0.442	3.66%	0.103	0.087	−15.53%	3.892	3.916	0.62%
7.301	4.504	6.120	3.043	2.694	−11.48%	0.514	0.538	4.63%	0.049	0.057	16.10%	3.639	3.673	0.94%
8.05	4.966	6.748	3.043	2.750	−9.64%	0.589	0.604	2.41%	0.169	0.181	6.87%	3.304	3.327	0.70%

C07														
v [m/s]	Fr_B	Fr_∇	τ_{Exp} [deg]	τ_{CFD} [deg]	$E_\tau\%$	$\dfrac{R_{Exp}}{\Delta}$	$\dfrac{R_{CFD}}{\Delta}$	$E_R\%$	$\dfrac{(Z_G)_{Exp}}{\nabla^{1/3}}$	$\dfrac{(Z_G)_{CFD}}{\nabla^{1/3}}$	$E_{Z_G}\%$	$\dfrac{(S_W)_{Exp}}{\nabla^{2/3}}$	$\dfrac{(S_W)_{CFD}}{\nabla^{2/3}}$	$E_{S_W}\%$
1.29	0.796	1.081	1.949	1.790	−8.17%	0.098	0.089	9.65%	0.080	−0.071	−12.09%	5.740	6.403	11.55%
2.357	1.454	1.976	3.326	3.148	−5.35%	0.168	0.189	−11.19%	0.005	−0.004	−17.06%	5.506	6.075	10.35%
3.131	1.931	2.625	3.154	3.420	8.43%	0.254	0.294	−13.45%	−0.045	0.046	4.45%	5.170	4.673	−9.60%
4.631	2.857	3.882	3.211	3.122	−2.78%	0.259	0.279	−7.25%	−0.150	0.123	−17.84%	4.644	4.309	−7.22%
5.368	3.311	4.500	3.208	2.874	−10.41%	0.296	0.308	−3.76%	−0.128	0.129	0.82%	4.245	4.066	−4.23%
6.34	3.911	5.314	2.751	2.638	−4.10%	0.404	0.406	−0.43%	−0.148	0.150	0.97%	3.754	3.944	5.06%
7.301	4.504	6.120	2.522	2.647	4.96%	0.508	0.519	−2.04%	−0.147	0.174	18.27%	3.271	3.131	−4.27%
8.05	4.966	6.748	2.407	2.608	8.34%	0.586	0.599	−2.05%	−0.154	0.189	22.26%	2.913	2.813	−3.43%

C08														
v [m/s]	Fr_B	Fr_∇	τ_{Exp} [deg]	τ_{CFD} [deg]	$E_\tau\%$	$\dfrac{R_{Exp}}{\Delta}$	$\dfrac{R_{CFD}}{\Delta}$	$E_R\%$	$\dfrac{(Z_G)_{Exp}}{\nabla^{1/3}}$	$\dfrac{(Z_G)_{CFD}}{\nabla^{1/3}}$	$E_{Z_G}\%$	$\dfrac{(S_W)_{Exp}}{\nabla^{2/3}}$	$\dfrac{(S_W)_{CFD}}{\nabla^{2/3}}$	$E_{S_W}\%$
1.29	0.796	1.081	2.417	2.587	7.02%	0.101	0.105	4.24%	−0.058	−0.067	15.57%	5.758	6.356	10.37%
2.357	1.454	1.976	3.742	4.218	12.73%	0.175	0.171	−2.42%	−0.002	−0.002	12.50%	5.591	5.963	6.66%

(*continued on next page*)

13

(*continued*)

C02														
ν [m/s]	Fr_B	Fr_∇	τ_{Exp} [deg]	τ_{CFD} [deg]	E_τ%	$\dfrac{R_{Exp}}{\Delta}$	$\dfrac{R_{CFD}}{\Delta}$	E_R%	$\dfrac{(Z_G)_{Exp}}{\nabla^{1/3}}$	$\dfrac{(Z_G)_{CFD}}{\nabla^{1/3}}$	E_{Z_G}%	$\dfrac{(S_W)_{Exp}}{\nabla^{2/3}}$	$\dfrac{(S_W)_{CFD}}{\nabla^{2/3}}$	E_{S_W}%
3.131	1.931	2.625	4.545	4.570	0.56%	0.216	0.209	−3.14%	0.065	0.056	−13.52%	4.923	5.253	6.70%
4.631	2.857	3.882	3.276	3.487	−0.48%	0.296	0.300	1.43%	0.143	0.119	−16.86%	4.183	4.300	2.79%
5.368	3.311	4.500	2.817	3.045	8.11%	0.347	0.356	2.75%	0.132	0.135	2.19%	4.014	4.103	2.22%
6.34	3.911	5.314	2.642	2.785	5.42%	0.419	0.435	3.87%	0.137	0.155	13.30%	3.845	4.103	6.71%
7.301	4.504	6.120	2.584	2.725	5.44%	0.485	0.509	5.06%	0.147	0.173	17.92%	3.418	3.692	8.00%
8.05	4.966	6.748	2.642	2.757	4.36%	0.536	0.553	3.28%	0.193	0.186	−3.56%	3.044	3.356	10.23%
C09														
ν [m/s]	Fr_B	Fr_∇	τ_{Exp} [deg]	τ_{CFD} [deg]	E_τ%	$\dfrac{R_{Exp}}{\Delta}$	$\dfrac{R_{CFD}}{\Delta}$	E_R%	$\dfrac{(Z_G)_{Exp}}{\nabla^{1/3}}$	$\dfrac{(Z_G)_{CFD}}{\nabla^{1/3}}$	E_{Z_G}%	$\dfrac{(S_W)_{Exp}}{\nabla^{2/3}}$	$\dfrac{(S_W)_{CFD}}{\nabla^{2/3}}$	E_{S_W}%
1.29	0.796	1.081	1.548	1.830	18.21%	0.090	0.101	12.94%	−0.071	−0.082	15.89%	6.641	7.384	11.18%
2.357	1.454	1.976	3.326	3.700	11.25%	0.188	0.170	−9.78%	0.002	0.002	13.02%	6.448	6.814	5.68%
3.131	1.931	2.625	3.326	3.510	5.53%	0.213	0.198	−7.20%	0.032	0.035	10.68%	3.777	4.094	8.40%
4.631	2.857	3.882	3.326	2.940	−11.61%	0.285	0.271	−4.92%	0.100	0.093	−6.74%	2.884	3.094	7.28%
5.368	3.311	4.500	3.097	2.810	−9.27%	0.319	0.354	11.17%	0.117	0.110	−6.44%	2.441	2.832	16.02%
6.34	3.911	5.314	3.040	2.580	−15.13%	0.393	0.421	7.03%	0.145	0.130	−10.07%	2.244	2.458	9.56%
7.301	4.504	6.120	2.696	2.612	−3.12%	0.535	0.541	1.13%	0.167	0.152	−8.94%	2.140	2.299	7.44%
8.05	4.966	6.748	2.639	2.450	−7.16%	0.614	0.619	0.78%	0.187	0.161	−13.80%	1.995	2.140	7.30%

References

Becker, C., Loreto, A., Shell, J., 2008. A Systematic Study of Stepped Planing Hulls. Webb Institute, Glen Cove, NY.

Begovic, E., Bertorello, C., 2012. Resistance assessment of warped hullform. Ocean Eng. 56, 28–42.

Benen, L., 1966. General Resistance Test of a Shallow Step Planing Hull with Application to a Hydrofoil Configuration, vol. 2169. DTMB Report.

Benen, L., 1967. General Resistance Test of a Stepped Planing Hull with Application to a Hydrofoil Configuration, vol. 2320. NSRDC Report.

Blount, D.L., Codega, L.T., 1992. Dynamic stability of planing boats. Mar. Technol. 29 (1), 4–12.

Brizzolara, S., Federici, A., 2013. Designing of planing hulls with longitudinal steps: CFD in support of traditional semi-empirical methods. In: Proceedings, Design, Construction & Operation of Super and Mega Yachts Conference. Genoa, Italy. May 8–9.

Clement, E.P., 1967. Effect of Length-Beam Ratio on the Performance of a Stepped Planing Boat with an Adjustable Stern Stabilizer. NSRDC Report 2552.

Cucinotta, F., Guglielmino, E., Sfravara, F., Strasser, C., 2018. Numerical and experimental investigation of a planing Air Cavity Ship and its air layer evolution. Ocean Eng. 152, 130–144.

Cucinotta, F., Eugenio, G., Felice, S., 2019. A critical CAE analysis of the bottom shape of a multi stepped air cavity planing hull. Appl. Ocean Res. 82, 130–142.

Danielsson, J., Strumquist, J., 2012. Conceptual Design of a High-Speed Superyacht Tender Hull Form Analysis and Structural Optimization [thesis]. Marina System Centre for Naval Architecture, KTH University, Stockholm.

Dashtimanesh, A., Tavakoli, S., Sahoo, P., 2017. A simplified method to calculate trim and resistance of a two-stepped planing hull. Ships Offshore Struct. 12, S317–S329.

Dashtimanesh, A., Esfandiari, A., Mancini, S., 2018. Performance prediction of two-stepped planing hulls using morphing mesh approach. J. Ship Prod. Des. 34 (3), 236–248.

Dashtimanesh, A., Roshan, F., Tavakoli, S., Kohansal, A., Barmala, B., 2019. Effects of step configuration on hydrodynamic performance of one-and doubled-stepped planing flat plates: a numerical simulation. In: Proceedings of the Institution of Mechanical Engineers. Journal of Engineering for the Maritime Environment, Part M. https://doi.org/10.1177/1475090219851917 (Published Online).

De Marco, A., Mancini, S., Miranda, S., Scognamiglio, R., Vitiello, L., 2017. Experimental and numerical hydrodynamic analysis of a stepped planing hull. Appl. Ocean Res. 64, 135–154.

Doctors, L.J., 1985. Hydrodynamics of High-Speed Small Craft. No. 292.

Filing, J., 1993. Experimental Procedure and Analysis of Stepped Planing Hulls with Applications to Motor Yachts, Patrol Vessels, and Fast Ferries. Webb Institute, Glen Cove, NY.

Garland, W.R., 2010. Stepped Planing Hull Investigation. United States Naval Academy.

Gassman, W., Kartinen, S., 1994. An Investigation into the Effects of the Step Location and the Longitudinal Center of Gravity Location on the Performance of Stepped Planing Hulls. Webb Institute, Glen Cove, NY.

Husser, N.A., 2023. Experimental and Numerical Investigation of Forward and Aft Swept Stepped Planing Hulls in Calm Water and Regular Waves. Doctoral dissertation. Virginia Tech.

ITTC, 2014. Practical Guidelines for Ship CFD Applications 7.5-03-02-03, Rev. 01.

Lee, E., Pavkov, M., McCue-Weil, L., 2014. The systematic variation of step configuration and displacement for a double-step planing craft. J. Ship Prod. Des. 30 (2), 89–97.

Molchanov, B., Lundmark, S., Fürth, M., Green, M., 2019. Experimental validation of spray deflectors for high speed craft. Ocean Eng. 191, 106482.

Morabito, M.G., Pavkov, M.E., 2014. Experiments with stepped planing hulls for special operations craft. Trans. Royal Inst. of Naval Architects. Part B–Int. J. Small Craft Technol. 156 (B2), 87–98.

Niazmand Bilandi, R., Dashtimanesh, A., Tavakoli, S., 2019. Development of a 2D+T theory for performance prediction of double-stepped planing hulls in calm water, Proceedings of the Institution of Mechanical Engineers, Part M. J. Eng. Marit. Environ. 233 (3), 886–904.

Niazmand Bilandi, R., Dashtimanesh, A., Tavakoli, S., 2020a. Hydrodynamic study of heeled double-stepped planing hulls using CFD and 2D+ T method. Ocean Eng. 196, 106813.

Niazmand Bilandi, R., Tavakoli, S., Dashtimanesh, A., 2021. Seakeeping of double-stepped planing hulls. Ocean Eng. 236, 109475.

Nourghasemi, H., Bakhtiari, M., Ghassemi, H., 2017. Numerical study of step forward swept angle effects on the hydrodynamic performance of a planing hull. In: Zeszyty Naukowe Akademii Morskiej w Szczecinie.

Park, S., Wang, Z., Stern, F., Husser, N., Brizzolara, S., Morabito, M., Lee, E., 2022. Single-and two-phase CFD V&V for high-speed stepped planing hulls. Ocean Eng. 261, 112047.

Ricks, A., Morabito, M.G., Datla, R., 2022. Effect of ventilation on cavity formation on stepped planing hulls. J. Ship Res. 1–16.

Rodstrom, R., Edstrand, H., Bratt, H., 1953. The Transverse Stability and Resistance of Single-step Boats when Planing, Nr. 25. The Swedish State Shipbuilding Experimental Tank, Goteborg, Sweden.

Savitsky, D., 1964. Hydrodynamic design of planing hulls. Mar. Technol. SNAME News 1, 71–95, 04.

Savitsky, D., Morabito, M., 2010. Surface wave contours associated with the forebody wake of stepped planing hulls. Mar. Technol. 47 (1), 1–16.

Savitsky, D., Morabito, M., 2011. Origin and characteristics of the spray patterns generated by planing hulls. J. Ship Prod. Des. 27, 63–83.

Sheingart, Z., 2014. Hydrodynamics of High-Speed Planing Hulls with Partially Ventilated Bottom and Hydrofoils, Master of Science Thesis. Department of Mechanical Engineering, Massachusetts Institute of Technology, Cambridge.

Siemens, P.L.M., 2022. STAR CCM+ User's Guide Version 17.02.007.

Taunton, D.J., Hudson, D.A., Shenoi, R.A., 2010. Characteristics of a series of high speed hard chine planing hulls-part 1: performance in calm water. Int. J. Small Craft Technol. 152, 55–75.

Taunton, D.J., Hudson, D.A., Shenoi, R.A., 2011. Characteristics of a series of high speed hard chine planing hulls-part II: performance in waves. Int. J. Small Craft Technol. 153, B1–B22.

Vitiello, L., Mancini, S., Niazmand Bilandi, R., Dashtimanesh, A., De Luca, F., Nappo, V., 2022. A comprehensive stepped planing hull systematic series: Part 1 - resistance test. Ocean Eng. 266, 112242.

White, G., Beaver, W., 2010. Stepped-hull High-Speed Boat Model Test EW-07-10. U.S. Naval Academy, Annapolis, MD, USA.

White, G., BeaverW, Vann D., 2012. An experimental analysis of the effects of steps on high speed planing boats. In: Paper Presented at: the 3rd Chesapeake Power Boat Symposium; Annapolis (MD), USA.

Wielgosz, C., Rosen, A., Datla, R., Chung, U., Danielsson, J., 2020. Experimental modelling of spray deflection influence on planing craft performance in calm water and waves. Proc. IME M J. Eng. Marit. Environ. 234 (2), 399–408.

Husser, N., Brizzolara, S., 2021. The impact of sweep angle on stepped planing hull performance. In: SNAME International Conference on Fast Sea Transportation, 26-27 October 2021. Providence, Rhode Island, USA.

Appendix 4 (Publication IV)

[P4] Niazmand Bilandi, R., Mancini, S., Dashtimanesh, A., Tavakoli, S. (2024). A revisited verification and validation analysis for URANS simulation of planing hulls in calm water. Ocean Engineering, 293, 116589. https://doi.org/10.1016/j.oceaneng.2023.116589

Research paper

A revisited verification and validation analysis for URANS simulation of planing hulls in calm water

Rasul Niazmand Bilandi [a,*], Simone Mancini [b,c], Abbas Dashtimanesh [d], Sasan Tavakoli [e,f]

[a] Estonian Maritime Academy, Tallinn University of Technology, 11712, Tallinn, Estonia
[b] Department of Industrial Engineering, Università degli Studi di Napoli " Federico II", 80125, Naples, Italy
[c] Department of Hydro and Aerodynamics, FORCE Technology, 2800, Kgs. Lyngby, Denmark
[d] School of Engineering Science, Engineering Mechanics Department, KTH Royal Institute of Technology, SE-100 44, Stockholm, Sweden
[e] Department of Infrastructure Engineering, The University of Melbourne, Parkville, 3052, VIC, Australia
[f] Marine and Arctic Technology Group, Department of Mechanical Engineering, Aalto University, Espoo 0073, Finland

ARTICLE INFO

ABSTRACT

Verification and Validation (V&V) is the foremost analysis which is carried out for evaluation of the accuracy level and dependability of computational fluid dynamic (CFD) simulations. The present study investigates the V&V of CFD models in predicting the dynamic trim and hull resistance of high-speed planing hulls with an aim to provide a deeper understanding of V&V analysis in this specific field of application. Two different planing hulls, namely the C05 stepped hull and the C1 interceptor hull, are analyzed with four different grids and time-steps using two mesh motion techniques, namely overset and morphing approach. The discretization (grid) and time-step uncertainties for each CFD simulation are estimated using the least squares method. The results indicate that the overset mesh approach performs better than the morphing grid method in terms of numerical uncertainty and validation achieved for both hulls. The error of both techniques in the prediction of resistance and trim angle of the boat shows an acceptable range of accuracy. The findings provide valuable insights for simulation-based designing and optimizing high-speed planing hulls, specifically by identifying the optimal mesh technique, cell number, and time-step for accurate prediction of wetted surface shape, ventilation formation, running attitude, and resistance.

1. Introduction

Computational Fluid Dynamics (CFD) has gradually turned into a very important hydrodynamic tool in the marine industry and ocean engineering, which can be used for analyzing and designing ships, offshore structures and ocean renewable energy converters (Hosseini et al., 2021; Roshan et al., 2020). The accuracy and reliability of CFD simulations are assessed through verification and validation (V&V) procedures which are two important but challenging steps in the CFD simulations. They help us to ensure that the numerical data obtained through CFD modeling are trustworthy and valid enough to be used for different aims (such as design, optimization or study of physics).

In recent decade, a growing number of studies have been carried out to numerically simulate hydrodynamic of various types of planing hulls using CFD simulations. Planing hulls are a special type of watercraft that ride on the water surface and may operate at relatively high speeds.

Stepped hulls are also identified as a special type of planing hulls, which have been introduced through modifications of the vessel by adding stepped configurations on the bottom. Step(s) may cause air ventilation and would highly increase lift over drag ratio of the vessel, leading to a more efficient design.

The use of CFD in simulating air-water flow around planing hulls dates to the 2000s. Researchers limited their studies to prismatic hulls fixed in heave and pitch directions. Such studies would be very valuable as they informed us with the way a CFD model/code would give lift over drag ratio of a planing hull. But their application is limited as they cannot model the actual ride of a planing hull advancing in calm water condition. In a calm water environment, the vessel is free in vertical direction, and under the action of the fluid forces, including hydrodynamic and hydrostatic forces, its bow is pushed up and its center of gravity would be lifted upward. This necessitates consideration of dynamic mesh motion, which would introduce many more challenges to

---

* Corresponding author.
  E-mail address: rasul.niazmand@taltech.ee (R. Niazmand Bilandi).

CFD modeling. One of the first studies highlighting the ride of a planing hull on calm water was done by Fu et al. (2014). Fu et al. (2014) used a CFD code to simulate the hydrodynamic forces and flow around planing craft in calm water and waves on a laboratory scale, while Judge et al. (2020) compared experimental and simulation results for a high-speed deep-V planing hull in calm water and in waves. Both of these studies targeted stepless planing hulls. Gray-Stephens et al. (2020) assessed the accuracy of CFD in modeling the nearfield longitudinal wake profiles of a high-speed planing hull, concluding that CFD is a reliable and precise method for modeling these profiles. Tavakoli et al. (2020) investigated the unsteady planing motion in waves using different approaches, including towing tank tests, CFD, and the 2D + T model, with results suggesting that the 2D + T model may over-predict vertical acceleration due to negative sectional forces near the bow of the vessel at short waves, but CFD models would outperform for the reason they would not give such negative forces.

Stepped hull simulations using different methods have been extensively carried out in recent years. This is due that fact that these hulls have attracted attentions of boat designers over last decade. It has led to introduction of different systematic experimental tests that can be found in literature (e.g. Lee et al., 2014; Taunton et al., 2010, 2011; Vitiello et al., 2022). Several researchers have investigated the accuracy of CFD in replication of calm water ride of stepped planing hulls. De Marco et al. (2017) used Star-CCM + software with an overset mesh approach to predict drag for a forward-swept single-stepped fast planing hull. Their study involved towing tank tests, Reynolds Averaged Navier-Stokes (RANS), and Large Eddy Simulations (LES) using different moving mesh techniques. The observations indicated that the overset/chimera grid approach was the most effective method. Understanding these phenomena is important for optimizing the effectiveness of stepped hull designs. Dashtimanesh et al. (2018) investigated the motion characteristics of a two-stepped planing hull with transverse steps in calm water using three-dimensional numerical simulations. The study found that transverse steps reduced resistance and improved lift over drag ratio and that the CFD simulations would help us to accurately predict resistance, trim, and lift as compared to model test data. It is important to note that Dashtimanesh et al. (2018) used a morphing mesh approach to conduct their CFD simulations and did not cover the choice of dynamic mesh approaches (i.e. they did not compare whether another mesh motion approach would influence the predictions or not). Vitiello et al. (2020) evaluated the reliability of full-scale CFD simulations for a double-stepped hull by comparing the results to towing tank tests and sea trials. It was found that CFD simulations could accurately predict the performance of stepped hulls, but it was noted that further investigation and verification are necessary due to the lack of reliable sea trial data. The full-scale CFD simulations in Vitiello et al. (2020) overestimated resistance by an average of 17.3% as compared to data collected in actual sea, while the experimental towing tank test results overestimated hull resistance by an average of 27.5%. Despite this, CFD simulations are still viewed as a highly reliable hydrodynamic tool for predicting calm water performance of high-speed stepped planing hulls, and in general any type of planing hulls. Niazmand Bilandi et al. (2020a, 2023b, 2021) used numerical simulations to validate the performance predictions of heeled planing hulls in calm water and motion predictions in waves. They used overset method for solving the problems and showed that the results of CFD runs would be more accurate as compared to mathematical models developed based on 2D + t method.

Park et al. (2022) evaluated the accuracy of single- and two-phase RANS solvers for predicting the hydrodynamic characteristics of high-speed stepped planing hulls in calm water. The results suggested that both solvers predicted the experimental trends with comparable errors to those for non-stepped hulls but with larger errors for trim and wetted areas. Niazmand Bilandi et al. (2023a) conducted a comparative analysis between towing tank test results and CFD simulations to examine the calm water behavior of swept-stepped planing hulls. By employing an overset mesh approach and Adaptive Mesh Refinement

(AMR) in their CFD simulations, they aimed to gain a deeper understanding of the hydrodynamic characteristics and flow patterns associated with such hulls. The study involved a systematic series of eight models, each representing different step configurations, step heights, and step positions. Through this investigation, they assessed the influence of these factors on the prediction of resistance, wetted surface pattern, and ventilation length.

Moreover, researchers have designed optimized stepless and stepped hull designs using analytical and CFD-based methods. Although analytical methods can be used to calculate performance predictions and motion in waves in the early-stage design, the use of CFD simulation can offer a higher level of accuracy, and would be favored in last stages of design, where more accurate predictions are required. Di Caterino et al. (2018) studied the performance and stability of a stepless hull at high speeds by employing an analytical/CFD-based method. Their results were promising and were validated it against the Savitsky method and CFD full-scale analysis. They also performed a porpoising analysis for the non-stepped hull. This combined set of CFD simulations provides efficient way to analyze and compare performance of various planing surfaces. Niazmand Bilandi et al. (2019; 2020b) developed an analytical 2D + t method alongside CFD simulation to predict the performance of stepped planing hulls in calm water and waves. Wang et al. (2023) developed a new semi-empirical method, called the modified M-S method, to accurately predict the trim angle, CG rise-up and resistance of planing hulls riding in calm water. Their method is based on Morabito's empirical equations, which give pressure distribution over the wet surface of a planing surface. The hydrodynamic characteristics of a planing hull free in have and pitch directions were investigated using numerical simulations of viscous fluid flow around the vessel which were which were built by the SST k-ω turbulence model and the Volume of Fluid scheme. The study compared the results with experimental data, which confirmed the good accuracy level of the CFD model and its setup. Overall, the aforementioned studies provide pieces of evidence of the high value of analytical and CFD-based methods in the optimization process of different types of planing hulls. As observed in most of these studies, CFD and 2D + t models offer efficient and accurate solutions for calm water performance of a planing surface, that can be directly used for hydrodynamic design of the vessel, the output of which may also be used for structural design of the marine vehicle.

Similarly, interceptor hulls are identified as a group of planing surfaces that has gained popularity owing to their higher lift-over-drag ratio, as compared to a typical deep-V planing surface. Interceptors are energy saving devices originally used in aeronautic and automotive fields, which have been considered as an alternative to wedges, stern flaps, and trim tabs in Naval Architecture community. Studies suggest that interceptors can lead to resistance reduction over a wide range of speeds, but their effectiveness is dependent on the deadrise angle of the vessel, the longitudinal center of gravity, and the interceptor geometry itself, which is not surprising. De Luca and Pensa (2012) experimentally investigated the effects of deadrise angle, longitudinal center of gravity, and interceptor geometry on the effectiveness of interceptors. It was found that interceptors generate high lift force and can reduce dynamic trim of the vessel, and the study showed how resistance reductions can be maximized by combining the position of the center of gravity with the depth of interceptors. Additionally, this study proposed two unconventional interceptors that may lead to significant reduction of resistance, allowing the vessel to reach higher speeds. Apart from that, the interceptor has been seen to be effective in semi-displacement mode, De Luca et al. (2015).

In recent studies, researchers have investigated the hydrodynamic effects of interceptors on the performance of high-speed planing hulls using CFD and experimental methods. Mansoori and Fernandes (2017) found that combining an interceptor with a trim tab improves performance compared to using a single interceptor. They also showed that interceptor height is an important factor in efficiency and should be chosen based on the vessel's length and boundary layer thickness at the

Fig. 1. Set-up of resistance towing tank tests for the C1 interceptor hull (left) and the C05 stepped hull (right) at the *Università degli Studi di Napoli "Federico II"* Towing Tank (De Luca and Pensa, 2017; Vitiello et al., 2022).

transom region. Similarly, Suneela et al. (2021) and Jangam (2021) found that interceptor height affects vessel performance and that adding an interceptor to the vessel can reduce trim and resistance in the planing regime. Jangam (2022) investigated the use of an interceptor-flap combination and found significant reductions in resistance and trim. Sahin et al. (2022) studied the effect of interceptor layout and blade height on hydrodynamic performance of the planing vessel and showed that interceptors can reduce dynamic trim, sinkage, and resistance in regular waves. All aforementioned studies used CFD simulations to analyze the problem. Overall, the findings suggest that interceptors can be an effective means of improving planing hull performance, but the height and proper placement of the interceptor must be carefully considered for an optimal calm-water ride.

As explained, most of studies highlighting the performance of planing hulls, either the stepped hull ones, or the ones equipped with the interceptor, have been performed through CFD simulations. Ensuring the accuracy of CFD simulations is important in various engineering applications. One widely known organization that recognizes the significance of verification and validation (V&V) procedures in CFD simulations is the International Towing Tank Conference (ITTC) (ITTC 75-03-01-01 Rev 04, 2021). The ITTC recommends several procedures to ensure reliable estimation of errors and uncertainties such as the Correction Factor (CF) (and its modifications, e.g. Stern et al. (2001) and Wilson et al. (2004)) or Factor of Safety (FS) (Roache, 1998). One of these procedures is the Least Squares Root method (LSR). As noted by Eca et al. (2010) and Larsson et al. (2014), LSR is particularly useful in situations where the numerical solutions exhibit scatter, such as in complex flows with relatively coarse grids, or when using unstructured grids lead to variability in the grids. By estimating the error using LSR, the accuracy of the simulation results can be significantly improved.

In recent years, there has been a surge of research focused on conventional and stepped planing hulls using CFD methods. However, to ensure the accuracy of the numerical simulations, it is essential to validate the results by comparing them with experimental data (the validation and calibration process). This is particularly important when dealing with hulls that have discontinuities, such as stepped hulls and hulls with interceptors since these features can introduce challenges in CFD simulations. They may lead to artificial errors, and can be a source of uncertainty due to the complex flow patterns they create. Stepped hulls present a unique challenge in calculating resistance and wetted surface due to the intricate fluid dynamics around the steps. Conversely, interceptor-equipped hulls pose heightened challenges in calculating trim angles owing to the complexities of the fluid dynamics in the vicinity of the interceptor. The aim of the present paper is to investigate the error and uncertainty associated with spatial discretization (grid) in CFD simulations of calm water performance of a stepped hull and a hull equipped with an interceptor. This study will shed light on the difficulties in CFD simulations of these types of planing hulls and the way we can overcome them.

This paper covers the validation and verification analysis of planing hull modeling in calm water environment using CFD simulations. The verification mesh results are obtained using the CFD commercial software SIEMENS PLM Star-CCM+, with two different mesh motion techniques, that are used to integrate rigid dynamic motions into the CFD tank, i.e. overset/chimera and morphing mesh methods. Discretization uncertainties for each CFD simulation are estimated using a least squares method, implemented in a Matlab-based code. To validate the results, towing tank tests conducted by De Luca and Pensa (2017) and Vitiello et al. (2022) are used for comparison.

The present paper is structured as follows: Section 2 presents a description of the hulls and towing tank set-up. Section 3 provides details the CFD models and setups, including the computational domain, boundary conditions, and mesh settings for the domain, hull, and free surface. Section 4 outlines the procedure used for estimating numerical uncertainty errors, along with the algorithm flowchart depicting the method. In Sections 5 and 6, the verification and validation of the C05 stepped hull and C1 interceptor hull are analyzed. Finally, Section 7 presents the concluding remarks. Appendices A and E compare CFD results of the running attitudes and resistance with towing tank data for the C05 stepped hull and C1 interceptor hull, respectively. Appendices B and C depict grid uncertainty analyses for the trim and resistance values of the C05 stepped hull. Appendix D presents the analysis of the wetted surface and ventilation formation of the C05 stepped hull by CFD and towing tank test. Appendixes F and G illustrate grid uncertainty analyses for the trim and resistance values of the C01 interceptor hull. Finally, Appendix H presents the spray and wave formation for the C1 interceptor hull by CFD and towing tank tests.

2. Cases description

Numerical simulations have been conducted using different cell numbers for two sets of planing models to validate and verify the analysis. These models have been previously designed and tested by De Luca and Pensa (2017) and Vitiello et al. (2022). In these two research papers, performance of these two planing models are reported. The use of these models in this study provides an opportunity to investigate the error/uncertainty related to the spatial discretization (grid) for hulls with discontinuities; stepped and interceptor hulls. It is worth noting that such sharp geometrical discontinues on solid boundaries would cause numerical challenges and may cause artificial effects, such as ripple generation, energy damping, etc. Two mesh techniques were implemented in the simulations, the overset and morphing mesh, respectively. These two meshing strategies represent the two most common approaches implemented for planing hull simulations (e.g. De Marco et al., 2017; Dashtimanesh et al., 2018).

The tests for both models were carried out in the towing tank of the *Dipartimento di Ingegneria Industriale (DII)* at the *Università degli Studi di Napoli "Federico II"*. The towing tank has main dimensions of $136 \times 9.0 \times 4.5$ m (Length, Width, and Depth), and the setup of calm water towing tank tests for the C1 interceptor hull and the C05 stepped hull are depicted in Fig. 1.

The first set of planing models, designed by De Luca and Pensa (2017) at the *Università degli Studi di Napoli "Federico II"*, investigated the effects of interceptor on performance of Systematic Series of hard
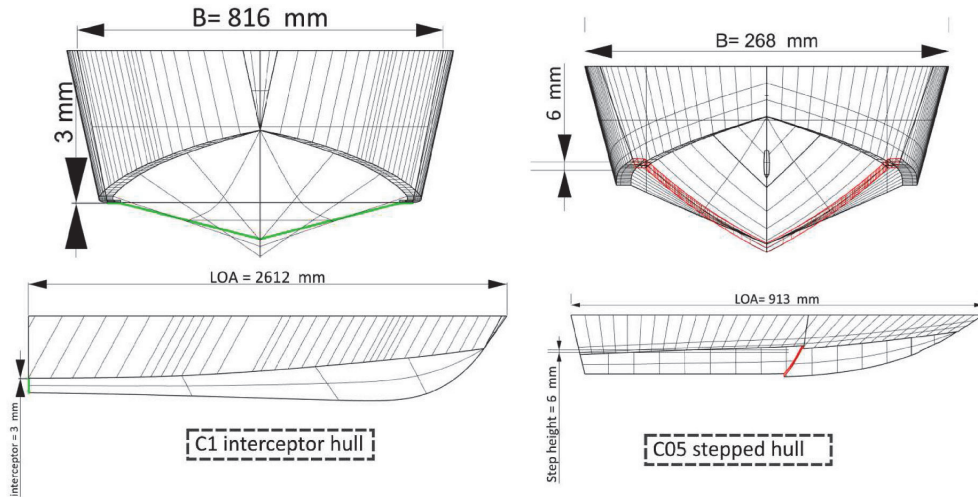
Fig. 2. Body plans of the models: (Left) C1 interceptor hull with green highlighting of the position and height of the interceptor, and (Right) C05 single-stepped hull with red highlighting of the position and height of the step.

Table 1
Principal characteristics of C1 interceptor hull and C05 stepped hull.

Model Characteristics	Description	C1	C05
L (m)	Length over all	2.612	0.91
L_{WL} (m)	Waterline Length	2.387	0.76
B (m)	Beam	0.816	0.268
β (°)	Deadrise	23.7	23
$\Delta/\rho g B^3$	Ratio of the displacement	0.02	0.163
$L/\nabla^{1/3}$	Length-displacement ratio	5.5	6.24
L_{CB} ($\tau_s = 0$)	Longitudinal center of buoyancy from transom	0.943	0.286
Position of step (m)	–	–	0.441
Height of step (mm)	–	–	6
Hight of interceptor (mm)	–	3	–
Fr_B	Beam Froude number	0.88–1.94	1.93–4.97

chine hulls in planing and semi-planing speed ranges. This systematic hard-chine planing hulls are named NSS. The chosen vessel is a warped hull with a length of 2.612 m and a mean deadrise angle of 23.7°.

The second set of planing models, designed and tested by the same institution (Vitiello et al., 2022), was developed to study the effects of the forward swept step position and height on the performance of stepped planing hulls. This systematic set of planing hull series is named VMV. For this research, one of the models, named C05, was selected,

which has one step with a height of 0.024B. The body plans of the two studied models are shown in Fig. 2, and their dimensions and other principal characteristics are listed in Table 1. In Table 1, τ_s represents static trim, which defines the ship's balanced hull orientation when at rest in calm waters, ensuring it remains level without tilting forward or backward.

For the cases description, it is important to emphasize that both hull types under investigation share a common characteristic, the presence of bottom 'discontinuities' leading to flow separation. This commonality serves as a significant rationale for analyzing both hulls together. By doing so, we aim to investigate the effects of these 'discontinuities' on hydrodynamic behavior. In essence, considering both hull types enriches the scope of our Verification and Validation (V&V) study, enabling us to achieve a deeper understanding of the impact of bottom discontinuities on the overall hydrodynamic response, thereby contributing to a more comprehensive analysis.

Further details of the towing tank tests can be found in the papers by De Luca and Pensa (2017) and Vitiello et al. (2022).

3. Numerical computational settings

Fluid motions are modeled by the RANS equations, and conservation of a volume fraction field, which helps us to capture the free surface deformation. For sake of beverity, governing equaitons are not presented in this study. They can be found in most of the CFD text books or

Table 2
Solver settings.

Item	Overset for C05	Overset for C1	Morphing for C05	Morphing for C1
solver	Implicit unsteady	Implicit unsteady	Implicit unsteady	Implicit unsteady
Convection term	2nd order	2nd order	2nd order	2nd order
Turbulence model	k-Omega SST	k-Omega SST	k-Omega SST	k-Omega SST
Time step (s)	$0.004 \sim 0.011 \frac{L_{wl}}{\nu}$	$0.004 \sim 0.011 \frac{L_{wl}}{\nu}$	$0.004 \sim 0.011 \frac{L_{wl}}{\nu}$	$0.004 \sim 0.011 \frac{L_{wl}}{\nu}$
Temporal Discretization	1st order	1st order	1st order	1st order
Iteration per time step	5	10	5	10
Mesh motion	Overset	Overset	Morphing	Morphing
Overset Interpolation scheme	Linear	Linear	–	–
Wall treatment	All y + wall treat	All y + wall treat	All y + wall treat	All y + wall treat
Water density	1000 kg/m³	998.09 kg/m³	1000 kg/m³	998.09 kg/m³
Water viscosity	0.000934 Pa-s	0.000997 Pa-s	0.000934 Pa-s	0.000997 Pa-s

Table 3
Comparative analysis of k-Omega SST and k-Epsilon turbulent models for C05 stepped hull with mesh configurations 15.4M (overset) and 15.17M (morphing) at maximum Froude number of 4.97, and for C1 interceptor hull with mesh configurations 14.9M (overset) and 13.2M (morphing) at maximum Froude number of 1.94.

C05 stepped hull										
$Fr_B = 4.97$	θ (deg.)					R/Δ				
	Exp.	k-Omega SST	$E\%$	k-Epsilon	$E\%$	Exp.	k-Omega SST	$E\%$	k-Epsilon	$E\%$
Overset	1.606	1.790	−11.49%	1.798	−11.99%	0.525	0.559	−6.56%	0.532	−1.43%
Morphing	1.606	1.819	−13.30%	1.816	−13.11%	0.525	0.53	−1.03%	0.504	3.86%
C1 interceptor hull										
$Fr_B = 1.94$	θ (deg.)					R/Δ				
	Exp.	k-Omega SST	$E\%$	k-Epsilon	$E\%$	Exp.	k-Omega SST	$E\%$	k-Epsilon	$E\%$
Overset	−0.091	−0.089	2.20%	−0.13	−42.86%	0.178	0.1647	7.55%	0.156	12.46%
Morphing	−0.091	−0.100	9.89%	−0.16	−75.82%	0.178	0.169	5.13%	0.165	7.17%

references (e.g. in Ferziger et al., 2019; Reynolds, 1997). Rigid body motions of the vessel are gvoverned by Newtons' Second Law, where forces are foung through integrating pressure and shear stresses over the surface of the hull. These equations are also not presented in this research for the same reason that fluid equations are not presented. Resaders intrested to know more about the equations governing the dynamic motion of a planing hull are referred to Su et al. (2012), and Tavakoli et al. (2020).

All CFD simulations in this study utilize the Finite-Volume Method (FVM) and the Volume-Of-Fluid (VOF) model to handle two-phase flows. The free surface between air and water is reproduced with the two-phase VOF method, with a High-Resolution Interface Capturing (HRIC) scheme based on the Compressive Interface Capturing Scheme for Arbitrary Mesh (CICSAM), and both fluids are considered incompressible Newtonian fluids. A Semi-Implicit Method for Pressure-Linked Equations (SIMPLE) was used to conjugate the pressure and velocity fields, and then solves the discretized equations that model the fluid motion over a single time step. A segregated flow solver approach was applied for all simulations. The numerical method and solver details can be found in the Siemens PLM Star-CCM + User's Guide, version 17.02.007 (SIEMENS, 2022). Additional information about the numerical solver used in the study is provided in Table 2. According to Table 2, a 1st-order temporal discretization is employed. Utilizing 1st-order accuracy in time provides time-averaged results, whereas the necessity for 2nd-order accuracy might not be as critical, particularly given the pseudo-unsteady nature of the resistance test. While higher-order accuracy in time could potentially benefit in handling dynamic instabilities, simulations did not encounter such instabilities.

To select the appropriate turbulent model, a comparative analysis was conducted between the k-Omega SST and k-Epsilon turbulence models for both hulls, utilizing finer meshes at their respective maximum Froude numbers. The findings for trim (θ) and resistance ratio (R/Δ) are summarized in Table 3. The results indicate that the k-Omega SST model exhibits a lower comparison error when compared to the k-Epsilon model. Consequently, the k-Omega SST turbulence model was chosen to accurately account for turbulence effects in the flow. Note that this finding is limited to the targeted hulls, and cannot be generalized for all planing hull models. The selection process excluded other turbulence models such as SA-DES, SARC-DES, SARC, DES, DDES, LES, or RSM, focusing on widely implemented CFD turbulence models frequently employed in practical design applications. While these excluded models

have value and applicability across various fluid flow scenarios, prior assessments and investigations led to the conclusion that the k-Omega SST model better captured the flow physics and phenomena relevant to the specific hull configurations and hydrodynamic conditions studied.

In this study, the variables employed to assess performance are integrated quantities, analogous to the method used in the towing tank procedure. The forces (and moments) are determined as the integration (summation) of the pressure and shear forces acting on the cell surfaces. The hull is configured using DFBI (Dynamic Fluid Body Interaction), enabling movement in the heave and pitch directions based on the exerted forces and moments. The vessel in the end is placed at an equilibrium condition, where the pitching moment is zero and weight force equals the external force caused by water pressure.

To accommodate the movements of the hull in the computational domain, both overset meshes and morphing techniques have been implemented with an aiming to compare these two meshing techniques. In both overset and morphing methods, four grids of different sizes are generated, with the same settings but with different base size of the mesh. This approach helps us conduct a discretization uncertainty analysis, which could include the use of the LSR method. Tables 4 and 5 summarize the number of cells and corresponding refinement ratio (with the finest grid referred to as 1). The refinement ratio, denoted by h, can be expressed as:

$$\frac{h_i}{h_f} = \frac{N_{cell_f}}{N_{cell_i}} \tag{1}$$

where N_{cell_i} denotes the number of cells in the grid i, while N_{cell_f} represents the number of cells in the finest grid.

The overset setup integrates hull motions into the fluid domain by using dynamic boundaries surrounding the hull, moving with it. It suits complex geometries but is computationally expensive, preferable for high vessel motions. Conversely, the morphing setup technique offers a more efficient alternative by taking into account the hull motions with a single domain modifying the position of nodes. This technique avoids the need for multiple grid domains and boundary conditions associated with overset methods, which can simplify the simulation setup and reduce computational effort. However, morphing mesh methods may require careful consideration of mesh quality and deformation to ensure the accuracy and stability of the simulation results. In Star-CCM+, a set of grid nodes (also called control vertices) define the initial movement

Table 4
Number of cells and grid refinement ratio for verification study of C05 stepped planing hull.

Overset						Morphing				
Grid no.	N_{cell_i}	h_i	Base size background	Base size overset	Ave. Y+	Grid no.	N_{cell_i}	h_i	Base size	Ave. Y+
8.9M	8,968,525	1.72	1.025 L_{WL}	0.615 L_{WL}	83	6.47M	6,474,763	2.34	0.535 L_{WL}	81
11.2M	11,245,013	1.37	1.025 L_{WL}	0.559 L_{WL}	77	8.8M	8,832,117	1.72	0.473 L_{WL}	75
12.9M	12,948,438	1.19	1.025 L_{WL}	0.549 L_{WL}	70	11.05M	11,054,112	1.37	0.439 L_{WL}	62
15.4M	15,449,886	1	1.025 L_{WL}	0.513 L_{WL}	65	15.17M	15,172,514	1	0.384 L_{WL}	45

Table 5
Number of Cells and Grid Refinement Ratio for Verification Study of C01 interceptor Planing Hull.

Overset						Morphing				
Grid no.	N_{cell_i}	h_i	Base size background	Base size overset	Ave. Y+	Grid no.	N_{cell_i}	h_i	Base size	Ave. Y+
8.8M	8,817,154	1.69	0.670 L_{WL}	0.430 L_{WL}	0.9	6.2M	6,275,120	2.11	0.437 L_{WL}	0.8
11.2M	11,225,477	1.33	0.670 L_{WL}	0.366 L_{WL}	0.77	8.1M	8,106,302	1.64	0.387 L_{WL}	0.65
12.9M	12,902,835	1.16	0.670 L_{WL}	0.335 L_{WL}	0.65	10.6M	10,645,546	1.25	0.335 L_{WL}	0.5
14.9M	14,942,391	1	0.670 L_{WL}	0.251 L_{WL}	0.4	13.2M	13,274,303	1	0.265 L_{WL}	0.25
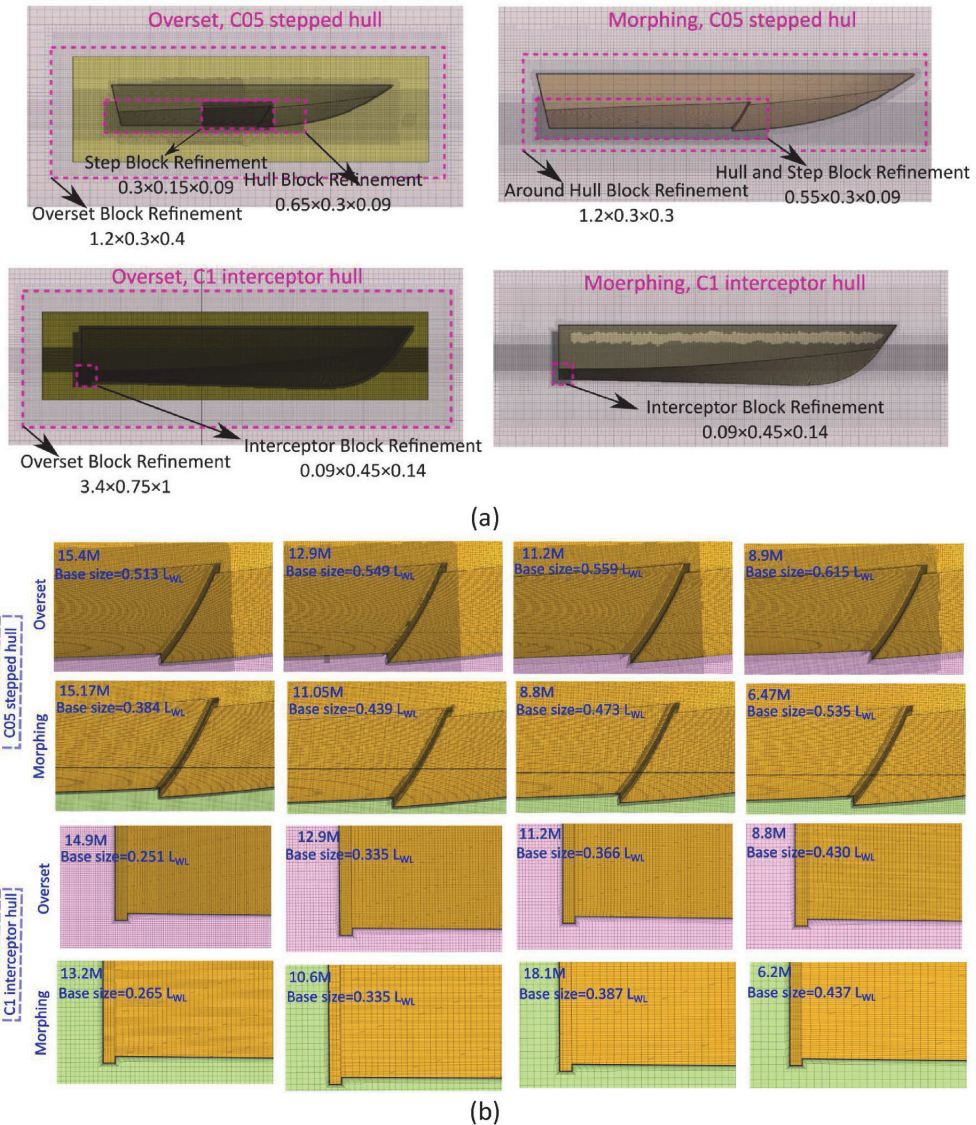
Fig. 3. (a) Block refinement around the hulls and extend of each block, (b) Mesh configuration around the step and interceptor for different mesh densities.

that the morphing solver imposes on the mesh. Each control vertex is associated with a displacement vector that the morphing solver uses to move the nearby vertices. The morphing solver utilizes Radial Basis Functions (RBF) to modify the grid according to hull motion. Details of the morphing solver procedures can be found in Dashtimanesh et al. (2018).

In this study, the meshing approach involved the utilization of various tools for overset setup and morphing configurations. The primer
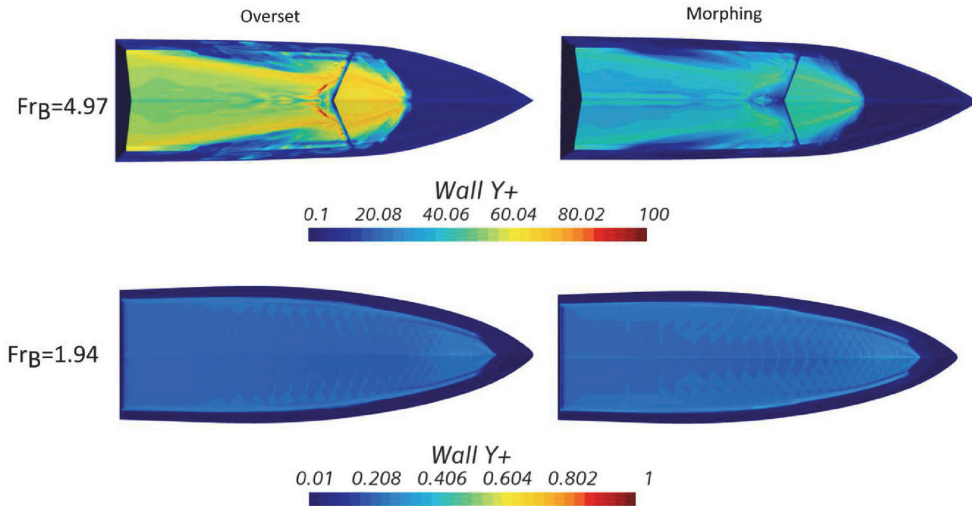
Fig. 4. The wall y + values of the walls for Overset and Morphing Mesh Motion of stepped hull and interceptor hull at maximum speed. For the C05 stepped hull, a time-step of $0.006L_{wl}/v$ was utilized, while for the C1 interceptor hull, a value of $0.009L_{wl}/v$ was employed.
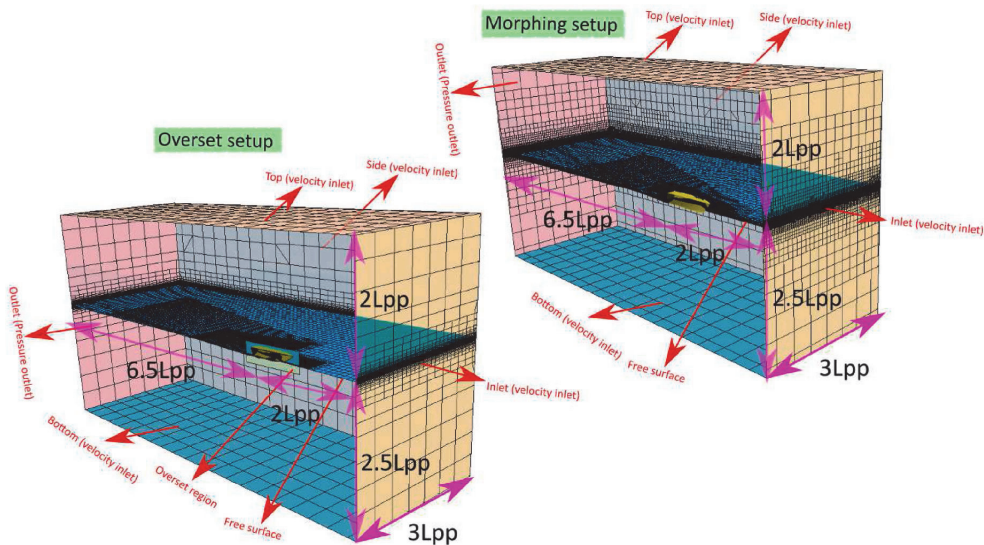
Fig. 5. Computational Domain, Boundary Conditions Settings, and Mesh on the domain, around the Hull and Free Surface for Overset (for C05 stepped hull) and Morphing (for C1 interceptor hull) Mesh Motion.

layer mesher, surface remesher, and trimmer were employed to facilitate this process. Specifically, for the C05 hull, nine prism layers with a near-wall thickness of 5.0E-5 were used, while the C1 interceptor hull utilized thirteen prism layers with a near-wall thickness of 2.0E-5. To mesh the hull surface, the triangle meshing method was applied. Additionally, mesh refinement was strategically implemented around specific areas, including the hulls, spray area, free surface, steps for the C05 hull, and the interceptor for the C1 hull. The overset setup ensured consistency in cell sizes between the overset and background regions, maintaining a uniform surface growth rate of 1.3 for both tanks. Similarly, a surface growth rate of 1.3 was applied to the Tank domain in the morphing setup. Notably, adaptive meshing techniques were not employed for the

grid overset or morphing processes. In Fig. 3, mesh refinement is depicted around the most critical areas, which are the stepped area for C05 and the interceptor area for C1.

A wall function treatment, specifically the All wall y + approach, has been employed in the simulation in order to describe the viscous sub-layer near the wall of the hull. The y + parameter employs a hybrid approach in the viscous sublayer region that emulates the low-y + wall (wall y+ < 1) value for fine resolution of the near wall zone and the high-y+ (wall y+ > 30) value for coarse resolution of the near wall zone. This approach provides an effective compromise between the two wall treatment methods. The results section demonstrates the effectiveness of the y + value in improving the accuracy of the simulations. Fig. 4

provides an overview of the wall y + values for the hulls with a finer mesh at maximum speeds.

A numerical tank with six boundaries is generated to simulate the fluid flow around each hull, as shown in Fig. 5. The inlet, up, side, and bottom boundaries utilize the velocity inlet boundary condition, while the outlet boundary has a specified hydrostatic pressure. To force flow symmetry, the center plane is set to be governed by symmetric boundary conditions. The non-slip boundary condition is set on the hull surfaces, forcing the friction between the hull and air-water flow.

In this study, the meshing technique utilized is carefully designed to capture the complex flow behavior around the stepped planing hull and interceptor planing hull, accurately. The accuracy of the simulations is evaluated by comparing the results obtained from both overset meshes and morphing techniques with experimental data at different mesh and Froude numbers. The comparison results for the C05 stepped hull and the C1 interceptor planing hull are available in Appendix A and Appendix C, respectively. The use of overset meshes and morphing techniques improves the accuracy of the simulations, although one technique may be more effective than the other depending on the specific scenario (De Marco et al., 2017; Hosseini et al., 2021; Nimmagadda et al., 2020). The meshing strategy employed in this study is instrumental in achieving reliable and promising results, which will facilitate further investigations into the hydrodynamic behavior of these hulls. In the following section, a discretization (grid) uncertainty analysis will be introduced, which can be used for evaluation of the performance of both techniques when different cell numbers are generated.

4. Proposed procedure for numerical uncertainty estimation

Discretization (temporal and spatial) errors are believed to be the main source of numerical error in most CFD simulations, and there are two primary approaches for quantifying this error. The first method involves performing spatial grid refinement studies to estimate the exact solution, the order of grid convergence, and the discretization error. The second method calculates the discretization error directly from an error transport equation. Although the first approach requires multiple solutions and grids, the second method estimates the residual/error with greater accuracy than that used in the discretization of the governing equations. After calculating the discretization error, both strategies estimate the grid uncertainty. In this paper, a method introduced by Eça and Hoekstra (Eca and Hoekstra, 2014) is employed for calculation of grid uncertainty using spatial grid refinement.

The estimation of the discretization error ($\mathcal{E}$) is achieved by utilizing a truncated power series expansion (Richardson Extrapolation), as follows:

$$\mathcal{E} \equiv \delta_{RE} = f_i - f_0 = \alpha h_i^{\mathbb{P}} \tag{2}$$

Here f_i is any data derived from the numerical solution of grid i, f_0 is the estimation of the exact solution, α is the error constant, $\mathbb{P}$ is the observed order of grid convergence.

The Least Squares Method is used to determine the values of f_0, α, and $\mathbb{P}$ in Eq. (2). This involves minimizing the sum of deviations between f_i and the model function $f_0 + \alpha h_i^{\mathbb{P}}$. If desired, the equation can be weighted to account for the greater accuracy and significance of data obtained from finer grids compared to coarser grids. This results in a weighted least squares version of the equation.

$$S_{RE}(f_0, \alpha, \mathbb{P}) = \sqrt{\sum_{i=1}^{n} \left(f_i - \left(f_0 + \alpha h_i^{\mathbb{P}} \right) \right)^2} \xrightarrow{minimum}$$

$$\sigma_{RE} = \frac{\sqrt{\sum_{i=1}^{n} \left(f_i - \left(f_0 + \alpha h_i^{\mathbb{P}} \right) \right)^2}}{(n-3)} \tag{3}$$

$$S_{RE}^w(f_0, \alpha, \mathbb{P}) = \sqrt{\sum_{i=1}^{n} w_i \left(f_i - \left(f_0 + \alpha h_i^{\mathbb{P}} \right) \right)^2} \xrightarrow{minimum}$$

$$\sigma_{RE}^w = \frac{\sqrt{\sum_{i=1}^{n} n w_i \left(f_i - \left(f_0 + \alpha h_i^{\mathbb{P}} \right) \right)^2}}{(n-3)} \tag{4}$$

where the weights (w_i) are determined based on the grid spacing, h_i:

$$w_i = \frac{1/h_i}{\sum_{i=1}^{n} 1/h_i} \tag{5}$$

The observed order of grid convergence ($\mathbb{P}$) can be determined by solving both equations (Eq. (3) and Eq. (4)) and identifying the minimum value. If both equations yield positive values of $\mathbb{P}$, the solution with the minimum standard deviation is chosen as the best fit. However, if one of the solutions results in a negative $\mathbb{P}$ value, it is disregarded as it does not represent a physically meaningful solution. If both solutions result in a negative $\mathbb{P}$ value, the data behavior is considered anomalous, indicating the presence of numerical artifacts or other issues.

If the apparent order of grid convergence falls within an acceptable range ($0.5 < \mathbb{P} < 2$) and the standard deviation (σ) is small, a corresponding grid uncertainty can be calculated based on the estimated discretization error, $\mathcal{E}$. Within this range, the discretization error can be computed using Eq. (2) and the minimum standard value of Eq. (3) and Eq. (4).

If $\mathbb{P}$ is greater than 2, δ_{RE} (Eq. (2)) is not used and instead, either δ_1 or δ_2, is used based on the following procedure:

$$\mathcal{E} \equiv \delta_1 = f_i - f_0 = \alpha h_i \tag{6}$$

$$\mathcal{E} \equiv \delta_2 = f_i - f_0 = \alpha h_i^2 \tag{7}$$

To estimate the values of f_0 and α, one can identify the best fit with the smallest standard deviation σ among the four possible fits.

$$S_1(f_0, \alpha) = \sqrt{\sum_{i=1}^{n} \left(f_i - \left(f_0 + \alpha h_i^1 \right) \right)^2} \xrightarrow{minimum}$$

$$\sigma_{RE} = \frac{\sqrt{\sum_{i=1}^{n} \left(f_i - \left(f_0 + \alpha h_i^1 \right) \right)^2}}{(n-2)} \tag{8}$$

$$S_2(f_0, \alpha) = \sqrt{\sum_{i=1}^{n} \left(f_i - \left(f_0 + \alpha h_i^2 \right) \right)^2} \xrightarrow{minimum}$$

$$\sigma_{RE} = \frac{\sqrt{\sum_{i=1}^{n} \left(f_i - \left(f_0 + \alpha h_i^2 \right) \right)^2}}{(n-2)} \tag{9}$$

$$S_1^w(f_0, \alpha) = \sqrt{\sum_{i=1}^{n} w_i \left(f_i - \left(f_0 + \alpha h_i^1 \right) \right)^2} \xrightarrow{minimum}$$

$$\sigma_{RE}^w = \frac{\sqrt{\sum_{i=1}^{n} n w_i \left(f_i - \left(f_0 + \alpha h_i^1 \right) \right)^2}}{(n-2)} \tag{10}$$

$$S_2^w(f_0, \alpha) = \sqrt{\sum_{i=1}^{n} w_i \left(f_i - \left(f_0 + \alpha h_i^2 \right) \right)^2} \xrightarrow{minimum}$$

$$\sigma_{RE}^w = \frac{\sqrt{\sum_{i=1}^{n} n w_i \left(f_i - \left(f_0 + \alpha h_i^2 \right) \right)^2}}{(n-2)} \tag{11}$$
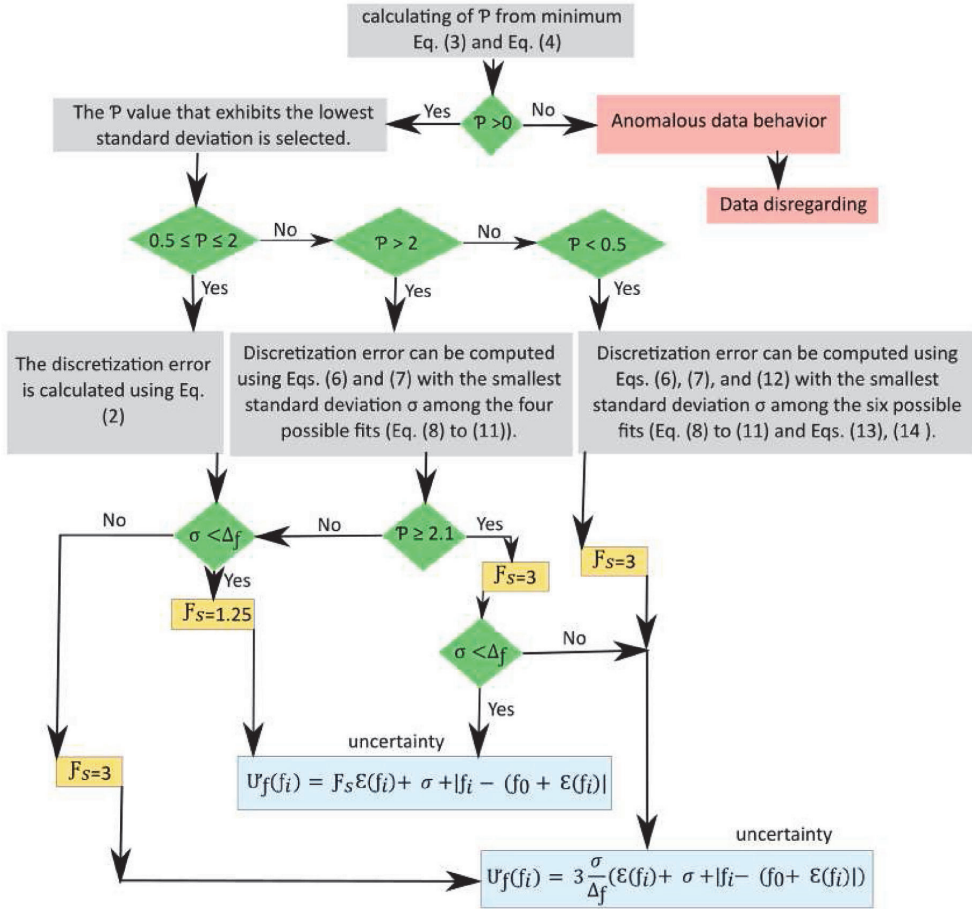
Fig. 6. Block diagram of the Least squares method used in the present research.

A high value of P can lead to an unrealistic error estimate, known as "noisy grid convergence".

If P is less than 0.5, such small P values can lead to overly conservative error estimates, which are commonly known as "overly pessimistic grid convergence". To address this issue, the discretization error is estimated using not only δ1 in Eq. (6) and δ2 in Eq. (7), but also the following equation:

$$\mathcal{E} \equiv \delta_{12} = f_i - f_0 = \alpha_1 h_i + \alpha_2 h_i^2 \tag{12}$$

In order to determine the values of f_0 and α, two additional fits are used in addition to the four fits specified in equation (8) through (11). Among the six possible fits, the one with the smallest standard deviation σ is selected:

$$S_{12}(f_0, \alpha_1, \alpha_2) = \sqrt{\sum_{i=1}^{n} \left(f_i - \left(f_0 + \alpha_1 h_i^1 + \alpha_2 h_i^2\right)\right)^2} \xrightarrow{minimum}$$

$$\sigma_{12} = \frac{\sqrt{\sum_{i=1}^{n}\left(f_i - \left(f_0 + \alpha h_i^1 + \alpha_2 h_i^2\right)\right)^2}}{(n-3)} \tag{13}$$

$$S_{12}^w(f_0, \alpha_1, \alpha_2) = \sqrt{\sum_{i=1}^{n} w_i\left(f_i - \left(f_0 + \alpha_1 h_i^1 + \alpha_2 h_i^2\right)\right)^2} \xrightarrow{minimum}$$

$$\sigma_{12}^w = \frac{\sqrt{\sum_{i=1}^{n} nw_i\left(f_i - \left(f_0 + \alpha_1 h_i^1 + \alpha_2 h_i^2\right)\right)^2}}{(n-3)} \tag{14}$$

Once the discretization error is calculated, the numerical uncertainty U_f can be determined. This involves defining a data range parameter Δ_f to assess the quality of the data fits:

$$\Delta_f = \frac{(f_i)_{max} - (f_i)_{min}}{n-1} \tag{15}$$

If the solution converges monotonically within the range of $0.5 < P < 2.1$ and Δ_f is greater than σ, then the error estimate is considered reliable, and the safety factor is set to $F_s = 1.25$. However, if the error estimate is not reliable, then the safety factor is increased to $F_s = 3$. Next, the uncertainty is calculated by taking into account the value of Δ_f:

If $\sigma < \Delta_f \quad \rightarrow U_f(f_i) = F_s\mathcal{E}(f_i) + \sigma + |f_i - (f_0 + \mathcal{E}(f_i))|$ (16)

If $\sigma \geq \Delta_f \quad \rightarrow U_f(f_i) = 3\frac{\sigma}{\Delta_f}(\mathcal{E}(f_i) + \sigma + |f_i - (f_0 + \mathcal{E}(f_i))|)$ (17)

Table 6
Differing time step settings for C05 stepped hull with mesh configurations 15.4M (overset) and 15.17M (morphing) at maximum Froude number of 4.97, and for C1 interceptor hull with mesh configurations 14.9M (overset) and 13.2M (morphing) at maximum Froude number of 1.94.

C05 stepped hull		C1 interceptor hull	
Time-step	t_i	Time-step	t_i
$0.007 \frac{L_{wl}}{v}$	0.606	$0.011 \frac{L_{wl}}{v}$	0.578
$0.006 \frac{L_{wl}}{v}$	0.707	$0.009 \frac{L_{wl}}{v}$	0.707
$0.00495 \frac{L_{wl}}{v}$	0.857	$0.00778 \frac{L_{wl}}{v}$	0.817
$0.00424 \frac{L_{wl}}{v}$	1	$0.00636 \frac{L_{wl}}{v}$	1

The least-squares method is a powerful tool in numerical simulations that accurately estimates discretization uncertainty by accounting for errors introduced during the numerical discretization process. The method's versatility enables its application to any scalar quantity, making it an essential technique for a wide range of applications. However, to obtain precise estimates of grid uncertainty, it is recommended to apply the method to quantities requiring minimal post-processing, such as the force/moment on planing hulls or their instantaneous displacement. Additionally, trim and resistance are also suitable options for estimating grid uncertainty. Sinkage was not included in the V&V process of this study due to the lack of experimental uncertainty estimation for the C1 hull with interceptor.

The flow phenomena around planing hulls especially stepped hulls and hulls with interceptors, are complex and can result in nonlinear effects (especially at the air-water interface) that significantly impact the solution of the RANS equations. These complex flow phenomena require the use of finer or coarser meshes, which may lead to nonlinear changes in the solution. Furthermore, the mesh structure can influence the behavior of the turbulence model, causing changes in the solution that are not mostly due to discretization errors. Despite these

aforementioned challenges, the least-squares method remains a reliable approach for estimating grid uncertainty. By considering errors introduced during the numerical discretization process, the method provides a systematic and versatile way to quantify the uncertainty in the solution, which is vital for making informed decisions based on the reliability of simulations.

A block diagram of the Least squares method is presented in Fig. 6, illustrating the systematic steps involved in the implementation of the method. The ability of method to estimate grid uncertainty accurately makes it an essential tool in numerical simulations, especially when it comes to complex flow phenomena, where the accuracy and reliability of the simulation results are important.

5. Discretization errors and uncertainties

This section presents a detailed grid uncertainty analysis of the quantity of trim and resistance for both the C05 stepped hull and C1 interceptor hull using overset and morphing mesh techniques with four different grids. The discretization error/uncertainty related to the grid is considered the main source of uncertainty for the resistance simulations rather than the iterations (iterative error/uncertainty) and time-step (temporal discretization error/uncertainty), as mentioned in several studies e.g. De Luca et al. (2016), Lee et al. (2017) where these errors/uncertainties are found to be an order of magnitude lower than the grid one.

The results of the analysis are presented through figures that show the fitted convergence trends based on least squares methods and Equation (2), along with the estimated grid uncertainties for each CFD simulation.

Before presenting the grid uncertainty of each hull, a preliminary investigation into time-step uncertainty is carried out. This exploration aims to evaluate how variations in the time step used in simulations may affect the accuracy and stability of the simulations. To address time-step uncertainty, sensitivity analyses are performed using four distinct time-step values through the LSR method. These analyses assess the effects of
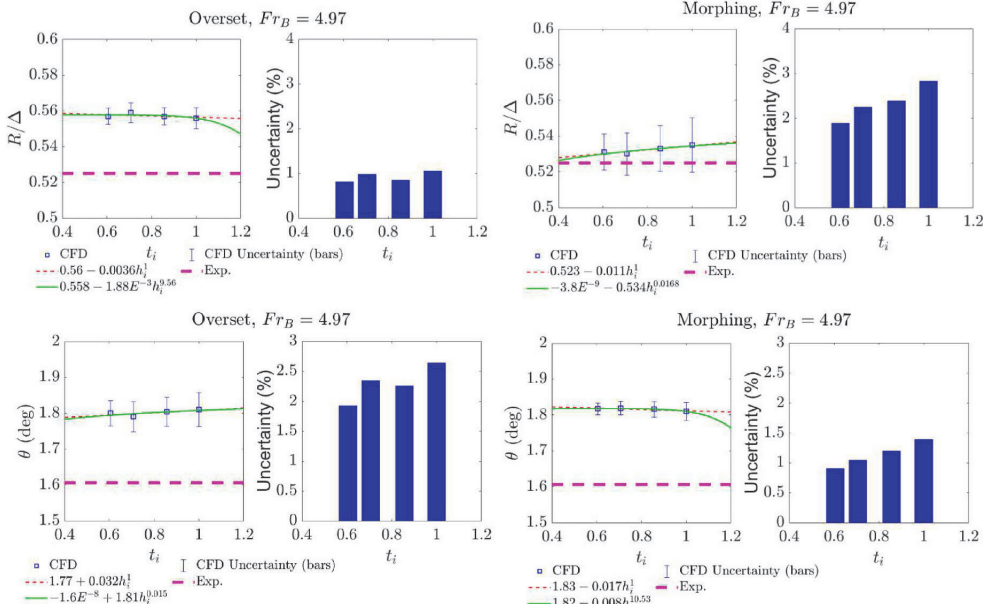

Fig. 7. Time-step uncertainty error assessment using the least squares method for trim and resistance values of the C05 stepped hull. The analysis employs overset and morphing mesh techniques at a Froude Number of 4.97, utilizing 15.4M and 15.17M Mesh Configurations for both mesh techniques, respectively.
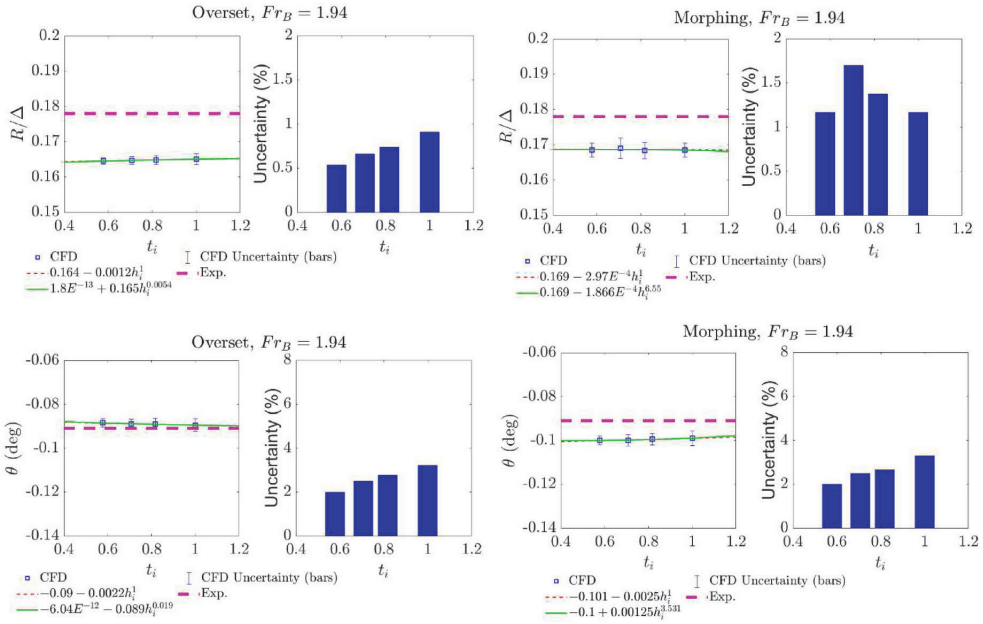
Fig. 8. Same as Fig. 7, but for the C1 Interceptor Hull at a Froude Number of 1.94, incorporating 14.9M and 13.2M Mesh Configurations for both overset and morphing mesh techniques, respectively.
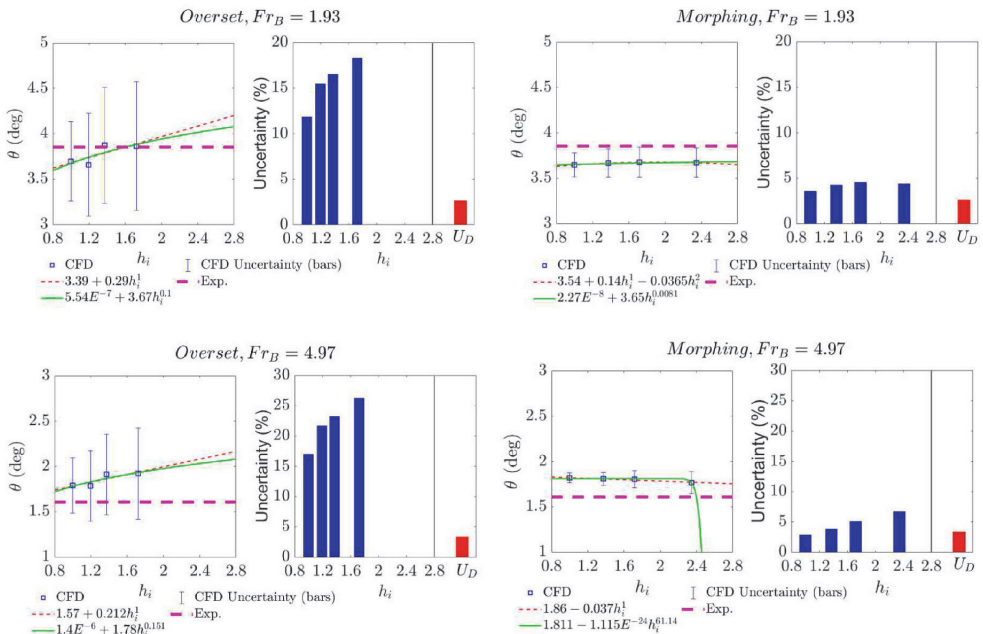

Fig. 9. Grid uncertainty analysis using the Least Squares Method for the trim value of C05 stepped hull with overset and morphing mesh techniques, revealing the order of convergence and estimation of errors at minimum Froude numbers 1.93, and Maximum Froude number 4.97. Additional Froude numbers, 2.86, 3.31, 3.91, and 4.5, are provided in Appendix B. U_D is experimental uncertainty.

Table 7
Comparison error and grid uncertainty for the trim value of the C05 stepped hull for finest mesh configurations 14.9M (Overset) and 13.2M (Morphing).

Fr_B	Overset						Morphing					
	1.93	2.86	3.31	3.91	4.5	4.97	1.93	2.86	3.31	3.91	4.5	4.97
$E_t\%$	4.06%	1.48%	0.67%	−7.92%	−5.24%	−11.49%	5.36%	3.19%	0.76%	−5.78%	−4.59%	−13.30%
$U_{G_T}\%$	11.85%	18.55%	25.55%	22.5%	17.52%	17.00%	3.29%	2.12%	4.60%	3.49%	1.96%	2.91%

variations on the results. Variations in the time step and the refinement ratio are summarized in Table 6, with the lowest time step designated as " *l*." The refinement ratio, denoted as *t*, can be mathematically expressed as follows:

$$\frac{t_i}{t_l} = \frac{\left[0.004 \sim 0.011 \frac{L_{wl}}{v}\right]_l}{\left[0.004 \sim 0.011 \frac{L_{wl}}{v}\right]_i} \qquad (18)$$

Figs. 7 and 8 show the effects of time-step uncertainty on trim and resistance values of two hulls studied in the present research. In Fig. 7, a thorough evaluation of time-step uncertainty errors of the C05 stepped hull is shown. The analysis is done for both results found using overset and morphing mesh techniques, with consistent mesh configurations of 15.4M for overset and 15.17M for morphing. All results correspond to beam Froude Number of 4.97. The analysis reveals that the average time-step uncertainty error for predicting resistance and trim of the C05 stepped hull is approximately 0.93% and 2.29%, respectively, when employing the overset technique. Meanwhile, utilizing the morphing mesh technique yields slightly higher average errors of 2.34% for resistance prediction and 1.14% for trim prediction. The conclusion derived from the analysis suggests that altering the time-step in the configuration of the C05 stepped hull has a limited impact on the results. In the context of stepped hulls, it is important to note that the uncertainty error in resistance carries more significance than that of trim. Consequently, when it comes to temporal discretization, overset

techniques demonstrate lower uncertainty as compared to morphing mesh methods. However, it is crucial to emphasize that the choice of the most accurate technique depends on other factors such as grid uncertainty and experimental uncertainty. Section 6 will provide a more detailed exploration of these considerations.

In Fig. 8, the results of a similar investigation carried out for the C1 interceptor hull are shown. This investigation was done for Froude Number of 1.94, and again the results of both overset and morphing mesh strategies are analyzed. These simulations adopt a uniform mesh configuration, specifically 14.9M for overset and 13.2M for morphing. Notably, the average time-step uncertainty error for predicting resistance and trim of the C1 interceptor hull through the overset technique is approximately 0.71% and 2.63%, respectively. When utilizing the morphing mesh technique, these figures increase to around 1.36% for resistance and 2.62% for trim prediction.

Similar to the C05 stepped hull, adjusting the time-step in the setup of the C1 interceptor hull has a minimal influence on the CFD results. For the interceptor hull, it is important to note that trim uncertainty carries more significance than resistance. This is because one of the primary objectives in installing an interceptor on the hull is to reduce trim angles and minimize motion. Therefore, accurately predicting the fluid around the interceptor is first priority. Yet accurate prediction of resistance is still important.

Both techniques provide trim values within a similar range of uncertainty when considering time-step uncertainty. However, the overset technique exhibits slightly lower uncertainty, in predicting resistance.
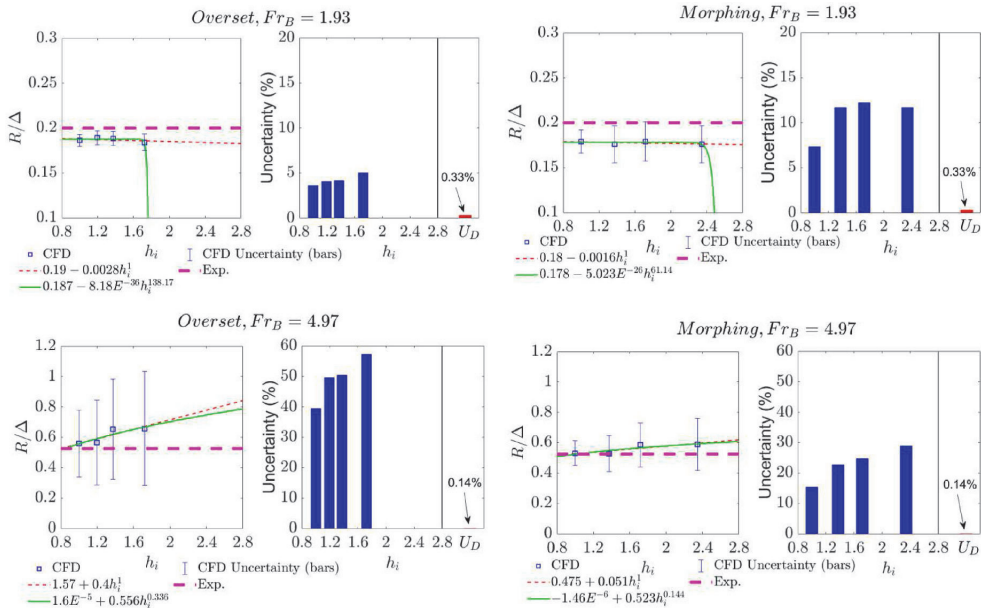

Fig. 10. Grid uncertainty analysis using the Least Squares Method for the resistance value of C05 stepped hull with overset and morphing mesh techniques, revealing the order of convergence and estimation of errors at minimum Froude numbers 1.93, and Maximum Froude number 4.97. Additional Froude numbers, 2.86, 3.31, 3.91, and 4.5, are provided in Appendix C. U_D is experimental uncertainty.

Table 8
Comparison error and grid uncertainty for the resistance value of the C05 stepped hull for finest mesh configurations 14.9M (Overset) and 13.2M (Morphing).

Fr_B	Overset						Morphing					
	1.93	2.86	3.31	3.91	4.5	4.97	1.93	2.86	3.31	3.91	4.5	4.97
$E_R\%$	7.10%	3.84%	2.09%	−1.65%	−5.97%	−6.47%	10.55%	6.37%	5.23%	3.23%	0.28%	−1.11%
$U_{GR}\%$	3.70%	12.19%	16.23%	23.45%	28.18%	39.51%	7.34%	1.71%	4.30%	4.36%	16.34%	15.42%

As per ITTC 7.5–03–02–03 (2011) guidelines, standard pseudo-transient resistance computations should use time steps ranging from $\Delta t = 0.005$ to $0.01\ L_{wl}/\nu$. In addition, certain research studies, such as Tezdogan et al. (2015), highlight the significance of adhering to the ITTC 7.5–03–02–03 (2011) time-step guidelines. This study followed these guidelines by employing four time steps within this recommended range. Furthermore, since implicit scheme was adopted in the unsteady simulations, the time step is more determined by the flow properties rather than the other parameters (e.g. Courant number). The suggested ranging of time steps represents also a way to balance accuracy and running time. Figs. 7 and 8 reveal a noticeable trend where in smaller time-step sizes occasionally demonstrate increased uncertainty. This observation could stem from several factors, including the complex nature of hull configurations, specific hydrodynamic conditions, or other simulation-related aspects (e.g. mesh densities). Smaller time steps may lead to numerical instabilities. Indeed, smaller time steps might capture more transient or oscillatory flow features, potentially introducing (relatively) higher uncertainty values.

In the following section, discretization error for the grid is undertaken. A time-step of $0.006 L_{wl}/\nu$ is adopted for the C05 stepped hull, while a value of $0.009 L_{wl}/\nu$ is employed for the C1 interceptor hull.

5.1. Grid uncertainty analysis for the C05 stepped hull

Fig. 9 shows the grid uncertainty analysis of the trim for the C05 stepped hull. U_D, in The Figures is experimental or data uncertainty. The fitting apparent order of convergence, ℙ, is less than 0.5 for the overset mesh technique, while for the morphing mesh technique, the order of convergence, ℙ, is greater than 2 for all Froude numbers except Froude numbers 1.93 and 3.91. Therefore, most of the errors are quantified using an error estimator with first order, except for Froude number 1.93, which is quantified using an error estimator with first and second orders. The compilation error between the CFD results and towing tank test data is shown in Appendix A. With an increase in speed (beam Froude Number), the error between numerical results and the experimental in the 8.9M and 11.2M mesh setup grows, mostly in the overset mesh technique. The discrepancy can be attributed to a stronger turbulent flow, consequently introducing greater uncertainty. Fig. 9 shows the grid uncertainty analysis at minimum Froude numbers 1.93 and the maximum Froude number 4.97. Additional Froude numbers, namely 2.86, 3.31, 3.91, and 4.5, are detailed in Appendix B.

Table 7 presents a comparison of the error in resistance for the C05 stepped hull obtained from CFD simulations using both mesh techniques for the towing tank test data. The table also includes data on grid uncertainty for resistance values obtained using a fine mesh for each technique. The results indicate that the error in resistance ranges from 0.67% to 11.49% for overset mesh and 0.76%–13.30% for the morphing technique. The grid uncertainty in resistance, U_τ, is higher for the overset mesh technique, with a range of 11.85%–25.55%, compared to the morphing mesh technique, which has a range of 1.96%–4.6%. The error in prediction of trim angle would be less when the overset technique is used, though the uncertainty associated to morphing method is less. The overset method highly depends on the way the interpolation between overset and background regions is done. Thus, the uncertainty would be much larger as compared to morphing.

Based on Fig. 9, when the parameter ℙ is below 0.5, the red line plot denoting Richardson extrapolation indicates convergence, allowing for
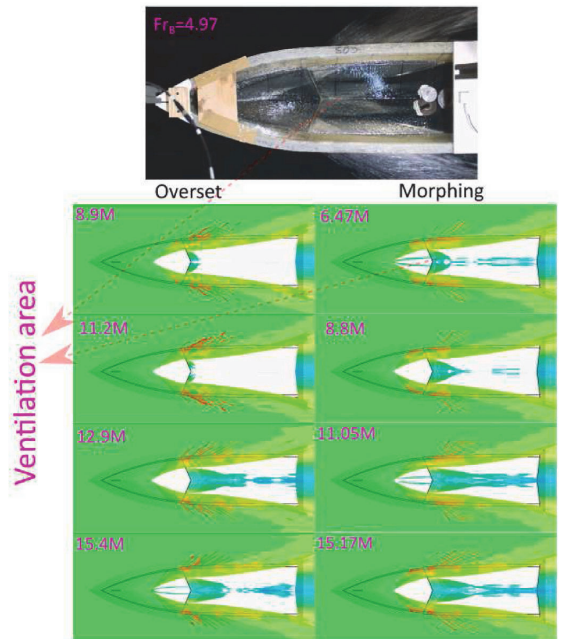

Fig. 11. Effect of mesh number on wetted surface area and ventilation in CFD simulations of stepped C05 hull compared to towing tank test at Froude number 4.94. Please refer to Appendix D for results at other Froude numbers.

a selection of the number of cells below the minimum mesh. However, the plots reveal instances of divergence in error estimation when ℙ exceeds 2. This situation leads to an unrealistically low error estimate. Consequently, the divergence suggests that having a number of cells below the minimum mesh requirement for this particular hull at this speed will result in a high discretization error.

Fig. 10 presents the results of the uncertainty analysis of CFD model in prediction of resistance of the C05 stepped hull at minimum Froude numbers 1.93 and the maximum Froude number 4.97. Additional Froude numbers, namely 2.86, 3.31, 3.91, and 4.5, are detailed in Appendix C. The overset mesh technique shows a fitting apparent order of convergence, ℙ, less than 0.5, while the morphing mesh technique has an order of convergence, ℙ, greater than 2 for all Froude numbers except for Froude numbers 3.31, 3.91, and 4.97, for which ℙ is observed to be lower than 0.5. Hence, a first-order error estimator is used to estimate all errors.

Table 8 presents the error in comparison to the towing tank test data and the grid uncertainty error of the CFD models in prediction of resistance of the C05 stepped hull. The table shows the results for fine cell numbers in each technique. The error in resistance ranges from 1.65% to 7.10% for the overset mesh technique and from 0.28% to 10.55% for the morphing mesh technique. The last row of the table outlines the grid uncertainty data, U_R, which is the range of uncertainty in the numerical results due to discretization errors. The grid uncertainty
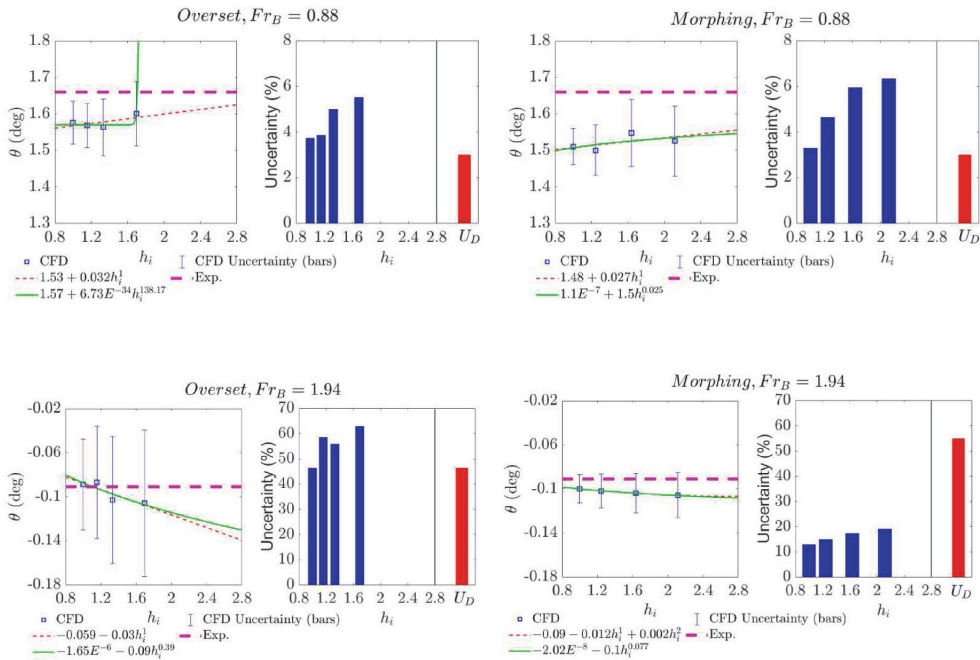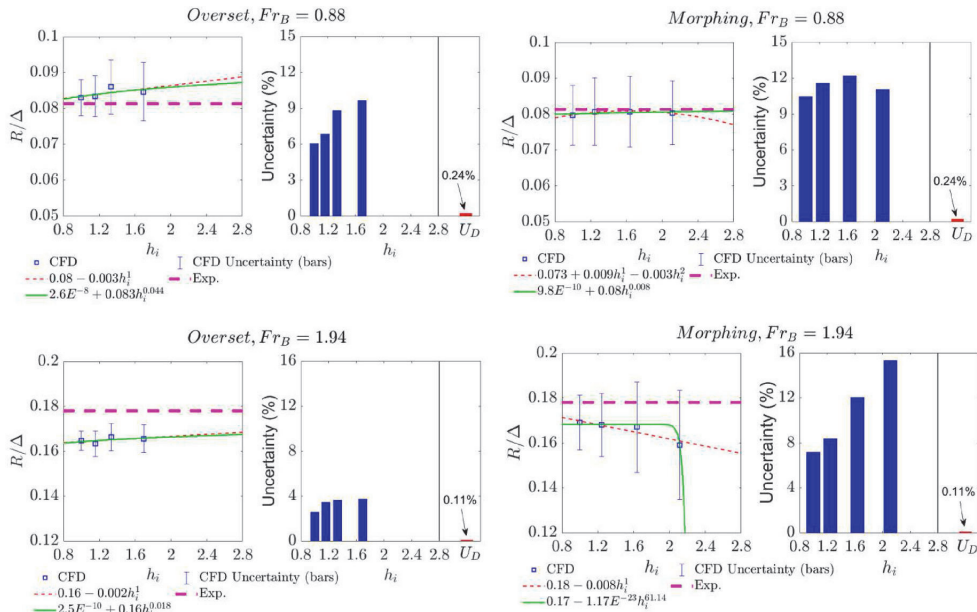
Fig. 12. Grid uncertainty analysis using the Least Squares Method for the trim value of C1 interceptor hull with overset and morphing mesh techniques, revealing the order of convergence and estimation of errors at minimum Froude numbers 0.88, and Maximum Froude number 1.94. Additional Froude numbers, 1.06, 1.24, 1.41, 1.6, and 1.77 are provided in Appendix F. U_D is experimental uncertainty.

ranges from 3.7% to 39.51% for the overset mesh technique and 1.71%–16.34% for the morphing mesh technique. The grid uncertainty values surpass the errors for all Froude numbers except 1.93 when employing the overset mesh technique. This observation was also made in prediction of trim angle of the stepped hull. This well shows that trim angle and resistance force are linked, which is not surprising. Hence, it provides another piece of evidence for what was explained before. The interconnection between trim angle and resistance force often reveals itself within hydrodynamic studies highlighting performance of planing hulls (e.g. Savitsky, 1964) due to their relationship in hull equilibrium. These findings emphasize the significance of their correlation, elucidating the mutual interdependency between dynamic trim angle and the opposing resistance force in hydrodynamic performance assessments. The overset method, while can be more accurate in calculation of trim and resistance, can introduce more uncertainty. However, when using the morphing mesh technique, the grid uncertainty values only exceed the errors for Froude numbers greater than or equal to 3.91. In the following section, the numerical uncertainty will be calculated using these values, and a comparison with the error in trim and resistance will be conducted to assess the validity and reliability of the CFD simulations for the C05 stepped hull.

Similar to Fig. 9, divergence is observed in the plots of resistance in Fig. 10 for most morphing techniques when P surpasses 2. This divergence implies that employing a number of cells below the minimum mesh requirement for this specific hull at this speed will lead to an oversized discretization error.

Fig. 11 presents a qualitative comparison of the wetted surface area observed in towing tank tests and the one monitored in CFD simulations. The results of both mesh motions are shown, and this Figure only covers Froude Number of 4.94. The figure also shows the effect of cell number on the ventilation area. The results corresponding to other Froude numbers are visualized, but they are provided in Appendix D.

The overset mesh technique does not capture ventilation when simulations are run with cell numbers 8.9M and 11.2M, while the ventilation area is well formed when higher two cell numbers are used (The ventilation area refers to the space behind the step where, at sufficiently high speeds, the water flow is detached from the bottom and draws air from the hull sides, inducing a "cavity" called ventilation area and its longitudinal extension is the ventilation length). Note that ventilation was observed to be well developed during the towing tank tests. On the other hand, the morphing mesh technique captures ventilation when run with all considered cell numbers. Yet a partial ventilation area is given by CFD model based on overset technique when two lower spatial resolutions are used.

Overall, upon qualitatively comparing the ventilation area developed through CFD simulations with those observed on the towing tank tests, it is concluded that the morphing mesh technique consistently outperforms the overset mesh technique in capturing the ventilation area in lower mesh numbers. The variation in the ventilation area between the morphing and overset meshes, particularly at lower speeds, might be attributed to the differing definitions or implementations of these methods. Furthermore, at high speeds, even small discrepancies in the trim angle could significantly impact the wetted surface distribution and spray distribution, potentially influencing the observed differences between overset and morphing results. This effect could be related to the nuanced handling of hull motions and their influence on the computational fluid dynamics (CFD) simulations at different Froude numbers.

These findings signify the importance of selecting an appropriate mesh technique and mesh number to accurately capture the ventilation emerging under bottom of a stepped planing surface. The morphing mesh technique is found to be a valuable tool for simulating the flow characteristics of planing hulls, especially in cases ventilation phenomena would emerge. It has the potential to enhance our understanding and facilitate the design optimization of such vessels.

Table 9

Comparison error and grid uncertainty for the trim value of the C1 interceptor hull for finest mesh configurations 14.9M (Overset) and 13.2M (Morphing).

	Overset							Morphing						
Fr_B	0.88	1.06	1.24	1.41	1.59	1.77	1.94	0.88	1.06	1.24	1.41	1.59	1.77	1.94
$E_\tau\%$	5.06%	0.34%	2.60%	6.04%	1.06%	3.20%	2.20%	9.04%	0.58%	2.44%	4.58%	3.17%	9.11%	9.89%
$U_{G\tau}\%$	3.73%	14.27%	13.94%	8.42%	8.22%	15.28%	46.37%	3.31%	11.66%	20.18%	5.32%	11.40%	74.47%	12.99%

Fig. 13. Grid uncertainty analysis using the Least Squares Method for the resistance value of C1 interceptor hull with overset and morphing mesh techniques, revealing the order of convergence and estimation of errors at minimum Froude numbers 0.88, and Maximum Froude number 1.94. Additional Froude numbers, 1.06, 1.24, 1.41, 1.6, and 1.77 are provided in Appendix G. U_D is experimental uncertainty.

5.2. Uncertainty analysis for C1 interceptor hull

Fig. 12 presents the uncertainty of simulations in prediction of the trim angle of the C1 interceptor hull. Appendix E documents a comparison of the errors of the CFD method in prediction of trim angle. The uncertainty of simulations in the prediction of the trim angle is investigated at various Froude numbers, including the minimum values of 0.88 and maximum value of 1.94. The findings for additional Froude numbers (1.06, 1.24, 1.41, 1.6, and 1.77) are included in Appendix F. As observed (Fig. 12), the overset mesh technique exhibits a fitting apparent order of convergence, ℙ, higher than 2 for all considered Froude numbers, except for Froude number of 1.94, for which the ℙ value is seen to be lower than 0.5. The morphing mesh technique has an order of convergence, ℙ, lower than 0.5 for almost of considered Froude numbers, which are 0.88, 1.41, 1.6, 1.77, and 1.94. For Froude numbers of 1.06 and 1.24, ℙ values are found to be greater than 2. Hence, a first-order error estimator is used to estimate the errors corresponding to all Froude Numbers of overset and morphing mesh techniques. But the exceptional case is the simulations done using morphing mesh approach for Froude number of 1.94 for which a second-order error estimator is used.

Table 9 gives the error of CFD simulations in calculations of the trim angles of C1 interceptor hull. In addition, the grid uncertainty values of the trim angles of this hull are also reported in this Table. The error is expressed as a percentage difference between the numerical and experimental values, while the grid uncertainty represents the

uncertainty associated with the numerical solution. For the overset mesh technique, the error, $E_\tau\%$, is seen to range in between 0.34% and 6.04% across the different cell numbers. The grid uncertainty associated to this method, $U_\tau\%$ is observed to range from 3.73% to 46.37%. The errors of the morphing technique are seen to be relatively grater as compared to the overset technique. The lower limit of the errors of morphing mesh in prediction of trim angle of C1 interceptor hull is 0.58%, and the upper limit 9.89%. The grid uncertainty associated to C1 interceptor hull has seen to be larger than those of the overset method, varying from 3.31% to 74.47%. This is opposite to what was observed in the uncertainty associated to simulations done for the stepped hull. The morphing method was seen to have a better level of certainty as compared to the overset method, when the calm water ride of the stepped hull was modeled. The absence of the ventilation area under the bottom surface of the vessel is likely to be the reason. When the overset method is used to solve the fluid motion around the stepped hull, the interpolation of different fields would be done in between a background region filled with water and an overset region free of water, which may introduce uncertainty. But for a hull with no step, both of these regions are filled with water and thus the uncertainty level would be lower.

Similar to the divergence observed in the plots of C05 stepped hulls (Figs. 9 and 10), a similar pattern emerges for C1 interceptor hulls in Figs. 11 and 12 when ℙ exceeds 2. This divergence indicates that utilizing a number of cells below the minimum mesh requirement for this specific hull at this speed will lead to a substantial discretization error.

Lastly, the grid uncertainty in predicting the trim angle of the C1 hull

Table 10
Comparison error and grid uncertainty for the resistance value of the C1 interceptor hull for finest mesh configurations 14.9M (Overset) and 13.2M (Morphing).

Fr_B	Overset							Morphing						
	0.88	1.06	1.24	1.41	1.59	1.77	1.94	0.88	1.06	1.24	1.41	1.59	1.77	1.94
E_R%	2.12%	5.47%	6.60%	6.55%	5.74%	1.66%	7.54%	1.97%	2.43%	2.94%	4.98%	6.56%	8.48%	5.12%
U_{GR}%	6.09%	14.87%	19.64%	15.75%	17.07%	6.07%	2.60%	10.47%	1.65%	7.90%	4.10%	1.69%	0.60%	7.19%
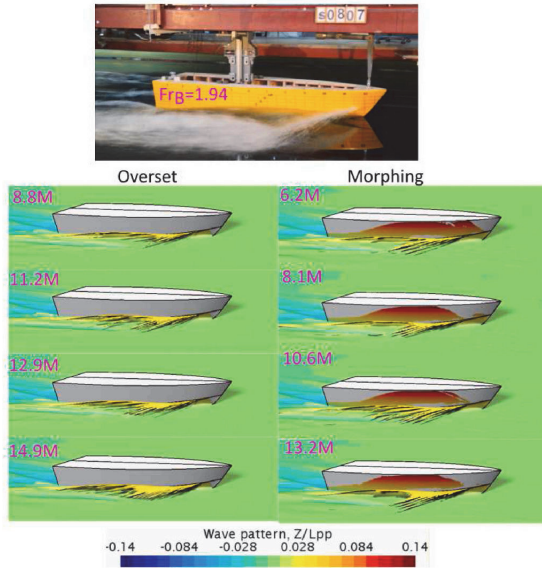
Fig. 14. A qualitative comparison of spray and wave formation around the C1 interceptor planing hull using different CFD mesh motion techniques and towing tank tests, with varying cell numbers at Froude number 1.94. Please refer to Appendix H for results at other Froude numbers.

exceeds the error for all Froude numbers, except for a Froude number of 0.88, where the grid uncertainty in predicting the trim angle is lower than the error generated by both mesh techniques. It is important to note that when the grid uncertainty level falls below the error level, it may indicate a potential lack of validation due to the models implemented in the simulations (ITTC 75-03-01-01 Rev 04, 2021) under these specific conditions. However, this aspect will be further explained and correlated with experimental values in Section 6 of the paper.

Moving on to Fig. 13, it presents the grid uncertainty analysis in prediction of the resistance of the C1 interceptor hull. This analysis encompasses several Froude numbers, ranging from the minimum value of 0.88 to the maximum value of 1.94. Additional findings for Froude numbers (1.06, 1.24, 1.41, 1.6, and 1.77) are detailed in Appendix G. The overset mesh technique shows a fitting apparent order of convergence, ₱, greater than 2 for Froude numbers of 1.06, 1.41, 1.6, 1.77. The

fitting apparent orders of overset method corresponding to Froude numbers 0.88, 1.24, and 1.94 are below 0.5. For the morphing mesh technique, the order of convergence, ₱, is found to be greater than 2 for all Froude numbers, except 0.88, 1.41, and 1.6. For these three aforementioned Froude Numbers, the orders of convergence are found to be lower than 0.5. As a result, for the morphing mesh, a first-order error estimator is used to calculate errors associated to all Froude Numbers, except the one corresponding to Froude number 0.88 for the morphing mesh technique. The errors associated to overset method are found using a first-order estimator at all Froude Numbers except $Fr_B = 1.24$, for which a first and second-order error estimator is embarked.

Table 10 presents the comparison of the error and the grid uncertainty in prediction of the resistance of the C1 interceptor hull. The errors of overset method in prediction of resistance vary from 1.66% to 7.54%, and the associated grid uncertainty ranges from 2.60% to 19.64%. Notably, the grid uncertainty surpasses the error for all Froude numbers, except at 1.94.

The range of errors of morphing mesh technique in prediction of resistance of C1 interceptor hull is relatively close to those of overset method. The range is in between 1.97% and 8.48. This shows that both methods would offer similar level of accuracy in prediction of resistance force. Interestingly, the grid uncertainty level of morphing mesh in prediction of resistance force is lower than those of overset method, and ranges from 0.60% to 10.47%. It is worth noting that the grid uncertainty of the morphing mesh exceeds the error at three of considered Froude numbers, which are 0.88, 1.24, and 1.94. But for overset method, the grid uncertainty level is larger than the errors at all Froude Numbers except the last one which is 1.94.

Fig. 14 qualitatively compares the water spray generated around the C1 interceptor planing hull using different CFD mesh motion techniques and towing tank tests, with varying cell numbers at Froude number 1.94. Results for other Froude numbers are provided in Appendix H. The overset mesh technique properly captures the formation main spray around the hull. The simulations done using morphing mesh technique, however, may give a greater spray volume and larger wave surface deformation around the hull. Therefore, for the C1 interceptor hull, the overset mesh technique is preferred over the morphing mesh technique if the target is to monitor the free surface deformation around the hull.

It is of note that a very small volume of air-water spray also emerges in simulations done using the morphing (above the chine). This volume of air-water spray above the chine seems very visible as the snapshots are colored using the water surface deformation. The presence of this negligible volume of air-water does not mean that the morphing mesh does not capture the water detachment from the chine as main spray (which is visible in Fig. 14) only forms if water is detached from the chines (Morabito, 2010; Savitsky and Morabito, 2011).

Table 11
Simulation Uncertainty Error of C05 stepped hull for Mesh Configurations 15.4M (Overset) and 15.17M (Morphing).

Fr_B	Overset						Morphing					
	U_{GR}%	U_{TSR}%	U_{SNR}%	U_{G_T}%	U_{TS_T}%	U_{SN_T}%	U_{GR}%	U_{TSR}%	U_{SNR}%	U_{G_T}%	U_{TS_T}%	U_{SN_T}%
1.93	3.70%	0.93%	3.82%	11.85%	2.29%	12.07%	7.34%	2.34%	7.70%	3.29%	1.14%	3.48%
2.86	12.19%	0.93%	12.23%	18.55%	2.29%	18.69%	1.71%	2.34%	2.90%	2.12%	1.14%	2.41%
3.31	16.23%	0.93%	16.26%	25.55%	2.29%	25.65%	4.30%	2.34%	4.90%	4.60%	1.14%	4.74%
3.91	23.45%	0.93%	23.47%	5.87%	2.29%	6.30%	4.36%	2.34%	4.95%	3.49%	1.14%	3.67%
4.50	28.18%	0.93%	28.20%	17.52%	2.29%	17.67%	16.34%	2.34%	16.51%	1.96%	1.14%	2.27%
4.97	39.51%	0.93%	39.52%	17.00%	2.29%	17.15%	15.42%	2.34%	15.60%	2.91%	1.14%	3.13%

Table 12
Uncertainty Error of C1 interceptor hull for Mesh Configurations 14.9M (Overset) and 13.2M (Morphing).

Fr_B	Overset						Morphing					
	U_{G_R}%	U_{TS_R}%	U_{SN_R}%	U_{G_τ}%	U_{TS_τ}%	U_{SN_τ}%	U_{G_R}%	U_{TS_R}%	U_{SN_R}%	U_{G_τ}%	U_{TS_τ}%	U_{SN_τ}%
0.88	6.09%	0.71%	6.13%	3.73%	2.63%	4.56%	10.47%	1.36%	10.56%	3.31%	2.62%	4.22%
1.06	14.87%	0.71%	14.89%	14.27%	2.63%	14.51%	1.65%	1.36%	2.14%	11.66%	2.62%	11.95%
1.24	19.64%	0.71%	19.65%	13.94%	2.63%	14.18%	7.90%	1.36%	8.02%	20.18%	2.62%	20.35%
1.41	15.75%	0.71%	15.77%	8.42%	2.63%	8.82%	4.10%	1.36%	4.32%	5.32%	2.62%	5.93%
1.60	17.07%	0.71%	17.08%	8.22%	2.63%	8.63%	1.69%	1.36%	2.17%	11.40%	2.62%	11.70%
1.77	6.07%	0.71%	6.11%	15.28%	2.63%	15.50%	0.60%	1.36%	1.49%	74.47%	2.62%	74.52%
1.94	2.60%	0.71%	2.70%	46.37%	2.63%	46.44%	7.19%	1.36%	7.32%	12.99%	2.62%	13.25%

5.3. Simulation uncertainty for both hulls

To perform a more complete analysis on the CFD simulations done using both methods, grid uncertainty error is considered, and an assumption is made that the time step uncertainty error remains constant for all speeds, equating to the values found at the highest speed (within the same mesh number where the time step uncertainty is conducted). This assumption allows for the estimation of simulation uncertainty to be defined as follows:

$$U_{SN}^2 = U_{TS}^2 + U_G^2 \qquad (19)$$

Where, U_{SN} signifies the estimation of simulation uncertainty, U_G represents grid uncertainty error, and U_{TS} stands for uncertainty time step error.

As previously noted, by assuming a constant U_{TS} across all speeds and equating it to that of the highest speed value ($Fr_B = 4.97$), uncertainty of both CFD setups in prediction of the trim angle and resistance force of C05 hull are calculated and then listed in Table 11. These errors are showcased for Mesh Configurations 15.4M (Overset) and 15.17M (Morphing) in accordance with Equation (19). In Table 11, across all Froude numbers, the simulation uncertainty error (U_{SN}) for the Morphing technique remains relatively lower compared to the Overset method for both resistance and trim, except at Froude number 1.93 for resistance values. As the Froude number increases to 4.97, these uncertainty percentages notably rise for both mesh configurations. However, the increase in uncertainty values for the Overset technique is higher as compared to Morphing method, reaching up to 39.52% for resistance values and 17.15% for trim values. This notable increase implies higher uncertainty in computational results as hydrodynamic conditions become more intricate at higher Froude numbers for stepped planing hulls.

Table 12 shows similar values (uncertainty errors) associated to both CFD models in prediction of trim angle and resistance of C1 Interceptor Hull, focusing on two refined mesh configurations: 14.9M using the Overset approach and 13.2M employing the Morphing technique. The table demonstrates the disparities in Uncertainty Error percentages across various Froude numbers, encompassing both grid and time-step variations. In Table 12, the simulation uncertainty error varies noticeably across different Froude numbers for both the overset and morphing techniques applied to the C1 interceptor hull. At the lowest Froude number (0.88) and the highest (1.94), the simulation uncertainty error in the resistance value is lower for the overset mesh compared to the morphing technique. However, for the other Froude numbers, the simulation uncertainty in prediction of the resistance is higher with the overset technique compared to that of morphing method. When considering the simulation uncertainty in trim values, at Froude numbers 1.24, 1.6, and 1.77, the simulation uncertainty with the overset technique is lower than with the morphing technique. On the contrary, for the remaining Froude numbers, the simulation uncertainty in the overset technique is higher than in the morphing technique.

Table 13
Scenarios of U_V and $|E|$ relationships in validation analysis (Coleman and Stern, 1997; ITTC 75-03-01-01 Rev 04, 2021).

Situation points	Validation achieved	Description
$U_V > |E|$	Yes	it indicates that the computational model aligns sufficiently well with experimental data and that the results fall within an acceptable range of accuracy.
$U_V \gg |E|$	Yes, at UV level of Uncertainty	the validation is achieved with a level of uncertainty that suggests that the results are overly noisy.
$U_V < |E|$	No	it implies that the computational model falls short of validation. In this case, the level of uncertainty in the simulation is greater than what is deemed acceptable based on the experimental data, indicating the presence of modeling issues or that the mesh configurations used are distant from the expected asymptotic trends.

6. Validation analysis (for both hulls)

To properly perform data validation study on CFD setups used in the present research, a crucial indicator termed Uncertainty Value, shown by U_V the, is introduced. U_V is found using the following equation:

$$U_V^2 = U_D^2 + U_{SN}^2 \qquad (20)$$

where, U_D, is experimental or data uncertainty, and U_{SN}, is the simulation uncertainty. This uncertainty value is essential because both hulls, the C05 stepped hull and the C1 interceptor hull, present unique challenges in simulation due to their complexity. The C05 stepped hull poses difficulties in prediction of resistance and wetted surface using CFD models mainly because it requires an exceptionally fine mesh, especially in proximity of the step. On the other hand, simulation of the fluid flow around the C1 interceptor hull is particularly challenging when it comes to predicting the trim angles, since it demands a very fine mesh setup and a precise prism layer around the interceptor. Therefore, both hulls present their own set of complexities in the simulation process.

The validation process relies on the relationship between U_V and another parameter, denoted as E, representing the percentage comparison, which is found as (EXP-CFD)/EXP (EXP refers to Experimental value and CFD refers to CFD value). Table 13 shows three scenarios that help us interpret the relationships between U_V and $|E|$ in the validation analysis. Each scenario describes different conditions and outcomes, providing insights into the accuracy level of the CFD model and dependability of computational simulations when compared to the value collected in experimental tests.

Tables 14–16 list a summary of the validation studies conducted for both the C05 stepped hull and the C1 interceptor hull. These tables interpret the assessment of validation. This analysis categorizes validation outcomes into "yes" or "yes, at UV level of Uncertainty" to signify achieved validation, while "no" indicates validation is not achieved. "Yes, at UV level of Uncertainty" implies validation accomplishment,

Table 14

Validation of resistance studies for C05 stepped hull with mesh configurations 15.4M (Overset) and 15.17M (Morphing) across all speeds.

Fr_B	Overset					Morphing				
	$E_R\%$	$U_{DR}\%$	$U_{SNR}\%$	$U_{VR}\%$	validation achieved	$E_R\%$	$U_{DR}\%$	$U_{SNR}\%$	$U_{VR}\%$	validation achieved
1.93	7.10%	0.33%	3.82%	3.83%	No	10.55%	0.33%	7.70%	7.71%	No
2.86	3.84%	0.27%	12.23%	12.23%	Yes, at UV level of Uncertainty	6.37%	0.27%	2.90%	2.91%	No
3.31	2.09%	0.22%	16.26%	16.26%	Yes, at UV level of Uncertainty	5.23%	0.22%	4.90%	4.90%	No
3.91	−1.65%	0.18%	23.47%	23.47%	Yes, at UV level of Uncertainty	3.23%	0.18%	4.95%	4.95%	Yes
4.50	−5.97%	0.15%	28.20%	28.20%	Yes, at UV level of Uncertainty	0.28%	0.15%	16.51%	16.51%	Yes, at UV level of Uncertainty
4.97	−6.47%	0.14%	39.52%	39.52%	Yes, at UV level of Uncertainty	−1.11%	0.14%	15.60%	15.60%	Yes, at UV level of Uncertainty

Table 15

Validation of trim studies for C05 stepped hull with mesh configurations 15.4M (Overset) and 15.17M (Morphing) across all speeds.

Fr_B	Overset					Morphing				
	$E_\tau\%$	$U_{D\tau}\%$	$U_{SN\tau}\%$	$U_{V\tau}\%$	validation achieved	$E_\tau\%$	$U_{D\tau}\%$	$U_{SN\tau}\%$	$U_{V\tau}\%$	validation achieved
1.93	4.06%	2.65%	12.07%	12.36%	Yes, at UV level of Uncertainty	5.36%	2.65%	3.48%	4.38%	No
2.86	1.48%	2.65%	18.69%	18.88%	Yes, at UV level of Uncertainty	3.19%	2.65%	2.41%	3.58%	Yes
3.31	0.67%	3.04%	25.83%	25.83%	Yes, at UV level of Uncertainty	0.76%	3.04%	4.74%	5.63%	Yes, at UV level of Uncertainty
3.91	−7.92%	3.26%	22.5%	22.73%	Yes, at UV level of Uncertainty	−5.78%	3.26%	3.67%	4.91%	No
4.50	−5.24%	3.47%	17.67%	18.01%	Yes, at UV level of Uncertainty	−4.59%	3.47%	2.27%	4.15%	No
4.97	−11.49%	3.39%	17.15%	17.49%	Yes	−13.30%	3.39%	3.13%	4.61%	No

but with the assumption that the UV value is twice the |E|. The experimental uncertainty for C05 stepped hull is taken from Vitiello et al. (2022) and for the C1 interceptor hull is derived from De Luca et al. (2016). Again, readers interested in more details regarding these experiments are referred to these two papers.

According to Tables 14 and 15, resistance validation of C05 with the CFD model built using the overset technique was found to be successfully achieved for all Froude numbers, except for $Fr_B = 1.93$, where the computational model suffers short of validation. Conversely, for the CFD model built based on the morphing mesh method, the resistance validation was only achieved for Froude numbers greater than or equal 3.91. For lower Froude numbers, the computational model was seen to be failed to be validated.

The overset technique was seen to reach a secured validation in prediction of the trim angle of C05 across all considered Froude numbers. The morphing mesh technique, was seen to be well validated for Froude numbers 2.86 and 3.31, but was seen to be failed in passing the validation criteria for other Froude numbers.

According to Tables 16 and 17, validation criteria of overset mesh method in the prediction of resistance force of C1 interceptor hull was seen to be well passed for all Froude numbers, except for the maximum one, which is 1.94. The morphing mesh passed this validation criteria for three different Froude Numbers of 0.88, 1.24, and 1.94.

The validation of the CFD model, based on the overset technique, accurately predicted the trim angle of C1 for all Froude Numbers considered. However, the morphing mesh technique struggled more in comparison to the overset method. The validation criteria were met by the morphing mesh for all Froude numbers except for $Fr_B = 0.88$.

In general, the overset mesh technique shows better performance compared to the morphing mesh technique in terms of numerical uncertainty and validation achieved through performing the Validation and Verification analysis. It is worth noting that both techniques exhibit relatively low error in prediction of trim angle and resistance with the towing tank test data. For the C05 stepped hull, the overset method showcased resistance and trim yield errors compared to the experiment, ranging from 1.6 to 7.1% and 0.7–11.5%, respectively. In contrast,

Table 16

Validation of resistance studies for C1 interceptor hull with mesh configurations 14.9M (Overset) and 13.2M (Morphing) across all speeds.

Fr_B	Overset					Morphing				
	$E_R\%$	$U_{DR}\%$	$U_{SNR}\%$	$U_{VR}\%$	validation achieved	$E_R\%$	$U_{DR}\%$	$U_{SNR}\%$	$U_{VR}\%$	validation achieved
0.88	2.12%	0.24%	6.13%	6.14%	Yes, at UV level of Uncertainty	1.97%	0.24%	10.56%	10.56%	Yes, at UV level of Uncertainty
1.06	5.47%	0.19%	14.89%	14.89%	Yes, at UV level of Uncertainty	2.43%	0.19%	2.14%	2.15%	No
1.24	6.60%	0.17%	19.65%	19.65%	Yes, at UV level of Uncertainty	2.94%	0.17%	8.02%	8.02%	Yes
1.41	6.55%	0.16%	15.77%	15.77%	Yes, at UV level of Uncertainty	4.98%	0.16%	4.32%	4.32%	No
1.59	5.74%	0.15%	17.08%	17.09%	Yes, at UV level of Uncertainty	6.56%	0.15%	2.17%	2.17%	No
1.77	1.66%	0.13%	6.11%	6.11%	Yes, at UV level of Uncertainty	8.48%	0.13%	1.49%	1.49%	No
1.94	7.54%	0.11%	2.70%	2.70%	No	5.12%	0.11%	7.32%	7.32%	Yes

Table 17

Validation of trim studies for C1 interceptor hull with mesh configurations 14.9M (Overset) and 13.2M (Morphing) across all speeds.

Fr_B	Overset					Morphing				
	$E_\tau\%$	$U_{D\tau}\%$	$U_{SN\tau}\%$	$U_{V\tau}\%$	validation achieved	$E_\tau\%$	$U_{D\tau}\%$	$U_{SN\tau}\%$	$U_{V\tau}\%$	validation achieved
0.88	5.06%	3.01%	4.56%	5.46%	Yes	9.04%	3.01%	4.22%	5.18%	No
1.06	0.34%	2.43%	14.51%	14.71%	Yes, at UV level of Uncertainty	0.58%	2.43%	11.95%	12.20%	Yes, at UV level of Uncertainty
1.24	2.60%	2.71%	14.18%	14.44%	Yes, at UV level of Uncertainty	2.44%	2.71%	20.35%	20.53%	Yes, at UV level of Uncertainty
1.41	6.04%	3.47%	8.82%	9.48%	Yes	4.58%	3.47%	5.93%	6.87%	Yes
1.59	1.06%	5.86%	8.63%	10.43%	Yes, at UV level of Uncertainty	3.17%	5.86%	11.70%	13.08%	Yes, at UV level of Uncertainty
1.77	3.20%	12.32%	15.50%	19.80%	Yes, at UV level of Uncertainty	9.11%	12.32%	74.52%	75.53%	Yes, at UV level of Uncertainty
1.94	2.20%	54.95%	46.44%	71.95%	Yes, at UV level of Uncertainty	9.89%	54.95%	13.25%	56.53%	Yes, at UV level of Uncertainty

morphing errors varied from 0.3 to 10.5% and 0.8–13.3%, respectively. Concerning the C1 interceptor hull, estimation errors for resistance and trim yield, in comparison to the experiment, ranged from 1.7 to 7.5% and 0.3–6%, respectively, using the overset method. Meanwhile, morphing errors spanned from 2 to 8.5% and 0.6–10%, respectively. These numerical uncertainty values can be further utilized to establish a confidence interval for the CFD simulations and to evaluate the sensitivity of the results to changes in numerical parameters.

7. Conclusion

To ensure accurate and reliable predictions of calm water ride of a planing hull, an uncertainty analysis is necessary for CFD simulations. The present paper explored the uncertainty of CFD models in predicting the dynamic trim and hull resistance of two different planing hull shapes, the C05 stepped hull and C1 interceptor hull using four different grids, and two different mesh motion approaches, namely overset, and morphing mesh. Fitted convergence trends based on the least squares method were used to estimate the grid and time step uncertainties for each CFD simulation, which was found to be the most robust method for obtaining these estimates. The algorithm flowchart of the LSR method was explained in the present paper, providing a detailed description of the steps involved in quantifying and assessing the uncertainties associated with the CFD simulations. By following this algorithm, researchers can gain useful insights into the reliability and accuracy of the results obtained from the simulations.

The comparative analysis showed that the choice of mesh technique and number of cells significantly affects the accuracy level of CFD simulations. Across a wider range of Froude Numbers examined in the validation analysis for both the C05 stepped hull and C1 interceptor hull (mostly validated at the UV level of Uncertainty), the overset mesh technique exhibited better performance. However, the numerical uncertainty linked with the morphing method consistently maintained lower values than those observed with the overset technique, with error values below the UV threshold, implying non-validated outcomes. However, cases, where validation was achieved with a validation uncertainty much greater than the comparison error, were an indication of

the fact that the numerical "signal" of CFD simulations is still noisier than the ideal level and the simulation modeling needs to be further improved. The improvement of CFD simulations can be pursued through various means, including the exploration of alternative turbulence models such as Detached Eddy Simulation (DES), addressing artificial ventilation, and fine-tuning various simulation parameters to reduce noise and enhance the overall accuracy of the results.

To summarize, this analysis highlights the potential and constraints of CFD models in predicting planing hull performance in calm water conditions. However, it is important to consider various factors such as flow conditions, grid density, time-step size, turbulence models, and meshing techniques, as they may greatly influence the results. The computed results exhibiting oscillatory and non-monotonic behavior, provide once again evidence that the verification and validation analysis represents a crucial point in the use of CFD models when comes to design and industrial applications as well.

CRediT authorship contribution statement

Rasul Niazmand Bilandi: Conceptualization, Data curation, Formal analysis, Investigation, Methodology, Resources, Software, Validation, Visualization, Writing – original draft. **Simone Mancini:** Conceptualization, Data curation, Formal analysis, Investigation, Methodology, Software, Writing – review & editing. **Abbas Dashtimanesh:** Funding acquisition, Supervision, Writing – review & editing. **Sasan Tavakoli:** Formal analysis, Writing – review & editing.

Declaration of competing interest

The authors declare that they have no known competing financial interests or personal relationships that could have appeared to influence the work reported in this paper.

Data availability

No data was used for the research described in the article.

Appendix A. Comparison of Errors between CFD and Towing Tank Test Results of single stepped planing hull, C05 at Different Cell Numbers in Predicting the Running Attitudes and Resistance

Table 18
Number of Cells for Verification Study of C05 Stepped Planing Hull.

Overset		Morphing	
Grid no.	Cell count	Grid no.	Cell count
8.9M	8,968,525	6.47M	6,474,763
11.2M	11,245,013	8.8M	8,832,117
12.9M	12,948,438	11.05M	11,054,112
15.4M	15,449,886	15.17M	15,172,514

Table 19
Comparison of Errors between CFD and Towing Tank Test Results of C05 hull at Different Cell Numbers in Predicting trim angle.

v [m/s]	Fr_B	τ_{Exp} [deg]	τ_{CFD} [deg]								Morphing							
			Overset															
			8.9M	$E\%$	11.2M	$E\%$	12.9M	$E\%$	15.4M	$E_R\%$	6.47M	$E\%$	8.8M	$E_R\%$	11.05M	$E_R\%$	15.17M	$E_R\%$
3.131	1.931	3.853	3.863	−0.27%	3.871	−0.48%	3.658	5.05%	3.696	4.06%	3.670	4.74%	3.676	4.58%	3.665	4.87%	3.646	5.36%
4.631	2.857	2.584	2.726	−5.48%	2.738	−5.95%	2.507	2.99%	2.546	1.48%	2.525	2.30%	2.526	2.26%	2.478	4.11%	2.502	3.19%
5.368	3.311	2.181	2.382	−9.24%	2.413	−10.66%	2.142	1.77%	2.166	0.67%	2.210	−1.35%	2.179	0.07%	2.110	3.24%	2.164	0.76%
6.34	3.911	1.777	2.092	−17.71%	2.091	−17.65%	1.896	−6.68%	1.918	−7.92%	1.929	−8.53%	1.931	−8.65%	1.893	−6.51%	1.880	−5.78%
7.301	4.504	1.700	1.910	−12.36%	1.922	−13.07%	1.769	−4.06%	1.789	−5.24%	1.754	−3.18%	1.810	−6.48%	1.784	−4.95%	1.778	−4.59%
8.05	4.966	1.606	1.920	−19.59%	1.910	−18.96%	1.784	−11.12%	1.790	−11.49%	1.765	−9.93%	1.802	−12.24%	1.806	−12.49%	1.819	−13.30%

20

Table 20
Comparison of Errors between CFD and Towing Tank Test Results of C05 hull at Different Cell Numbers in Predicting resistance.

v [m/s]	Fr_B	$\frac{R_{Exp}}{\Delta}$	$\frac{R_{CFD}}{\Delta}$	Overset								Morphing							
				8.9M	$E\%$	11.2M	$E\%$	12.9M	$E\%$	15.4M	$E_R\%$	6.47M	$E\%$	8.8M	$E_R\%$	11.05M	$E_R\%$	15.17M	$E_R\%$
3.131	1.931	0.200		0.184	8.27%	0.188	5.93%	0.189	5.80%	0.186	7.10%	0.176	12.17%	0.179	10.45%	0.176	11.94%	0.179	10.55%
4.631	2.857	0.258		0.261	−1.52%	0.259	−0.46%	0.247	4.27%	0.248	3.84%	0.244	5.36%	0.241	6.22%	0.240	6.80%	0.241	6.37%
5.368	3.311	0.301		0.314	−4.38%	0.320	−6.37%	0.301	0.08%	0.295	2.09%	0.296	1.49%	0.293	2.57%	0.287	4.73%	0.285	5.23%
6.34	3.911	0.378		0.412	−9.03%	0.439	−16.08%	0.386	−2.19%	0.384	−1.65%	0.383	−1.34%	0.375	0.81%	0.371	1.85%	0.366	3.23%
7.301	4.504	0.453		0.538	−18.80%	0.527	−16.39%	0.474	−4.76%	0.480	−5.97%	0.518	−14.52%	0.471	−4.07%	0.454	−0.32%	0.451	0.28%
8.05	4.966	0.525		0.657	−25.31%	0.653	−24.45%	0.565	−7.63%	0.559	−6.47%	0.588	−12.00%	0.584	−11.31%	0.527	−0.36%	0.530	−1.11%

Table 21
Comparison of Errors between CFD and Towing Tank Test Results of C05 hull at Different Cell Numbers in Predicting sinkage.

v [m/s]	Fr_B	$\frac{(Z_G)_{Exp}}{\nabla^{1/3}}$	$\frac{(Z_G)_{CFD}}{\nabla^{1/3}}$									Morphing							
			Overset																
			8.9M	$E\%$	11.2M	$E\%$	12.9M	$E\%$	15.4M	$E_R\%$	6.47M	$E\%$	8.8M	$E_R\%$	11.05M	$E_R\%$	15.17M	$E_R\%$
3.131	1.931	0.091	0.066	27.64%	0.066	27.79%	0.065	28.05%	0.065	28.32%	0.064	29.93%	0.064	29.75%	0.064	29.59%	0.064	29.95%
4.631	2.857	0.131	0.120	8.20%	0.121	7.81%	0.119	9.28%	0.120	8.74%	0.118	9.72%	0.118	9.88%	0.117	10.56%	0.118	10.03%
5.368	3.311	0.133	0.135	−1.76%	0.136	−2.11%	0.134	−0.60%	0.135	−1.32%	0.134	−1.09%	0.133	−0.07%	0.133	0.10%	0.134	−0.86%
6.34	3.911	0.148	0.151	−1.94%	0.150	−1.34%	0.150	−1.56%	0.151	−1.73%	0.149	−0.92%	0.151	−1.85%	0.150	−1.54%	0.151	−1.98%
7.301	4.504	0.216	0.163	24.74%	0.164	24.23%	0.165	23.79%	0.164	24.17%	0.161	25.66%	0.163	24.53%	0.164	23.91%	0.165	23.52%
8.05	4.966	0.189	0.175	7.62%	0.174	7.84%	0.174	7.69%	0.174	7.69%	0.172	8.95%	0.173	8.34%	0.175	7.19%	0.176	6.85%

Table 22
Comparison of Errors between CFD and Towing Tank Test Results of C05 hull at Different Cell Numbers in Predicting wetted surface.

v [m/s]	Fr_B	$\frac{(S_W)_{Exp}}{\nabla^{2/3}}$	$\frac{(S_W)_{CFD}}{\nabla^{2/3}}$														
			Overset								Morphing							
			8.9M	$E\%$	11.2M	$E\%$	12.9M	$E\%$	15.4M	$E_R\%$	6.47M	$E\%$	8.8M	$E_R\%$	11.05M	$E_R\%$	15.17M	$E_R\%$
3.131	1.931	4.939	4.502	8.84%	4.921	0.36%	5.113	−3.52%	4.744	3.95%	4.645	5.94%	5.290	−7.12%	5.085	−2.95%	5.262	−6.55%
4.631	2.857	4.180	3.991	4.51%	3.954	5.41%	4.000	4.29%	4.356	−4.21%	4.412	−5.55%	4.187	−0.18%	4.272	−2.20%	4.234	−1.30%
5.368	3.311	3.807	3.655	4.00%	3.795	0.31%	3.823	−0.42%	3.860	−1.41%	3.729	2.03%	3.776	0.80%	3.757	1.30%	4.141	−8.77%
6.34	3.911	3.315	3.776	−13.91%	3.879	−17.02%	3.505	−5.74%	3.365	−1.51%	3.692	−11.38%	3.542	−6.87%	3.430	−3.48%	3.542	−6.87%
7.301	4.504	2.829	4.187	−48.04%	3.972	−40.44%	3.038	−7.39%	3.019	−6.73%	3.421	−20.94%	3.296	−16.51%	2.926	−3.43%	3.038	−7.39%
8.05	4.966	2.450	3.440	−40.42%	3.290	−34.31%	2.524	−3.02%	2.580	−5.31%	2.991	−22.10%	2.898	−18.29%	2.664	−8.75%	2.636	−7.60%

Appendix B. Grid uncertainty analysis for the trim value of C05 stepped hull
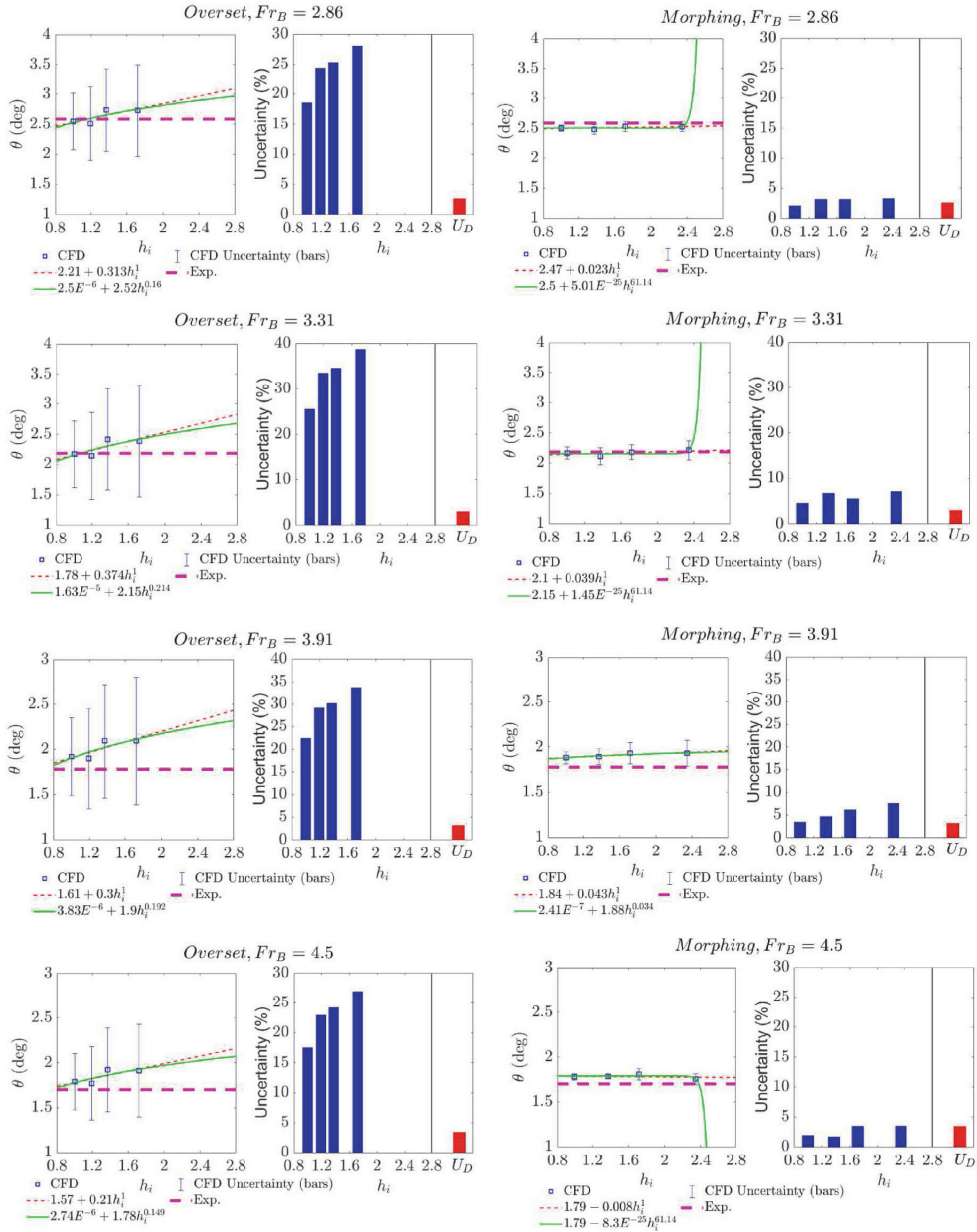
Fig. 15. Grid uncertainty analysis using the Least Squares Method for the trim value of C05 stepped hull with overset and morphing mesh techniques, revealing the order of convergence and estimation of errors at Froude numbers 2.86, 3.31, 3.91, and 4.5.

Appendix C. Grid uncertainty analysis for the resistance value of C05 stepped hull
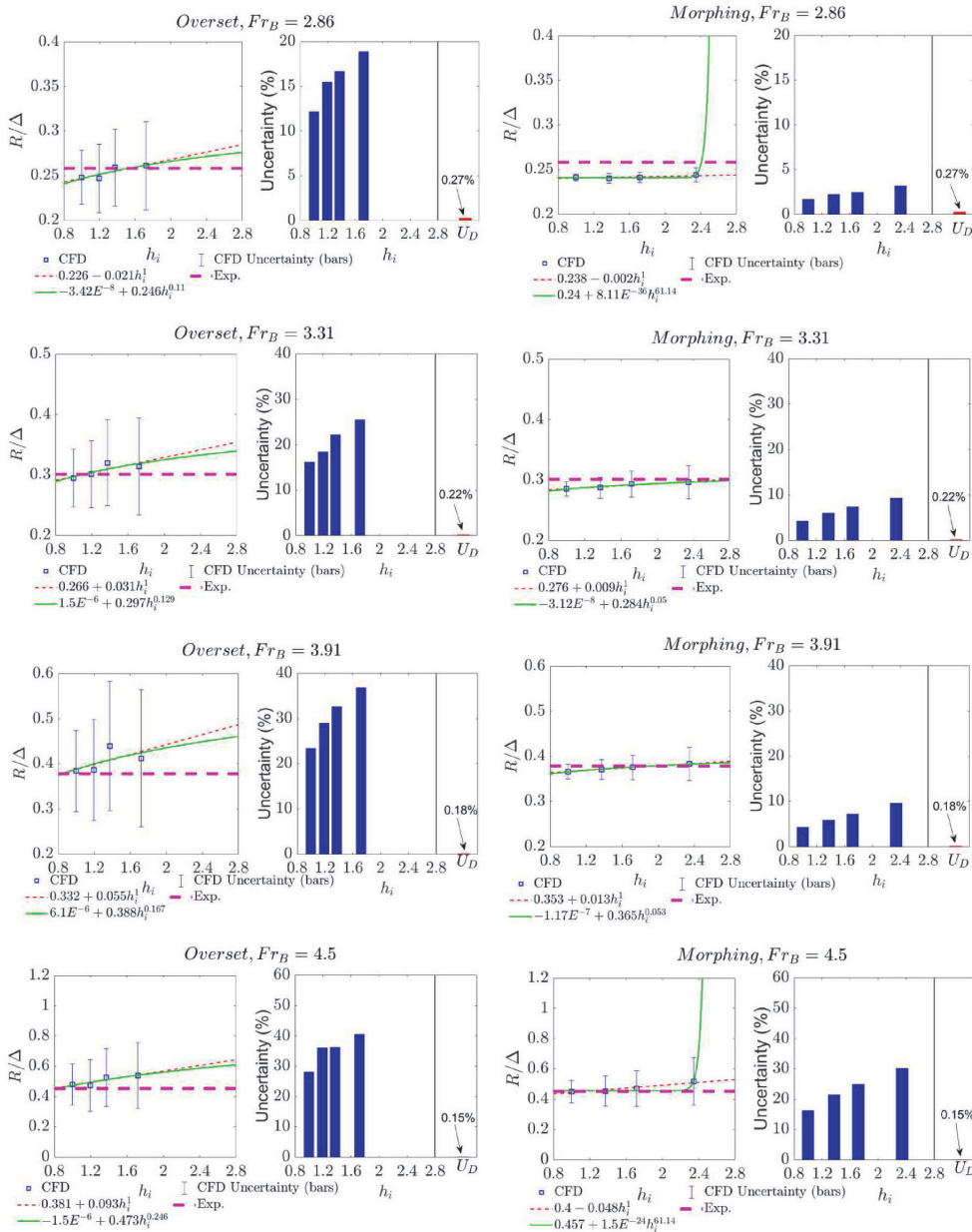
Fig. 16. Grid uncertainty analysis using the Least Squares Method for the resistance value of C05 stepped hull with overset and morphing mesh techniques, revealing the order of convergence and estimation of errors at Froude numbers 2.86, 3.31, 3.91, and 4.5.

Appendix D. Comparative Analysis of Wetted Surface and Ventilation Formation of C05 Stepped Hull Using Various CFD Mesh Techniques and Numbers at Different Froude Numbers Compared to Towing Tank Test Results

This appendix presents a comparative analysis of the wetted surface and ventilation formation in C05 stepped hulls using different CFD mesh techniques and numbers at various Froude numbers, in comparison to the results obtained from towing tank tests. The aim of this analysis is to investigate the accuracy of different CFD mesh techniques and numbers in predicting the wetted surface shape and ventilation formation and to identify the optimal mesh technique and number for accurate prediction
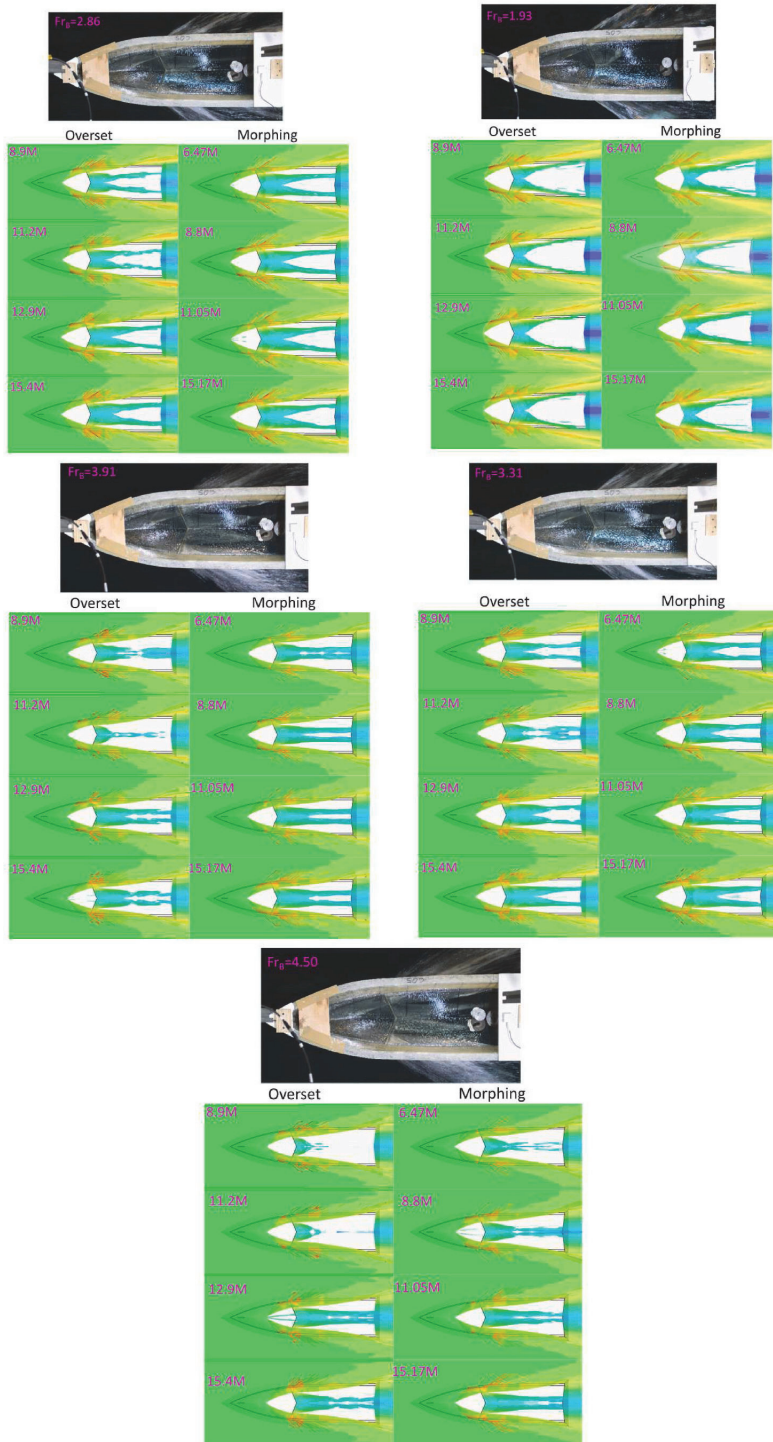
Fig. 17. Comparison of wetted surface and ventilation formation in CFD simulations of the C05 stepped hull using different cell numbers and techniques, compared to towing tank test results, at various Froude numbers.

Appendix E. Comparative Analysis of Running Attitudes and Resistance Prediction Errors Between Various CFD Mesh Techniques and Towing Tank Test Results for Interceptor Planing Hull, C1, at Various Froude Numbers

Table 23
Number of Cells for Verification Study of C1 interceptor planing Hull.

Overset		Morphing	
Grid no.	Cell count	Grid no.	Cell count
8.8M	8,817,154	6.2M	6,275,120
11.2M	11,225,477	8.1M	8,106,302
12.9M	12,902,835	10.6	10,645,546
14.9M	14,942,391	13.2	13,274,303

Table 24

Comparison of Errors between CFD and Towing Tank Test Results of C1 hull at Different Cell Numbers in Predicting trim angle.

v [m/s]	Fr_B	τ_{Exp} [deg]	τ_{CFD} [deg]								Morphing							
			Overset															
			8.8M	E%	11.2M	E%	12.9M	E%	14.9M	E_R%	6.2M	E%	8.1M	E_R%	10.6M	E_R%	13.2M	E_R%
2.5	0.88	1.660	1.600	3.61%	1.563	5.84%	1.568	5.54%	1.576	5.06%	1.525	8.13%	1.548	6.75%	1.500	9.64%	1.510	9.04%
3	1.06	2.057	2.013	2.14%	2.000	2.77%	2.000	2.77%	2.050	0.34%	1.997	2.92%	2.040	0.83%	1.990	3.26%	2.045	0.58%
3.5	1.24	1.847	1.861	−0.76%	1.850	−0.16%	1.850	−0.16%	1.895	−2.60%	1.835	0.65%	1.890	−2.33%	1.780	3.63%	1.892	−2.44%
4	1.41	1.440	1.334	7.36%	1.342	6.81%	1.328	7.78%	1.353	6.04%	1.372	4.72%	1.420	1.39%	1.330	7.64%	1.374	4.58%
4.5	1.6	0.853	0.839	1.64%	0.827	3.05%	0.869	−1.88%	0.862	−1.06%	0.878	−2.93%	0.920	−7.85%	0.871	−2.11%	0.880	−3.17%
5	1.77	0.406	0.391	3.69%	0.393	3.20%	0.387	4.68%	0.419	−3.20%	0.460	−13.30%	0.450	−10.84%	0.367	9.61%	0.443	−9.11%
5.5	1.94	−0.091	−0.106	−16.48%	−0.103	−13.19%	−0.087	4.40%	−0.089	2.20%	−0.106	−16.48%	−0.104	−14.29%	−0.102	−12.09%	−0.100	−9.89%

Table 25

Comparison of Errors between CFD and Towing Tank Test Results of C1 hull at Different Cell Numbers in Predicting resistance.

v [m/s]	Fr_B	$\frac{R_{Exp}}{\Delta}$	$\frac{R_{CFD}}{\Delta}$																
			Overset								Morphing								
			8.8M	E%	11.2M	E%	12.9M	E%	14.9M	E_R%	6.2M	E%	8.1M	E_R%	10.6M	E_R%	13.2M	E_R%
2.5	0.88	0.081	0.0846	−4.08%	0.0860	−5.76%	0.0834	−2.59%	0.0830	−2.12%	0.0803	1.19%	0.0807	0.70%	0.0807	0.70%	0.0797	1.97%
3	1.06	0.100	0.1029	−2.65%	0.1097	−9.42%	0.1011	−0.79%	0.1058	−5.47%	0.0964	3.85%	0.0970	3.26%	0.0974	2.89%	0.0978	2.43%
3.5	1.24	0.110	0.1239	−12.56%	0.1211	−10.10%	0.1192	−8.35%	0.1173	−6.60%	0.1052	4.39%	0.1060	3.67%	0.1045	5.04%	0.1068	2.94%
4	1.41	0.118	0.1165	1.47%	0.1267	−7.10%	0.1261	−6.66%	0.1260	−6.55%	0.1123	5.01%	0.1124	5.00%	0.1112	6.00%	0.1124	4.98%
4.5	1.6	0.132	0.1279	2.91%	0.1400	−6.27%	0.1394	−5.80%	0.1393	−5.74%	0.1231	6.57%	0.1231	6.54%	0.1226	6.95%	0.1231	6.56%
5	1.77	0.150	0.1444	4.05%	0.1492	0.85%	0.1494	0.72%	0.1480	1.66%	0.1380	8.28%	0.1378	8.47%	0.1373	8.77%	0.1377	8.48%
5.5	1.94	0.178	0.1656	7.02%	0.1663	6.66%	0.1633	8.34%	0.1647	7.54%	0.1590	10.76%	0.1670	6.27%	0.1680	5.69%	0.1690	5.12%

Table 26
Comparison of Errors between CFD and Towing Tank Test Results of C1 hull at Different Cell Numbers in Predicting sinkage.

v [m/s]	Fr_B	$\frac{(Z_G)_{Exp}}{\nabla^{1/3}}$	Overset								Morphing							
			8.8M	$E\%$	11.2M	$E\%$	12.9M	$E\%$	14.9M	$E_R\%$	6.2M	$E\%$	8.1M	$E_R\%$	10.6M	$E_R\%$	13.2M	$E_R\%$
2.5	0.88	−0.037	−0.03950	−6.05%	−0.04028	−8.15%	−0.03990	−7.13%	−0.03969	−6.56%	−0.03779	−1.46%	−0.03933	−5.60%	−0.04165	−11.84%	−0.04053	−8.83%
3	1.06	−0.022	−0.02113	2.71%	−0.02213	−1.86%	−0.02166	0.28%	−0.02033	6.40%	−0.02120	2.42%	−0.02115	2.61%	−0.02044	5.92%	−0.02295	−5.65%
3.5	1.24	0.001	0.00148	−15.13%	0.00141	−10.20%	0.00135	−5.26%	0.00133	−3.62%	0.00110	14.47%	0.00112	12.83%	0.00127	1.32%	0.00118	7.89%
4	1.41	0.018	0.01820	1.40%	0.01993	−7.98%	0.02014	−9.13%	0.02025	−9.70%	0.01904	−3.18%	0.01978	−7.18%	0.02044	−10.73%	0.01902	−3.07%
4.5	1.6	0.028	0.02840	−2.15%	0.03074	−10.58%	0.03061	−10.12%	0.03051	−9.74%	0.02951	−6.17%	0.02992	−7.62%	0.03040	−9.36%	0.02974	−6.98%
5	1.77	0.032	0.03604	−13.32%	0.03600	−13.18%	0.03380	−6.28%	0.03384	−6.41%	0.03519	−10.66%	0.03559	−11.92%	0.03505	−10.20%	0.03378	−6.21%
5.5	1.94	0.029	0.03287	−13.62%	0.03239	−11.95%	0.03177	−9.83%	0.03171	−9.61%	0.03315	−14.57%	0.03209	−10.92%	0.02918	−0.85%	0.03061	−5.82%

Table 27

Comparison of Errors between CFD and Towing Tank Test Results of C1 hull at Different Cell Numbers in Predicting wetted surface.

v [m/s]	Fr_B	$\frac{(S_W)_{Exp}}{\nabla^{2/3}}$	Overset								Morphing							
			$\frac{(S_W)_{CFD}}{\nabla^{2/3}}$															
			8.8M	$E\%$	11.2M	$E\%$	12.9M	$E\%$	14.9M	$E_R\%$	6.2M	$E\%$	8.1M	$E_R\%$	10.6M	$E_R\%$	13.2M	$E_R\%$
2.5	0.88	7.387	7.042	4.67%	7.220	2.25%	7.033	4.79%	7.167	2.98%	8.825	−19.47%	8.736	−18.26%	8.558	−15.85%	8.468	−14.64%
3	1.06	7.257	7.461	−2.81%	7.488	−3.18%	7.524	−3.67%	7.452	−2.69%	8.647	−19.15%	8.647	−19.15%	8.379	−15.46%	8.201	−13.01%
3.5	1.24	7.103	7.443	−4.78%	7.515	−5.79%	7.515	−5.79%	7.470	−5.16%	8.513	−19.84%	8.558	−20.47%	8.201	−15.45%	8.112	−14.20%
4	1.41	7.010	7.265	−3.63%	7.390	−5.41%	7.443	−6.18%	7.381	−5.29%	8.290	−18.26%	8.468	−20.80%	8.112	−15.71%	8.023	−14.44%
4.5	1.6	6.908	7.292	−5.55%	7.452	−7.87%	7.818	−13.16%	7.426	−7.48%	8.112	−17.42%	8.023	−16.13%	7.755	−12.26%	7.844	−13.55%
5	1.77	6.861	7.310	−6.53%	7.426	−8.22%	7.764	−13.16%	7.417	−8.09%	8.201	−19.53%	8.112	−18.23%	7.844	−14.33%	7.934	−15.63%
5.5	1.94	6.984	7.310	−4.66%	7.345	−5.17%	7.417	−6.19%	7.301	−4.53%	8.290	−18.70%	8.112	−16.14%	7.844	−12.32%	7.934	−13.59%

Appendix F. Grid uncertainty analysis for the trim value of C1 interceptor hull
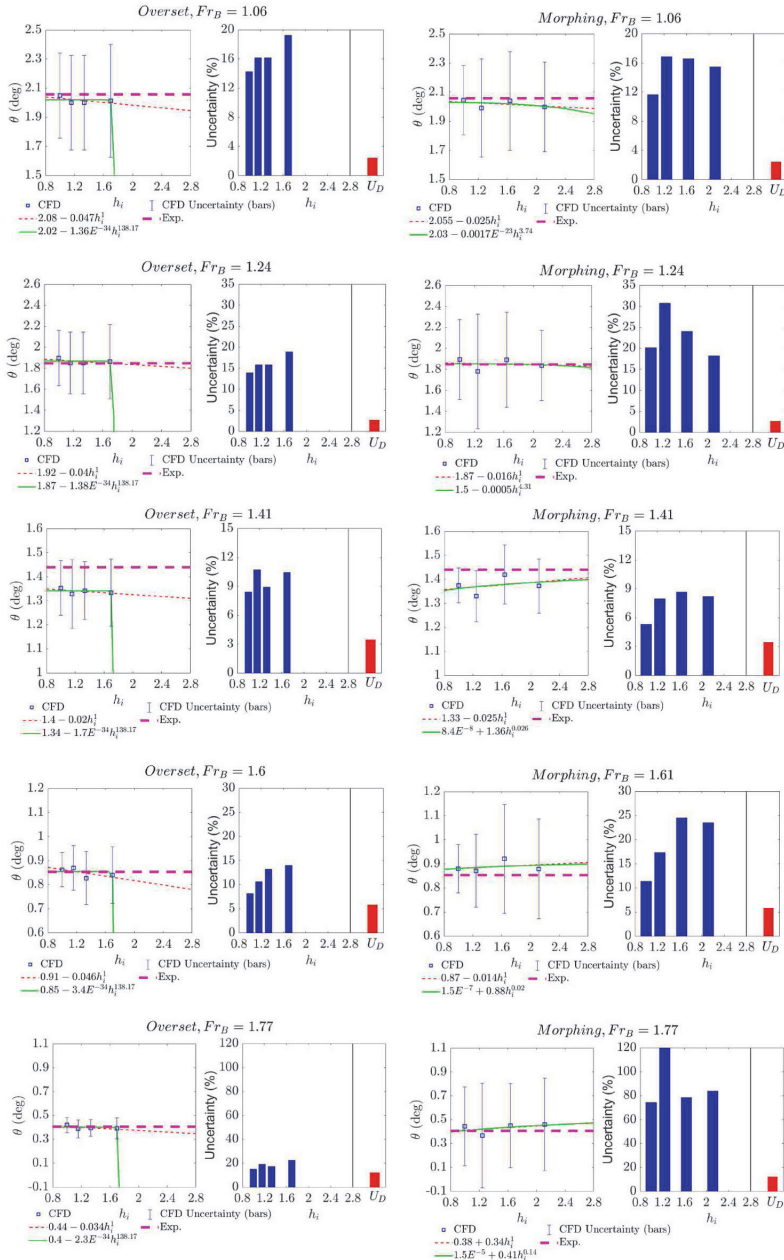
Fig. 18. Grid uncertainty analysis using the Least Squares Method for the trim value of C1 interceptor hull with overset and morphing mesh techniques, revealing the order of convergence and estimation of errors at Froude numbers 1.06, 1.24, 1.41, 1.6, and 1.77.

Appendix G. Grid uncertainty analysis for the resistance value of C1 interceptor hull
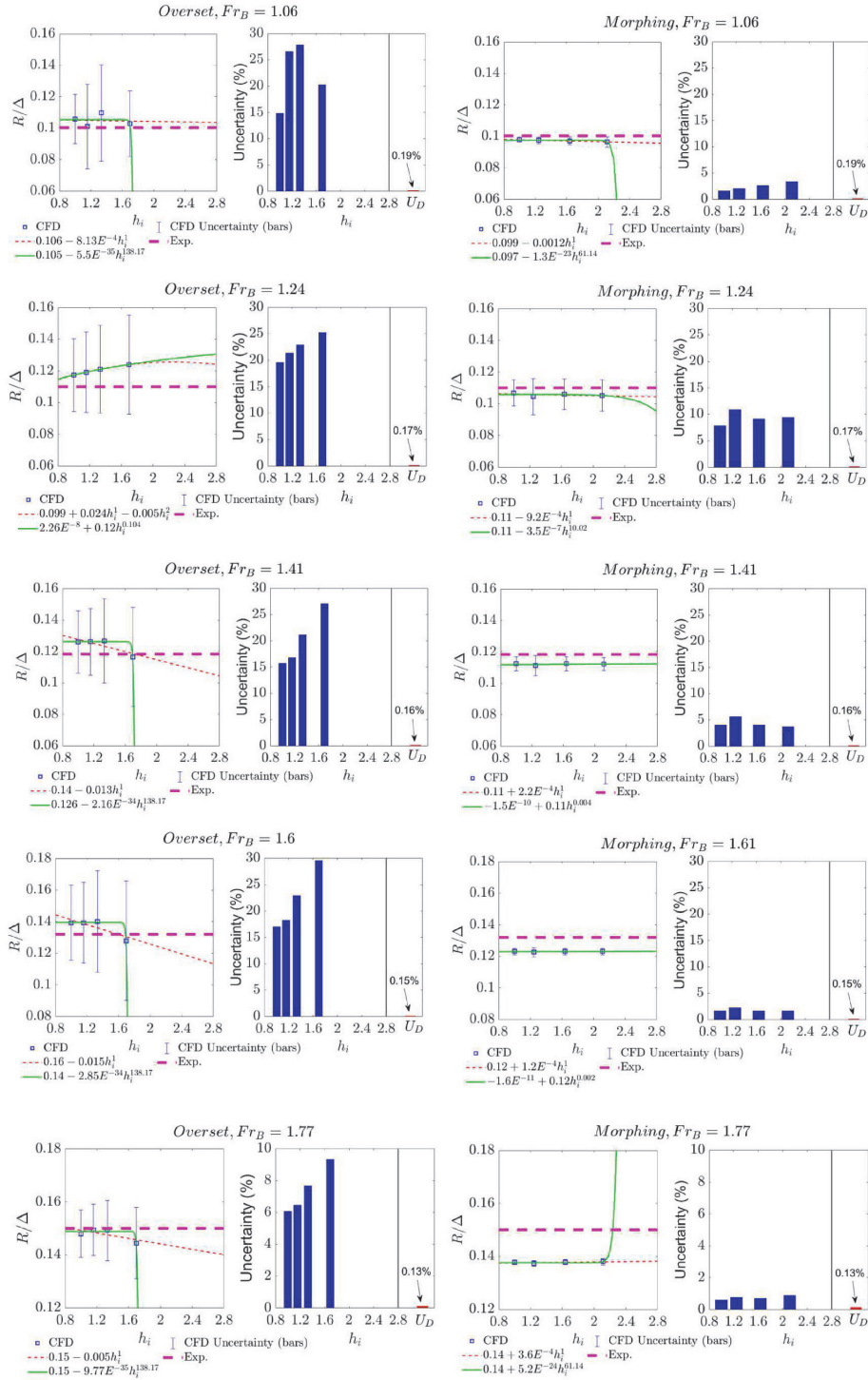
Fig. 19. Grid uncertainty analysis using the Least Squares Method for the resistance value of C1 interceptor hull with overset and morphing mesh techniques, revealing the order of convergence and estimation of errors at Froude numbers 1.06, 1.24, 1.41, 1.6, and 1.77.

Appendix H. Comparison of Spray and Wave Formation for C1 Interceptor Planing Hull Using Various CFD Mesh Techniques and Towing Tank Test Results at Different Froude Numbers

This appendix presents a comparison of spray formation around the C1 interceptor planing hull, at various Froude numbers, using CFD simulations and towing tank tests. Two mesh motion techniques, overset and morphing, are compared to evaluate their accuracy in capturing spray formation. The investigation includes the effect of cell numbers on the accuracy of spray formation prediction. The findings of this study can provide valuable insights into the suitability and limitations of CFD simulations and towing tank tests for studying the spray formation of interceptor planing hulls. The results can aid in the development of more accurate and efficient design methods for high-speed marine vessels.
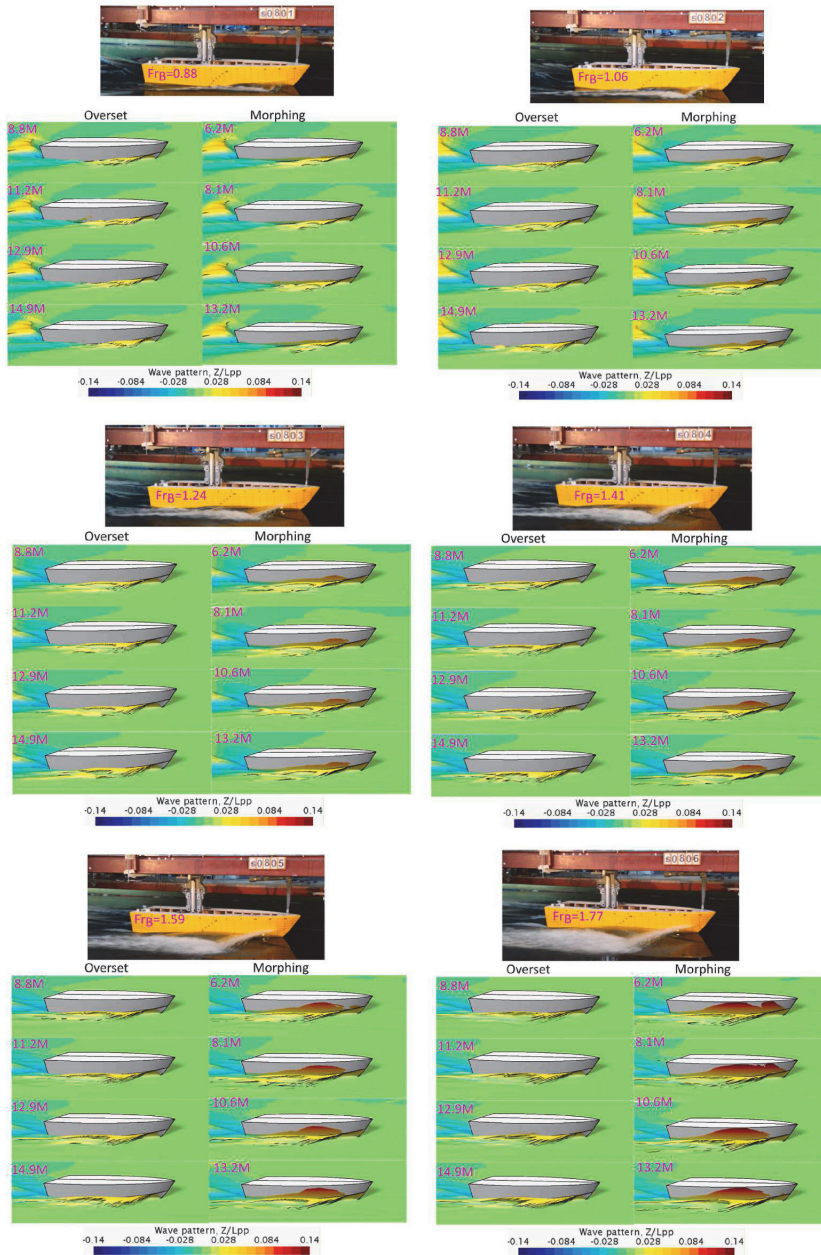
Fig. 20. Comparison of spray and wave formation around the C1 interceptor planing hull using different CFD mesh motion techniques and towing tank tests, with varying cell numbers at different Froude numbers.

References

Coleman, H.W., Stern, F., 1997. Uncertainties and CFD code validation. J. Fluid Eng. 119 (4), 795–803. https://doi.org/10.1115/1.2819500.

Dashtimanesh, A., Esfandiari, A., Mancini, S., 2018. Performance prediction of two-stepped planing hulls using morphing mesh approach. J. Ship Prod. Des. 34 (3), 236–248. https://doi.org/10.5957/JSPD.160046.

De Luca, F., Mancini, S., Manfredini, A., Pensa, C., Scognamiglio, R., 2015. Interceptor Device for a High-Speed Displacing Craft (Comparison between CFD Simulation and Experimental Data), pp. 906–915.

De Luca, F., Mancini, S., Miranda, S., Pensa, C., 2016. An extended verification and validation study of CFD simulations for planing hulls. J. Ship Res. 60 (2), 101–118. https://doi.org/10.5957/jsr.2016.60.2.101.

De Luca, F., Pensa, C., 2012. Experimental investigation on conventional and unconventional interceptors. Transactions of the Royal Institution of Naval Architects Part B: International Journal of Small Craft Technology 154, B65–B72. https://doi.org/10.3940/rina.ijsct.2012.b2.129.

De Luca, F., Pensa, C., 2017. The Naples warped hard chine hulls systematic series. Ocean Eng. 139, 205–236. https://doi.org/10.1016/j.oceaneng.2017.04.038.

De Marco, A., Mancini, S., Miranda, S., Scognamiglio, R., Vitiello, L., 2017. Experimental and numerical hydrodynamic analysis of a stepped planing hull. Appl. Ocean Res. 64, 135–154. https://doi.org/10.1016/j.apor.2017.02.004.

Di Caterino, F., Niazmand Bilandi, R., Mancini, S., Dashtimanesh, A., Carlini, M., 2018. A Numerical Way for a Stepped Planing Hull Design and Optimization. https://doi.org/10.3233/978-1-61499-870-9-220.

Eca, L., Vaz, G., Hoekstra, M., 2010. In: Code Verification, Solution Verification and Validation in RANS Solvers. https://doi.org/10.1115/OMAE2010-20338, 597–605.

Eca, L., Hoekstra, M., 2014. A procedure for the estimation of the numerical uncertainty of CFD calculations based on grid refinement studies. J. Comput. Phys. 262, 104–130. https://doi.org/10.1016/j.jcp.2014.01.006.

Ferziger, J.H., Perić, M., Street, R.L., 2019. Computational Methods for Fluid Dynamics. Springer.

Fu, T., Brucker, K., Mousaviraad, M., Ikeda-Gilbert, C., Lee, E.J., O'Shea, T.T., Wang, Z., Stern, F., Judge, C., 2014. An Assessment of Computational Fluid Dynamics Predictions of the Hydrodynamics of High-Speed Planing Craft in Calm Water and Waves.

Gray-Stephens, A., Tezdogan, T., Day, S., 2020. Numerical modelling of the nearfield longitudinal wake profiles of a high-speed planing hull. J. Mar. Sci. Eng. 8 (7) https://doi.org/10.3390/jmse8070516. Article 7.

Hosseini, A., Tavakoli, S., Dashtimanesh, A., Sahoo, P.K., Kõrgesaar, M., 2021. Performance prediction of a hard-chine planing hull by employing different CFD models. J. Mar. Sci. Eng. 9 (5) https://doi.org/10.3390/jmse9050481. Article 5.

ITTC 7.5-03-02-03, 2011. Recommended Procedures and Guidelines: Practical Guidelines for Ship CFD.

ITTC 75-03-01-01 Rev 04, 2021. Uncertainty Analysis in CFD Verification and Validation, Methodology and Procedures.

Jangam, S., 2021. Pressure distribution on planing hull bottom with stern interceptor. Appl. Ocean Res. 117, 102953 https://doi.org/10.1016/j.apor.2021.102953.

Jangam, S., 2022. CFD based prediction on hydrodynamic effects of Interceptor and flap combination on planing hull. Ocean Eng. 264, 112523 https://doi.org/10.1016/j.oceaneng.2022.112523.

Judge, C., Mousaviraad, M., Stern, F., Lee, E., Fullerton, A., Geiser, J., Schleicher, C., Merrill, C., Weil, C., Morin, J., Jiang, M., Ikeda, C., 2020. Experiments and CFD of a high-speed deep-V planing hull—Part I: calm water. Appl. Ocean Res. 96, 102060 https://doi.org/10.1016/j.apor.2020.102060.

Larsson, L., Stern, F., Visonneau, M. (Eds.), 2014. Numerical Ship Hydrodynamics: an Assessment of the Gothenburg 2010 Workshop. Springer Netherlands. https://doi.org/10.1007/978-94-007-7189-5.

Lee, E.J., Schleicher, C.C., Merrill, C.F., Fullerton, A.M., Geiser, J.S., Weil, C.R., Morin, J. R., Jiang, M.J., Stern, F., Mousaviraad, S.M., Judge, C.Q., 2017. Benchmark testing of generic prismatic planing hull (GPPH) for validation of CFD tools. In: SNAME 30th American Towing Tank Conference. https://doi.org/10.5957/ATTC-2017-0023.

Lee, E., Pavkov, M., McCue-Weil, L., 2014. The systematic variation of step configuration and displacement for a double-step planing craft. Journal of Ship Production and Design 30 (2), 89–97. https://doi.org/10.5957/jspd.2014.30.2.89.

Mansoori, M., Fernandes, A.C., 2017. Interceptor and trim tab combination to prevent interceptor's unfit effects. Ocean Eng. 134, 140–156. https://doi.org/10.1016/j.oceaneng.2017.02.024.

Morabito, M.G., 2010. On the Spray and Bottom Pressures of Planing Surfaces. Stevens Institute of Technology.

Niazmand Bilandi, R., Dashtimanesh, A., Mancini, S., Vitiello, L., 2023a. Comparative study of experimental and CFD results for stepped planing hulls. Ocean Eng. 280, 114887 https://doi.org/10.1016/j.oceaneng.2023.114887.

Niazmand Bilandi, R., Dashtimanesh, A., Tavakoli, S., 2020a. Hydrodynamic study of heeled double-stepped planing hulls using CFD and 2D+T method. Ocean Eng. 196, 106813 https://doi.org/10.1016/j.oceaneng.2019.106813.

Niazmand Bilandi, R., Dashtimanesh, A., Tavakoli, S., 2023b. Stepped Hulls Early Stage Design by Implementing 2D+T Method. IOS Press, pp. 23–32. https://doi.org/10.3233/PMST230005. *HSMV 2023*.

Niazmand Bilandi, R., Mancini, S., Dashtimanesh, A., Tavakoli, S., De Carlini, M., 2019. A Numerical and Analytical Way for Double-Stepped Planing Hull in Regular Wave, pp. 417–427. https://upcommons.upc.edu/handle/2117/330006.

Niazmand Bilandi, R., Tavakoli, S., Dashtimanesh, A., 2021. Seakeeping of double-stepped planing hulls. Ocean Eng. 236, 109475 https://doi.org/10.1016/j.oceaneng.2021.109475.

Niazmand Bilandi, R., Vitiello, L., Mancini, S., Nappo, V., Roshan, F., Tavakoli, S., Dashtimanesh, A., 2020b. Calm-water performance of a boat with two swept steps at high-speeds: laboratory measurements and mathematical modeling. Procedia Manuf. 42, 467–474. https://doi.org/10.1016/j.promfg.2020.02.046.

Nimmagadda, N.V.R., Polisetty, L.R., Vaidyanatha Iyer, A.S., 2020. Simulation of air–water interface effects for high-speed planing hull. J. Mar. Sci. Appl. 19 (3), 398–414. https://doi.org/10.1007/s11804-020-00172-0.

Park, S., Wang, Z., Stern, F., Husser, N., Brizzolara, S., Morabito, M., Lee, E., 2022. Single- and two-phase CFD V&V for high-speed stepped planing hulls. Ocean Eng. 261, 112047 https://doi.org/10.1016/j.oceaneng.2022.112047.

Reynolds, O., 1997. IV. On the dynamical theory of incompressible viscous fluids and the determination of the criterion. Phil. Trans. Roy. Soc. Lond. 186, 123–164. https://doi.org/10.1098/rsta.1895.0004.

Roache, P.J., 1998. Verification and Validation in Computational Science and Engineering. Hermosa Publishers, Albuquerque, New Mexico.

Roshan, F., Dashtimanesh, A., Bilandi, R.N., 2020. Hydrodynamic characteristics of tunneled planing hulls in calm water. Brodogradnja : Teorija i Praksa Brodogradnje i Pomorske Tehnike 71 (1), 19–38. https://doi.org/10.21278/brod71102.

Sahin, O.S., Kahramanoglu, E., Cakici, F., 2022. Numerical evaluation on the effects of interceptor layout and blade heights for a prismatic planing hull. Appl. Ocean Res. 127, 103302 https://doi.org/10.1016/j.apor.2022.103302.

Savitsky, D., 1964. Hydrodynamic design of planing hulls. Marine Technology and SNAME News 1 (4), 71–95. https://doi.org/10.5957/mt1.1964.1.4.71.

Savitsky, D., Morabito, M, 2011. Origin and characteristics of the spray patterns generated by planing hulls. Journal of Ship Production and Design 27 (2), 63–83. https://doi.org/10.5957/jspd.2011.27.2.63.

SIEMENS, P.L.M., 2022. STAR CCM+ User's Guide Version 17.02.007.

Stern, F., Wilson, R.V., Coleman, H.W., Paterson, E.G., 2001. Comprehensive approach to verification and validation of CFD simulations—Part 1: methodology and procedures. J. Fluid Eng. 123 (4), 793–802. https://doi.org/10.1115/1.1412235.

Su, Y., Chen, Q., Shen, H., Lu, W., 2012. Numerical simulation of a planing vessel at high speed. J. Mar. Sci. Appl. 11 (2), 178–183. https://doi.org/10.1007/s11804-012-1120-7.

Suneela, J., Krishnankutty, P., Subramanian, V.A., 2021. Hydrodynamic performance of planing craft with interceptor-flap hybrid combination. J. Ocean Eng. Mar. 7 (4), 421–438. https://doi.org/10.1007/s40722-021-00211-0.

Taunton, D.J., Hudson, D.A., Shenoi, R.A., 2010. Characteristics of a series of high speed hard chine planing hulls - part 1: performance in calm water. Int. J. Small Craft Technol. 152, 55–75. https://doi.org/10.3940/rina.ijsct.2010.b2.96.

Taunton, D.J., Hudson, D.A., Shenoi, R.A., 2011. Characteristics of a series of high speed hard chine planing hulls - part II: performance in waves. Int. J. Small Craft Technol. 153 https://doi.org/10.3940/rina.ijsct.2011.b1.97. B1–B22.

Tavakoli, S., Niazmand Bilandi, R., Mancini, S., De Luca, F., Dashtimanesh, A., 2020. Dynamic of a planing hull in regular waves: comparison of experimental, numerical and mathematical methods. Ocean Eng. 217, 107959 https://doi.org/10.1016/j.oceaneng.2020.107959.

Tezdogan, T., Demirel, Y.K., Kellett, P., Khorasanchi, M., Incecik, A., Turan, O., 2015. Full-scale unsteady RANS CFD simulations of ship behaviour and performance in head seas due to slow steaming. Ocean Eng. 97, 186–206. https://doi.org/10.1016/j.oceaneng.2015.01.011.

Vitiello, L., Mancini, S., Niazmand Bilandi, R., Dashtimanesh, A., De Luca, F., Nappo, V., 2022. A comprehensive stepped planing hull systematic series: Part 1 - resistance test. Ocean Eng. 266, 112242 https://doi.org/10.1016/j.oceaneng.2022.112242.

Vitiello, L., Mancini, S., Niazmand Bilandi, R., Nappo, V., 2020. In: An Overview of Stepped Hull Performance Evaluation: Sea Trial Data vs Full-Scale CFD Simulation https://doi.org/10.3233/PMST200026.

Wang, H., Zhu, R., Huang, S., Zha, L., Gu, M., 2023. A study on hydrodynamic characteristics of a planing hull by CFD simulation and modified M-S method. Ships Offshore Struct. 18 (2), 157–174. https://doi.org/10.1080/17445302.2022.2032995.

Wilson, R., Shao, J., Stern, F., 2004. Discussion: criticisms of the "correction factor" verification method 1. J. Fluid Eng. 126 (4), 704–706. https://doi.org/10.1115/1.1780171.

Appendix 5 (Publication V)

[P5] Niazmand Bilandi, R., Tavakoli, S., Mancini, S., Dashtimanesh, A. (2024). Dynamic Motion Analysis of Stepless and Stepped Planing Hulls in Random Waves: A CFD Model Perspective. Applied Ocean Research 149:104046. doi: 10.1016/j.apor.2024.104046

Research paper

Dynamic motion analysis of stepless and stepped planing hulls in random waves: A CFD model perspective

Rasul Niazmand Bilandi [a,*], Sasan Tavakoli [b,c], Simone Mancini [d], Abbas Dashtimanesh [e]

[a] *Estonian Maritime Academy, Tallinn University of Technology, 11712, Tallinn, Estonia*
[b] *Department of Infrastructure Engineering, The University of Melbourne, Parkville, 3052, VIC, Australia*
[c] *Marine and Arctic Technology Group, Department of Mechanical Engineering, Aalto University, Espoo, 02150, Finland*
[d] *Department of Industrial Engineering, University of Napoli" Federico II", 80125, Napoli, Italy*
[e] *Engineering Mechanics Department, School of Engineering Science, KTH Royal Institute of Technology, 100 44 Stockholm, Sweden*

ARTICLE INFO

ABSTRACT

Predicting the dynamic responses of planing hulls in real sea conditions is important for identifying how basic design factors influence their seakeeping performance. Hence, there is a pressing need to provide high-fidelity models for predicting the motions of these hulls in random waves, representing actual seas. In this article, a computational-based model for solving viscous fluid flow around the vessel is built to address this problem. Three different planing hulls, denoted as C, C1, and C2, each distinguished by the number of steps incorporated on their bottom surfaces (1 and 2 indicating the respective step count, with case C being the stepless hull), are modeled in a Computational Fluid Dynamics (CFD) tank, allowing for analysis of the effects of steps on dynamic responses of a planing surface operating in random waves. CFD data is compared against those collected in towing tank tests, revealing a satisfactory level of accuracy. Extreme value and gamma distributions are shown to give probabilities of maxima/minima of displacements and vertical acceleration at the center of gravity (CG) for all three hulls. It is shown that the stepless boat may be exposed to lower vertical acceleration at an early planing speed, but at higher planing speeds, a double-stepped design mitigates the vertical acceleration. Nevertheless, the double-stepped hull would experience more significant extreme heave responses across all speeds and may be exposed to less significant extreme pitch responses during the ride at the highest speed compared to the stepless and one-stepped hulls. The skewness of heave and pitch is evaluated, and it is found that the heave response tends to skew toward positive values (upward). This skewness becomes more noticeable with increasing speed but remains insensitive to wave steepness. Additionally, the pitch response at lower planing speeds shows a partial skew towards negative values (bow-down), but eventually, they may also be partially skewed towards positive values at higher speeds. Moreover, a correlation is observed between the kurtosis of responses of different hulls and the occurrence of the 1/100 highest responses, indicating that a kurtosis greater than 3.0 would result in more extreme responses. Overall, this analysis offers practical insights into planing hull behavior in actual sea conditions from a CFD model perspective, highlighting the potential of CFD in simulating this complex problem.

1. Introduction

Planing hulls represent an interesting innovation in naval architecture, identified by their ability to lift and glide on the water surface. This allows them to reach relatively high speeds in calm water conditions. These hulls have extensive applications across a wide range of maritime activities, spanning from high-speed recreational boats to search and rescue missions (Savitsky, 1985). The hydrodynamic performance of planing hulls while navigating through waves is important (Camilleri et al., 2018; Rosén and Garme, 2004). Operating a planing hull under actual sea conditions at high speeds results in large motions, such as vertical acceleration, which directly affects the vessel's seaworthiness level, stability, crew safety, and the structural fatigue life of the craft (Rosén et al., 2017). Furthermore, the interaction between a planing hull and irregular waves introduces nonlinear rigid body motions, particularly within the planing regime (Begovic et al., 2014b). This nonlinearity becomes increasingly strong as the operational speed increases, posing

* Corresponding author.
E-mail address: rasul.niazmand@taltech.ee (R.N. Bilandi).

Nomenclature

A	Rigid body boundary.
B	Maximum Beam of the boat (m).
$\mathbf{F} = [F_x, F_y, F_z]$	Fluid force acting on the vessel (N). Different components refer to the surge, sway and heave forces.
$Fr_B = u/(gB)^{-1}$	Beam Froude Number (-).
$\mathbf{f_b}$	Body force (N).
g	Gravity acceleration (m/s^2).
H_s	Significant wave height (m).
H_{s1}	Forward step height (m).
H_{s2}	Aft step height (m).
$\overline{H}$	Average wave height.
I	Mass moment of inertia (Kg-m^2).
k	Wave number (m^{-1}).
K	Kurtosis.
k_{yy}	Pitch radius of gyration (m).
κ	Wave steepness.
L_{CG}	The longitudinal position of the centre of gravity (CG) for transom (m).
LOA	Length Overall.
L_{s1}	Forward step position with respect to CG (m).
L_{s2}	Aft step position with respect to CG (m).
Δ	Mass of the boat (Kg).
m_n	nth order spectral moment.
$\mathbf{n}$	Normal unite vector.
p	Fluid pressure (N/m^2).
r	Ratio of negative values among the maxima values divided by the total number of maxima values. Similarly, for the minima values, represents the ratio of positive values among the minima values divided by the total number of minima values.
$\boldsymbol{r}_0$	Position vector from a reference point.
$\boldsymbol{r}_G$	Position vector of the center of gravity
S	Skewness.
t	Time (s).
T_{in}	Wave period (s).
T_p	Peak wave period (s).
$\overline{T}$	Mean wave height.
u	Boat speed (m/s).
$\boldsymbol{U} = [v_x, v_y, v_z]$	Velocity field in the fluid domain (m/s).

$Z, \dot{Z}, \ddot{Z}$	Heave displacement (m), speed (m/s), and acceleration (m/s^2).
Z_{Hmean}	Mean of highest height of heave (m).
$Z_{H1/n}$	Mean of 1/n highest height of heave (m).
$\ddot{Z}_{Hmean}$	Mean of highest height of CG acceleration (m/s^2).
$\ddot{Z}_{H1/n}$	Mean of 1/n highest height of CG acceleration (m/s^2).
η	Water surface elevation (m).
$\theta, \dot{\theta}, \ddot{\theta}$	Pitch angle (rad), velocity (rad/s), and acceleration (rad/s^2).
θ_{Hmean}	Mean of highest height of pitch angle (rad).
$\theta_{H1/n}$	Mean of 1/n highest height of pitch angle (rad).
μ	Dynamic viscosity (Kg/m-s).
μ_a	Air viscosity (Kg/m-s).
μ_{eff}	Viscosity of the mixture of water (μ_a) and air (μ_a) at any point in the domain (Kg/m-s).
μ_t	Turbulent viscosity of the flow (Kg/m-s).
μ_w	Water viscosity (Kg/m-s).
ρ_{eff}	Density of the mixture of water (ρ_w) and air (ρ_a) at any point in the domain (Kg/m^3).
ρ_a	Density of the air (Kg/m^3).
ρ	Density of the water (Kg/m^3).
$\boldsymbol{\varphi}$	Normal stress tensor.
Ψ	Volume fraction of the water-air flow (-).
ω	Wave angular frequency (rad/s).
ω_p	Peak wave angular frequency (rad/s).

Abbreviation

CFD	Computation Fluid Dynamics
CICSAM	Compressive Interface Capturing Scheme for Arbitrary Mesh
CG	Center of Gravity
EPF	Exceedance Probability Function
Exp	Experimental data
FFT	Fast Fourier Transform
FVM	Finite Volume Method
HRIC	High-Resolution Interface Capturing
ITTC	International Towing Tank Conference
PDF	Probability Density Functions
RANS	Reynolds Average Navier-Stokes
RMS	Root-Mean-Square
SIMPLE	Semi-Implicit Method for Pressure-Linked Equations

substantial challenges for both designers and operators. Therefore, a deep analysis of these motions can provide a valuable understanding of operational limits, structural risks and possible solutions (Taunton et al., 2011). To gain a comprehensive understanding of this phenomenon, a combination of methodologies, such as towing tank tests, Computational Fluid Dynamics (CFD), and mathematical modeling have been used.

The most reliable approach used for analysing the motions of any vessel operating in waves is laboratory tank testing. Waves are mechanically generated by wave makers in a tank/basin and the vessel is towed in the tank at a constant speed. This allows for sampling the temporal motions of the vessel and may provide valuable seakeeping data, that can be used on both small and actual scales. However, the availability of experimental data on the seakeeping performance of high-speed planing hulls is limited. The physical testing of unsteady planing motion in waves has been done since the 1950s, but the first set of systematic tests was done by Fridsma in the late 1960s and early 1970s. In specific, Fridsma's work in 1971 (Fridsma, 1971) marked the initiation of experimental investigations into the dynamic behavior of prismatic planing boats in irregular waves. Through systematic model tests, Fridsma explored the influence of various parameters, such as hull

design factors, dynamic trim, load, length over beam ratio, bow form, speed and wave conditions, on the seakeeping performance of prismatic planing hulls (Fridsma, 1971). Fridsma showed that planing boats exhibit non-linear behavior throughout the majority of their operational range, signifying that the use of response amplitude operators can be ineffective over some frequencies. Consequently, he advocated for the adoption of statistical methods to study the dependence of motion and acceleration responses of prismatic planing hulls towed in irregular waves. Throughout his analyses, Fridsma employed an exponential probability distribution function for vertical accelerations and showed that either a Generalized Rayleigh or Cartwright and Longuet-Higgins distribution can represent the statistical behaviour of heave and pitch displacements.

Since Fridsma's pioneering work in 1971, there have been notable systematic research papers highlighting planing hull seakeeping. However, there have also been some significant contributions emerged over the years. For instance, In 1981, Zarnick and Turner (1981) extended Fridsma's experiments by conducting tests on prismatic hulls with high length-to-beam (L/B) ratios of 7 and 9 in irregular waves. In addition, Klosinski & Brown (1993) investigated the influence of both the length

over beam ratio (L/B) and the longitudinal center of gravity (LCG) position on seakeeping performance. Meanwhile, Keuning & Pinkster (1995) introduced the concept of an "enlarged ship concept" (ESC), to enhance the seakeeping characteristics of planing craft.

Subsequently, a series of systematic studies conducted by Soletic (2010), Taunton et al. (2011), Begovic et al. (2014a, 2016), and De Luca & Pensa (2019) have made significant contributions to the understanding of the physics of planing hull seakeeping. Taunton et al. (2011) introduced a systematic series involving four monohedral planing hulls tested in irregular head seas at various speeds. This comprehensive study aimed to explore the impact of parameters such as $(L/\Delta)^{1/3}$, transverse steps, radius of gyration, wave height, and peak wave period on the motions of the vessel operating in random waves (irregular waves). They conducted statistical analyses of motions' maxima (crests of the recorded time histories of displacement) and minima (troughs the recorded time histories of displacement), as well as accelerations at the center of gravity and the bow. The findings favored the use of the Gamma distribution for analyzing vertical accelerations statistically and confirmed the suitability of the Cartwright probability density function for analyzing heave and pitch motions. In another set of experimental tests, Begovic et al. (2014a, 2016) conducted experimental tests on monohedral and warped hull motions in irregular head sea waves. Their research included descriptions of heave and pitch maxima and minima, along with the utilization of three different probability density functions (PDFs). These datasets were fitted with various statistical functions, including Normal, CLH, extreme value, Exponential, Gamma, and Weibull, for analyzing motion responses. They reported that sea state and deadrise angle had a greater influence on vertical acceleration compared to speed. More recently, De Luca & Pensa (2019) investigated the dynamic behavior of the Naples Systematic Series (NSS) in irregular head seas. Their study employed statistical approaches, including Cartwright Lounguet Higgins, extreme value, and normal distribution fittings for heave and pitch maxima and minima, as well as gamma and extreme value distributions for acceleration at the center of gravity and the bow. This stream of studies covered a wide range of hull designs, statistical analyses, and wave conditions, providing valuable insights into motion responses, acceleration characteristics, and probability density functions. These studies collectively contribute to our understanding of unsteady planing. But they are mostly limited to stepless planing hulls.

At the outset of the design process, researchers often seek streamlined approaches due to the potential cost and time constraints associated with planing hull tests. These complexities arise from the need to build a scale model and procure specialized infrastructure for motion measurement and mechanical wave generation in a tank/basin. Furthermore, is worth mentioning that the model scale for seakeeping tests is different from the model scale for resistance/self-propulsion tests.

A significant breakthrough in the pursuit of accurate planing hull simulations in rough sea conditions came from the research carried out by Zarnick in 1979 (Zarnick, 1979). Zarnick pioneered the development of a nonlinear mathematical model to describe the vertical motion of planing hulls in regular waves using the 2D+t method. Expanding upon this work, Zarnick extended the mathematical model to accommodate irregular waves. Zarnick's contributions set a valuable precedent, prompting many researchers to adopt his method, resulting in improved accuracy in predicting planing hull motions. Notable examples include the works of Akers (1999), Blake & Wilson (2001), Garme (2005), Garme & Rosén (2003), Hicks et al. (1995), Keuning (1994), Payne (1994), Sebastiani et al. (2009), Troesch & Hicks (1994), and van Deyzen (2008).

Furthermore, Tavakoli et al. (2015) extended the 2D+t method to

model roll motion, while Tavakoli & Dashtimanesh (2019), Tavakoli & Dashtimanesh (2017), and Algarín & Bula (2021) applied it to the maneuvering of planing hulls in six-degrees of freedom. Additionally, Niazmand Bilandi et al. (2020a; 2019, , 2023a; 2020b) extended this method to various designs of planing vessels, including stepped boats.

Despite the flexibility and promising accuracy of the 2D+t method, as well as its usefulness for parametric studies (Di Caterino et al., 2018), it has limitations in monitoring all fluid phenomena around the hull advancing in planing mode. This may limit its range of application especially when the fluid motion becomes turbulent, and the water surface exhibits strong non-linear behavior (such as wave breaking). As a result, Computational Fluid Dynamics (CFD), solving RANS (Reynolds-Averaged Navier Stokes Equations) has emerged as a reliable hydrodynamic tool for modeling planing problems (Niazmand Bilandi et al., 2024). CFD has been instrumental in performance prediction of planing hulls (Dashtimanesh et al., 2018; De Marco et al., 2017; Judge et al., 2020b; Niazmand Bilandi et al., 2023b; Putra and Suzuki, 2024; Roshan et al., 2020), motion prediction of planing hulls in regular waves (Capasso et al., 2023; Esfandiari et al., 2020; Jin et al., 2023; Niazmand Bilandi et al., 2021; Tavakoli et al., 2020), and the measurement of slamming pressures (C. Judge et al., 2020a; Lee et al., 2024; Mousaviraad et al., 2015).

However, it is important to note that research focusing on dynamic motion simulations of planing hulls in irregular waves using CFD codes is still relatively scarce and our understanding of the statistical behaviour of planing hull advancing in irregular wave is very limited. On top of that, the effects of step on this statistical behaviour are not well addressed. The only set of tests covering the dynamic motions of stepped planing hulls in waves was performed by Taunton et al. in 2011, who only reported the maximum and minimum heave/pitch movements of stepless, stepped, and double-stepped hulls (statistical analysis was performed only on vertical acceleration). This leaves us with several questions: 1) how the time history of motions differs between stepless and stepped planing hulls, 2) which statistical indicators (such as kurtosis or skewness) can affect the extreme response of stepless and stepped planing hulls, and 3) how different the spectral density of stepless and stepped planing hulls can be. The answers to these questions can be found by reproducing the motions of stepless and stepped planing hulls using a CFD code. Currently, the development of a well-calibrated and accurate numerical simulation setup is challenging but yet crucial. In particular, setting up models for random wave conditions is invaluable but currently absent. With advances in CFD simulations, obtaining data for highly accurate predictions in a wider range of wave conditions has become possible. These datasets are invaluable for characterizing the nonlinear dynamics of planing hulls, often aided by machine learning algorithms to predict vessel motions without the need for expensive models (e.g. in Marlantes and Maki, 2022, 2021).

Therefore, in this paper, the aim is to present a CFD model that can be used for simulating dynamic motions of stepless and stepped planing hulls in random waves. Furthermore, the simulation data are utilized to provide a thorough understanding of statistical behaviour of stepless and stepped planing hulls through analyzing the highest values, analyzing the exceedance probability of motions, and finding the link between the behaviour of exceedance probabilities and statistical indexes including skewness and kurtosis of the motions. Our hypothesis is that skewness and kurtosis of the motions of stepless and stepped hull can permit understanding of the extreme responses of these boats, and also, they would inform us about the time history of motions (skewness of each motion would let us know how skewed the motion is during each cycle and kurtosis would provide us with a general understanding of peakedness). Moreover, the aim is also to provide an understanding of

spectra of heave, pitch, and accelerations of stepless and stepped planing hulls and these have not been fully addressed in the literature so far, as stated before.

To reach the mentioned scope, a commercial CFD code is employed to model the dynamic behavior of a planing hull in irregular waves. The C model family, designed by Taunton et al. (2011) is chosen for this study due to the availability of experimental data for this model in irregular waves and investigations into the effects of one/two steps on its seakeeping performance. This allows us to compare the dynamic motions of stepless boats against those of single-stepped and double-stepped boats, which is lacking in the literature. There is an open question about the effects of adding steps on the seakeeping performance of a planing craft. In parallel, this research aims to build a CFD model that solves the dynamic motion of planing hulls in random waves, and then analyze the effects of adding steps on the performance of the vessel, which is also missing in the literature. In a broader sense, the CFD itself will benefit the naval architecture community as it provides a better understanding of how the motions of any vessel exposed to random waves can be modelled in a CFD tank.

The rest of the present paper is organized as follows. Section 2 introduces the hull planing models that are studied in the present research. Section 3 briefly introduces the fluid assumptions and governing equations, and then details the numerical scheme used to replicate the motions of the hulls in a numerical tank. Section 4 investigates the comparative analysis between Computational Fluid Dynamics (CFD) data and results obtained from towing tank tests, employing a local Maxima/Minima approach to identify peaks and troughs in time series. Section 5 presents the statistical analysis of heave, pitch, and CG acceleration under varying operational conditions, dissecting a range of statistical indicators. Additionally, it explores the probability distributions of heave, pitch motions, and center of gravity (CG) acceleration, examining their conformity to specific distribution functions. Furthermore, Section 6 investigates skewness and kurtosis in these motions to provide a better understanding of the response of planing hulls in random waves. Moreover, Section 7 focuses on the Exceedance Probability Functions (EPF) for wave profiles, heave, pitch, and CG acceleration, providing insights into extreme event occurrences. Finally, Section 8 investigates a detailed analysis of the spectral characteristics of heave, pitch, and CG acceleration. Concluding remarks are presented in Section 9.

2. Hull models details

There is a notable scarcity of systematic experimental data documenting the seakeeping performance and motions of high-speed planing hulls in water waves, especially with regard to stepped hulls, as explained in the literature review. Consequently, the use of CFD codes simulating and investigating planing hull motions in waves remains limited. As mentioned in the Introduction section, one of the aims of the present research is to bridge this gap by establishing a CFD setup to replicate the motion of planing hulls in random wave conditions. This may help in evaluating the wave-induced motions of a planing surface over a wide range of frequencies. It also allows statistical analysis of the motion of planing hulls, which is still very limited in our understanding.

To carry out this research, a hard-chine hull, named "C," has been selected. This hull was previously subjected to testing in GKN Westland Aerospace No.3 Test Tank by Taunton et al. (2011). The choice of hull "C" is based on the wide range of calm and rough water testing it has undergone within the planing regime.

When a single step is added to the bottom surface, the hull is properly termed "C1" (1 refers to single-step design). This step is positioned 31%

Table 1
Principal characteristics of models (C, C1, and C2).

Parameter	C
LOA (m)	2
B (m)	0.46
β (°)	22.5
$\Delta/\rho g B^3$	0.026
k_{yy}	0.16LOA
LCG (%L, forward transom)	32.9
L_{s1} (%L, forward transom) (for C1 and C2)	31
L_{s2} (%L, forward transom) (only for C2)	18.5
H_{s1} (%B) (for C1 and C2)	2.17
H_{s2} (%B) (only for C2)	2.17
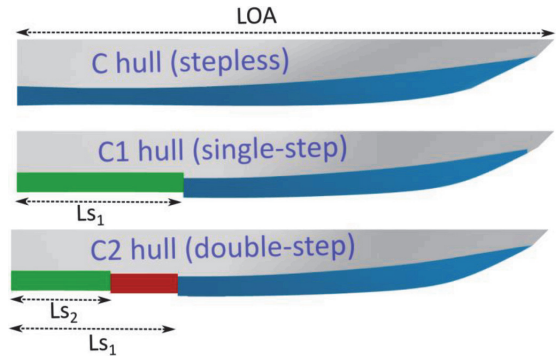
Fig. 1. Geometry of hull models.

L forward of the transom and has a height equal to 2.17 % B, which is a typical step height in stepped planing hull design. A second step, identical in height to the first, is introduced between the initial step and the transom of the C1 hull, 18.5% L forward the transom. This hull is named "C2" (2 refers to double-step design). Table 1 outlines a detailed summary of the particulars of these three modes, and Fig. 1 shows the body profiles of these three hulls.

The models underwent testing in irregular head waves at beam Froude numbers of 2.94, 4.71, and 5.67 (Here beam Froude Number is defined as $Fr_B = \frac{u}{\sqrt{gB}}$, where u is the operation speed, g is gravity acceleration and B is the beam). For the experimental tests, the wave spectra chosen were derived from metocean data obtained from wave buoy measurements conducted in the vicinity of the Isle of Wight, U.K., over a one-year period spanning from March 2006 to March 2007. For additional information regarding the experimental tests, readers are referred to the paper by Taunton et al. (2011). One notable concern regarding the experimental results is the relatively short duration of the experiments for all hulls, along with the absence of specified result uncertainties.

3. Numerical model

In this study, motions of planing hulls in random wave conditions are simulated using the commercial CFD software SIEMENS PLM STAR-CCM+, version 17.02.007. The simulation employs an implicit Unsteady Reynolds-Averaged Navier-Stokes (URANS) solver to model the hydrodynamics of a planing hull (Reynolds, 1895). This involves solving the three-dimensional RANS equations with a Realizable k-epsilon

turbulence model, ensuring the conservation of mass and momentum for incompressible turbulent flow. The continuity and momentum conservation equations are defined as follows (Ferziger et al., 2019):

$$\nabla.\boldsymbol{U} = 0, \tag{1}$$

$$\partial(\rho\boldsymbol{U})\Big/\partial t + \nabla.(\rho\boldsymbol{U}\boldsymbol{U}) - \nabla.\left(\mu_{eff}\nabla\boldsymbol{U}\right) = -\nabla p + \mathbf{f_b} + \nabla\boldsymbol{U}.\nabla\mu_{eff}. \tag{2}$$

Where, $\boldsymbol{U}$ is the fluid velocity vector, p is the fluid pressure, $\mathbf{f_B} = (0, 0, -g)$ is the body force, ρ is density, and μ_{eff} show the viscosity of the mixture of water and air at any point in the domain, that is defined:

$$\mu_{eff} = \mu + \mu_t, \tag{3}$$

here, μ represents dynamic viscosity, and μ_t signifies the turbulent viscosity, the latter of which depends on the chosen turbulence model. The k-ε turbulence model is employed to simulate turbulent flow within the domain. The turbulent viscosity equation for the $k - \varepsilon$ turbulence model is defined as follows:

$$\mu_t = C_\mu \frac{k^2}{\varepsilon}, \tag{4}$$

where C_μ is constant that is equal to 0.09, k is the turbulent kinetic energy, and ε is the turbulent dissipation rate. The equations for turbulent kinetic energy (k) and its dissipation rate (ε) in the $k - \varepsilon$ turbulence model are as follows:

$$\partial(\rho k)\Big/\partial t + \nabla.(\rho \boldsymbol{U} k) = \nabla.\left(\underbrace{\left(\mu + \frac{\mu_t}{\sigma_k}\right)\nabla k}_{\mu_{eff}}\right) + P_k - \rho\varepsilon, \tag{5}$$

$$\partial(\rho\varepsilon)\Big/\partial t + \nabla.(\rho \boldsymbol{U}\varepsilon) = \nabla.\left(\underbrace{\left(\mu + \frac{\mu_t}{\sigma_\varepsilon}\right)\nabla\varepsilon}_{\mu_{eff}}\right) + C_{\varepsilon 1}\frac{\varepsilon}{k}P_k - C_{\varepsilon 2}\rho\frac{\varepsilon^2}{k}. \tag{6}$$

The empirical constants $C_{\varepsilon 1}$, and $C_{\varepsilon 2}$ are utilized to model the production and dissipation of turbulent kinetic energy, and are assigned values of 1.44 and 1.92, respectively. Similarly, σ_k, and σ_ε represent the turbulent Prandtl numbers for k and ε, respectively, with typical values around 1.0.

The simulation of the air-water flow employs the Volume of Fluid (VOF) technique (Hirt and Nichols, 1981). This method utilizes a volume fraction parameter, denoted as Ψ, to determine the effective properties of the mixture. Ψ ranges from 0 to 1, representing pure air and pure water, respectively. The effective density and viscosity of the mixture are calculated as a combination of the properties of air and water, determined by

$$\rho_{eff} = \Psi.\rho_w + (1 - \Psi).\rho_a, \tag{7}$$

$$\mu_{eff} = \Psi.\mu_w + (1 - \Psi).\mu_a, \tag{8}$$

where, the subscript w signifies the parameters associated with water, while Ψ corresponds to those linked with air. The governing equation governing the volume fraction parameter is represented as follows:

$$\partial(\Psi)/\partial t + \nabla . (\Psi\boldsymbol{U}) = 0. \tag{9}$$

The solver used in this study utilizes the Finite Volume Method (FVM) to discretize the integral form of the Navier-Stokes equations for numerical analysis of incompressible viscous flows. For temporal

Table 2
Solver settings.

Item	
solver	Implicit unsteady
Implicit scheme	SIMPLE
Convection term	2nd order
VOF scheme	HRIC
Turbulence model	Realizable $k - \varepsilon$
Temporal Discretization	2nd order
Iteration per time step	10
Mesh motion	Overset
Overset Interpolation scheme	Distance-weighted interpolation
Wall treatment	All $y+$ wall treat
Water density	1000 kg/m^3
Water viscosity	0.000934 Pa-s

discretization of the transient terms, a second-order implicit backward Euler scheme was employed. Spatial discretization involved using a second-order upwind scheme for convection terms and a second-order centered scheme for diffusive terms. To couple pressure and velocity, the SIMPLE (Semi-Implicit Method for Pressure-Linked Equations) algorithm was adopted.

The time step for simulations is determined using the one suggested in ITTC 7.5–03–02–03 (2021), which recommends a time step of at least 100-time steps per period for the shortest waves. The DFBI approach is employed in the Siemens PLM Star-CCM+ solver to solve the forces and moments acting on the stepped planing hull in two degrees of freedom (pitch and heave). The motion equations can be solved by employing rigid body equations over time. The forces acting on the planing body are then computed accordingly:

$$\boldsymbol{F} = \iint_A (p + \boldsymbol{\varphi}).\boldsymbol{n}dA, \tag{10}$$

$$\boldsymbol{M} = \iint_A (p + \boldsymbol{\varphi}).\boldsymbol{n} \times (\boldsymbol{r}_0 - \boldsymbol{r}_G) \ dA, \tag{11}$$

where φ is the normal stress tensor, A represents the total area of the boat, and $\mathbf{n}$ is the unit normal vector. Some details of the numerical methods and solvers are provided in Table 2, with additional information available in the Siemens PLM STAR-CCM+ User's Guide, version 17.02.007 (SIEMENS PLM, 2022).

The overset setup approach is used to integrate the rigid body motions of the hull into the fluid domain. The overset domain has a dimension of $2.5L \times 3.0\text{B} \times 6.0\text{T}$. This has been done by introducing an overset region surrounding the hull, which is placed in the background region. Distance-weighted interpolation is utilized as the method for the integration of fluid motion in this sub-domain into the background domain. This approach is particularly advantageous due to its robustness, especially in scenarios involving significant relative motions (SIEMENS PLM, 2022). While the linear interpolation scheme suggested by De Luca et al. (2016) may provide benefits in certain contexts, such as pseudo-transient resistance computations, the distance-weighted technique is deemed more appropriate for simulating unsteady motions like seakeeping and maneuvering. The overset boundaries are dynamic and rigidly move with the hull, while other boundaries remain static. This approach allows for the simulation of complex hull geometries and motions. This method is mostly favored when the motions of the vessel are relatively high.

Fig. 2 provides a comprehensive overview of the different boundaries employed in the simulations and the mesh used for overset mesh motion. The mesh study results are presented in Appendix A. Moreover, the
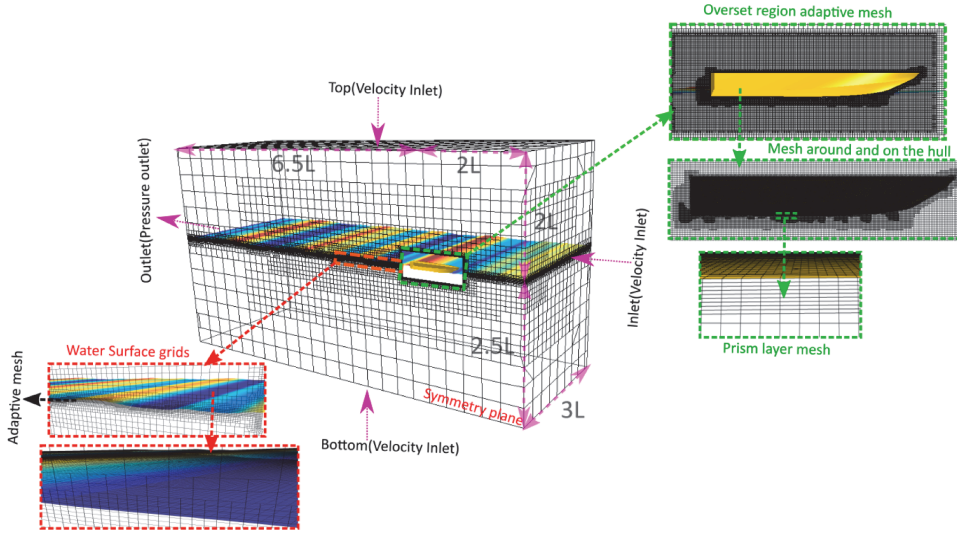
Fig. 2. The computational domain, including imposed boundary conditions and the grid, for simulating a planing hull using an overset grid.

Table 3
The boundary conditions.

	No-slip (wall)	Symmetry	Velocity inlet	Pressure outlet
Velocity	$v_x = v_y = v_z = 0$	$\boldsymbol{U} = 0$	$\boldsymbol{U} = v_x$	$\frac{\partial \boldsymbol{U}}{\partial \boldsymbol{n}} = 0$
Pressure	$\frac{\partial p}{\partial \boldsymbol{n}} = 0$	$\frac{\partial p}{\partial \boldsymbol{n}} = 0$	$\frac{\partial p}{\partial \boldsymbol{n}} = 0$	$p = 0$
Volume fraction	$\frac{\partial \Psi}{\partial \boldsymbol{n}} = 0$	$\frac{\partial \Psi}{\partial \boldsymbol{n}} = 0$	$\Psi = 1$, for water; $\frac{\partial \Psi}{\partial \boldsymbol{n}} = 0$, for air	$\Psi = 1$, for water; $\frac{\partial \Psi}{\partial \boldsymbol{n}} = 0$, for air
Turbulent kinetic energy (k)	$k = 0$	$k = 0$	$k = $ constant	$k = $ constant
dissipation rate (ε)	$\varepsilon = 0$	$\varepsilon = 0$	$\varepsilon = $ constant	$\varepsilon = $ constant

initial location of the free surface is determined based on the draft obtained from the hydrostatic analysis to ensure the accurate capture and simulation of the free surface in the numerical model. In the context of this study, the boundary conditions were established as follows: In the background region, the inlet, top, bottom, and side boundaries were designated as the velocity inlet, and the outlet was configured as a pressure outlet. Additionally, the middle longitudinal section was specified as a symmetry plane. Within the overset region, the mid-ship section retained its role as a symmetry plane, while the surrounding planes were assigned as overset mesh boundaries. Lastly, a non-slip wall boundary condition is set for the vessel's surface. These boundary conditions were set to support the computational simulations and analyses conducted in this research. A summary of boundaries is shown in Table 3.

The simulations were conducted utilizing the High-Performance Computing (HPC) cluster available at Tallinn University of Technology. The HPC cluster featured nodes equipped with 40 cores and a memory capacity of 80 GB. Each simulation run, representative of the planing hull dynamics in random waves, required an average of 25 days

to complete the simulation for 40 s of physical time.

3.1. Wave-generating method

In this study, the interface between air and water is accurately simulated using the Volume of Fluid (VOF) approach to replicate random incident waves. The implementation includes a High-Resolution Interface Capturing (HRIC) scheme based on the Compressive Interface Capturing Scheme for Arbitrary Mesh (CICSAM). This technique permits precise tracking of the air-water surface by monitoring volume fractions within individual cells. Both fluids are treated as incompressible Newtonian fluids, ensuring an accurate representation of the free surface dynamics. The software's forcing capability was employed at the upstream and downstream boundaries as well as the side wall boundaries to cancel out undesired wave reflections. For generating irregular waves in the numerical tank, a unidirectional version of the JONSWAP spectrum is used. This spectrum, derived from observations made in the North Sea and described by Hasselmann et al. (1973), was used to represent the irregular waves in the analysis. The JONSWAP spectrum applied in this study is given by

$$S(\omega) = A_\gamma \frac{5}{16} \left(\frac{H_s^2 \omega_p^4}{\omega^5}\right) \exp\left[-\frac{5}{4}\left(\frac{\omega}{\omega_p}\right)^{-4}\right] \gamma^{\exp\left[-(\omega-\omega_p)^2/(2\sigma^2\omega_p^2)\right]}, \quad (12)$$

where $A_\gamma = 1 - 0.287\ln(\gamma)$, is the normalizing factor, $\gamma = 3.3$, is the peak enhancement factor referring to the non-dimensional peak-enhancement factor, ω is the wave frequency, ω_p is the peak wave frequency, H_s is the significant wave height, and σ represents the spectral width parameter and can be expressed as follows:

$$\sigma = \begin{cases} 0.07 & (\omega_p \geq \omega) \\ 0.09 & (\omega_p < \omega) \end{cases}. \quad (13)$$

The values of the parameters used in the input wave spectrum for each hull are summarized in Table 4, providing a detailed reference for the wave characteristics under consideration.

Table 4

Details of seakeeping model simulation in irregular waves (Taunton et al., 2011).

Configuration	Model	u (m/s)	Fr_B	Hs (m)	T_P (s)	k (m^{-1})	$\kappa = kHs/2$
case 12	C	6.25	2.94	0.092	2.57	0.609	0.028
case 13	C	10.1	4.71	0.092	2.57	0.609	0.028
case 14	C	12.05	5.67	0.092	2.57	0.609	0.028
case 15	C	12.05	5.67	0.092	1.72	1.360	0.063
case 16	C	12.05	5.67	0.046	2.57	0.609	0.014
case 17	C	12.05	5.67	0.138	2.57	0.609	0.042
case 19	C	6.25	2.94	0.092	1.72	1.360	0.063
case 27	C1	6.25	2.94	0.092	2.57	0.609	0.028
case 28	C1	10.1	4.71	0.092	2.57	0.609	0.028
case 29	C1	12.05	5.67	0.092	2.57	0.609	0.028
case 30	C2	6.25	2.94	0.092	2.57	0.609	0.028
case 31	C2	10.1	4.71	0.092	2.57	0.609	0.028
case 32	C2	12.05	5.67	0.092	2.57	0.609	0.028
case 33	C2	12.05	5.67	0.092	1.72	1.360	0.063

Fig. 3. (a) Time history of wave elevation for irregular head sea conditions at recorded by the numerical wave probe. (b) Comparison of wave spectra among a static probe in the towing tank, the theoretical JONSWAP spectrum, and the CFD results for sea state T_P=2.57s, H_s=0.09 m.

Table 5

Comparison of wave characteristics between theoretical JONSWAP, experimental, and current CFD.

	Theoretical	CFD	Error CFD with theoretical	Exp.
H_S (m)	0.092	0.086	6.5 %	0.109
$\overline{H}$ (m)	0.0575	0.054	6 %	0.0687
$\overline{T}$(s)	2.15	2.075	3.5 %	2.21

It is important to ensure that a sufficiently large number of waves are encountered during computations to accurately calculate statistical characteristics in irregular seas. In this simulation, the background domain (without hull) was generated using the same grid configuration employed in seakeeping simulations of hulls. Within the simulation, a wave probe, positioned 1.30 L forward of the hull, recorded wave elevations to monitor the formation of irregular waves generated by the numerical wave maker. Fig. 3-a displays the time history of wave elevations as observed by the probe. Using the Fast Fourier Transform (FFT), the wave spectrum of the water surface elevation recorded at this probe is found, which is shown in Fig. 3-b. The spectrum found through CFD simulations is compared against those measured in the tank tests and the theoretical JONSWAP spectrum. The results correspond to a peak period of T_P=2.57 s and a significant wave height of Hs=0.09 m (this corresponds to a wave steepness of 0.028). With the wave spectrum determined, various statistical wave parameters can be calculated using spectral moments, which can be expressed as follows:

$$m_n = \int_0^\infty \omega^n S(\omega) d\omega. \tag{14}$$

As a result, specific wave characteristics, calculated using spectral moments, are listed in Table 4, along with a comparison between the
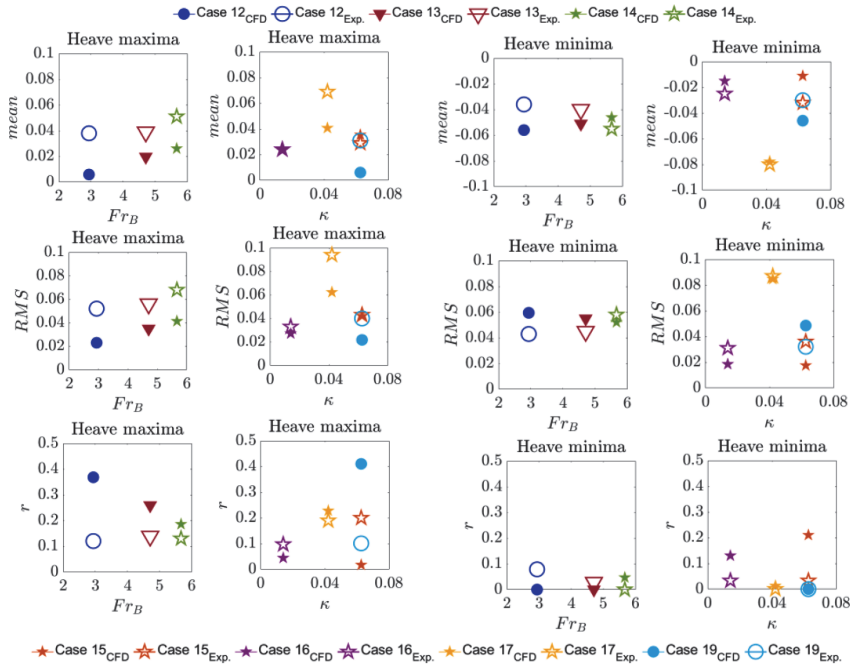
Fig. 4. A comparison between experimental (unfilled) and CFD (filled) distribution parameters of heave motion extremes (Maxima and Minima) for C hull under various operating conditions. Here heave is in meters.
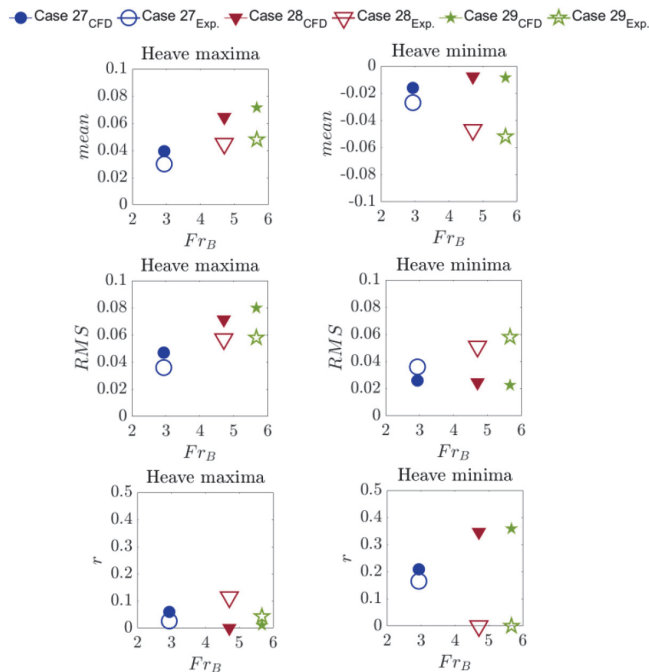
Fig. 5. A comparison between experimental (unfilled) and CFD (filled) distribution parameters of heave motion extremes (Maxima and Minima) for C1 hull under various operating conditions. Here heave is in meters.
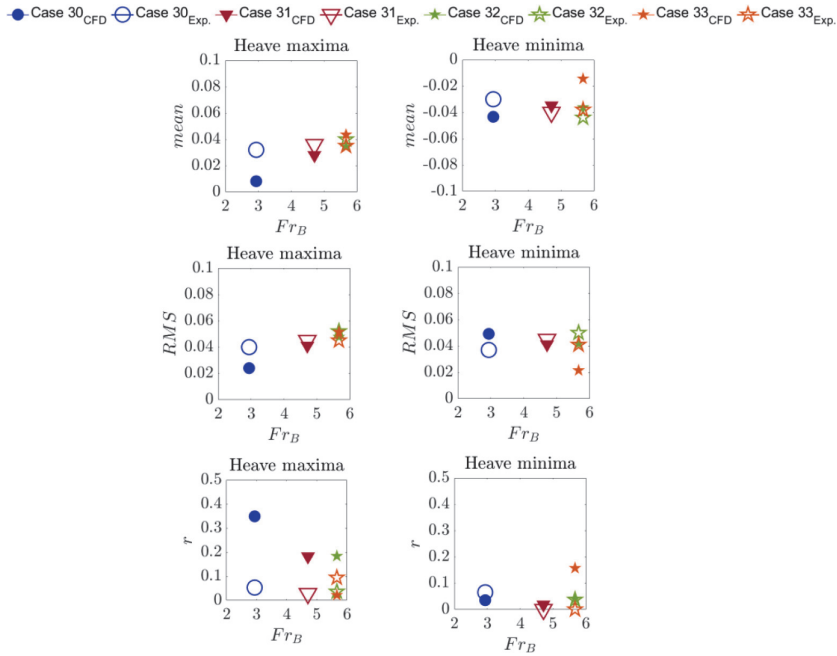
Fig. 6. A comparison between experimental (unfilled) and CFD (filled) distribution parameters of heave motion extremes (Maxima and Minima) for C2 hull under various operating conditions. Here heave is in meters.
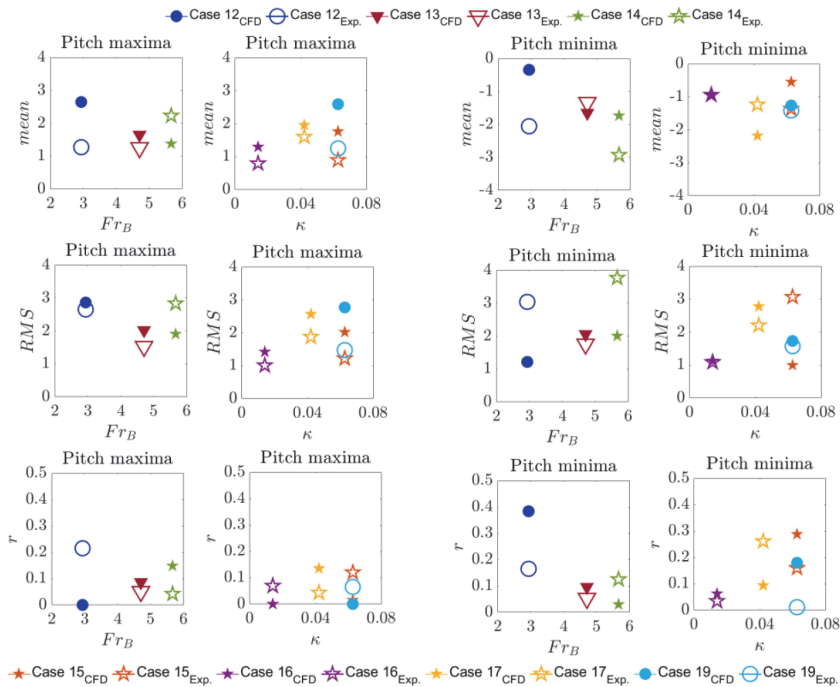
Fig. 7. A Comparison between experimental (unfilled) and CFD (filled) distribution parameters of pitch motion extremes (Maxima and Minima) for C hull under various operating conditions. Here pitch is in degrees.
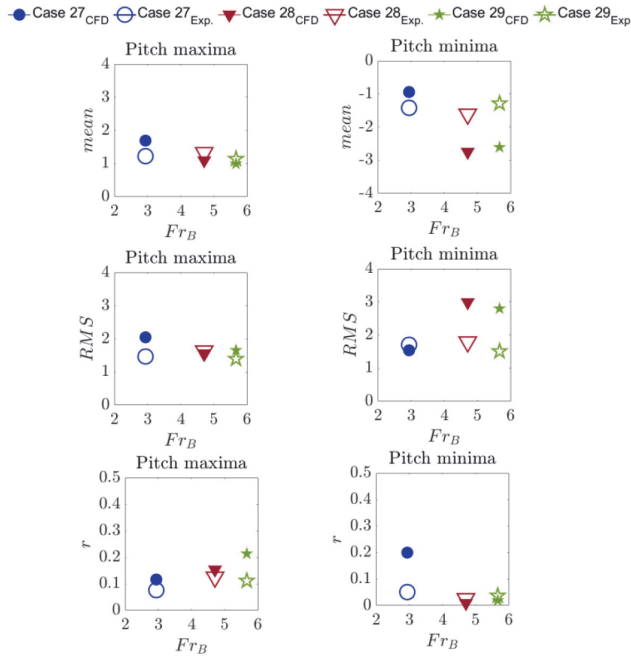
Fig. 8. A Comparison between experimental (unfilled) and CFD (filled) distribution parameters of pitch motion extremes (Maxima and Minima) for C1 hull under various operating conditions. Here pitch is in degrees.
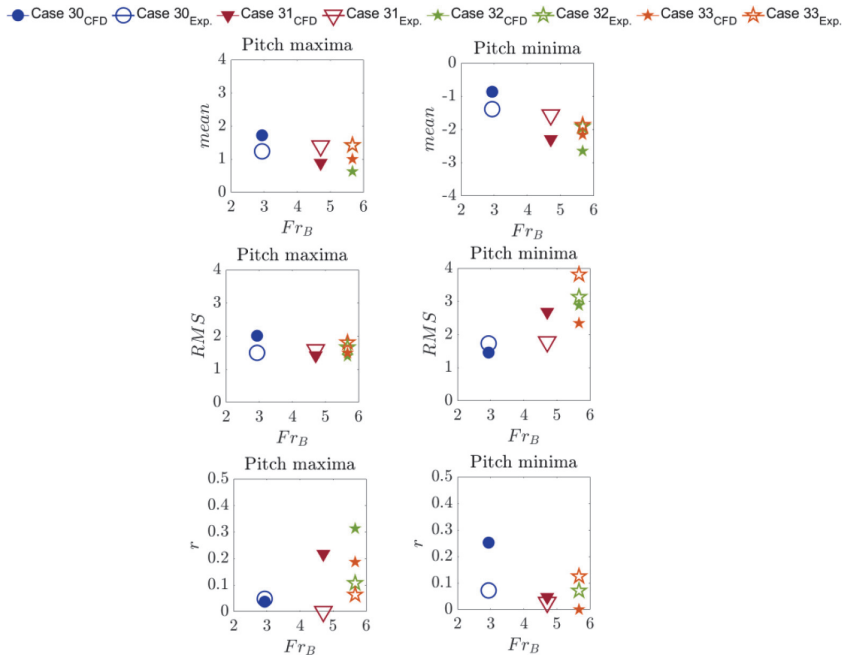
Fig. 9. A Comparison between experimental (unfilled) and CFD (filled) distribution parameters of pitch motion extremes (Maxima and Minima) for C2 hull under various operating conditions. Here pitch is in degrees.
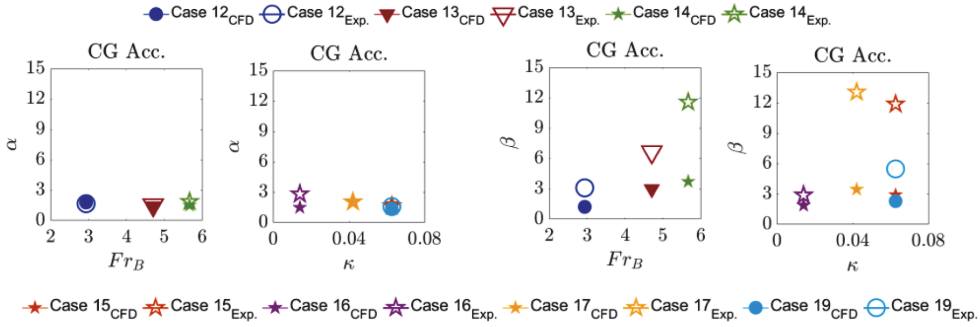
Fig. 10. A Comparison between experimental (unfilled) and CFD (filled) Gama distribution parameters of minima CG acceleration for C hull under various operating conditions.
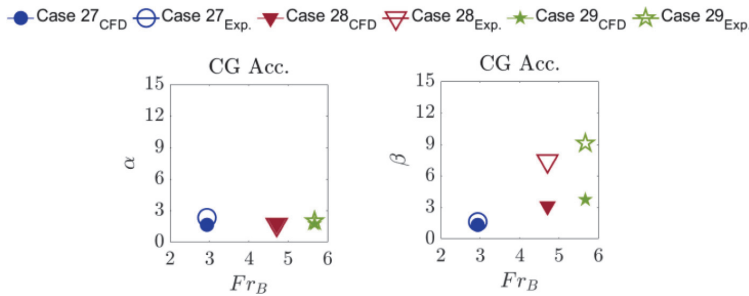
Fig. 11. Comparison between experimental (unfilled) and CFD (filled) Gama distribution parameters of minima CG acceleration for C1 hull under various operating conditions.
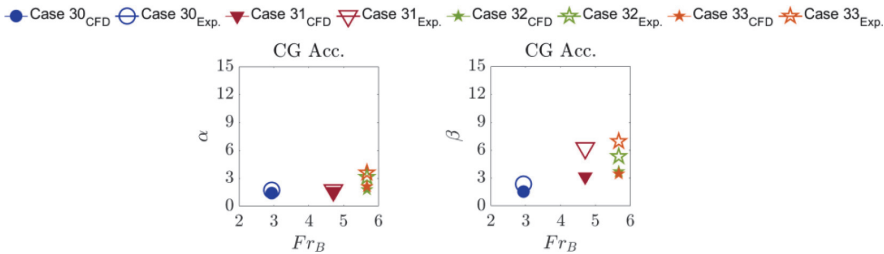
Fig. 12. Comparison between experimental (unfilled) and CFD (filled) Gama distribution parameters of minima CG acceleration for C2 hull under various operating conditions.

theoretical JONSWAP spectrum, experimental data, and the current CFD model (It is noteworthy that the experimental data points were extracted from the plot of Taunton et al. (2011), albeit we did not have access to actual values). In the Table 5, $Hs = 4\sqrt{m_0}$, is significant wave height, $\overline{H} = 2.5\sqrt{m_0}$, represents average wave height, and $\overline{T} = 2\pi m_0/m_1$, denotes mean wave period.

The observed differences between the wave spectra from CFD simulations and the JONSWAP spectrum, particularly at lower frequencies, are notable. While the spectra found through simulations and those found in the measurement align well over higher frequencies, indicating satisfactory capture of relevant components for high-speed planing hull

behavior, there is a discrepancy in the low-frequency range. This peak may be attributed to potential artificial effects in the computational setup, such as the simulation of air-water flow to achieve a specific speed. However, its impact on motion spectra of heave, pitch, and acceleration, seems negligible (See Section 8, Figs. 29-31). Thus, concerns about its influence on hull behavior are minimal. Nonetheless, addressing this discrepancy remains a priority for future studies (focusing on identifying and implementing potential solutions to mitigate the observed local peak in the wave spectrum) and is out of the scope of present research.
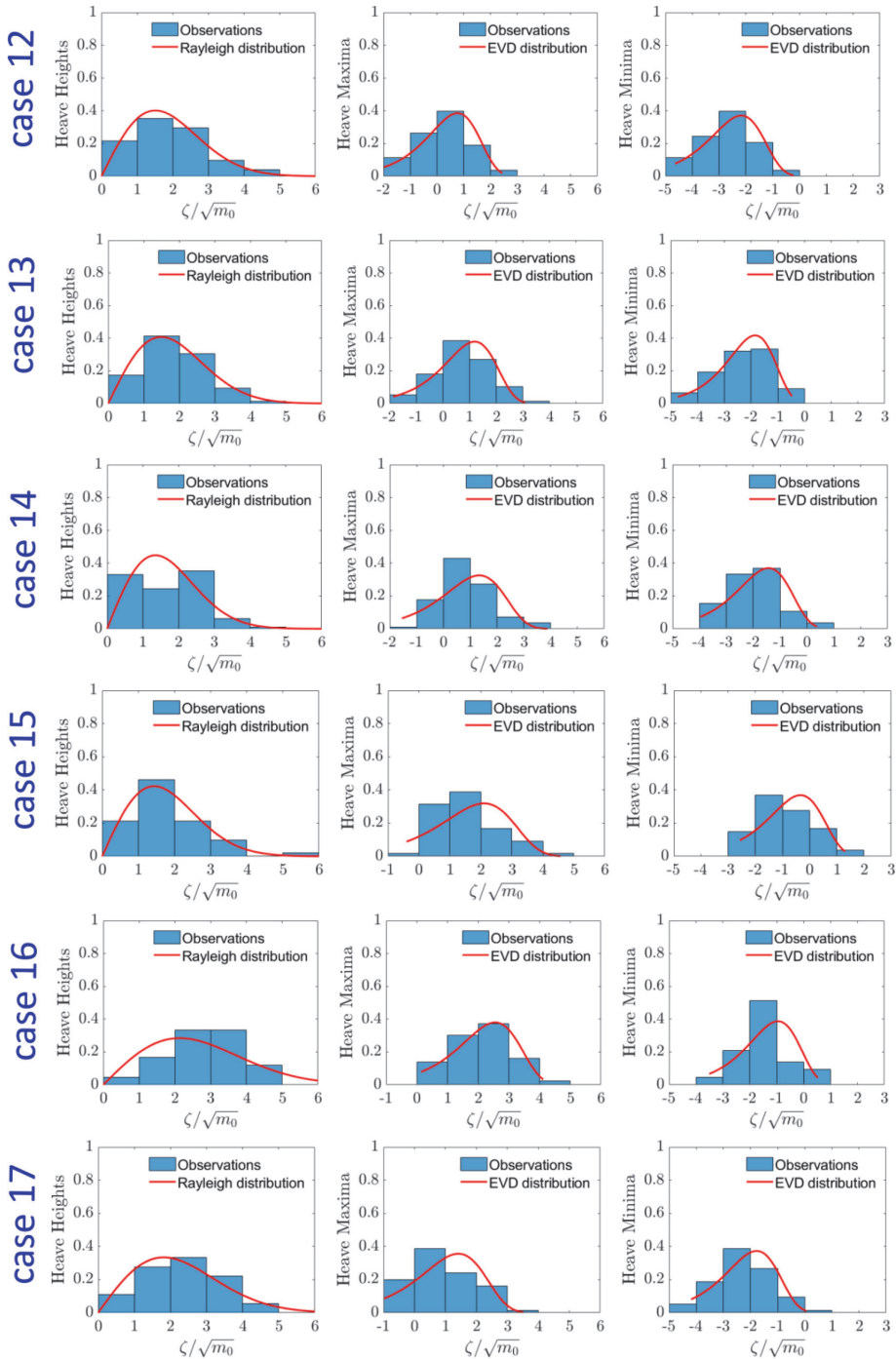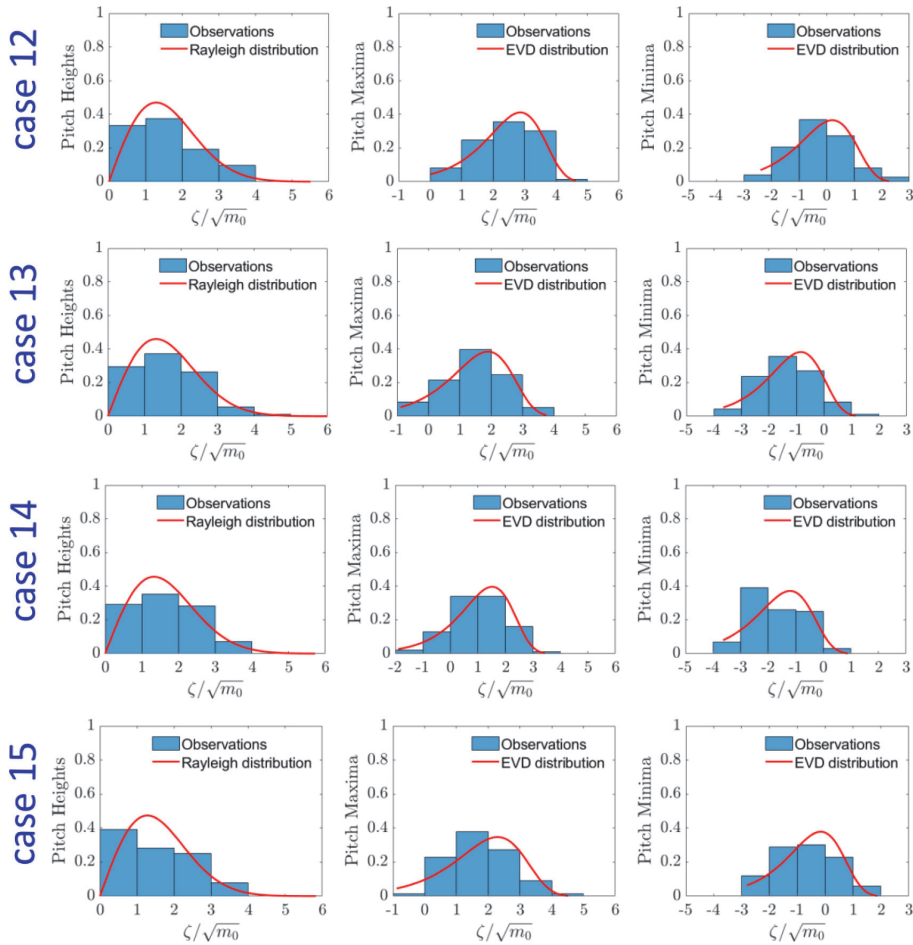
Fig. 13. Statistics of normalized heights, maxima, and minima for heave motions of the three hulls at different cases: a) C, b) C1, and c) C2.
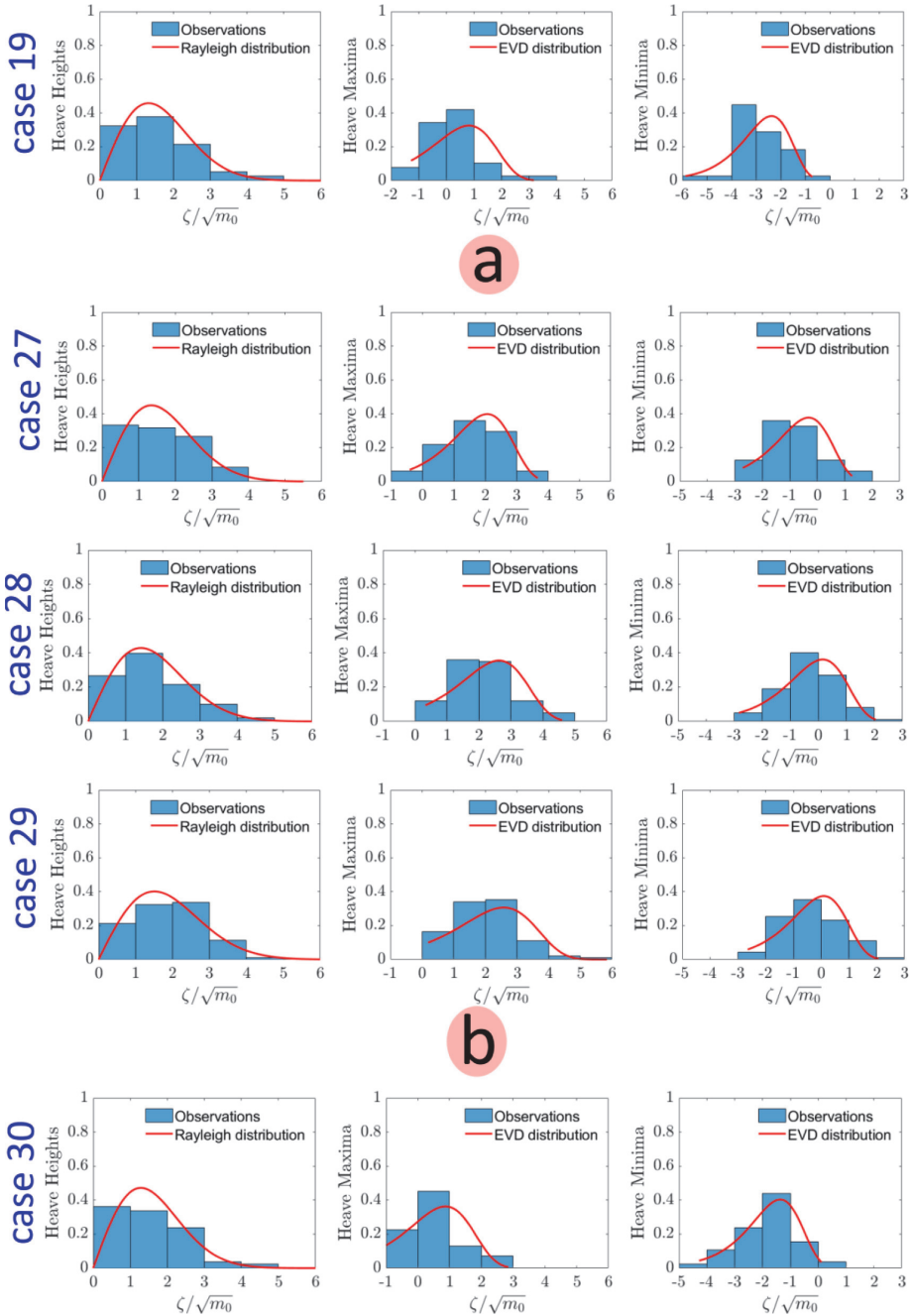
Fig. 13. (*continued*).

4. Analyzing discrepancies: computational fluid dynamics vs experimental results

As a first step, the CFD data is compared against those recorded in towing tank tests (Taunton et al., 2011). Time histories of heave, pitch, and CG vertical acceleration for the C (case 13), C1 (case 28), and C2

(case 31) hulls, along with cross-sections of the wetted surface and hull pressure at various times, are displayed in Appendix B. This study employs a local Maxima/Minima approach to identify peaks and troughs of the time series. In this method, peaks and troughs are recognized as local maxima or minima within a specified neighbourhood. The data is then scanned, and the highest or lowest values within the window are
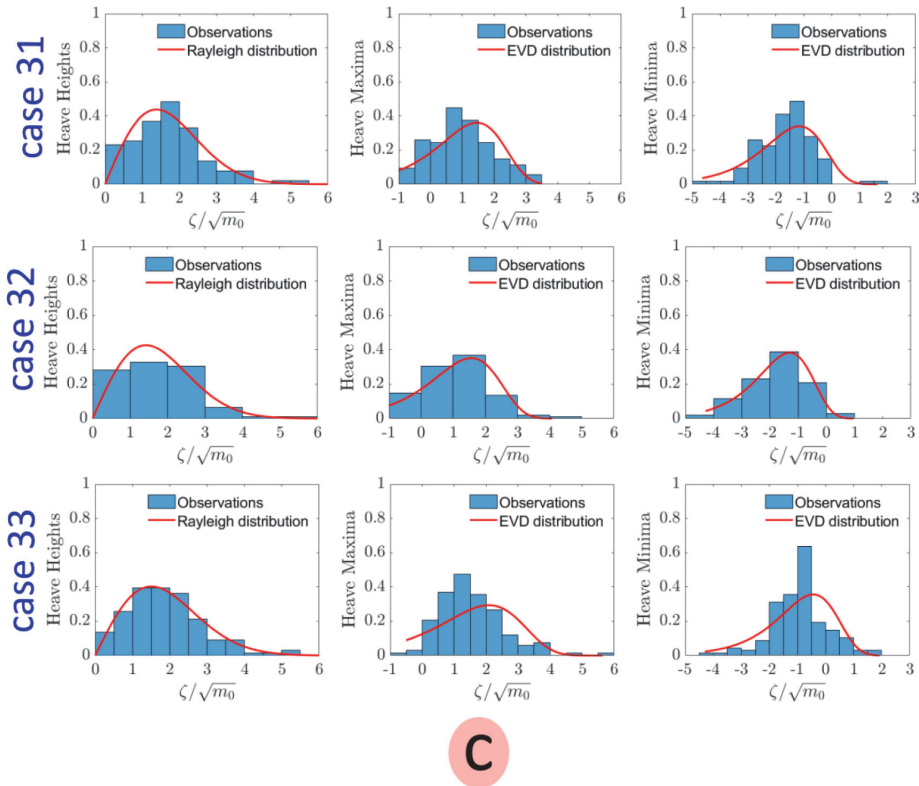
Fig. 13. (*continued*).

considered as the peak or trough. Subsequently, the amplitudes (maxima or minima) of pitch and heave motions, as well as the CG acceleration relative to the mean value, are determined from the time histories of these motions. Finally, the Mean, RMS, and ratio (r) for crests and troughs are computed and compared to the values obtained from the experimental data. The parameter 'r' represents the ratio of negative values among the maxima values divided by the total number of maxima values. Similarly, for the minima values, 'r' represents the ratio of positive values among the minima values divided by the total number of minima values.

Figs. 4, 5, and 6 provide a quantitative comparison between the distribution parameters of heave motion extremes (Maxima and Minima) obtained from experimental tests and CFD runs for three different hulls: C, C1, and C2, under various operating conditions outlined in Table 4. Detailed data can be found in Appendix C, Table 7. For the stepless case, data is once plotted as a function of Froude Number, and once as a function of wave steepness value to provide a better understanding of the effects of these two parameters on motions (note that for the stepped cases there is not much variety in the steepness value). Table 7 presents the values of maximum, minima and RMS of heave motion of three different hulls, as found through both CFD simulation and experimental tests.

The results illustrate that CFD predictions of heave motion for non-stepped C hull, one-stepped C1 hull, and two-stepped C2 hull are reasonably accurate, although the accuracy varies across different speeds and wave conditions. Given the randomness of the waves and the limited time duration of experimental tests, it is very challenging to reach a perfect match between CFD data and the experimental data.

Due to the nonlinear nature of vertical motions in random waves, RMS values of CFD runs align more closely with experimental data as compared to mean values, particularly for C2. The largest errors of CFD simulations in the prediction of RMS of heave maxima of C and C2 are seen at the lowest speed, though the largest errors of CFD simulations in the prediction of RMS of heave maxima of C1 are seen at the $Fr_B = 5.67$. The largest errors of the CFD model in the prediction of the heave minima of C are seen at the lowest speed, but for the stepped cases, the largest errors are seen at the largest speed.

In cases where the hulls are exposed to similar random waves at various speeds (e.g., Cases 12, 13, 14 for C hull; Cases 27, 28, 29 for C1; and Cases 30, 31, 32 for C2), the addition of steps to the hull leads to a reduction in the RMS of heave maxima and minima. This reduction is more noticeable for the hull with two steps, especially at higher speeds. Note that a deeper discussion on the effects of step on wave-induced heave, pitch, and vertical acceleration is available in Section 5.

High-speed planing hulls demonstrate nonlinear behavior, especially in the relationship between local wave elevation and craft motions. This nonlinearity becomes more pronounced as the speed increases, resulting in distinct characteristics in the time histories of motions and

Fig. 14. Statistics of normalized heights, maxima, and minima for pitch motions of the three hulls at different cases: a) C, b) C1, and c) C2.

accelerations. C. Judge et al. (2020) emphasizes the importance of utilizing time history data of mechanically generated wave for generating irregular waves in the CFD tank, rather than relying solely on spectra, to accurately simulate such conditions. Additionally, ensuring occurrence of a similar number of motions between CFD and experimental data is crucial for meaningful comparisons. If experimental work and CFD models did not record the same number of motions, it can affect parameters like 1/3 and 1/10 values, particularly in cases with larger motions. The lack of comprehensive experimental data on the time history of generated wave and number of recorded motions along with lack of verification studies on irregular seas further complicates the matter, as replicating these conditions and conducting repeated tests for statistical analysis are resource-intensive tasks. Consequently, even minor variations in wave elevation time histories, despite matching energy spectra and significant wave height, can significantly affect response parameters such as heave, pitch, and center of gravity

acceleration. Therefore, observed differences between experimental data and CFD simulations in mean, RMS, and the parameter r for maxima and minima of heave and pitch values are believed to be attributable to these inherent differences in wave elevation time histories and response characteristics that were not available. To comprehensively analyze these differences, detailed attention should be paid to the response characteristics of towing tank tests, including having a time history of waves and the number of motions, probability distributions of responses, individual maxima and minima, and statistical analysis values such as 1/3, 1/10, and 1/100 of individual peaks. Incorporating these analyses would provide a clearer understanding of the observed discrepancies in the response parameters among different cases.

The pitch motion extremes, maxima and minima, predicted by the presented CFD setup and those collected in experiments for hulls C, C1, and C2 are shown in Figs. 7, 8, and 9, with their corresponding values presented in Appendix C, Table 8.
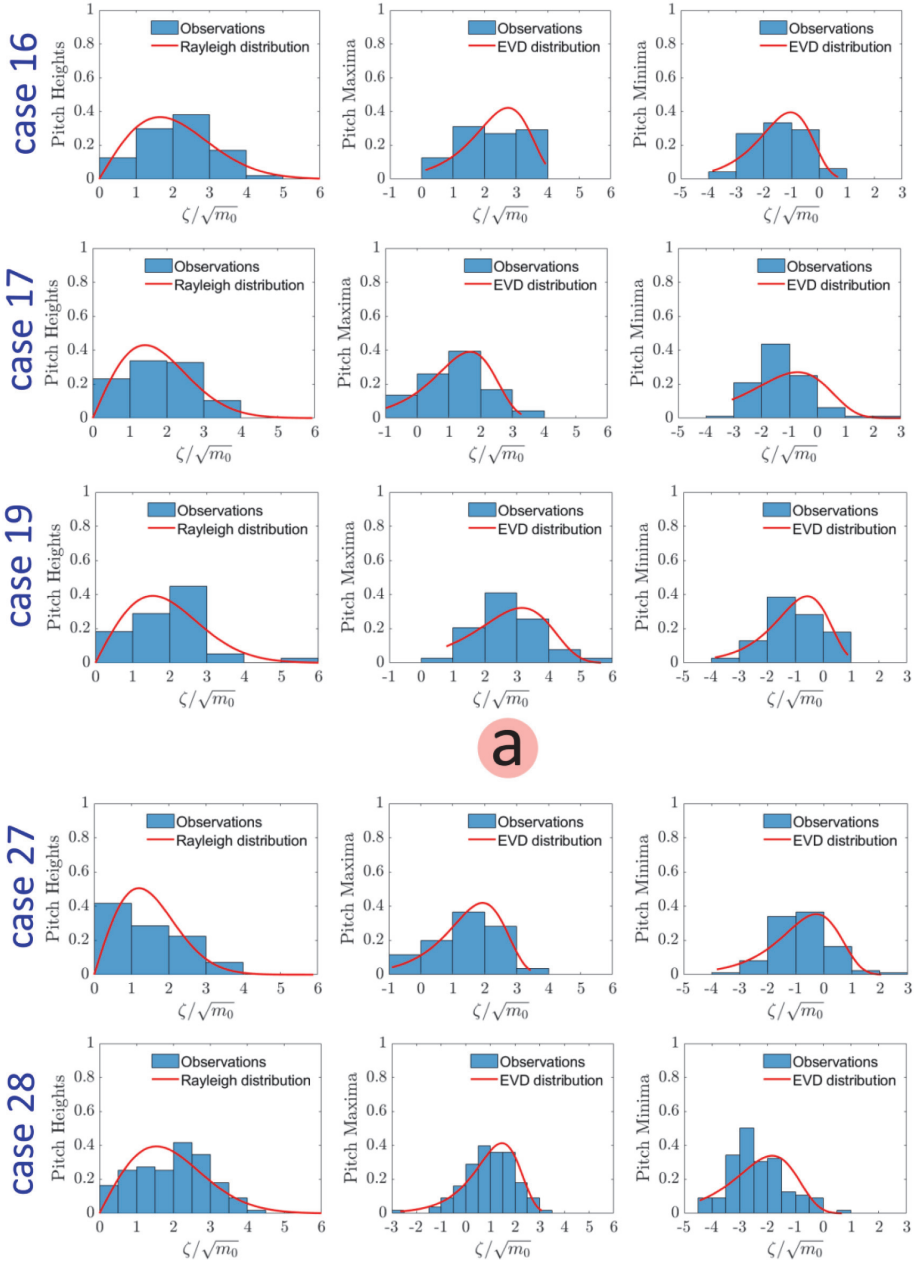
Fig. 14. (*continued*).

The largest errors in CFD simulations in the prediction of the RMS of pitch maxima of C1 and C2 are observed at the lowest speed. However, the largest errors of the CFD simulations in predicting the pitch maxima

of C are found at Froude numbers 2.94 and 5.67, which are observed to be more remarkable for larger wave steepness values.

CFD model has larger errors in the prediction of the RMS of pitch
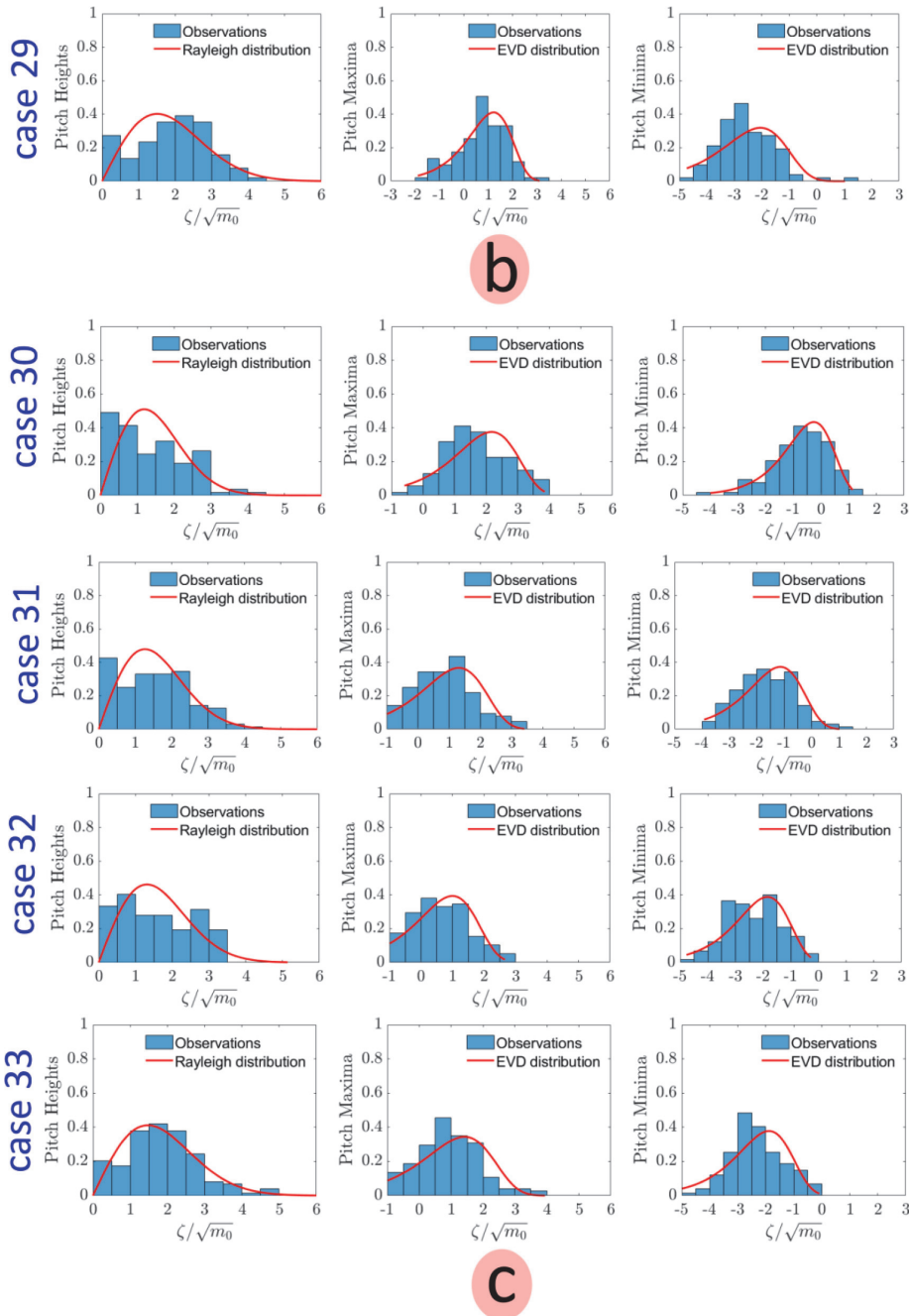
Fig. 14. (*continued*).

minima of C at Fr_B = 2.94 and 5.67, which is similar to what was observed for RMS of pitch maxima. The errors are seen to increase under the increase of the wave steepness. However, for the stepped cases, the largest errors in the prediction of the RMS of pitch minima are observed at the highest speed. The accuracy of the CFD model in the prediction of

RMS of pitch minima of both stepped hulls is promising. For C1, all cases are run for a unique value of wave steepness (see Table 4), C2 hull, Cases 32 and 33 are run for different wave steepness values. This helps us to also analyze the effects of wave steepness on the accuracy level of the CFD model in the prediction of the motions of the double-stepped hull.
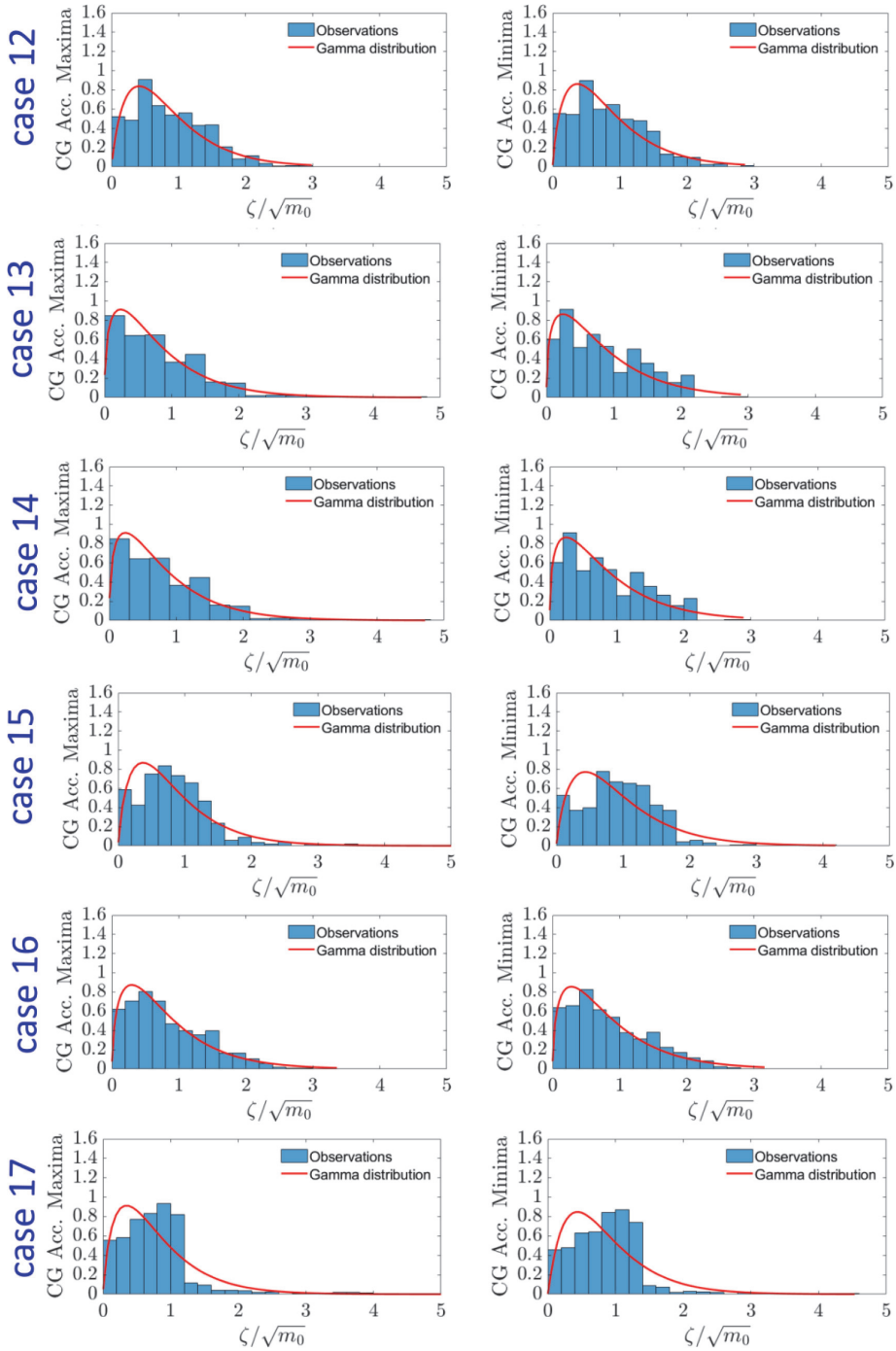
Fig. 15. Normalized maxima, and minima probability distributions, for CG acceleration of the three hulls at different cases: a) C, b) C1, and c) C2.

Interestingly, an increase in wave steepness would lead to a higher level of accuracy in the prediction of the pitch motion of C2.

The acceleration data exhibit distinct characteristics compared to the motions, allowing for the use of another analysis approach. The experimental data is exclusively available for minima and specifically for the gamma distribution parameters alpha (shape factor) and beta (scale
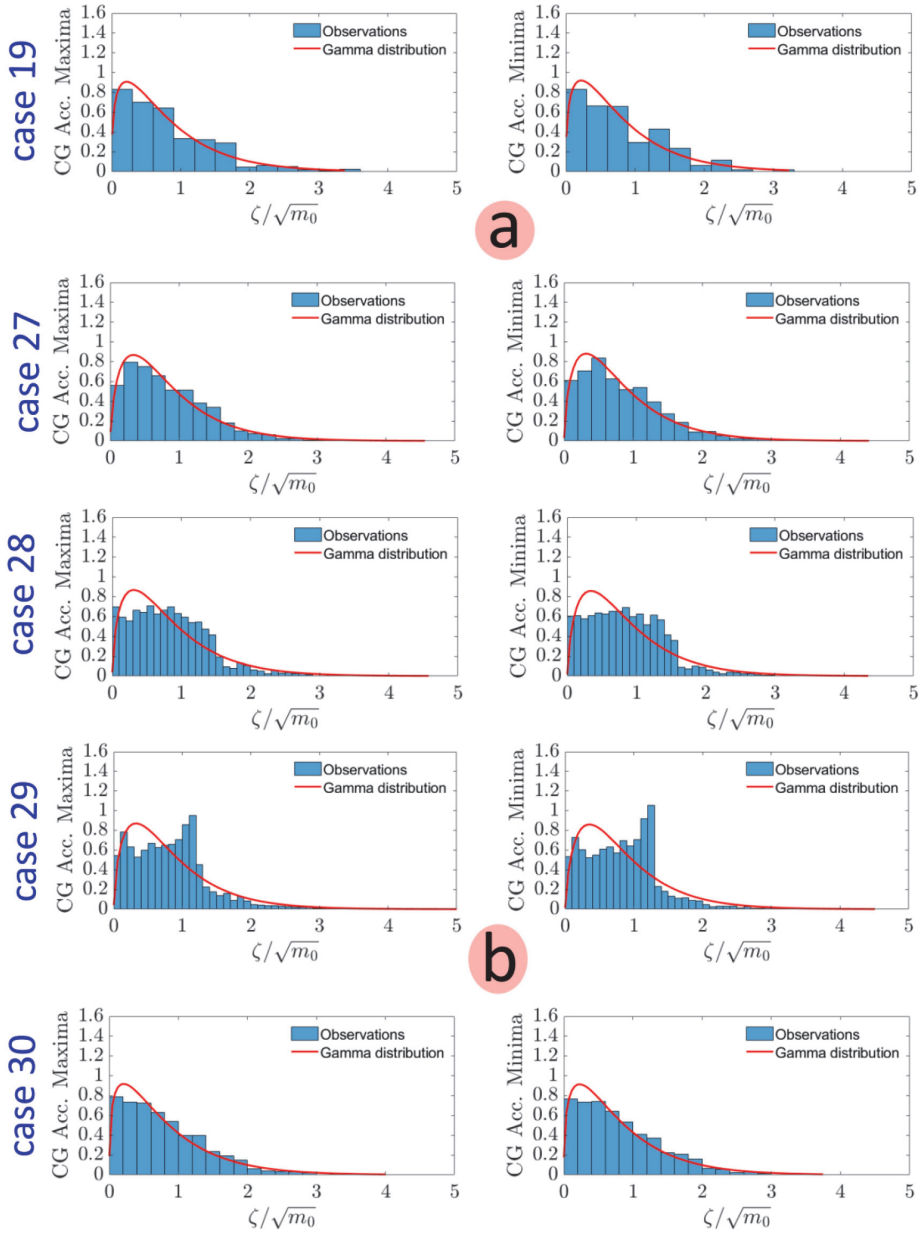
Fig. 15. (*continued*).

factor).

A comparison between the experimental and CFD gamma distribution parameters of the minima CG acceleration for hulls C, C1, and C2 is illustrated in Figs. 10, 11, and 12, with corresponding forcing conditions listed in Appendix C, Table 9. The values of alpha (shape factor) closely

align with the experimental results for almost all three hulls, although discrepancies are observed in certain cases for beta (scale factor). Detailed statistical analyses for the acceleration data, as well as heave and pitch motion, will be presented in the following section. Furthermore, the subsequent section will explain the probability distribution for
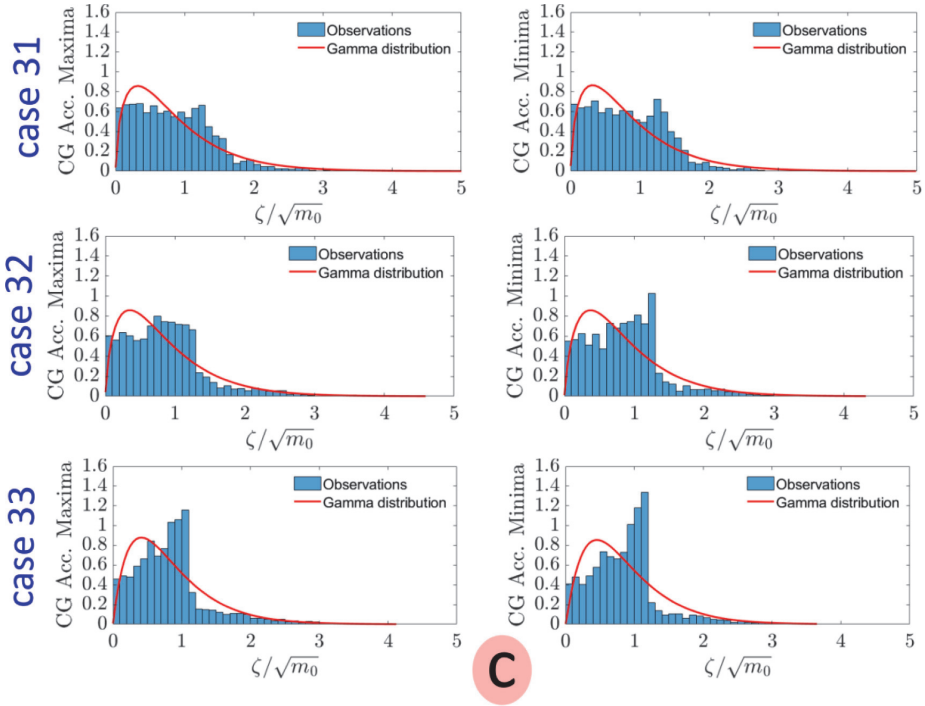
Fig. 15. (*continued*).
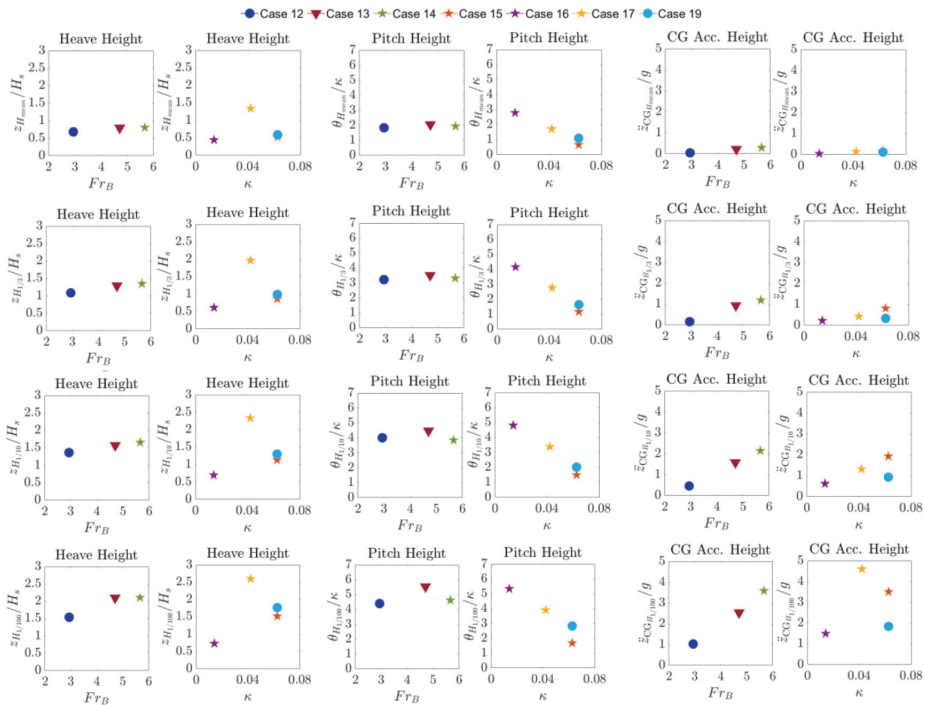
Fig. 16. Statistics of heave, pitch, and CG vertical acceleration measurements of C hull.
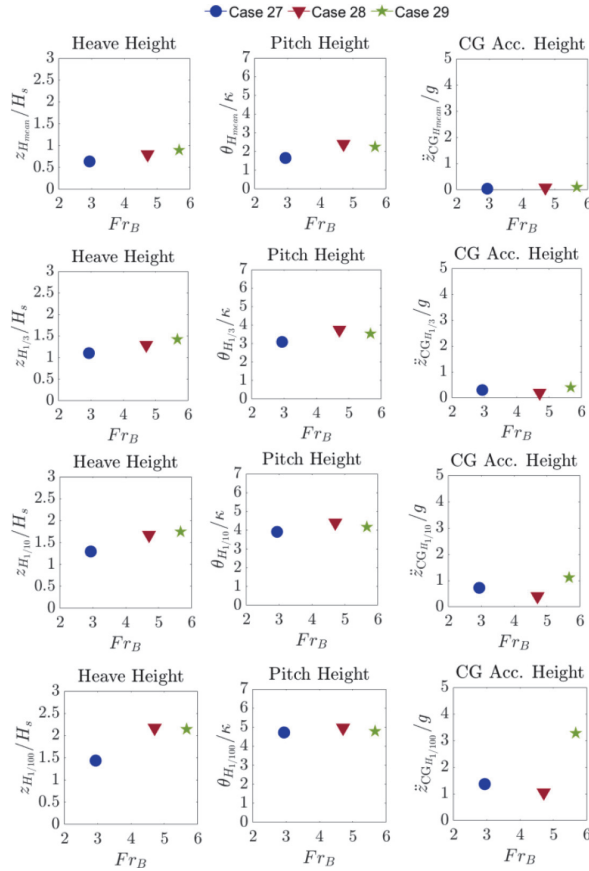
Fig. 17. Statistics of heave, pitch, and CG vertical acceleration measurements of C1 hull.

heave, pitch motions, and CG acceleration. Observations made in Figs. 10, 11, and 12 provide good evidence for the favorable accuracy level of the present CFD model in capturing the statistical behaviour of acceleration of stepless and stepped hulls.

5. Statistical analysis of heave, pitch, and center of gravity acceleration

5.1. Probability distributions

In this section, the probability distribution of heave and pitch motions along CG accelerations found in CFD simulations are calculated and it is shown what probability distribution function would match them. Heights, maxima and minima of heave/pitch motions and vertical accelerations, ζ are normalized using the Root-Mean-Square (RMS) of the data (shown by Begovic et al., 2016), as per

$$\eta = \zeta/\sqrt{m_0}, \tag{15}$$

where the relevant bandwidth parameter ε is defined as:

$$\varepsilon^2 = 1 - (1 - 2r)^2. \tag{16}$$

The normalized heights of heave/pitch motions are seen to fit the Rayleigh distribution. However, the normalized maxima and minima of heave/pitch motions are observed to fit using the Extreme Value Distribution (EVD), as demonstrated in Figs. 13 and 14. As for vertical accelerations, the normalized maxima and minima are found to fit the Gamma distribution, as shown in Fig. 15.

Seakeeping aspects are of paramount importance in the context of high-speed vessels, primarily due to the significant accelerations experienced during operation. These high accelerations not only affect passenger and crew comfort but also pose operational challenges for cargo. Furthermore, events such as slamming can induce substantial loads and impact the fatigue life of the vessel's construction. One key distinction between the seakeeping behavior of high-speed vessels and conventional ships lies in the nonlinear relationship between local wave elevation and vessel motions and accelerations. Time histories of motions and accelerations often exhibit complex characteristics, such as sharp peaks or flat troughs, rendering them unsuitable for linear analysis methods (ITTC, 7.5–02–04–05, 2014, 2014). This nonlinearity
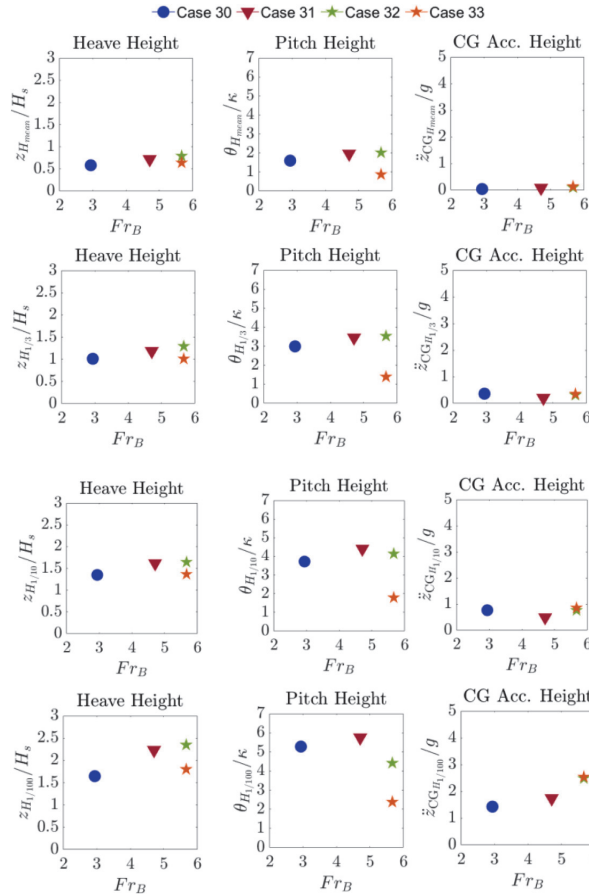
Fig. 18. Statistics of heave, pitch, and CG vertical acceleration measurements of C2 hull.

intensifies with the increase in speed. Semi-planing mono-hulls, operating at lower speeds, generally exhibit less complex responses. However, in our study, where hulls operated within the planing regime (defined by Fr_B values greater than 1.5), the time histories of heave, pitch, and acceleration displayed intricate characteristics, making them challenging to fit into distributions. Consequently, deviations from expected distributions, as observed in Figs. 13, 14, and 15 for heave, pitch, and CG acceleration, can be attributed to the presence of sharp peaks or flat troughs in the time histories, reflecting the nonlinear nature of high-speed vessel responses. These findings align with prior research by Fridsma (1971), Begovic et al. (2016), and De Luca and Pensa (2019).

5.2. Statistics of CFD measurements

In this sub-section, the statistical analysis is carried out to investigate how heave and pitch motion, along with CG vertical acceleration would be affected by the change in speed and wave steepness. A range of statistical indicators, including the mean, 1/3, 1/10, and 1/100 highest values are considered. The statistical analysis for heave and pitch

motion, as well as CG vertical acceleration, encompassing the mean, 1/3, 1/10, and 1/100 highest values for hulls C, C1, and C2, is depicted in Figs. 16, 17, and 18. Detailed data can be found in Appendix D, Table 10.

The mean value, as a statistical indicator, shows the central tendency of the data, helping us understand the typical dynamic response exhibited by each hull. The 1/3 highest values provide an understanding of the extreme or upper-tail behavior of the recorded motions. The 1/10 highest values can provide a better understanding of extreme events happening during the ride of the vessel. And finally, by narrowing down the threshold of defining extreme values, the 1/100 of largest values can be found, which informs us of the most extreme outliers. To sum up, analysis on the 1/3, 1/10, or 1/100 of highest values enables us to identify critical behaviors of the hulls riding in random waves.

The mean values of heave responses for hulls C, C1, and C2 slightly increase with speed, with C2 consistently exhibiting lower values compared to C and C1. Notably, a wave steepness of 0.042, which corresponds to the highest significant wave height, results in larger heave responses. Conversely, at wave steepness values of 0.028 and 0.063, the responses are very close. For C2, runs were only performed for wave
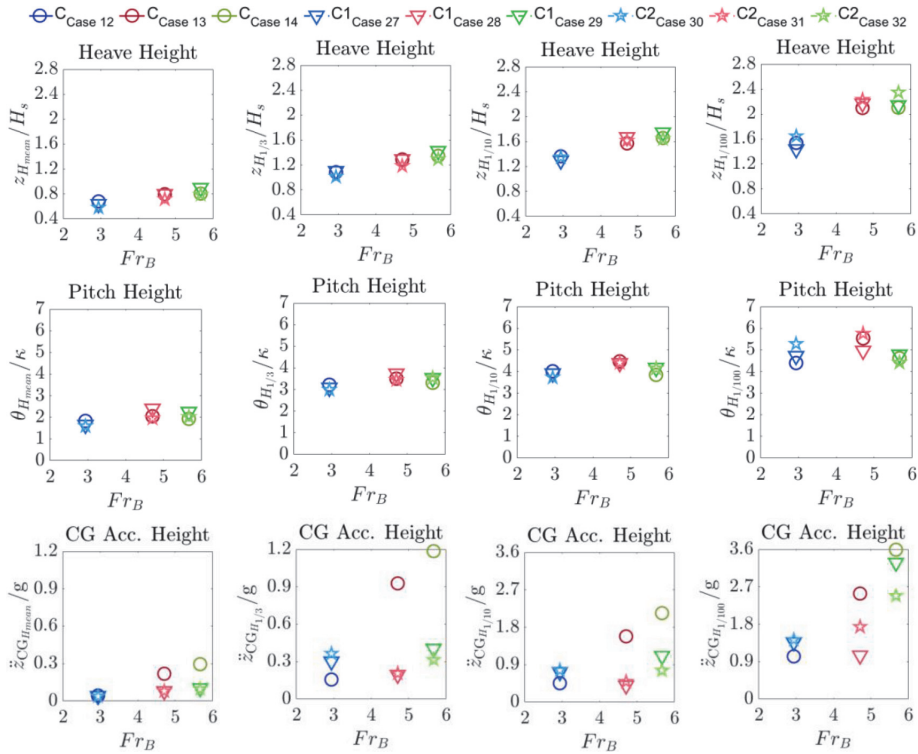
Fig. 19. Effect of step configurations on heave, pitch, and CG acceleration statistics with increasing Froude numbers in identical irregular wave conditions.

steepness values of 0.028 and 0.063, and larger waves can lead to lower mean values of heave response.

The 1/3 and 1/10 highest heave responses follow a similar pattern observed in the mean values, slightly increasing with speed. However, the 1/100 highest heave response behaves differently, exhibiting an abrupt increase from Froude number 2.92 to 4.71, flattening out at $Fr_B > 4.71$. For C2 slightly larger values may be recorded at 4.71 compared to higher speeds, but for C and C1, the 1/100 highest heave response of the two greater speeds are nearly equal.

For pitch responses, the mean and 1/3 highest pitch response of hulls C, C1, and C2 show insensitivity to speed. However, the 1/10 and 1/100 values may reach lower values at the highest speed, which is noticeable for C2 (i.e., case 32). An increase in wave steepness results in decreased mean and extreme pitch values for C and C2 (case 32 and case 33), with C1 showing less sensitivity to speed.

The mean values of CG vertical acceleration responses for C, C1, and C2 are slightly increased by speed (but not very significantly), with C consistently exhibiting higher values than C1 and C2. The 1/3, 1/10, and 1/100 highest CG vertical acceleration responses for C exhibit an abrupt increase from Froude number 2.92 to 5.67. An increase in wave steepness at the same speed leads to an increase in CG vertical acceleration responses, except for 1/100 highest CG vertical accelerations, which decrease after wave steepness goes beyond 0.042 (it peaks at this wave steepness, which is similar to what was observed for heave response, see the first column of Fig. 16). The 1/3, 1/10, and 1/100 of CG vertical acceleration responses for C1 and C2 decrease up to

Fr_B=4.71 but increase thereafter, with C1 showing more pronounced changes.

In Fig. 19, the effects of adding steps to the bottom of the vessel on statistical parameters, are explored. Results of this Figure correspond to data collected for cases in which similar speeds and waves were modeled (Cases 12, 13, 14 for the C hull; Cases 27, 28, 29 for C1; and Cases 30, 31, 32 for C2).

The mean, 1/3, and 1/10 highest heave and pitch heights among the three hulls exhibit similar behaviour at different speeds. There might be some slight differences which are not significant. For example, the mean amplitude of heave and pitch of a one-stepped hull are seen to be slightly larger than those of a double-stepped hull and a non-stepped hull at the largest speed. The other example is the mean heave and pitch responses observed at the lowest speed, which are seen to be slightly larger when no step is incorporated on the bottom. However, when focusing on the 1/100 highest values of recorded heave and pitch motions, differences become more significant. The two-stepped hull may have higher extreme heave and pitch motions compared to the other hulls. The 1/100 highest heave responses of this double-stepped hull are larger than those of the other cases at all three speeds. The 1/100 highest pitch response of the double-stepped hull is larger than those of the stepless and single-stepped hull at the early planing speed, but the highest planing speed, 1/100 highest pitch response of the double-stepped hull becomes lower than those of the two other hulls. This is a very interesting point, showing that adding two steps on the bottom of the hull may cause more extreme heave motions and less extreme pitch motions
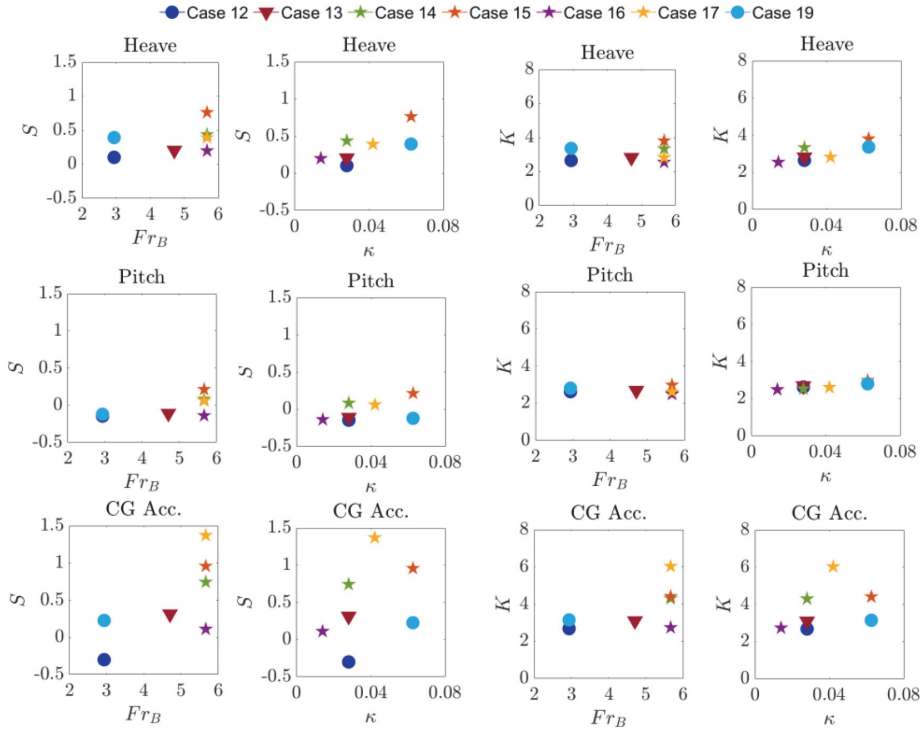
Fig. 20. Exploring Kurtosis (K) and Skewness (S) variations in heave, pitch, and CG vertical acceleration for a C hull under various operating conditions.

at the highest speed. It may be related to the fact that a double-stepped hull may be more sensitive to longer waves, which may cause larger heave motion, but lower pitch motion.

Additionally, the mean, 1/3, 1/10, and 1/100 highest values of CG vertical acceleration for stepped hulls are lower than those for non-stepped hulls, except at the minimum speed. For instance, at Fr_B=5.67, the 1/100 highest values of CG vertical acceleration of the two-stepped hull (C2) are 31 % lower compared to the non-stepped hull (C). But interestingly, at the lowest speed (corresponding to Fr_B=2.94), the 1/100 highest values of CG vertical acceleration of the non-stepped hull are seen to be relatively lower than those of the stepped hull. This shows that a stepped design would decrease the vertical accelerations mostly at higher speeds. This might be due to the fact that the wetted surface decreases under the increase of speed which would possibly decrease the acceleration, but a moderate planing speed would not benefit the vessel as a larger maximum pressure area would appear on the bottom of the vessel.

6. Exploring skewness and kurtosis in heave, pitch motions, and CG acceleration

The skewness and kurtosis of heave, pitch motions, and CG acceleration may inform the general behavior pattern of the vessel riding in random waves. Skewness measures the asymmetry pattern of each cycle of the response, and kurtosis assesses its peakedness. High values of kurtosis may inform about the likelihood of extreme events.

In general, it is expected that CG acceleration does not follow a normal distribution. In addition, a high kurtosis value of CG acceleration may indicate a greater chance of experiencing extreme CG acceleration events, potentially causing discomfort, injury, or damage. A positive value of CG acceleration would indicate that large acceleration is mostly in the upward direction.

Figs 20, 21 and 22 display the kurtosis (K) and skewness (S) variations for heave, pitch, and CG vertical acceleration in three distinct hull types: C, C1, and C2. The corresponding values can be found in Appendix E, Table 11. Skewness values of heave motions of a stepless boat mostly range between 0 and 1, and those of its pitch motion vary between −0.2 and 0.2. The skewness of the heave response of a non-stepped planing hull is seen to be insensitive to speed, though it is increased under the increase of wave steepness. The skewness of heave and pitch responses of stepped hulls, however, are seen to increase under the increase of speed, while growing under the increase of wave steepness. This shows that all planing boats may show stronger non-linear heave and pitch motions when waves become larger. But only speed may affect the nonlinear behavior (asymmetric pattern of each cycle) of heave and pitch motions of stepped hulls.

The skewness of CG acceleration of all three hulls is seen to increase under the increase of speed and wave steepness values, as it was expected. The nonlinearity associated with vertical acceleration is much stronger as compared to those of heave and pitch displacement and is always intensified under the increase in speed.

Kurtosis values of heave and pitch displacement are seen to be nearly 3 in most of the cases with wave steepness value below 0.04. When wave steepness exceeds this value, kurtosis of heave displacement may reach
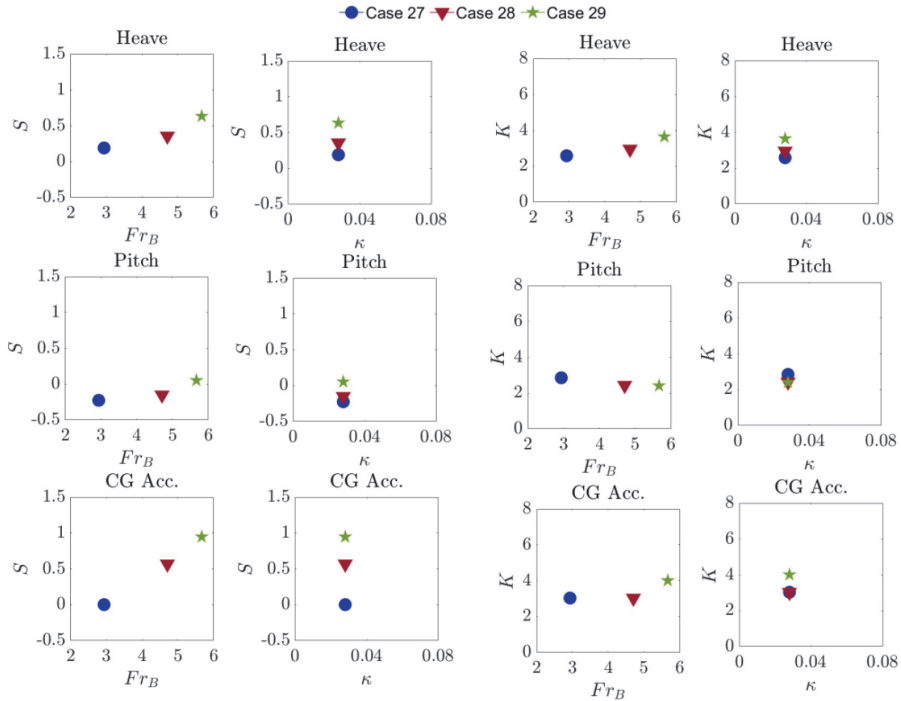
Fig. 21. Exploring Kurtosis (K) and Skewness (S) variations in heave, pitch, and CG vertical acceleration for a C1 hull under various operating conditions.
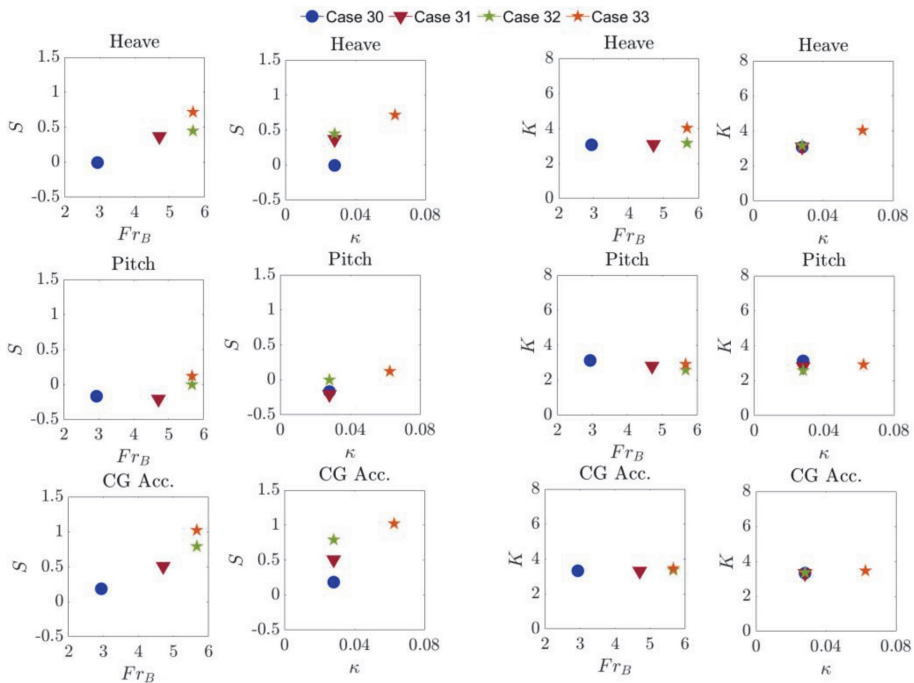

Fig. 22. Exploring Kurtosis (K) and Skewness (S) variations in heave, pitch, and CG vertical acceleration for a C2 hull under various operating conditions.
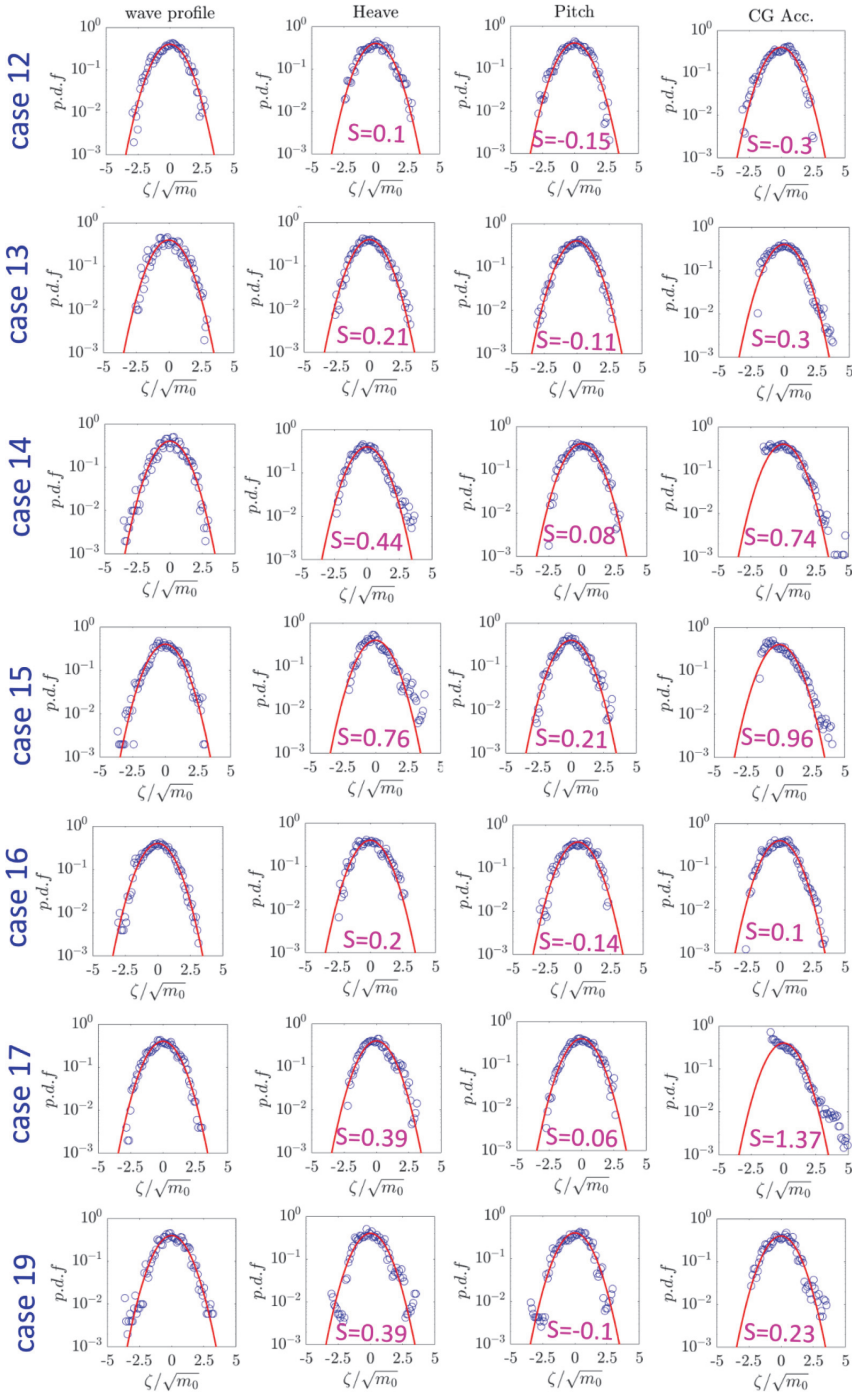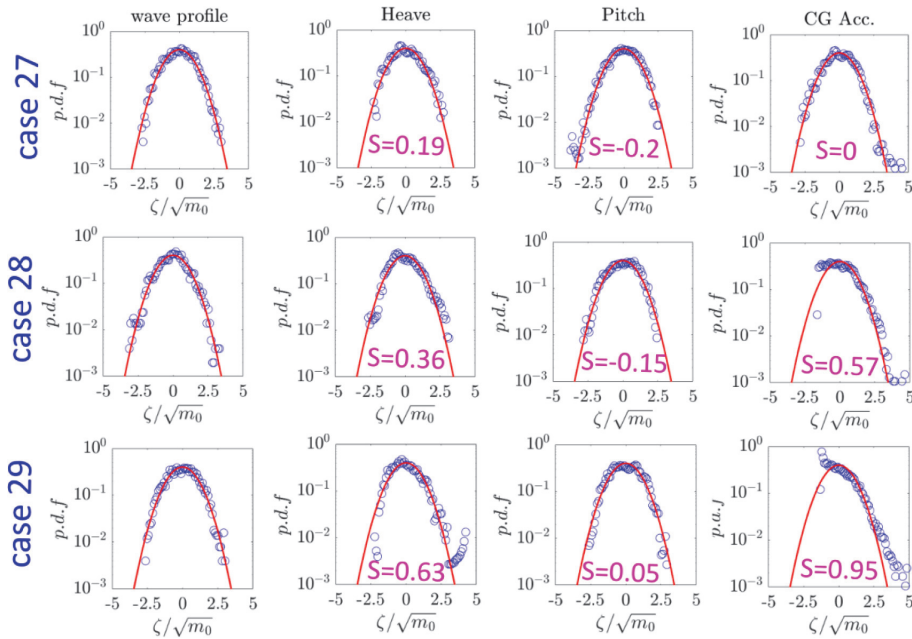
Fig. 23. Probability Density Functions for wave profiles, heave, pitch, and CG acceleration of the C planing hull under various operating conditions. The solid red curve represents a Gaussian distribution.

Fig. 24. Probability Density Functions for wave profiles, heave, pitch, and CG acceleration of the C1 planing hull under various operating conditions. The solid red curve represents a Gaussian distribution.

up to 4.0 and this may cause a sharper crest and shallower trough. Kurtosis of vertical acceleration is seen to slightly increase under the increase of speed. For the double-stepped hull, the kurtosis of vertical acceleration is seen to be insensitive to wave steepness, but for the stepless hull, kurtosis increases under the increase of wave steepness reaching a peak value at wave steepness of 0.04. This may lead to very extreme vertical accelerations, which shall be discussed later.

The interesting point is about the kurtosis of different hulls. At the lowest speed, the kurtosis of CG acceleration for C is lower than that of C1 and C2. This aligns well with the observations of the 1/100 highest CG acceleration at this speed, as depicted in Fig. 19. As was observed, hull C was exposed to lower values of 1/100 highest CG acceleration at this speed. However, at the highest speed, a shift occurs: the kurtosis of C2 is the lowest, whereas that of C is the largest. This pattern is consistent with the findings in Fig. 19, where the 1/100 highest CG acceleration of C2 was recorded as the lowest, and that of C was the largest at this speed.

7. Exceedance probability of wave profiles, heave, pitch, and CG acceleration

Figs. 23, 24, and 25 show the probability density functions (PDF) of wave profiles, heave, pitch, and CG acceleration of planing hulls C, C1, and C2 under various operational conditions. In these plots, the solid red curve represents a Gaussian distribution, with the highest point on the curve corresponding to the mean value. If a PDF follows this Gaussian distribution, it imposes that the recorded signal shows a Gaussian behavior.

As seen in the PDFs recorded water waves, generated in the numerical tank are in line with the Gaussian distribution, suggesting that

no nonlinearity has emerged in waves propagating across the numerical tank. PDFs of recorded heave motions is skewed towards positive values for the cases for which the skewness was found to be relatively large (for example: highest speed for all hulls). The PDF of pitch motion of all cases are seen to nearly match with Gaussian distribution but partially skewed toward negative values at the two lowest speeds. The PDFs of the vertical acceleration of all three hulls is seen to be skewed toward positive values at two higher speeds. The very interesting point is about the PDF of the vertical acceleration of the stepless boat at the lowest speed, which is skewed toward negative values (with negative skewness).

In Figs. 26, 27, and 28, the Exceedance Probability Function (EPF) for crest height in wave profiles, heave, pitch, and CG acceleration of planing hulls C, C1, and C2 under varying Froude numbers and random wave conditions is presented. The solid red curve represents the Rayleigh distribution function. When the data diverges more the from Rayleigh distribution curve, nonlinearities are stronger and resulting extreme events are more probable. Most of the cases for wave profiles, heave and pitch closely follow the Rayleigh distribution in the analysis.

However, when the EPF data deviates from the mean value and diverges further from the Rayleigh distribution curve, it suggests that the data is not accurately represented by the Rayleigh distribution. In cases 15, 19, 29, and 33, the heave motion shows distinct behavior from the tail of pure Rayleigh distribution. This suggests that these cases experience conditions that result in unfavorable heave responses (this behavior has also been demonstrated in the Fridsma (1971) report). The reasons for this divergence could be attributed to the nonlinear motion of the vessel which correlates with the kurtosis value. A kurtosis value greater than 3.0 would cause the data to diverge from a normal EPF to a higher degree. Additionally, this deviation is most prominent in the CG vertical acceleration data, especially for case 17, where the vertical
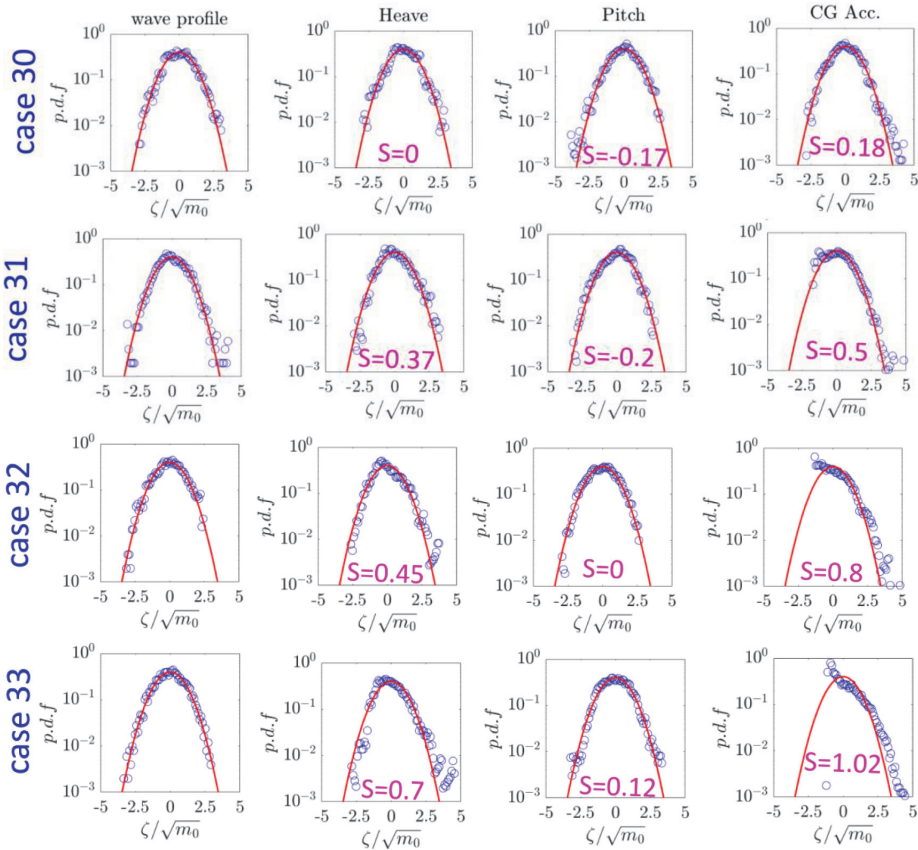
Fig. 25. Probability Density Functions for wave profiles, heave, pitch, and CG acceleration of the C2 planing hull under various operating conditions. The solid red curve represents a Gaussian distribution.

acceleration is notably the largest among all cases and the related Kurtosis value is greater than 6.0.

8. Examining hull motion and CG acceleration through spectrum analysis

Figs. 29, 30, and 31 show spectra of heave, pitch, and CG acceleration of C, C1, and C2. The spectrum is found using Fast Fourier Transform (FFT). The curves are presented on a logarithmic scale. This allows us to understand the slope of the tail of the spectrum, and compare it against that of the JONSWAP spectrum, decay of which is proportional to ω^{-5}. The more the spectrum of the motion deviates from the ω^{-5} and decays with a larger, the more that response deviates from the tail of the spectrum. If the tail of spectrum decays with a lower rate, it means response is more sensitive to the shorter wave as expected. Here, we need to note that the reason for focusing on the tail of the spectrum is that it is related to shorter waves (shorter periods), which happen more frequently. In addition, it is observed that there are no local peaks in the spectra of heave, pitch, and CG acceleration over low frequencies, which ensures that the local peak observed in the wave spectrum (Fig. 3) is not a cause for concern.

The tail of the heave and pitch spectra are seen to slightly follow and be relatively (not completely) proportional to ω^{-5}, as compared to vertical acceleration. This indicates that these responses would be responded to shorter waves to some degrees. Over the larger frequency ($\frac{\omega}{\omega_p} > 1.5$) the tail of spectrum may deviate from ω^{-5} and decreases with a lower rate, which means some non-linear effects may shift the energy of motions towards very short periods. The tail of heave spectrum of stepless boat is seen to deviate more from ω^{-5} at the lowest considered speed and decreases with a greater rate than ω^{-5}, it well aligns to ω^{-5} at the medium speed, and again it may deviate from ω^{-5} at the largest speed, but this deviation is less significant as compared to the lowest speed. Interestingly, there is a correlation between this deviation and the mean value of the heave response (please see the circle markers in Fig. 19, mean heave panel). The larger the deviation, the smaller the mean heave. The tails of the heave spectrum of stepped hulls (C1 and C2) deviate more from ω^{-5} at lower speeds, and then its slopes converge to ω^{-5} as the speed increases. It is different from what was observed for the stepless hull. But the interesting point is that a link between the deviation of the tail of spectrum from ω^{-5} and mean values of heave response can be seen.
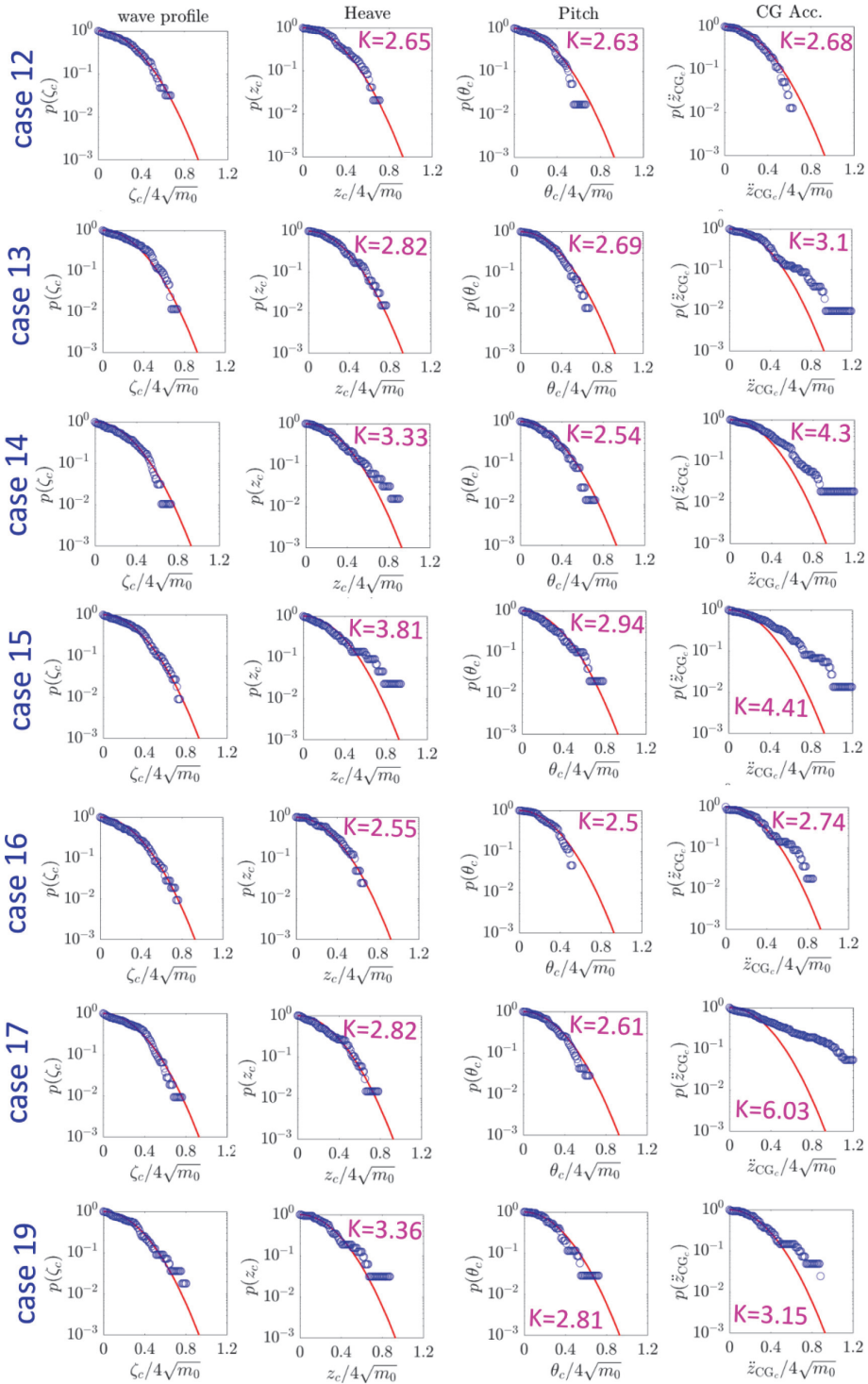
Fig. 26. Exceedance Probability Functions for crest height in wave profiles, heave, pitch, and CG acceleration of the C planing hull under different Froude numbers and random wave conditions. The solid red curve represents the Rayleigh distribution function.
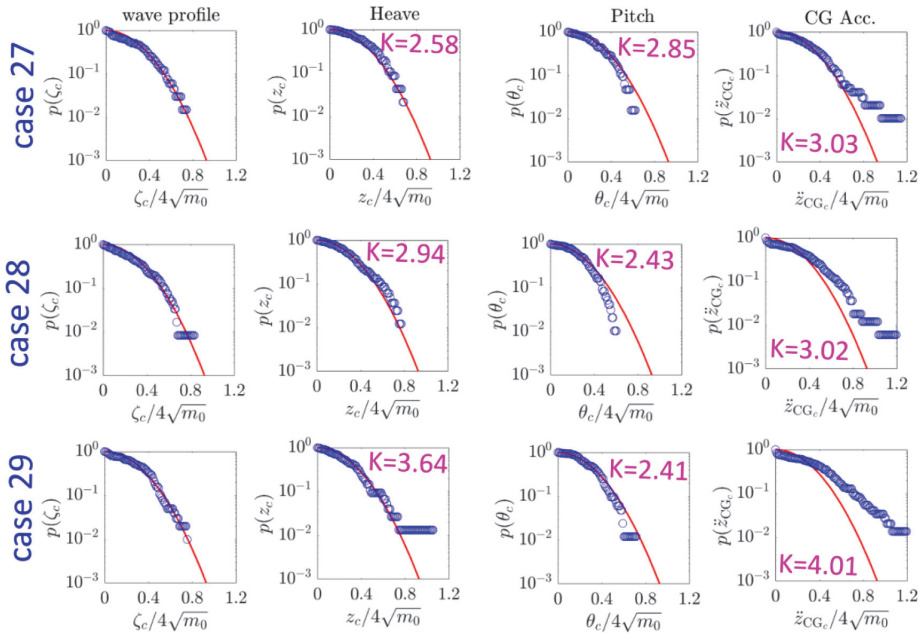
Fig. 27. Exceedance Probability Functions for crest height in wave profiles, heave, pitch, and CG acceleration of the C1 planing hull under different Froude numbers and random wave conditions. The solid red curve represents the Rayleigh distribution function.

The tails of pitch spectra of all three boats are seen to decay with a slightly larger rate than ω^{-5} at the lowest speed, then they nearly decay with rates of $\approx \omega^{-5}$ at the medium speed, and at the largest speed, they decay with a slightly lower rate than ω^{-5} at the largest speed.

The slop of the tail of the CG acceleration spectrum deviates from ω^{-5} across all cases as compared to heave and pitch responses. Interestingly the slope of the tail of CG acceleration spectra is lower than ω^{-5}. These deviations signify that vertical acceleration with a relatively short period is more sensible on the boat as compared to heave and pitch displacement and energy associated with acceleration may be highly transferred to larger frequencies.

9. Conclusions

In this study, the Siemens PLM STAR-CCM+ software, version 17.02.007, was employed to conduct simulations of planing hulls in varying wave conditions. Utilizing an implicit Unsteady Reynolds-Averaged Navier-Stokes (URANS) solver, the hydrodynamics of planing hulls were modeled, particularly focusing on their behavior in random wave environments. Through the application of the Finite Volume Method (FVM), the integral form of the Navier-Stokes equations was discretized to facilitate numerical simulation of incompressible viscous flows around the stepless and stepped planing hulls. Specifically, the DFBI approach within the Siemens PLM STAR-CCM+ solver was employed, allowing for the resolution of forces and moments acting on the stepped planing hull in both pitch and heave degrees of freedom.

This research focused on analyzing planing hull behavior in irregular waves through Computational Fluid Dynamics (CFD) modelling. Investigating the models C, C1 and C2 which are from Taunton systematic series enabled a comparative analysis between dynamic responses of stepless, single-stepped, and double-stepped hulls, offering insights into their dynamic motions in random waves. The study aimed to statistically analyze CFD results in random waves, lacking in existing literature, and aimed to build a promising CFD model capable of simulating planing

motion in real sea conditions. The paper presented an in-depth analysis of probability distributions, statistical indicators, skewness, kurtosis, Exceedance Probability Functions (EPF), and spectral characteristics of heave, pitch, and CG acceleration of C (stepless hull), C1 (single-stepped hull), and C2 (double-stepped hull). The findings contribute to a better understanding of planing hull dynamics in irregular waves, benefiting future naval architecture designs and bolstering the use of CFD simulations in this domain.

Time histories of motions and accelerations in non-stepped and stepped high-speed planing hulls were displayed intricate characteristics like sharp peaks or flat troughs, making them unsuitable for linear analysis methods. This nonlinear relationship contrasts with conventional ships, where the relationship between local wave elevation and vessel motions and accelerations tends to be linear. Deviations from expected distributions observed in the data underscore the complex nature of high-speed vessel responses. These findings, consistent with observations of previous studies, provide valuable insights into the behavior of high-speed vessels in irregular wave conditions.

In general, it was shown that adding steps to the bottom of the vessel can significantly affect the hull behaviour in waves, particularly influencing heave, pitch, and CG vertical acceleration heights, which vary depending on speed and wave steepness. These observations suggest that the incorporation of steps on the vessel's bottom influences the overall characteristics of heave, pitch, and CG vertical acceleration. The difference in step configurations notably alters extreme motions, as evidenced by the significantly higher extreme heave motion observed in the two-stepped hull across all speeds, while the 1/100 highest pitch responses decrease at the highest speed. This shows the significance of hull design in managing extreme motions during high-speed operation. Additionally, stepped hulls generally exhibit lower CG vertical acceleration values, except at the lowest considered speed, where non-stepped hulls display relatively lower 1/100 highest CG vertical acceleration values compared to stepped hulls. For instance, at $Fr_B = 5.67$, the 1/100 highest values of CG vertical acceleration of the two-stepped hull (C2) are 31 % lower than those of the non-stepped hull (C), highlighting the
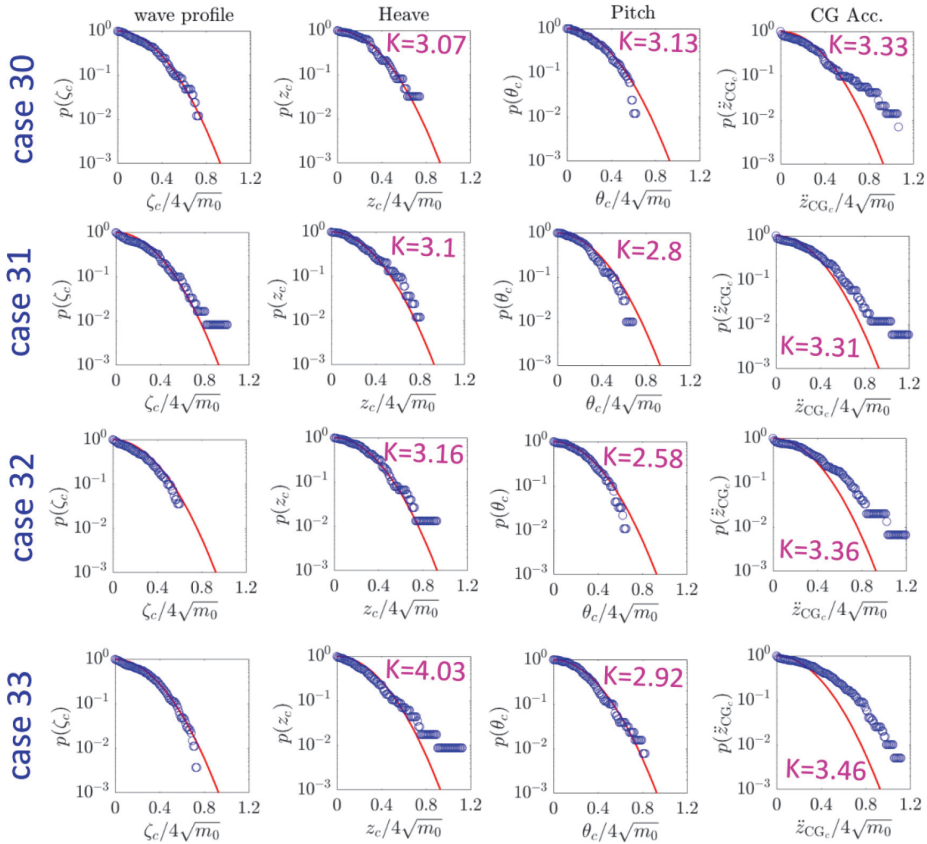
Fig. 28. Exceedance Probability Functions for crest height in wave profiles, heave, pitch, and CG acceleration of the C2 planing hull under different Froude numbers and random wave conditions. The solid red curve represents the Rayleigh distribution function.

influence of step configurations on motion characteristics.

Statistical analysis showed that the heave and pitch displacement deviate from the pure Rayleigh distribution over higher Froude Numbers, and their corresponding time series may not follow Gaussian distribution. Pitch response was found to be skewed toward negative values at low two speeds, which was more remarkable for the stepless case, and heave response was seen to be skewed towards positive values, which was observed to be more significant under the increase of speed. A Correlation between 1/100 highest values of responses of the stepped hull and stepless hull one. The tail of heave and pitch spectra deviate less from ω^{-5}, while that of CG acceleration spectrum was seen to highly deviate from ω^{-5}, decaying with a very lower rate.

In the present investigation of simulating high-speed planing hulls in irregular waves using STAR-CCM+ software, it is crucial to recognize several inherent limitations. Firstly, CFD simulations rely on various assumptions and simplifications to model complex fluid flow phenomena. These assumptions and simplifications encompass factors such as turbulence modeling, boundary conditions, and numerical discretization methods, which may not fully capture the actual fluid dynamics. Additionally, the motions of planing hulls are strongly nonlinear, posing

challenges in accurately capturing their behavior using any non-physical model. Simulating irregular seas presents further difficulties due to the complex nature of wave groups. Moreover, the lack of comprehensive experimental and systematic data and verification studies on planing hulls in irregular seas compounds these challenges. Replicating irregular sea conditions in experimental tests is challenging, and conducting multiple runs for statistical analysis in towing tanks is resource-intensive. These limitations underscore the complexities involved in accurately simulating high-speed planing hulls in irregular waves and emphasize the need for cautious interpretation of results. Furthermore, the present model is not developed to consider fluid-solid interactions and related hydroelastic responses, which adds another layer of limitation to the current computational model. Additionally, our study is limited to head sea conditions, and the hull is restricted in heave and pitch free motion. Finally, the present results and CFD model do not consider bio-model sea and interaction of different wave groups.

The present CFD setup holds promise for assessing the design phase performance of fast boats in rough water conditions. Future studies should focus on developing a mathematical model to predict the sea-keeping performance of planing hulls in real sea conditions and advance
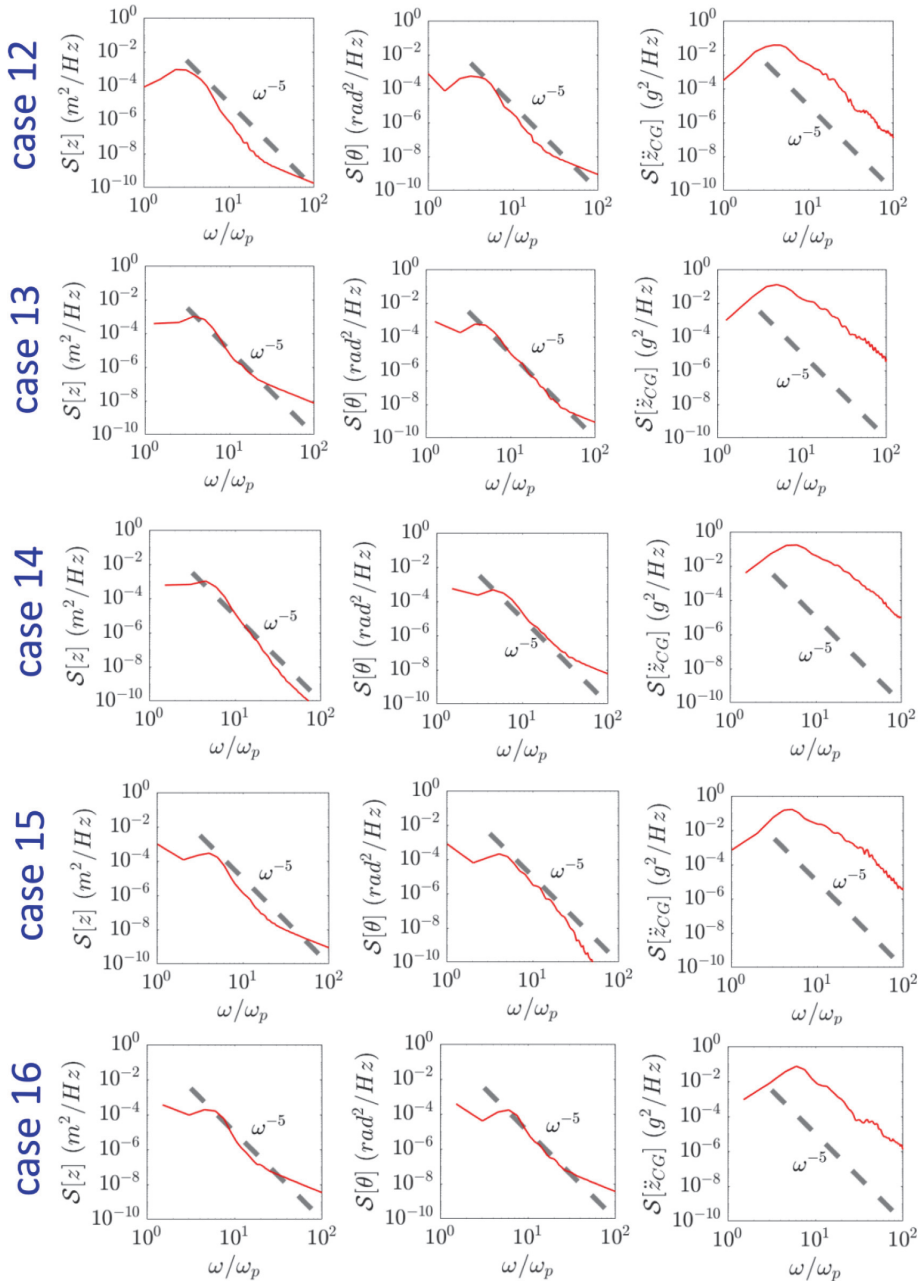
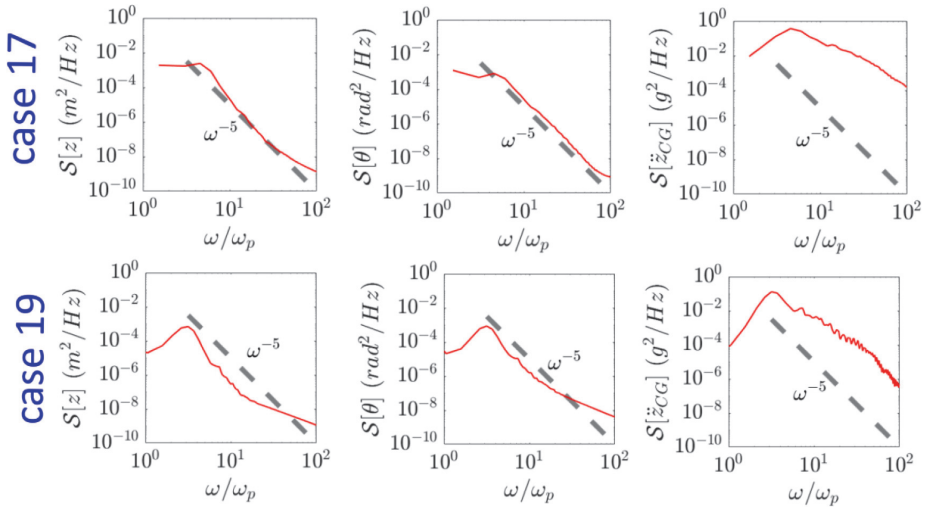**Fig. 29.** Spectrum of heave, pitch, and CG acceleration of C hull under various operating conditions.
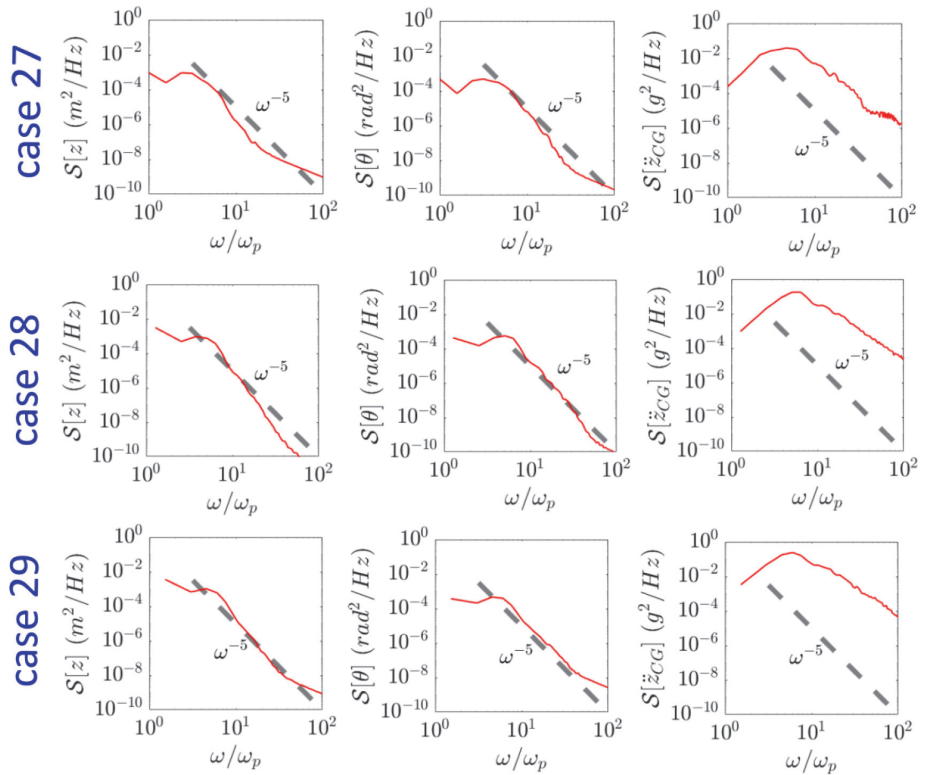
Fig. 29. (*continued*).

Fig. 30. Spectrum of heave, pitch, and CG acceleration of C1 hull under various operating conditions.
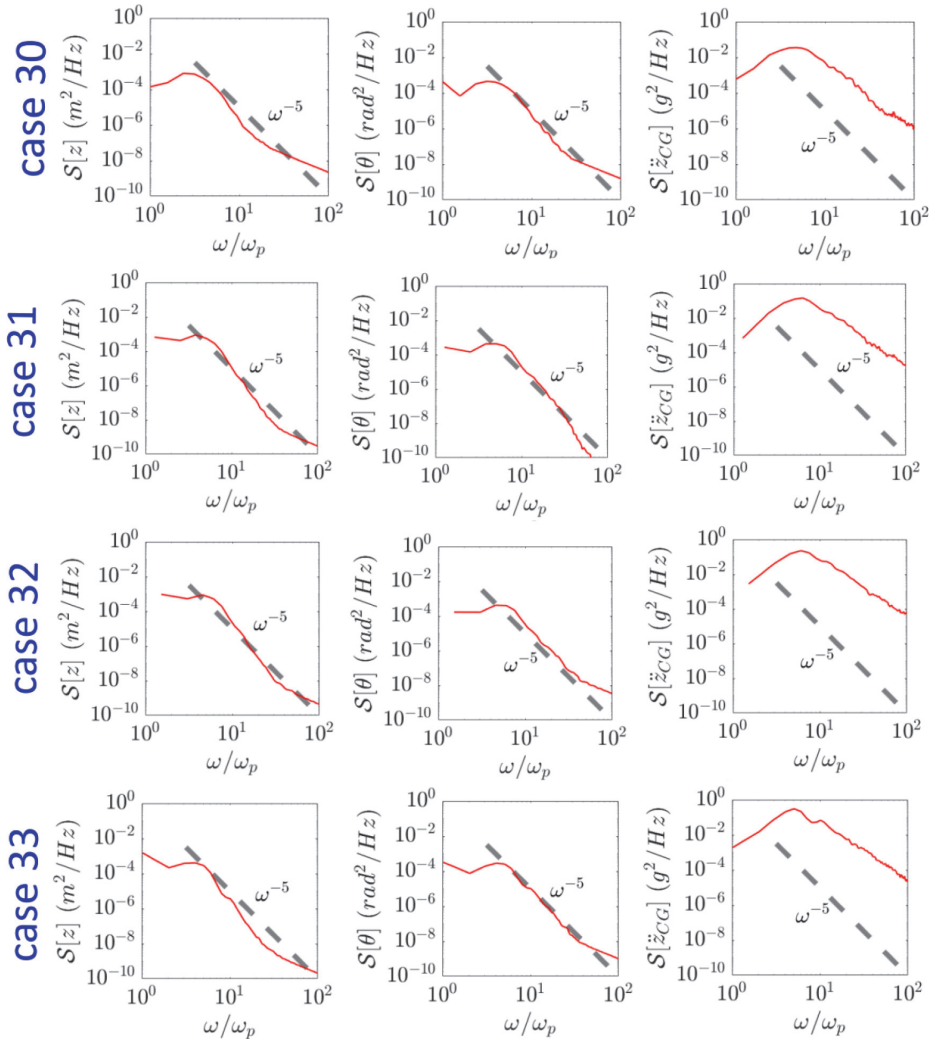
Fig. 31. Spectrum of heave, pitch, and CG acceleration of C2 hull under various operating conditions.

CFD modeling for their maneuvering in random waves. Furthermore, future investigations will involve conducting simulations for a single hull using a CFD/mathematical model over various time durations (ranging from 100 to 400 s) to assess the sensitivity of parameters such as 1/3 and 1/10 values to the duration and number of motions.

CRediT authorship contribution statement

Rasul Niazmand Bilandi: Writing – original draft, Visualization, Validation, Software, Resources, Methodology, Investigation, Formal analysis, Data curation, Conceptualization. **Sasan Tavakoli:** Writing – review & editing, Investigation, Formal analysis, Resources. **Simone Mancini:** Writing – review & editing, Software, Resources, Formal analysis. **Abbas Dashtimanesh:** Writing – review & editing, Supervision.

Declaration of competing interest

The authors declare that they have no known competing financial interests or personal relationships that could have appeared to influence the work reported in this paper.

Data availability

No data was used for the research described in the article.

Appendix A: CFD Model Mesh Independence Study

A mesh independence study was conducted to determine the most suitable mesh for numerical experiments in CFD modeling. Results from numerical simulations indicate that the optimal choice for simulations is a fine grid containing almost 3.9 million of cells. All the CFD data presented in this paper were computed using G3. The results shown in Figs. 32 and 33 confirm that the heave and pitch response converge across all three hulls. Table 6 displays the four grid sizes utilized in this grid study.

Table 6
Generated grids.

Grid Name	Number of cells in Million		
	C	C1	C2
G1	1,981,889	2,012,145	2,080,656
G2	2,798,441	2,812,650	2,840,122
G3	3,928,571	3,971,462	3,979,812
G4	5,212,945	5,321,456	5,362,321

Fig. 32. Mesh convergence study for the CFD model. The data demonstrate the convergence of the mean highest values of heave and the distribution parameters of heave motion extremes (Maxima and Minima) for hulls C, C1, and C2, operating at a maximum beam Froude Number of 5.67 and a wave steepness of 0.028.
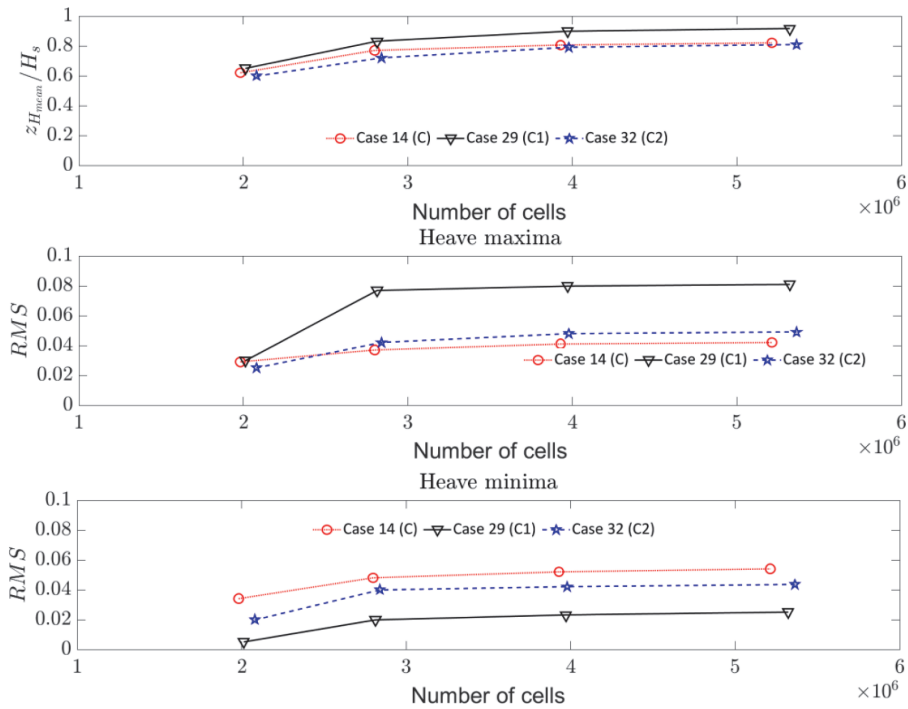
Fig. 33. Mesh convergence study for the CFD model. The data demonstrate the convergence of the mean highest values of pitch and the distribution parameters of pitch motion extremes (Maxima and Minima) for hulls C, C1, and C2, operating at a maximum beam Froude Number of 5.67 and a wave steepness of 0.028.
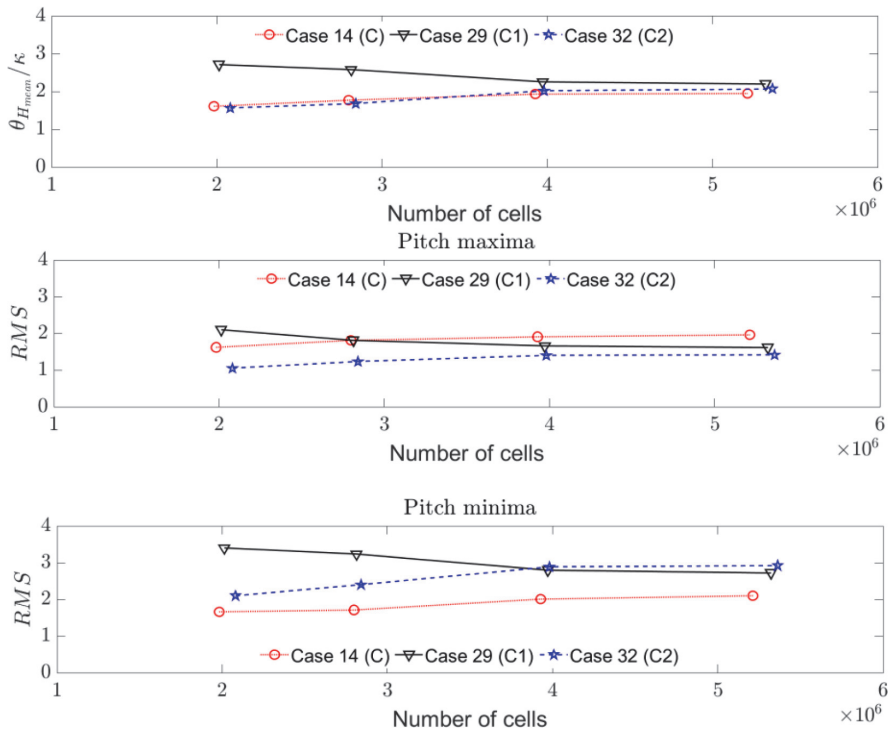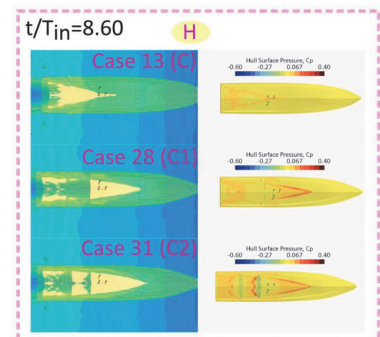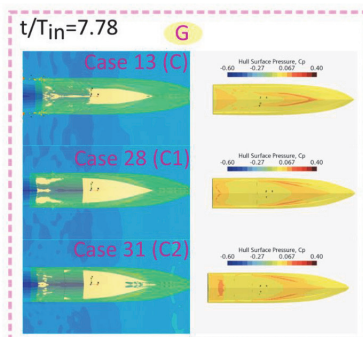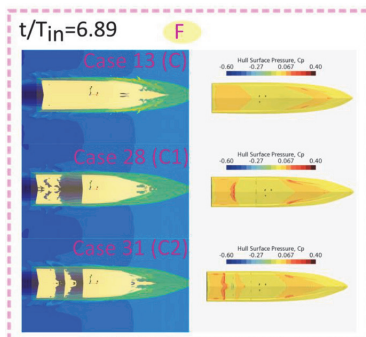
Appendix B: Time histories of heave, pitch, and CG vertical acceleration for C, C1, and C2 hulls
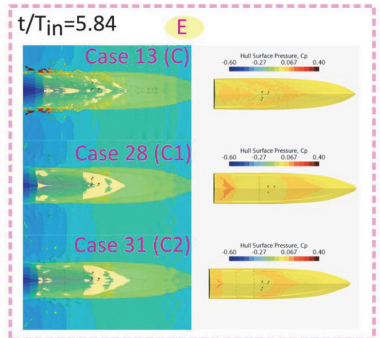
Appendix C: Distribution parameters

Table 7
Distribution parameters for maxima and minima of heave motion.

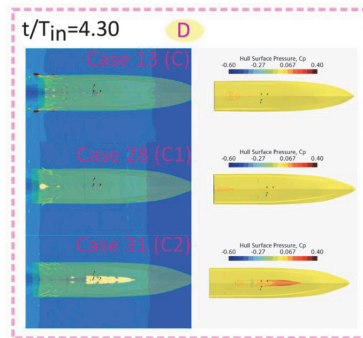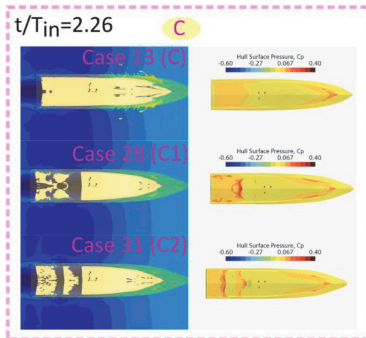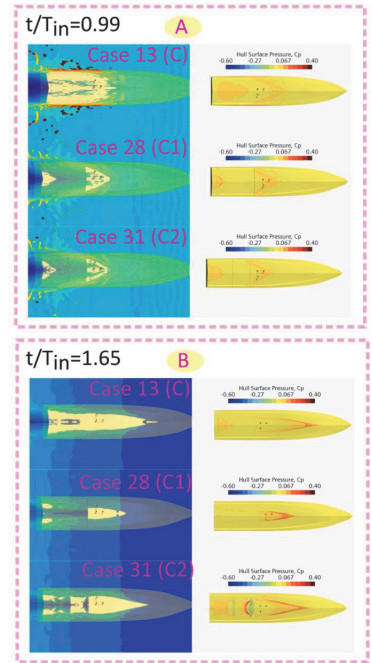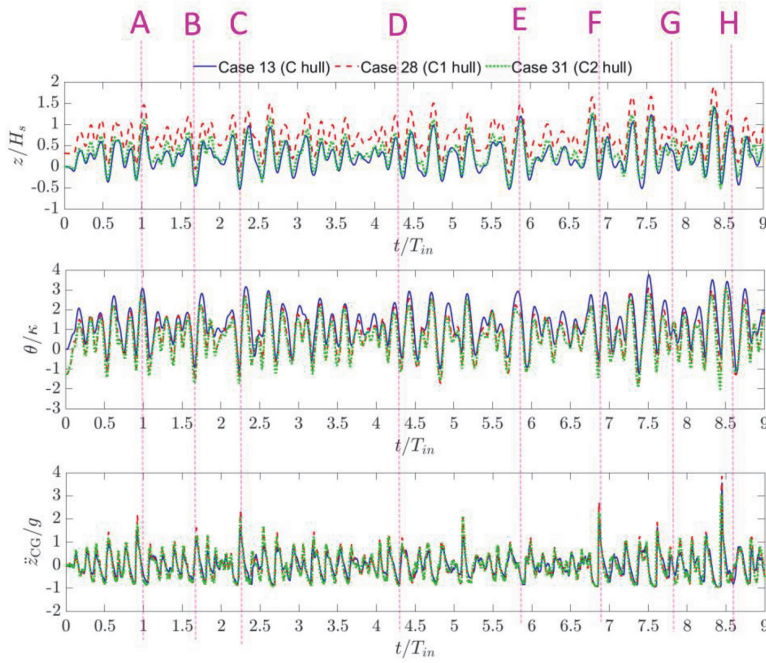| Cases	Heave maxima						Heave minima					
	EXP			CFD			EXP			CFD		
	Mean	RMS	r	Mean	RMS	r	Mean	RMS	r	Mean	RMS	r
C												
12	1.273	2.654	0.215	2.646	2.863	0.000	−0.036	0.043	0.079	−0.056	0.059	0.000
13	1.259	1.530	0.051	1.648	2.020	0.086	−0.040	0.045	0.028	−0.051	0.055	0.000
14	2.229	2.833	0.042	1.379	1.907	0.149	−0.055	0.058	0.000	−0.046	0.052	0.047
15	0.894	1.217	0.120	1.763	2.019	0.015	−0.032	0.036	0.033	−0.011	0.018	0.211
16	0.795	1.007	0.069	1.297	1.418	0.000	−0.025	0.031	0.033	−0.015	0.019	0.130
17	1.602	1.874	0.043	1.958	2.567	0.135	−0.080	0.087	0.000	−0.078	0.085	0.013
19	1.252	1.473	0.065	2.592	2.768	0.000	−0.030	0.032	0.000	−0.046	0.049	0.000
C1												
27	0.030	0.036	0.026	0.039	0.047	0.060	−0.027	0.036	0.165	−0.016	0.026	0.209
28	0.045	0.057	0.114	0.065	0.071	0.000	−0.047	0.051	0.000	−0.008	0.025	0.346
29	0.048	0.058	0.043	0.072	0.080	0.011	−0.052	0.058	0.000	−0.009	0.023	0.359
C2												
30	0.032	0.040	0.053	0.008	0.024	0.349	−0.030	0.037	0.065	−0.043	0.049	0.035
31	0.036	0.045	0.028	0.028	0.041	0.182	−0.040	0.045	0.000	−0.035	0.041	0.018
32	0.040	0.052	0.036	0.034	0.048	0.184	−0.044	0.050	0.037	−0.036	0.042	0.041
33	0.035	0.045	0.094	0.044	0.052	0.022	−0.038	0.041	0.000	−0.014	0.021	0.157

Table 8
Distribution parameters for maxima and minima of pitch motion.

Cases	Pitch maxima						Pitch minima					
	EXP			CFD			EXP			CFD		
	Mean	RMS	r	Mean	RMS	r	Mean	RMS	r	Mean	RMS	r
C												
12	0.038	0.052	0.12	0.006	0.023	0.368	−2.056	3.039	0.165	−0.343	1.216	0.384
13	0.039	0.056	0.139	0.020	0.035	0.259	−1.335	1.755	0.053	−1.653	2.055	0.096
14	0.051	0.068	0.13	0.026	0.041	0.186	−2.929	3.767	0.125	−1.733	2.006	0.030
15	0.029	0.043	0.200	0.035	0.042	0.018	−1.363	3.067	0.160	−0.549	0.995	0.288
16	0.024	0.033	0.097	0.024	0.027	0.044	−0.941	1.087	0.034	−0.945	1.127	0.063
17	0.069	0.094	0.190	0.041	0.062	0.228	−1.239	2.203	0.261	−2.180	2.777	0.094
19	0.031	0.040	0.101	0.006	0.022	0.410	−1.414	1.570	0.011	−1.264	1.730	0.179
C1												
27	1.223	1.465	0.076	1.694	2.047	0.116	- 1.419	1.704	0.051	−0.941	1.540	0.200
28	1.329	1.633	0.125	1.096	1.555	0.153	−1.611	1.790	0.026	−2.750	2.986	0.009
29	1.142	1.393	0.111	0.996	1.656	0.214	−1.287	1.507	0.037	−2.609	2.797	0.019
C2												
30	1.24	1.498	0.048	1.722	2.010	0.037	−1.387	1.732	0.072	−0.863	1.459	0.252
31	1.402	1.587	0.000	0.888	1.416	0.217	−1.563	1.780	0.027	−2.296	2.681	0.047
32	1.419	1.658	0.107	0.633	1.398	0.313	- 1.915	3.133	0.071	−2.650	2.880	0.000
33	1.426	1.809	0.063	1.004	1.495	0.187	−1.864	3.808	0.125	−2.159	2.342	0.000

Table 9
Gamma distribution parameters for minima CG vertical acceleration.

Cases	$\alpha_{Exp.}$	$\beta_{Exp.}$	α_{CFD}	β_{CFD}
C				
12	1.657	3.094	1.776	1.215
13	1.538	6.636	1.400	2.970
14	1.864	11.56	1.491	3.715
15	1.644	11.874	1.857	2.905
16	2.810	2.879	1.488	1.874
17	2.043	13.063	2.015	3.459
19	1.577	5.475	1.377	2.288
C1				
27	2.318	1.620	1.637	1.325
28	1.666	7.415	1.680	3.112
29	2.005	9.101	1.724	3.743
C2				
30	1.706	2.344	1.395	1.536

Table 9 (*continued*)

Cases	$\alpha_{Exp.}$	$\beta_{Exp.}$	α_{CFD}	β_{CFD}
31	1.707	6.208	1.589	3.130
32	3.114	5.326	1.777	3.695
33	3.590	6.937	2.105	3.446

Appendix D: The statistical analysis for heave and pitch motions, and CG vertical acceleration

Table 10

Statistics of heave, pitch and CG vertical acceleration measurements of C, C1, and C2 hull.

Cases	$\dfrac{z_{H_{mean}}}{H_s}$	$\dfrac{z_{H_{1/3}}}{H_s}$	$\dfrac{z_{H_{1/10}}}{H_s}$	$\dfrac{z_{H_{1/100}}}{H_s}$	$\dfrac{\theta_{H_{mean}}}{\kappa}$	$\dfrac{\theta_{H_{1/3}}}{\kappa}$	$\dfrac{\theta_{H_{1/10}}}{\kappa}$	$\dfrac{\theta_{H_{1/100}}}{\kappa}$	$\dfrac{CG_{H_{mean}}}{g}$	$\dfrac{CG_{H_{1/3}}}{g}$	$\dfrac{CG_{H_{1/10}}}{g}$	$\dfrac{CG_{H_{1/100}}}{g}$
C												
12	0.682	1.086	1.363	1.538	1.836	3.220	4.009	4.395	0.045	0.156	0.454	1.026
13	0.797	1.291	1.571	2.098	2.052	3.505	4.469	5.537	0.219	0.927	1.580	2.537
14	0.806	1.347	1.657	2.104	1.933	3.314	3.843	4.616	0.296	1.186	2.140	3.592
15	0.527	0.862	1.131	1.518	0.655	1.164	1.487	1.680	0.153	0.813	1.929	3.506
16	0.441	0.611	0.696	0.728	2.785	4.160	4.811	5.344	0.040	0.222	0.622	1.493
17	1.340	1.968	2.332	2.598	1.713	2.768	3.383	3.910	0.145	0.428	1.312	4.601
19	0.587	0.991	1.300	1.767	1.090	1.641	2.019	2.836	0.113	0.332	0.931	1.838
C1												
27	0.638	1.105	1.296	1.437	1.656	3.089	3.915	4.719	0.042	0.301	0.725	1.369
28	0.800	1.294	1.671	2.172	2.401	3.743	4.393	4.964	0.080	0.195	0.401	1.049
29	0.898	1.424	1.746	2.144	2.254	3.533	4.171	4.784	0.104	0.404	1.113	3.279
C2												
30	0.582	1.013	1.350	1.645	1.598	2.995	3.727	5.279	0.038	0.364	0.767	1.428
31	0.718	1.185	1.615	2.231	1.961	3.451	4.408	5.751	0.080	0.206	0.490	1.737
32	0.791	1.294	1.644	2.348	2.018	3.537	4.143	4.417	0.097	0.314	0.763	2.484
33	0.640	1.011	1.366	1.800	0.874	1.395	1.792	2.380	0.136	0.357	0.856	2.541

Appendix E: Kurtosis and skewness variations in heave, pitch, and CG vertical acceleration

Table 11

Kurtosis (K) and skewness (S) variations in heave, pitch, and CG vertical acceleration of C, C1, and C2 hull.

Skewness			Kurtosis		
Heave	Pitch	CG Acc.	Heave	Pitch	CG Acc.
C					
0.1027	−0.146	−0.3005	2.6475	2.6298	2.6814
0.2057	−0.1093	0.3131	2.818	2.6895	3.098
0.4368	0.0836	0.7432	3.333	2.536	4.3035
0.762	0.2141	0.9581	3.8098	2.9844	4.4119
0.1997	−0.1387	0.1112	2.5467	2.495	2.7372
0.3915	0.0613	1.371	2.8187	2.6155	6.0347
0.3931	−0.1213	0.2267	3.3605	2.8093	3.1474
C1					
0.1899	−0.2261	1.86E-04	2.5793	2.8541	3.0304
0.3559	−0.1517	0.5685	2.9453	2.4309	3.022
0.6343	0.053	0.9466	3.6414	2.4109	4.0101
C2					
−0.0052	−0.1669	0.1852	3.0715	3.1301	3.3307
0.3672	−0.2081	0.5058	3.0896	2.8041	3.3098
0.4479	−0.0012	0.7912	3.1659	2.5816	3.3632
0.7163	0.1217	1.0223	4.0307	2.9193	3.4649

References

Akers, R.H., 1999. Dynamic analysis of planing hulls in the vertical plane. In: Proceedings of the Society of Naval Architects and Marine Engineers. New England Section.

Algarín, R., Bula, A., 2021. A numeric study of the maneuverability of planing hulls with six degrees of freedom. Ocean Eng. 221, 108514 https://doi.org/10.1016/j.oceaneng.2020.108514.

Begovic, E., Bertorello, C., Pennino, S., 2014a. Experimental seakeeping assessment of a warped planing hull model series. Ocean Eng. 83, 1–15. https://doi.org/10.1016/j.oceaneng.2014.03.012.

Begovic, E., Bertorello, C., Pennino, S., 2014b. Planing hull seakeeping in irregular head seas. Trans. FAMENA 38 (3), 1–12.

Begovic, E., Bertorello, C., Pennino, S., Piscopo, V., Scamardella, A., 2016. Statistical analysis of planing hull motions and accelerations in irregular head sea. Ocean Eng. 112, 253–264. https://doi.org/10.1016/j.oceaneng.2015.12.012.

Blake, J.I.R., & Wilson, P.A. (2001). An analysis of planing craft vertical dynamics in calm water and waves. 77–90. https://eprints.soton.ac.uk/21656/.

Camilleri, J., Taunton, D.J., Temarel, P., 2018. Full-scale measurements of slamming loads and responses on high-speed planing craft in waves. J. Fluids Struct. 81, 201–229. https://doi.org/10.1016/j.jfluidstructs.2018.05.006.

Capasso, S., Tagliafierro, B., Mancini, S., Martínez-Estévez, I., Altomare, C., Domínguez, J.M., Viccione, G., 2023. Regular wave seakeeping analysis of a planing hull by smoothed particle hydrodynamics: a comprehensive validation. J. Mar. Sci. Eng. 11 (4), 4 https://doi.org/10.3390/jmse11040700.

Dashtimanesh, A., Esfandiari, A., Mancini, S., 2018. Performance prediction of two-stepped planing hulls using morphing mesh approach. J. Ship Product. Des. 34 (03), 236–248. https://doi.org/10.5957/JSPD.160046.

De Luca, F., Pensa, C., 2019. The naples systematic series – second part: irregular waves, seakeeping in head sea. Ocean Eng. 194, 106620 https://doi.org/10.1016/j.oceaneng.2019.106620.

De Marco, A., Mancini, S., Miranda, S., Scognamiglio, R., Vitiello, L., 2017. Experimental and numerical hydrodynamic analysis of a stepped planing hull. Appl. Ocean Res. 64, 135–154. https://doi.org/10.1016/j.apor.2017.02.004.

Di Caterino, F., Niazmand Bilandi, R., Mancini, S., Dashtimanesh, A., & Carlini, M. (2018, June 21). A numerical way for a stepped planing hull design and optimization. https://doi.org/10.3233/978-1-61499-870-9-220.

Esfandiari, A., Tavakoli, S., Dashtimanesh, A., 2020. Comparison between the dynamic behavior of the non-stepped and double-stepped planing hulls in rough water: a numerical study. J. Ship Prod. Des. 36 (01), 52–66. https://doi.org/10.5957/jspd.2020.36.1.52.

Ferziger, J.H., Perić, M., Street, R.L., 2019. Computational Methods for Fluid Dynamics. Springer.

Fridsma, G., 1971. A systematic study of the rough-water performance of Planing Boats. Irregular Waves—Part 2. https://apps.dtic.mil/sti/citations/AD0728788.

Garme, K., 2005. Improved time domain simulation of planing hulls in waves by correction of the near-transom lift. Int. Shipbuild. Progr. 52 (3), 201–230.

Garme, K., Rosén, A., 2003. TIME-Domain simulations and full-scale trials on planing craft in waves. Int. Shipbuild. Progr. 50 (3), 177–208.

Hasselmann, K., Barnett, T.P., Bouws, E., Carlson, H., Cartwright, D.E., Enke, K., Ewing, J.A., Gienapp, A., Hasselmann, D.E., Kruseman, P., Meerburg, A., Müller, P., Olbers, D.J., Richter, K., Sell, W., Walden, H., 1973. Measurements of Wind-Wave Growth and Swell Decay During the Joint North Sea Wave Project (JONSWAP). Ergänzungsheft Zur Deutschen Hydrographischen Zeitschrift. Reihe A, Nr. 12. https://pure.mpg.de/pubman/faces/ViewItemOverviewPage.jsp?itemId=item_3262854.

Hicks, J.D., Troesch, A.W., Jiang, C., 1995. Simulation and nonlinear dynamics analysis of planing hulls. J. Offshore Mech. Arctic Eng. 117 (1), 38–45. https://doi.org/10.1115/1.2826989.

Hirt, C.W., Nichols, B.D., 1981. Volume of fluid (VOF) method for the dynamics of free boundaries. J. Comput. Phys. 39 (1), 201–225. https://doi.org/10.1016/0021-9991(81)90145-5.

ITTC, 7.5-02-04-05, 2014. ITTC – Recommended Procedures and Guidelines. Seakeeping Tests.

ITTC, 7.5-02-07-02.1, 2014. ITTC – Recommended Procedures and Guidelines. Seakeeping Experiments.

ITTC 7.5-03-02-03. (2021). Recommended procedures and guidelines: practical guidelines for ship CFD.

Jin, S., Peng, H.(Heather), Qiu, W., Hunter, R., Thompson, S., 2023. Numerical simulation of planing hull motions in calm water and waves with overset grid. Ocean Eng. 287, 115858 https://doi.org/10.1016/j.oceaneng.2023.115858.

Judge, C., Mousaviraad, M., Stern, F., Lee, E., Fullerton, A., Geiser, J., Schleicher, C., Merrill, C., Weil, C., Morin, J., Jiang, M., Ikeda, C., 2020b. Experiments and CFD of a high-speed deep-V planing hull—Part I: calm water. Appl. Ocean Res. 96, 102060 https://doi.org/10.1016/j.apor.2020.102060.

Judge, C., Mousaviraad, M., Stern, F., Lee, E., Fullerton, A., Geiser, J., Schleicher, C., Merrill, C., Weil, C., Morin, J., 2020a. Experiments and CFD of a high-speed deep-V planing hull–part II: slamming in waves. Appl. Ocean Res. 97, 102059.

Keuning, J.A. (1994). Nonlinear Behaviour of Fast Monohulls in Head Waves. https://repository.tudelft.nl/islandora/object/uuid%3Aa2d52ad2-29b7-498e-b030-9306052ca1f5.

Keuning, J.A., & Pinkster, J. (1995). Optimisation of the seakeeping behaviour of a fast monohull. https://trid.trb.org/view/479814.

Klosinski, W.E., & Brown, P.W. (1993). Additional seakeeping model tests of two U.S. coast guard notional designs of 110 FT And 120 FT WPB hulls; final Rept (USCG-d-18-93). Article USCG-d-18-93. https://trid.trb.org/view/406002.

Lee, E.J., Diez, M., Harrison, E.L., Jiang, M.J., Snyder, L.A., Powers, A.M.R., Bay, R.J., Serani, A., Nadal, M.L., Kubina, E.R., Stern, F., 2024. Experimental and computational fluid-structure interaction analysis and optimization of Deep-V planing-hull grillage panels subject to slamming loads – Part II: irregular waves. Ocean Eng. 292, 116346 https://doi.org/10.1016/j.oceaneng.2023.116346.

Marlantes, K.E., Maki, K.J., 2021. Modeling Vertical Planing Boat Motions using a Neural-Corrector Method. In: SNAME International Conference on Fast Sea Transportation. https://doi.org/10.5957/FAST-2021-014.

Marlantes, K.E., Maki, K.J., 2022. A neural-corrector method for prediction of the vertical motions of a high-speed craft. Ocean Eng. 262, 112300 https://doi.org/10.1016/j.oceaneng.2022.112300.

Mousaviraad, S.M., Wang, Z., Stern, F., 2015. URANS studies of hydrodynamic performance and slamming loads on high-speed planing hulls in calm water and waves for deep and shallow conditions. Appl. Ocean Res. 51, 222–240. https://doi.org/10.1016/j.apor.2015.04.007.

Niazmand Bilandi, R., Dashtimanesh, A., Mancini, S., Vitiello, L, 2023b. Comparative study of experimental and CFD results for stepped planing hulls. Ocean Eng. 280, 114887 https://doi.org/10.1016/j.oceaneng.2023.114887.

Niazmand Bilandi, R., Dashtimanesh, A., Tavakoli, S, 2019. Development of a 2D+T theory for performance prediction of double-stepped planing hulls in calm water. Proc. Insti. Mech. Eng., Part M: J. Eng. Maritime Environ. 233 (3), 886–904. https://doi.org/10.1177/1475090218797784.

Niazmand Bilandi, R., Dashtimanesh, A., Tavakoli, S, 2020a. Hydrodynamic study of heeled double-stepped planing hulls using CFD and 2D+T method. Ocean Eng. 196, 106813 https://doi.org/10.1016/j.oceaneng.2019.106813.

Niazmand Bilandi, R., Dashtimanesh, A., Tavakoli, S, 2023a. Stepped hulls early stage design by implementing 2D+T method. HSMV 2023. IOS Press, pp. 23–32. https://doi.org/10.3233/PMST230005.

Niazmand Bilandi, R., Mancini, S., Dashtimanesh, A., Tavakoli, S, 2024. A revisited verification and validation analysis for URANS simulation of planing hulls in calm water. Ocean Eng. 293, 116589 https://doi.org/10.1016/j.oceaneng.2023.116589.

Niazmand Bilandi, R., Tavakoli, S., Dashtimanesh, A, 2021. Seakeeping of double-stepped planing hulls. Ocean Eng. 236, 109475 https://doi.org/10.1016/j.oceaneng.2021.109475.

Niazmand Bilandi, R., Vitiello, L., Mancini, S., Nappo, V., Roshan, F., Tavakoli, S., Dashtimanesh, A, 2020b. Calm-water performance of a boat with two swept steps at high-speeds: laboratory measurements and mathematical modeling. Procedia Manuf. 42, 467–474. https://doi.org/10.1016/j.promfg.2020.02.046.

Payne, P.R., 1994. Recent developments in "added-mass" planing theory. Ocean Eng. 21 (3), 257–309. https://doi.org/10.1016/0029-8018(94)90002-7.

Putra, A.M.F., Suzuki, H., 2024. Experimental and numerical study on the high-speed ship hydrodynamics influenced by an interceptor with varied angle of attack. Int. J. Naval Architect. Ocean Eng. 16, 100566 https://doi.org/10.1016/j.ijnaoe.2023.100566.

Reynolds, O., 1895. IV. On the dynamical theory of incompressible viscous fluids and the determination of the criterion. Philos. Trans. R. Soc. Lond. 186, 123–164. https://doi.org/10.1098/rsta.1895.0004.

Rosén, A., Begovic, E., Razola, M., Garme, K., 2017. High-speed craft dynamics in waves: challenges and opportunities related to the current safety philosophy. In: 16th International Ship Stability Workshop (ISSW 2017). Belgrade, Serbia, 2017. https://urn.kb.se/resolve?urn=urn:nbn:se:kth:diva-240876.

Rosén, A., Garme, K., 2004. Model experiment addressing the impact pressure distribution on planing craft in waves. Int. J. Small Craft Technol. 146.

Roshan, F., Dashtimanesh, A., Bilandi, R.N., 2020. Hydrodynamic characteristics of tunneled planing hulls in calm water. Brodogradnja : Teorija i Praksa Brodogradnje i Pomorske Tehnike 71 (1), 19–38. https://doi.org/10.21278/brod71102.

Savitsky, D., 1985. Planing Craft. Naval Eng. J. 97 (2), 113–141. https://doi.org/10.1111/j.1559-3584.1985.tb03397.x.

Sebastiani, L., Bruzzone, D., Gualeni, P., Rambaldi, G., Ruscelli, D., & Viviani, M. (2009). A practical method for the prediction of planing craft motions in regular and irregular waves. 687–696. https://doi.org/10.1115/OMAE2008-57946.

SIEMENS PLM. (2022). STAR CCM+ User's Guide Version 17.02.007.

Soletic, L., 2010. In: Seakeeping of a Systematic Series of Planing Hulls. The 2 nd Chesapeake Power Boat Symposium. Annapolis, Maryland.

Taunton, D.J., Hudson, D.A., Shenoi, R.A., 2011. Characteristics of a series of high speed hard chine planing hulls - part II: performance in waves. Int J Small Craft Technol 153, B1–B22. https://doi.org/10.3940/rina.ijsct.2011.b1.97.

Tavakoli, S., Dashtimanesh, A., 2017. Running attitudes of yawed planing hulls in calm water: development of an oblique 2D+T approach. Ships Offshore Struct. 12 (8), 1086–1099. https://doi.org/10.1080/17445302.2017.1316555.

Tavakoli, S., Dashtimanesh, A., 2019. A six-DOF theoretical model for steady turning maneuver of a planing hull. Ocean Eng. 189, 106328 https://doi.org/10.1016/j.oceaneng.2019.106328.

Tavakoli, S., Ghadimi, P., Dashtimanesh, A., Sahoo, P.K., 2015. Determination of hydrodynamic coefficients in roll motion of high-speed planing hulls. In: SNAME 13th International Conference on Fast Sea Transportation. https://doi.org/10.5957/FAST-2015-052.

Tavakoli, S., Niazmand Bilandi, R., Mancini, S., De Luca, F., Dashtimanesh, A., 2020. Dynamic of a planing hull in regular waves: comparison of experimental, numerical and mathematical methods. Ocean Eng. 217, 107959 https://doi.org/10.1016/j.oceaneng.2020.107959.

Troesch, A.W., Hicks, J.D., 1994. The efficient use of simulation in planing hull motion analysis. Naval Eng. J. 106 (1), 75–85. https://doi.org/10.1111/j.1559-3584.1994.tb02799.x.

van Deyzen, A.F.J, 2008. A nonlinear mathematical model of motions of a planning monohull in head seas. Delft University of Technology, Department of Marine Technology, Ship Hydromechanics Laboratory, Report No. 1595-P. In: Proceedings of the 6th International Conference on High-Performance Marine Vehicles, HIPER'08. University of Naples. ISBN: 88-901174-9-4. https://repository.tudelft.nl/islandora/object/uuid%3A7e524531-132c-4c4a-84d5-42fd0f2a1320.

Zarnick, E., 1979. A Nonlinear Mathematical Model of Motions of a Planing Boat in Irregular Waves (Technical Report DTNSRDC/SPD-0867-01). David Taylor Naval Ship Research and Development Center. https://apps.dtic.mil/sti/citations/ADA078605.

Zarnick, E.E., Turner, C.R., 1981. Rough Water Performance of High Length to Beam Ratio Planing Boats (DTNSRDC/SPD-0973-01). David W. Taylor Naval Ship Research and Development Center. https://apps.dtic.mil/sti/citations/ADA108815.

Curriculum vitae

Personal data

Name:	Rasul Niazmand Bilandi ETIS, ORCID, SCOPUS
Date of birth:	09.09.1991
Place of birth:	Gonabad, Iran
Citizenship:	Iran

Contact data

E-mail:	rasul.niazmand@taltech.ee

Education

2021–2024	Tallinn University of Technology, Estonian Maritime Academy, Engineering Sciences, PhD.
2015–2018	Persian Gulf University, School of Engineering, Naval Architecture, Hydromechanics, MSc.
2010–2014	Petroleum University of Technology, Mahmood Abad Faculty of Marine Sciences, Ship Engineering, Engine, BSc.

Language competence

English	Fluent
Estonian	A1
Persian	Native

Fields of research

ETIS RESEARCH FIELD: 4. Natural Sciences and Engineering; 4.13. Mechanical Engineering, Automation Technology and Manufacturing Technology; CERCS RESEARCH FIELD: T210 Mechanical engineering, hydraulics, vacuum technology, vibration acoustic engineering; SPECIFICATION: Ship Hydrodynamics, CFD Simulation, High Speed Craft, Fuel efficiency.

Professional employment

2021–2024	Tallinn University of Technology, Estonian Maritime Academy, Early-stage Researcher.
2019–2021	Lecturer, Engineering Department, Persian Gulf University.
2017–2024	Researcher and remote CFD engineer at Eurisco Consulting Srls Italy Company Group, R&D Company.
2016–2018	Field Engineer, Survey Engineer at DP vessel.
2015–2015	Third engineer at pipe laying barge (4 month).
2014–2014	Fifth engineer at Islamic Republic of Iran Shipping Lines (IRISL) (6 month).

Completed projects

VIR20039 "Green Cruising for High-speed Small Craft in The Baltic Sea" (1.10.2020–30.09.2021); Principal Investigator: Abbas Dashtimanesh; Tallinn University of Technology, Estonian Maritime Academy; Financier: IB.SH - Investitionbank Schleswig-Holstein; Financing: 19 000 EUR.

Visiting activities:

27.11.2023–08.12.2023	Visiting researcher at KTH Royal Institute of Technology, Department of Engineering Mechanics, SCI by Erasmus+ scholarship.
01.05.2024–30.09.2024	Visiting researcher at University of Naples "Federico II", Department of Industrial Engineering by Erasmus+ scholarship.

Workshop:

2024	DNV Nordic Maritime Universities Workshop 2024 at Aalto University. The abstract I have presented is titled "Modeling Planing Hull Motion in Waves."
2024	Model and Full-scale Resistance Prediction and Comparison Workshop (CFD Workshop, Jores Project, Chalmers University)

Teaching experience:

2022	Teaching assistant in Ship seagoing characteristics and optimization of ship handling at Tallinn University of Technology, Estonian Maritime Academy.
2020	Taught Numerical Analysis using MATLAB at Persian Gulf University, Engineering Department.
2019	Taught Computer Programming using MATLAB at Persian Gulf University, Engineering Department.

Publications

2024

Niazmand Bilandi, R., Tavakoli, S., Mancini, S., and Dashtimanesh, A. (2024). Dynamic Motion Analysis of Stepless and Stepped Planing Hulls in Random Waves: A CFD Model Perspective. Applied Ocean Research 149:104046. doi: 10.1016/j.apor.2024.104046.

Niazmand Bilandi, R., Mancini, S., Dashtimanesh, A., Tavakoli, S. (2024). A revisited verification and validation analysis for URANS simulation of planing hulls in calm water. Ocean Engineering, 293, 116589. https://doi.org/10.1016/j.oceaneng.2023.116589.

Sulman, M., Mancini, S., **Niazmand Bilandi, R.** (2024). Numerical Investigation of Single and Double Steps in Planing Hulls. Journal of Marine Science and Engineering, 12(4), Article 4. https://doi.org/10.3390/jmse12040614.

2023

Niazmand Bilandi, R., Dashtimanesh, A., Mancini, S. and Vitiello, L., (2023). Comparative study of experimental and CFD results for stepped planing hulls. Ocean Engineering, 280, p.114887. DOI: https://doi.org/10.1016/j.oceaneng.2023.114887.

Niazmand Bilandi, R., Dashtimanesh, A., Tavakoli, S. (2023). Stepped Hulls Early Stage Design by Implementing 2D+t Method. In *HSMV 2023* (pp. 23–32). IOS Press. https://doi.org/10.3233/PMST230005.

Niazmand Bilandi, R., Mancini, S., Dashtimanesh, A., Lakatos, M. (2023). How to Improve Full-Scale Self-Propulsion Simulations? A Case Study on a Semi-Displacement Hull. In HSMV 2023 (pp. 265–274). IOS Press. https://doi.org/10.3233/PMST230034.

2022

Vitiello, L., Mancini, S., **Niazmand Bilandi, R.,** Dashtimanesh, A., De Luca, F. and Nappo, V. (2022). A comprehensive stepped planing hull systematic series: Part 1- Resistance test. Ocean Engineering, 266, p.112242. DOI: https://doi.org/10.1016/j.oceaneng.2022.112242.

Spinelli, F., Mancini, S., Vitiello, L., **Niazmand Bilandi, R.,** De Carlini, M. (2022). Shipping Decarbonization: An Overview of the Different Stern Hydrodynamic Energy Saving Devices. Journal of Marine Science and Engineering, 10 (5), 574. DOI: 10.3390/jmse10050574.

Dashtimanesh, A., Ghaemi, M. H., Wang, Y., Karczewski, A., **Niazmand Bilandi, R.,** Hirdaris, S. (2022). Digitalization of High Speed Craft Design and Operation Challenges and Opportunities. Procedia Computer Science, 200, 566–576. DOI: 10.1016/j.procs.2022.01.254.

2021

Niazmand Bilandi, R., Tavakoli, S., Dashtimanesh, A. (2021). Seakeeping of double-stepped planing hulls. Ocean Engineering, 236, 109475. DOI: 10.1016/j.oceaneng.2021.109475.

2020

Tavakoli, S., **Niazmand Bilandi, R.,** Mancini, S., De Luca, F., Dashtimanesh, A. (2020). Dynamic of a planing hull in regular waves: Comparison of experimental, numerical and mathematical methods. Ocean Engineering, 217, 1–24. DOI: 10.1016/j.oceaneng.2020.107959.

Niazmand Bilandi, R., Dashtimanesh, A., Tavakoli, S. (2020). Hydrodynamic study of heeled double-stepped planing hulls using CFD and 2D+t method. Ocean Engineering, 196, #106813. DOI: 10.1016/j.oceaneng.2019.106813.

Roshan, F., Dashtimanesh, A., **Niazmand Bilandi, R.,** (2020). Hydrodynamic characteristic of tunneled planing hulls in calm water. Brodogradnja, 71 (1), 19–38. DOI: 10.21278/brod71102.

Jamei, S.; Adi, J., **Niazmand Bilandi, R.,** Azwadi, N., Mancini, S., Vitiello, L., De Carlini, M. (2020). Wake behind a compound wing in ground effect. Journal of Marine Science and Engineering, 8 (3), 156. DOI: 10.3390/jmse8030156.

Roshan, F., Dashtimanesh, A., Tavakoli, S., **Niazmand Bilandi, R.,** Abyn, H. (2020). Hull–propeller interaction for planing boats: a numerical study. Ships and Offshore Structures, 1–13. DOI: 10.1080/17445302.2020.1790295.

Niazmand Bilandi, R., Vitiello, L., Mancini, S., Nappo, V., Roshan, F., Tavakoli, S., Dashtimanesh, A. (2020). Calm-water performance of a boat with two swept steps at high-speeds: Laboratory measurements and mathematical modeling. *Procedia Manufacturing, 42*, 467–474. DOI: 10.1016/j.promfg.2020.02.046.

Vitiello, L., Mancini, S., **Niazmand Bilandi, R.**, Nappo, V. (2020). *An Overview of Stepped Hull Performance Evaluation: Sea Trial Data vs Full-Scale CFD Simulation*. HSMV 2020 (2020): 58-65. https://doi.org/10.3233/PMST200026

2019

Niazmand Bilandi, R., Dashtimanesh, A., Tavakoli, S. (2019). Development of a 2D+t theory for performance prediction of double-stepped planing hulls in calm water. Proceedings of the Institution of Mechanical Engineers Part M Journal of Engineering for the Maritime Environment, 233 (3), 886–904. DOI: 10.1177/1475090218797784.

Mancini, S., Pensa, C., Vitiello, L., **Niazmand Bilandi, R.** (2019). The Failed Project of the "Heavy" MAS. *International Conference on Nautical and Maritime Culture: International Conference on Nautical and Maritime Culture, Nautical and Maritime Culture, from the Past to the Future, Naples, Italy, 14-15 November.* IOS Press, 159–169. DOI: 10.3233/PMST190017.

2018

Niazmand Bilandi, R., Jamei, S., Roshan, F., Azizi, M. (2018). Numerical simulation of vertical water impact of asymmetric wedges by using a finite volume method combined with a volume-of-fluid technique. Ocean Engineering, 160, 119–131. DOI: 10.1016/j.oceaneng.2018.04.043.

Niazmand Bilandi, R., Mancini, S., Vitiello, L., Miranda, S., De Carlini, M. (2018). A validation of symmetric 2D + T model based on single-stepped planing hull towing tank tests. Journal of Marine Science and Engineering, 6 (4), 136. DOI: 10.3390/jmse6040136.

Di Caterino, F., **Niazmand Bilandi, R.,** Mancini, S., Dashtimanesh, A., De Carlini, M. (2018). A numerical way for a stepped planing hull design and optimization. *Technology and Science for the Ships of the Future: Proceedings of NAV 2018: 19th International Conference on Ship & Maritime Research: Technology and Science for the Ships of the Future: Proceedings of NAV 2018: 19th International Conference on Ship & Maritime Research, 20-22 June 2018, Trieste, Italy.* IOS Press, 220–229. DOI: 10.3233/978-1-61499-870-9-220.

Elulookirjeldus

Isikuandmed

Nimi:	Rasul Niazmand Bilandi ETIS, ORCID, SCOPUS
Sünniaeg:	09.09.1991
Sünnikoht:	Gonabad, Iraan
Kodakondsus:	Iraani

Kontaktandmed

E-post:	rasul.niazmand@taltech.ee

Hariduskäik

2021–2024	Tallinna Tehnikaülikool, Eesti Mereakadeemia, Tehnikateadused, PhD.
2015–2018	Pärsia Lahe Ülikool, Inseneriteaduskond, Laevaehitus, Hüdromehaanika, MSc.
2010–2014	Nafta Tehnikaülikool, Mahmood Abadi Mereaineteaduskond, Laevainsener, Masin, BSc.

Keelteoskus

Inglise keel	Kõrgtase
Eesti keel	A1
Pärsia keel	Emakeel

Teadustöö põhisuunad

ETIS TEADUSVALDKOND: 4. Loodusteadused ja tehnika; 4.13. Masinaehitus, automaatikatehnika ja tootmistehnika; CERCS TEADUSVALDKOND: T210 Masinaehitus, hüdraulika, vaakumtehnika, vibratsiooniakustika; SPETSIFIKATSIOON: Laevade hüdrodünaamika, CFD simulatsioon, Kiirekäiguline laev, Kütuse tõhusus.

Teenistuskäik

2021–2024	Tallinna Tehnikaülikool, Eesti Mereakadeemia, nooremteadur.
2019–2021	Lektor, Inseneriteaduskond, Pärsia Lahe Ülikool.
2017–2024	Teadur ja kaug-CFD insener Eurisco Consulting Srls Itaalia Firmagrupis, R&D ettevõttes.
2016–2018	Välisinsener, Uurimisinsener DP laeval.
2015–2015	Kolmas insener torupaigalduspargil (4 kuud).
2014–2014	Viies insener Iraani Islamivabariigi Laevandusliinides (IRISL) (6 kuud).

Lõppenud projektid

VIR20039 "Keskkonnasäästlikud väikesed kiirlaevad Läänemerel" (1.10.2020–30.09.2021); Vastutav täitja: Abbas Dashtimanesh; Tallinna Tehnikaülikool, Eesti Mereakadeemia; Finantseerija: IB.SH - Investitionbank Schleswig-Holstein; Eraldatud summa: 19 000 EUR.

Külastustegevused

27.11.2023–08.12.2023	Külalisteadur KTH Kuninglikus Tehnoloogiainstituudis, Insenerimehaanika osakonnas, SCI Erasmus+ stipendiumiga.
01.05.2024–30.09.2024	Külalisteadur Napoli Ülikoolis "Federico II", Tööstusinseneri osakonnas Erasmus+ stipendiumiga.

Töötuba:

2024	DNV Nordic Maritime Universities Workshop 2024, Aalto Ülikool. Minu esitatud abstrakt kannab pealkirja" Modeling Planing Hull Motion in Waves."
2024	Model and Full-scale Resistance Prediction and Comparison Workshop (CFD Workshop, Jores Project), Chalmersi Ülikool.

Külastustegevused

2022	Õpetamisassistent Laeva meresõiduomaduste ja laevajuhtimise optimeerimise kursusel Tallinna Tehnikaülikoolis, Eesti Mereakadeemias.
2020	Õpetas numbrilist analüüsi kasutades MATLABi Pärsia Lahe Ülikoolis, Inseneriteaduskonnas.
2019	Õpetas Arvutiprogrammeerimist kasutades MATLABi Pärsia Lahe Ülikoolis, Inseneriteaduskonnas.

Publikatsioonid

Avaldatud teadusartiklite, muude publikatsioonide ja peetud konverentsiettekannete loetelu on lisatud ingliskeelsele elulookirjeldusele.